CENTER FOR TRANSPORTATION INFRASTRUCTURE AND SAFETY

Design and Evaluation of High-Volume Fly Ash (HVFA) Concrete Mixes

by

Jeffery S. Volz, SE, PE, PhD (Principal Investigator)
John J. Myers, PE, PhD (Co-Principal Investigator)
David N. Richardson, PE, PhD (Co-Principal Investigator)
Mahdi Arezoumandi
Karl Beckemeier
Drew Davis
Kyle Holman
Trevor Looney
Brian Tucker

NUTC R268

Disclaimer

The contents of this report reflect the views of the author(s), who are responsible for the facts and the accuracy of information presented herein. This document is disseminated under the sponsorship of the Department of Transportation, University Transportation Centers Program and the Center for Transportation Infrastructure and Safety NUTC program at the Missouri University of Science and Technology, in the interest of information exchange. The U.S. Government and Center for Transportation Infrastructure and Safety assumes no liability for the contents or use thereof.

Technical Report Documentation Page

1. Report No. NUTC R268	2. Government Accession No.	3. Recipient's Catalog No.
4. Title and Subtitle Design and Evaluation of High-Volume Fly Ash (HVFA) Concrete Mixes		5. Report Date October 2012
		6. Performing Organization Code
7. Author/s Jeffery S. Volz, SE, PE, PhD (Principal Investigator) , John J. Myers, PE, PhD (Co-Principal Investigator) , David N. Richardson, PE, PhD (Co-Principal Investigator), Mahdi Arezoumandi Karl Beckemeier, Drew Davis, Kyle Holman, Trevor Looney, Brian Tucker		8. Performing Organization Report No. 00033573
9. Performing Organization Name and Address Center for Transportation Infrastructure and Safety/NUTC program Missouri University of Science and Technology 220 Engineering Research Lab Rolla, MO 65409		10. Work Unit No. (TRAIS)
		11. Contract or Grant No. DTRT06-G-0014
12. Sponsoring Organization Name and Address U.S. Department of Transportation Research and Innovative Technology Administration 1200 New Jersey Avenue, SE Washington, DC 20590		13. Type of Report and Period Covered Final
		14. Sponsoring Agency Code

15. Supplementary Notes

16. Abstract

Concrete is the world's most consumed man-made material. Unfortunately, the production of portland cement, the active ingredient in concrete, generates a significant amount of carbon dioxide. For each pound of cement produced, approximately one pound of carbon dioxide is released into the atmosphere. With cement production reaching nearly 6 billion tons per year worldwide, the sustainability of concrete is a very real concern.

Since the 1930's, fly ash – a pozzolanic material – has been used as a partial replacement of portland cement in concrete to improve the material's strength and durability, while also limiting the amount of early heat generation. From an environmental perspective, replacing cement with fly ash reduces concrete's overall carbon footprint and diverts an industrial by-product from the solid waste stream (currently, about 40 percent of fly ash is reclaimed for beneficial reuse and 60 percent is disposed of in landfills).

Traditional specifications limit the amount of fly ash to 25 or 30 percent cement replacement. Recent studies, including those by the investigators, have shown that higher cement replacement percentages – even up to 75 percent – can result in excellent concrete in terms of both strength and durability. Referred to as high-volume fly ash (HVFA) concrete, this material offers a viable alternative to traditional portland cement concrete and is significantly more sustainable. By nearly doubling the use of reclaimed fly ash in concrete, HVFA concrete aligns well with MoDOT's green initiative on recycling.

However, HVFA concrete is not without its problems. At all replacement rates, fly ash generally slows down the setting time and hardening rates of concrete at early ages, especially under cold weather conditions, and when less reactive fly ashes are used. Furthermore, with industrial by-products, some variability in physical and chemical characteristics will normally occur, not only between power plants but also within the same plant. Consequently, to achieve the benefits of HVFA concrete, guidelines are needed for its proper application in bridges, roadways, culverts, retaining walls, and other transportation-related infrastructure components. The objective of this research was to design, test, and evaluate HVFA concrete mixtures. The study focused on the hardened properties of HVFA concrete containing aggregates and fly ash indigenous to the state of Missouri and developed guidelines on its use in infrastructure elements for MoDOT.

17. Key Words		18. Distribution Statement		
Cement, Concrete, Flexural Behavior, Fly Ash, High-Volume Fly Ash Concrete, Mix Design, Mix Optimization, Reinforcing Bond, Reinforced Concrete, Shear Behavior, Sustainability.		No restrictions. This document is available to the public through the National Technical Information Service, Springfield, Virginia 22161.		
19. Security Classification (of this report) unclassified		20. Security Classification (of this page) unclassified	21. No. Of Pages 819	22. Price

<div align="center">Form DOT F 1700.7 (8-72)</div>

EXECUTIVE SUMMARY

On behalf of the Missouri Department of Transportation (MoDOT), Missouri University of Science and Technology (Missouri S&T) completed a research study on high-volume fly ash (HVFA) concrete using fly ashes and aggregates indigenous to the State of Missouri. The report, entitled *Design and Evaluation of High-Volume Fly Ash (HVFA) Concrete Mixes*, consists of a summary report followed by five detailed technical reports. Taken together, these reports document the background, detailed approaches, experimental procedures and processes, results, findings, conclusions, and recommendations of the study.

The research work plan included eight tasks consisting of the following: (1) Task 1: Literature Review, (2) Task 2: Mix Development, (3) Task 3: Hardened Properties of HVFA Concrete Mixes, (4) Task 4: Bond and Development of Mild Steel, (5) Task 5: Full Scale Specimen Tests, (6) Task 6: AASHTO & ACI Code Comparison of Test Results, (7) Task 7: Recommendations & Specifications for Implementing HVFA Concrete, and (8) Task 8: Value to MoDOT and Stakeholders to Implementing HVFA Concrete.

Based on the results of Tasks 1 through 6, the researchers recommend the implementation of HVFA concrete in the construction of transportation-related infrastructure in the State of Missouri. However, the investigators also recommend initially limiting the fly ash replacement levels to 50% and avoiding applications subjected to direct deicing chemicals, such as bridge decks and pavements, due to potential scaling issues.

To alleviate any potential construction delays due to low early-age strength gains, the researchers recommend two approaches: (1) lowering the water-cementitious materials (*w/cm*) ratio compared to equivalent conventional concrete mixes or (2) adding powder activators such as gypsum, lime, and rapid-set cement. In general, the gypsum and lime powder activators offer the greatest benefits to early-age strength gain, with recommended dosages of 4% gypsum and 10% lime as a function of the amount of fly ash. At the recommended initial levels of 50% fly ash replacement, lowering the *w/cm* ratio is also a very viable approach to any early-age strength gain issues, particularly since the high amount of fly ash will significantly improve workability even without water-reducing admixtures.

On average, replacing even 50% of the cement used in concrete with fly ash will reduce the annual amount of greenhouse gas emissions by nearly 1.8 billion tons worldwide. Furthermore, this change would also eliminate more than 20 billion cubic feet of landfill space each year. In terms of energy consumption, this fly ash replacement level would save the equivalent of 6.7 trillion cubic feet of natural gas annually.

There are additional benefits of using fly ash to replace a significant portion of the cement in concrete. In terms of monetary savings, fly ash costs approximately one-half the amount for cement. For the same workability, fly ash reduces the amount of potable mixing water by approximately 20%. Even more importantly, fly ash increases the durability of concrete beyond what can be attained with portland cement alone. Increased durability translates into increased sustainability by extending the useful life of the material.

ACKNOWLEDGEMENTS

TABLE OF CONTENTS

LIST OF ILLUSTRATIONS

LIST OF TABLES

1. INTRODUCTION

1.1. REPORT ORGANIZATION

The following report documents a research project on high-volume fly ash (HVFA) concrete performed by Missouri University of Science and Technology (Missouri S&T) on behalf of the Missouri Department of Transportation (MoDOT). The report consists of a Summary Report followed by five detailed technical reports. Section 1 of the Summary Report presents the report organization and background for the study. The project work plan is presented in Section 2 to familiarize the reader with the overall objectives, project tasks, and scope of the research study. Following the project work plan, the summary findings, conclusions, and recommendations are presented task by task in Section 3. Detailed Technical Reports A through E are attached following the Summary Report, which provides the detailed specifics undertaken in this research investigation. The Summary Report is designed to provide the reader with the project highlights in terms of findings, conclusions, and recommendations, while Technical Reports A through E provide the background, detailed approaches, experimental procedures and processes, results, findings, conclusions, and recommendations.

1.2. BACKGROUND

Concrete is the world's most consumed man-made material. Unfortunately, the production of portland cement, the active ingredient in concrete, generates a significant amount of carbon dioxide. For each pound of cement produced, approximately one pound of carbon dioxide is released into the atmosphere. With cement production reaching

nearly 6 billion tons per year worldwide, the sustainability of concrete is a very real concern.

Since the 1930's, fly ash – a pozzolanic material – has been used as a partial replacement of portland cement in concrete to improve the material's strength and durability, while also limiting the amount of early heat generation. From an environmental perspective, replacing cement with fly ash reduces concrete's overall carbon footprint and diverts an industrial by-product from the solid waste stream (currently, about 40 percent of fly ash is reclaimed for beneficial reuse and 60 percent is disposed of in landfills).

Traditional specifications limit the amount of fly ash to 25 or 30 percent cement replacement. Recent studies, including those by the investigators, have shown that higher cement replacement percentages – even up to 75 percent – can result in excellent concrete in terms of both strength and durability. Referred to as HVFA concrete, this material offers a viable alternative to traditional portland cement concrete and is significantly more sustainable. By nearly doubling the use of reclaimed fly ash in concrete, HVFA concrete aligns well with MoDOT's green initiative on recycling ("MoDOT Keeps Billions of Pounds of Waste from Landfills," MoDOT News Release, September 20, 2010).

However, HVFA concrete is not without its problems. At all replacement rates, fly ash generally slows down the setting time and hardening rates of concrete at early ages, especially under cold weather conditions, and when less reactive fly ashes are used. Furthermore, with industrial by-products, some variability in physical and chemical characteristics will normally occur, not only between power plants but also within the

same plant. Consequently, to achieve the benefits of HVFA concrete, guidelines are

needed for its proper application in bridges, roadways, culverts, retaining walls, and other

transportation-related infrastructure components.

2. PROJECT WORK PLAN

As with most research projects, the project work plan evolved during the course of the study as results became available. The work plan described below reflects the work as completed on the project.

The *objective* of the research was to design, test, and evaluate HVFA concrete mixtures. The study focused on the hardened properties of HVFA concrete containing aggregates and fly ash indigenous to the state of Missouri and developed guidelines on its use in infrastructure elements for MoDOT. The *project work plan* included eight (8) tasks necessary to reach this goal and consisted of the following:

1. Task 1: Literature Review

2. Task 2: Mix Development

3. Task 3: Hardened Properties of HVFA Concrete Mixes

4. Task 4: Bond and Development of Mild Steel

5. Task 5: Full Scale Specimen Tests

6. Task 6: AASHTO & ACI Code Comparison of Test Results

7. Task 7: Recommendations & Specifications for Implementing HVFA Concrete

8. Task 8: Value to MoDOT and Stakeholders to Implementing HVFA Concrete

The following sections discuss each of these individual tasks.

2.1. TASK 1: LITERATURE REVIEW

The purpose of this task was to conduct a comprehensive and critical literature review of past experiences and previous research on HVFA concrete, with particular

attention to the impact that these findings may have on the work plan. Specifically, the literature review focused on studies involving the hardened properties of HVFA concrete that affect structural performance (e.g., compressive strength, bond, shear strength) and durability (e.g., freeze-thaw resistance, permeability), particularly the role of local aggregates and fly ash sources. Furthermore, to establish a solid background for the study, the investigators also reviewed literature on HVFA concrete related to fresh properties, admixtures, and mix design methods.

2.2. TASK 2: MIX DEVELOPMENT

The aim of this task was to develop several HVFA concrete mix designs that maximized the percentage of fly ash yet still fulfill typical construction needs, such as early strength development. These mix designs will then serve as the basis for the subsequent research. One (1) traditional concrete mix design served as a control during the research. Concrete properties, particularly at higher strengths, are very dependent on aggregate type, so comparison mixes were necessary to allow an unbiased assessment of HVFA concrete mixes containing Missouri aggregates. This task involved three (3) subtasks.

2.2.1. Subtask 2a: Characterize Missouri Fly Ash Sources. The investigators obtained fly ash samples from a variety of coal-fired power plants in Missouri, including Ameren's Labadie, Meramec, and Rush Island plants and Kansas City Power & Light's LaCygne, and Nearman plants (the Iatan plant had a shutdown during the course of the project). All of these plants produce an ASTM C 618 (AASHTO M 295) Class C fly ash.

However, studies have shown that the pozzolanic and cementitious quality of fly ash can vary significantly between sources and even within the same plant.

As a result, in addition to the traditional oxide analyses, the investigators performed x-ray diffraction (XRD) and scanning electron microscopy (SEM) techniques to characterize the mineralogical composition of the different fly ash sources. This step was necessary in order to characterize the amount and composition of the glassy phases, as well as the amount of calcium silicates and calcium aluminates present in the fly ash. Both of these factors have a significant influence on the pozzolanic and cementitious properties of the fly ash, and the maximum percentages that can be successfully used in the HVFA concrete mixes.

2.2.2. Subtask 2b: Establish Maximum Fly Ash Replacement Percentages.

The Class C fly ash produced in Missouri has significant potential for HVFA concrete mixtures. In a previous study for the Ameren Corporation, the investigators successfully developed a 75 percent fly ash concrete with a 28-day compressive strength of 4,250 psi. More importantly, the concrete reached 910 psi in one (1) day and 2,880 psi in seven (7) days, which is conducive to a traditional construction environment. To reach these early strength gains, the investigators added gypsum, calcium hydroxide, and calcium sulfoaluminate cements to the fly ash and Type I portland cement mixture. This part of the study used paste mixes to arrive at the optimum combinations and percentages of several additives to maximize the percentage of fly ash. The primary criteria at this stage of the research was set time and rate of strength gain. The results from this subtask formed the basis of Subtask 2c.

2.2.3. Subtask 2c: Develop HVFA Concrete Mixes. Based on the results of Subtask 2b, the investigators developed several HVFA concrete mix designs that maximized the percentage of fly ash yet still fulfill typical construction needs, such as early strength development. The results of Subtask 2b determined whether each of the Missouri fly ash sources required a different formulation to maximize the fly ash percentage yet still achieve similar set times and strength gains. Consequently, the number of HVFA concrete mix designs depended on the results of Subtask 2b. Subtask 2c also evaluated the impact of Missouri aggregates on the properties of HVFA concrete. The primary criteria at this stage of the research was set time and rate of strength gain. The final mix design choices and target strength levels were approved by MoDOT prior to the start of test specimen construction.

2.3. TASK 3: HARDENED PROPERTIES OF HVFA CONCRETE MIXES

The objective of the proposed research was to design, test, and evaluate HVFA concrete mixtures containing aggregates and fly ash indigenous to the state of Missouri. As such, in Task 3, the investigators focused on the hardened properties of HVFA concrete as compared to traditional concrete mixes. Task 3 involved three (3) subtasks.

2.3.1. Subtask 3a: Test Matrix. **Table 1** represents the test matrix for this research study based on MoDOT's requirements and the opinions of the investigators. Broadly speaking, the tests are classified into four (4) main categories: fresh concrete properties (*e.g.*, slump), hardened mechanical properties (*e.g.*, compressive strength, shrinkage), durability (*e.g.*, freeze-thaw resistance), and structural performance (*e.g.*, bond, shear strength).

Table 1 – Concrete Test Methods and Protocols

PROPERTY	TEST METHOD	TEST TITLE/DESCRIPTION	TASK
FRESH CONCRETE PROPERTY TESTS			
Unit Weight	ASTM C 138	Standard Test Method for Density (Unit Weight).	MSTR
Air Content	ASTM C 231	Standard Test Method for Air Content of Freshly Mixed Concrete by the Pressure Method.	MSTR
Slump	ASTM C 143	Standard Test Method for Slump of Hydraulic-Cement Concrete.	MSTR
Time of Set	ASTM C 403	Standard Test Method for Time of Setting of Concrete Mixtures by Penetration Resistance.	MSTR
Miniature Slump Test	Non-ASTM	A method to study rheological properties of cement pastes.	MSTR
Calorimetry	Non-ASTM	A method to study rate of set and strength gain based on heat evolution of paste, mortar, and concrete mixtures.	MSTR
HARDENED MECHANICAL PROPERTY TESTS			
Compressive Strength	ASTM C 39	Standard Test Method for Compressive Strength of Cylindrical Concrete Specimens.	3
Splitting Tensile Strength	ASTM C 496	Standard Test Method for Splitting Tensile Strength of Cylindrical Concrete Specimens.	3
Flexural Strength	ASTM C 78	Standard Test Method for Flexural Strength of Concrete.	3
Modulus of Elasticity	ASTM C 469	Standard Test Method for Static Modulus of Elasticity.	3
Creep/Shrinkage	ASTMC 512	Standard Test Method for Creep of Concrete in Compression.	3
DURABILITY TESTS			
Chloride Permeability	ASTM C 1202	Standard Test Method for Electrical Indication of Concrete's Ability to Resist Chloride Ion Penetration.	3
Chloride Permeability	ASTM C 1543	Standard Test Method for Determining the Penetration of Chloride Ion into Concrete by Ponding.	3
Concrete Resistivity	Non-ASTM	A method to determine the ability of concrete to protect steel from corroding.	3
Rapid Freeze Thaw Resistance	ASTM C 666	Standard Test Method for Resistance of Concrete to Rapid Freezing and Thawing.	3
Scaling Resistance	ASTM C 672	Standard Test Method for Scaling Resistance of Concrete Surfaces Exposed to Deicing Chemicals	3
Wear Resistance	ASTM C 944	Standard Test Method for Abrasion Resistance of Concrete or Mortar Surfaces by the Rotating-Cutter Method.	3
MILD STEEL BOND AND DEVELOPMENT TESTS			
Direct Pull-out Tests	RILEM 7-II-128	A comparative test that evaluates direct bond strength while minimizing the effect of confining pressures as in previous direct pull-out test methods, see Fig. 1.	4
4-Point Loading Beam Splice Test Specimens	Non-ASTM	Generally regarded as the most realistic test method for development length and splice length, see Fig. 2.	4
FULL SCALE SPECIMEN TESTS			
Shear Test Specimens	Non-ASTM	Full-scale tests to study the shear behavior of HVFA concrete beams and evaluate the contributions from the concrete, V_c, and transverse (shear) reinforcement, V_s, see Fig. 3.	5
Flexural Test Specimens	Non-ASTM	Full-scale tests to study the flexural behavior of HVFA concrete beams, see Fig. 3.	5
Table Notes: **Non-ASTM** – refers to a test method that is not a standard ASTM test. The test is either generally accepted research practice or a standard undertaken at Missouri S&T for similar studies. **MSTR** – refers to a Missouri S&T recommended test for this project.			

2.3.2. Subtask 3b: Test Results. This subtask was critical to a successful

research program and involved more than simply compiling the test results. In reality,

this subtask involved adapting the test matrix as necessary during the course of testing. In

other words, if a particular property turned out to be critical to the overall performance of

HVFA concrete, more or different tests may have been warranted, and the testing plan

was adapted accordingly.

2.3.2. Subtask 3c: Conclusions & Recommendations. The investigators

developed conclusions and recommendations based on the test results. In addition to

evaluating the different HVFA concrete mixes for performance, these conclusions and

recommendations formed the basis of the draft specifications developed as part of Task 7.

2.4. TASK 4: BOND AND DEVELOPMENT OF MILD STEEL

The issue to be addressed under this task was to determine whether the current

AASHTO LRFD Bridge Design Specifications[1] for development length are appropriate

for HVFA concrete. In other words, does HVFA concrete enhance, compromise, or not

affect the relationship between development length and compressive strength as

previously formulated for conventional portland cement concrete. Although the design

equations are currently valid for fly ash replacement rates up to 35 percent, the micro-

and macro-structure of the cementitious system may well change with significantly

higher fly ash percentages. This task involved two (2) subtasks. Details regarding the test

methods to be investigated are summarized in **Table 1**.

2.4.1. Subtask 4a: Direct Pull-out Tests. Although there are a variety of bond

and development length testing protocols available, a direct pull-out test offers several

advantages, including test specimens that are easy to construct and a testing method that is relatively simple to perform. The downside is a lack of direct comparison with actual structures and the development of compressive and confinement stresses generated due to the reaction plate.

However, modifications suggested in RILEM 7-II-128[2] reduce some of these problems and result in a simplified test that offers relative comparisons between concrete or reinforcement types. **Figure 1** is a schematic of the test specimen based on the RILEM specifications. Bond between the reinforcing bar and the concrete only occurs in the upper half of the concrete block, through the addition of a PVC tube in the lower portion, significantly reducing the effect of any confinement pressure generated as a result of friction between the specimen and the reaction plate.
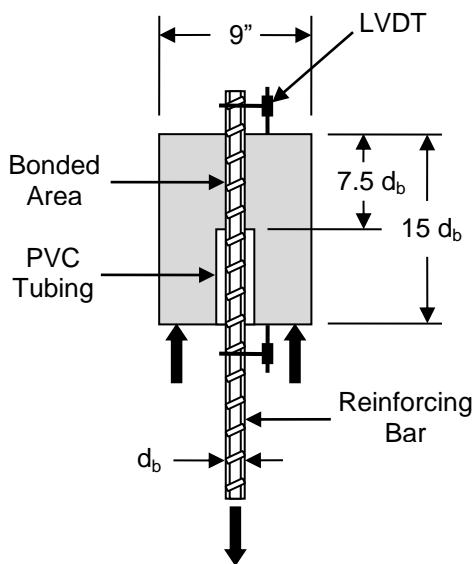
Figure 1 – Direct Pull-out Test Setup

The investigators constructed and instrumented several direct pull-out specimens for testing as shown in **Fig. 1**. The variables included bar size and concrete type (HVFA or conventional concrete). Data recorded during the test included load and bar slip.

2.4.2. Subtask 4b: Mild Steel Bond and Development. This subtask investigated development length of mild steel in both HVFA concrete and conventional concrete mixes. Although there are a variety of bond and development length testing protocols available, the beam splice specimen shown in **Fig. 2** is generally regarded as the most realistic test method.[3, 4] Current ACI 318 design provisions for development length and splice length are based primarily on data from this type of test setup.[4]
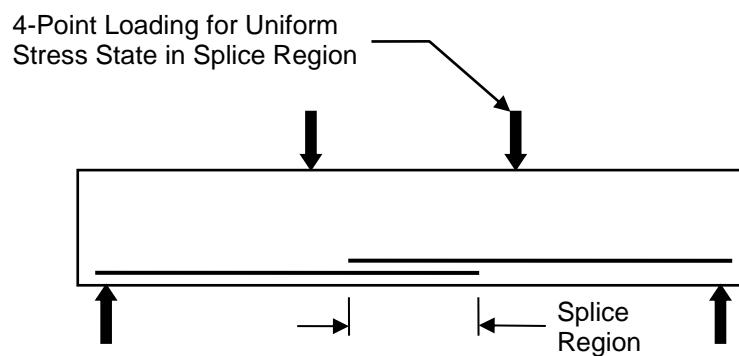
Figure 2 – Beam Splice Test Setup

The investigators constructed and instrumented rectangular beams for splice specimen testing as shown in **Fig. 2**. The variables included bar size, lap length, and concrete type (HVFA or conventional concrete). To evaluate the top bar effect, several beams were cast upside-down with at least 12 inches of concrete below the bars. Specimen instrumentation consisted of strain gauges placed at the start of each lap. Data recorded during the tests included load and deflection of the specimen as it was tested to flexural or bond failure.

2.5. TASK 5: FULL SCALE SPECIMEN TESTS

This task involved testing of full-scale specimens to demonstrate the potential of HVFA concrete construction. The specimens were constructed with HVFA concrete from the local Ready Mix Concrete plant to confirm the ability to successfully transfer the mix designs from the laboratory to the field. The testing also included control specimens constructed from conventional concrete. The full-scale tests consisted of beam specimens for both shear and flexural testing. This task involved two (2) subtasks. Details regarding the test methods to be investigated are summarized in **Table 1**.

At the beginning of the research project, there was a possibility of a MoDOT pilot project using HVFA concrete that the research team could monitor and evaluate as part of this research study. Unfortunately, due to timing issues, this aspect did not occur.

2.5.1. Subtask 5a: Full-Scale Beam Shear Tests. This subtask involved full-scale beam tests to study the shear behavior of HVFA concrete beams and evaluate the contributions from the concrete and transverse (shear) reinforcement. The investigators constructed, instrumented, and tested rectangular beams in the configuration shown in **Fig. 3**, which applies a uniform shear over a significant portion of the beam. The variables included amount of transverse (shear) reinforcement and concrete type (HVFA or conventional concrete). Specimen instrumentation consisted of strain gauges, demountable mechanical strain gauges (DEMEC gauges), and linear variable displacement transducers (LVDTs). Data recorded during the tests also included load and deflection of the specimen as it was tested to shear failure.

2.5.2. Subtask 5b: Full-Scale Beam Flexural Tests. This subtask involved full-scale beam tests to study the flexural behavior of HVFA concrete beams. The

investigators constructed, instrumented, and tested rectangular beams in the configuration

shown in **Fig. 3**, which applies a uniform moment over a significant portion of the beam.

The variables included amount of longitudinal (flexural) reinforcement and concrete type

(HVFA or conventional concrete). Specimen instrumentation consisted of strain gauges,

DEMEC gauges, and LVDTs. Data recorded during the tests also included load and

deflection of the specimen as it was tested to flexural failure.
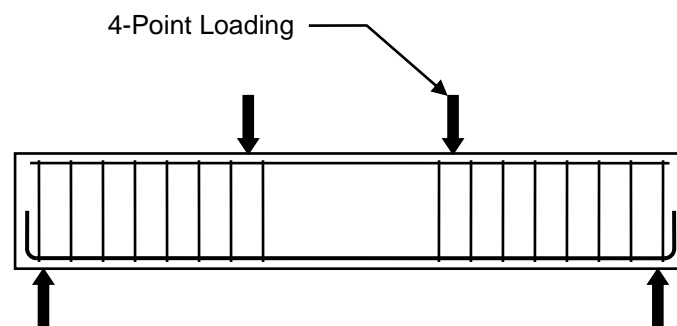
Figure 3 – Full Scale Beam Test Setup

2.6. TASK 6: AASHTO & ACI CODE COMPARISON OF TEST RESULTS

The purpose of this task was to compare the test results from Tasks 3, 4, and 5

with the design provisions and relationships in the current AASHTO LRFD Bridge

Design Specifications. Although the design equations are currently valid for fly ash

replacement rates up to 35 percent, the micro- and macro-structure of the cementitious

system may well change with significantly higher fly ash percentages. The comparisons

ranged from relatively simple relationships – such as modulus of elasticity based on

compressive strength – to complex design relationships – such as bond, development

length, and shear strength. As necessary, the investigators also compared the test results

with prediction equations and relationships from other publications, such as the various

ACI committee documents and the CEB-FIP Model Code.[5] The results of this task

assessed whether or not the current design provisions are applicable to HVFA concrete.

2.7. TASK 7: RECOMMENDATIONS & SPECIFICATIONS FOR IMPLEMENTING HVFA CONCRETE

Based on the results of Tasks 1 through 6, the investigators developed

recommendations for the use of HVFA concrete in infrastructure elements. Based on

these recommendations and the results of this research study, the investigators also

developed a suggested MoDOT specification for the use of HVFA concrete in

transportation-related infrastructure.

2.8. TASK 8: VALUE TO MODOT AND STAKEHOLDERS TO IMPLEMENTING HVFA CONCRETE

The issue to be addressed under this task was to quantify the benefit to MoDOT

of applying the results of this research project – specifically, to determine a "value to

MoDOT and the residents of Missouri" in the event that HVFA concrete is incorporated

into construction of the State's transportation-related infrastructure. From an

environmental perspective, replacing cement with fly ash reduces concrete's overall

carbon footprint and diverts an industrial by-product from the solid waste stream

(currently, about 40 percent of fly ash is reclaimed for beneficial reuse and 60 percent is

disposed of in landfills). This value aligns with both MoDOT's Tangible Result of being

environmentally and socially responsible[6] and MoDOT's Research Need for strategies to

reduce energy consumption.[7] The investigators determined the reduction in energy and

greenhouse gas emissions and the amount of material recycled by implementing HVFA concrete.

Furthermore, increased use of fly ash has several other benefits to MoDOT and the residents of Missouri. These benefits include less need for concrete mixing water – as fly ash reduces the water demand to obtain the same level of workability – and increased concrete durability – resulting in longer life and reduced life-cycle costs. The investigators evaluated qualitative and quantitative measures for both of these benefits.

Overall, this task sought to establish a basis for whether or not HVFA concrete should be used by MoDOT, based upon the results from Tasks 1 through 6.

3. TASK SUMMARIES: FINDINGS, CONCLUSIONS, AND RECOMMENDATIONS

The following descriptions summarize the major findings, conclusions, and recommendations for project Tasks 1 through 8. Each sub-section refers to the specific Technical Report A through E where the background, detailed approach, experimental procedures and processes, results, findings, conclusions, and recommendations may be referenced for much greater detail. Report designations (*i.e.*, "Report A") are provided as a reference such that the specific detailed report located in the appendix may be consulted to gain an improved understanding of how this particular finding or conclusion was established.

3.1. TASK 1: LITERATURE REVIEW

Detailed Technical Reports A through E each provide a thorough literature review related to the topic of study at hand. The reader is referred to the detailed technical reports for topic specific literature reviews on HVFA concrete. However, the more notable general findings include the following:

Technical Reports A through E:

- Research on hydration of HVFA concrete has found that if not enough sulfate is present, ettringite will be unable to slow the reaction of tricalcium aluminate, which will consume the calcium in solution, slowing or stopping hydration of the silicates, resulting in retardation of set or failure to set.

- Research on hydration of HVFA concrete has shown that the reactivity of the particular fly ash combined with the amount of calcium hydroxide present is critical to optimum hydration of the HVFA concrete mixture.

- Research on plastic properties of HVFA concrete has shown increased slump, decreased rate of set, and potential air entraining issues depending on the particular fly ash used in the mixture.

- Research on hardened properties of HVFA concrete has shown decreased rate of strength gain compared with conventional concrete but that the differences are reduced over time, particularly at ages of 56 days and beyond. Flexural strength and splitting tensile strengths tended to track with concrete strength, but modulus of elasticity was found to be higher for HVFA concrete, possibly due to unreacted glassy fly ash particles acting as aggregate and increasing the rigidity of the material.

- Research on creep and shrinkage of concrete with fly ash has been studied extensively, except that the vast majority of studies have been limited to Class F fly ash and fly ash replacement levels of 50% or less.

- Research on durability of HVFA concrete has shown decreased permeability and increased freeze-thaw resistance but decreased scaling resistance compared with conventional concrete.

- Research on bond of mild steel in HVFA concrete has been very limited, with most studies performing only pull-out tests, tests on small-scale specimens, or limiting the fly ash replacement levels below 50%, which is the traditional cutoff for HVFA concrete.

- Research on shear strength of HVFA concrete has been very limited, with most studies performing tests on small-scale specimens, beams with shear span-to-depth ratios that classify the specimens as deep beams, or limiting the fly ash replacement levels to between 40% and 50%.

3.2. TASK 2: MIX DEVELOPMENT

This portion of the study involved working with cementitious paste mixtures to examine the effect of water reducer dosages, fly ash substitution rates, cement brands, fly ash sources, and powder activator types and amounts. Based on the results of the paste study, the researchers developed the concrete mixes used to study the fresh and hardened properties of HVFA concrete. The findings and conclusions from this task consist of the following:

Technical Report A:

- The position of the calorimetry curve was reflected in setting time, early strength achieved, and tendency for early stiffening, offering a valuable tool to assess different combinations of cement, fly ash, powder activators, and chemical admixtures.

- At high levels of CaO and low levels of aluminate, alkali, and aluminate/sulfate ratio, as fly ash increased, the calorimetry curves were increasingly delayed and the peaks were shorter.

- As the CaO dropped and the aluminate, alkali, and aluminate/sulfate ratio increased to more moderate levels, the curves became shorter and broader, sometimes exhibiting two peaks.

- When the CaO was low and the aluminate, alkali, and aluminate/sulfate ratio was high, the curves reversed and occurred earlier than straight portland cement curves.

- Fly ash effects on initial setting time were mixed. At 25% replacement, retardation usually occurred. At 50% replacement, both retardation and acceleration occurred. At 70% replacement, many times acceleration occurred.

- To improve early strengths, lime, rapid set cement (RSC), or gypsum by themselves were not particularly helpful. However, gypsum and lime together were effective, but lowered later strengths. Gypsum-RSC improved strengths at all ages. Gypsum by itself helped restore (retarded) the fly ash-accelerated HVFA calorimeter curve positions, as did gypsum-RSC. Gypsum-lime restored the curves almost to the zero fly ash positions. Early stiffening tendencies were alleviated by gypsum and gypsum-lime, but made worse by gypsum-RSC.

- The dosages chosen for the concrete study were 4% gypsum because it controlled the fly ash-accelerated reactions best, 10% lime because in combination with the 4% gypsum, it controlled the accelerated reactions best, and 20% RSC because it improved one day strengths best.

3.3. TASK 3: HARDENED PROPERTIES OF HVFA CONCRETE MIXES

This portion of the study involved scaling up the most promising powder activator combinations from paste to concrete and evaluating the mixtures in terms of plastic and hardened properties. The mixture matrix included two portland cement-fly ash blends and fly ash replacement at three levels (zero, 50% and 70%) with the water reducer dosage, gypsum content (4%), lime content (10%), and RSC content (20%) held constant.

Additional studies were also completed on two HVFA concrete mixtures that used 70% replacement of cement with fly ash as well as gypsum and lime as the powder activators. One mix used a relatively high total cementitious content of 756 lb/yd^3 (448 kg/m^3), and the other had a relatively low total cementitious content of 564 lb/yd^3 (335 kg/m^3). A conventional concrete mix was used as a control for comparison. The findings and conclusions from this task consist of the following:

Technical Report A (hardened properties):

- For reaction time (calorimeter curve time, setting time, stiffening time), the value varied as a function of the characteristics of the OPC and fly ash in conjunction with each other, type and level of powder activators used, dosage of WR/HRWR, and the type of test method used for evaluation.

- For compressive strength, at the 50% fly ash level, one day strengths were low no matter what powder activator was used, but 1000 psi (6.9 MPa) was reached in a number of OPC-fly ash blends, with and without powder activators. Good strengths can be achieved at 3 days. At the 70% fly ash level, concrete is weaker, but reasonable strengths can be reached at 28 days.

- For flexural strength, and with all tests conducted at 28 days, depending on the blend, the 50% fly ash mixtures were about the same strength as the OPC mixture, or somewhat below, although the weakest was still greater than 600 psi (4.1 MPa). At the 70% fly ash level, strengths dropped below the 50% fly ash level. Only one mixture achieved 550 psi (3.8 MPa).

- For splitting tensile strength, and with all tests conducted at 28 days, at the 50% fly ash level, the strengths either slightly exceeded or were a bit below the OPC strengths. The 70% fly ash level mixtures were weaker than 50% fly ash mixtures.

- For modulus of elasticity, as a general rule, the 50% fly ash values were close to, and in some cases slightly greater than the OPC strengths. As expected, the 70 % mixtures had lower modulus of elasticity values.

- For drying shrinkage, the HVFA concrete mixtures shrink less than their OPC counterparts.

Technical Report A (durability):

- For chloride resistance, in comparison to the OPC mixtures, rapid chloride permeability is lower for the 50% fly ash mixtures, but the 70% fly ash mixtures are more permeable, possibly due to the 28-day testing time as the fly ash will continue to hydrate.

- For freeze-thaw resistance, all HVFA concrete mixtures had greater durability factors than the OPC mixtures.

- For scaling resistance, all fly ash mixtures did poorly in regard to salt scaling.

- For abrasion resistance, at 50% fly ash replacement, resistance is somewhat lower. At 70% replacement, the effect is much worse, but usually tracks with compressive strength.

Technical Report D (creep and shrinkage):

- The HVFA concrete mixes that used 70% replacement of cement with fly ash showed significantly less shrinkage strain compared to the control mix.

- As expected, the HVFA concrete with the lower cementitious content had noticeably less shrinkage than the higher cementitious content mix.

- Both HVFA concrete mixes compared favorably with previous research results on shrinkage of HVFA concrete.

- Existing shrinkage models for conventional concrete overestimated the shrinkage strains for the HVFA concrete specimens.

- Both HVFA concrete mixes outperformed the conventional concrete mix in terms of creep strain, with both mixes experiencing significantly less creep strain at 126 days after loading than the conventional concrete mix.

- Creep strain data may be misleading due to the fact that HVFA concrete specimens were loaded at lower levels than conventional concrete due to their decreased compressive strengths at the time of loading. To normalize results, specific creep can be examined. The high cementitious HVFA concrete mix performed poorly in creep when taken in terms of specific creep. As the specimens got older, however, specific creep of the high cementitious HVFA concrete mix got closer to that of the conventional concrete.

- The two HVFA concrete mixes and the conventional concrete mix showed similar behavior under load, however, as the specimens aged, the advantage of the HVFA concrete mixes over the conventional mix became more apparent. This is demonstrated best by the percentage of 126 day creep. The data shows that during the

first two weeks of loading, the HVFA concrete specimens experienced a greater percentage of their ultimate creep strain than did the conventional concrete specimens. However, due to the tendency of HVFA concrete to gain strength at later ages, creep performance improved as the specimens aged.

Technical Report E (hardened properties):

- For compressive strength, both of the 70% fly ash level HVFA concretes trailed behind the conventional concrete mix in terms of rate of strength gain and 28-day strength. Minimal improvement occurred at 56 days most likely due to depletion of the available calcium hydroxide.

- For flexural strength, in all but one instance, the 70% fly ash level HVFA concretes exceeded the conventional concrete mix even though the compressive strength of the conventional concrete significantly exceeded that of the HVFA concrete mixes. Consequently, when normalized for concrete strength, the HVFA concrete mixes significantly outperformed the conventional concrete mix.

- For splitting tensile strength, the conventional concrete mix outperformed the HVFA concrete mixes.

- For modulus of elasticity, in all but one instance, the 70% fly ash level HVFA concretes exceeded the conventional concrete mix even though the compressive strength of the conventional concrete significantly exceeded that of the HVFA concrete mixes. Consequently, when normalized for concrete strength, the HVFA concrete mixes significantly outperformed the conventional concrete mix.

Technical Report E (durability):

- For chloride resistance as measured by the rapid chloride permeability test, the 70% HVFA concrete mixtures could not complete the test due to excessive voltage buildup or excessive current. However, previous research has established that the rapid chloride permeability test may not be applicable to concretes with very high fly ash replacement levels.

- For chloride resistance as measured by ponding, the 70% HVFA concrete mixtures had lower chloride levels than the conventional concrete mix.

- For freeze-thaw resistance, the 70% HVFA concrete mixtures had greater durability factors than the conventional concrete mix.

- For scaling resistance, all fly ash mixtures did poorly in regard to salt scaling.

3.4. TASK 4: BOND AND DEVELOPMENT OF MILD STEEL

The mix designs tested for bond and development consisted of two HVFA concrete mixtures that used 70% replacement of cement with fly ash, with gypsum and lime as the powder activators, and one conventional concrete mix for the control. One of the HVFA concrete mixes used a relatively high total cementitious content of 756 lb/yd^3 (448 kg/m^3), and the other HVFA concrete mix had a relatively low total cementitious content of 564 lb/yd^3 (335 kg/m^3), with the mixes denoted as HVFA-70H and HVFA-70L, respectively.

Two test methods were used for bond strength comparisons. The first was a direct pull-out test based on RILEM 7-II-128[2] "RC6: Bond test for reinforcing steel. 1. Pull-out test." The second test method consisted of full-scale beam splice test specimens subjected

to a four-point loading until failure of the splice. The findings and conclusions from this task consist of the following:

Technical Report B:

- The average peak load for the #4 (#13), HVFA-70H and HVFA-70L pull-out specimens was 0.7% lower and 2.3% higher than that of the control, respectively. The average peak load for the #6 (#19), HVFA-70H and HVFA-70L pull-out specimens was 11.3% and 9.9% higher than that of the control, respectively.

- A total of nine test specimens with 3#6 (#19) longitudinal reinforcing bars spliced at midspan were constructed for the HVFA concrete bond test program – three for each concrete type. The average peak bar stress for the HVFA-70H and HVFA-70L bottom splice beam specimens was 29.5% and 15.2% higher than that of the control specimens, respectively. The peak bar stress for the HVFA-70H and HVFA-70L top splice beam specimens was 48.7% and 23.1% higher than that of the control specimens, respectively.

- Based on an analysis of the test results, particularly those for the more realistic beam splice specimens, the HVFA concrete has significantly improved bond strength compared to conventional concrete.

3.5. TASK 5: FULL SCALE SPECIMEN TESTS

The mix designs tested in the full-scale specimens for shear and flexure consisted of two HVFA concrete mixtures that used 70% replacement of cement with fly ash, with gypsum and lime as the powder activators, and two corresponding conventional concrete

mixtures for the controls. One of the HVFA concrete mixes used a relatively high total cementitious content of 756 lb/yd^3 (448 kg/m^3), and the other HVFA concrete mix had a relatively low total cementitious content of 564 lb/yd^3 (335 kg/m^3), with the mixes denoted as HVFA-70H and HVFA-70L, respectively.

Most research to date has consisted only of the evaluation of the strength and durability of HVFA concrete mixtures, while only a limited number of studies have implemented full-scale testing of specimens constructed with HVFA concrete to determine its potential use in the industry. For this research, a laboratory testing program was developed to investigate the shear and flexural performance of reinforced concrete (RC) beams constructed with HVFA concrete. The experimental program consisted of 36 tests performed on full-scale RC beams. The findings and conclusions from this task consist of the following:

Technical Report C:
- In terms of crack morphology, crack progression, and load-deflection response, the behavior of the HVFA concrete and conventional concrete beams was virtually identical.
- Existing design standards (AASHTO, ACI, CSA) conservatively predicted the shear and flexural capacities of the HVFA concrete beams.
- The total cementitious content had little effect on the shear and flexural behavior of the HVFA concrete beams.
- In general, the HVFA concrete beams exceeded the code predicted shear strengths by a larger margin than the conventional concrete beams.

- Statistical data analyses – both parametric and nonparametric – showed that the HVFA concrete beams had higher normalized shear capacities than the conventional concrete beams.

- The HVFA concrete and conventional concrete test results fall within a 95% confidence interval of a nonlinear regression curve fit of a shear test database of conventional concrete specimens.

- A significant majority of the HVFA concrete test results fall at or above the nonlinear regression curve fit of the conventional concrete shear test database.

3.6. TASK 6: AASHTO & ACI CODE COMPARISON OF TEST RESULTS

The test results from Tasks 3, 4, and 5 were compared with the design provisions and relationships in the current AASHTO LRFD Bridge Design Specifications and ACI Building Code. The comparisons ranged from relatively simple relationships – such as modulus of elasticity based on compressive strength – to complex design relationships – such as bond, development length, and shear strength. In general, the current AASHTO and ACI design provisions and relationships for conventional concrete are equally applicable or conservative for HVFA concrete with fly ash replacement levels up to 70%. These provisions include mechanical properties, creep and shrinkage behavior, bond and development of reinforcing steel, and shear and flexural strength. Refer to detailed Technical Reports A through E for the in-depth comparisons and evaluations.

3.7. TASK 7: RECOMMENDATIONS & SPECIFICATIONS FOR IMPLEMENTING HVFA CONCRETE

Based on the results of Tasks 1 through 6, the investigators recommend the implementation of HVFA concrete in the construction of transportation-related infrastructure in the State of Missouri. However, the investigators also recommend initially limiting the fly ash replacement levels to 50% and avoiding applications subjected to direct deicing chemicals, such as bridge decks and pavements, due to potential scaling issues. To accomplish this, the following requirements are recommended for incorporation into MoDOT's standard specifications or job specific provisions.

<u>HIGH-VOLUME FLY ASH CONCRETE FOR CAST-IN-PLACE CONSTRUCTION</u>

1.0 Description. High-Volume Fly Ash (HVFA) concrete is concrete with at least 50 percent of the cement replaced with fly ash. All material, proportioning, mixing and transporting of concrete shall be in accordance with Sec 501, except as specified herein.

2.0 Concrete Mix Design. At least 120 days prior to using HVFA concrete, the contractor shall submit a mix design for approval to Construction and Materials. The HVFA concrete mix shall be designed by absolute volume methods or an optimized mix design method such as Shilstone or other recognized optimization method.

2.1 Required Information. The mix design shall contain the following information:

(a) Source, type and specific gravity of Portland cement

(b) Source, type (class, grade, etc.) and specific gravity of fly ash

(c) Source, name, type and amount of admixture

(d) Source, type (formation, etc.), ledge number if applicable, and gradation of the aggregate

(e) Specific gravity and absorption of each fraction in accordance with AASHTO T 85 for coarse aggregate and AASHTO T 84 for fine aggregate, including raw data

(f) Unit weight of each fraction in accordance with AASHTO T 19

(g) The design air content and target slump

(h) Batch weights of Portland cement and fly ash

(i) Batch weights of coarse, intermediate and fine aggregates

(j) Batch weight of water

(k) Compressive strength at 1-, 3-, 7-, and 28 days

2.2 Fly Ash. The fly ash shall be in accordance with Sec 1018, except as noted herein. The HVFA concrete mix shall use only Class C fly ash as the supplementary cementitious material. The amount of fly as a percentage of total cementitious material shall be as shown on the contract documents.

2.3 Water Amount. The water/cementitious materials ratio shall meet the following requirements:

Water/Cementitious Materials Ratio	
Minimum	Maximum
0.30	0.40

2.4 Minimum Cementitious Material Amount. The total amount of cementitious materials shall not be below 600 pounds per cubic yard.

2.5 Air Content. Air content shall be determined in accordance with AASHTO T 152. The minimum air content shall be as shown on the contract documents.

2.6 Compressive Strength. Compressive strength shall be determined in accordance with AASHTO T 22. Concrete shall have 1-, 3-, 7-, and 28-day minimum compressive strengths as shown on the contract documents.

3.0 Batching Sequence Plan. The contractor shall submit a Batching Sequence Plan outlining how the HVFA concrete mix will be batched and mixed. The Batching Sequence Plan shall be submitted to the Engineer for approval.

4.0 Trial Batch. A trial batch shall be done at least 90 days prior to HVFA concrete being used to ensure the mix is in accordance with this special provision. The HVFA concrete mix design shall not be used until all of the specified criteria have been met. The trial batch shall be at least 3 cubic yards. The MoDOT Field Materials Engineer shall be present during the trial batch. The HVFA concrete mix shall be tested for air content, unit weight, slump, and compressive strength.

4.1 Compressive Strength. Compressive strength testing shall be conducted in accordance with AASHTO T 22. Concrete shall have 1-, 3-, 7-, and 28-day minimum compressive strengths as shown on the contract documents.

5.0 Production. HVFA concrete mix shall not be used until the concrete mix, the Batching Sequence Plan, and the trial batch have been approved. The HVFA concrete mix shall not vary from the mix design submitted for approval. Any changes in material sources, aggregate gradations, or material content shall require a new HVFA concrete mix be resubmitted for approval. Changes to the water content and chemical admixture dosages will be allowed by the MoDOT Field Materials Engineer to handle changes in environmental conditions.

3.8. TASK 8: VALUE TO MODOT AND STAKEHOLDERS TO IMPLEMENTING HVFA CONCRETE

From an environmental perspective, replacing cement with fly ash reduces concrete's overall carbon footprint and diverts an industrial by-product from the solid waste stream (currently, about 40 percent of fly ash is reclaimed for beneficial reuse and 60 percent is disposed of in landfills). These values align with both MoDOT's Tangible Result of being environmentally and socially responsible[6] and MoDOT's Research Need for strategies to reduce energy consumption.[7]

Concrete is the most widely used man-made material on earth, with nearly three tons produced annually for each man, woman, and child, and accounts for over 5% of the carbon dioxide released into the atmosphere each year. On average, replacing even 50% of the cement used in concrete with fly ash will reduce the annual amount of greenhouse gas emissions by nearly 1.8 billion tons worldwide. Furthermore, this change would also eliminate more than 20 billion cubic feet of landfill space each year. In terms of energy consumption, this fly ash replacement level would save the equivalent of 6.7 trillion cubic feet of natural gas annually.

There are additional benefits of using fly ash to replace a significant portion of the cement in concrete. In terms of monetary savings, fly ash costs approximately one-half the amount for cement. For the same workability, fly ash reduces the amount of potable mixing water by approximately 20%. Even more importantly, fly ash increases the durability of concrete beyond what can be attained with portland cement alone. Increased durability translates into increased sustainability by extending the useful life of the material.

4. REFERENCES

1. AASHTO (2010). *AASHTO LRFD Bridge Design Specifications*, 5th edition, Washington, D.C.

2. RILEM (1994). "RC5: Bond Test for Reinforcing Steel. 1. Pullout test," *RILEM Technicial Recommendations for the Testing and Use of Construction Materials, 7-II-128*, E & FN Spon, London, U.K.

3. Ramirez, J.A. and Russell, B.W. (2008). *Splice Length for Strand/Reinforcement in High-Strength Concrete*, NCHRP Project 12-60 Report, Transportation Research Board, Washington, D.C.

4. ACI Committee 408 (2003). "Bond and Development of Straight Reinforcing Bars in Tension (408R-03)," *Technical Documents*, American Concrete Institute, Farmington Hills, MI.

5. Comité Euro-Internationale du Bèton (1993). "CEB-FIP Model Code 1990," Bulletin d'Information, No. 213/214, Lausanne, Switzerland.

6. MoDOT Tangible Results – Environmentally and Socially Responsible, http://www.modot.mo.gov/about/MissionValuesTangibleResults.htm.

7. Stone, W. (2010). "Update on MoDOT's Research Activities and Needs," http://library.modot.mo.gov/RDT/Forum/y10/BillStoneLunchDiscussion.pdf.

5. TESTING STANDARDS

1. AASHTO – American Association of State Highway Transportation Officials: http://www.trasportation.org

2. ACI – American Concrete Institute: http://www.concrete.org

3. ASTM International – American Society of Testing Methods: http://www.astm.org

4. PCI – Prestressed/Precast Concrete Institute: http://www.pci.org

APPENDIX A

APPENDIX B

APPENDIX C

APPENDIX D

APPENDIX E

FINAL Report A

TRyy1110

**Project Title: Design and Evaluation of High-Volume
Fly Ash (HVFA) Concrete Mixes**

**Report A: Evaluation of HVFA Cementitious Paste and
Concrete Mixtures**

Prepared for
Missouri Department of Transportation
Construction and Materials

Missouri University of Science and Technology, Rolla, Missouri

October 2012

ABSTRACT

In the Paste Screening Study, 25 combinations of five Type I/II portland cements and five Class C fly ashes commonly used in Missouri were tested in paste form with no chemical or powder additives. Testing procedures included semi-adiabatic calorimetry, Vicat setting time, miniature slump, and compressive strength at one and 28 days. The two most reactive and two least reactive combinations (defined by one day strengths) were further evaluated in the Paste Main Effects Study. Eighty mixtures were examined.

In the Paste Main Effects Study, the effects of two levels each of WR/HRWR, gypsum, calcium hydroxide (lime), rapid set cement (RSC), and gypsum-lime, and gypsum-RSC were determined. Except for the WR/HRWR dosage level experiment, all other mixtures contained a low WR/HRWR dosage. Except for the gypsum level experiment, all other mixtures contained 4% gypsum. The lime levels were 5 and 10% and the RSC levels were 10 and 20%. All percentages are by mass of fly ash. Sixty-four mixtures were examined.

The objective of the Concrete Properties Study was to scale up from paste to concrete the most promising powder additive combinations and then evaluate the mixtures in terms of plastic and hardened properties. Thus the mixture matrix included ordinary portland cement (OPC)-fly ash blends at two levels (same as in the Paste Main Effects Study) and fly ash at three levels (zero, 50 and 70%). WR dosage (nominal dosage), gypsum content (4%), lime content (10%), and RSC content (20%) were held constant. Ten concrete mixtures were evaluated.

At the 50% fly ash level, one day strengths were low no matter which powder additives was used, but good strengths were achieved by day 3. At the 70% fly ash level,

the concrete was weaker than at zero and 50% fly ash, but reasonable strengths were reached at 28 days. At 50% fly ash, abrasion resistance was somewhat lower. At 70% the effect was much worse. In regard to drying shrinkage, it appears that HVFA mixtures shrink less than their OPC counterparts. In a comparison to OPC mixtures, rapid chloride permeability (RCP) was lower for 50% fly ash mixtures, but 70% fly ash mixtures are more permeable. All HVFA mixtures had greater freeze-thaw Durability Factors than the OPC mixtures, and were at 93 or above. However, all fly ash mixtures did poorly in regard to salt scaling. Reaction time (calorimeter curve time, setting time, stiffening time) varied as a function of characteristics of the OPC and fly ash in conjunction with each other, type and level of powder additives used, dosage of WR/HRWR, and the type of test method used for evaluation.

TABLE OF CONTENTS

LIST OF ILLUSTRATIONS

LIST OF TABLES

1. INTRODUCTION

1.1. BACKGROUND

Missouri S&T was contracted by MoDOT to determine the feasibility of using high substitution rates of fly ash for portland cement in concrete used for structural purposes. Using a large amount of fly ash in concrete typically results in slower setting times, reduced early strength (and sometimes reduced ultimate strength), salt scaling issues, and incompatibilities with other concrete components which sometimes result in unexpected and severe early stiffening and delayed strength gain. Although concrete with high replacement levels of fly ash were studied over 30 years ago, methods of mitigation of these problems has recently centered on use of activator powders. The current interest in HVFA concrete stems from an increased interest in sustainability, determining the upper limit of replacement level issues that can be mitigated, and dealing with incompatibilities, especially for materials common in Missouri. As a part of the overall study being conducted by Missouri S&T, the present portion of the study deals with producing a variety of mixture designs and determining the plastic and hardened properties of the high volume fly ash (HVFA) concrete.

1.2. OBJECTIVES

The objectives of this portion of the study was to select portland cement, fly ash, and several powder activators for use in HVFA concrete, and to develop several mixtures for further testing.

1.3. SCOPE

The scope of this study was limited to sources of portland cement and fly ash commonly used in Missouri. The powder activators were limited to gypsum, hydrated lime, and commercially available rapid set cement, and to specific percentages as used in previous studies (Marlay, 2011), which have been shown to be effective in reducing the harmful effects of high volumes of fly ash in concrete (Bentz, 2010).

2. LITERATURE REVIEW

2.1. HIGH VOLUME FLY ASH MIXTURES

2.1.1. High Volume Fly Ash Hydration. High volume fly ash (HVFA) concrete mixes are typically defined as concrete mixes containing larger than normal replacements of cement with fly ash. This replacement is typically greater than or equal to 30% replacement (Naik, et al., 1995). Others have defined HVFA as 50% fly ash or more. Replacing large volumes of cement with fly ash in this manner, however, drastically influences the hydration curve of the cementitious system. Wang, et al. investigated the effects of fly ash and admixtures on the hydration curve of cement. They replaced Type I and II cement with 20% of Class F and Class C fly ash. Class F fly ash served only to reduce the heat release, while Class C fly ash reduced the heat release as well as delaying the peak of the hydration curve, effectively serving to retard the set of the concrete mixture. When combining substitution of fly ash with the addition of a water reducing (WR) admixture and a retarding admixture, the Class C mixes were more significantly affected than any other combination, impeding hydration for an extended time (Wang, et al., 2006).

Sulfate is required in order to force the reaction of tricalcium aluminate (C_3A) and tetracalcium aluminoferrite (C_4AF) to ettringite. Ettringite requires a significant concentration of sulfate in order to form and remain stable—once the sulfate level drops below the level required to maintain stable formation of ettringite, it undergoes conversion to monosulfate. In addition, the sulfate level affects the reaction of the silicates (tricalcium silicate, C_3S and dicalcium silicate, C_2S) in cement, more fully hydrating the silicates and resulting in higher strengths. If not enough sulfate is present

in the cement, ettringite will be unable to slow the reaction of C_3A, which will consume the calcium in solution, slowing or stopping the hydration of silicates, and resulting in retardation of set, or failure to set (Roberts & Taylor, 2007).

In regard to WR, as dosages of water reducing admixtures increase, the silicate hydration peak is retarded, resulting in retarded set. Beyond a point, the sulfate depletion occurs before the silicate hydration peak, resulting in the formation of monosulfate, and the consumption of calcium in C_3A hydration, leading the silicate peak to be severely retarded and depressed. Combining this effect with substitution of Class C fly ash, which depresses the silicate hydration peak, set may not occur (Roberts and Taylor, 2007).

Jiang, et al. investigated the hydration of HVFA pastes using replacement rates of 40% or greater. They found that as the fly ash content increased and as the *w/cm* increased, the total porosity increased. At a fly ash content of 70%, mixes with a larger *w/cm* showed a higher permeability, suggesting that the fly ash content should be limited to less than 70% in HFVA concrete. However, with increase of age, the porosity decreased, with pore volumes in HVFA mixes being of a smaller size. This was because the hydration of fly ash particles leads to a denser microstructure with an improved pore size distribution. However, using a scanning electron microscope, the authors noted that even at 90 days, many unreacted fly ash particles were found embedded in hydration products, which suggests that the fly ash in HVFA concrete cannot be fully hydrated (Jiang, et al., 1999).

Hübert, et al. examined the hydration products in HVFA binders. Three blended cements were examined containing 60%, 70%, and 85% replacement of portland cement by weight with two different fly ashes. Hydration was halted after 3, 7, 28, 90, and 300

days to characterize the hydration products. For every HVFA mix the calcium hydroxide

content was lower than the baseline cement-only mix at all ages. For several of the

mixes, complete depletion of calcium hydroxide occurred, likely due to the high

reactivity of the fly ash. Ettringite content was also examined in the mixes, with

evidence that ettringite was also a product of the hydration of the fly ash in these systems.

The two different fly ashes showed that differing fly ash contents were required to attain

the greatest amount of additional C-S-H. This is likely due to the varying consumption of

calcium hydroxide. The reactivity of the fly ash used in a concrete mix needs to be

adapted to the amount of available calcium hydroxide for optimal increase in strength

(Hübert, et al., 2001). This leads to an examination of the concept of adding

supplementary powder additives.

     2.1.2. Powder Activators. Bentz examined HVFA mixes with a 50%

replacement of cement with Class C fly ash, which resulted in a loss of compressive

strength in the paste cubes. The addition of one and five % gypsum increased early age

hydration and strength but did nothing to influence the retardation in set. Powder

additions are necessary to restore the "normal" hydration and strength development,

though some may not serve to mitigate the retardation influence of the fly ash. Bentz

examined several powder additions with the intent of mitigating the retardation. Dosages

for these powders were in percentage of total solids of the mix. A dosage of 5% of the

mass of total solids of limestone powder showed a minimal effect on the hydration curve.

Ten% aluminum hydroxide increased the heights of the hydration peaks, but did not

accelerate the occurrence of the peaks. In particular, aluminum hydroxide increased the

height of the second peak, corresponding to secondary aluminate hydration. A dosage of

10% cement kiln dust only accelerated the curves minimally, though Bentz notes that it increased the early-age hydration. Five % condensed silica fume accelerated the hydration, but failed to restore the curve to the condition of the baseline curve. Of the powders examined, the two that showed a marked degree of success in restoring the normal hydration were calcium hydroxide and rapid set cement (Bentz, 2010). It has been shown that that these two activators serve to decrease set times of HVFA mixes back to set times similar to a control mix, or in some cases resulting in faster setting than the baseline, while still resulting in an initial set of greater than three hours, allowing for time to transport and place the concrete (Bentz and Ferraris, 2010).

2.1.2.1. Calcium Hydroxide. If insufficient calcium is available and is consumed by C_3A reactions, the silicate reactions will be slowed or halted. The addition of calcium hydroxide, then, provides a source of calcium ions to restore the normal silicate reactions (Roberts and Taylor, 2007). Calcium is already being restored to the mixture in the form of gypsum, however, it is likely that the calcium and sulfate provided by gypsum are both being utilized in aluminate reactions, leading to the formation of ettringite rather than aiding in the silicate hydration. In Bentz' study of 5% calcium hydroxide addition, the hydration curve accelerated by 1.5 hours; this acceleration increased when a high range water reducer (HRWR) was present in the mixture, nearly restoring the curve to the same position as the control mixture. However, it was suggested that calcium hydroxide may reduce compressive strengths (Bentz, 2010).

2.1.2.2. Rapid Set Cement. Rapid set cement contains calcium sulfoaluminate, dicalcium silicate, and gypsum. The chemistry of rapid set cement may be unaffected by the retarding action of the fly ash. A three-component blend would utilize rapid set

cement to contribute to early age strength development and set, while fly ash would contribute to the longer term performance and strength gain. Rapid set cement was used at a dosage of 10% of the total mass of cementitious materials. Rapid set cement provides two separate contributions to the mix: both the hydration reactions of the rapid set cement, and the accelerated hydration of the cement/fly ash mixture due to the rapid set cement. With a HRWR, retardation was reduced by four hours, with the rapid set cement reacting nearly immediately after contact with water. In addition, he writes that initial compressive strengths were five % greater than those with no rapid set cement addition at 28 days. There is some concern that at a replacement level of 20%, the hydration may be excessive, and lead to setting occurring too rapidly (Bentz, 2010).

2.1.3. Mixture Proportioning. Bentz, et al. present a method for optimizing HVFA concrete mixes; the method consists of four stages: checking compatibility, attaining acceptable setting times, attaining acceptable strengths, and attaining acceptable autogenous shrinkage. After selecting potential fly ash and cement sources, compatibility should be determined by calorimetry. If the cement and fly ash combination are deemed incompatible, then this incompatibility must be rectified by addition of gypsum in order to optimize sulfate balance. Then, retardation should be mitigated by means of either powder addition to the mix, or admixture replacement. Calcium hydroxide and rapid set cement have been found to have potential for restoring setting time at levels of 5% to 10% per mass of binder. Adjustment of the dosage of water reducer, if applicable, may be necessary at this level. Though long term strengths of HVFA mixtures may approach or exceed those of control mixtures, short term strengths may suffer. If higher one day strengths are required from the HVFA mix, switching to a Type III cement may provide

increased early strengths. Changing from a Type II/V cement to a Type III cement

resulted in a compressive strength increase of 60% at one day. It is critical to maintain

saturation of the capillary pores in order to not only hydrate the long term strength

products, but also to reduce autogenous shrinkage. External curing may not be enough,

due to the limited travel distance of water once the capillary porosity becomes severely

limited due to hydration. Internal curing seems effective in providing a long term source

of hydration for pozzolanic reactions. However, if this method is chosen, the cost of

materials will significantly increase. By following this method of proportioning HVFA

concrete mixes, benefits will include a lowered tendency toward thermal cracking due to

the lower heat release of HVFA concrete mixes, as well as a cost savings at the time of

placement and over a life-cycle (Bentz, et al., 2010).

2.2. PASTE CONSIDERATIONS

2.2.1. Compressive Strength. The rate of strength gain in mixtures containing

high volumes of Class C fly ash will be slower due to the slow rate of the pozzolanic

reaction. This results in lower early strengths. However, the pozzolanic reaction will also

generally produce greater strengths at later ages. This is due to the replacement of the

weak CH products with C-S-H, which is stronger, and the filling of pores with pozzolanic

reaction products, which reduces the overall porosity of the paste and leads to an increase

in strength (Detwiler, et al., 1996).

2.2.2. Methods of Evaluating Heat Evolution. There are many calorimetry

methods and tools used to evaluate the heat evolution of cementitious mixtures. Some of

the more widely used calorimeters include isothermal, semi-adiabatic, adiabatic, and

solution calorimeters. The type of calorimetry device, mixing method, temperature of mixing environment, and sample size can all affect the results for a given mixture. Also, calorimetry results are reported in different ways, depending on the type of calorimeter being used. Therefore, it is necessary to have an understanding of the method behind varying calorimetry techniques when interpreting the results of heat of hydration experiments (Wang, 2006).

2.2.2.1. Isothermal Calorimetry. Isothermal calorimetry is used to measure the rate of heat production of a specimen kept at near-isothermal conditions. This means that the temperature of the specimen is kept at a near constant temperature during hydration. A typical isothermal calorimeter employs two heat flow sensors, each with an attached specimen vial holder, and a heat sink with a thermostat. A prepared sample is placed in one of the vials and an inert specimen is placed in the other vial. Each vial is then placed into one of the vial holders. The heat released during hydration then passes to the heat flow sensors. The output of the inert specimen sensor is subtracted from the output of the test specimen sensor to result in the calorimeter output. The heat production is measured in watts (W) or joules per second (J/s). The results are usually reported in relation to the specimen mass as mW/g or J/s/g (ASTM C 1679, 2009). Isothermal calorimetry is used as a precise means of determining the heat produced solely by the cementitious materials at a given temperature. The results are generally used quantitatively.

2.2.2.2. Semi-Adiabatic Calorimetry. Semi-adiabatic calorimetry measures the temperature of a partially insulated specimen over time. There are a variety of semi-adiabatic systems available that differ in the size of sample used and the degree of insulation. The objective for a given system is to insulate the sample in a way that

minimizes the influence of the ambient temperature, but also does not retain excessive heat that would accelerate the hydration of the specimen and distort the thermal profile. One common system uses plastic cylinder molds as the specimen container. The container is placed in a cylindrical receptacle in the device, which consists of an insulated box with a thermocouple at the bottom, so that the thermal readings are taken from the bottom of the specimen. Another common method uses thermocouples or thermistors, which are inserted into the center of the specimen. With this method, the specimen container is anything that can hold an appropriately sized sample, such as plastic cylinders or even coffee cups (Cost, 2009).

Semi-adiabatic calorimetry is generally used as an economical alternative to isothermal calorimetry that can also be used in field conditions. The results are generally used for comparative and qualitative evaluation. However, some researchers have used more elaborate semi-adiabatic methods to achieve quantitative results, such as the adiabatic temperature rise or predicted setting times. Also, semi-adiabatic conditions may provide a better model for the thermal conditions inside a non-massive concrete structure, where gradual heat loss occurs.

2.2.2.3. Adiabatic Calorimetry. In adiabatic calorimetry, there is no heat loss or gain experienced by the specimen and the temperature of the specimen is measured during hydration. An economical adiabatic calorimeter used by Gibbon, et al. consisted of a large tank with heater elements, a temperature probe, and stirrers. Inside of the tank, the specimen container was placed with a temperature probe inserted in the center of the specimen. The water temperature was controlled to be maintained at the same temperature as the hydrating sample. After completion of a test, the temperature readings

were used to determine the specific heat and heat of hydration. The heat of hydration curve was then integrated to give a plot of total heat produced over time (Gibbon, et al., 1997).

This type of calorimetry is often used to determine the cumulative temperature rise of the concrete over time. It provides a model of the heat conditions in massive concrete structures, where there is little or no dissipation of heat.

2.2.2.4. Solution Calorimetry. Solution calorimetry is most often used to determine the adherence of a hydraulic cement to ASTM specifications on heat of hydration requirements at 7 and 28 days. However, it may also be used for research purposes to determine the heat of hydration at any age. The method involves dissolving two samples in a solution of nitric acid and hydrofluoric acid. One of the samples consists of the dry cementitious materials, while the other is a corresponding, partially hydrated paste specimen. The paste specimen is prepared ahead of time and stored in a sealed vial and placed in a water bath. At the time of testing, the paste specimen is removed from the vial and crushed with a mortar and pestle until all of the material passes through a No. 20 sieve. The heat of solution of the dissolving specimens is measured and the difference between the dry and partially hydrated specimens is taken as the heat of hydration (ASTM C 186, 2005).

2.2.3. Evaluation of Heat Evolution to Avoid Incompatibilities. The composition of mineral admixtures varies considerably, even between those that fall under the same classification. This leads to complexity in cementitious systems, as the use of one or more mineral admixtures in a single concrete mixture is commonplace. Due to this complexity, problems such as slump loss, delayed setting, and slow rates of

strength gain, are more likely to occur as a result of incompatibilities between the materials. The most common cause of incompatibility is related to the sulfate concentration in a system. If there is not a sufficient amount of sulfate, the aluminates (C_3A and C_4AF) will react rapidly and consume a large portion of the available calcium in the system. This will cause the hydration of the silicates (C_3S and C_2S) to slow down and possibly stop completely. Using isothermal calorimetry, Lerch (1946) illustrated the effect of insufficient sulfate levels on cement. The results showed that as the sulfate level decreased, the second peak of the hydration curve decreased. This was attributed to a depletion of available calcium for hydration of the silicates. A similar effect was found by Roberts and Taylor (2007) for concrete mixtures with Class C fly ash, which is known to commonly cause incompatibility related problems, due to relatively high levels of aluminates. The results show a decrease and delay in the silicate hydration curve.

Cost and Knight (2007) also discussed the use of Class C fly ash as a common cause of abnormal behavior in concrete, due to increased aluminate levels, along with high temperatures, sulfate levels, chemical admixtures, and hot-weather concreting practices. It was noted that the potential for erratic behavior may increase in hot-weather concrete operations if the dosage of Class C fly ash is increased to utilize the retarding effect of the material. As part of the study, the heat generation of several paste mixtures was evaluated, using semi-adiabatic calorimetry, to detect incompatibilities. The concrete was made with a Type II cement at varying sulfate levels and a Class C fly ash at varying replacement levels. The results showed that the only combination to generate a typical silicate peak was the 3.3% sulfate cement with 10% fly ash. The combinations of this cement with 25% and 35% fly ash both showed extremely depressed silicate hydration

peaks. The 3.7% sulfate cement with 25% fly ash showed improvement in the silicate peak, but at 35% fly ash only a small peak was developed. To investigate an additional increase in sulfate, the sulfate content of the cement was increased to 4.1% in combination with the 35% replacement level of Class C fly ash. This seemed to somewhat restore the silicate peak, but it was delayed significantly (Cost and Knight, 2007).

As can be seen, the use of Class C fly ash can cause significant problems in concrete when the sulfate balance has been compromised. High temperatures and the use of chemical admixtures, such as water reducers, can increase the magnitude of incompatibility related problems as these can affect the solubility and reaction rate of compounds in the system (Cost and Knight, 2007). Generally, the adverse effects of incompatibilities are accompanied by changes in heat evolution. Therefore, investigating the heat producing behavior of cementitious system can assist in avoiding incompatibilities in the field.

2.2.4. Miniature Slump. Kantro (1980) discussed the use of the miniature slump test as a rapid means of determining the effects of admixtures on the rheological properties of cement pastes. In this study, a miniature slump cone was made of Lucite with a height of 2.25 inches, top diameter of 0.75 inches, and bottom diameter of 1.50 inches. These dimensions were chosen to be in proportion to the dimensions of the traditional slump cone used for ASTM C 143. After performing the test, the area of the paste pat was determined. The miniature slump test was used on paste mixtures with varying water-cement ratios and various admixtures. It was found that the method was suitable for comparative testing and evaluating loss in workability. Also, though it was

determined that the miniature slump test was more sensitive, it was found that the overall

effects observed with the paste testing correlated with the results of corresponding

concrete testing.

Other researchers have utilized the miniature slump cone to evaluate the early

stiffening behavior of pastes (Bhattacharja and Tang, 2001; Roberts and Taylor, 2007). In

these studies, the paste was mixed following a standard procedure and the miniature

slump test was performed at 2, 5, 15, and 30 minutes after the start of mixing. It was

noted that later times, such as 45 minutes, may also be used. Roberts and Taylor

discussed the use of an early stiffening index, which was calculated by dividing the pat

area at 30 minutes by the pat area at 5 minutes. They noted that calculated indices less

than 0.85 are generally considered to indicate rapid stiffening behavior. It was also noted

by these researchers that since pastes are more sensitive to incompatibilities, paste

systems that indicated potential problems may behave normally in concrete mixtures.

2.3. PLASTIC CONCRETE PROPERTIES

2.3.1. Slump. In a study involving the influence of varying fly ash contents on

slump and required dosage of HRWR, the mix using unground fly ash required less

HRWR to achieve a given slump than the mix using fly ash which had been interground

with the cement. The increase in required HRWR was due primarily to the increased

fineness of the interground fly ash (Bouzoubaa, et al., 2001).

Bouzoubaa, et al. (2007) investigated the use of 30%, 40%, and 50% by mass

replacement of cement with fly ash. Three concrete mixtures were of different grades:

20, 40, and 60 MPa achieved by varying the cement content. As fly ash content

increased, the water requirement to attain a given slump decreased, and consequently the

w/cm decreased as well (Bouzoubaa, et al., 2007).

2.3.2. Air Content. In regard to the influence of varying fly ash content on air

content and required dosage of air entraining agents, fly ash which had been interground

with the cement required a higher dosage of air entraining agent than the mix using an

unground fly ash. This was also primarily due to the increased fineness of the interground

fly ash (Bouzoubaa, et al., 2001).

Bilodeau, et al. noted that the amount of air entraining agent required to attain the

desired air content was greatly influenced by both the fly ash and the cement used in the

mix. Differing dosages were due to the carbon, alkali contents, and the fineness of the fly

ash, and the alkali content of the cement used (Bilodeau, et al., 1994).

2.3.3. Time of Set. Mehta and Monteiro note that the initial setting and final

setting times are arbitrarily defined in test methods, and they do not mark a specific

physical or chemical change in the cement paste, but rather "the former defines the limit

of handling and the latter defines the beginning of development of mechanical strength".

In a study of HVFA concretes, the setting times for HVFA concrete mixtures

were 30 minutes to 3 ½ hours longer than those of the baseline mixes. The fly ash mixes

used in this study consisted of 45% by mass of cement, and 55% by mass of a Class F fly

ash (Bouzoubaa, et al., 2001).

2.3.4. Microwave Water Content. The method used for determining water

content of fresh concrete by the microwave method comes from work done by Nagi and

Whiting. The authors used a 900 W microwave oven to dry a 1500 g sample of concrete.

They developed a schedule for microwaving the sample and breaking it up in order to

achieve full recovery of water content within a reasonable amount of time. A delay of up to 30 minutes from initial mixing showed no effect on the results of microwave water content determination. There was good agreement between multiple operators after only a brief instruction in the test method. In addition to being reproducible, the test is also independent of absorption of aggregates or the consistency of the concrete, having tested it on mixes ranging from a 0.2 in. (5 mm) slump to a 6.6 in. (168 mm) slump (Nagi and Whiting, 1994).

2.4. HARDENED CONCRETE PROPERTIES

2.4.1. Compressive Strength. Compressive strength of HVFA mixtures typically suffers in the short term, as highly reactive cement is replaced with less reactive fly ash. One study showed 55% Class F fly ash mixtures obtained around half the strength of ordinary portland cement (OPC) mixtures at one day. The fly ash mixtures only begin to match or exceed the strength of control mixes between 14 and 28 days, with substantial strength gains still occurring out to one year. This is due to the pozzolanic activity of the fly ash present in the mix reacting to continue to form C-S-H (Bouzoubaa, et al., 2001).

Another study showed strengths of Class F fly ash mixes at 30%, 40%, and 50% replacement by mass of cement with fly ash lagging behind their control mix counterpart in strengths. The difference between the control mix and the HVFA mixtures lessens as the specimens age, and at one year of age, the 40% fly ash mix has exceeded the control mix in compressive strength (Galeota, et al., 1995).

In regard to long term effects of high volumes of both Class C and Class F fly ashes on concrete mixtures, it has been found that increasing volumes of both Class C

and Class F fly ashes resulted in a similar decrease in early strengths, although Class F

fly ashes show a better long term strength gain correlation with increased fly ash volume.

Class C fly ashes performed better at early age strength gain than Class F fly ashes, due

to the pozzolanic activity imparted by the higher calcium content of Class C fly ashes

(Naik, et al., 2003).

      2.4.2. Flexural Strength. Bouzoubaa, et al. investigated the use of 30%, 40%,

and 50% by mass replacement of cement with fly ash. Three concrete mixtures of

different grades were studied: 20 MPa, 40 MPa, and 60 MPa. Splitting tensile and

flexural strength increased with age and with increasing grade of concrete, however, the

effect of fly ash was more varied. At the 20 MPa grade, fly ash content did not seem to

affect the flexural strength significantly until 91 days of age, however at 40 MPa there

were noticeably higher flexural strengths compared to the control concrete, and at 60

MPa, higher fly ash content resulted in a general decrease in flexural strengths

(Bouzoubaa, et al., 2007).

      A study by Naik, et al. examined three different fly ash mixes: 20% Class C fly

ash, 50% Class C fly ash, and 40% Class F fly ash. As fly ash content increased for Class

C ashes, the flexural strength suffered at earlier ages, though as the age approached a year

the flexural strength of the 50% Class C fly ash mix approached and then exceeded the

flexural strength seen by the 20% Class C fly ash mix. Flexural strength development

curves followed a similar curve shape as that of compressive strength (Naik, et al., 1995).

      2.4.3. Splitting Tensile Strength. Bouzoubaa, et al. investigated the use of 30%,

40%, and 50% by mass replacement of cement with fly ash. Three concrete mixtures of

different grades were studied: 20 MPa, 40 MPa, and 60 MPa. Splitting tensile and

flexural strength increased with age and with increasing grade of concrete, however, the effect of fly ash was more varied. At the 20 MPa grade, fly ash content did not seem to affect the splitting tensile strength significantly, however at 40 MPa there were noticeably higher splitting tensile strengths compared to the control concrete, and at 60 MPa, higher fly ash content resulted in a decrease in splitting tensile strengths, with lower splitting tensile strengths than the control concrete at 91 days of age (Bouzoubaa, et al., 2007).

Rivest, et al. cast large monoliths of control concretes and a 56% fly ash HVFA mixture with accompanying specimens to test mechanical properties. Splitting tensile strengths were expected to fall in the range of 8% to 10% of the compressive strength as published data predicted (Rivest, et al., 2004).

A study by Naik, et al. examined three different fly ash mixtures: 20% Class C fly ash, 50% Class C fly ash, and 40% Class F fly ash. As fly ash content increased for Class C ashes, splitting tensile strengths decreased, following similar strength development curves as expected of compressive strength (Naik, et al., 1995).

2.4.4. Modulus of Elasticity. Rivest et al. found that the modulus of elasticity for the HVFA concrete mix was generally higher than both control concretes made with Type I and with Type II cement. They suggest that this is due to unreacted glassy fly ash particles acting as very fine aggregates rather than hydration products, thereby increasing the rigidity of the concrete. Also, the filler effect of the fly ash contributes to a stronger transition zone, subsequently increasing the rigidity of the concrete (Rivest, et al., 2004).

2.4.5. Abrasion Resistance. Cabrera and Atis note that there are no guidelines on values from abrasion tests that ensure whether a concrete will perform adequately or

not, thus, abrasion results may only be used on a comparative basis. The authors used a British abrasion standard typically used for abrasion characteristics of aggregates in their study; findings confirmed other studies that abrasion is closely related to compressive strength (Cabrera & Atis, 1999).

Three Class C fly ashes were investigated in concrete mixes at replacement rates of 40%, 50%, and 60%. A modified version of ASTM C 944 involved the addition of silica sand to the surface at one minute intervals while abrading the specimen, and measuring the resulting depth of wear with time. The resistance to abrasion increased with age, and decreased with both time abraded and fly ash content, although a 40% replacement of cement with fly ash seemed to perform as well as the control mixture with no ash. A correlation between abrasion resistance and compressive strength existed. The source of fly ash showed a significant effect on hardened concrete properties, though no definite trend was established by the authors between fly ash properties and abrasion resistance (Naik, et al., 2002).

2.4.6. Rapid Chloride Permeability. Rapid Chloride Permeability is measured by means of ASTM C 1202, which notes that the test measures electrical conductance of concrete, which is a rapid method of indicating concrete's resistance to chloride ion penetration, not a direct measure of chloride ion penetration (ASTM, 2012).

Gu, et al. examined the performance of steel reinforcement in HVFA concretes when exposed to chloride solutions. Two mixes in this study incorporated 58% by mass of both Class F and Class C fly ash. There was greater resistance to chloride ion permeability than control concretes, even at only 28 days of age (Gu, et al., 1999).

HVFA concrete mixes containing 58% replacement of cement by mass with fly ash were studied by Bilodeau et al. The resistance of concrete to chloride ion penetration from 28 days out to 1 year showed high resistance to chloride ion penetration, with values at one year being rated 'very low', or less than 1000 coulombs passed. There was a relationship between chloride ion penetration and compressive strength of concrete. The differences between two mixes using two different cements were likely due to differences in porosity as a result of differing rates of hydration and pozzolanic reaction in different cement and fly ash combinations (Bilodeau, et al., 1994).

Bouzoubaa, et al. investigated the use of 30%, 40%, and 50% by mass replacement of cement with fly ash with three concrete mixtures of different grades. While satisfactory chloride ion permeability could be achieved simply by reducing the *w/cm* ratio, the addition of fly ash drastically reduced chloride ion permeability as soon as 28 days, with 91 day tests showing coulomb values of less than 300, or almost negligible permeability (Bouzoubaa, et al., 2007).

2.4.7. Freeze-Thaw Resistance. Bilodeau, et al. examined a number of HVFA (58% fly ash) concrete mixes. After 300 cycles of freezing and thawing, all combinations of cement and fly ash showed durability factors of greater than or equal to 96. Freezing and thawing tests were extended to 1000 cycles, an extremely severe condition, and all but one mix retained durability factors of greater than or equal to 93 (Bilodeau, et al., 1994).

Galeota, et al. examined four concrete mixtures—one control mix with no fly ash, and three HVFA concrete mixes—at 30%, 40%, and 50% replacement of cement with fly ash. A Class F fly ash was used with no air entrainment. The control mixture with no fly

ash and the 30% fly ash mix failed earlier than did their counterparts containing more fly ash, showing that increased fly ash content seems to increase freeze-thaw resistance (Galeota, et al., 1995).

2.4.8. Scaling Resistance. The freeze-thaw resistance of concrete when in contact with deicing salts is generally lower than the resistance to freezing and thawing alone, with the most damage occurring to concrete surfaces at a salt concentration of 4-5 percent (Mehta & Montiero, 1993). Rosli and Harnik examined the possible reasons for scaling to occur when concrete is subjected to a combination of freezing and deicing salts. The inhomogeneity of concrete at the surface, namely that the cement gel, fine aggregate particles, and capillarity, is more concentrated than through the rest of the concrete, and there are less coarse aggregate particles. This means that concrete properties differ at this 'transitional zone', including *w/cm*, modulus of elasticity, and pore volume.

There are several gradients in concrete, leading to a "layer by layer" freezing effect which can cause cracking and spalling of the concrete when subjected to deicing salts and freezing. The first gradient is water content, with the highest concentration of water being present at the surface of the concrete, with the gradient tapering off further into the concrete due to the lowered permeability of concrete. The presence of this gradient means that a "water front" will form. This water front is the boundary between frozen and unfrozen concrete, as the outer saturated layer will freeze earlier than the less saturated inner layers. Ice formation, then, is restrained to the outer layer until the temperature drops enough to freeze the inner layers of the concrete, which contributes to surface damage of the concrete.

The second gradient is the gradient of salt concentration. Salt concentration is typically low directly on the surface of the concrete, as salt is generally washed off of the surface of the concrete by rain. The peak salt concentration, then, exists within the concrete due to chloride diffusion through the concrete. Upon freezing, the outer layers will be able to freeze sooner, due to lower chloride content, and the higher chloride content inner layers will remain unfrozen. This freezing mechanism also contributes to damage of the outer layers.

The final gradient is the thermal gradient through the concrete. Concrete surfaces undergo "temperature shock" when ice is rapidly thawed by salt, as the heat required for spontaneous melting of ice is extracted from the concrete. This "temperature shock" leads to the formation of a large thermal gradient within the concrete. The conclusion is that this rapid cooling causes tensile stresses on the order of the tensile strength of the concrete, contributing to microcracking which could lead to macrocracks after occurring repeatedly. The inhomogeneous properties of the outer layers of the concrete, combined with the three gradients discussed lead to the deterioration of the concrete in the form of scaling (Rosli & Harnik, 1980).

Bilodeau, et al. examined a number of HVFA (58% fly ash) concrete mixes. When examining resistance to deicer salt scaling, it was found that all HVFA concretes showed a poor resistance to deicer salt scaling. All tested combinations of cement and fly ash by Bilodeau et al. showed a rating of 5 at 50 cycles, or severe scaling, with the exception of one mix showing a rating of 4, or moderate to severe scaling. The specimens were all air entrained, and showed good performance against repeated freezing and thawing, as well as showing good air void parameters in specimens cut from concrete

prisms. There were no observable difference between concrete made with different cement brands, although the scaling residue collected differed considerably depending upon the fly ash used (Bilodeau, et al., 1994).

Naik, et al. investigated long term pavement performance of HVFA concrete pavements containing up to 70% cement replacement with Class C fly ash, and up to 67% cement replacement with Class F fly ash. To the contrary of Bilodeau et al.'s results, Naik et al. found comparatively less scaling. Through a visual observation of the surface of in-use pavements, an 18 year old pavement containing 70% Class C fly ash rated at 3+, or moderate to heavy scaling, and a 12 year old pavement containing 50% Class C fly ash received a rating of 2, representing very slight to slight scaling. These results indicate a difference in field performance and laboratory scaling results (Naik, et al., 2003).

Another study reveals the scaling susceptibility of a 55% fly ash mix exhibited severe scaling, showing a visual rating (ASTM C672) of 5. However, experimental HVFA concrete sidewalks in Halifax, Canada were subjected to four winters and over 400 freezing and thawing cycles, combined with numerous applications of deicing salts, but have shown satisfactory performance. It was suggested that ASTM C 672 may be overly severe in its assessment of concrete's performance in field applications (Bouzoubaa, et al., 2001).

2.4.9. Shrinkage. In a study of a 56% fly ash HVFA mix with accompanying specimens, shrinkage strains were recorded out to one year for the HVFA concrete mix as well as control mixes made with Type I and Type II cement. The control concretes showed more shrinkage (strains of 0.069 and 0.059 mm/mm respectively) compared to

the HVFA concrete, which had a strain of only 0.048 mm/mm. It was suggested that this was due to the lower water content requirement of HVFA concretes, as well as greater unhydrated cementitious material in the HVFA mix which serves to act as aggregate, restraining shrinkage (Rivest, et al., 2004).

   2.4.10. Summary. High replacement rate of cement with fly ash tends to lower the water requirement to achieve slump, reduce early strength, retard setting times, increase slump loss, but increase later strengths. Restoration of strength of may occur as early as 14 days. Beneficial consequences of up to 50% replacement can be increased modulus of elasticity and freeze-thaw durability, lower rapid chloride permeability and less shrinkage. Typical detrimental effects are lower abrasion resistance and laboratory salt scaling resistance, although field studies do not wholly support problems with scaling. Sometimes incompatibilities arise in the cement-fly ash-water reducer system. Severe retardation or even acceleration of set time, extremely low early strengths and delayed or severely diminished later strengths may occur. These problems are many times related to an imbalance of aluminate/sulfate brought on by significant levels of aluminate in some Class C fly ashes, which consumes the available calcium, making it unavailable for silicate reactions. Various powder activators have been tried to address the above issues. The most promising appear to be calcium hydroxide and rapid set cement.

3. TECHNICAL APPROACH

The study was divided into two parts, termed Phase I and Phase II. Phase 1 involved working with cementitious paste mixtures to examine the effect of water reducer dosages, fly ash substitution rates, cement brands, fly ash sources, and powder additive types and amounts. Once the paste results pointed the way toward the optimum levels of these components, Phase II began, which dealt with examining the effect of the above variables on the plastic and hardened properties of concrete.

4. PHASE I – PASTE STUDY

4.1. EXPERIMENTAL DESIGN

A variety of decisions had to be made in setting up the experimental design. Fly ash class, source, percent replacement, cement type and source, *w/cm*, admixture type and dosage, powder activator types and contents, test types, test equipment, and paste mixing methods were variables that needed to be examined.

Ultimately, it was decided to use fly ash and cement sources that were commonly used in MoDOT projects. Thus, five type I/II cement brands all were chosen, three from the east side of the state and two from the west side. The predominant fly ash class produced by Missouri power plants is Class C. Five sources were chosen, three from plants from the east side of the state, and two from the west side. Because the present study was in many ways a continuation of a previous study done at Missouri S&T, replacement levels for the HVFA were set at 50 and 70% by mass of total cementitious material. Additionally, the literature has shown that about 25% replacement is the upper bound on "normal" behavior of concrete, and is a common maximum allowable value in many specifications, including MoDOT's. Including the straight ordinary portland cement (OPC) control mixture, the fly ash levels were zero, 25, 50, and 70% replacement. The five cements were designated as numbers 1 through 5, and the fly ashes the same. Thus, a combination of cement 1 and fly ash 3 was termed combination "1-3".

The choice of *w/cm* involved several factors: workability, choice of admixture, early and late strength, and realism. The literature showed that other studies utilized fairly low *w/cm's*, in the range of 0.26 to 0.50. A review of typical structural and paving mixtures used on MoDOT projects revealed *w/cm's* of 0.45 and 0.40, respectively.

Because there was a concern that at 70% fly ash substitution strengths would be low, it was preferred that a somewhat low *w/cm* should be used, but not unrealistically low. Thus, a *w/cm* of 0.40 was chosen. The total cementitious material content of 564 lbs (255 kg) was used, which is a typical value used by contractors on MoDOT projects (and exceeds MoDOT specifications for both structural and pavement mixtures).

Recognizing that mixtures of this *w/cm* would encounter workability issues for the straight OPC mixtures, it was decided to use a water reducer (WR). Although a traditional Type A may have been less problematic, a WR was chosen that was advertised as being able to function as both an A and as an F high range water reducer (HRWR). Because it has been shown that WR will affect setting time (usually retard), and may cause early stiffening because of an interaction with a particular sources of cement and fly ash, it was decided to explore the effect of several levels of WR. Three dosage levels were selected: zero, low, and high. "Low" was defined as the dosage necessary to achieve the required design slump of the concrete control mix. The "high" level was selected at an arbitrarily greater value compared to the low dosage. Actual dosages were determined experimentally and are discussed later in this report.

As mentioned, the previous HVFA study conducted on campus was based on work done by Bentz (Bentz, 2010). As a continuation of both studies, the type and initial amounts of powder additives were fixed: gypsum, calcium hydroxide, and rapid set cement (RSC). Gypsum was used to restore the aluminate/sulfate balance in the HVFA mixtures made necessary because of the high aluminate-low sulfate levels in fly ash which would upset the carefully determined proper balance in straight OPC's. Calcium hydroxide has been used to restore the delayed setting time from use of large

substitutions of fly ash in mixtures. The third powder admixture was rapid set cement (calcium sulfoaluminate-dicalcium silicate- gypsum) and has been used to restore early strengths in HVFA mixtures. Several levels of each were utilized, again based on the previous studies: 2 and 4 % gypsum, 5 and 10% lime, and 10 and 20% RSC. Percents refer to percent of fly ash, not total cementitious material. This is an important distinction from other studies reported in the literature, where the latter definition is used. Thus, 4% in this study would be a numerically smaller value if reported as others have done (e.g. 1.87 to 2.63%). In **Table 4.1** is shown a comparison of percentages as defined by the two methods. Mixtures in this study are designated as follows:

PC-FA-%FA-%PC-%G-%L-%RSC-WR

An example would be for cement #4, fly ash #1, 70% fly ash, 30% cement, 4% gypsum, 5% lime, zero % RSC, zero WR/HRWR dosage:

4-1-70-30-4-5-0-Z

Table 4.1 - Percentages of powder admixtures by mass of fly ash and by total cementitious material

Mixture	Powder	% by Fly ash mass	% by TCM mass
PC-FA-50-50-0-5-0-Z	lime	5.0	2.44
PC-FA-70-30-0-5-0-Z	lime	5.0	3.38
PC-FA-50-50-0-10-0-Z	lime	10.0	4.76
PC-FA-70-30-0-10-0-Z	lime	10.0	6.54
PC-FA-50-50-0-0-10-Z	RSC	10.0	4.76
PC-FA-70-30-0-0-10-Z	RSC	10.0	6.54
PC-FA-50-50-0-0-20-Z	RSC	20.0	9.09
PC-FA-70-30-0-0-20-Z	RSC	20.0	12.28
PC-FA-50-50-4-0-0-Z	Gyp	4.0	1.96
PC-FA-70-30-4-0-0-Z	Gyp	4.0	1.96
PC-FA-50-50-4-5-0-Z	Gyp & lime	4.0, 5.0	1.91, 2.39
PC-FA-70-30-4-5-0-Z	Gyp & lime	4.0, 5.0	2.63, 3.29
PC-FA-50-50-4-10-0-Z	Gyp & lime	4.0, 10.0	1.87, 4.67
PC-FA-70-30-4-10-0-Z	Gyp & lime	4.0, 10.0	2.55, 6.37
PC-FA-50-50-4-0-10-Z	Gyp & RSC	4.0, 10.0	1.87, 4.67
PC-FA-70-30-4-0-10-Z	Gyp & RSC	4.0, 10.0	2.55, 6.37
PC-FA-50-50-4-0-20-Z	Gyp & RSC	4.0, 20.0	1.79, 8.93
PC-FA-70-30-4-0-20-Z	Gyp & RSC	4.0, 20.0	2.40, 11.99

The properties of the paste that were of interest included some measure of early stiffening and fluidity, setting time, strength at a full range of ages, and reaction characteristics. Based on recommendations in the literature (NCPTC, 2007), the test

methods chosen were the miniature slump for fluidity and early stiffening, Vicat setting

time, compressive strengths using 2 in. (50 mm) cubes at ages between one and 56 days,

and semi-adiabatic calorimetry. The semi-adiabatic method was selected because of its

relative low cost equipment, ease of use, and general acceptance of use in the literature

for comparative studies such as the present study. Thus, behavior over a full range of

time would be provided, as shown in **Figure 4.1**.
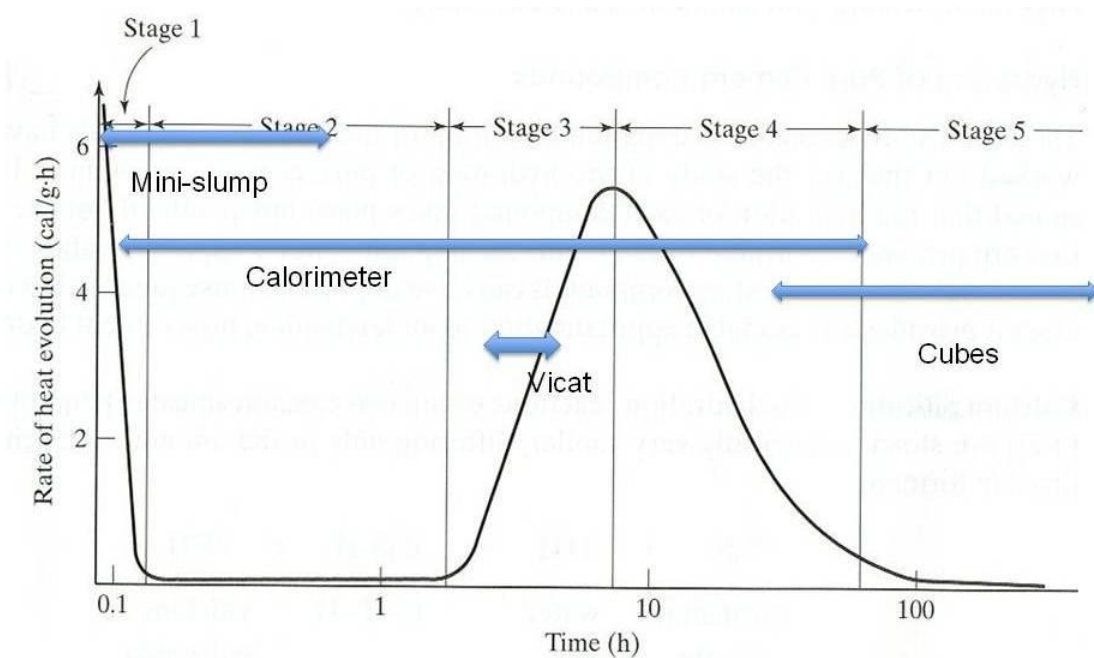
Figure 4.1- Typical calorimeter curve with testing intervals shown

The literature showed that the type of mixing method used for the cementitious

paste has a significant effect on the test results. After a review of previous studies and

consulting with experts in the field, it was decided to batch the cubes, mini-slump, and

calorimeter specimens together using a hand-held kitchen-type mixer and bowl in a very

prescribed and controlled time-wise method, and to use the standard Hobart-type mixer

for the Vicat setting time specimens.

Because a full factorial experiment involving five levels of cement source, five levels of fly ash source, four levels of fly ash replacement rate, three levels of gypsum, three levels of lime, three levels of RSC, and three levels of WR/HRWR would result in over a thousand different mixtures, it was decided to use a screening study followed by more specific examination of effects. The screening study was designed to narrow the combinations of cement source and fly ash source to two: the most reactive and the least reactive. Reactivity was defined as one day compressive strengths at 70% fly ash replacement without any powder additives or WR/HRWR. The other paste tests were also performed (mini-slump, Vicat setting time, and 28 day compressive strengths) for additional information. All five cements and all five fly ashes in combination with each were tested, along with the five cements by themselves, at zero, 25, 50, and 70% fly ash replacements, resulting in 80 mixtures. Details of the testing are discussed later in this report.

Once the two combinations were determined, the second portion of the paste study was initiated (Main Effects Study). In this effort, the levels of fly ash were limited to zero, 50, and 70%. All mixtures contained the "low" WR/HRWR dosage level, because this had been determined in a different part of the study to be necessary to bring the control concrete mixture to the design slump. However, a greater level of WR/HRWR was also tested (at all four levels of fly ash but with no powder additives). Two levels of gypsum (2 and 4 %) were tried at the 50 and 70% fly ash rates to determine the optimum level of gypsum. Four % was chosen. Finally, at the low level of WR/HRWR and at 4% gypsum, the level of lime (5 and 10 %) and RSC (10 and 20%) was varied for fly ash levels of zero, 50, and 70%. This partial factorial experimental design resulted in 48

mixtures. An additional 16 mixture experiment with no gypsum was also conducted (eight with lime, eight with RSC at 50 and 70% fly ash). Thus, including the screening study, 144 mixtures were examined in Phase I (the paste study). The test methods were the same as in the screening study: miniature slump, Vicat setting time, calorimetry, and compressive strength. However, the compressive strength testing was expanded to include more ages: 1, 3, 7, 28, and 56 days. From all this, 10 concrete mixtures were selected for Phase II with the optimum WR/HRWR, gypsum, lime, and RSC levels at zero, 50, and 70% fly ash levels.

4.2. REPLICATE SPECIMENS

For each mixture, there were three replicate specimens for both compressive strength and calorimeter testing, with one mini-slump and one Vicat specimens.

4.3. MATERIALS

4.3.1. Portland Cement. The five portland cements (all Type I/II) were ones that have been commonly used on MoDOT projects. Preliminary chemical and physical analyses were obtained from MoDOT. Later, mill certifications from the producers, which are more specific to the materials used in this study, were supplied when the cements were delivered. Additionally, the research team at Missouri S&T's department of Civil, Architectural, and Environmental Engineering (CArE) did some physical testing as well. Interestingly, no two laboratories performed the exact same set of test methods. In **Table 4.2** are the results from the cement producers. The cement oxide analyses were

performed on materials that were produced at a similar time as those received during the

first shipment of materials.

Table 4.2 – Analyses from cement producer mill certifications (Screening Study)

Cement	SiO_2 %	Al_2O_3 %	Fe_2O_3 %	CaO %	SO_3 %	Na_2O %	K_2O %	EqAlk %	C_3S %	C_3A %	Fineness cm^2/g
1	20.4	4.21	3.62	63.83	2.49	0.20	0.45	0.52	58	5	3980
2	19.90	5.1	3.8	62.6	3.00	---	---	0.5	62	7.1	3920
3	20.3	4.69	3.22	63.0	2.82	---	---	0.50	56	7	3839
4	19.85	4.63	3.23	64.08	3.28	0.177	0.481	0.493	60	7	3856
5	19.8	4.8	3.1	63.2	3.1	---	---	0.55	53	8	3710

A second shipment of Cement 1 and Cement 4 were received approximately six

months after the first delivery, shown in **Table 4.3**. As can be seen, the analyses are quite

similar.

Table 4.3 – Analyses from cement producer mill certifications (Main Effects Study)

Cement	SiO_2 %	Al_2O_3 %	Fe_2O_3 %	CaO %	SO_3 %	Na_2O %	K_2O %	EqAlk %	C_3S %	C_3A %	Fineness cm^2/g
1	20.29	4.05	3.64	63.43	2.91	0.20	0.47	0.54	57	4	4000
4	20.0	4.6	3.1	63.9	3.1	---	---	0.53	61	7	3900

4.3.2. Fly Ash. The five Class C fly ash sources were also ones that were

commonly used on MoDOT projects. Preliminary chemical and physical analyses were

obtained from MoDOT; more specific mill certifications were supplied from some of the

producers upon delivery of materials. Additionally, the Materials Research Center (MRC) at Missouri S&T performed chemical analyses and the particle size distributions were analyzed by the Ash Grove Cement Company Technical Center on the initial shipment of materials.

In **Table 4.4** are the oxide results from the MRC and the PSD results from the Ash Grove laboratories. The Missouri S&T results are from the delivered materials. All of the fly ashes conformed to the requirements for ASTM Class C fly ash.

Table 4.4 – MRC and Ash Grove laboratory analyses of fly ashes

Fly ash	SiO_2 %	Al_2O_3 %	Fe_2O_3 %	CaO %	SO_3 %	Na_2O %	K_2O %	EqAlk %	Retained #325 %	LOI %
1	33.72	21.9	7.15	25.31	2.25	1.40	0.41	1.68	11.16	0.37
2	33.34	20.57	6.15	26.34	1.87	1.63	0.43	1.92	11.17	0.49
3	35.42	16.88	7.97	23.21	3.46	1.40	0.56	1.78	19.37	3.05
4	30.55	18.78	7.48	28.43	3.33	1.50	0.45	1.81	10.17	0.57
5	32.26	19.03	6.24	27.94	2.40	2.20	0.33	2.43	13.04	0.26

During the course of the study, several of the cements and fly ash stocks were exhausted and new samples obtained. These were not tested. A second shipment of Fly Ash 3 was received approximately six months after the first shipment and was used primarily in the Main Effects Study and in Phase II (concrete). Fly Ash 1 was continually resupplied from bulk shipments to Missouri S&T and was used primarily in the Main Effects Study and in Phase II (concrete).

4.3.3. Gypsum. Gypsum was used to restore the aluminate/sulfate balance in the HVFA mixtures made necessary because of the high aluminate-low sulfate levels in fly ash which would upset the carefully determined proper balance in straight OPC's. The gypsum was commercially available recycled drywall called "Ultrafine Gypsum", manufactured by USA Gypsum. The analysis provided in the company's literature states it is 96.0% calcium sulfate. It was assumed that the wallboard is essentially calcium sulfate dihydrate ($CaSO4·2 H20$), commonly known as gypsum.

4.3.4. Lime. Calcium hydroxide has been used to restore the delayed setting time from use of large substitutions of fly ash in mixtures. The calcium hydroxide used in this study was "Standard Hydrated Lime" as manufactured by Mississippi Lime. The advertised analysis was 98.0% $Ca(OH)_2$ with a specific gravity of 2.34. The calcium hydroxide will be referred to as "lime" in other parts of this study.

4.3.5. Rapid Set Cement. The third powder admixture was rapid set cement (calcium sulfoaluminate-dicalcium silicate- gypsum) and has been used to restore early strengths in HVFA mixtures. The particular material used in this study was called "Rapid Set Cement" as manufactured by CTS Cement Manufacturing Corporation. The advertised oxide analysis is shown in **Table 4.5**.

4.3.6. Water Reducer/High Range Water Reducer. The WR/HRWR was essentially a polycarboxylate material (BASF Glenium 7500) and was advertised as meeting both Type A and F admixture requirements.

4.3.7. Water. Deionized water was used throughout the paste study.

Table 4.5 - Oxide analysis of RSC

Parameter	Percent
Calcium oxide (CaO)	50.87
Silicon dioxide (SiO2)	15.40
Aluminum oxide (Al2O3)	13.74
Sulfur trioxide (SO3)	12.52
Iron oxide (FesO3)	2.38
Magnesium oxide (MgO)	1.26
Total alkalis (as Na2O)	0.56
Loss on ignition	2.84
Insoluble residue	0.78
Specific gravity	2.98

4.4. TEST EQUIPMENT AND PROCEDURES

4.4.1. Mixing for Compressive Strength, Calorimetry, and Miniature Slump

4.4.1.1 Pre-blending. Prior to mixing of the paste batches, the dry constituents of the mixture were pre-blended. This was performed by transferring no more than 1200 grams of the materials into a 4x8 in. (100x200 mm) plastic cylinder mold in similar proportions as used in the mixture. The cap was then placed on the cylinder and the cylinder was held horizontally with one hand on each end. The cylinder was then shaken 25 cycles using a six in. (150 mm) throw. This procedure is included in all of the test procedures in Appendix A.

4.4.1.2 Combined Test Method Mixing. The paste batches for semi-adiabatic calorimetry, compressive strength, and miniature slump testing were mixed using the

same procedure and equipment. The paste for all three test methods was typically mixed

in a single batch. As noted by Cost (2009), the use of equipment and methods other than

those given in ASTM C 305 (ASTM, 2006a) can successfully shorten mixing times to as

little as sixty seconds, which may be necessary when batches for multiple test methods

are made simultaneously. The choice of test method and equipment can render

significantly different test results. In order to mix the materials adequately and within the

time requirements of the tests being performed, a handheld kitchen mixer was used. The

batches were mixed using a 250-watt Black and Decker Model MX217 hand mixer with

egg beater-style paddles, shown in **Figure 4.2**, below.
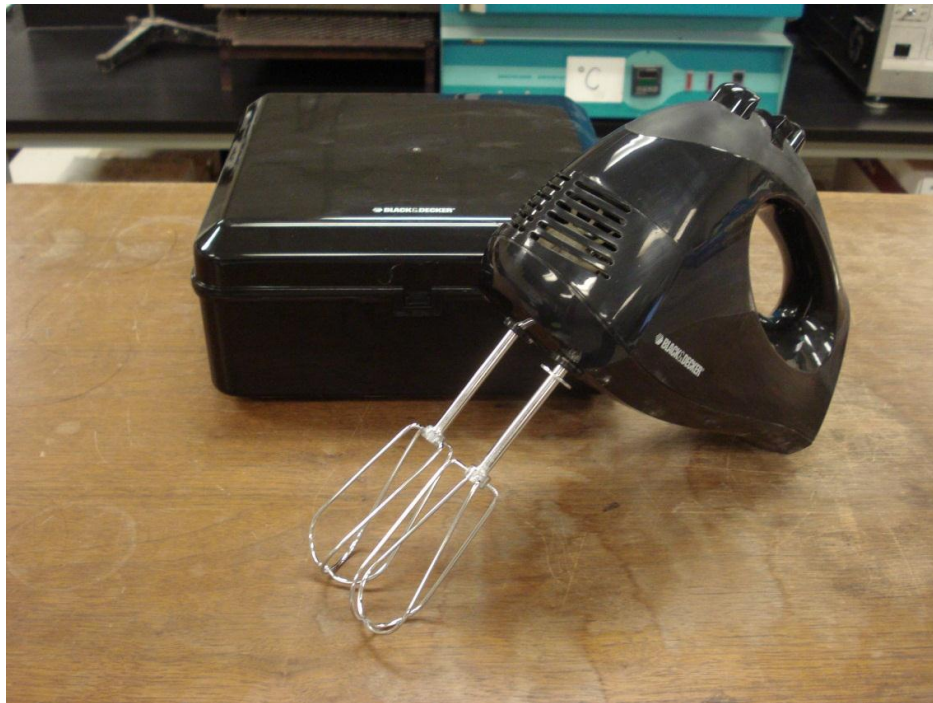
Figure 4.2 – Black and Decker hand mixer

The mixer had six speed settings along with a "Power Boost" option that would

increase the mixing speed when pushed. The rotational speeds were determined in the

following manner. An adjustable rate strobe light was used to determine the rotational speeds for the various settings on the handheld mixer. To do this, a piece of white tape was attached to a fin of one paddle and a piece of orange tape was placed on the other paddle. The mixer was then started and the strobe light was adjusted to flash at different rates until the tape on the paddles appeared to stop moving. It was also noted that each fin appeared to stop when the proper rate was set on the light. This rate was read in RPMs off of the dial used to adjust the flashing rate. The rates determined were between 390 and 700 RPM, which is a reasonable result for this appliance. Judgment had to be used to make sure that higher or lower speeds were not taken to be the actual speed of the blender, since the stopped-movement appearance can occur at higher or lower flashing rates on the strobe light that would be unreasonable for this type of device. The rotational speeds for the various settings are given below in **Table 4.6**.

Table 4.6 – Hand Mixer Rotational Speeds

Speed Setting	Rotational Speed (RPM)
1	390
2	440
3	490
4	540
5	600
6	670
Power Boost	700

The paste was mixed in a stainless steel mixing bowl from a Hobart Model A-200 mixer, which had a capacity of 20 quarts (19 l). Temperature measurements of the paste, after mixing, were made using an analog thermometer with a probe length of five in. (125

mm). Other equipment included a stopwatch for timing of the mixing procedure and a ladle to transport the paste mixture from the mixing bowl. **Figure 4.3**, below, shows the mixing bowl, thermometer, and other equipment used during mixing.

Figure 4.3 – Equipment used in the Combined Mixing Procedure

In this study, the initial mixing of the paste batch was performed in ninety seconds, which allowed the first miniature slump test to be performed at two minutes after mixing began. The initial mixing consisted of adding the water to the cementitious materials, allowing the cement to absorb the water for ten seconds, mixing for 20 seconds at Speed 2 (440 rpm), and then mixing for 60 seconds at Speed 6 (670 rpm). As noted by Kantro (1980), brief setting of the paste mixture can be avoided by remixing the paste. This was done in this study by remixing the paste for thirty seconds at Speed 2 prior to each miniature slump test. The calorimeter specimens were prepared and inserted into the calorimeter after the 5-minute miniature slump test, which allowed for early data

collection, and the cube specimens were molded after the 15-minute miniature slump test, so that molding began within 2 minutes and 30 seconds after remixing. In **Table 4.7**, on the following page, the complete sequence of testing can be seen.

It was critical to adhere to the schedule to reduce variability in test results. In some cases, not all of the tests were performed using a single batch of paste. For these cases, the same mixing and remixing sequences were followed with the tests being performed at their respective times in the combined mixing procedure.

Table 4.7 – Combined Mixing Procedure Sequence

Elapsed Time (mm:ss)	Action
0:00	Add water to mixing bowl with cementitious materials Record Time (Start Time)
0:10	Start mixing at Speed 2 (440 RPM)
0:30	Start mixing at Speed 6 (670 RPM)
1:30	Stop Mixing Record Temperature of Paste Prepare mini-slump test
2:00	Lift mini-slump cone
4:00	Remix paste at Speed 2
4:30	Prepare mini-slump test
5:00	Lift mini-slump cone Prepare calorimeter specimens Insert calorimeter specimens in F-Cal 4000
10:00	Close and latch the lid of the F-Cal 4000
13:00	Remix paste at Speed 2
13:30	Prepare mini-slump test
15:00	Lift mini-slump cone Mold cement cubes
28:00	Remix paste at Speed 2
28:30	Prepare mini-slump test
30:00	Lift mini-slump cone
43:00	Remix paste at Speed 2
43:30	Prepare mini-slump test
45:00	Lift mini-slump cone
60:00	Measure and record mini-slump diameters

4.4.2. Cube Compressive Strength. Three replicate specimens per mixture were molded. Steel and plastic molds were used to mold the two-in. (50 mm) paste cubes. All of the cube molds were sealed with vacuum grease to prevent the paste from leaking. Excess vacuum grease was removed from the interior of the molds to avoid deforming the shape of the cubes. The vacuum grease was Dow Corning High-Vacuum Grease. In **Figure 4.4** is shown the cube molding equipment. The molding of the specimens followed the filling, tamping, and leveling procedures outlined in ASTM C 109 with a deviation of the time at which molding began (ASTM, 2008a). ASTM C 109 states that specimen molding should begin within two minutes and thirty seconds after completion of the original mixing of the batch. In this study, molding started after completion of the 15-minute miniature slump test, which would mean that molding started approximately fourteen minutes after completion of the initial mixing. However, this molding time was within two minutes and thirty seconds after completion of the remixing for the 15-minute miniature slump test. Also, it was noted that the paste at this time was sufficiently fluid to allow for complete consolidation. Following the completion of the molding procedures, the specimens (still in the molds) were placed in the moist room which had a relative humidity maintained at 95% or greater. There was concern about breakage of some of the weaker specimens, so three days of curing was allowed before stripping. The paste cubes were removed from the molds and placed in buckets of water saturated with hydrated lime. The buckets had a capacity of five gal (19 l) and were placed back in the moist room.
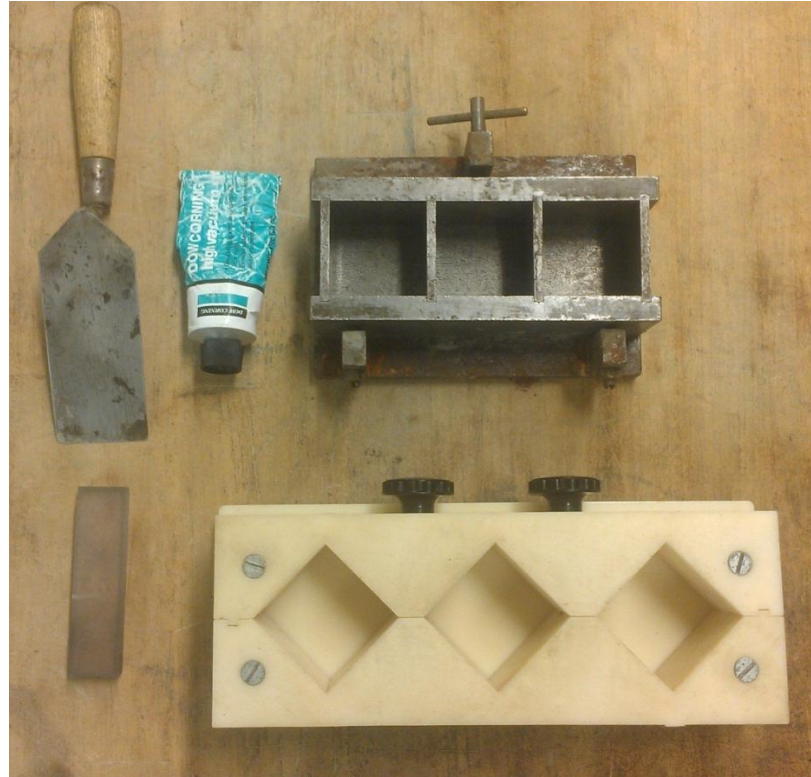
Figure 4.4 – Cube molding equipment

The two-in. (50 mm) cube specimens were tested for compressive strength on a hydraulic, Tinius-Olsen tension/compression machine with a capacity of 200,000 lbs (90,800 kg). The Tinius-Olsen is controlled using a desktop computer with MTestW software. It is important to match the loading platen size to the specimen size. Two loading platens were used to apply the load to the two loading faces of the cube specimens. The lower, square loading platen was about 12 in. tall and had a diagonal dimension of 3.5 in. (90 mm). It was attached to a larger, circular loading platen, typically used for cylinder testing, which rested on the lower table of the Tinius-Olsen machine. The upper, circular loading platen was about six in. (150 mm) tall and was attached to the upper crosshead of the Tinius-Olsen machine. The loading block of the upper platen was spherically seated and had a diameter of 3.5 in. (90 mm). **Figure 4.5**

shows the Tinius-Olsen machine with the loading platens and the computer used to control the machine.

Other equipment included digital calipers for measuring the dimensions of the specimen and sand paper to smooth the loading faces of the specimen. The sand paper had a grit size of 60.

Figure 4.5 – Tinius-Olsen load frame and computer

The compressive strengths of the cubes were tested at a load rate of 200 lbs/sec (91 kg/sec), which is within the range allowed by ASTM C 109. Prior to loading the specimens, the molded faces of the cubes that were to be loaded were sanded to provide flat loading surfaces. The cubes and the loading platens were cleaned of any debris prior to the start of loading.

4.4.3. Semi-adiabatic Calorimetry. Semi-adiabatic calorimetry was performed on the paste mixtures using an F-Cal 4000 calorimeter with CalCommander v1.3 Software Suite from Calmetrix, Inc. Temperature measurements were taken of hydrating paste specimens over time. The F-Cal 4000, shown in **Figure 4.6**, consists of four receptacles in an insulated box with thermistors at the bottom of each receptacle. The thermistors, along with a USB port, are connected to a single data logger. The receptacles are sized to hold standard 4x8 in. (100x150 mm) plastic cylinder molds.
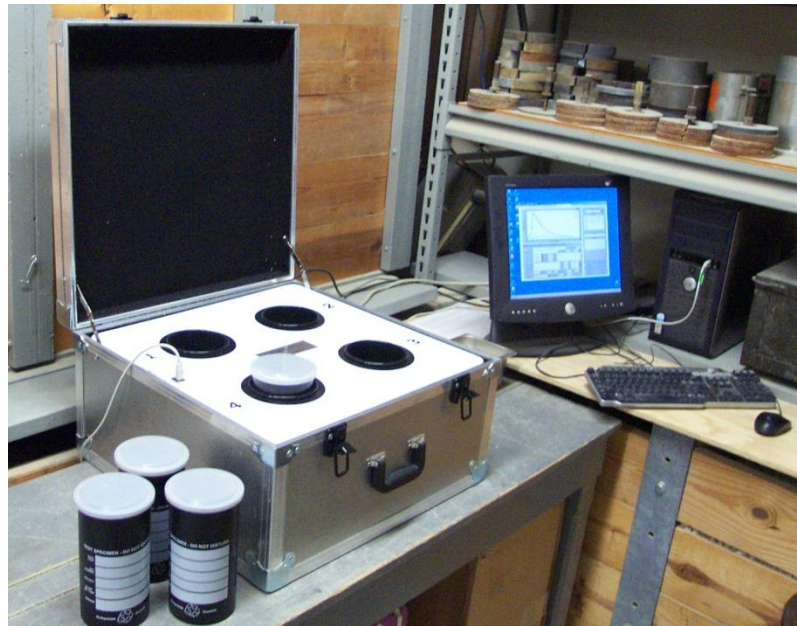
Figure 4.6 – F-Cal 4000, computer, and cylinder molds

Three specimens were inserted into the F-Cal 4000 for each mixture, with one receptacle containing the inert specimen. It was decided that three specimens should be used for each mixture, instead of testing multiple mixtures simultaneously, so that the results for a given specimen would not be affected by the temperature rise of the other specimens in the box with different compositions. The inert specimen consisted of high-

silica sand and deionized water with a water-to-sand ratio equal to the water-to-cementitious materials ratio of 0.40 and mass similar to the paste specimens. The use of a water and sand combination is intended to better simulate the thermal conductivity of the paste specimens, when compared to a dry sand inert specimen (T. Cost, personal communication, April 10, 2012). The mass of the inert specimen was 1250.0 grams and the masses of the paste specimens were 1250.0 grams with a tolerance of 10.0 grams. This mass is recommended in the F-Cal 4000/8000 User Manual and fills approximately one-third of the cylinder's volume. As noted in a draft ASTM standard for evaluating hydration using thermal measurements (ASTM, 2011a), the "masses of all specimens that will be compared with each other shall not differ by more than 5%". A tolerance of 10.0 grams was chosen since it was within this range, was easily accomplished, and could lessen the variability between specimens when compared to specimens differing in mass by 5%.

Prior to loading the specimens in the calorimeter, the cylinders were tapped ten times with an open hand to remove entrapped air from the paste. The cylinders were then capped and placed in the calorimeter. Logging typically continued for 48 hours after the start of the initial mixing. However, the logging time was shortened for mixtures that obtained the peak hydration curve in less than 48 hours and lengthened for mixtures that experience significant delays in hydration.

Once logging in the F-Cal 4000 was complete, the data was retrieved using the CalCommander software. The calorimeter was connected to a desktop computer with a USB cable. From the software, the data for each logging channel was exported as a separate Text Document (.txt) file. These were then imported into Microsoft Excel 2010

and the Signal-to-Noise ratio (S/N) was calculated for each of the three specimens. The Signal is the difference between the highest and lowest temperatures recorded for the sample being tested. The Noise is the difference between the highest and lowest temperatures recorded for the inert specimen. **Figure 4.7**, below, shows an example of the temperature versus time curves resulting from the raw data for a typical hydrating cement paste sample and corresponding inert specimen. The Signal and Noise quantities are indicated in the figure.

Cost (2009) noted that the curve generated for the inert specimen should be subtracted from the curve for the hydrating specimen, so that the resulting data represents only the heat evolution of the sample and not variances in the ambient temperature. Cost designated this quantity as ΔT, which is shown below in **Figure 4.8**. In this study, the curves for the three specimens were averaged to result in a single hydration curve for each paste mixture. The curve for the inert specimen was then subtracted from this averaged curve to result in a corrected average hydration curve.
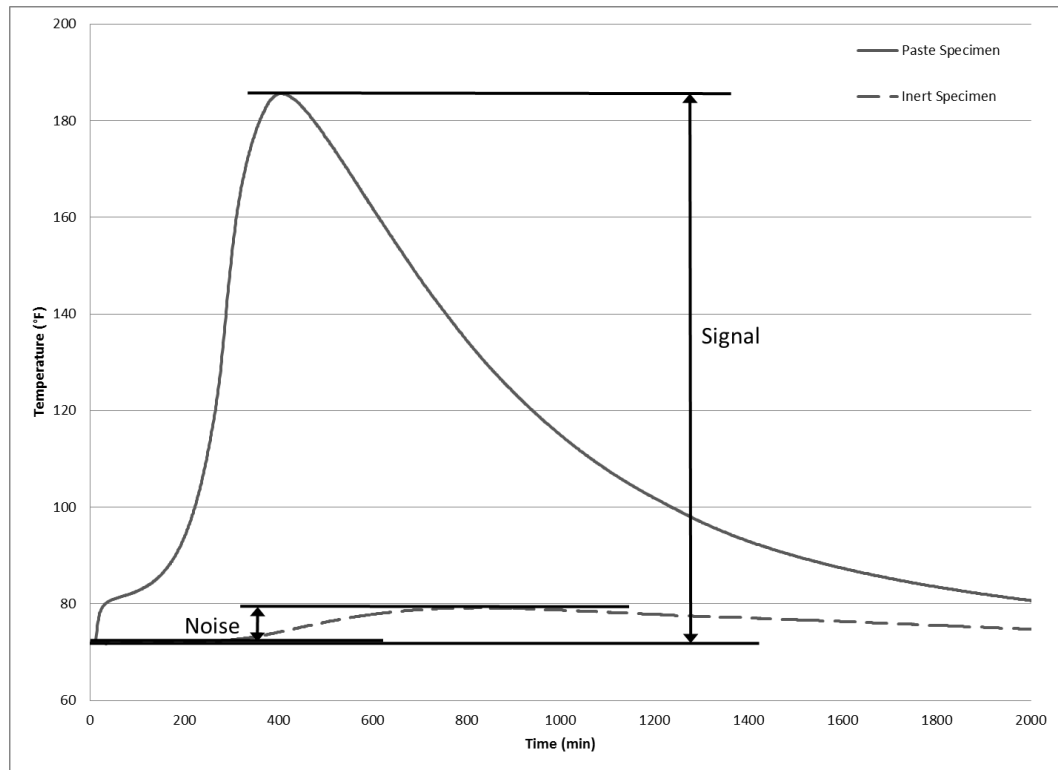
Figure 4.7. Examples of signal and noise quantities

This curve was then used to calculate predicted setting times using the Fractions

Method and Derivatives Method, as discussed by Sandberg and Liberman (2007). For the

Fractions Method, the main hydration response rise (M) is calculated, which is the

difference between the peak temperature of the main hydration curve and the lowest

temperature during the dormant period, and then two percentage values of the main

hydration response rise are chosen to represent the initial and final set times. For this

study, 20% of the main response was chosen for initial set and 50% was chosen for final

set. A representation of the calculated values for the Fractions Method is shown below in

Figure 4.9. For the Derivatives Method, initial set is taken as the time when the

maximum second derivative of the main hydration curve occurs and final set is taken as

the time when the maximum first derivative of the main hydration curve occurs.
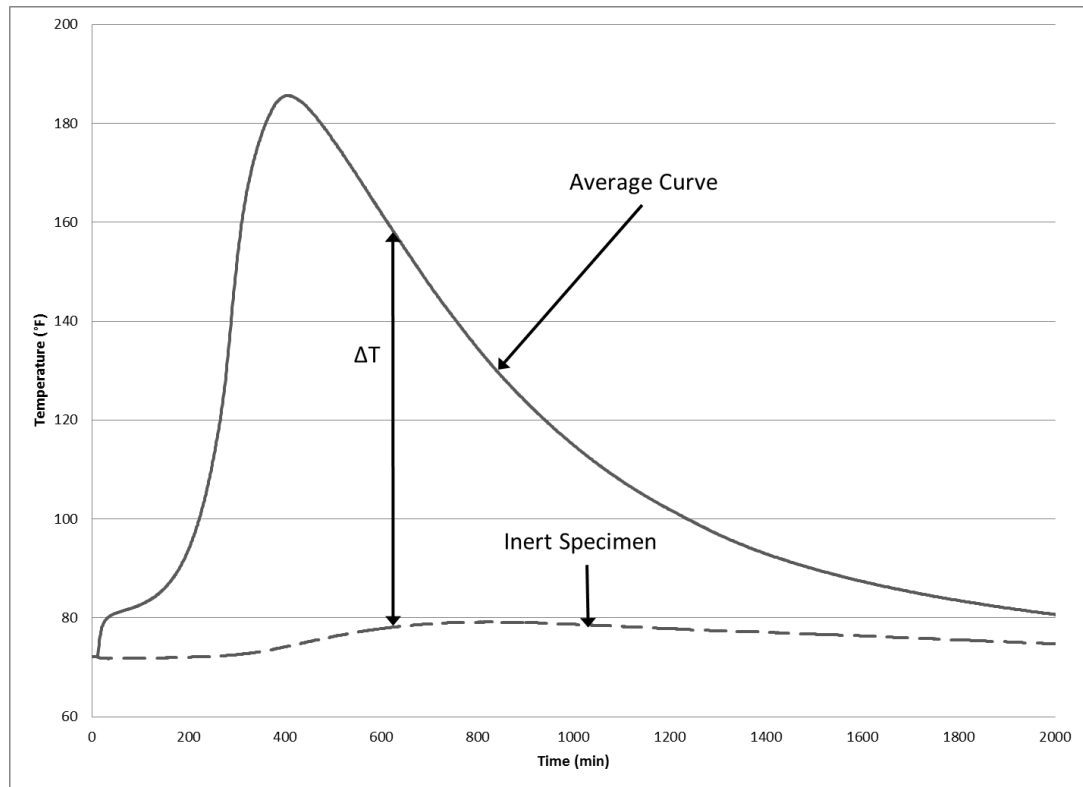
Figure 4.8. Representation of the ΔT quantity

The complete semi-adiabatic calorimetry procedure, including data reduction, is titled "Using the F-Cal 4000 & CalCommander Software for Testing Cement Paste" and is included in Appendix B.

After acquiring the F-Cal 4000, a verification of the internal connections was performed, as suggested in the F-Cal 4000/8000 User Manual, to ensure that the connections had not been damaged during shipping. This was done by filling four cylinders with water at 110°F (43.3 C) and inserting them into the F-Cal 4000. After 30 minutes, the temperature reading was checked for each of the sensors to ensure that no two sensors differed by more than 2°F (1.1 C).
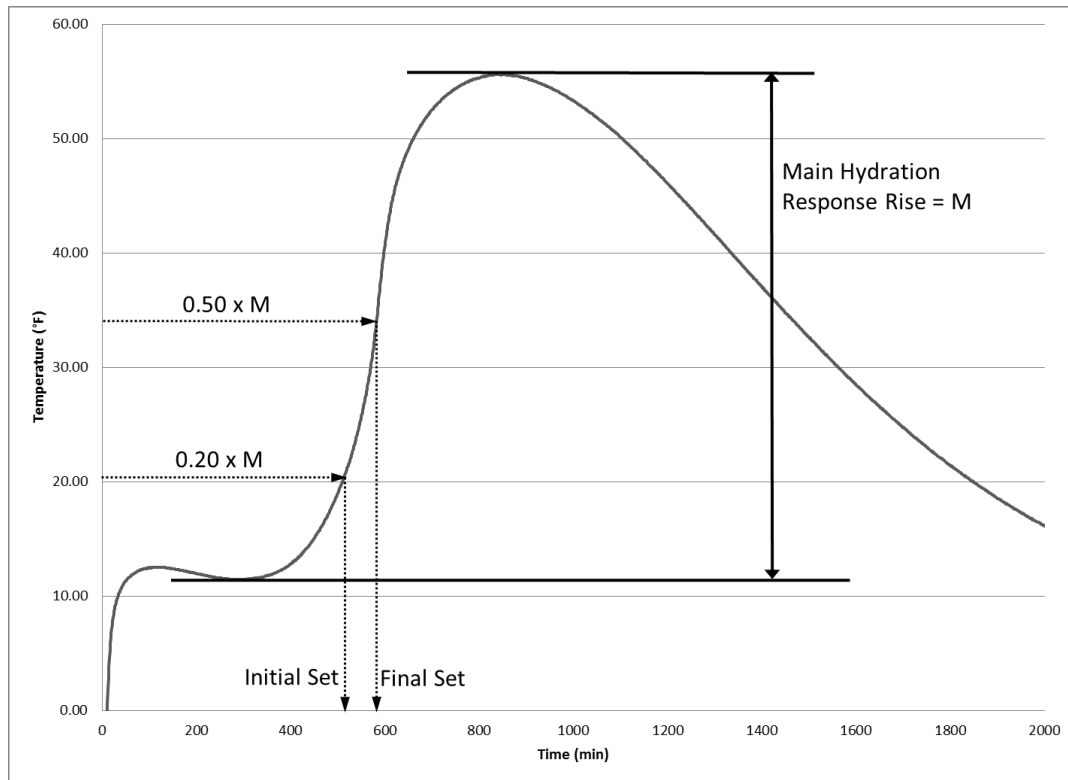
Figure 4.9. Example of setting time prediction by the fractions method

4.4.4. Miniature Slump. Two identical miniature slump cones were fabricated

from Plexiglas with the dimensions given by Kantro (1980). The inside of the cones had

dimensions in the same proportion as those specified for a standard slump cone as given

in ASTM C 143 (0.75 in.(19 mm) top diameter, 1.5 in. (38 mm) bottom diameter, and

2.25 in. (57 mm) height)(ASTM, 2010a).

Figure 4.10, shows the two cones used in this study, along with other equipment

used for performing this test, which included a Plexiglas board, plastic discs, and a

spatula.

Figure 4.10 – Miniature slump cones and equipment

The paste for the miniature slump test was mixed according to the combined mixing procedure previously discussed. The test was performed at 2, 5, 15, 30, and 45 minutes, as was done by Bhattacharja and Tang (2001). The tests at 2 and 5 minutes were performed 30 seconds after the end of mixing or remixing. The tests at 15, 30, and 45 minutes were performed one minute and thirty seconds after the end of remixing to allow for a longer period to fill the cone, which was needed for stiffer mixtures.

The cones were placed on thin plastic discs, as suggested by Bhattacharja and Tang (2001), to prevent leaking from the bottom of the cone. The discs had diameters of two inches and were cut from Zip-Lock sandwich bags.

Previous research (Kantro, 1980; Bhattacharja and Tang, 2001), discussed the use of a planimeter for measuring the area of the miniature slump pats. To do this, tracings of the pats were made on paper and measured after the pats had hardened and were removed. An alternative method uses multiple diameter measurements to obtain an average diameter from which the area is calculated. While the planimeter method gives somewhat more accurate results, time constraints and concerns about variability

introduced by the paper led to the use of diameter measurements for area determination. In this study, this involved taking four diameter measurements, separated by rotations of 45 degrees, to obtain an average diameter from which the area was calculated.

The diameter measurements were taken at 60 minutes after the start of mixing. This time was chosen to allow the later miniature slump tests time to stabilize without allowing sufficient time for the results of the earlier tests to be affected by shrinkage from hydration and drying.

The complete test procedure, which was adapted from procedures given by Kantro (1980) and Bhattacharja & Tang (2001), is titled "Miniature Slump Cone" and is included in Appendix C.

4.4.5. Normal Consistency and Vicat Time of Setting. The Vicat apparatus described in ASTM C 191 and ASTM C 187 was used for both the Vicat setting time and normal consistency tests (ASTM, 2008b, 2010b). In **Figure 4.11** is shown the apparatus.

The paste was mixed using a Hobart Model N50 mixer, bowl, and paddle, which conform to the requirements of ASTM C 305 (ASTM, 2006a). The mixer has three speeds and moves the paddle in both planetary and revolving motions. **Figure 4.12**, below, shows the mixer and bowl scraper.

The paste for the normal consistency test was mixed according the Procedure for Mixing Pastes given in ASTM C 305 with one deviation. In this study, the bowl and paddle were wetted before mixing commenced to provide a more constant surface condition of these items when multiple tests were run in succession. Care was taken to ensure that excess water was not present, which would affect the normal consistency

results. Following the mixing procedure, normal consistency was determined according to ASTM C 187.

Figure 4.11 – Vicat apparatus with ring and glass plate

The paste from the normal consistency test was used to determine the time of setting by the Vicat method according to ASTM C 191 with one deviation. The specimen was kept in the moist room between penetration measurements and was covered with a plastic sheet while in the moist room to prevent damage to the surface of the specimen from dripping water. Similar modifications to ASTM C 191 have been made by other researchers (Bentz and Ferraris, 2010) to prevent evaporation from the surface of the specimen during the test.

Figure 4.12 – Hobart mixer with bowl scraper

For specimens that experienced initial set prior to the first penetration reading at 30 minutes, a penetration of 1.57 in. (40 mm) was assumed at time zero. This made possible the interpolation of initial set at a penetration of 0.98 in. (25 mm), as described in ASTM C 191.

4.5. RESULTS AND DISCUSSION

4.5.1. Screening Study

4.5.1.1. General. The purpose of the Screening Study was to make a first pass through all five cements and all five fly ashes to find the most reactive and the least reactive combination. The two selected pairings would then be the subject to the Main Effects Study, where the effects of powder additives would be explored. Historically,

early strength is one of the properties of most concern for HVFA, and as fly ash content increases, early strength is anticipated to be more problematic. Therefore, "reactivity" was defined as one day compressive strengths at 70% fly ash replacement without any powder additives or WR/HRWR. The other paste tests were also performed (miniature slump, Vicat setting time, and 28 day compressive strengths) for additional information.

4.5.1.2. Compressive Strength. One and 28 day cube compressive strengths are tabulated in Appendix F. Of 480 cubes cast and tested, there were eight outliers, according to the procedure of ASTM E178. The results were discarded.

The effects of fly ash replacement level on each combination are shown in **Figures 4.13-4.17**.
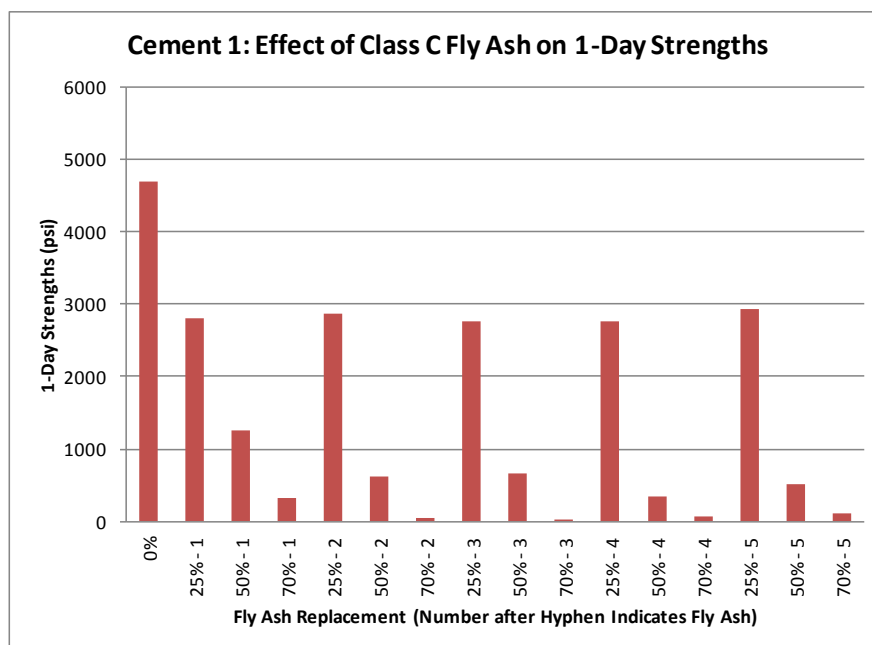
Figure 4.13 – Effect of Fly Ash Replacement Level on One Day Strengths of Cement 1 in Combination with Each Fly Ash
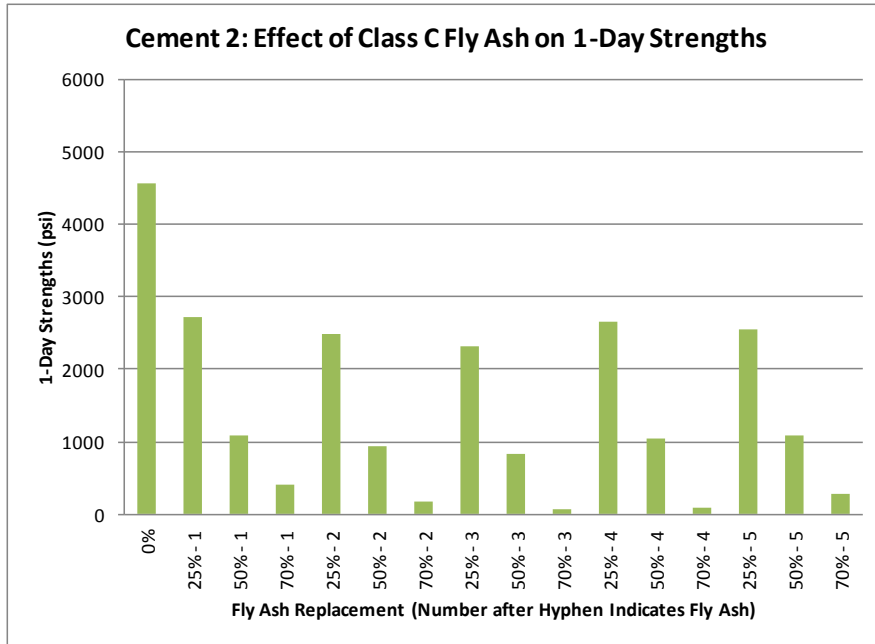
Figure 4.14 – Effect of Fly Ash Replacement Level on One Day Strengths of Cement 2 in Combination with Each Fly Ash
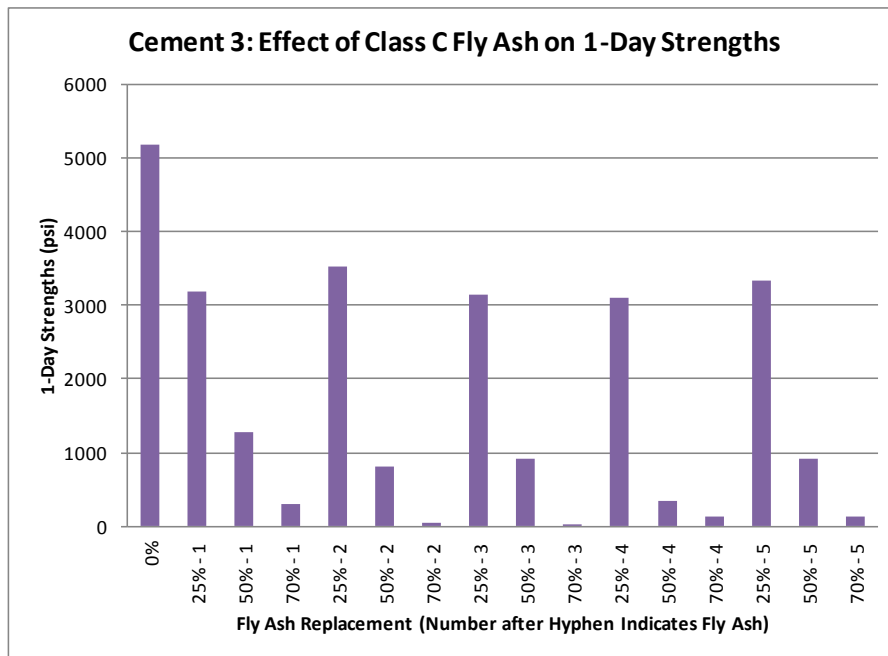
Figure 4.15 – Effect of Fly Ash Replacement Level on One Day Strengths of Cement 3 in Combination with Each Fly Ash
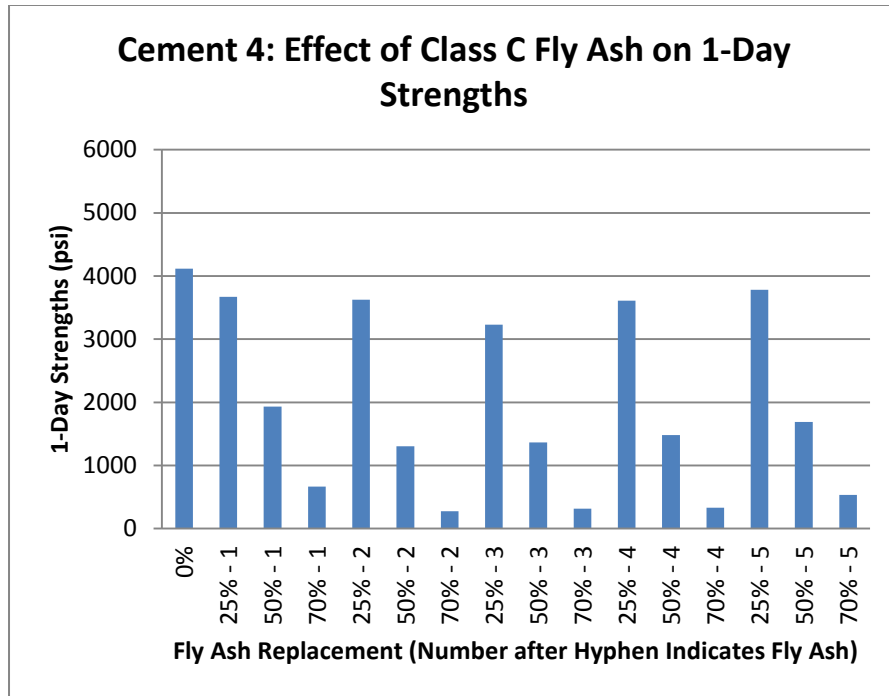
Figure 4.16 – Effect of Fly Ash Replacement Level on One Day Strengths of Cement 4 in Combination with Each Fly Ash
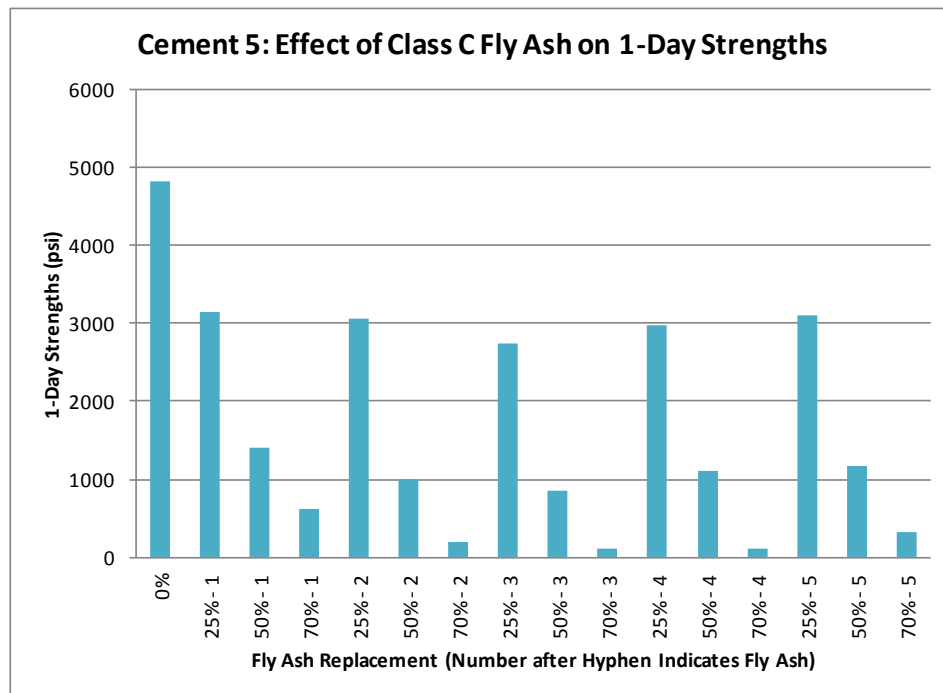
Figure 4.17 – Effect of Fly Ash Replacement Level on One Day Strengths of Cement 5 in Combination with Each Fly Ash

The general trend is as expected: as fly ash replacement level increases from 25% through 70%, one day strengths decreased. The specific combination of cement and fly ash sources also impacted the strengths. The combination of greatest one day strength at 70% replacement was Cement 4 with Fly Ash 1 (designated "4-1"). The lowest reactivity combination was Cement 1 with Fly Ash 3 (designated "1-3"). Fly Ash 3 was the lowest performer in almost every 70% combination. These two combinations were carried forward into the Main Effects Study. A value of 1000 psi (6.9 MPa) one day strength for concrete has been suggested as a minimum for acceptance (Cost and Knight, 2007). In this study, 1200 psi (8.3 MPa) paste strength corresponded to 1000 psi concrete strength. Of the 25 combinations, 12 exceeded 1200 psi.

The 28 day strengths of the different combinations are shown in **Figures 4.18-4.22.**

The general trend is as expected: as fly ash replacement level increases from 25% through 70%, 28 day strengths decreased. The specific combination of cement and fly ash sources also impacted the strengths. Fly ash 3 was the lowest performer in almost every 70% combination, although at 25 and 50%, other fly ashes exhibited lower strengths. The range of strengths for various replacement levels were: cement alone: 11,260-12,210 psi (77.7-84.2 MPa); at 25% fly ash: 5860-12,080 psi (40.4-83.3 MPa); at 50% fly ash: 4160-8800 psi (28.7-60.7 MPa); and 70% fly ash: 2350-6040 psi (16.2-41.6 MPa). So, the specific combination of cementitious materials at various ages is important to strength. In terms of pozzolanic action, only one combination at 25% fly ash level exceeded the straight OPC mixture, although seven combinations approached the zero fly ash controls within 1000 psi (6.9 MPa).
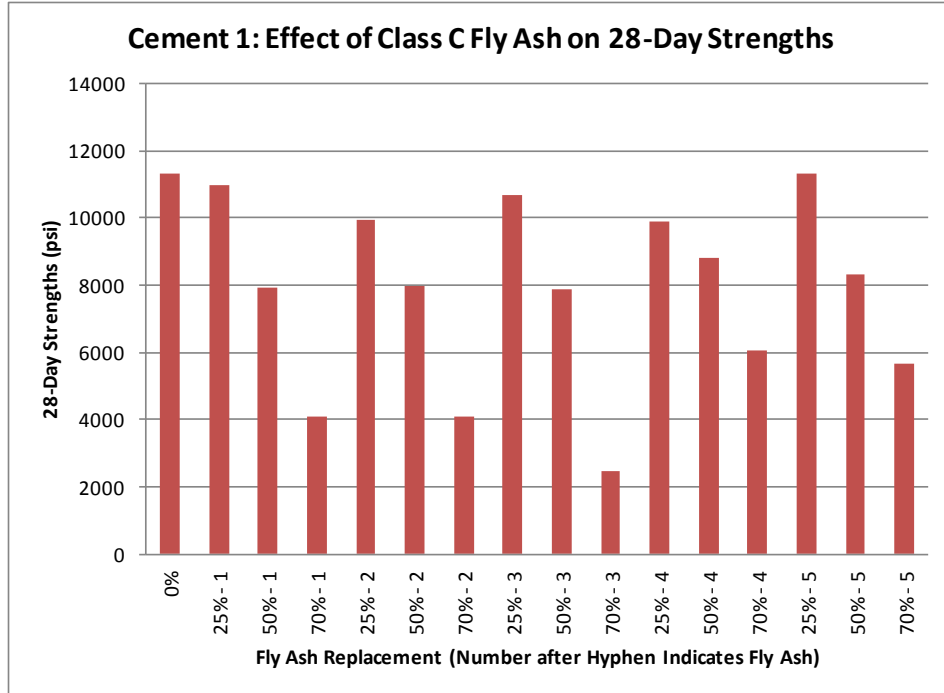
Figure 4.18 – Effect of Fly Ash Replacement Level on 28 Day Strengths of Cement 1 in Combination with Each Fly Ash
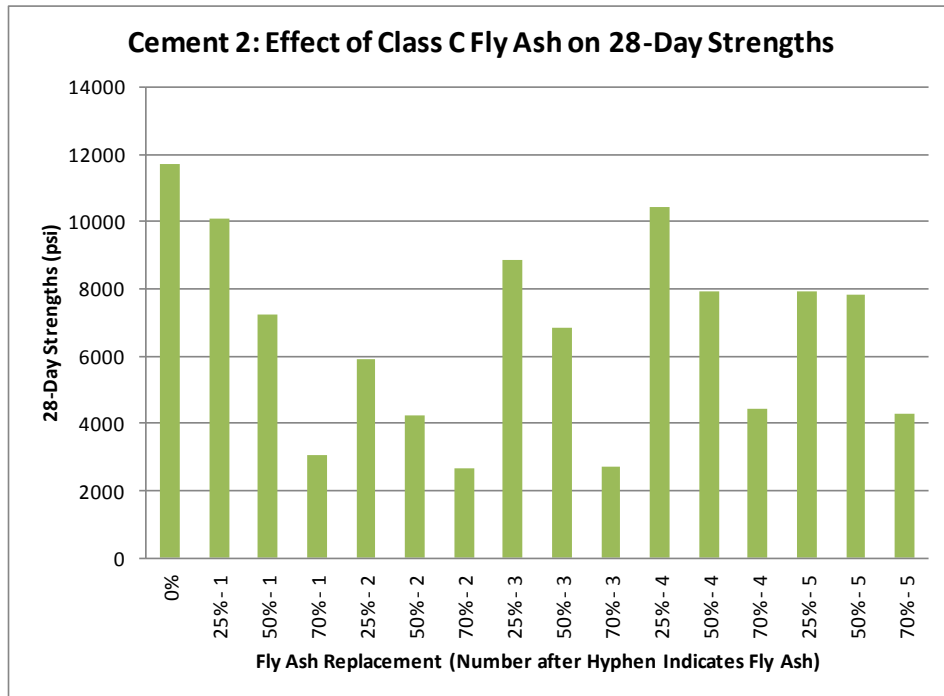
Figure 4.19 – Effect of Fly Ash Replacement Level on 28 Day Strengths of Cement 2 in Combination with Each Fly Ash
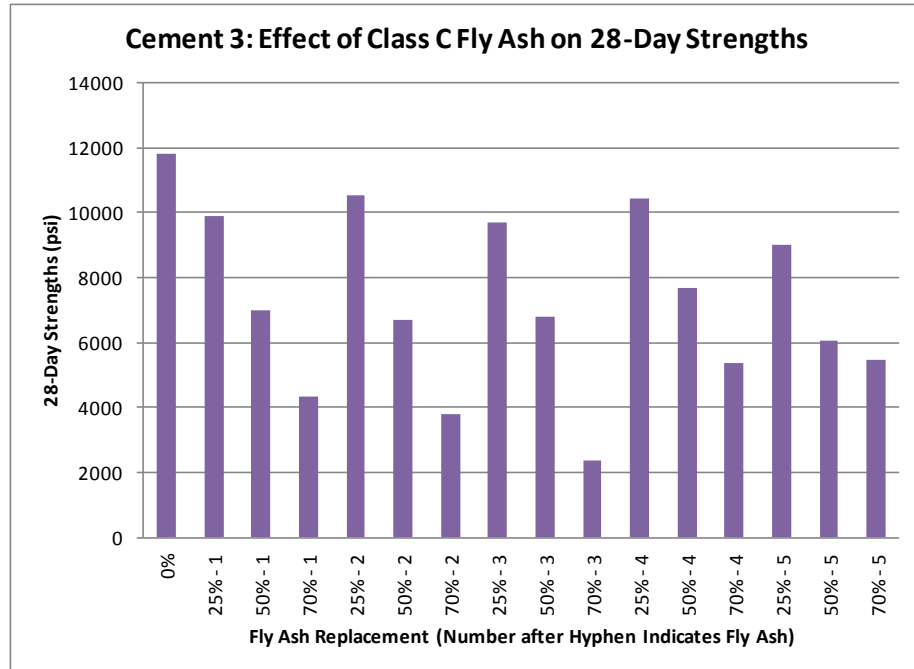
Figure 4.20 – Effect of Fly Ash Replacement Level on 28 Day Strengths of Cement 3 in Combination with Each Fly Ash
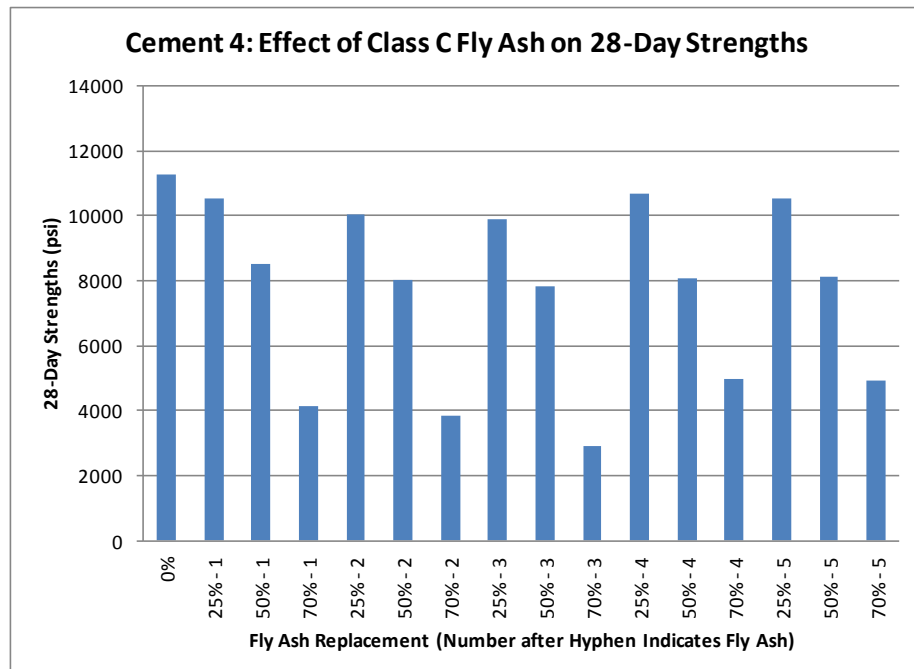
Figure 4.21 – Effect of Fly Ash Replacement Level on 28 Day Strengths of Cement 4 in Combination with Each Fly Ash
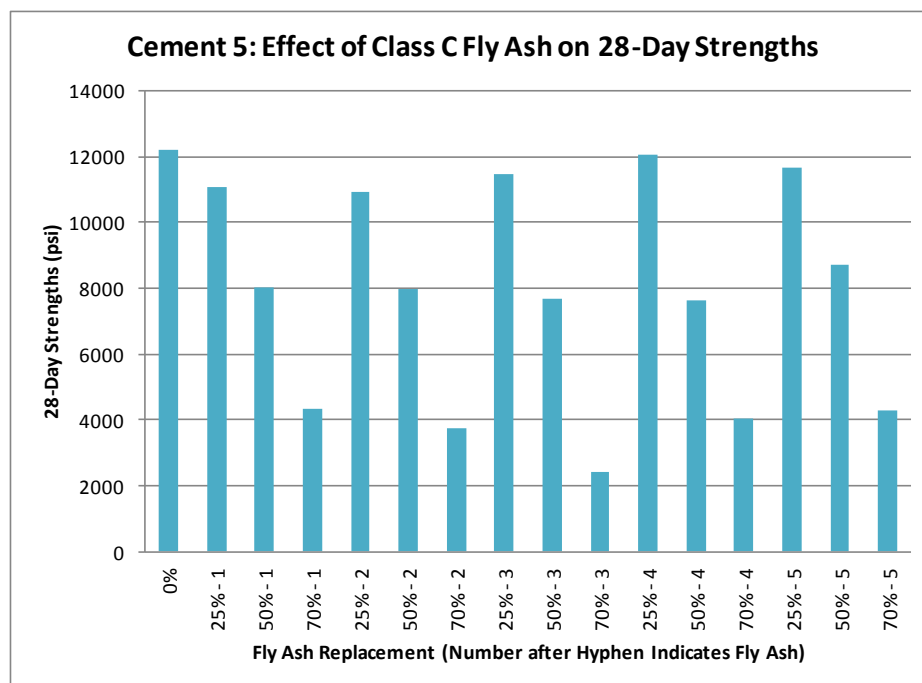
Figure 4.22 – Effect of Fly Ash Replacement Level on 28 Day Strengths of Cement 5 in Combination with Each Fly Ash

Various total oxide contents of each blend were calculated based on the individual cement and fly ash oxide analyses and their proportions (percentages) in the blend. For the combined Screening and Main Effects data, early strength is correlated to the total calcium oxide (CaO) (R= 0. 949), total aluminates (R= -0.872), and total equivalent alkalis (R= -0.898) in the OPC-fly ash system. These relationships are shown in **Figures 4.23-4.25**. Calcium ions are necessary for forming the main strength-producing hydration product, calcium silicate hydrate (C-S-H). High aluminate content systems react rapidly with calcium, thus reducing the calcium available to the silicate hydration reaction, lowering strengths. Likewise, high total equivalent alkalis increase the rate of reaction between the aluminates and the calcium.
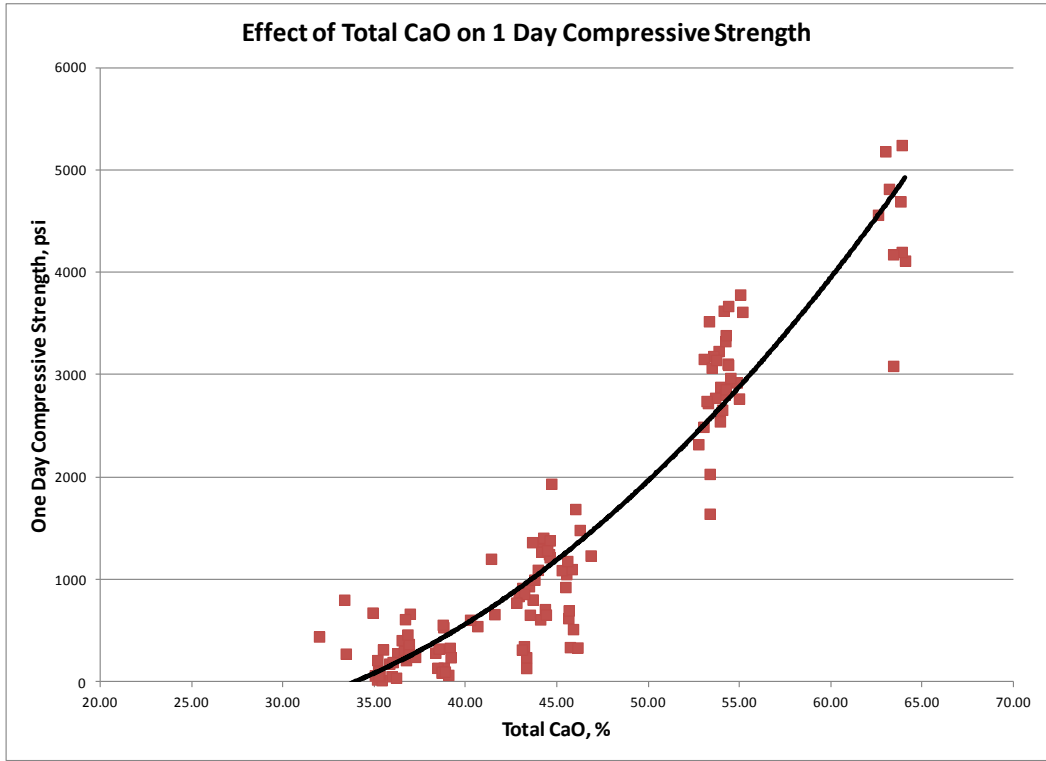
Figure 4.23 – Effect of Total CaO on One Day Compressive Strengths
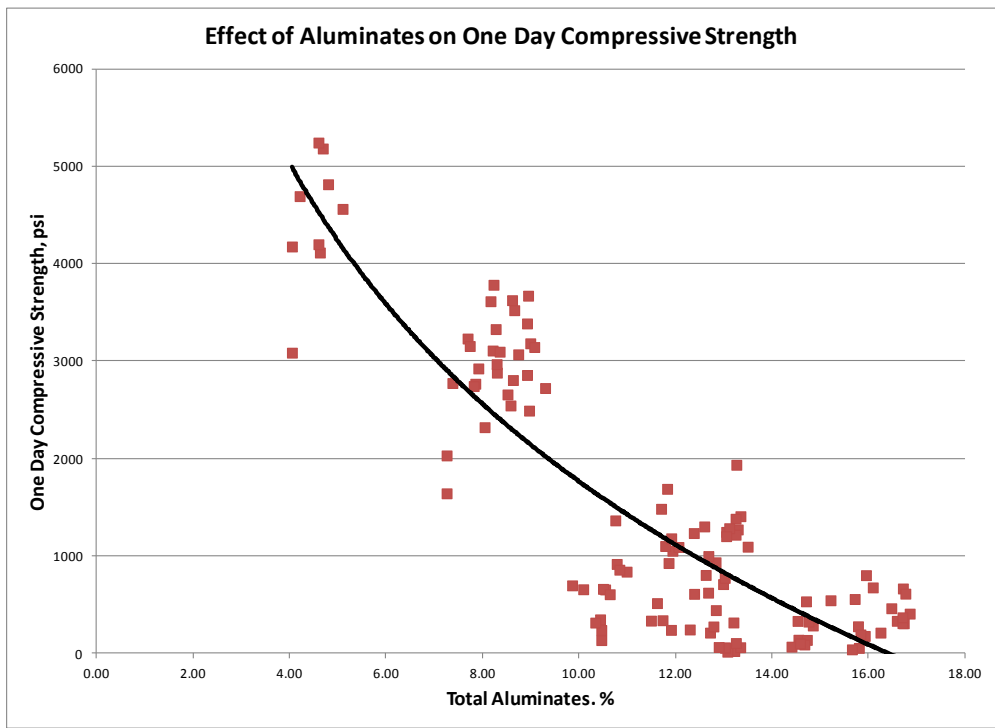
Figure 4.24 – Effect of Total Aluminates on One Day Compressive Strengths
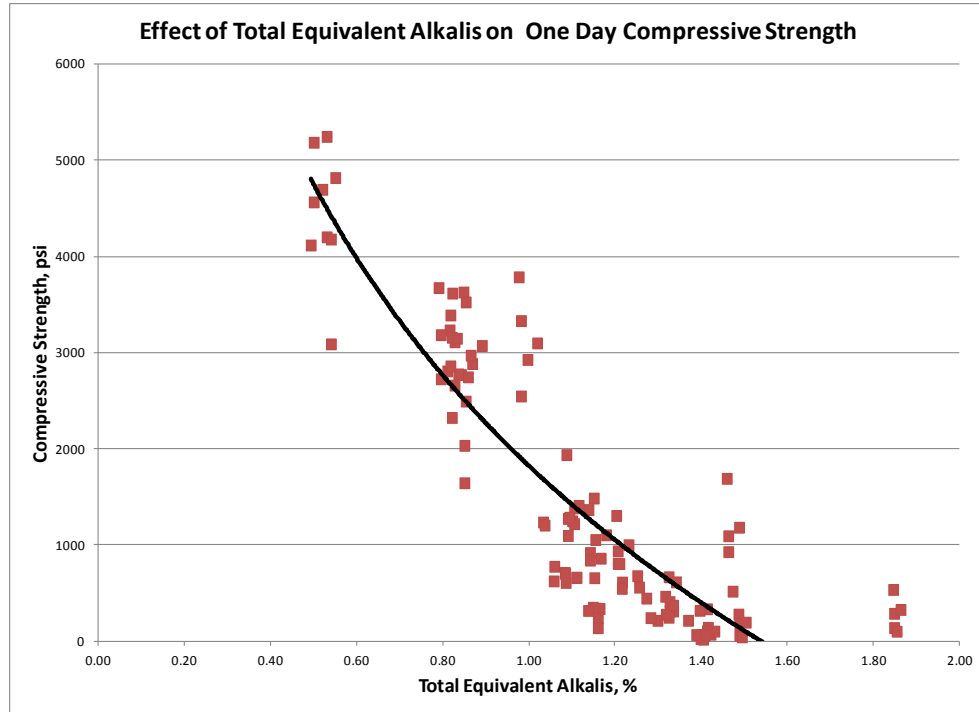
Figure 4.25 – Effect of Total Equivalent Alkalis on One Day Compressive Strengths

In a later section, the relationship of early compressive strength, calorimeter curves, and the oxide analyses will be explored.

The compressive strength results are tabulated in Appendix F.

4.5.1.3. Calorimetry. All 80 mixtures were subjected to semi-adiabatic calorimetry testing. The Signal/Noise ratio of each replicate was used to assess the occurrence of outliers. There were none in the screening study dataset. A typical set of results is shown in **Figure 4.26**.

Cement with Increasing Amounts of Fly Ash
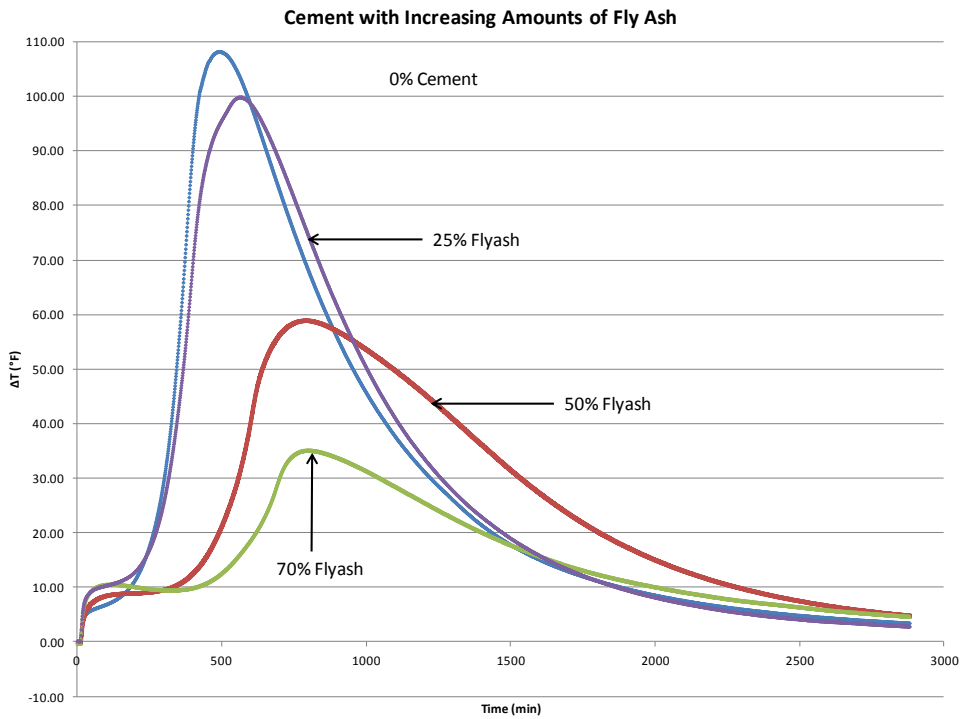
Figure 4.26 – Typical Calorimeter Curves

As shown, the expectations are that with increasing fly ash replacement, the peak of the temperature curve becomes lower, and occurs later because of the slower reaction of the fly ash compared to straight OPC. The peak temperature in this study is termed "NetTMax" and is shown in **Figure 4.27**.
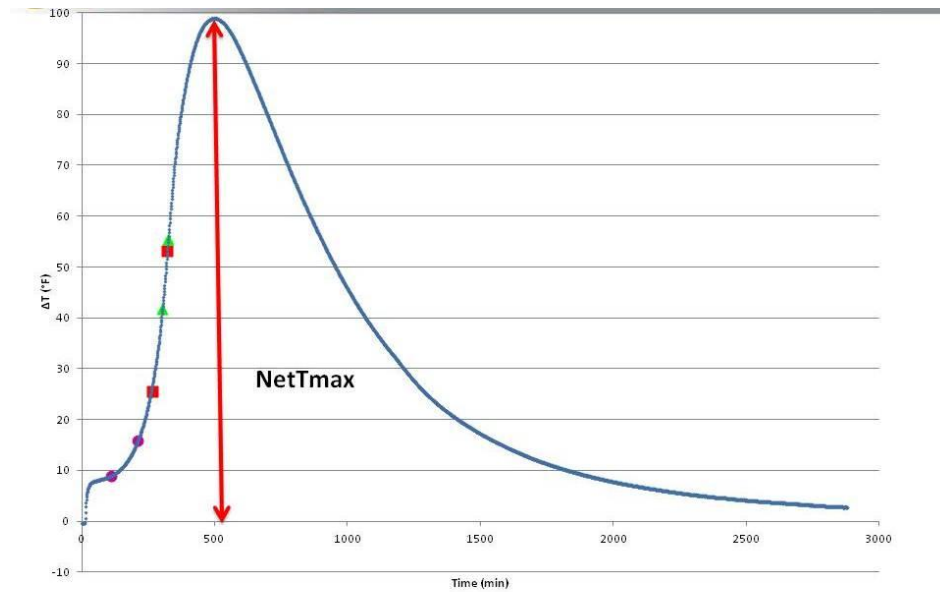
Figure 4.27 – Illustration of net peak temperature, NetTMax

A higher peak is associated with greater reactivity, especially at early ages (the reaction is typically during the first day of hydration). A correlation between NetTMax and one day compressive strength is shown in **Figure 4.28.** The correlation constant R is quite high (0.976). The data represents both the Screening Study and the Main Effects mixtures. In an earlier section, it was shown that one day compressive strengths were highly correlated to total calcium oxide, total aluminate, and total equivalent alkali contents. The same trends are in evidence for these oxides and NetTMax: total calcium oxide (R= 0.926), total aluminates (R= -0. 865), and total equivalent alkalis (R= -0.873).
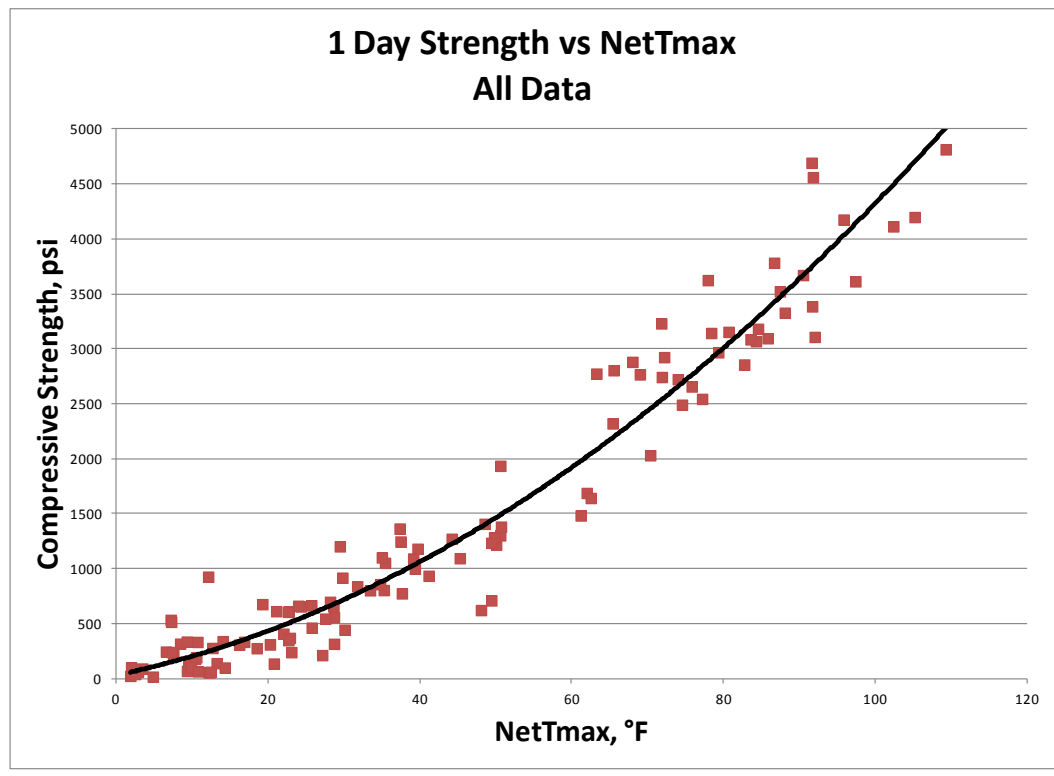
Figure 4.28 – Relationship of Calorimeter Peak Temperature NetTMax and One Day Compressive Strength

NetTMax also has a significant relationship with 28 day strength, although not as strong (R= 0.873), as shown in **Figure 4.29** (Screening and Main Effects data combined)**.**

The calorimeter results are tabulated in Appendix F.
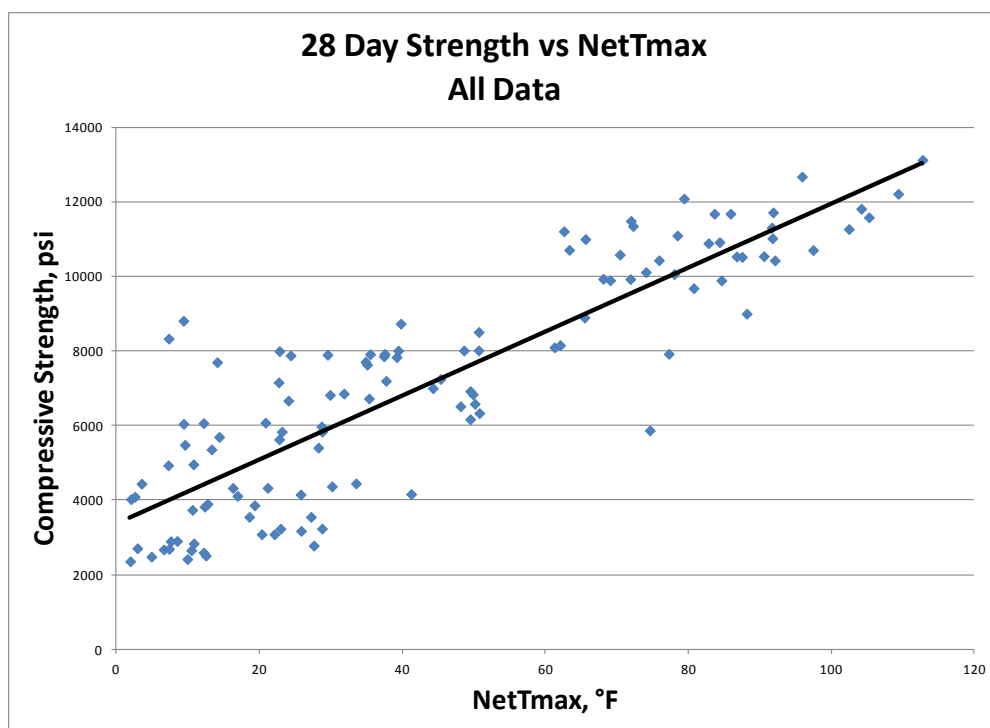
Figure 4.29 – Relationship of Calorimeter Peak Temperature NetTMax and 28 Day Compressive Strength

The calorimeter data was also examined in regard to prediction of setting time. This will be discussed in a later section.

Additionally, the calorimeter curves sometimes indicated abnormal behavior. This also will be discussed in a later section.

4.5.1.4. Miniature Slump. The miniature slump test is a measure of fluidity, and more importantly, a measure of early stiffening tendencies. The test interval spans the first 45 minutes of the life of the paste from the moment water contacts the cementitious materials through 45 minutes.

The effect on fluidity is as expected: as fly ash content increases, the mixture becomes more fluid, most likely because of the lubricating effect of the spherical nature of the fly ash particles. As shown in **Figure 4.30**, the 2 min. reading substantially

increases as the fly ash content varies from zero to 70%. The effect is also in evidence at

readings 5 and 15, but has died off between the 30 minute and the 45 min. time intervals.

The OPC line is essentially flat through the whole process, which is expected because the

cement hydration is in the usual dormant period.
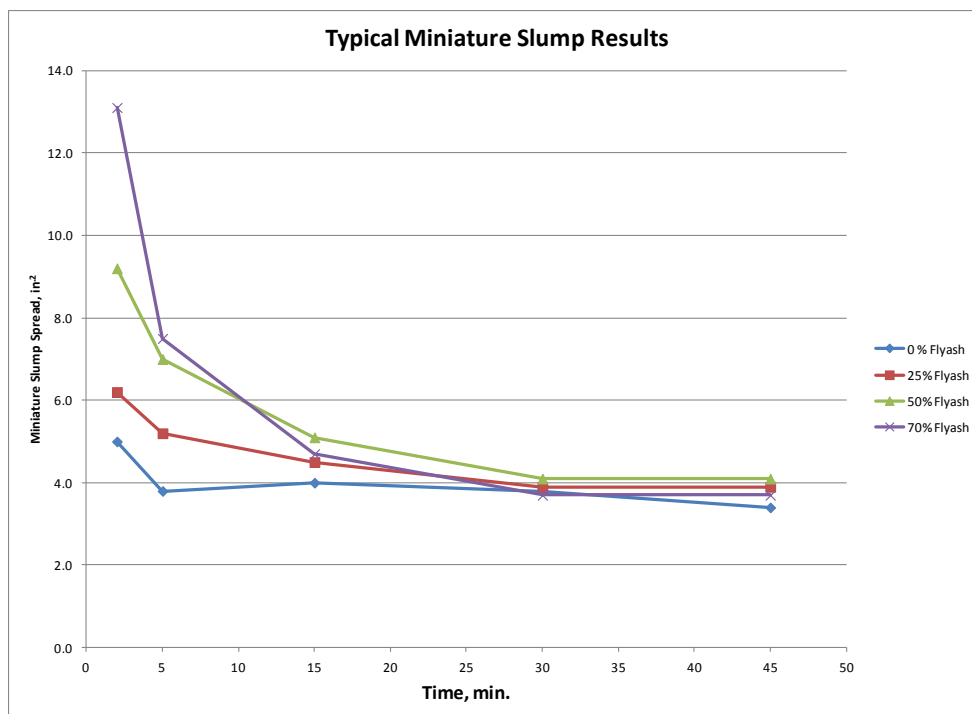
Figure 4.30 – Effect of Fly Ash Content on Miniature Slump Spread

It should be remembered that the paste was remixed immediately prior to each

reading. This action should destroy any false setting effects due to an excess of gypsum

precipitating out. In regard to the evaluation of early stiffening, several methods were

examined. One was to examine the slope of the line between the 5 and 15 minute

readings. A steeper slope would indicate a more rapid loss in slump. A second method as

reported by Roberts and Taylor (Roberts and Taylor, 2007) was to calculate the ratio of

the 30 min. spread to the 5 min. spread. As the ratio diminished, the paste would be

stiffening more rapidly. A correlation comparison with other indications of early reactivity such as initial set and 50%NetTMax time indicated that the ratio method resulted in a somewhat better correlation than the slope method. Roberts and Taylor recommend a minimum value of 0.85—below this, early stiffening is significant. However, they also warn that pastes are more sensitive to incompatibilities than concrete, so paste systems that indicate potential problems may behave normally in concrete.

In an attempt to explain the occurrence of early stiffening, correlations were performed with various total (OPC and fly ash) oxide amounts and ratios. The greatest correlations were with total equivalent alkali content (R = 0.859), shown in **Figure 4.31**, and total aluminate content (R= 0.739), which is shown in **Figure 4.32**. As total equivalent alkali content increases (greater fly ash content), more fly ash is activated, and the AR 5-30 ratio decreases, indicating an increase in stiffening. Likewise, as total aluminate content increases (because of an increase in fly ash content), the aluminate/gypsum balance is tilted toward more aluminates being free to react with water, thus causing a faster reaction.

An advantage of the miniature slump test as a diagnostic tool is its relatively quick time of obtaining results: 45 minutes as opposed to up to 10 hrs for Vicat setting time and up to three days for the calorimeter curve. Also, the equipment is simpler and the operator skill level is less demanding.

The miniature slump results are tabulated in Appendix F.
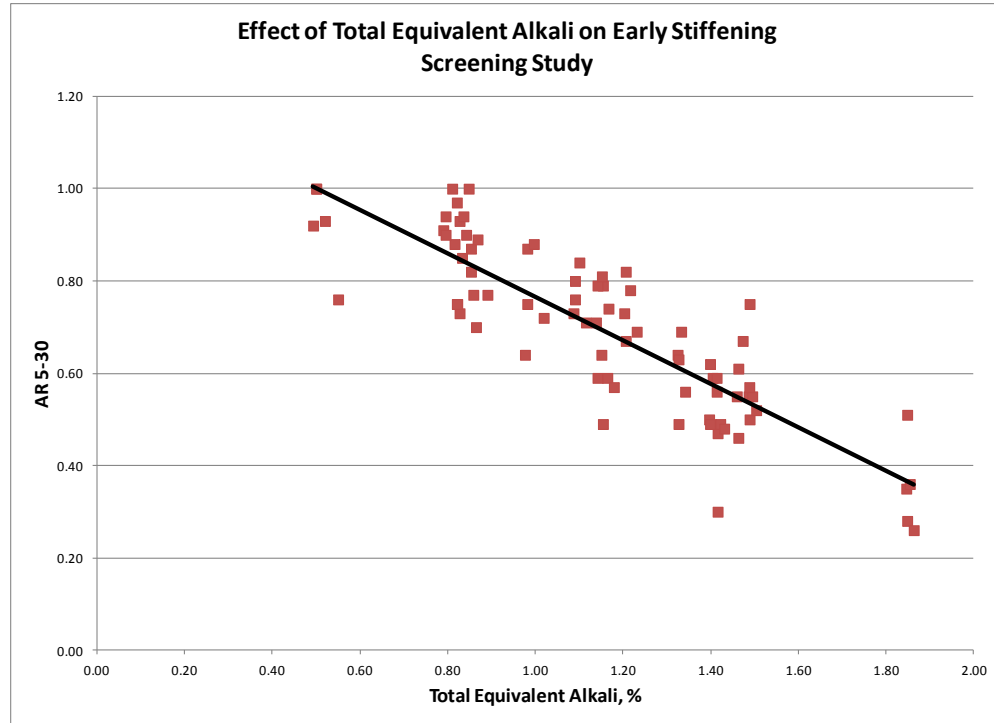
Figure 4.31 – Effect of Total Equivalent Alkali Content on Early Stiffening
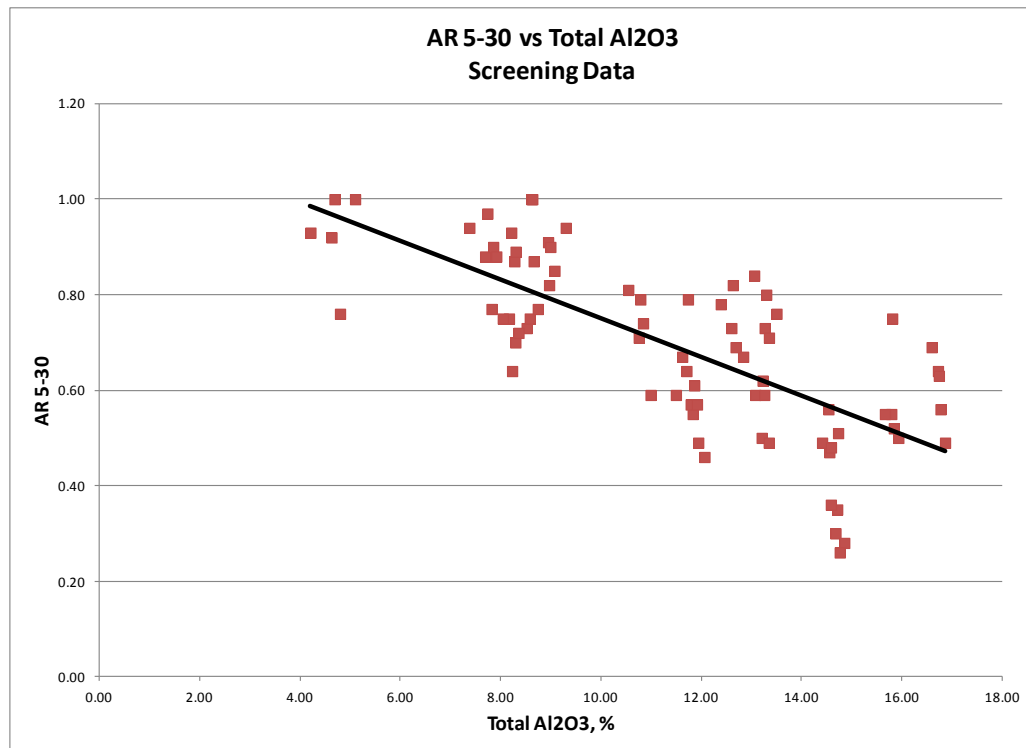
Figure 4.32 –Effect of Total Aluminate Content on Early Stiffening

4.5.1.5. Vicat Setting Time. Initial and final setting times of the pastes were determined by the Vicat method. Increasing levels of fly ash affect initial setting time. In 10 of the 25 combinations of OPC and fly ash sources (typical 1-4), there was a retarding effect at 25 and 50% fly ash levels as would be expected due to the slower reaction rates of fly ash compared to OPC. However, at 70% fly ash, there was acceleration, most likely due to the lack of gypsum and surplus of aluminate, causing a faster reaction. In nine of the combinations (typical 1-2), there was the expected retarding effect at 25% fly ash, but at 50 and 70%, there was an acceleration effect. In six combinations (typical 2-4), all levels of fly ash exhibited an accelerating effect. All three typical curve shapes are shown in **Figure 4.33**.
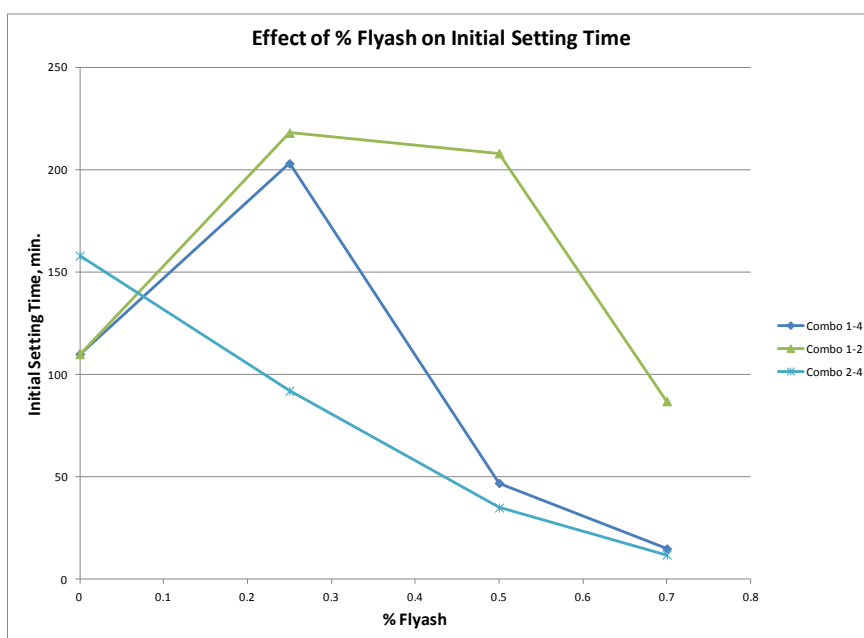
Figure 4.33 – Effect of Fly Ash level on Initial Setting Time

Although there were many OPC-fly ash blends that violated the recommended minimum initial setting time for straight OPC's of 45 min., there were only five blends

that exceeded the final setting time maximum limit of 8 hrs (480 min.). Four were at the

50% fly ash level and one was at 70%. The setting time results are tabulated in Appendix

F.

The performance of the Vicat setting time test is lengthy and subjective. It has

been postulated that setting time characteristics could be approximated by certain time

intervals associated with the calorimeter curve such as at inflection points (second and

first derivatives) and more arbitrarily at the 20 and 50% time intervals associated with the

time that the peak temperature occurs, as shown in **Figure 4.34.**
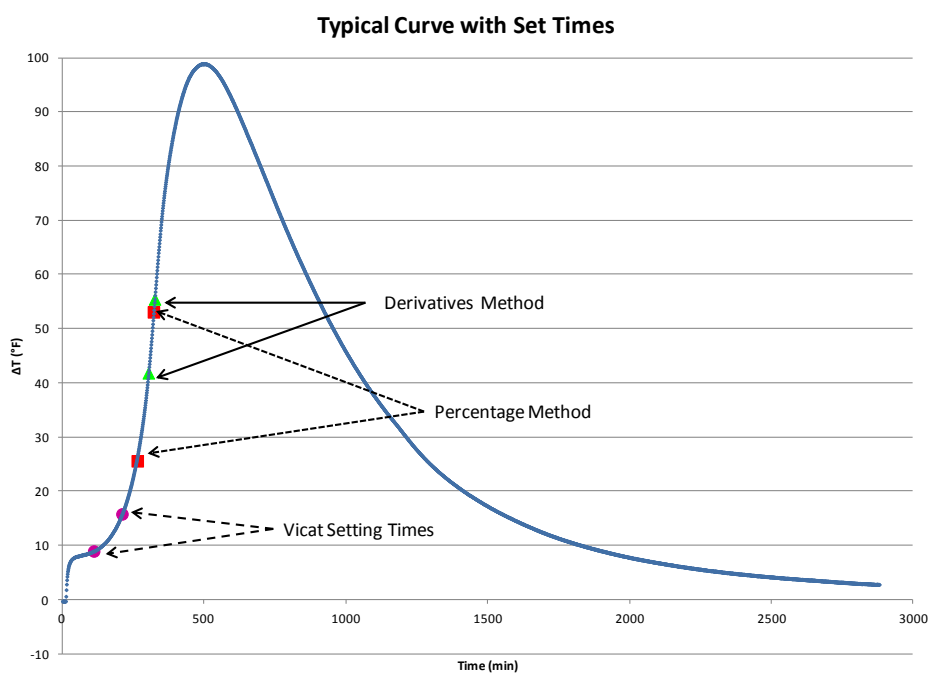
Figure 4.34 – Various Methods to Determine Setting Times

Initial set time and the following parameters had poor correlations: second

derivative, first derivative, 20% NetTMax, and 50% NetTMax. However, initial set time

and AR 5-30 had a fairly good correlation (0.781), as shown in **Figure 4.35.**
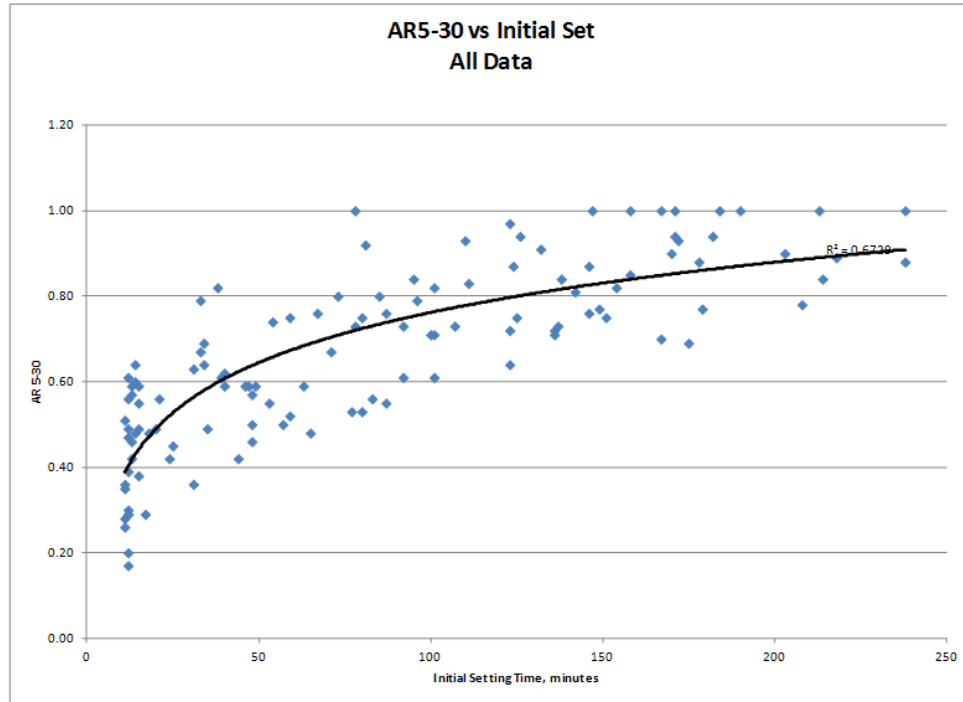
Figure 4.35 – Relationship of Early Stiffening and Initial Setting Time

Calorimeter curve characteristics, coupled with strength development, early stiffening, and setting time data, were examined in order to attempt to explain paste hydration behavior, especially potential incompatibilities among paste constituents. Seven different curve types were identified in this study and are shown in **Figures 4.36-4.42**. As explained earlier, the blend specimen temperature has been corrected for the inert specimen temperature.
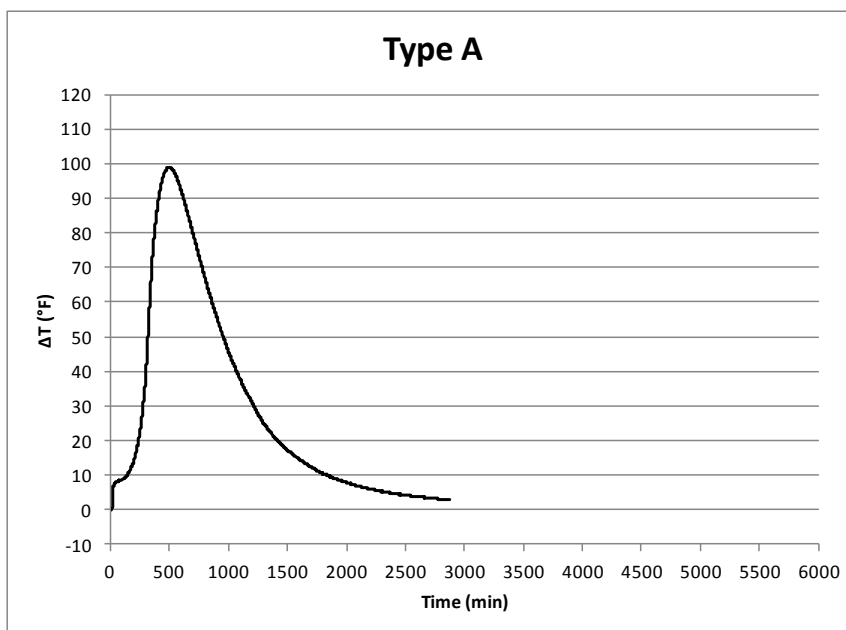
Figure 4.36 – Normally-shaped Type A Calorimeter Curve

The Type A curve is characterized by having a normal dormant period followed by a single tall hydration peak occurring at an average of 475 min. (OPC), 720 min. (25% fly ash), and 820 min. (50% fly ash), with no plateaus or shoulders. When water and cement come into contact, the aluminates go into solution rapidly, followed by the sulfate. The presence of the sulfate lowers the solubility of the aluminates, plus ettringite forms around the particles, both actions slowing hydration of the aluminate. A dormant period ensues until the pore solution is critically saturated with calcium ions, thus causing the silicates to react rapidly, releasing heat with a consequent rise in temperature and gain in strength. Type A curves had the greatest strengths, greatest CaO contents, lowest total equivalent alkalis, lowest total aluminates, and lowest total aluminate/total sulfate ratios. Type A curves were always exhibited by OPC and 25% fly ash mixtures, along with some of the 50% fly ash mixtures. Early stiffening was either not a problem or only

marginal (average AR 5-30 = 0.82). The silicate hydration and the aluminate reaction
(sulfate depletion) probably occurred relatively simultaneously.

Type B curves, shown in **Figure 4.37**, exhibited smaller magnitude in peak
heights and longer times-to-peak heights. The very short peak height curves were from
both 50% and 70% fly ash mixtures, with peak heights occurring later than Type A
curves, and times of around 860 min. Type B curves exhibited lower CaO contents,
greater total equivalent alkalis, greater total aluminates, and greater total aluminate/total
sulfate ratios than Types A, C, and D mixtures. B curves generally occurred sooner than
C and D curves (all 50% fly ash). The lower magnitude heights and delayed times were
to be expected from higher fly ash contents due to slower reactions and less calcium ions
available for reacting with the silicates producing calcium silicate hydrates. Early
stiffening (AR5-30= 0.60) was an issue.
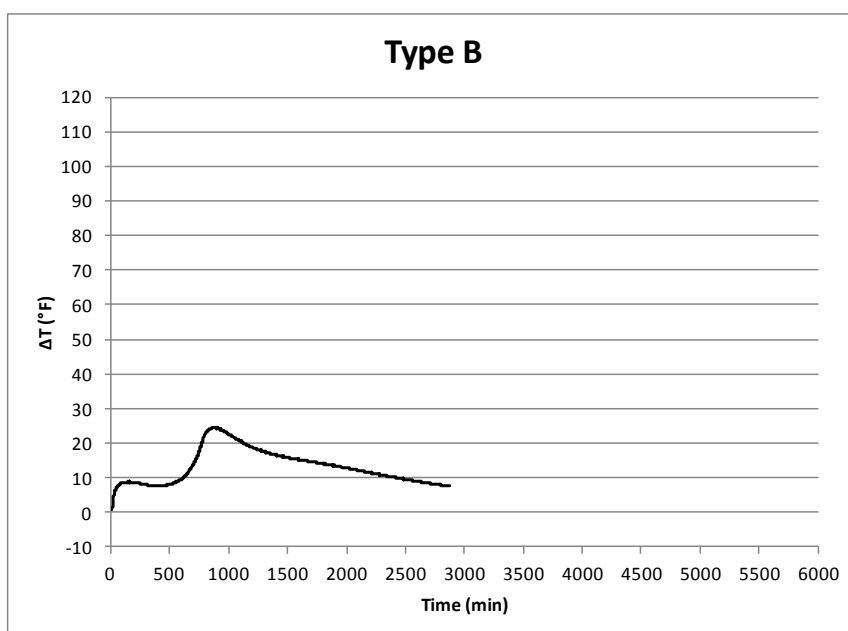
Figure 4.37 – Normally-shaped, Lower Magnitude Type B Calorimeter Curve

Type C curves were always associated with 50% fly ash mixtures and typically

had somewhat greater peak heights and were broader in nature than Type B curves,

which was to be expected (e.g. peak heights between Types A and B). However, peak

times occurred later than Type B's. Type C is shown in **Figure 4.38.** Compared to Type

A curves, C curve mixtures had less CaO, greater equivalent alkali and aluminate

contents, and greater aluminate/sulfate ratios. Early stiffening was either not a problem or

only marginal (average AR 5-30 = 0.80).
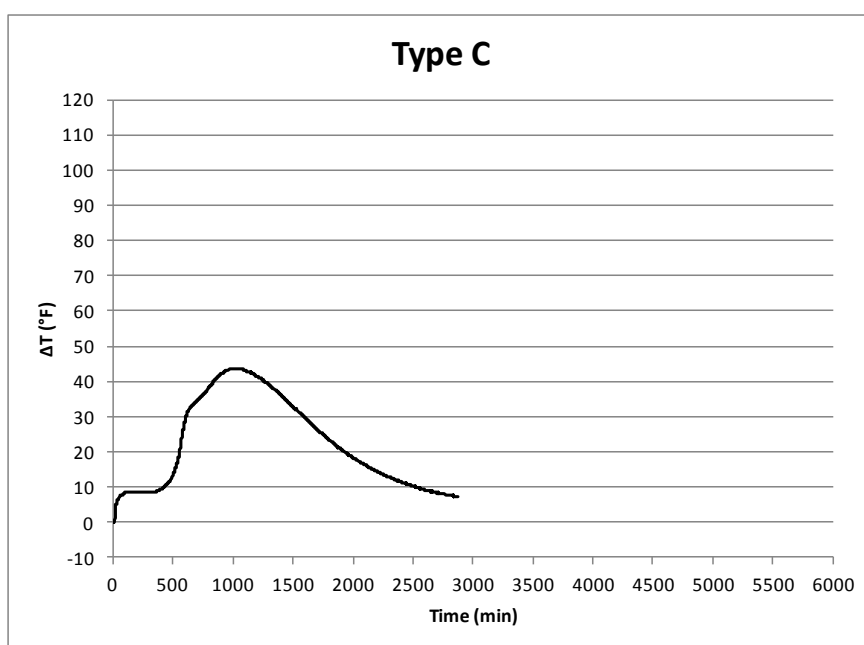
Figure 4.38 – Normally-shaped, Lower Magnitude, Broader Type C Calorimeter Curve

Type D curves (**Figure 4.39**) were always from 50% fly ash mixtures, but

involved a double peak. The second peak, thought to be the silicate reaction, was taller

than the first (aluminate reaction), and occurred after the first peak. The first peak

occurred around 625 min. on the average, (sometimes called a "delayed" aluminate peak,

meaning delayed from the normal position of being very early in the reaction) (Cost and

Knight, 2007) while the second peak was at about 1700 min. The second peak usually

occurred much later than Types A, B, and C curves, and was lower in magnitude than A

and C curves. Type D curve mixtures had moderate CaO contents, moderate equivalent

alkali contents, and moderate aluminate/sulfate ratios, but high aluminate contents. Early

stiffening (AR5-30= 0.62) was an issue.
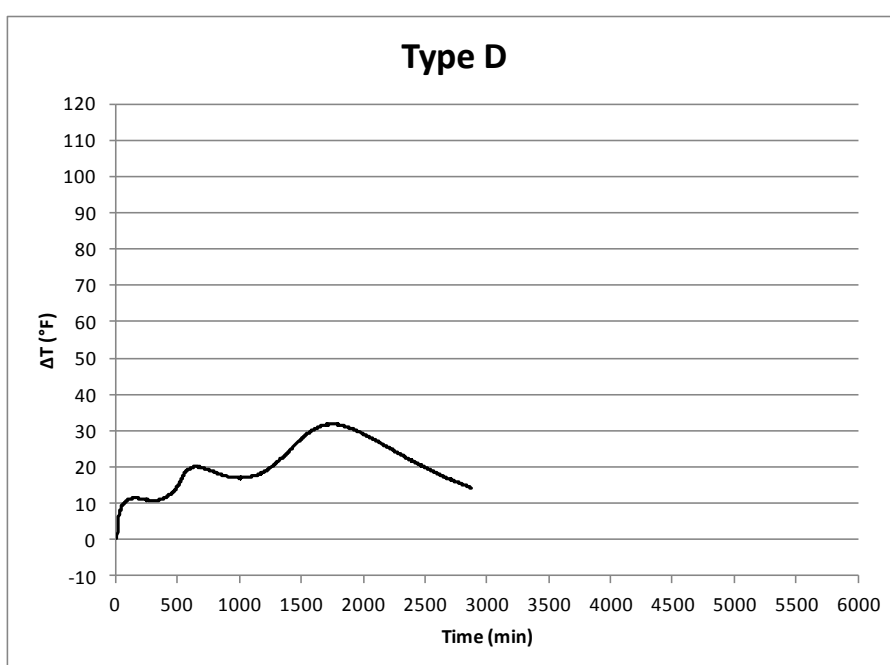
Figure 4.39 – Double Peak, Delayed Second Peak Type D Curve.

Type E curves (**Figure 4.40**) were of fairly low peak height magnitude but quite

broad in nature, or were a combination of two consecutive peaks but of equal height,

resulting in a long time of occurrence. Type E curves resulted from 70% fly ash mixtures.

The curves were accelerated compared to curves A through D. E curve mixtures were

low in CaO, and high in equivalent alkali, aluminate, and aluminate/sulfate. Early

stiffening (AR5-30= 0.47) was more of an issue than A through D and as bad as Types F

and G.
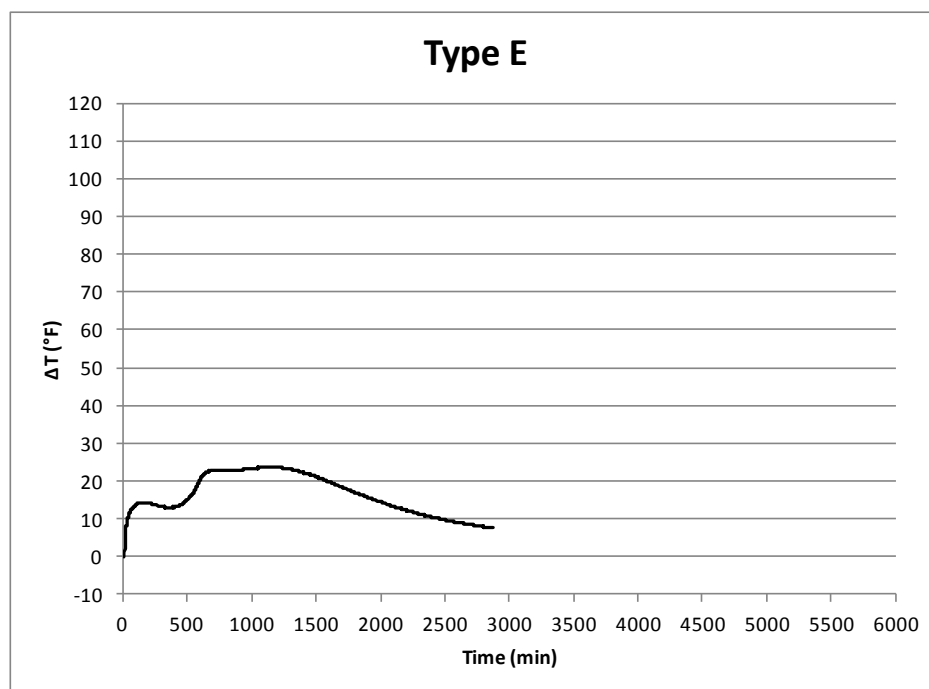
Figure 4.40 – Type E Curve Exhibiting Delayed, Broad or Equal Double Peaks

Type F curves (**Figure 4.41**) were drastically different than Types A through E in

that they developed very short magnitude peak heights (thought to be "delayed" initial

aluminate reactions) occurring at an average of 245 min., with no silicate peak. All Type

F curves were from 70% fly ash mixtures. F mixtures had the lowest one day strengths,

low CaO contents, and were high in total equivalent alkali, aluminate, and

aluminate/sulfate. Calcium ions are necessary for forming the main strength-producing

hydration product, calcium silicate hydrate (C-S-H). High aluminate content systems

react rapidly with calcium, thus reducing the calcium available to the silicate hydration

reaction, lowering strengths. Likewise, high total equivalent alkalis increase the rate of

reaction between the aluminates and the calcium. Apparently, the system was so low in available calcium ions after the initial aluminate reaction that the silicate reaction could not happen. Early stiffening (AR5-30= 0.49) was more of an issue than A through D mixtures.
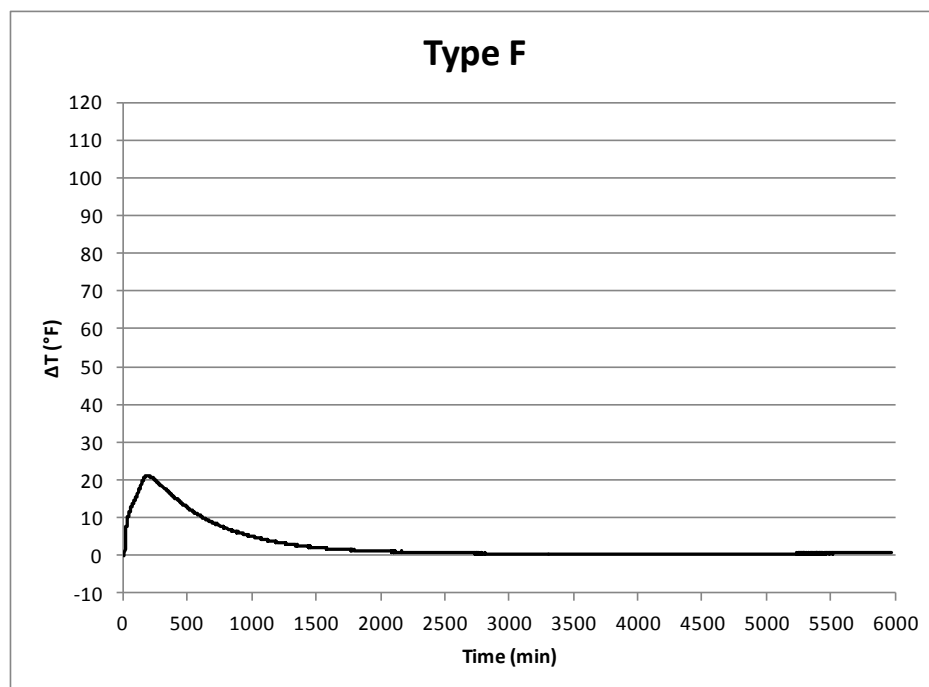
Figure 4.41 – Type F Curve Exhibiting Accelerated Time to Peak Height

Finally, Type G Curves (**Figure 4.42**) were similar to Type F curves with a first peak (average 370 min.), thought to be the "delayed" initial aluminate reaction, but with a very delayed second peak (average around 4020 min.), and thought to be the silicate reaction. Some of the mixtures labeled Type F may have been actually Type G, but early in the study the time in the calorimeter was prematurely terminated, thus missing a potential second curve. All Type G curves were from 70% fly ash mixtures.

An overlay plot of all seven typical curve types is shown in **Figure 4.43**.
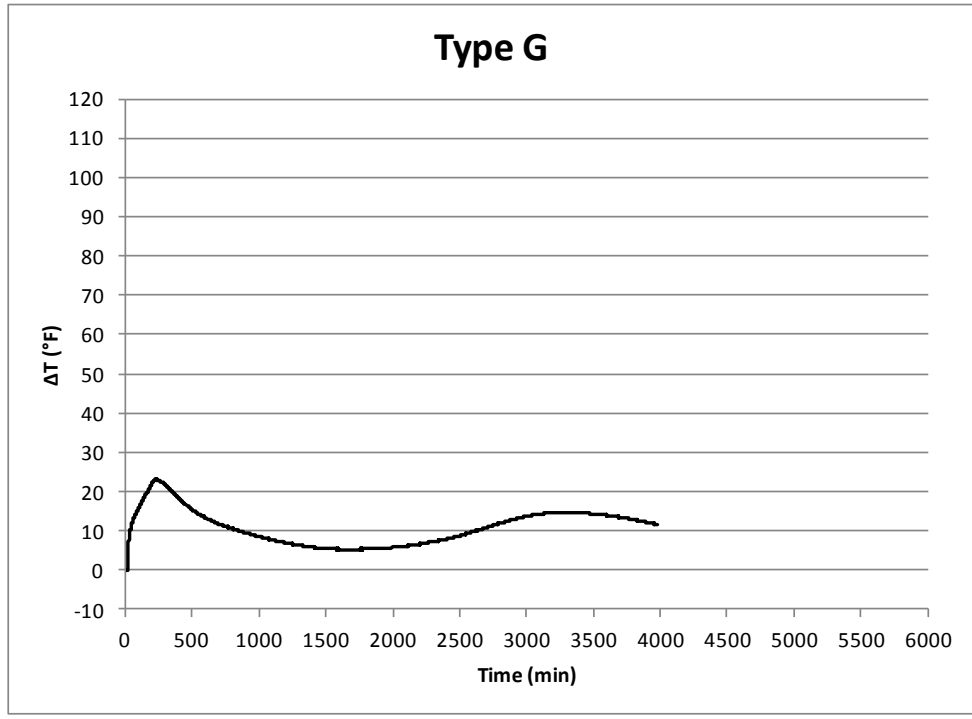
Figure 4.42 – Type G Curve Exhibiting Accelerated Time to Peak Height with Delayed Second Peak.
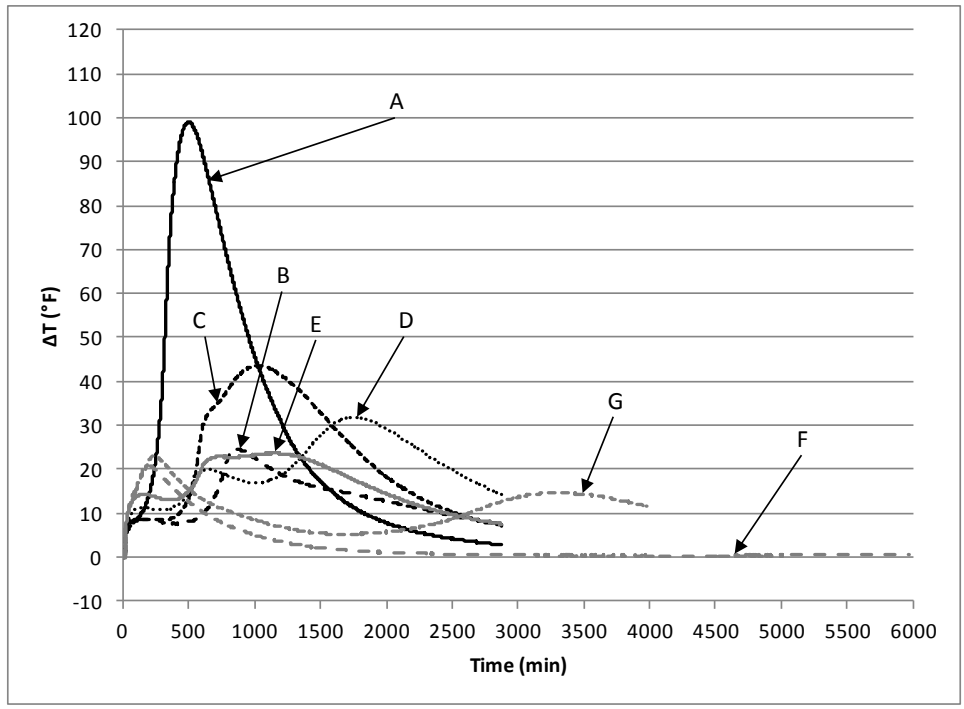
Figure 4.43 – All curve types (typical)

Thus, Types A, B, and C curves exhibited the expected peak height shortening and delay as expected from increased fly ash contents. Types F and G curves showed an unusual acceleration of the peak (along with the expected short peak heights) from some 70% fly ash mixtures. Early stiffening and flash setting were characteristics of these two curve types, indicating a possible incompatibility between the particular cement and the fly ash at the proportions in the mixture. The D and E types were unusual in that they too exhibited early stiffening and flash setting but had delayed silicate reaction curve occurrence times. All Screening Study mixture calorimetry curves are in Appendix D.

4.5.2 Main Effects Study

4.5.2.1. Mixture Designs. Once the least and most reactive combinations of cement plus fly ash were determined, the Main Effects portion of the paste study began, using combinations 4-1 and 1-3. In order, WR/HRWR dosage, gypsum content, and finally lime or RSC contents were explored, all at zero, 50% and 70% fly ash replacement levels. As in the Screening Study, the *w/cm* and total cementitious materials content was kept constant.

First, WR/HRWR dosage was chosen. As previously mentioned, recognizing that mixtures of the relatively low *w/cm* would encounter workability issues for the straight OPC mixtures, it was decided to use a water reducer (WR). Although a traditional Type A may have been less problematic, a WR was chosen that was advertised as being able to function as both an A and as an F high range water reducer (HRWR). Because it has been shown that WR will affect setting time (usually retard), and may cause early stiffening because of an interaction with a particular sources of cement and fly ash, it was decided to explore the effect of several levels of WR. Three dosage levels were selected: zero,

low, and high. "Low" was defined as the dosage necessary to achieve the required design slump of the concrete control mix. The "high" level was selected at an arbitrarily greater value compared to the low dosage. In an on-going parallel HVFA study, some work with concrete mixtures had been completed. From that, WR dosage between 2 and 3 fl oz/cwt was necessary to achieve a 5 in. slump. Thus, the WR dosage was selected as 2.75 fl oz/cwt.

Next, gypsum level was selected, based on previous studies by Bentz (2010), who used 2% gypsum by TCM mass. In the present study, for most mixtures, 4% by mass of fly ash was used. This translates into a range of 1.91 to 2.63% by TCM mass for the mixtures in this study, as shown earlier in **Table 4.1**. Additionally, the effect of 4% gypsum was compared to 2% (both by mass of fly ash).

Lime content was chosen in a similar manner. Bentz used 5 % lime by TCM mass. In the present study, 10% lime by weight of fly ash (4.67-6.54% by TCM mass) was studied. Additionally, the effect of 10% lime was compared to five %, both by mass of fly ash (5% ~2.39-3.38% by TCM mass).

Finally, RSC content was chosen. Bentz used 10% RSC by TCM mass. In the present study, 20% RSC by weight of fly ash (8.93-12.28% by TCM mass) was studied. Additionally, the effect of 20% RSC was compared to 10%, both by mass of fly ash (10% ~4.67-6.54% by TCM mass).

As stated earlier, at the low level of WR and at 4 % gypsum, the level of lime (5 and 10 %) and RSC (10 and 20%) was varied for fly ash levels of zero, 50, and 70%.This partial factorial experimental design resulted in 48 mixtures. An additional 16 mixture experiment with no gypsum was also conducted (eight with lime, eight with RSC at 50

and 70% fly ash). The test methods were the same as in the screening study: miniature slump, Vicat setting time, calorimetry, and compressive strength. However, the compressive strength testing was expanded to include more ages: 1, 3, 7, 28, and 56 days. From all this, 10 concrete mixtures were selected for Phase II with the optimum WR/HRWR, gypsum, lime, and RSC levels at zero, 50, and 70% fly ash levels.

4.5.2.2. Effect of Fly Ash. The effect of increasing fly ash content was evaluated in terms of calorimeter curve peak height and time, miniature slump early stiffening, early and later compressive strengths, and setting time.

As expected, strength at early ages was decreased as fly ash content increased. In most cases, strength of the fly ash mixtures were not fully equivalent to OPC mixtures as late as 56 days. This is shown in **Figures 4.44** and **4.45**. The effect of WR/HRWR is also shown: at up to seven days, WR has little effect, but at later ages, strength is increased somewhat. It should be noted that for combination 1-3 at 70% fly ash, strengths at ages up to 7 days was very low, indicating little activity.
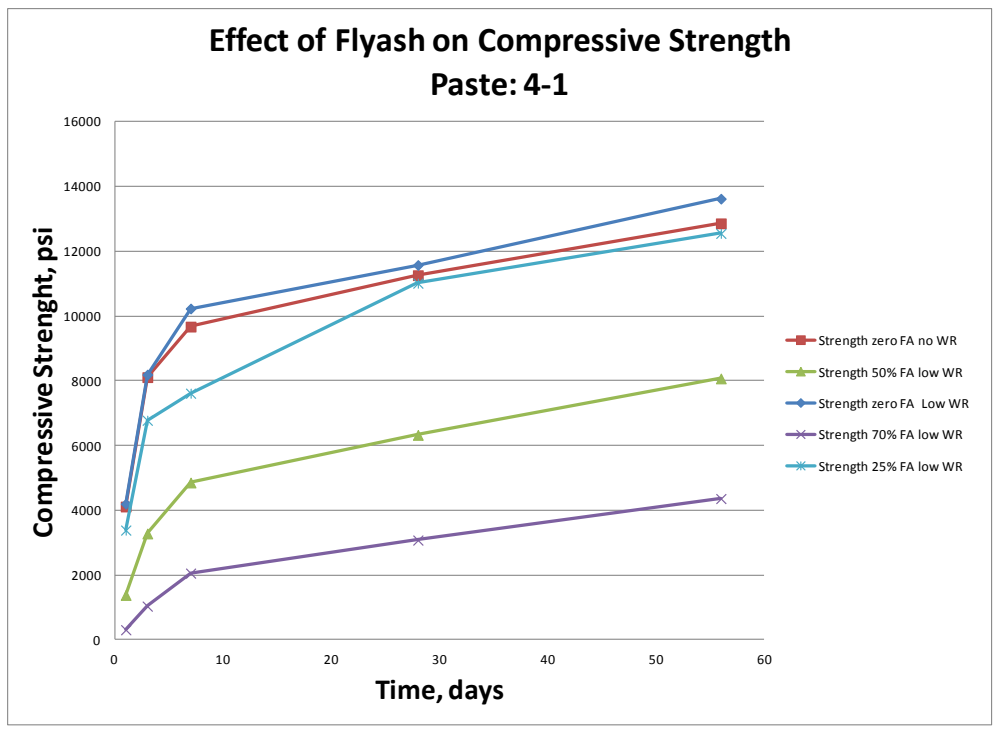
Figure 4.44 – Effect of Fly Ash Content and WR/HRWR on Compressive Strength, Combination 4-1
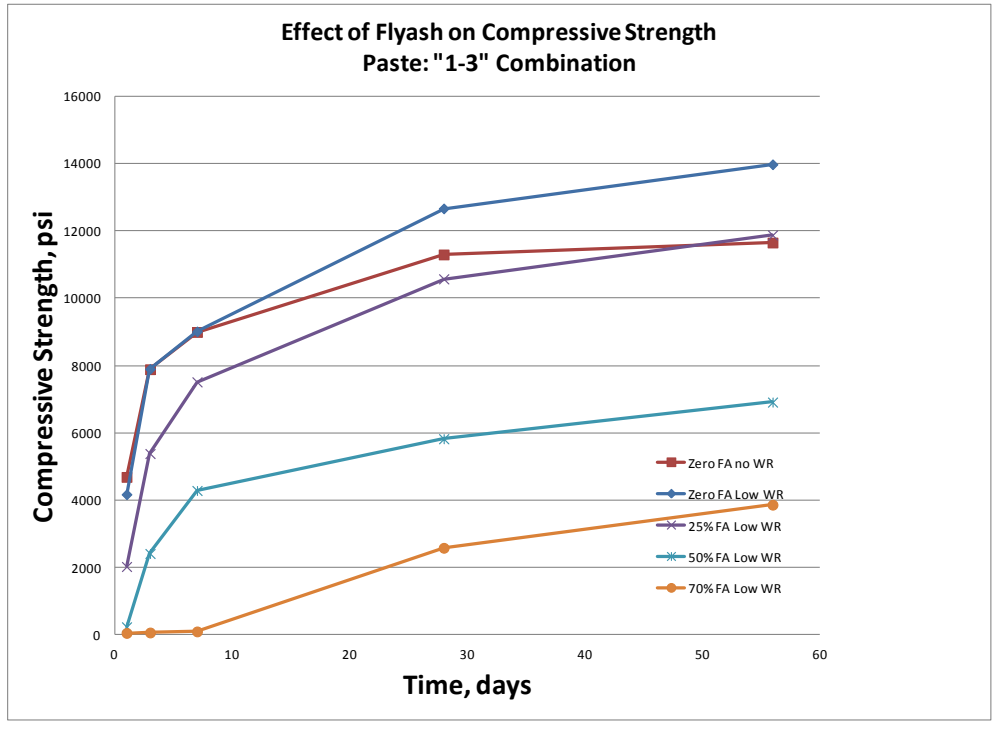
Figure 4.45 – Effect of Fly Ash Content and WR/HRWR on Compressive Strength, Combination 1-3

The effect of fly ash content and presence of WR/HRWR on reaction time as represented by the 50% NetTMax time of occurrence is shown in **Figure 4.46**. The admixture served to retard the curve position. In the case of the 4-1 combination, increasing fly ash content increasingly retarded the reaction. As for the 1-3 combination, 25% and 50% retarded increasingly. However, the 70% replacement level, the reaction was greatly accelerated, as seen in the Screening Study, indicating some kind of incompatibility.
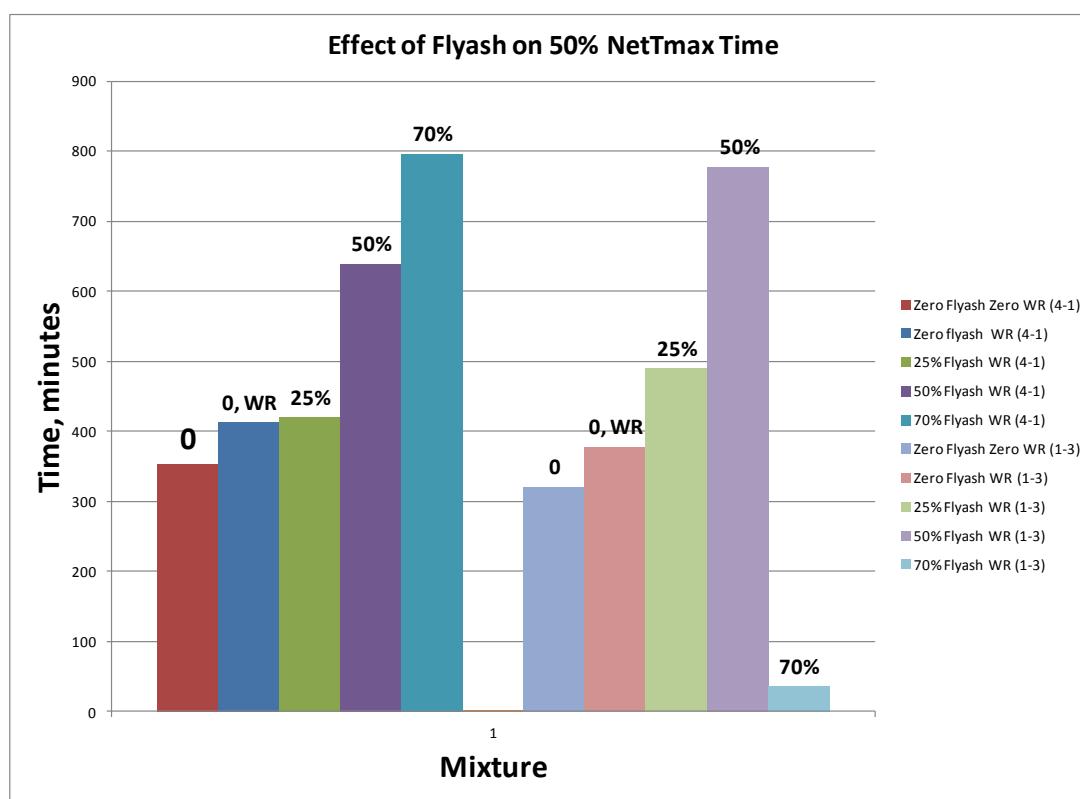
Figure 4.46 – Effect of Fly Ash Content and WR/HRWR on 50%NetTMax Time for Zero, 25, 50 and 70% Fly Ash Mixtures

The effect of fly ash on setting time is shown in **Figure 4.47.** For both cementitious combinations, 25% fly ash mixtures were retarded. For the 4-1 mixture, the

50% fly ash mixture also was retarded, but the 1-3 combination was accelerated. The 70% fly ash level accelerated setting time for both combinations, and was below the 45 min. threshold.

Only one mixture exceeded the ASTM C150 final setting time maximum limit of 480 min.: the 1-3 70% fly ash (525 min.).
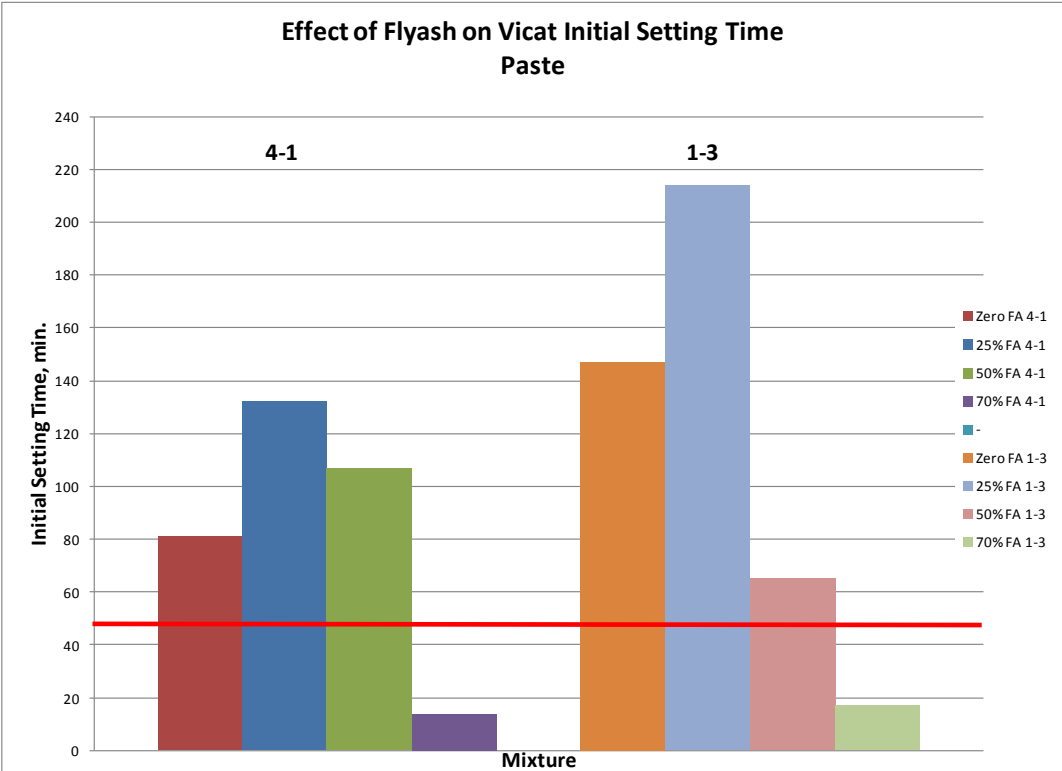
Figure 4.47 – Effect of Fly Ash Content on Initial Setting Time for Zero, 25, 50, and 70% Fly Ash Contents

The effect of fly ash on early stiffening is shown in **Figure 4.48.** Although increasing fly ash content increases fluidity (not shown), the fly ash causes an increase in early stiffening tendencies. The zero and 25% fly ash mixtures do not, but the 50% and especially the 70% fly ash mixtures fall below the threshold of 0.85.
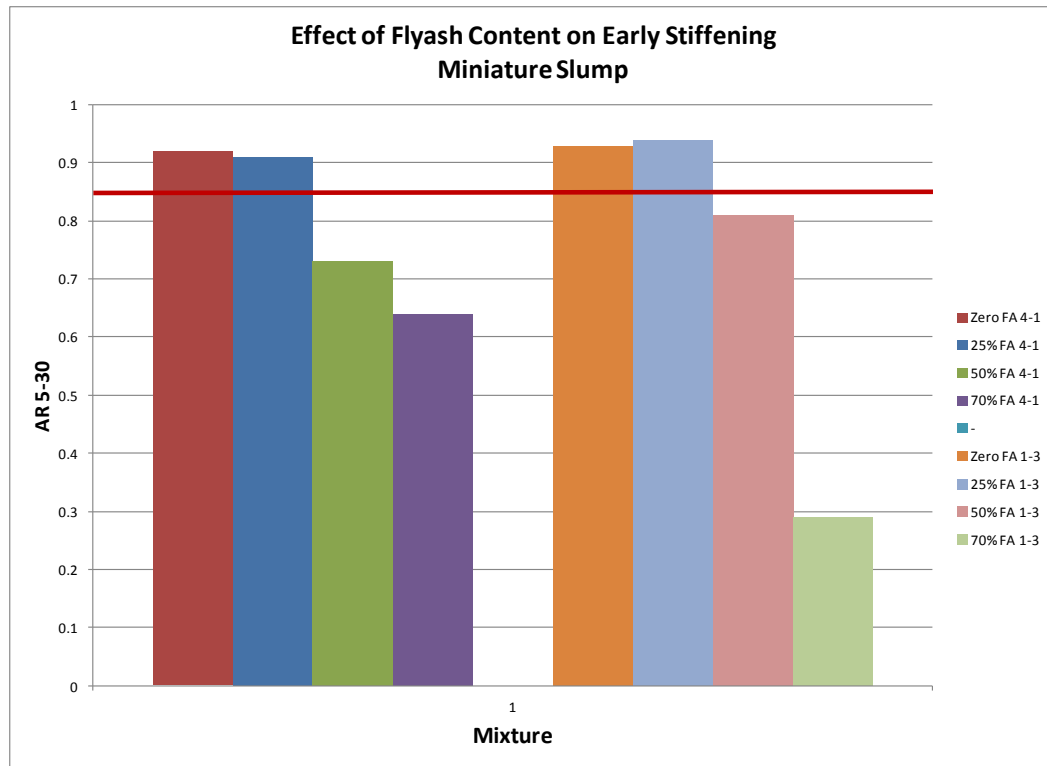
Figure 4.48 – Effect of Fly Ash Content on Early Stiffening for Zero, 25, 50 and 70% Fly Ash Mixtures

4.5.2.3. Effect of WR/HRWR. The effect of the WR/HRWR on compressive strength and 50% NetTMax time has been presented.

In **Figure 4.49** is shown a typical set of calorimeter curves with zero, low, and high dosages superimposed. In all cases, increasing dosage of WR/HRWR retarded the curves. All Main Effect study curves are in Appendix G.
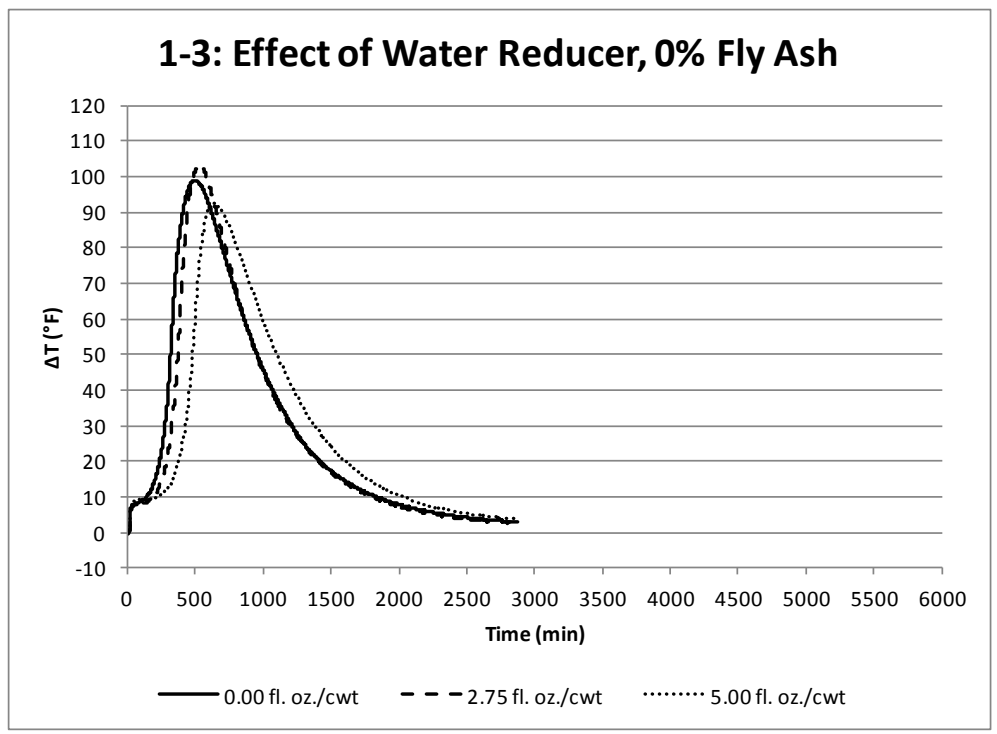
Figure 4.49 – Typical Effect of WR/HRWR Dosages on Calorimeter Curve Characteristics

The effect on initial setting time of zero and 50% fly ash mixtures is shown in

Figure 4.50. For the 100% OPC mixtures, the WR/HRWR retarded initial setting time

significantly. For the 50% fly ash mixtures, the effect was mixed. For the 4-1

combination, the low dosage (2.75 fl oz/cwt) retarded while the high dosage (5.0 fl

oz/cwt) accelerated. For the 1-3 combination, both dosages accelerated.
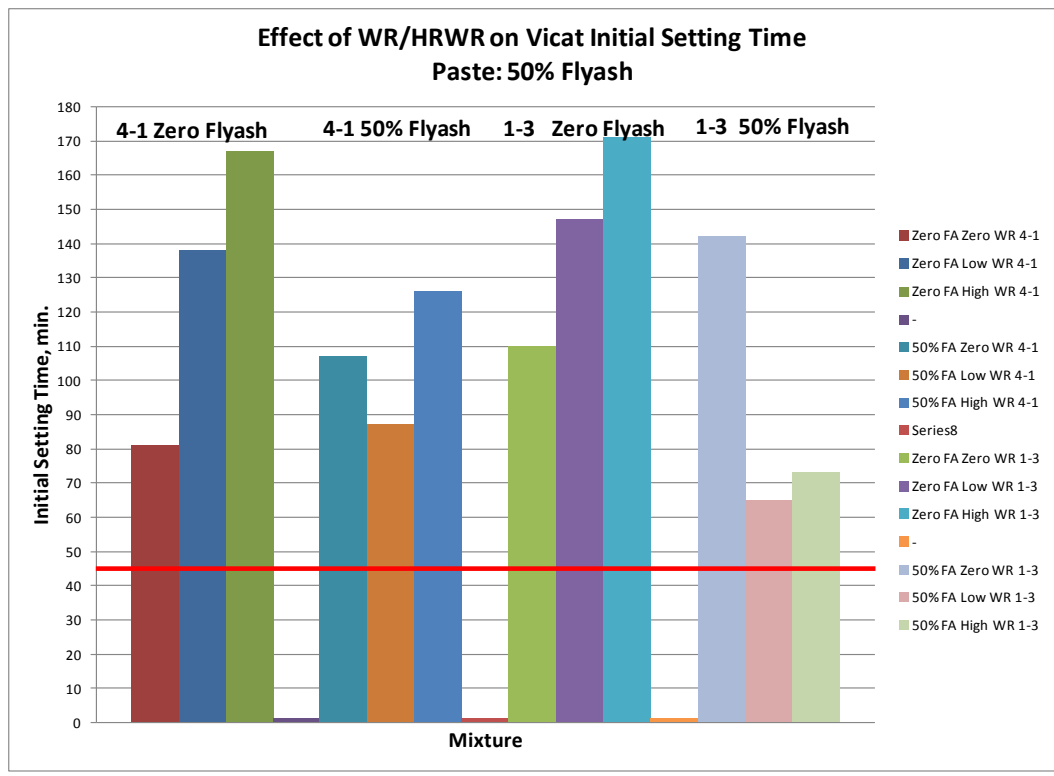
Figure 4.50 – Effect of WR/HRWR on Initial Setting Time, 50% Fly Ash Mixtures

The effect of WR/HRWR had opposite effects on the 70% fly ash mixtures, depending on combination of cementitious materials. The 4-1 combination shows retardation, while the 1-3 mixtures were accelerated, shown in **Figure 4.51**. Most mixtures set too quickly to meet the 45 min. minimum.
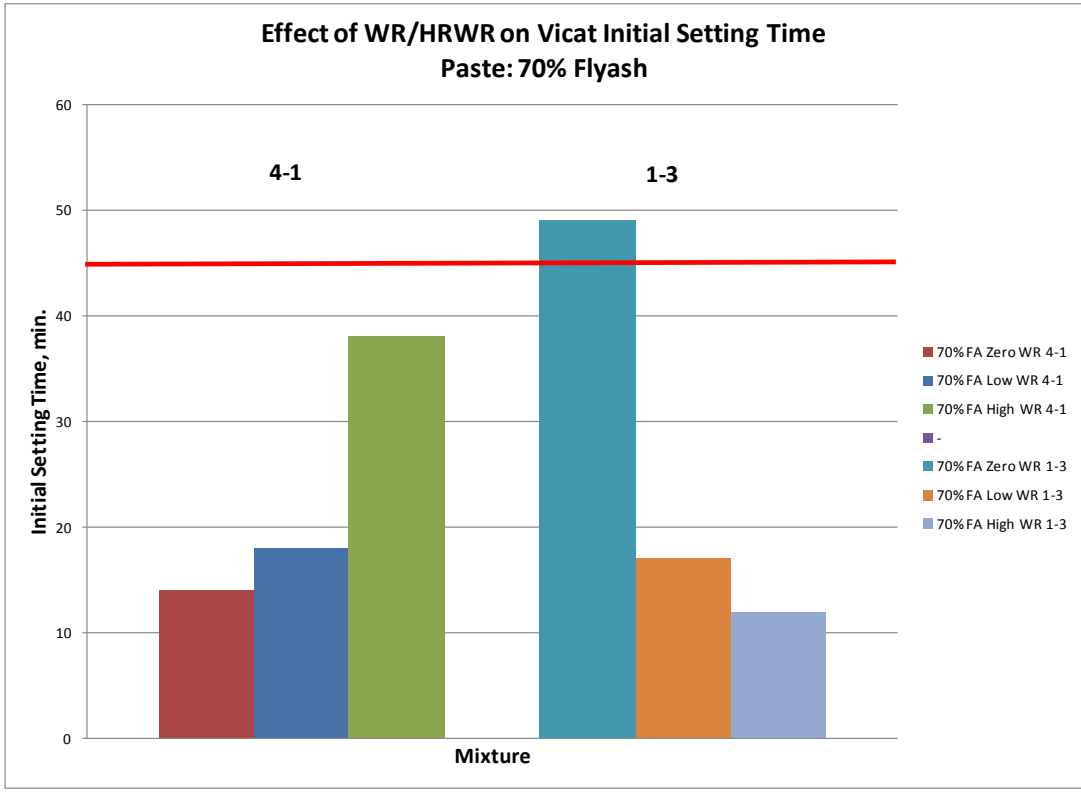
Figure 4.51 – Effect of WR/HRWR on Initial Setting Time, 70% Fly Ash Mixtures

The effect of WR/HRWR on early stiffening for combination 4-1 is shown in **Figure 4.52.** In general, the low dosage increased early stiffening tendencies while the high dosage did the opposite. The worst situation was 70% fly ash with the low WR/HRWR dosage. For the 1-3 combination (**Figure 4.53**), the low dosage generally made early stiffening worse. The high dosage alleviated or worsened the stiffening, depending on fly ash content.
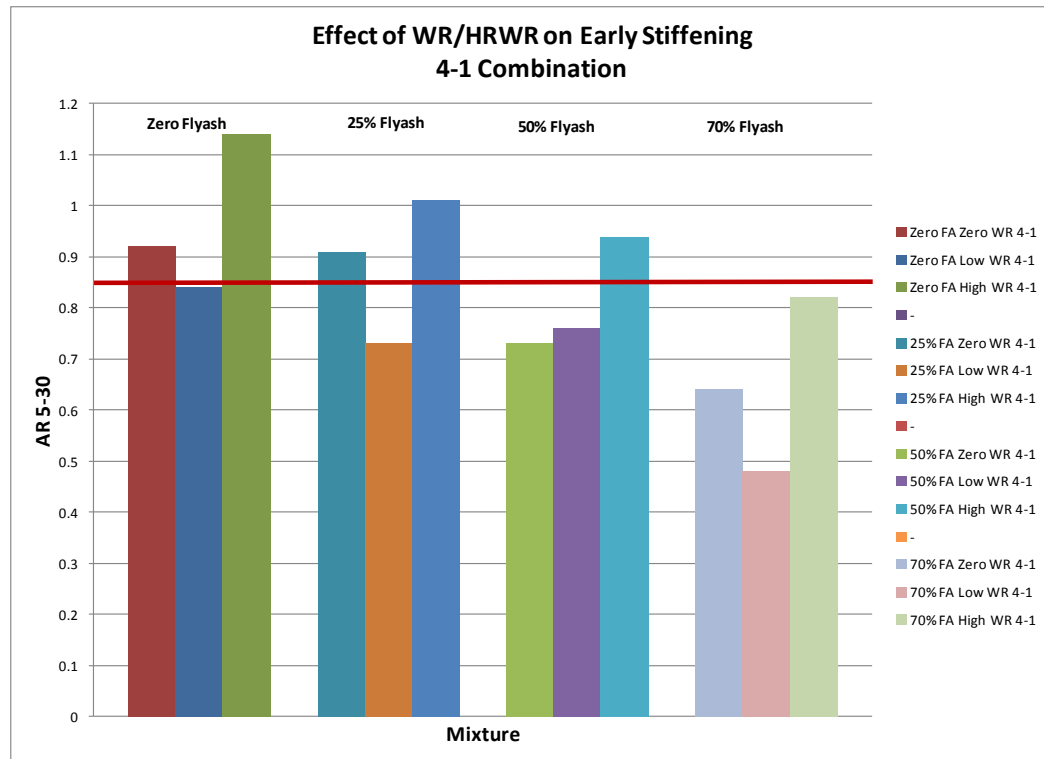
Figure 4.52 – Effect of WR/HRWR and Fly Ash Content on Early Stiffening for Zero, 25, 50 and 70% Fly Ash Mixtures (4-1 Combination)

Only three mixtures exceeded the ASTM C150 final setting time maximum limit of 480 min.: the 1-3 25% fly ash low WR (510 min.), the 1-3 25% fly ash high WR (555 min.), and the 1-3 50% fly ash high WR (510 min.).
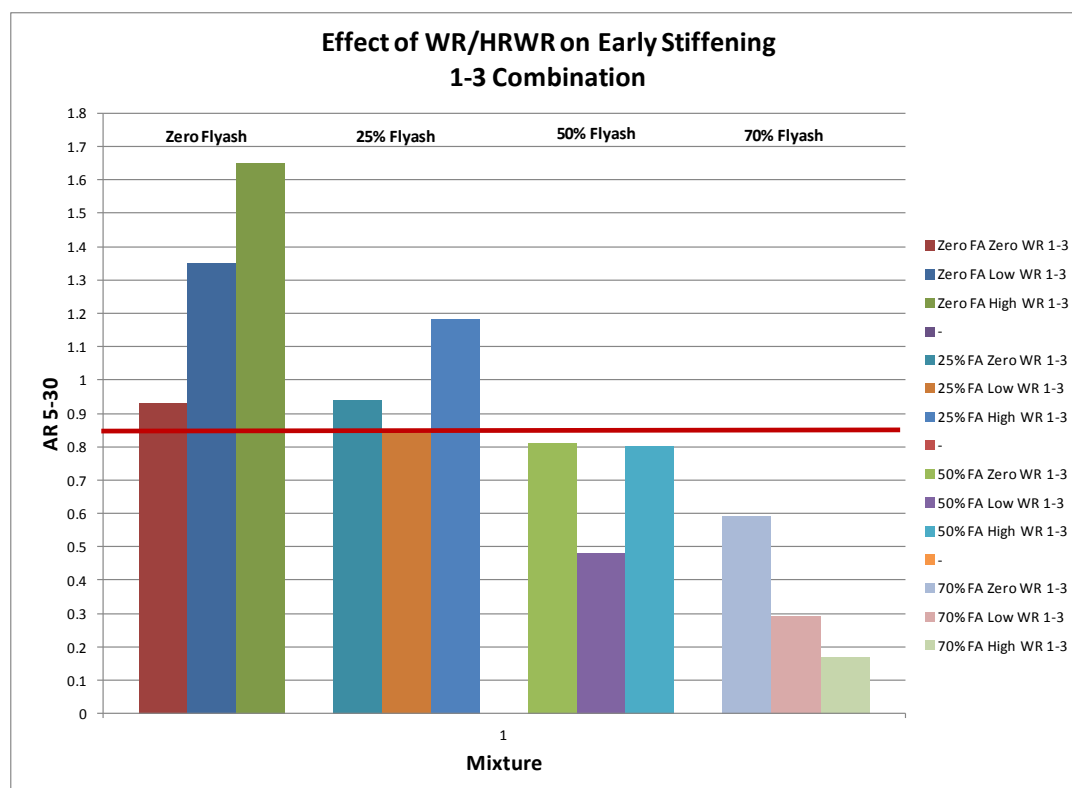
Figure 4.53 – Effect of WR/HRWR and Fly Ash Content on Early Stiffening for Zero, 25, 50 and 70% Fly Ash Mixtures (1-3 Combination)

All subsequent mixtures involving the effects of gypsum, lime, and RSC contained the low dosage (2.75 fl oz/cwt) of WR/HRWR because that is what the preliminary testing indicated would be the dosage for the concrete mixtures.

4.5.2.4. Effect of Gypsum. Initially, two levels of gypsum (2 and 4% by mass of fly ash) were examined at zero, 50, and 70% fly ash. The effect on reaction curve position is indicated by the effect on 50%NetTMax time, as shown in **Figure 4.54,** for the 50% fly ash content mixtures. As can be seen, for the 4-1 combination of OPC and fly ash, gypsum retarded the reaction and the effect increased with increasing gypsum content. For the 1-3 combination, the effect of gypsum accelerated the curve; however, the 2% content accelerated the reaction more than the 4% content. Also shown is the

50%NetTMax time for the zero fly ash mixtures. **Figure 4.55** shows the calorimeter curves for the 4-1 blend. As gypsum level increases, the curves shift increasingly rightward (delayed).
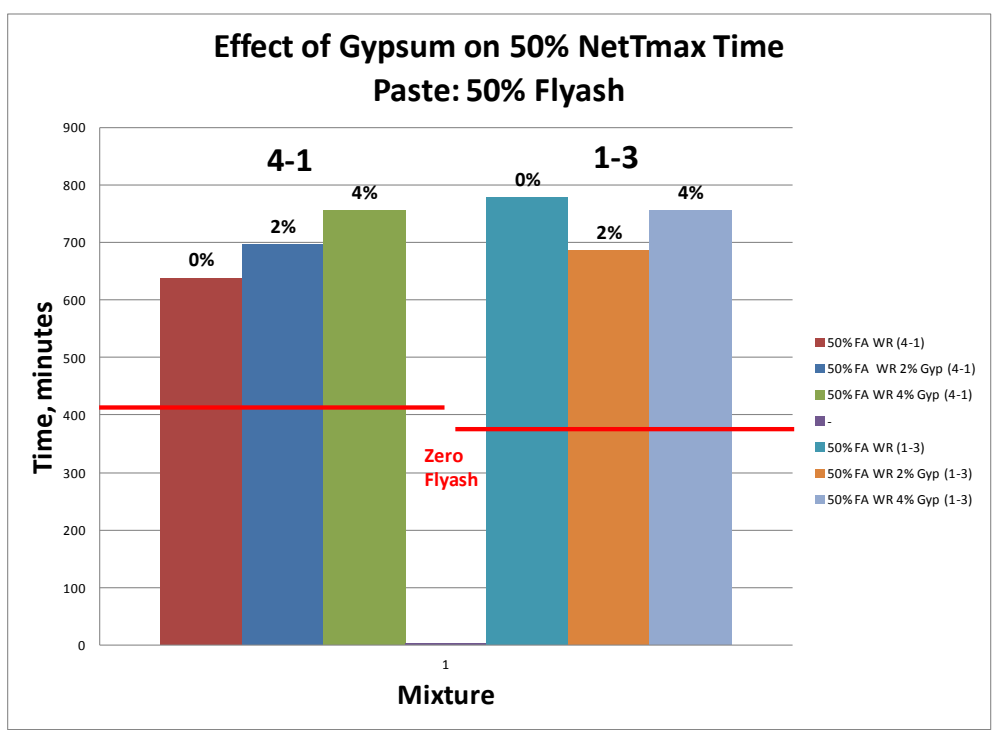
Figure 4.54 - Effect of Gypsum Content on 50%NetTMax Time for 50% Fly Ash Mixtures
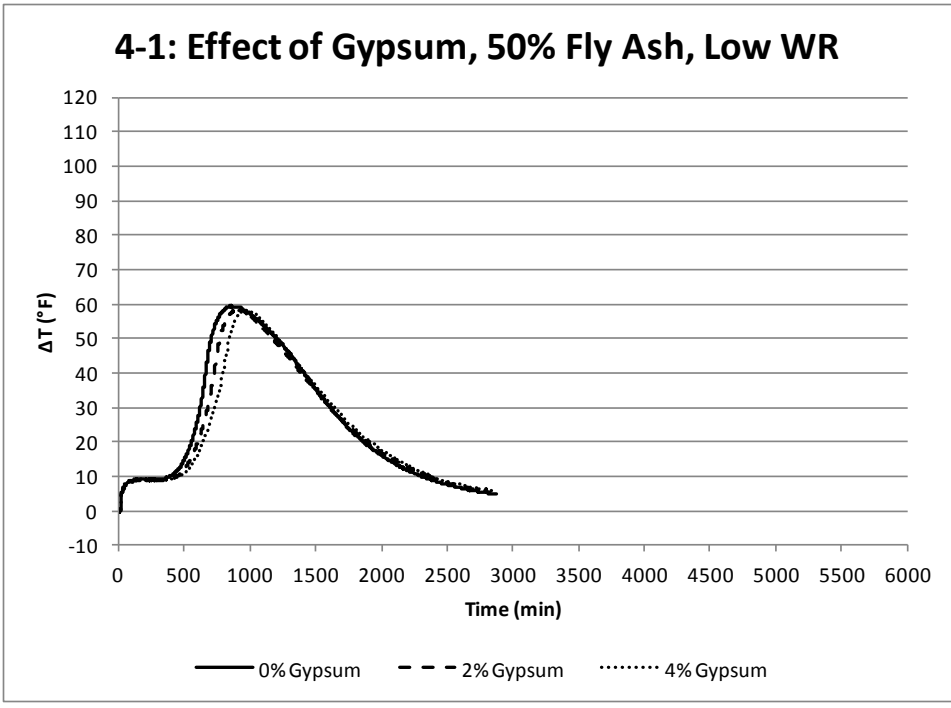
Figure 4.55– Typical Effect of Gypsum Content on Calorimeter Curve Characteristic

Figure 4.56 shows the same relationships for the 70% fly ash mixtures. The 4-1 combination at 70% fly ash acted in the same manner as at 50% fly ash: gypsum retarded the reaction and the effect increased with increasing gypsum content. The effect was more pronounced at 70% fly ash. For the 1-3 combination, the zero gypsum curve was greatly accelerated; the presence of gypsum appears to be negligible.
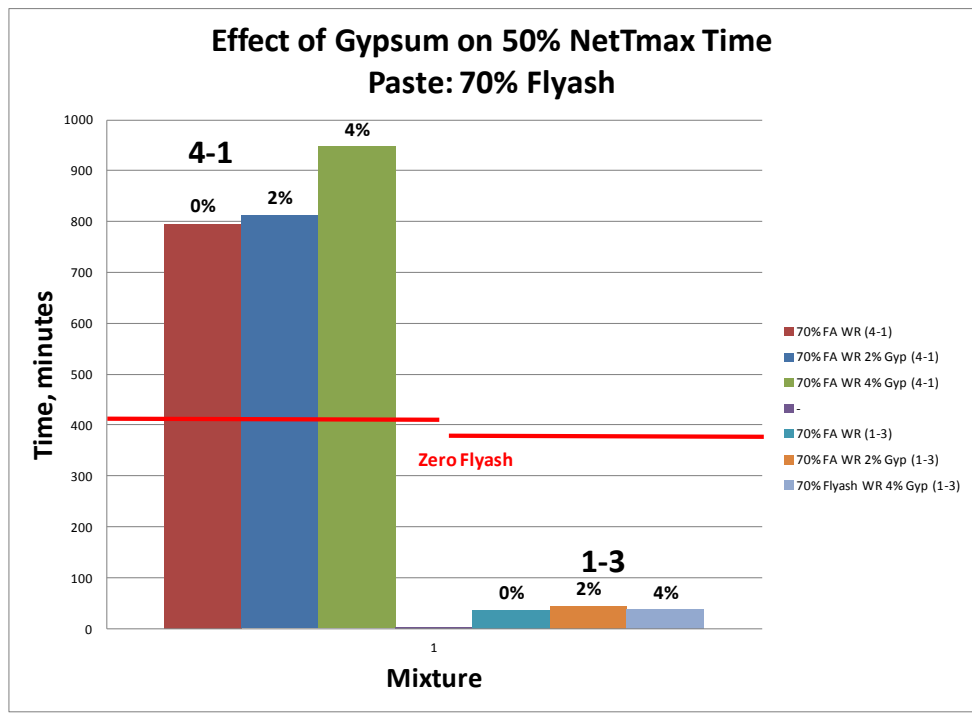
Figure 4.56 - Effect of Gypsum Content on 50%NetTMax Time, 70% Fly Ash Mixtures

The effect of gypsum on one day compressive strengths for the 50% fly ash mixtures is shown in **Figure 4.57.** As can be seen, 2% gypsum reduced the strength somewhat and the effect was greater with 4% gypsum for combination 4-1. For the 1-3 combination, gypsum increased strength marginally, with 2% slightly more than 4%.
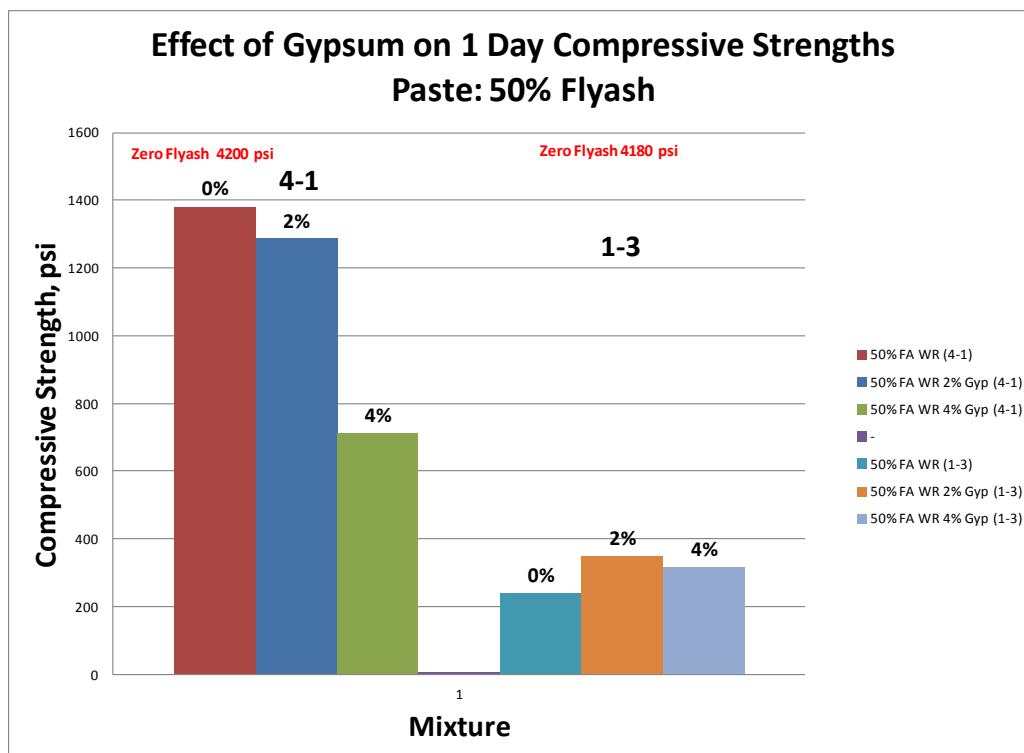
Figure 4.57 - Effect of Gypsum Content on One Day Compressive Strength for 50% Fly Ash Mixtures

For the 70% fly ash mixtures, the effect of gypsum was somewhat different, as shown in **Figure 4.58.** For the 4-1 combination, 2% gypsum increased strength while 4% decreased it. For the 1-3 combination, 2% gypsum had little effect while 4% increased strength. It is interesting to examine a calorimeter curve for the 1-3 70% mixture. As shown in **Figure 4.59**, the zero gypsum curve is of the F type which essentially has no silicate reaction curve. But, upon gypsum addition, some activity is spurred on as evidenced by the secondary peaks.
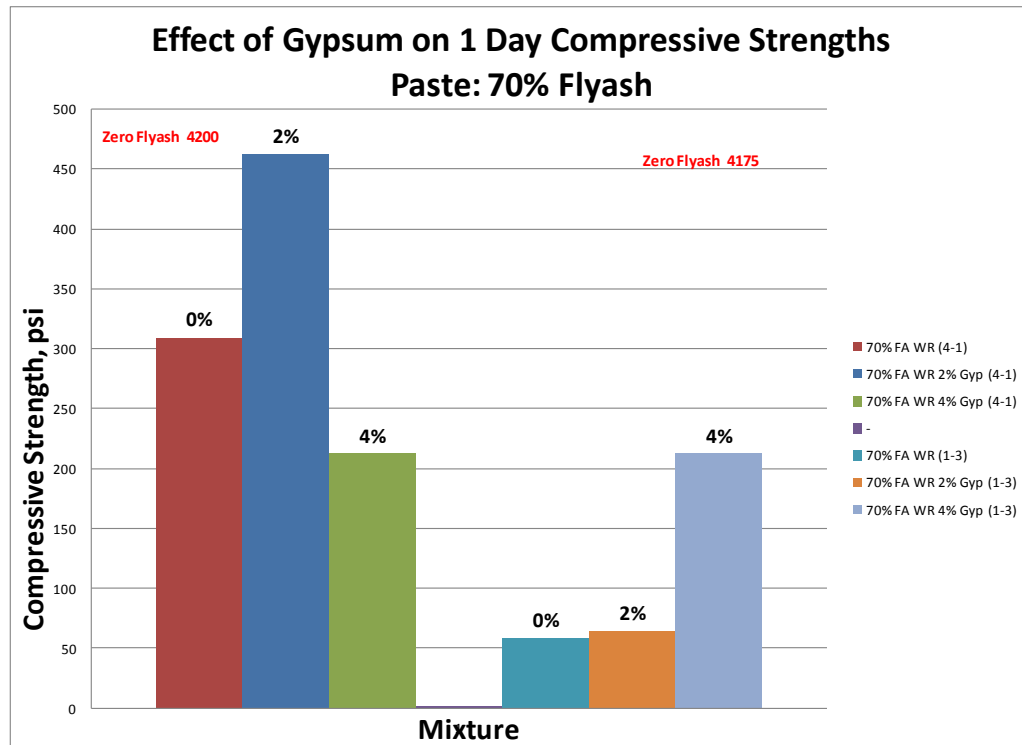
Figure 4.58 - Effect of Gypsum Content on One Day Compressive Strength for 70% Fly Ash Mixtures

At 56 days, **Figure 4.60** shows the effect of gypsum. The effect is negligible to marginal for all of the mixtures.

Finally, the effect of gypsum on 56 day strength for the 70% fly ash mixtures is shown in **Figure 4.61.** For most mixtures, the addition of gypsum reduced strength only marginally; however, at 2% for the 4-1 combination, the reduction was more significant.
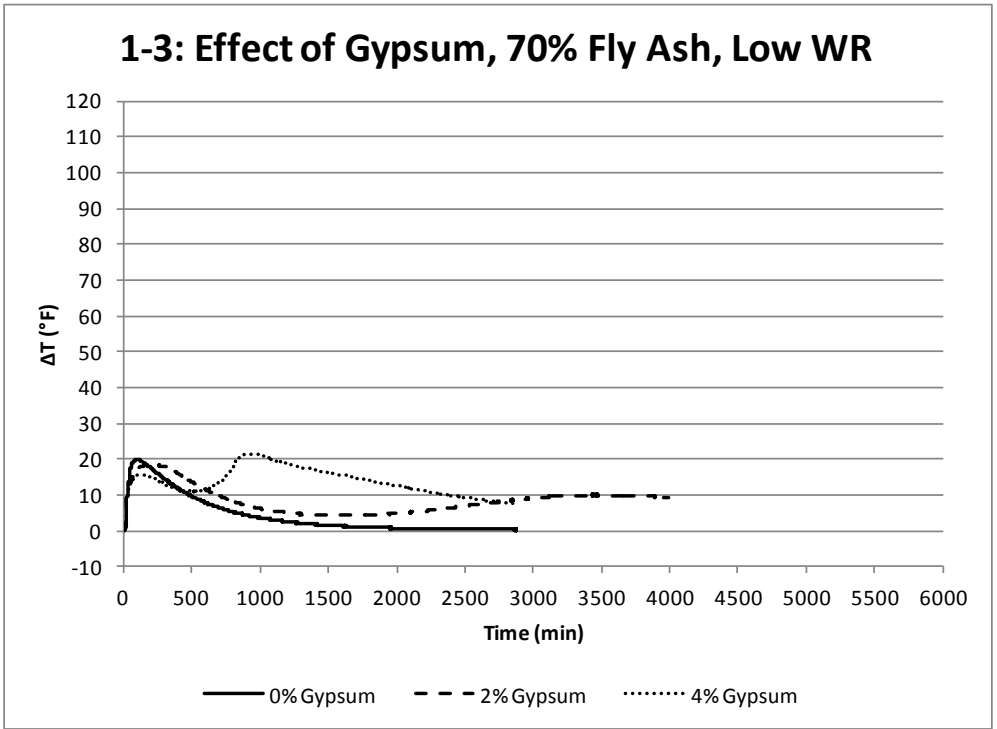
Figure 4.59– Typical Effect of Gypsum Content on Calorimeter Curve Characteristics
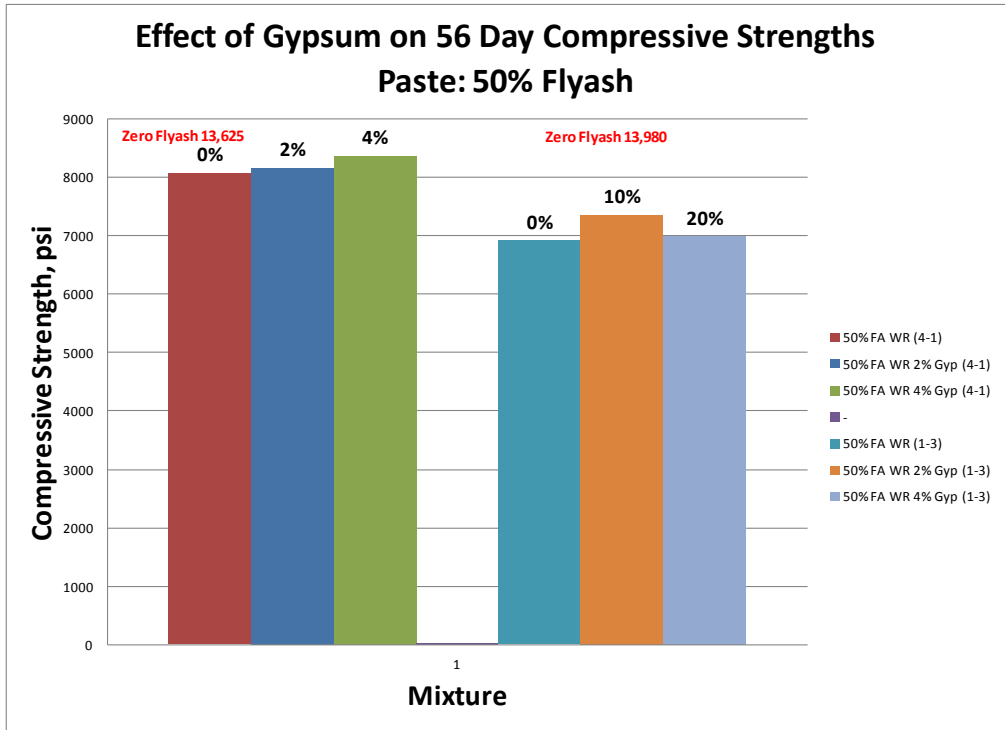
Figure 4.60 - Effect of Gypsum Content on 56 Day Compressive Strength for 50% Fly Ash Mixtures
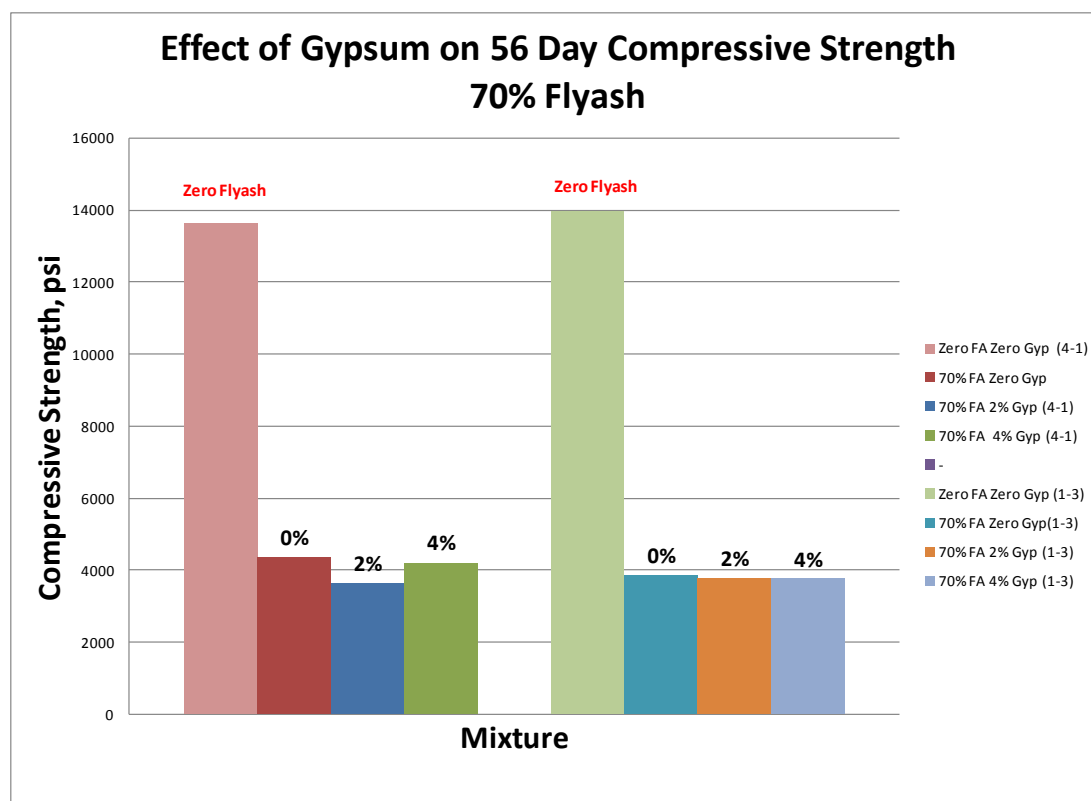
Figure 4.61 - Effect of Gypsum Content on 56 Day Compressive Strength for 70% Fly Ash Mixtures

The effect of gypsum on initial setting time (Vicat) for the 50% fly ash mixtures is shown in **Figure 4.62**. As can be seen, fly ash by itself accelerated the setting time significantly. When introduced, the gypsum retarded the set. In the case of the 4-1 combination, the setting time was essentially restored to the zero fly ash time, with 2% gypsum slightly more effective than the 4% level. For the 1-3 combination, the gypsum at both 2 and 4% levels only marginally retarded the setting time-it was still quite early. For the 70% fly ash mixtures (**Figure 4.63**), which were badly accelerated, in most cases the gypsum retarded the setting time (which is a good thing), but only to a small degree (10 minutes or less). As a point of reference, the ASTM C150 and C1157 minimum threshold

of 45 min. is shown. All 50% mixtures were greater than the minimum. However, only the 2% gypsum 4-1 mixture met the minimum. All the rest set up too quickly.
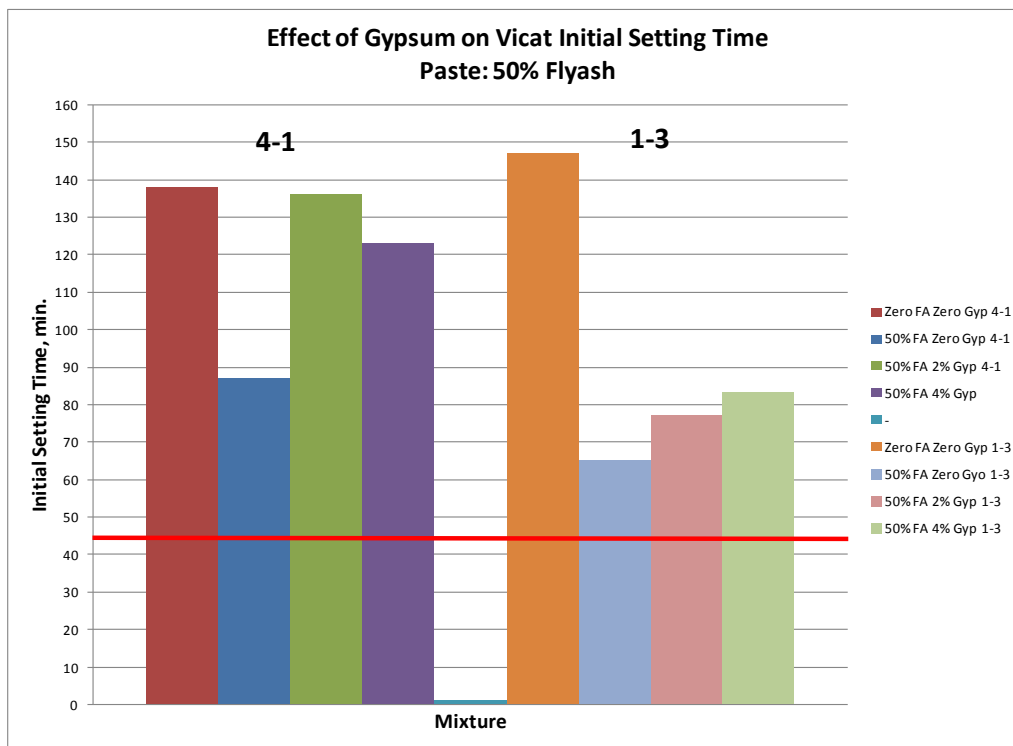
Figure 4.62 - Effect of Gypsum Content on Vicat Initial Setting Time for 50% Fly Ash Mixtures

Only three mixtures exceeded the ASTM C150 final setting time maximum limit of 480 min.: the 1-3 50% fly ash 2% gypsum (570 min.), the 4-1 50% fly ash 4% gypsum (540 min.), and the 1-3 50% fly ash 4% gypsum (675 min.).

Figure 4.64 depicts the effect of gypsum on early stiffening. In three of the four mixtures with fly ash, gypsum improved early stiffening tendencies. However, none of the effects of gypsum was more than marginal. All mixtures (with fly ash) were prone to early stiffening to some degree.
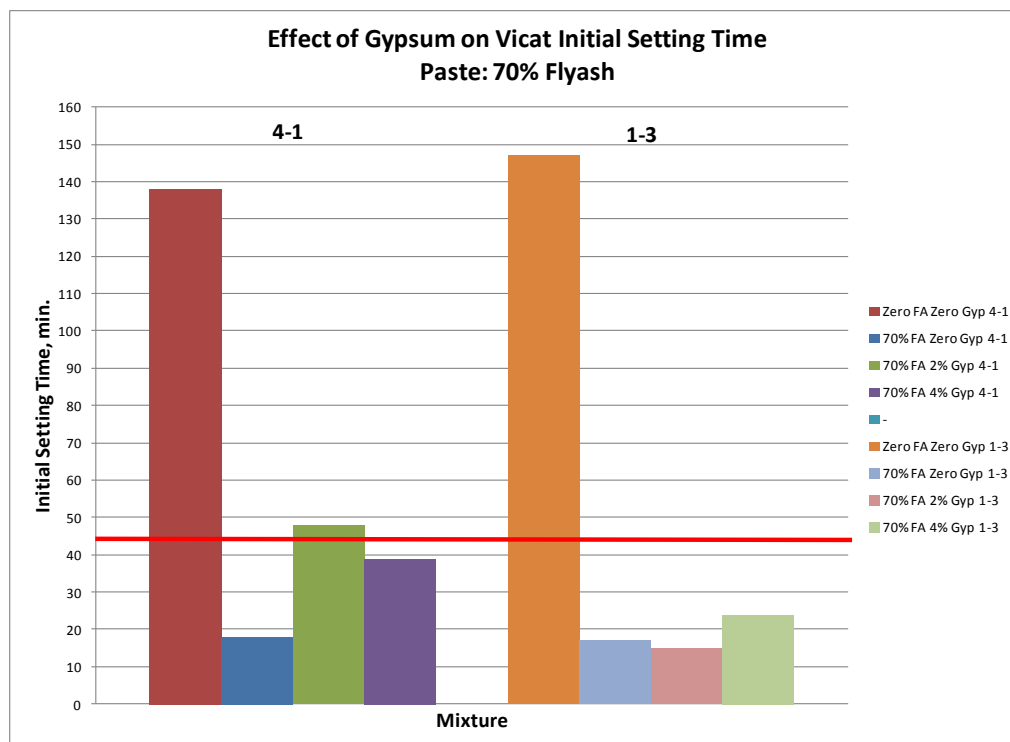
Figure 4.63 - Effect of Gypsum Content on Vicat Initial Setting Time for 70% Fly Ash Mixtures

4.5.2.5. Effect of Lime. A limited amount of testing was performed to examine the effect of lime by itself. **Figure 4.65** shows a comparison of compressive strength to that of OPC mixtures, all with the low dosage of WR/HRWR, for the 4-1 combination. Likewise, **Figure 4.66** depicts the 1-3 combination. The 5% lime improved strength somewhat for the 50% and 70% fly ash 4-1 mixture at later strengths; at other ages and fly ash contents there was no improvement, or even small decreases. The 10% lime strength generally was slightly lower than the 5% lime. For the 1-3 combination, there was little or no improvement for the 50% and 70% mixtures, but both lime percentages increased strength at 56 days for both the 50 and 70% fly ash mixtures. Also, both lime contents improved the seven day strengths of the 70% mixtures.
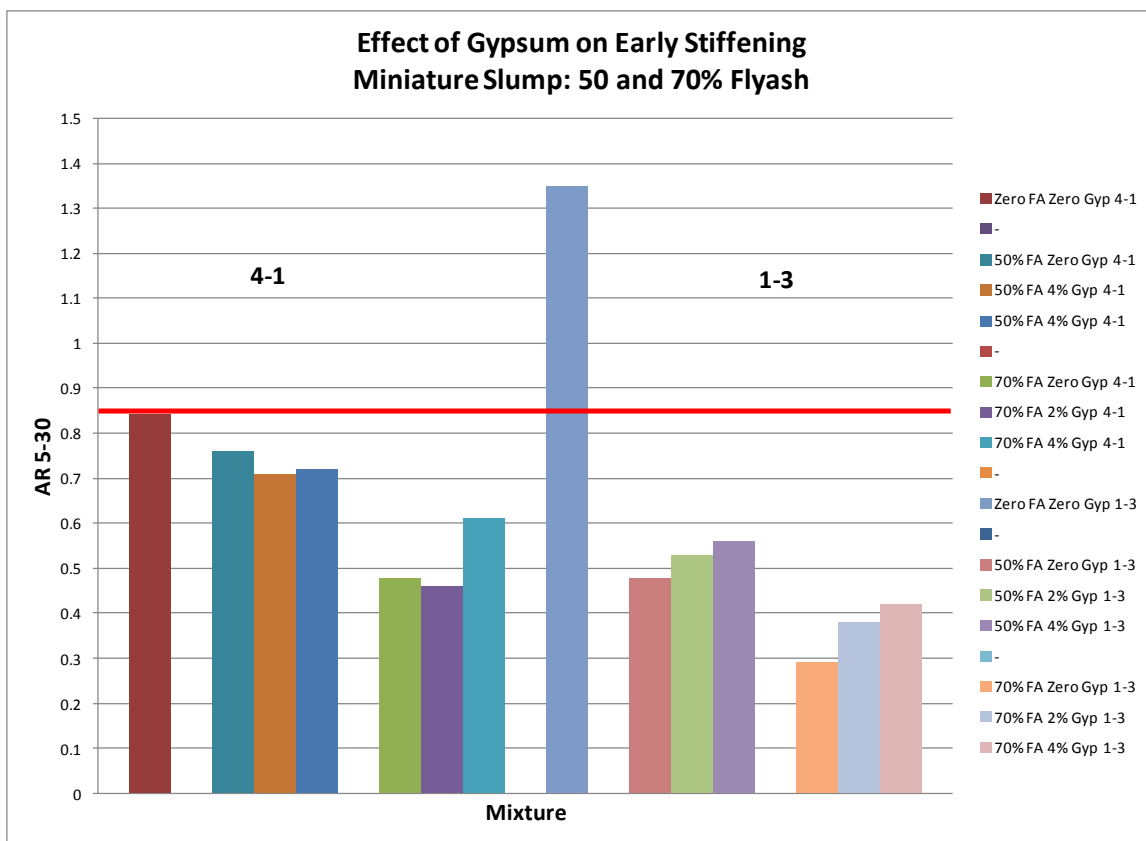
Figure 4.64 – Effect of Gypsum and Fly Ash Content on Early Stiffening for Zero, 50, and 70% Fly Ash Mixtures
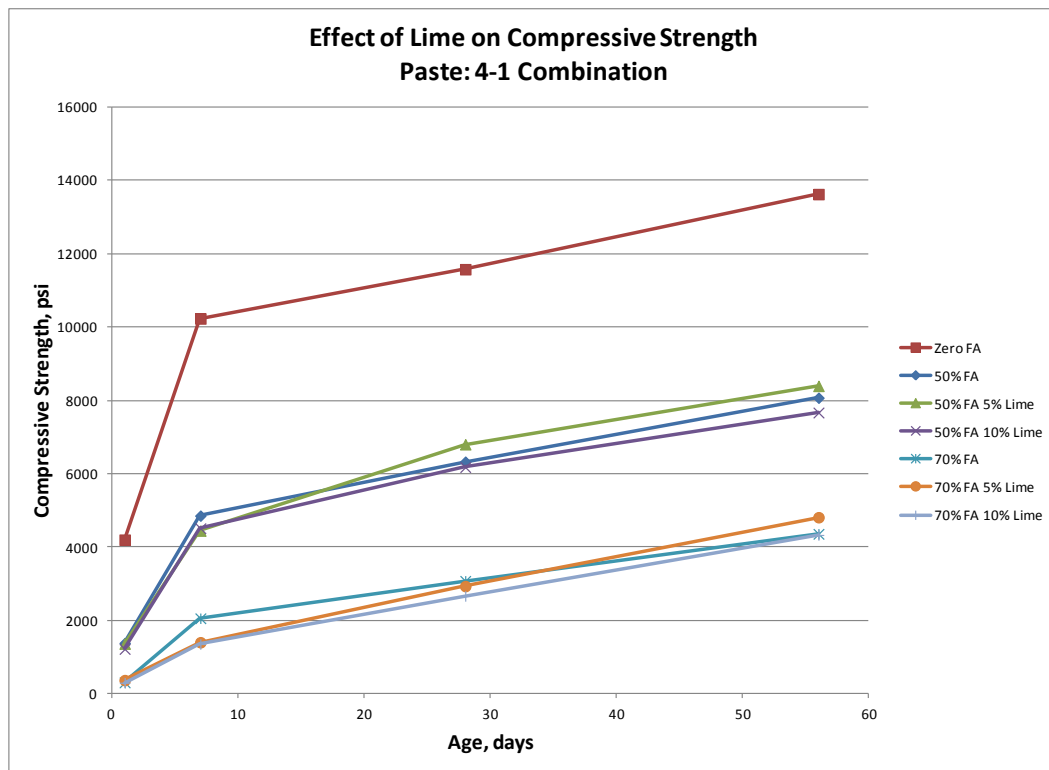
Figure 4.65 – Effect of Lime on Compressive Strength, 4-1 Combination
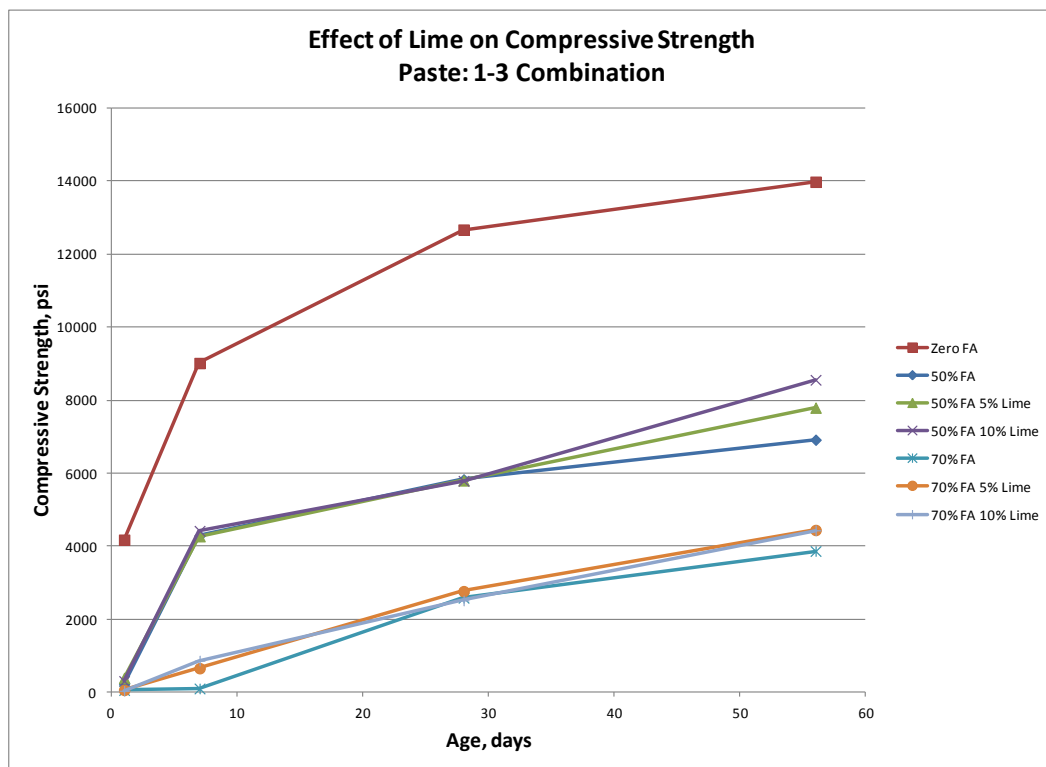
Figure 4.66 – Effect of Lime on Compressive Strength, 1-3 Combination

4.5.2.6. Effect of RSC. A limited amount of testing was performed to examine the effect of RSC by itself. **Figure 4.67** shows a comparison of compressive strength to that of OPC mixtures, all with the low dosage of WR/HRWR, for the 4-1 combination. Likewise, **Figure 4.68** depicts the 1-3 combination. RSC improved strengths for both cementitious combinations at ages of seven days and later, but only marginally at one day. Both RSC levels improved 56 day strengths somewhat, with the 20% RSC level faring better.
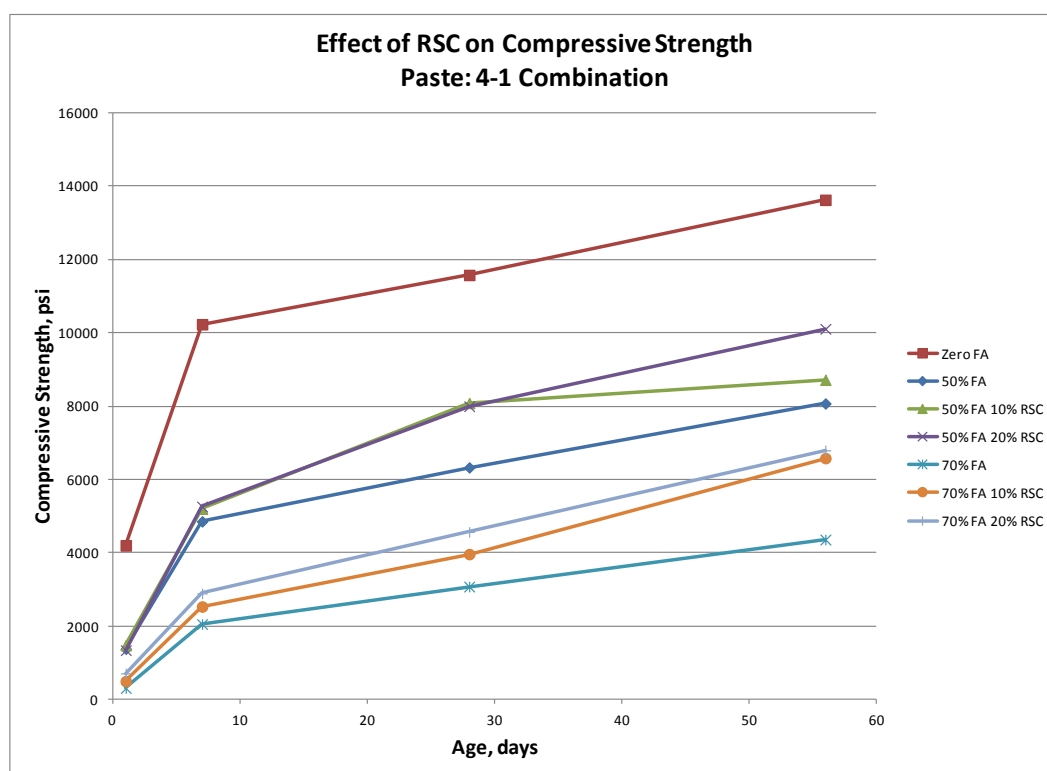
Figure 4.67 – Effect of RSC on Compressive Strength, 4-1 Combination
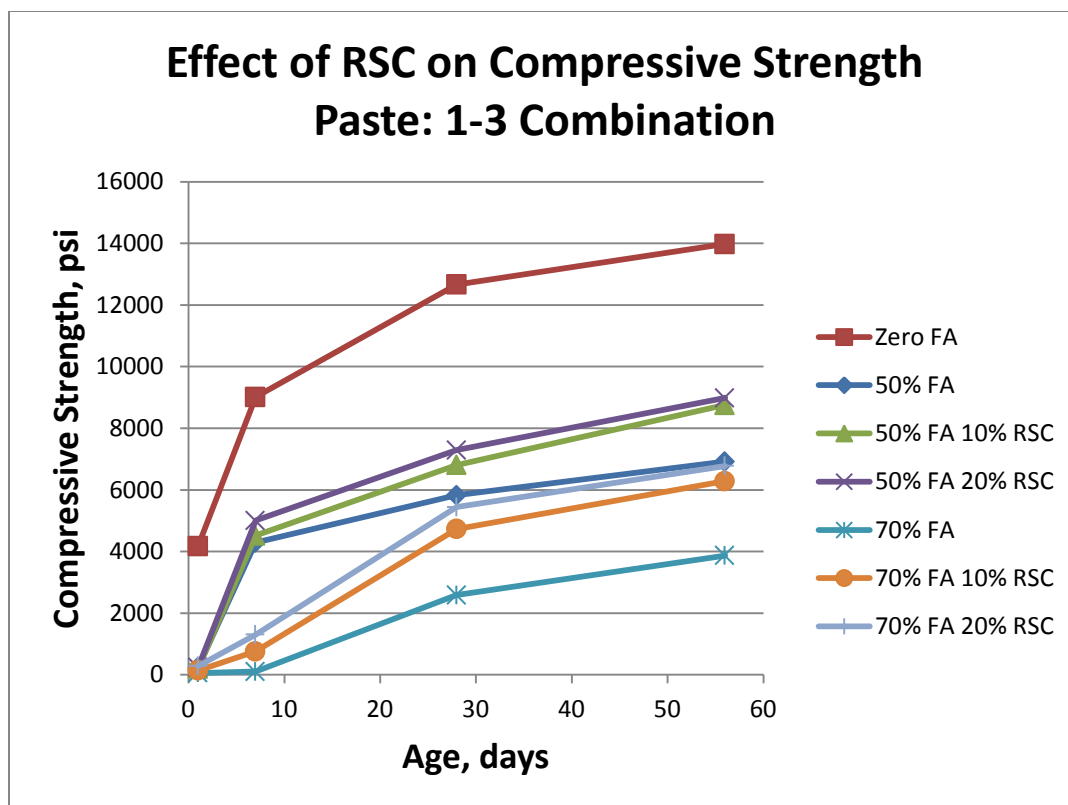
Figure 4.68 – Effect of RSC on Compressive Strength, 1-3 Combination

4.5.2.7. Effect of Gypsum-Lime. At the 4% gypsum level, two levels of lime were explored: 5 and 10%. **Figures 4.69** and **4.70** show the results of the effect of 50 and 70% fly ash contents, respectively, on one day strengths. The results are mixed: for the 50% fly ash 4-1 blend, gypsum-lime reduced strengths at both the 5 and 10% levels of lime. However, for the 50% fly ash mixtures 1-3 blend and both combinations at 70% fly ash, the gypsum-lime increased strengths. Dosage made little difference.
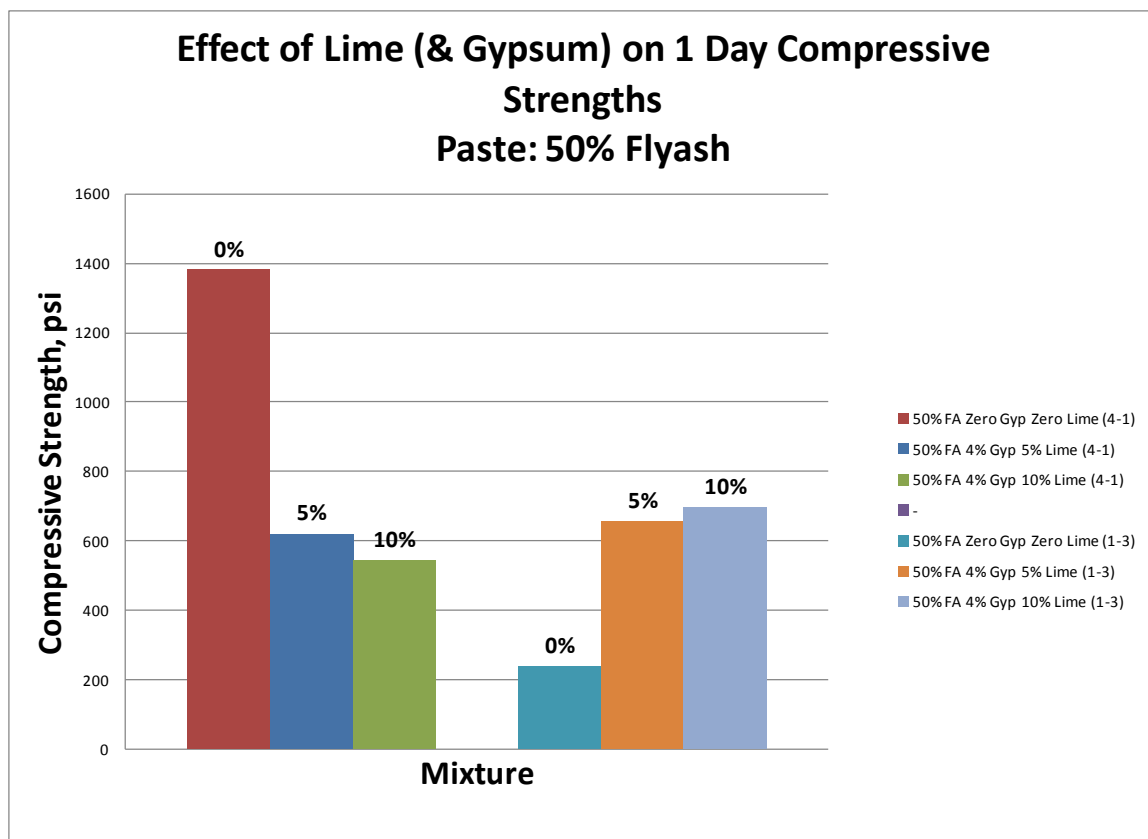
Figure 4.69 – Effect of Gypsum-Lime on One Day Compressive Strength for 50% Fly Ash Mixtures
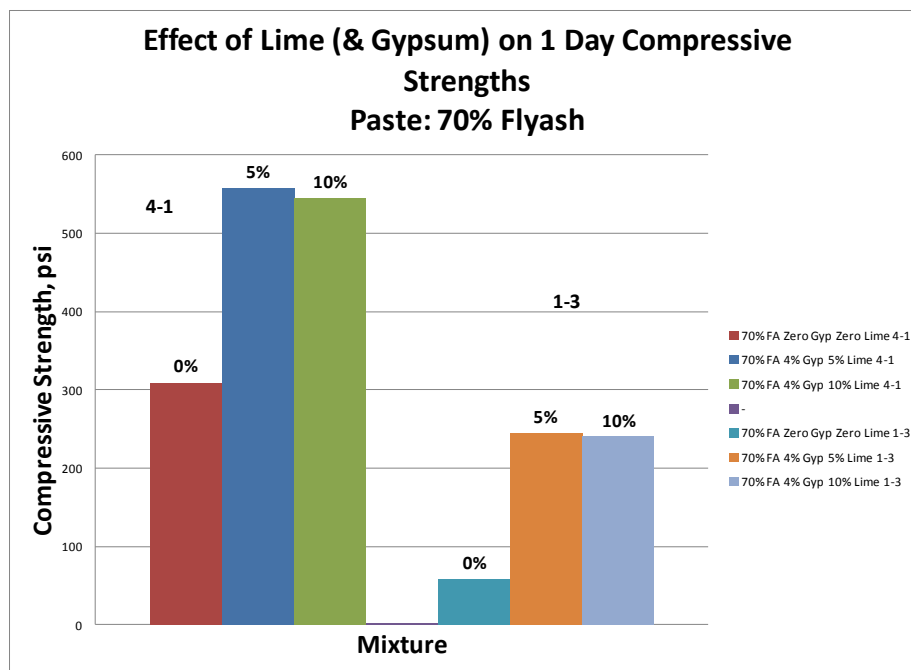
Figure 4.70 – Effect of Gypsum-Lime on One Day Compressive Strength for 70% Fly Ash Mixtures

At 56 days, **Figures 4.71** and **4.72** indicate that gypsum-lime reduced strengths. Again, dosage made little difference.
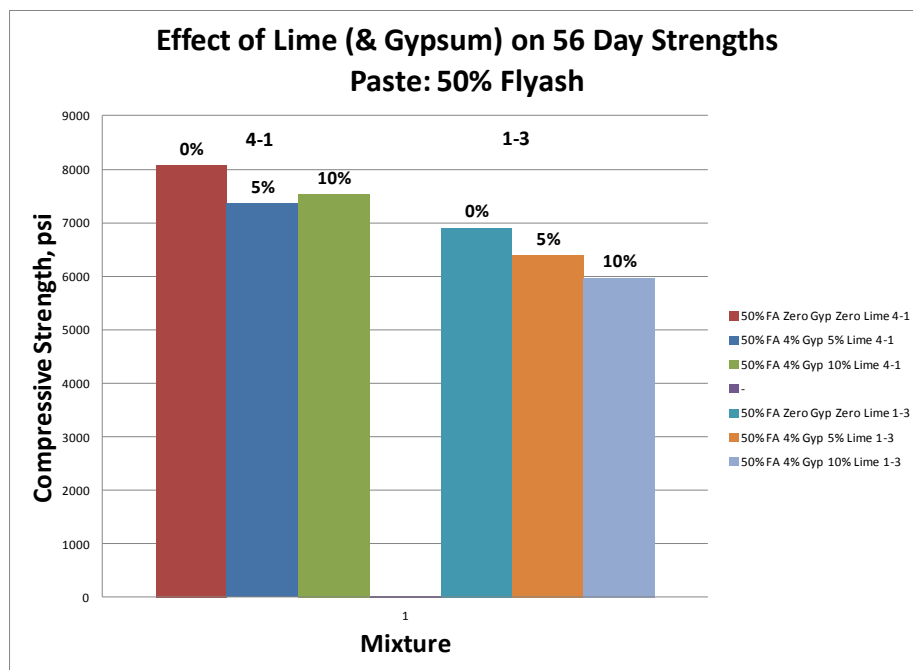
Figure 4.71 – Effect of Gypsum-Lime on 56 Day Compressive Strength for 50% Fly Ash Mixtures
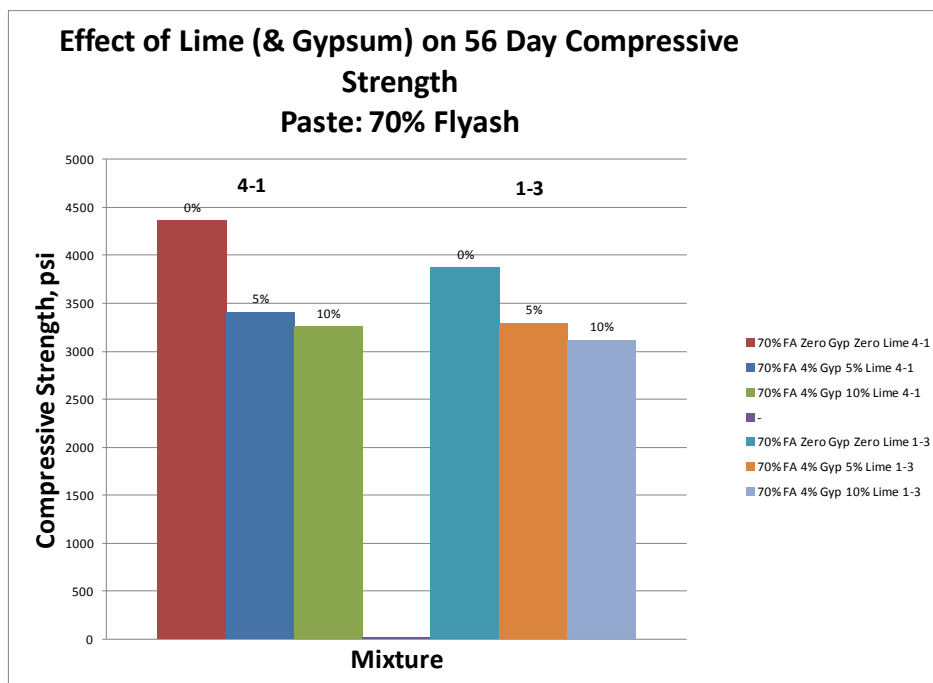
Figure 4.72 – Effect of Gypsum-Lime on 56 Day Compressive Strength for 70% Fly Ash Mixtures

The effect of 4% gypsum-lime (5 and 10%) on calorimetry (50%NetTMax time) results is shown in **Figures 4.73** and **4.74** for 50% and 70% fly ash, respectively.
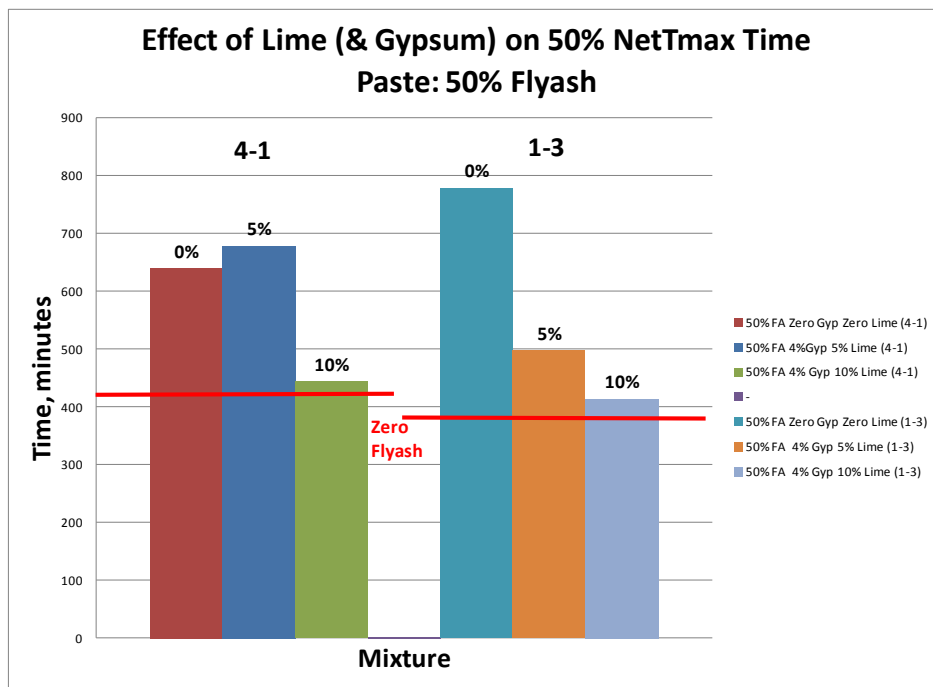
Figure 4.73 – Effect of Gypsum-Lime on 50%NetTMax Time for 50% Fly Ash Mixtures

In general, it appears that the curves are accelerated (50%NetTMax time decreases) quite significantly for the combination 4-1 at both the 50% and 70% fly ash contents, and for the 1-3 mixture at 50% fly ash. The optimum lime content is 10%.
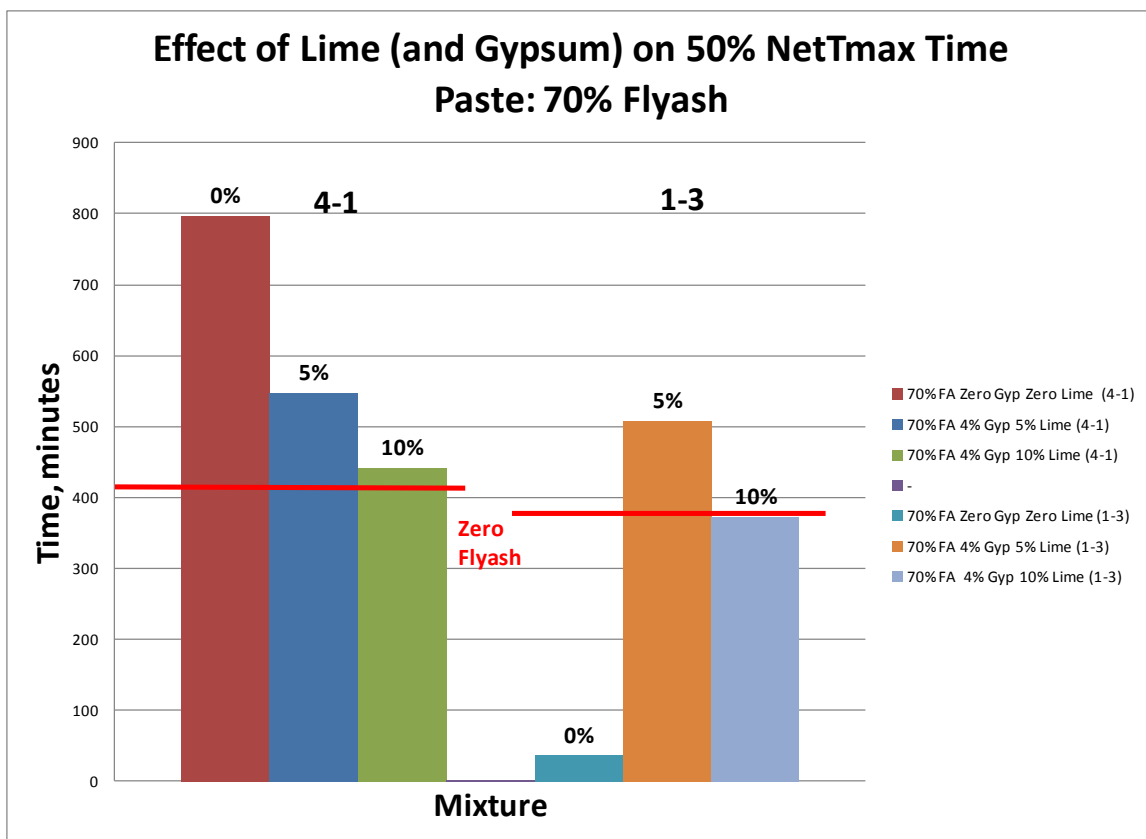
Figure 4.74 – Effect of Gypsum-Lime on 50%NetTMax Time for 70% Fly Ash Mixtures

A typical calorimeter set of curves showing all three levels of lime (zero, 5, and 10%) is depicted in **Figure 4.75**. It can be seen that the curves are shifted to the left with increasing amounts of lime, indicating an acceleration of the reactions.

4-1: Effect of Lime, 50% Fly Ash, 4% Gyp, Low WR
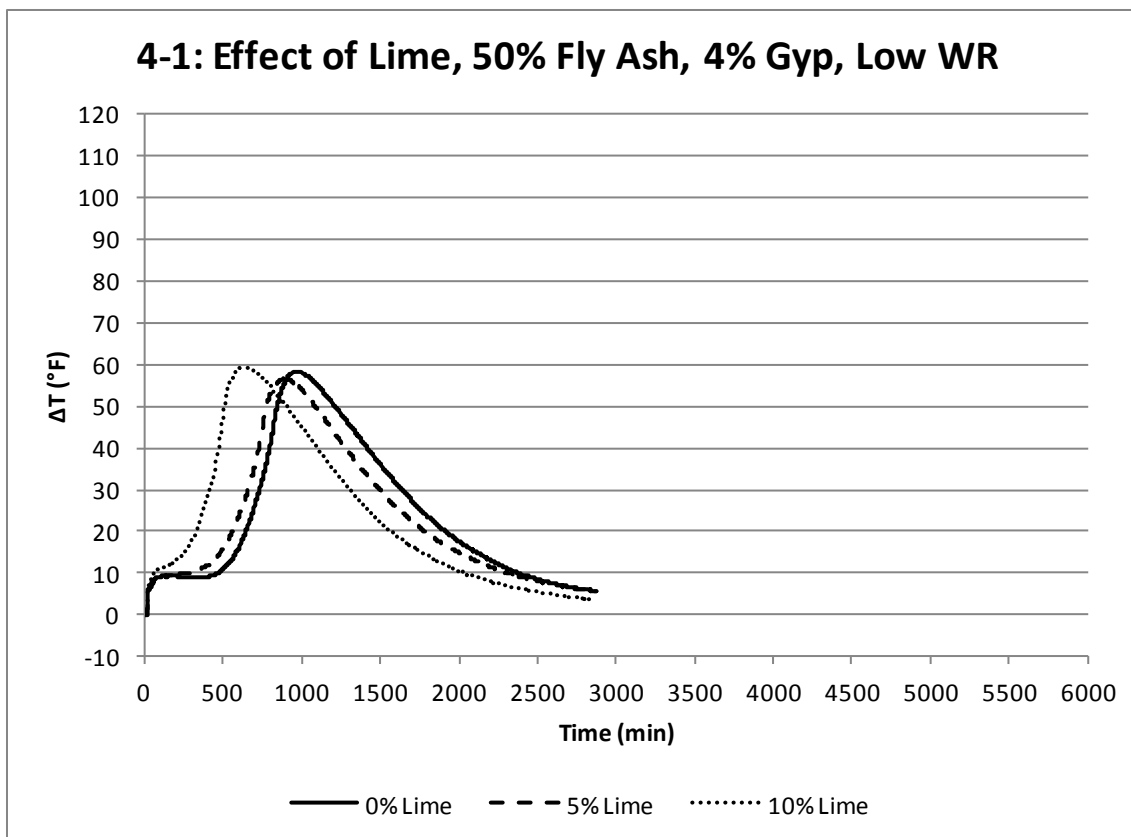
Figure 4.75– Typical Effect of Gypsum-Lime Content on Calorimeter Curve Characteristics

Referring back to **Figure 4.74**, for the 70% fly ash 1-3 blend, which is greatly accelerated without powder additives, the addition of gypsum-lime appears to retard the 50%NetTMax time to at or greater than the zero fly ash time. However, upon inspection of the calorimeter curves (**Figure 4.76**), the curves with the powder additives appear to shift to the left, as in all the other calorimeter curves with this treatment. This apparent non-agreement between the bar chart and the calorimeter curves points out the possibility of pulling off a single value (e.g. 50% NetTMax time) from oddly-shaped curves, where the data point may happen to be on the secondary curve.
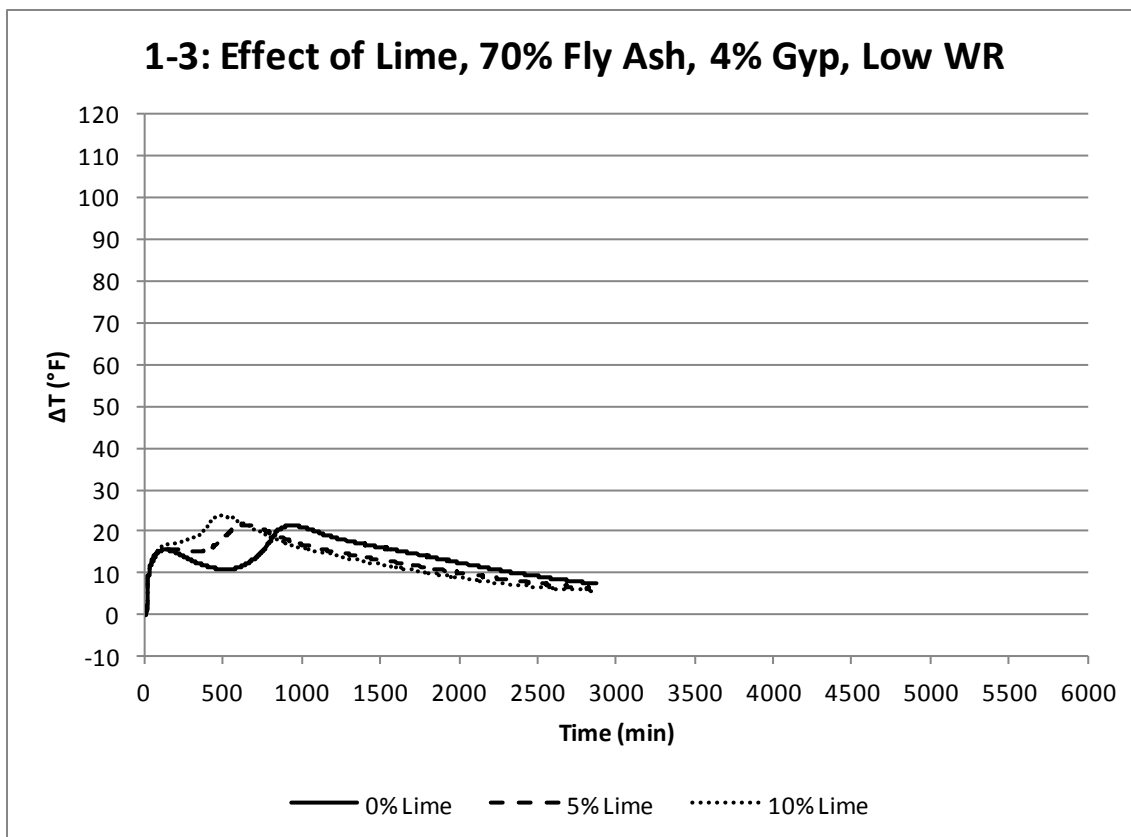
Figure 4.76– Gypsum-Lime Content Calorimeter Curve Showing Dilemma of Picking the 50%NetTMax Point

The effect of gypsum-lime on initial setting time is shown in Figures 4.77 and **4.78** for the 50 and 70% fly ash content mixtures, respectively. In the case of the 4-1 blend at 50% and 70 % fly ash, the gypsum-lime retarded the set, with no consistency between lime contents. However, for the 3-1 blends, the results were mixed, with retardation, acceleration, and no change. However, magnitudes were small.
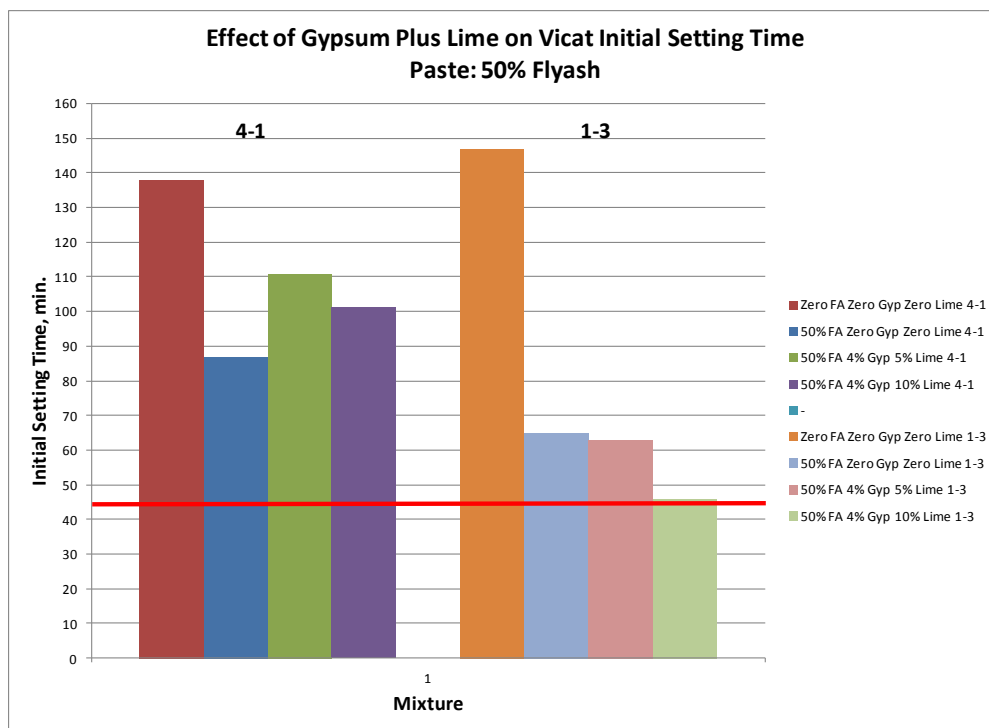
Figure 4.77 – Effect of Gypsum-Lime on Initial Setting Time, 50% Fly Ash
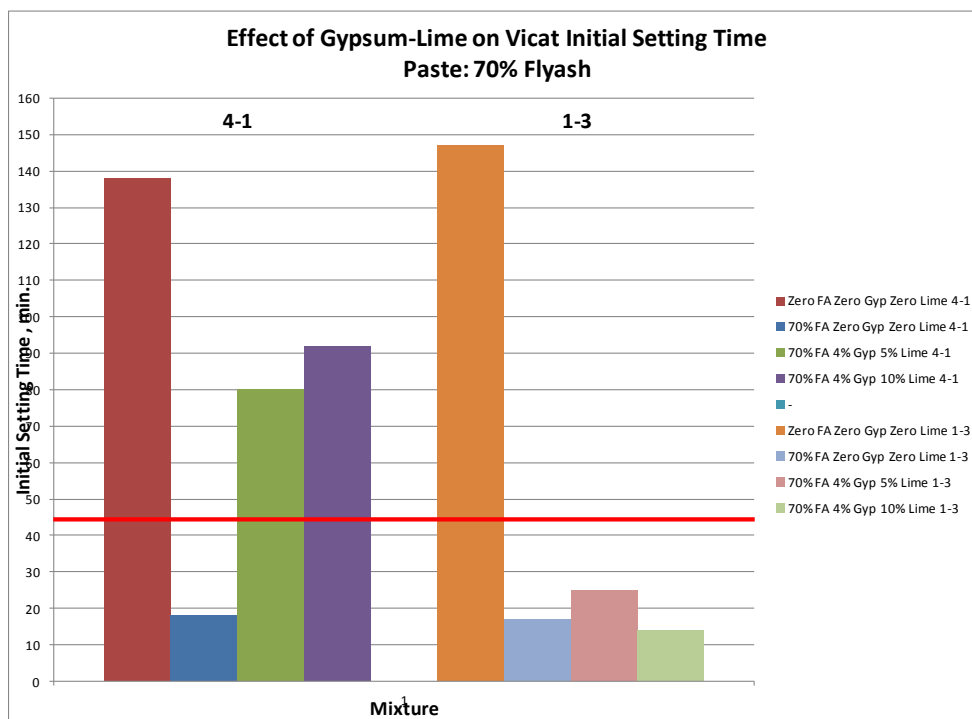
Figure 4.78 – Effect of Gypsum-Lime on Initial Setting Time, 70% Fly Ash

The effect of gypsum-lime on early stiffening is shown in **Figure 4.79**. In almost all cases, addition of the powder additives improved (increased AR 5-30) early stiffening behavior.
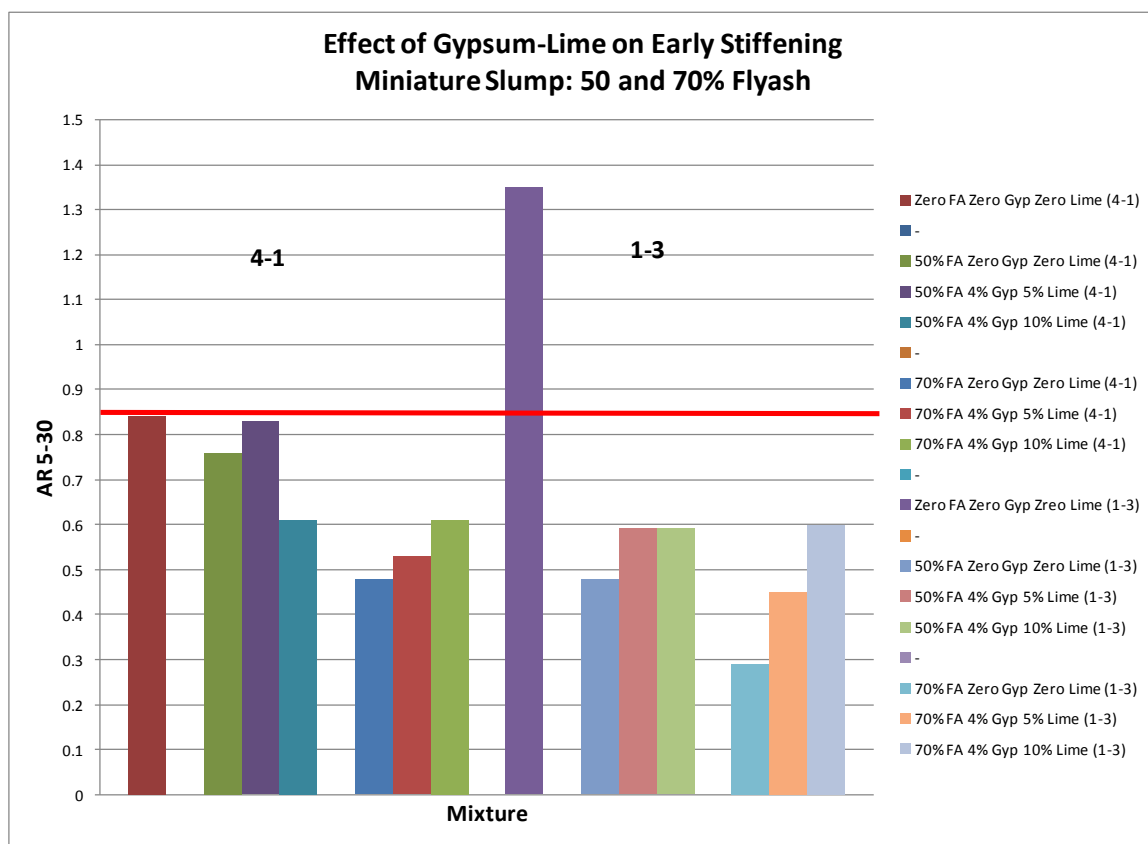
Figure 4.79 – Effect of Gypsum-Lime on Early Stiffening, 50 and 70% Fly Ash Contents

4.5.2.8. Effect of Gypsum-RSC. The effect of gypsum-RSC addition at 10 and 20% levels on one day compressive strength is shown in **Figure 4.80** and **4.81**. For the 1-3 blend, powder additives increased early strength both at 50 and 70% fly ash, with mixed results in terms of which dosage (10 or 20% RSC) is better. For the 4-1 blend, at 70% fly ash, both levels of powder additives improved strength, with 20% RSC being superior. However, the additives lowered strength at 50% fly ash.
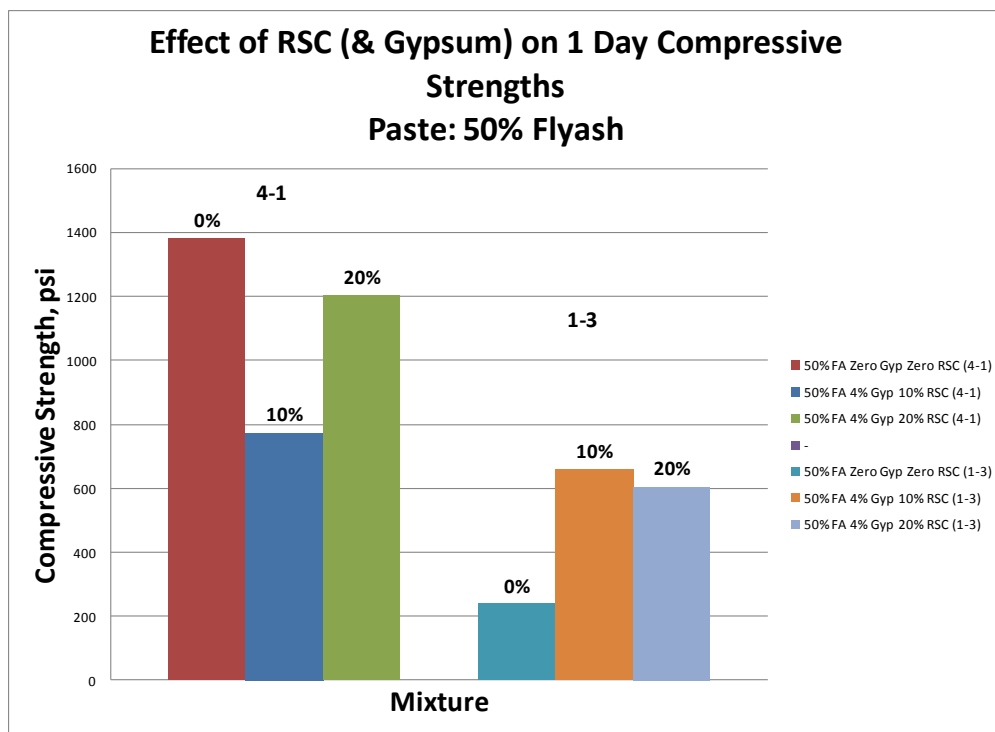
Figure 4.80 – Effect of Gypsum-RSC on One Day Compressive Strength, 50% Fly Ash
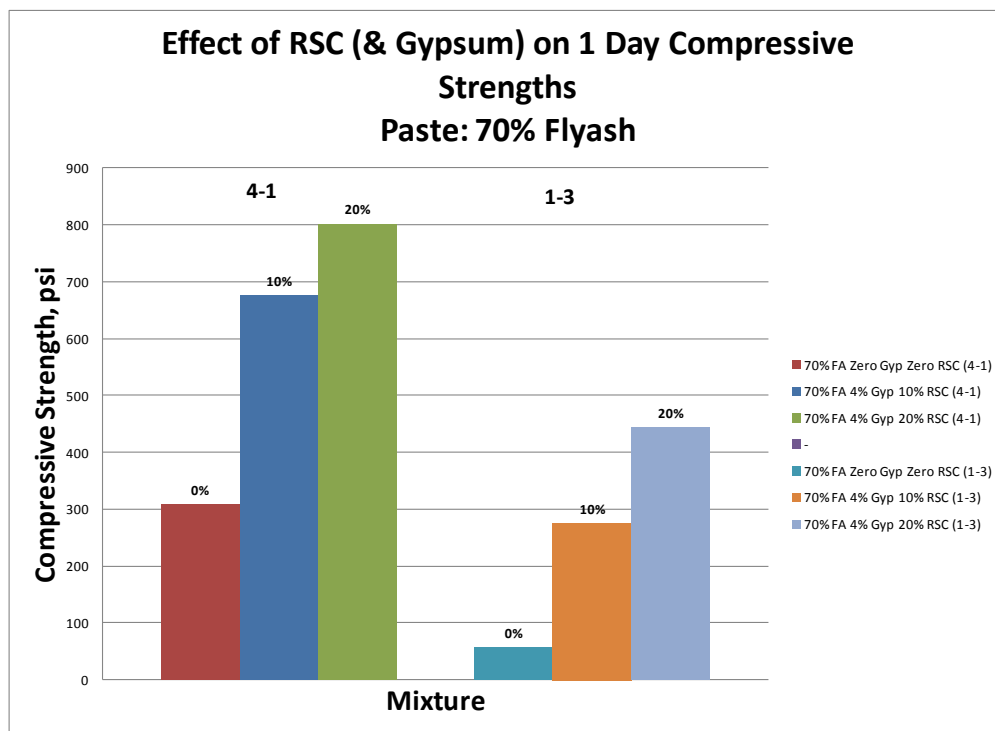
Figure 4.81 – Effect of Gypsum-RSC on One Day Compressive Strength, 70% Fly Ash

In regard to 56 day strengths, **Figures 4.82** and **4.83** depict the effects of the gypsum-RSC on both 50 and 70% mixtures. In every case, gypsum-RSC increased strength, with 20% being superior to 10%. In one case the improvement was only marginal, and in the others it was inconsistent as to which RSC level was more efficient.
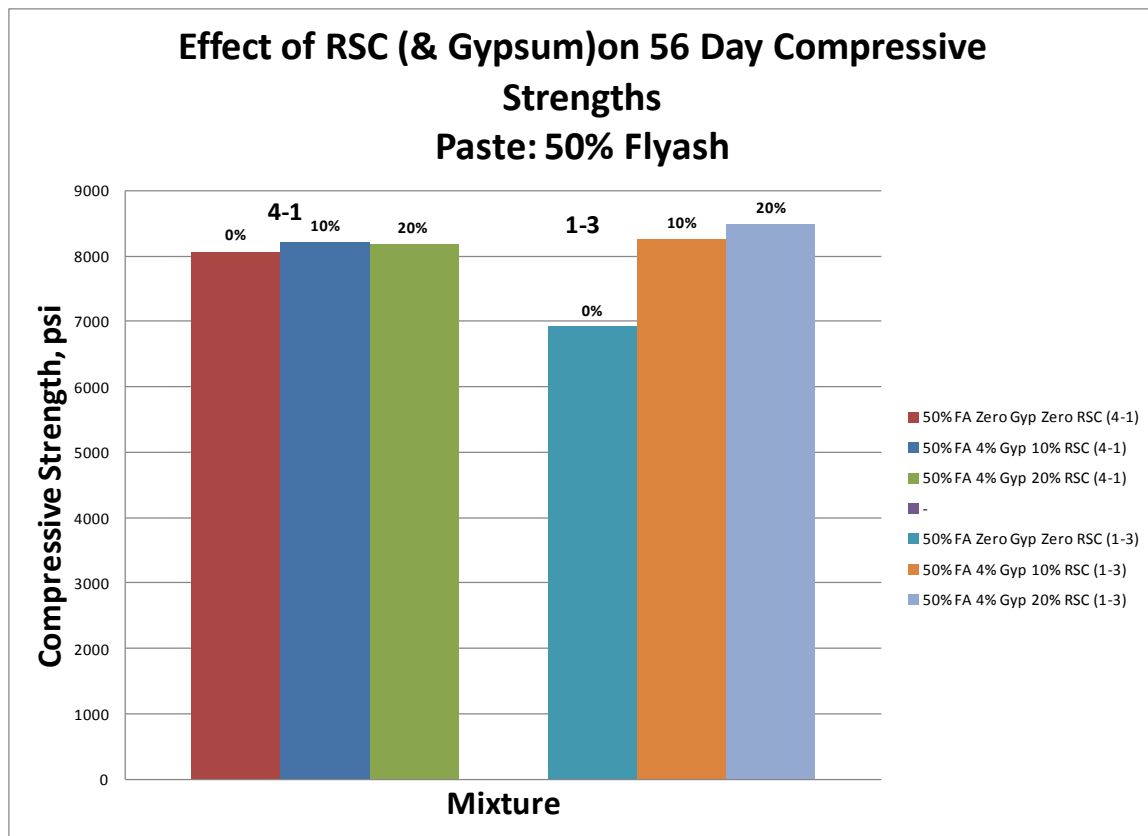
Figure 4.82 – Effect of Gypsum-RSC on 56 Day Compressive Strength, 50% Fly Ash
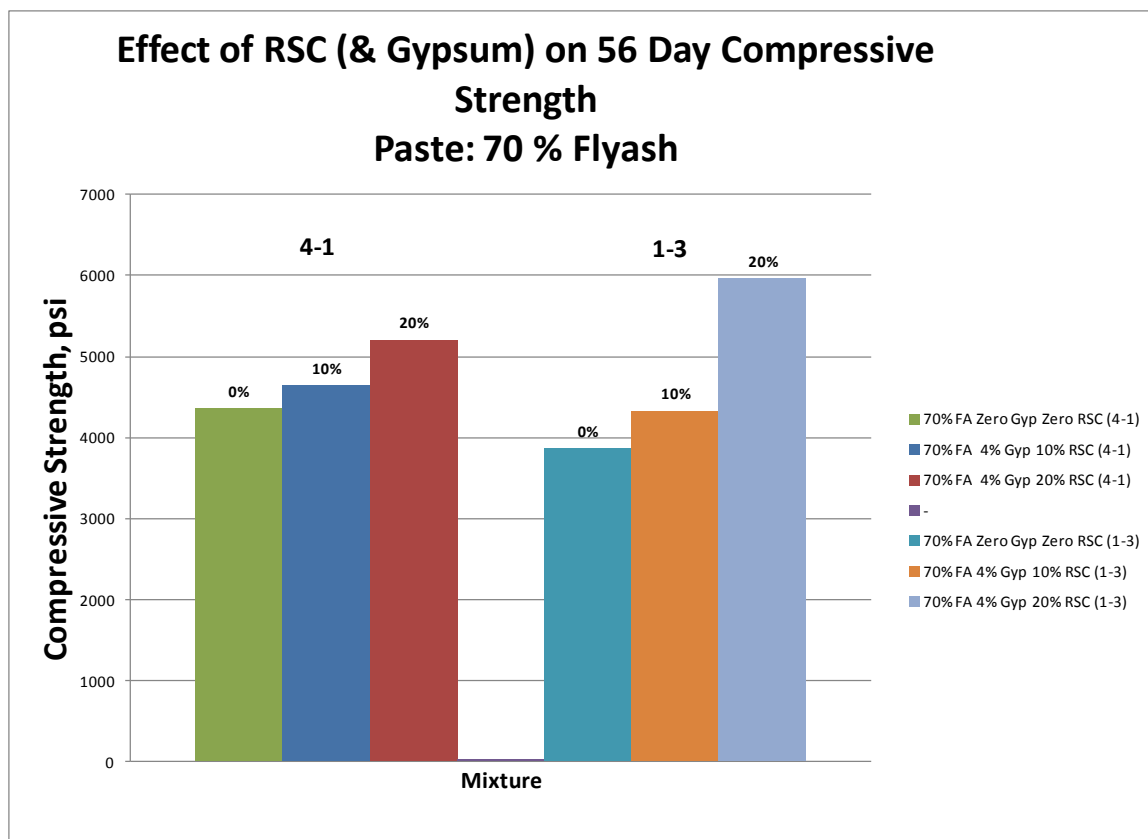
Figure 4.83 – Effect of Gypsum-RSC on 56 Day Compressive Strength, 70% Fly Ash

The effect of gypsum-RSC on calorimeter results (50%NetTMax time) is shown in **Figures 4.84** and **4.85**. For the 4-1 blend at 50 and 70% fly ash and the 1-3 blend at 50% fly ash, addition of gypsum-RSC reduced 50%NetTMax times. The 10% level times approached the zero fly ash times, but the 20% level accelerated the reaction excessively. This can be seen in **Figure 4.86**. For the 1-3 blend 70% fly ash mixture, even without the gypsum-RSC, the mixture reacted too quickly, and the powder admixtures did not change that.
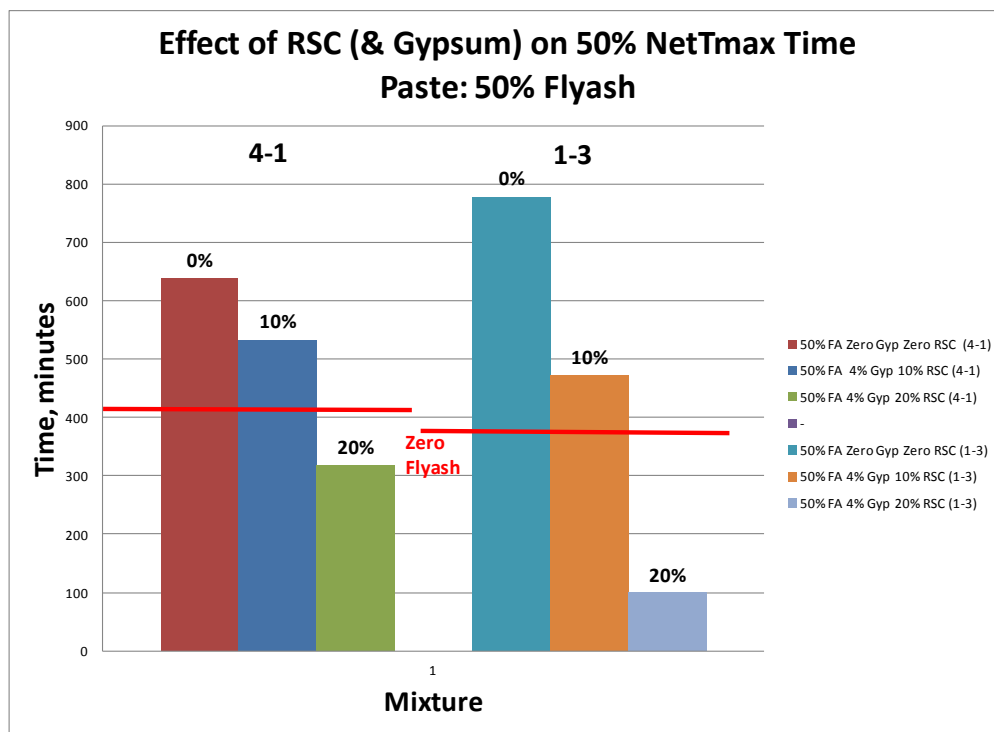
Figure 4.84 – Effect of Gypsum-RSC on 50%NetTMax Time for 50% Fly Ash Mixtures
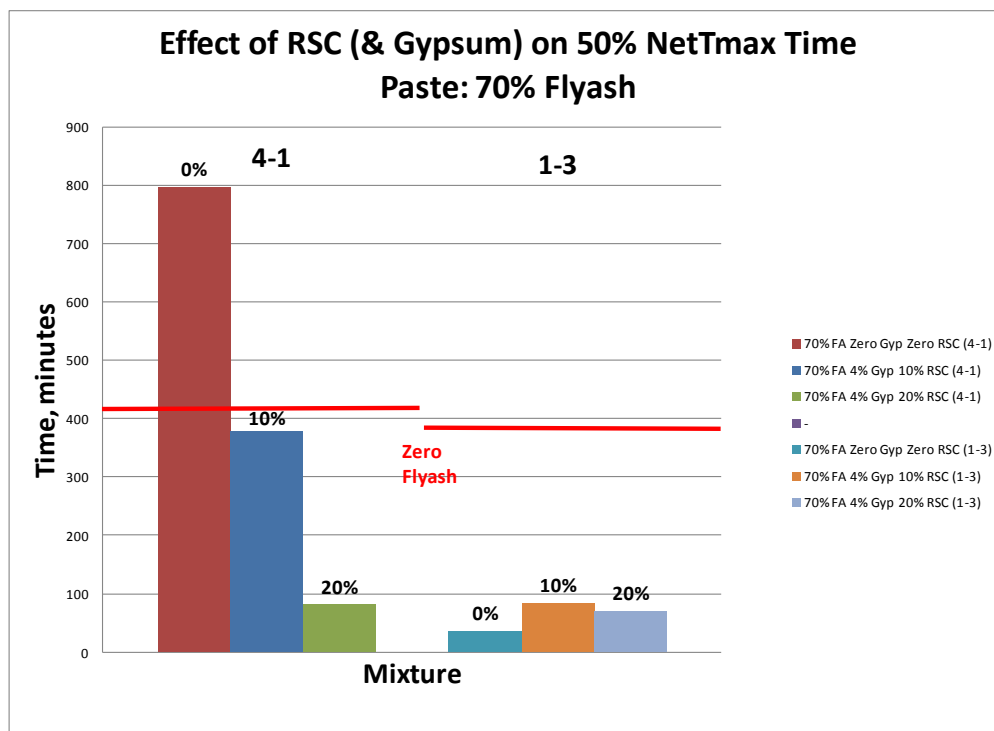
Figure 4.85 – Effect of Gypsum-RSC on 50%NetTMax Time for 70% Fly Ash Mixtures
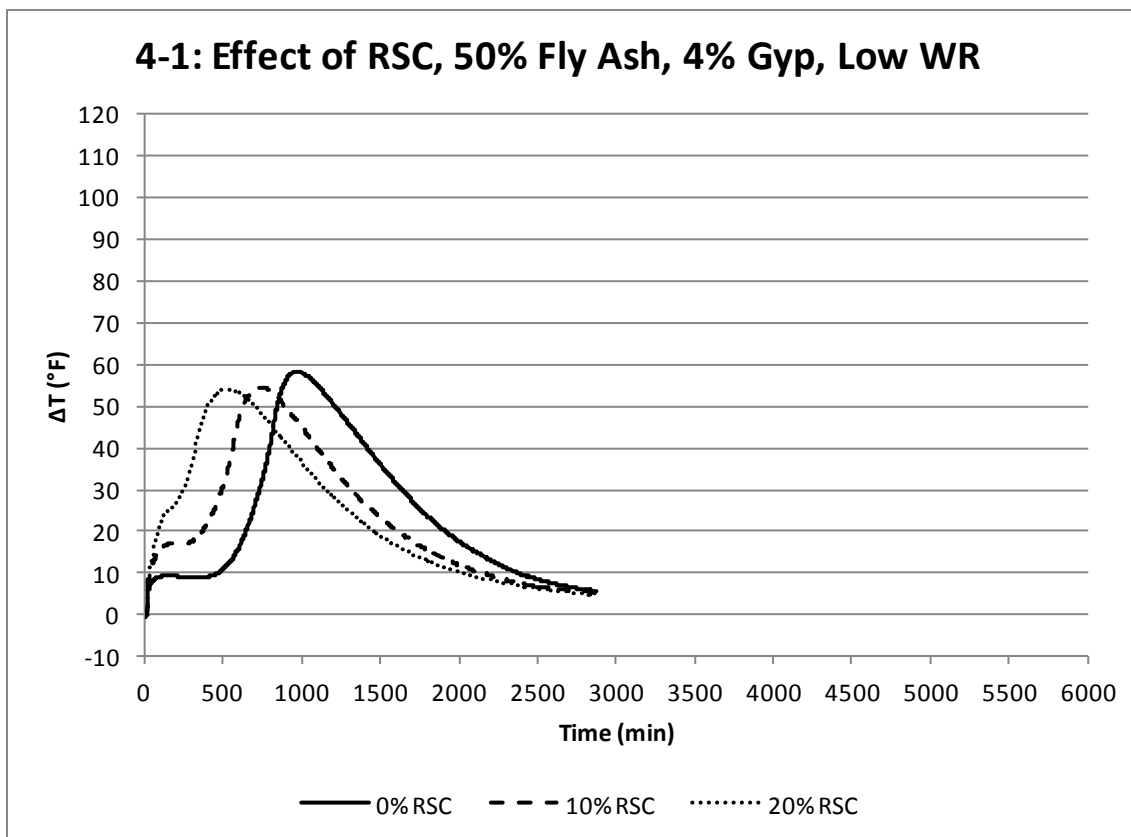
Figure 4.86– Typical Effect of Gypsum-RSC Content on Calorimeter Curve Characteristics

The effect of gypsum-RSC on initial setting time is seen in **Figure 4.87** and **4.88** for 50 and 70% fly ash contents, respectively. In 3 of the 4 cases, the mixtures were accelerated. The 1-3 blend 70% fly ash mixture was retarded somewhat.
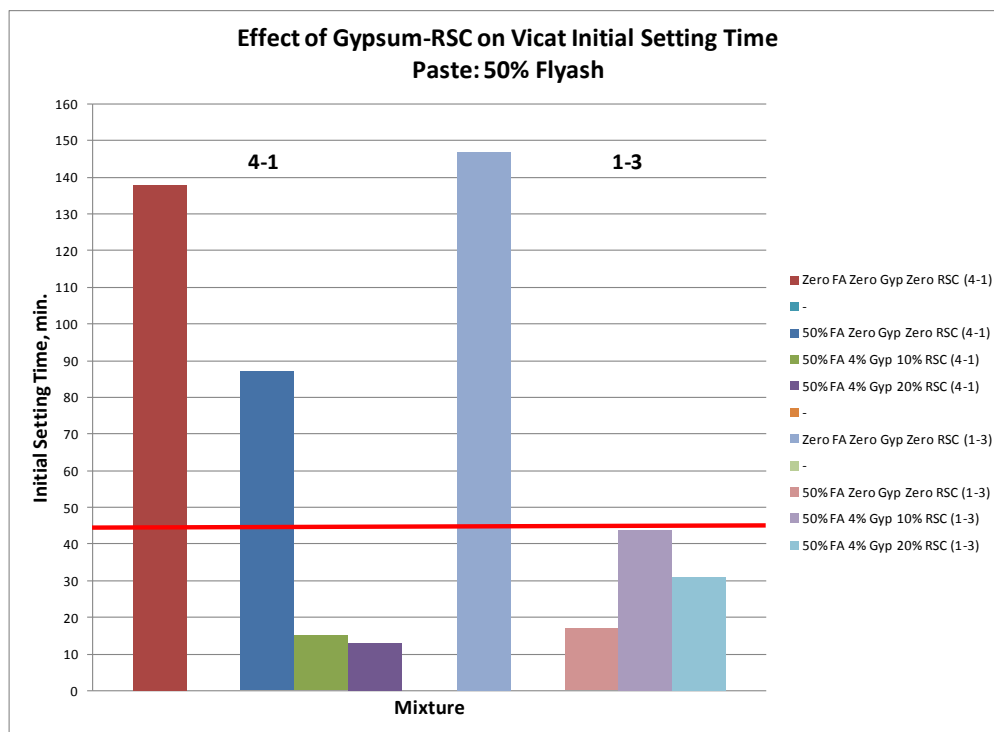
Figure 4.87 – Effect of Gypsum-RSC on Initial Setting Time, 50% Fly Ash Content
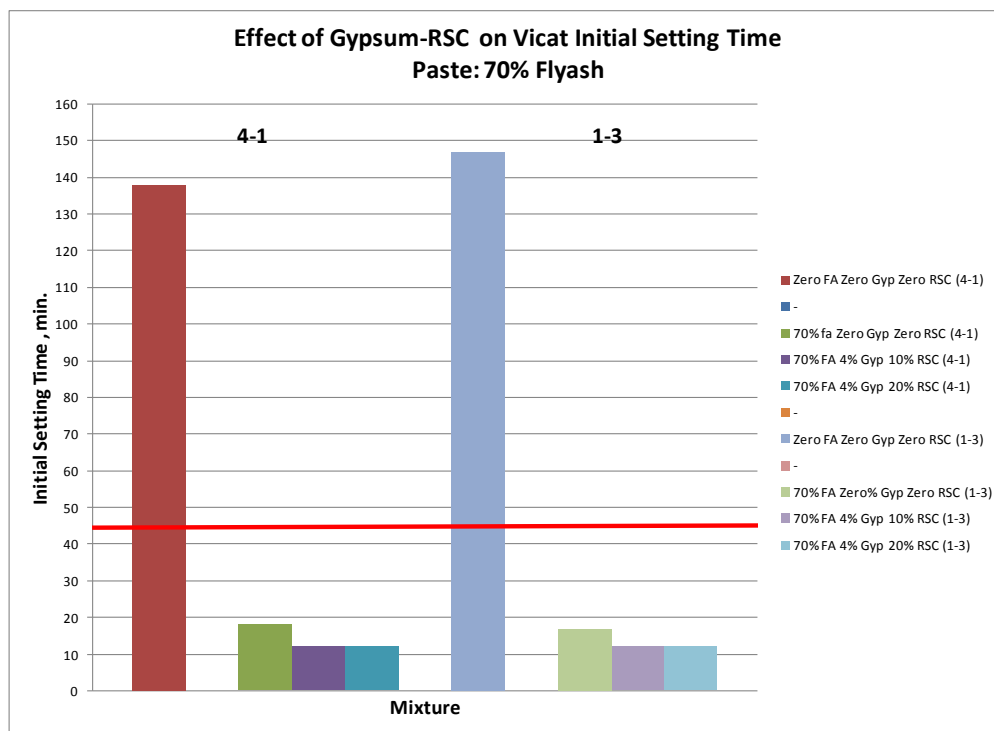
Figure 4.88 – Effect of Gypsum-RSC on Initial Setting Time, 70% Fly Ash Content

The effect of gypsum-RSC on early stiffening can be seen in **Figure 4.89**.

Generally, as RSC level increased from 10 to 20%, early stiffening potential increased.
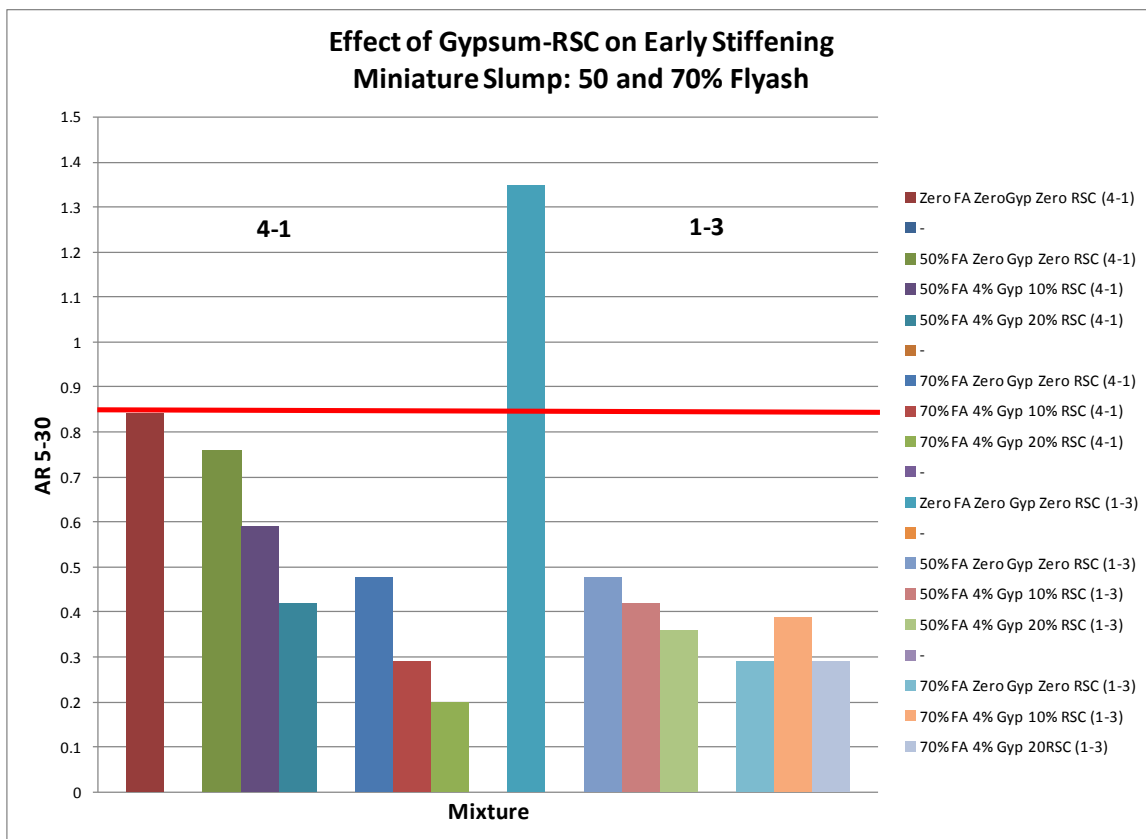
Figure 4.89 – Effect of Gypsum-RSC on Early Stiffening, 50 and 70% Fly Ash Contents

All Main Effects test results are tabulated in Appendix G.

4.5.2.9. Maximum Sulfur Trioxide Limit. The maximum sulfur trioxide (SO_3) limit for OPC and Class C fly ash is 3.0% and 5.0%, respectively for both current ASTM and the AASHTO specifications. In the mixtures in the Main Effects study, sources of SO_3 were OPC, fly ash, gypsum, and RSC. The combined SO_3 contents for the various mixtures (not including straight OPC base mixtures) ranged between 3.0 and 5.0 with one exception: the 1-3 blend at 70% fly ash, 4% gypsum, and 20% RSC. At a typical

maximum specification limit of 25% fly ash with OPC and fly ash at their maximum allowable SO_3 limits, the highest calculated combined SO_3 would be 3.5%. Thus, it is recommended that if a calculation of a given blend of materials shows a high combined SO_3 content, physical testing be conducted to assure that excessive expansion will not occur, especially if the concrete is going to be in a high sulfate service environment.

4.6. PASTE STUDY CONCLUSIONS

4.6.1. Background. In the Screening Study, 25 combinations of five Type I/II portland cements and five Class C fly ashes in paste form with no chemical or powder additives were tested by semi-adiabatic calorimetry, Vicat setting time, miniature slump, and compressive strength at one and 28 days. The two most reactive and least reactive combinations (defined by one day strengths) were further evaluated in the Main Effects Study.

In the Main Effects Study, the effects of two levels each of WR/HRWR, gypsum, lime, RSC, and gypsum-lime, and gypsum-RSC were determined. Except for the WR/HRWR experiment, all other mixtures contained the low (2.75 fl oz/cwt) dosage. Except for the gypsum level experiment, all other mixtures contained 4% gypsum by mass of fly ash. The lime levels were 5 and 10% and the RSC levels were 10 and 20%, both by mass of fly ash. Based on both the Screening Study and Main Effects Study, the following conclusions were drawn.

4.6.2. Fly Ash Replacement. In terms of the constituents (oxide content, etc) of the blends, as fly ash increased, CaO was reduced and aluminates, alkalis, and the aluminate/sulfate ratio increased. The total amount of the important oxides was a function

of the amounts present in the OPC, the individual fly ash, and the fly ash content of the blend.

In terms of when reactions occurred relative to straight OPC as characterized by calorimeter curve position, whether the curve was retarded or accelerated and the magnitude of reaction rate and peak height depended on the total chemistry of the blend. At high levels of CaO and low levels of aluminate, alkali, and aluminate/sulfate, as fly ash increased, the curves were increasingly delayed and the peaks were shorter. As the CaO dropped and the aluminate, alkali, and aluminate/sulfate increased to more moderate levels, the curves became shorter and broader, sometimes exhibiting two peaks. When the CaO was low and the aluminate, alkali, and aluminate/sulfate were high, the curves reversed and occurred earlier than straight OPC curves. The position of the curve was reflected in setting times, early strength achieved, and tendency for early stiffening. Thus, it is difficult to make general statements about what to expect with certain levels of fly ash in terms of physical properties without information on oxide contents, fineness, and glass content.

Fly ash reduced one day strengths at all levels of replacement. Fly ash usually reduced 56 day strengths at all levels of replacement, with one exception at 25%.

Fly ash effects on initial setting time were mixed. At 25%, retardation usually occurred. At 50%, both retardation and acceleration occurred. At 70%, many times acceleration occurred.

4.6.3. WR/HRWR. At the 0.40 *w/cm*, the use of WR/HRWR was necessary to restore workability. The effect of WR/HRWR generally was to slow down reactions and their outcomes. Calorimeter curves were usually delayed and one day strengths were

lower. However, the effect on setting times and early stiffening were mixed. Many times the setting time was accelerated, but sometimes retarded. Likewise, early stiffening was usually an issue, and but sometimes not. Beyond one day, strengths were usually increased. Overall, there was no clear advantage between the two dosage levels.

4.6.4. Gypsum. Gypsum addition generally usually delayed the calorimeter curves or was negligible. The higher dosage made a more pronounced effect. Setting time usually was retarded. Because in all four cases the setting time had been accelerated by the high fly ash substitution, retarding by gypsum was a positive benefit. Early stiffening tendencies were either improved or were negligibly affected. One day strengths were down, or negligibly affected, and 56 day strengths were not much affected. Overall, there was no clear advantage to either the 2 or 4% gypsum levels.

4.6.5. Lime. One day strengths were negligibly impacted, some severely low 7 day strengths were improved, and late strengths were negligibly impacted. The 5 % level of lime had a slight edge over the 10% level.

4.6.6. Rapid Set Cement. At all ages and fly ash contents at seven days and later, the addition of RSC significantly increased compressive strengths. At one day, strengths were increased, but marginally so. The 20% level usually was superior to the 10% level.

4.6.7. Gypsum-Lime. In three of the four cases, the gypsum-lime addition improved one day strengths, with little difference between the 5 and 10% levels. However, all 56 day strengths were lowered, with 10% level usually the worst by a small amount. The calorimeter curves were shifted to earlier times, with the 10% level earlier than the 5% level. The 10% lime mixture positions were almost restored back to where

the zero fly ash curves were. Initial setting times had been accelerated by the replacement of fly ash. Upon addition of gypsum-lime, the 4-1 blend was retarded at both levels of fly ash, approaching the zero fly ash values (an improvement), but there was little effect on the 1-3 blend setting times. The tendency to early stiffen was alleviated somewhat by gypsum-lime in every blend but one, with the 10% level usually better.

4.6.8. Gypsum-Rapid Set Cement. In all cases of gypsum-RSC addition, the calorimeter curves were accelerated. In three of the four cases, the gypsum-lime addition improved one day strengths, with a moderate advantage with the 20% RSC level. In all cases, the 56 day strengths were improved, some quite significantly. In regard to initial setting time, all four blends had been accelerated by the fly ash replacement, three of the four severely so. Unfortunately, addition of gypsum-RSC made it worse in one blend, was negligible in two others, and helped (retarded) somewhat in the fourth blend. Also, in almost all mixtures, the early stiffening tendencies were significantly worsened. It should be noted that the combined SO3 content in some of these mixtures is somewhat high.

4.6.9. Summary. To improve early strengths, lime, RSC, or gypsum by themselves were not particularly helpful. However, gypsum and lime together were effective, but lowered later strengths. Gypsum-RSC improved strengths at all ages. Gypsum by itself helped restore (retarded) the fly ash-accelerated HVFA calorimeter curve positions, as did gypsum-RSC. Gypsum-lime restored the curves almost to the zero fly ash positions. Early stiffening tendencies were alleviated by gypsum and gypsum-lime, but made worse by gypsum-RSC.

The dosages chosen for the concrete study were 4% (vs. 2%) gypsum because it controlled the fly ash-accelerated reactions best, 10% (vs. 5%) lime because in

combination with the 4% gypsum, it controlled the accelerated reactions best, and 20% (vs. 10%) RSC because it improved one day strengths best.

High calculated combined SO3 level mixtures should be checked via expansion testing for possible issues, especially if the concrete is going to be in a high sulfate service environment.

5. PHASE II – CONCRETE STUDY

5.1. EXPERIMENTAL DESIGN

5.1.1. Variables. The objective of the concrete properties study was to scale up the most promising powder additive combinations from paste to concrete and evaluate the mixtures in terms of plastic and hardened properties. Thus the mixture matrix included OPC-fly ash blends at two levels ("4-1" and "1-3) and fly ash at three levels (zero, 50 and 70%). WR dosage (nominal 2.75 fl oz/cwt), gypsum content (4%), lime content (10%), and RSC content (20%) were held constant.

5.1.2. Test Methods. Plastic concrete properties of interest were slump, air content, unit weight, concrete setting time, and water content (and *w/cm*). Hardened concrete properties were compressive strength, flexural strength (modulus of rupture = MOR), splitting tensile strength, modulus of elasticity (MOE), shrinkage, abrasion resistance, freeze-thaw resistance, permeability (rapid chloride penetration = RCP), and salt scaling resistance.

5.1.3. Mixture Designs. Because of concerns about possible salt scaling issues for pavements (PCCP), bridge decks (B-2 and MB-2), and barrier walls (B-1), it was decided to target the MoDOT structural mixture design (B). However, the mixture was designed to also meet the more stringent PCCP specification as a point of interest. After consulting MoDOT mixture design personnel for typical mixture designs that are approved by MoDOT, the design parameters were chosen.

Cement content and *w/cm* were chosen to not only meet specifications for mixtures B and PCCP, but to also be in line with typical approved mixtures. Choice of fly ash contents were carried forward from the paste study (50 and 70%).

In regard to slump, being locked into a certain water content by the fixed *w/cm* and fixed cementitious content rendered a stiff mixture (~1 in.) which would be practical for a slip-formed pavement mixture but not a structural mixture. The upper limit on fly ash was 70%; at this level, previous experience with the project materials indicated that the slump would be about 5 in. So, the mixture was locked in at 5 in. slump. To achieve a slump of 5 in. for the less-than-70% fly ash mixtures (zero and 50%), necessitated the use of admixtures: a combination of the required air entraining agent plus a WR.

It was anticipated that with a *w/cm* of 0.40, a WR, and a high quality coarse aggregate, would produce at least 4000 psi at 28 days for the base mixture (actual design was for 5170 psi (35.6 MPa)). Air content was the minimum required. Sand content was chosen at 40% which was typical for both mixture types. Choice of a coarse aggregate gradation was a D which would meet the 501 specification for the B concrete mixture, is used commonly for PCCP mixtures, and is readily available. A comparison of MoDOT 501 and 1005 (MoDOT, 2011) specifications, typical mixtures, and values used in this study are shown in **Table 5.1.**

The five mixture design proportions are given in **Table 5.2**. These were used for both the blends of OPC and fly ash, as the specific gravities of both cements were the same and both fly ashes were (surprisingly) the same.

Table 5.1 - Mixture Design Requirements, Typical Values, and Final Choices

	501 B	**Typical B**	**501 PCCP**	**Typical PCCP**	**Choice**
OPC, min., lbs/cy	525	535	535	564	564
Fly ash, at 25% max., lbs/cy	131	---	134	---	varied
w/cm, max.	0.51	0.45	0.50	0.40	0.40
Air content, min., %	5.0	6.0	5.0	6.0	5.0
Slump, max., in.	4	---	---	1.5	5
Comp. strength, min., psi	3000	---	4000	>4000	----
Sand, %	---	40	---	40	40
CA abs., max. , %	3.5	---	3.5	---	1.4
CA gradation	D or E	---	---	---	D
FA DRUW, lbs/cf	109	---	109	---	111.4

Table 5.2 - Proportions of Five Concrete Mixtures

Material	**Unit**	**Base Zero Fly Ash**	**Lime 50% Fly Ash**	**Lime 70% Fly Ash**	**RSC 50% Fly Ash**	**RSC 70% Fly Ash**
OPC	lbs	564	264	154	252	145
Fly ash	lbs	0	264	360	252	338
Gypsum	lbs	0	11	14	10	14
Lime	lbs	0	26	36	0	0
RSC	lbs	0	0	0	50	68
Water	lbs	226	226	226	226	226
CA, ssd	lbs	1877	1877	1877	1877	1877
FA,ssd	lbs	1249	1195	1175	1202	1186
Air (4-1)	fl oz/cwt	4.7	2.1	2.1	1.9	1.9
WR (4-1)	fl oz/cwt	5.3	2.8	1.9	3.6	2.8
Air (1-3)	fl oz/cwt	8.1	6.5	7.3	6.5	7.3
WR (1-3)	fl oz/cwt	5.0	4.0	4.9	5.3	6.2

5.2. REPLICATE SPECIMENS

For all plastic concrete tests only one specimen was tested. For the hardened concrete tests, usually three replicate specimens were tested. Two replicate cylinders were made for the RCP procedure, but each cylinder yielded two slices, thus totaling four replicate test values. There were two replicate shrinkage test specimens cast.

5.3. MATERIALS

5.3.1. General. The cement, fly ash, gypsum, lime, RSC, and WR/HRWR used in the concrete study were the same as were used in the paste study. Additional materials used in the concrete study are tap water, coarse aggregate, fine aggregate, and an air entraining agent. Cementitious material specific gravities are shown in **Table 5.3**.

Table 5.3 Cementitious Materials Specific Gravities

Cement 1	Cement 4	Fly Ash 1	Fly Ash 3	Gyp	Lime	RSC
3.15	3.15	2.686	2.685	2.00	2.34	2.98

5.3.2. Air Entrainment. The air entraining agent used was BASF MB AEA 90.

5.3.3. Aggregate. The coarse aggregate was St. Louis Limestone Formation, Ledges 1-7, Gradation D from Bluff City Minerals at Alton, Illinois. The fine aggregate was Missouri River sand. Aggregate properties are shown in **Table 5.4**.

5.4. TESTING EQUIPMENT AND PROCEDURES

5.4.1. Aggregate.

5.4.1.1. Specific Gravity and Absorption. Specific gravity of the coarse and fine aggregates was determined in accordance with ASTM C 127 and C 128, respectively (ASTM, 2012a; ASTM, 2012b).

5.4.1.2. Gradation. Sieve analyses coarse and fine aggregates was determined in accordance with ASTM C 136 and C117 (ASTM 2006b; ASTM, 2004).

5.4.2. Plastic Concrete.

5.4.2.1. Mixing. In order to assure uniform moisture contents in the aggregate used to mix fresh concrete, an aggregate preparation schedule was developed. First,

roughly 25 lbs (11 kg) of Jefferson City dolomite were tumbled in the concrete mixer for

five minutes in order to clean the drum out and loosen any hardened concrete on the fins

or in the drum. This aggregate was disposed of after tumbling. The drum mixer was a six

cu. ft. (0.17 m^3) capacity, variable speed mixer, pictured below in **Figure 5.1.**

Table 5.4 - Aggregate Characteristics

Test	Unit	CA	FA
Specific grav., ssd		2.66	2.64
Absorption	%	1.4	0.7
DRUW	lbs/cf	97.0	111.4
FM			2.73
NMS	in.	3/4	
Gradation	% passing		
1	in.	100	
¾	in.	92	
½	in.	53	
3/8	in.	26	100
#4		6	98.5
#8		4	92
#16			79
#30		3	50
#50			9
#100		3	1
#200		2.6	0.2

To prepare the aggregate for mixing, the coarse and fine aggregate were both

weighed, exceeding the estimated amount needed for a given batch by roughly 50 to 100

lbs. (23 to 46 kg). Coarse aggregate was mixed first, and then fine aggregate. Both

aggregates were mixed at a speed of "9" in the concrete drum for five minutes. Upon

completion of the mixing time, each aggregate was discharged into a separate mortar box,

mixed with a square pointed shovel, and then tightly covered with plastic sheeting.
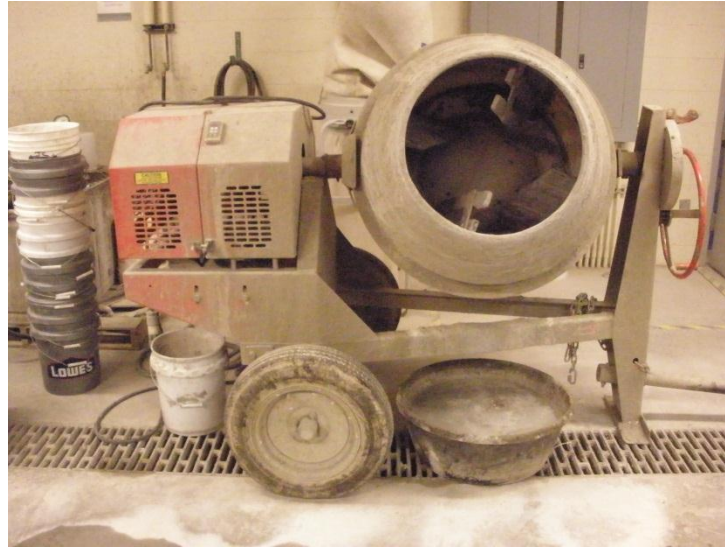
Figure 5.1- Six Cubic Foot Variable Speed Mixer

Three hours prior to mixing, the plastic sheet was momentarily removed in order to take moisture content samples. A shovel was used to mix the aggregate again, taking a moisture content sample from each aggregate bin. The plastic sheet was then replaced until it was time to batch out aggregates for the mix. Aggregate was dried for three hours in a forced air drying oven at 235 F (113 C). Immediately prior to concrete mixing, the moisture content samples were removed from the drying oven, weighed, and used to determine the necessary moisture content adjustments to be made to aggregate and batch water.

The mixing procedure used was a modified version of ASTM C 192 (ASTM, 2007). Prior to mixing fresh concrete, the mixer was "buttered" by adding several pounds of cementitious materials matching the mix design to the drum, adding water, and allowing this fluid to mix in the drum for at least five minutes, coating all surfaces of the inside of the drum. This fluid was discharged and wasted just prior to the beginning of fresh concrete mixing.

Batch water was separated into two buckets, one containing two thirds of the total batch water plus the total amount of air entraining agent, the other containing one third of the water, plus the water reducer. This procedure was recommended by the admixture technical representative to assist in loosening the very stiff mixture so that the Type A/F HRWR would have a chance of working properly. Next, the total amount of coarse aggregate was added to the drum, and the mixer was started on a speed setting of "12". The bucket of water containing air entrainment agent was then added, taking care to flush any fines on the sides of the mixer back into the aggregate. The sand was then added, and the mixer was run until the aggregates appeared well blended. Cement and the remaining water containing water reducer were then metered in so that the mix appeared uniform. After completion of addition of the mix constituents, the concrete was mixed at a speed setting of "15" for three minutes, subjected to a rest period of three minutes, and then remixed for a period of two minutes before discharging. Notably, the mixer was not covered during the three minute rest period as dictated in ASTM C 192.

Due to the large number of specimens combined with the limited capacity of the mixer, three batches were made for each mixture. The test methods assigned to each batch were chosen because of the potential for trying to correlate properties within the batch. Thus, one batch was for strength (compressive, flexural, and splitting) and modulus, the second for durability (freeze-thaw, rapid chloride penetration, salt scaling, and abrasion), and the third for shrinkage and setting time.

5.4.2.2. Temperature. Temperature of the concrete mixes was measured with an analog thermometer with a 5 in. (127 mm) probe length, and a resolution of one degree. Temperature of fresh concrete was conducted in accordance with ASTM C 1064 (ASTM,

2011b). The temperature of the batch was taken in a wheelbarrow immediately after discharge of the concrete from the drum.

5.4.2.3 Unit Weight. Air content of the concrete mixes was measured by means of a Type B pressure meter, and unit weight was measured in the air content bowl. Unit weight of fresh concrete was conducted in accordance with ASTM C 138 (ASTM 2012c). The same measure and concrete sample were used for the air content test immediately after determining the unit weight.

5.4.2.4. Slump. The slump of fresh concrete was determined in accordance with ASTM C 143 (ASTM, 2010a).

5.4.2.5. Air Content. The air content of fresh concrete was determined in accordance with ASTM C 231, using a type B pressure meter (ASTM, 2010c). This test was run upon the same measure and concrete sample used previously to determine unit weight. This often meant cleaning the rim of the bowl a second time after transporting it to a scale and back.

5.4.2.6. Water Content. A 1250 watt microwave from Panasonic was used to determine the microwave water content of fresh concrete. The sample was wrapped in a fiberglass cloth sheet approximately 20 in. x 20 in. (508 mm x 508 mm), and placed in a microwave-safe baking dish. A 1 in. (25 mm) wide metal scraper and a 2in. (25 mm) diameter ceramic pestle were used to break up the concrete sample. The microwave water content equipment is pictured below in **Figure 5.2**.

Figure 5.2 - Microwave Water Content Station

Microwave water content of fresh concrete was determined in accordance with AASHTO 318 (AASHTO, 2007). During the study, initially the sample was taken from the batch sometime after it had been discharged and during the time that the other tests specimen preparation had commenced. It was observed that after some time in the wheelbarrow, some batches would segregate, leading to areas of variable water contents in the batch. Sampling of this led to variable tested water contents. The results led to a refinement of the sampling/testing procedure. Ultimately, the sample for microwave water content was taken halfway through discharge of the drum and weighed immediately. The test was then conducted after the other fresh concrete tests had been completed.

In addition to determining the water content by the microwave method, it was also calculated based upon the amount of water actually batched. Using either of these two values, the *w/cm* can be calculated.

5.4.2.7. Setting Time of Concrete. The concrete time of set test was performed

using an Acme penetrometer from Humboldt. The concrete sample was passed over a #4

sieve, and collected in a 6 in. (150 mm) diameter cylinder mold, cut to a 6 in. (150 mm)

depth. Needles of varying diameter (1", ½", ¼", 1/10", 1/20", and 1/40") are attached to a

loading arm, and the load required to penetrate the concrete is recorded upon a dial gauge

on the penetrometer. The concrete time of set equipment is pictured below in **Figure 5.3**.

Concrete time of set was conducted in accordance with ASTM C 403 (ASTM, 2008c).

Samples were wet sieved over a #4 sieve after fresh concrete testing was completed, and

remixed by hand after a suitable amount of concrete had been sieved for the test.

Figure 5.3 - Concrete Time of Set Equipment

5.4.2.8. Curing Equipment. With the exception of freeze-thaw prisms, concrete

specimens were cured in a moist cure room at Missouri S&T. The moist cure room mists

water over the specimens in such a manner as to maintain at least 95% relative humidity at all times. Freeze-thaw prisms were cured in a saturated limewater bath, as were flexural strength beams for the final 24 hrs. before testing.

5.4.3. Hardened Concrete.

5.4.3.1. Compressive Strength. Four in. (100 mm) diameter concrete cylinders for compressive strength were cast in accordance with ASTM C 192 (ASTM, 2007). Placement consisted of two lifts, each being consolidated with 25 roddings with a 3/8 in. (9.5 mm) tamping rod, and 10 taps. Three replicate specimens were cast from each mixture, demolded after 24 hrs., moist-cured under standard curing conditions, and then tested at 28 days. Compressive strength of the 4x8 in. (100 mm x 200 mm) concrete cylinders was determined in accordance with ASTM C 39 (ASTM, 2012d). A 400,000 lb (181,600 kg) load frame from Forney was used in determining the compressive strength. Cylinders were capped with sulfur in accordance with ASTM 617 prior to testing. Cylinder diameter measurements were taken using calipers.

5.4.3.2. Modulus of Rupture. .Concrete beams were cast in accordance with ASTM C 192. Placement consisted of two layers, each layer rodded 72 times, tapped 12 times, and then spaded around the edges. Three replicate specimens were cast from each mixture, demolded after 24 hrs., moist-cured under standard curing conditions, and then tested at 28 days. Beams were cured in saturated limewater for the last 24 hours of curing prior to testing. Flexural strength of the concrete beams was determined in accordance with ASTM C 78 (ASTM, 2010d). A 200,000 lb. (90,800 kg) universal Tinius Olsen load frame was used in determining the flexural strength. An alignment jig constructed at Missouri S&T was used to ensure that the beam testing apparatus was aligned properly

with the top load being applied at third points. The flexural strength specimens were tested on a Test Mark third point loading beam testing apparatus. The testing apparatus is pictured in **Figure 5.4**.
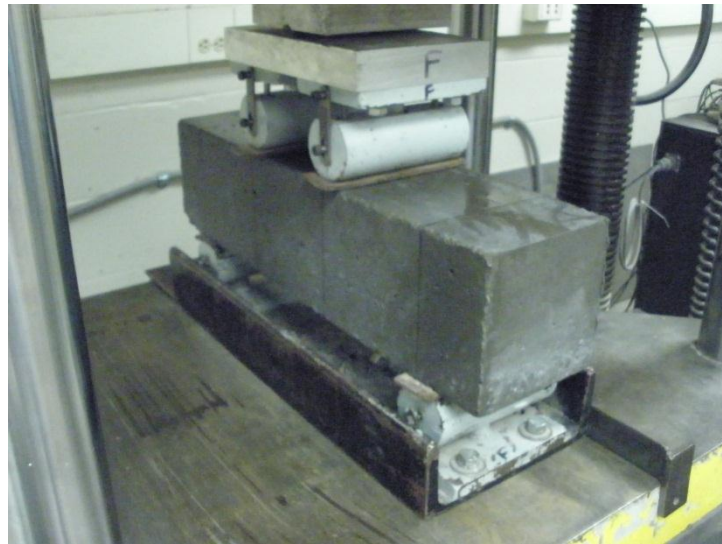
Figure 5.4 - Beam Testing Apparatus

5.4.3.3. Splitting Tensile Strength. Splitting tensile strength was determined on 6 in. (150 mm) diameter cylinders, cast in accordance with ASTM C 192. Placement consisted of three layers, each being consolidated with 25 roddings with a 5/8 in. (16 mm) tamping rod, and 10 taps. Three replicate specimens were cast from each mixture, demolded after 24 hrs., moist-cured under standard curing conditions, and then tested at 28 days. Splitting tensile strength was determined in accordance with ASTM C 496 using a 400,000 lb (181,600 kg) Forney compression load frame (ASTM, 2011c). A marking jig pictured below in **Figure 5.5** was used to mark diametral lines upon the specimens. The testing jig pictured in **Figure 5.6** was used to center and load the specimens. The testing jig was not available at the start of testing; therefore early testing was conducted

by manually centering the specimen below the crosshead, and using a piece of steel stock as a supplementary bearing block.

Figure 5.5 - Cylinder Marking Jig
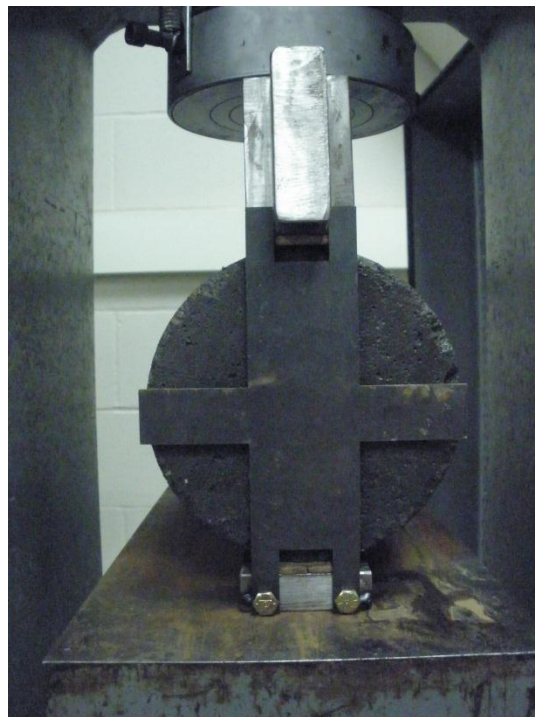
Figure 5.6 - Splitting Tensile Testing Jig

5.4.3.4. Modulus of Elasticity. Modulus of elasticity was determined on 6 in. (150 mm) diameter cylinders, cast in accordance with ASTM C 192. Placement consisted of three layers, each being consolidated with 25 roddings with a 5/8 in. (16 mm) tamping rod, and 10 taps. Three replicate specimens were cast from each mixture, demolded after 24 hrs., moist-cured under standard curing conditions, and then tested at 28 days. Modulus of elasticity was determined in accordance with ASTM C 469 (ASTM, 2010e). A 200,000 lb. (90,800 kg) Tinius Olsen universal load frame from was used. Each cylinder was secured in a yoke, which held an LVDT to measure axial compression during the test. Prior to testing, the concrete cylinders were sulfur capped to ensure planeness of loading surfaces.

5.4.3.5. Abrasion Resistance. Specimens for abrasion resistance were cast in one lift, consolidated with 96 roddings with a 5/8 in. (16 mm) diameter tamping rod, followed by 10 taps with a rubber mallet, and finally spaded around the edges. The specimens were 3.5 x 6 x 16 in. (89 x 150 x 406 mm). Two specimens were cast from each mixture, screeded with an aluminum float, demolded after 24 hrs., moist-cured under standard curing conditions, and then tested at 28 and 56 days. After the moist curing time, the specimens were surface dried using a towel. Abrasion testing was conducted in accordance with ASTM C 944 (ASTM, 2005a); however, the test was conducted at 300 rotations per minute instead of 200 rotations per minute, due to limitations of the drill press. A specialized abrasion head, constructed at Missouri S&T was used to abrade the concrete, and a weight was hung from the arm of the drill press, corresponding to a 44 lb. double load as noted in ASTM C 944. The abrasion testing equipment is pictured below in **Figure 5.7**.

Figure 5.7 - Abrasion Testing Equipment

The initial weight of each specimen slab was determined. A two min. abrasive action was applied to the specimen surface, the dust removed, and weight determined. Depth of wear was also determined at eight points at both the innermost and outermost abraded rings on the specimen using a digital caliper. This procedure was repeated twice more on the same spot, and the results averaged. Then, the whole procedure was repeated on two additional spots, for a total of three replicate tests. A typical tested specimen is shown in **Figure 5.8**. The abrasion resistance test procedure is included in Appendix H.
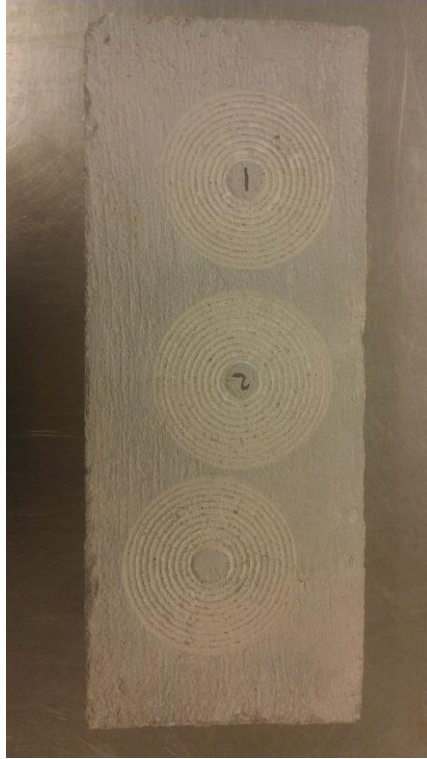
Figure 5.8 – Example of Abrasion Test Specimen

5.4.3.6. Drying Shrinkage. Two replicate specimens used to determine linear

shrinkage of concrete were cast in 4 in. (100 mm) inner diameter PVC molds, each 24 in.

(610 mm) long. Concrete was placed in two layers in the molds, and consolidated by

vibration. The next day, specimens were demolded by use of a Dremel tool with a

cutting head. DEMEC points were attached with a metal and concrete epoxy, and initial

readings were taken as soon as was feasible. Linear shrinkage of concrete was determined

in a modified version of ASTM C 157, using a cylindrical specimen with DEMEC points

attached (ASTM, 2008d). DEMEC points were attached with a metal and concrete epoxy

24 hours after casting. A DEMEC gauge was used in order to measure shrinkage of the

specimens. The specimens and DEMEC gauge are pictured below in **Figure 5.9**.

Figure 5.9 - DEMEC Gauge and Specimen

Initially, readings were taken daily, with increasing periods of time between readings as the rate of shrinkage of the specimens decreased. Data was then adjusted for the reference bar; the shrinkage was calculated in microstrain and plotted. The drying shrinkage test procedure is included in Appendix I.

5.4.3.7. Freeze-Thaw Durability. Freeze-thaw resistance, in terms of a Durability Factor, was determined in accordance with ASTM C 666 Method B (ASTM, 2008e). Durability factor (DF) is a relative measure, adjusting the relative dynamic modulus for the number of cycles that the specimen has undergone, relative to the total number of cycles it should undergo. Concrete prisms measuring 4.5 in. (114 mm) deep, 3.5 in. (89 mm) wide, and 16 in. (406 mm) long were cast with gauge studs at either end to Specimens were cast in two layers, and consolidated by means of 28 roddings, 10 tappings, and spading around the perimeter of the specimens. Three specimens were cast from each mixture. After demolding, freeze-thaw prisms were cured in a saturated limewater tank until the date of testing. The prisms were transported to MoDOT's

Central Testing Laboratory between 14 and 21 days of age, and were tested there at age 35 days. Testing was conducted according to ASTM C 666 Method B.

5.4.3.8. Salt Scaling. Three replicate specimens for salt scaling resistance were cast in molds 12 x 12 x 4 in. deep (300 x 300 x 100 mm) in one lift and rodded 72 times. Initially, specimens were cast at a full 4 in. (100 mm) depth with a broomed finish, and a 1 in. (25 mm) high, 1 in. (25 mm) wide mortar dam was built atop the finished surface with the aid of an angle iron backer. After consultation with technicians from MoDOT, however, the casting procedure was revised. The molds for scaling resistance specimens were under filled, and the concrete surface finished approximately an in. (25 mm) below the top surface of the mold. This surface was broomed, and a 1 in. (25 mm) high, 1 in. (25 mm) wide mortar dam was built atop the finished surface against the steel mold.

Scaling specimens were cured in the moist cure room for 14 days, after which they were subjected to a 14 day drying period prior to testing. Between 14 days and 21 days, the scaling specimens were transported to MoDOT central testing laboratories for testing in accordance with ASTM C 672 (ASTM, 2003). The mold and finished specimen are shown in **Figures 5.10** and **5.11.**

5.4.3.9. Rapid Chloride Penetration. Two replicate concrete cylinders 4 in. (100 mm) in diameter were cast for use in the rapid chloride permeability test. These cylinders were placed and consolidated in the same manner that the compressive strength cylinders were. Concrete was placed in two lifts, and each lift was rodded 25 times with a 3/8" diameter tamping rod before being tapped 10 times. Samples were transported to MoDOT Central Testing Laboratory between 14 and 21 days of age for testing according to ASTM C 1202 (ASTM, 2012e).

Figure 5.10 – Salt Scaling Mold

Figure 5.11 – Salt Scaling Specimen

5.5. RESULTS AND DISCUSSION

5.5.1. Plastic Concrete Test Results.

5.5.1.1. Slump. Glenium 7500 water reducer was used in all 10 concrete mixes in order to adjust the slump to 5±1 inches. In **Table 5.2** was shown the dosages used for each mix. For the 4-1 combination, as would be expected (Bouzoubaa, et al., 2007), less

water reducer was required to achieve a 5 in. (27 mm) slump as the amount of fly ash in the mix increased. Mixes with rapid set cement as an activator required more water reducer than did those with calcium hydroxide as an activator. The rapid hydration of rapid set cement led to a more rapid rate of slump loss than calcium hydroxide, and the dosage of rapid set cement was 20% by weight of fly ash, or twice that of the dosage used for calcium hydroxide.

For the 1-3 combination, the trend is not as clear. Mixes using rapid set cement as an activator required higher dosages of water reducer than those using calcium hydroxide for the same reasons outlined before. However, increasing fly ash content in these mixes led to an increase in the required dosage of water reducer. Rapid slump loss was noticed during mixing for fly ash mixes in the 1-3 combination, so it is possible that rapid aluminate reactions due to the fly ash meant that a higher dosage of water reducer was necessary in order to achieve a target slump. There were 35 batches made in the concrete study; the average slump was 5.1 in., with a range of 4 to 7 in.

5.5.1.2. Air Content. BASF's MB-AE-90 air entrainment admixture was used in all 10 concrete mixes in order to adjust the air content to $5\pm0.75\%$. In **Table 5.2** was shown the required dosages in oz/cwt to achieve this air content. For the 4-1 combination, the required dosage of air entrainment agent was lower at higher percentages of fly ash replacement. This is likely tied to the increased workability seen with these mixes, therefore requiring a lower dosage to entrain the same amount of air. Very little difference was noted in air entrainment dosages between those mixes utilizing calcium hydroxide as an activator and those utilizing rapid set cement as an activator.

For the 1-3 combination, again, no difference was noted in air entrainment dosages between those utilizing calcium hydroxide and those utilizing rapid set cement as activators. As in the case of the water reducer, fly ash mixes initially required less air entrainment agent to achieve a given air content, though the required dosage increased as the fly ash content increased from 50% to 70%. Again, this is partially due to the more rapid rate of slump loss. Additionally, the fly ash used in the 1-3 combination had a much greater Loss-on-Ignition (LOI) and was darker in color than that used in the 4-1 combination, indicating higher carbon content. Fly ash mixes with higher carbon content typically require more air entrainment admixture to achieve a given air content. For the 35 concrete batches, the average air content was 5.2% with no batches outside the target range of 4.0 to 6.0 %.

5.5.1.3. Microwave Water Content. Although great care was taken to correct the water content of each concrete batch for moisture content of the aggregate, it was decided to begin checking the water content by the microwave method, AASHTO T318 (AASHTO, 2002). Using the water content and knowing the cement content, the *w/cm* can be calculated. The average difference in *w/cm* in the concrete study was only 0.006, however, there was a fair amount of scatter in the results. As mentioned previously, as experience was gained, the sampling method was refined. Part of the reason for the scatter in results may have been due to the timing and location of the sampling. It was observed that waiting to sample from the completed batch sometime after mixing resulted in samples of varying consistency. From this limited experience, it is felt that the microwave method may be a practical tool for field checking of *w/cm* from ready mix

operations. The method is used routinely by such agencies as the New York and New Jersey Port Authority.

5.5.1.4. Time of Set. Time of set was determined on each of the 10 concrete mixtures tested for this project. **Figure 5.12** below details the initial and final set times determined for the 4-1 combination.
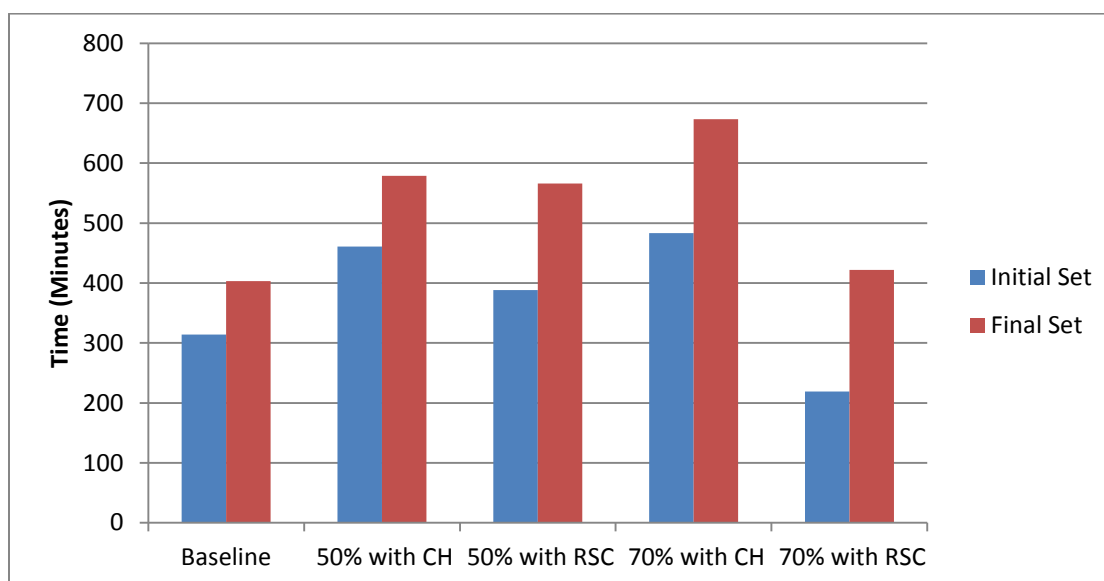
Figure 5.12 - Initial and Final Set Times for the 4-1 Combination

The addition of gypsum-lime to fly ash mixtures caused both the initial and final set to increase for mixes incorporating calcium hydroxide as an activator. The effect was more pronounced at the 70% fly ash replacement rate. Mixes incorporating rapid set cement as an activator fared better than their calcium hydroxide counterparts in reducing the lengthened time of set due to fly ash substitution. Notably, at 70% replacement of cement with fly ash, the rapid set cement mixture brought the time of set down considerably more than at 50% replacement of cement with fly ash. This discrepency is likely due to the fact that since activator levels are determined as a percentage of fly ash,

more rapid set cement is present in the 70% fly ash mixture than the 50% fly ash mix,

resulting in a decreased time of set.

The results of time of set tests on combination 1-3 are pictured below in **Figure
5.13**. Results on the 1-3 combination are very similar to those found for the 4-1

combination. At 50% fly ash replacement the rapid set cement mixture responds in a

similar way to the calcium hydroxide mix, whereas at 70% fly ash replacement, the rapid

set cement mixture exhibits a marked decrease in set time from the calcium hydroxide

mixture. The setting time results are tabulated in Appendix J.
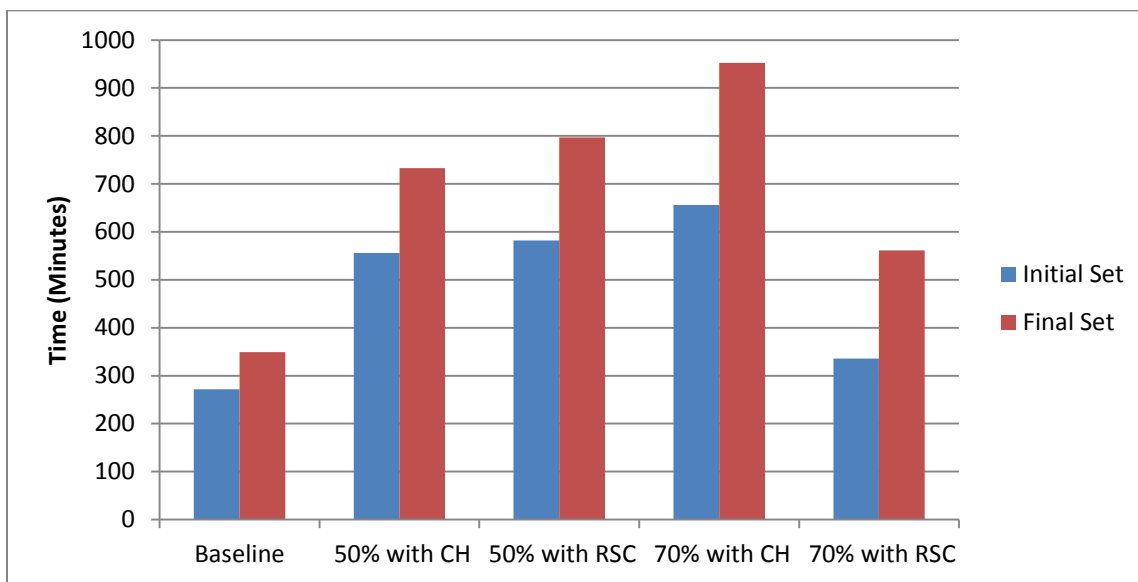
Figure 5.13 - Initial and Final Set Times for the 1-3 Combination

In most cases, powder additives retarded concrete setting time. This is in contrast

to the results of the paste study where in all cases the additives followed the acceleration

of the fly ash replacement for these particular cementitious blends. In the case of the 1-3

mixtures, the WR/HRWR dosage was greater than that used in the paste study. Whether

this had an effect is unclear.

5.5.2. Hardened Concrete Test Results.

5.5.2.1. Compressive Strength. An outlier analysis was performed in accordance with ASTM E178—there were two outlier test results, which were discarded. Results from the 4-1 combination are presented in **Figure 5.14**, below. All fly ash mixtures, regardless of replacement percentage, suffered in terms of short term strength gain compared to the baseline mixture. However, both 4-1 blends at 50% fly ash with either lime or RSC met or exceeded the 1000 psi (6.9 MPa) minimum threshold. By seven days of age, however, the 50% fly ash mixtures had begun to exhibit more reasonable strengths, exceeding 3000 psi (20.7 MPa)(the MoDOT structural B mixture min. 28 day strength). In fact, they reached 2750 psi (19.0 MPa) (a typical form removal minimum) in 5 to 6 days. They continued to gain strength, approximating the baseline mixture strengths by 28 days (exceeding 4000 psi (27.6 MPa) which is the PCCP mixture 28 day min.) and at 56 days exceeding baseline strengths, topping 5000 psi (34.5 MPa). Mixtures with 70% fly ash replacement exhibited greatly lowered strengths when compared to baseline mixtures, or even their 50% fly ash replacement counterparts at all ages, although they almost achieved 3000 psi (20.7 MPa) at 28 days and 3500 psi (24.1 MPa) at 56 days. The difference in strength due to activator selection was small at most ages, though mixtures using rapid set cement were always somewhat stronger than mixtures using calcium hydroxide as an activator. In comparison to the paste study results, the trends in strength for concrete followed the trends shown for paste, although the RSC's superiority was more pronounced in the paste results.
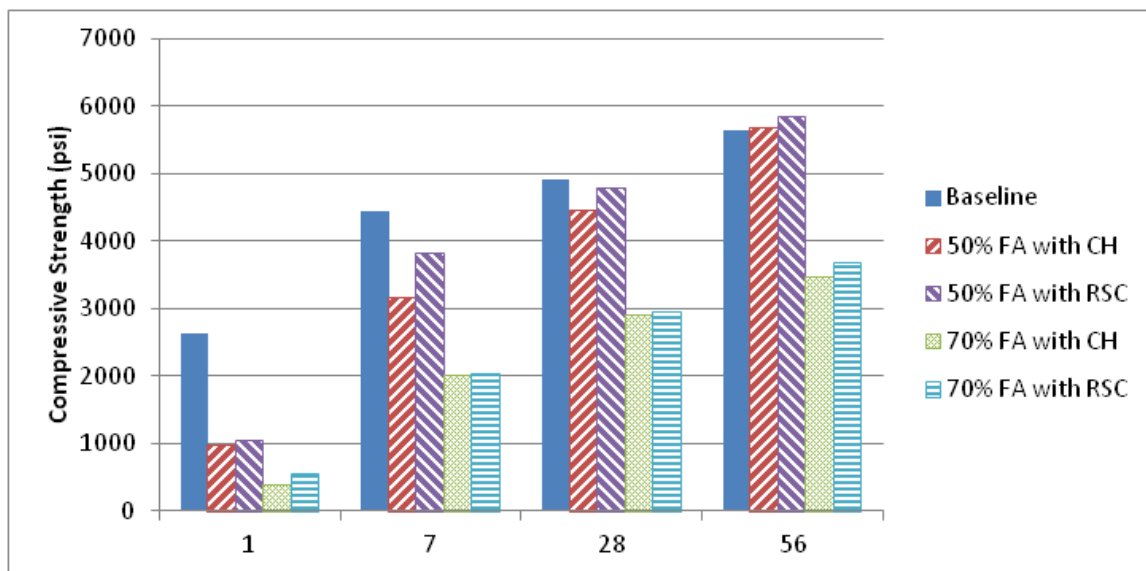
Figure 5.14 - Compressive Strengths for Combination 4-1

Results from the 1-3 combination are presented in Figure 5.15, below. All fly ash mixes for this combination exhibited lower strengths than the baseline concrete mixture at all ages. For the 50% fly ash replacement level, mixtures using calcium hydroxide as an activator showed slightly greater strengths than mixtures using rapid set cement as an activator. The 70% fly ash mixes displayed lower strengths than the 50% fly ash mixtures, as expected. None of the fly ash mixtures reached 1000 psi (6.9 MPa) at one day. The 50% fly ash mixtures reached 2750 psi (19.0 MPa)(a typical form removal minimum) in 5 to 6 days, exceeded 4000 psi (27.6 MPa) at 28 days, and were equal to or greater than 5000 psi (34.5 MPa) at 56 days. The 70% fly ash mixture with 20% RSC exceeded 3000 psi (20.7 MPa) at 28 days, and both activated 70% fly ash mixtures exceeded 3000 psi (20.7 MPa) at 56 days. In comparison to the paste study results, the trends in strength for concrete followed the trends shown for paste for lime, but RSC showed superior strengths at one and 56 days in the paste results.
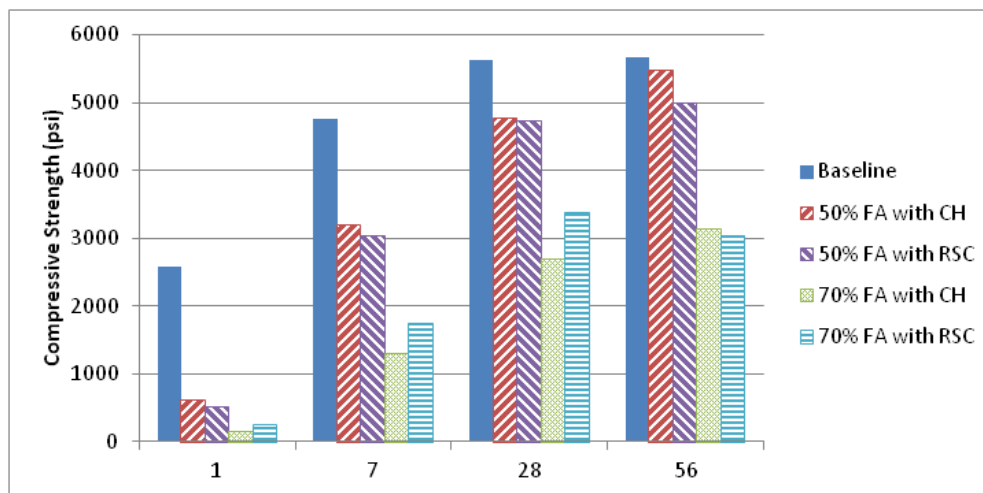
Figure 5.15 - Compressive Strengths for Combination 1-3

The compressive strength results are tabulated in Appendix J.

5.5.2.2. Flexural Strength (MOR). An outlier analysis was performed: there were no outlier test results. Results from the 4-1 combination are presented below in **Figure 5.16**. At 50% replacement of cement with fly ash with both activators, the 28 day flexural strengths were close to the base mixture and were at nearly 700 psi (4.8 MPa). At the 70% replacement level, there was a notable loss in flexural strength, more so with the calcium hydroxide mixture than the rapid set cement mixture.
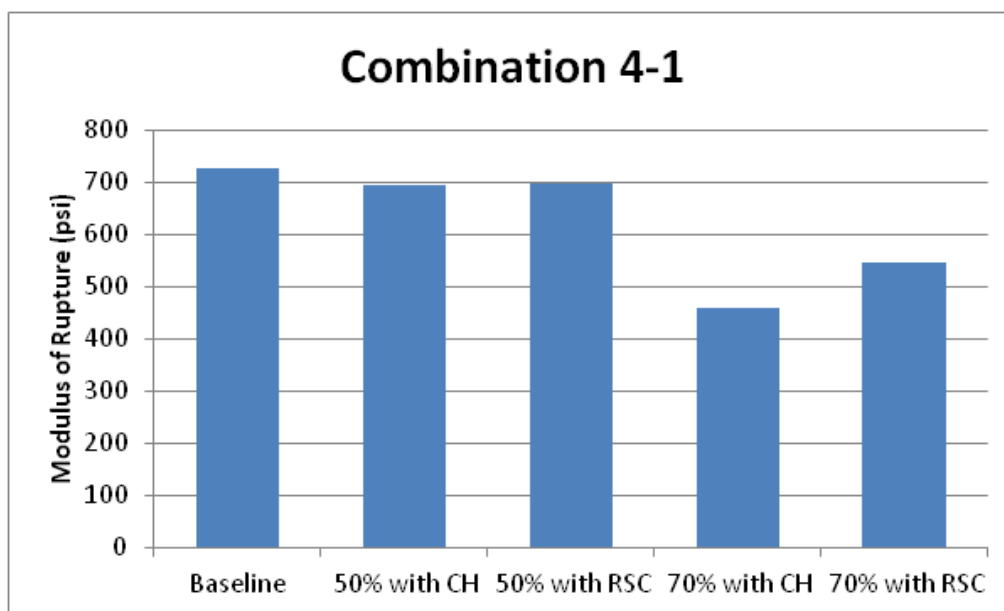
Figure 5.16 - Flexural Strength of Combination 4-1

Results from the 1-3 combination are presented below in **Figure 5.17**. At 50% replacement of cement with fly ash, calcium hydroxide and rapid set cement mixtures performed similarly, though a greater loss of strength was observed here than with combination 4-1. At 70%, another drop in strength is seen, with the rapid set cement mixture providing a greater flexural strength than the calcium hydroxide mixture. The flexural strength results are tabulated in Appendix J.

The loss of flexural strength moving from 50% fly ash replacement to 70% fly ash replacement is consistent with work by Naik, et al (1995), showing that as Class C fly ash content increases, the flexural strength suffers. It is possible, however, if the flexural strength testing had been conducted at later ages, that higher volume fly ash mixtures may have exhibited greater flexural strength in the longer term.
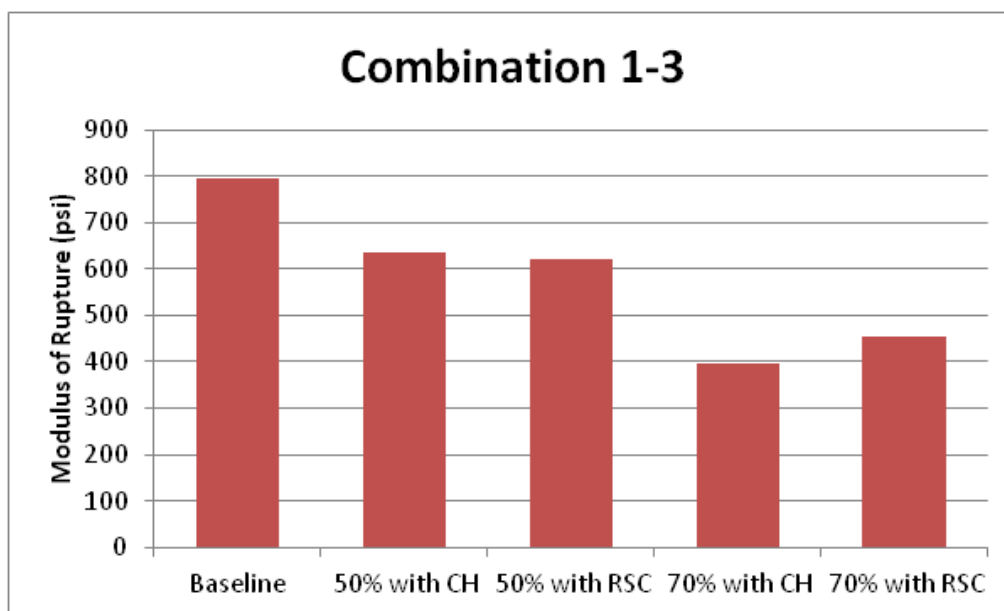
Figure 5.17 - Flexural Strength of Combination 1-3

5.5.2.3. Splitting Tensile Strength. An outlier analysis was performed which revealed that there was one outlier test result, which were discarded. Results from the 4-1 combination are shown below in **Figure 5.18**. At 50% fly ash substitution, splitting tensile strength results were greater than the baseline mixture, while at higher levels of fly ash substitution, the splitting tensile strength was reduced. Results from the 1-3 combination are shown in **Figure 5.19**. The 50% fly ash replacement mixes show a small loss in splitting tensile strength, with a larger loss present at 70% fly ash replacement. In both 4-1 and 1-3 combinations, rapid set cement appears to be a more effective activator at 70% replacement.

The drop in splitting tensile strength from 50% fly ash replacement to 70% fly ash replacement falls in line with previous research showing a lowered splitting tensile strength with increased Class C fly ash content (Naik, et al, 1995). The majority of the splitting tensile strengths at 28 days fall within 8.9% to 10.7% of the compressive

strength at 28 days, with one mix exhibiting a splitting tensile strength 12.8% of the

compressive strength. Previous research has shown that splitting tensile strengths are

expected to fall within 8% to 10% of the compressive strength of concrete, and this

appears to be fairly true (Rivest, et al, 2004). The splitting tensile strength results are

tabulated in Appendix J.
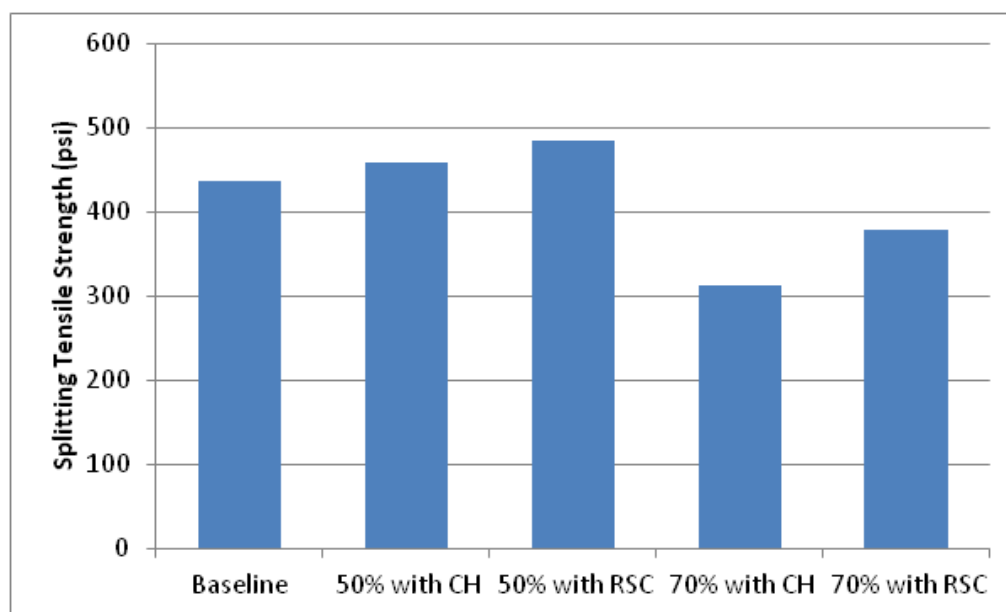
Figure 5.18 - Splitting Tensile Strength of Combination 4-1
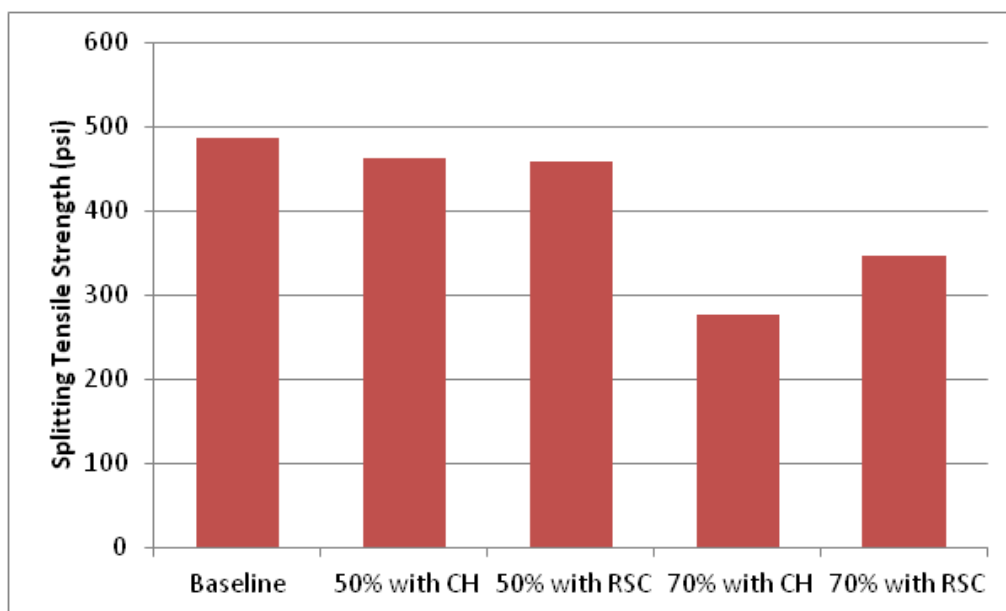
Figure 5.19 - Splitting Tensile Strength of Combination 1-3

5.5.2.4. Modulus of Elasticity. No outliers were found in the MOE dataset.

Results from the 4-1 combination are shown in **Figure 5.20**, and from the 1-3

combination in **Figure 5.21**. In both the 4-1 and 1-3 combinations, the 50% fly ash

mixes show a similar or slightly increased modulus of elasticity, indicating a stiffer

concrete. At 70% replacement of cement with fly ash, all concrete mixtures exhibit a

lower modulus of elasticity, with those 70% fly ash mixtures using rapid set cement as an

activator suffering the smallest loss in modulus.

It has been suggested that the increased modulus of elasticity of the high volume

fly ash concretes could be due to unreacted particles acting as fine aggregates to

contribute to the rigidity of the concrete (Rivest, et al, 2004). This could likely explain

why even the 70% fly ash concrete mixtures exhibited a modulus of elasticity around 4

million psi, despite a drastically lowered compressive strength. The modulus of elasticity

results are tabulated in Appendix J.
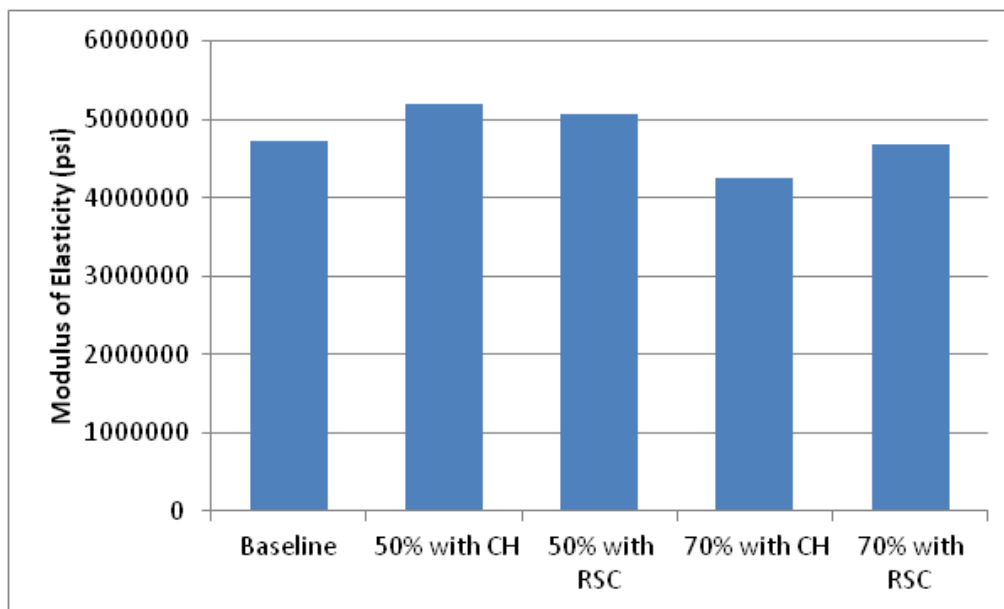
Figure 5.20 - Combination 4-1 Modulus of Elasticity
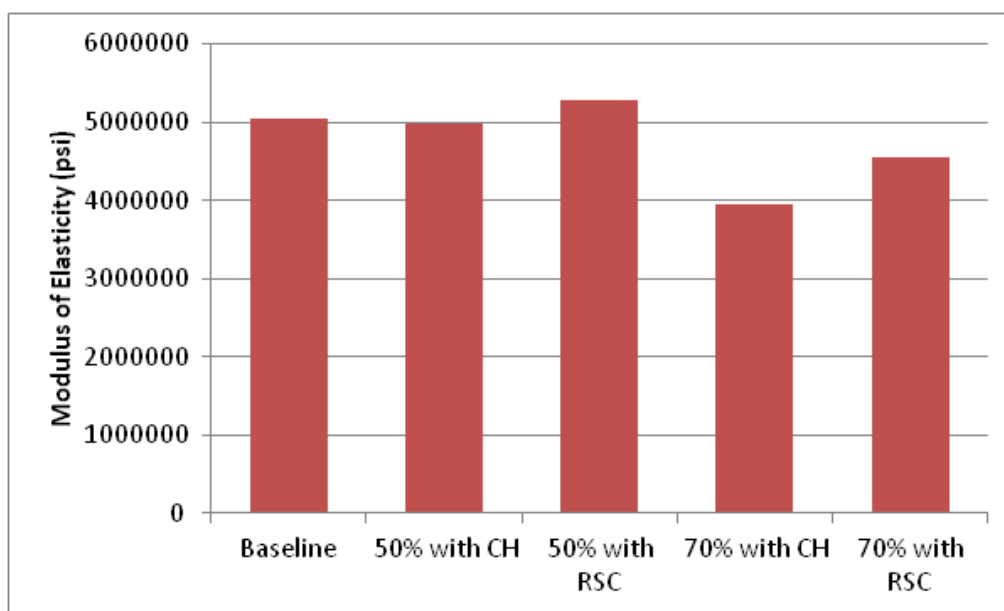
Figure 5.21 - Combination 1-3 Modulus of Elasticity

5.5.2.5. Abrasion Resistance. Outlier analyses of abrasion data showed one mass test and one depth of wear test result to be outliers—these were discarded. Abrasion resistance was measured in both mass loss and depth of wear of the abrasion specimens

in three replicates. **Figure 5.22** shows a strong correlation between the two measured methods of abrasion resistance.
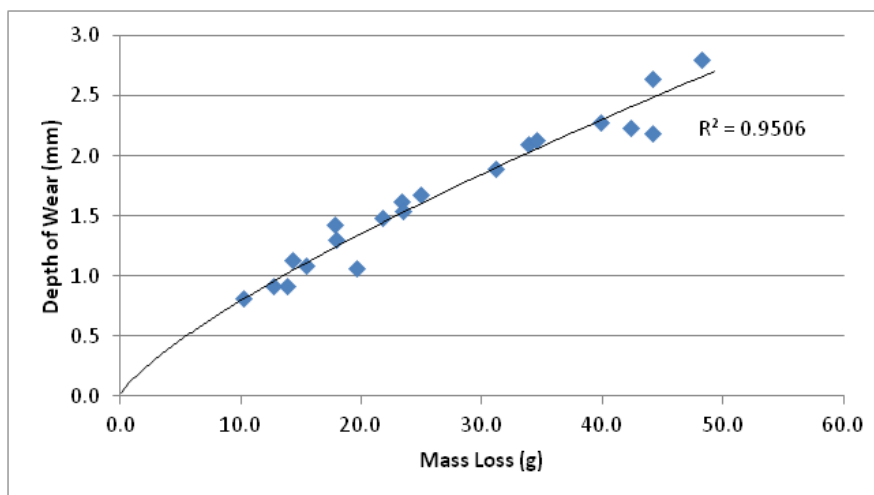
Figure 5.22 - Mass Loss/Depth of Wear Correlation

In all cases, HVFA concrete mixes showed less resistance to abrasion than their baseline counterparts. Between 28 days and 56 days of age, the HVFA concrete mixes did gain some abrasion resistance, though in every case they still fared more poorly than their baseline counterparts. For combinations 4-1, the 50% fly ash mix using calcium hydroxide as an activator came closest to matching the performance of the baseline concrete, while for 1-3 the RSC activator did better. Mass loss for each mix at 28 and 56 days is plotted in **Figure 5.23** for combination 4-1, and in **Figure 5.24** for combination 1-3. Some scatter is evident in the baseline mixture data, as made apparent by 56 day abrasion tests of the baseline mixes being quite similar or higher than 28 day abrasion tests despite having higher compressive strengths at 56 days. The abrasion results are tabulated in Appendix J.
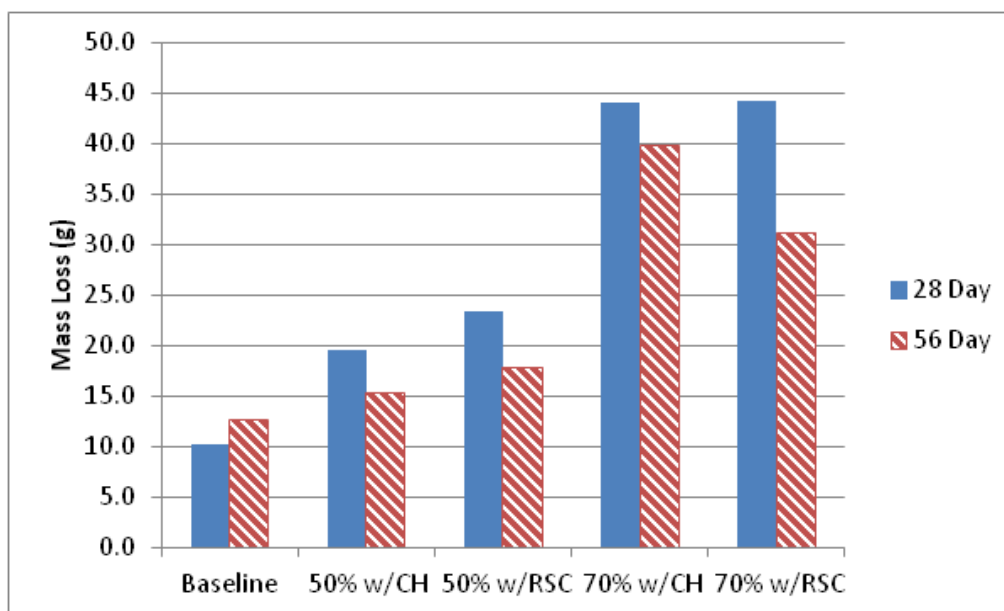
Figure 5.23 - Abrasion Resistance Mass Loss for 4-1
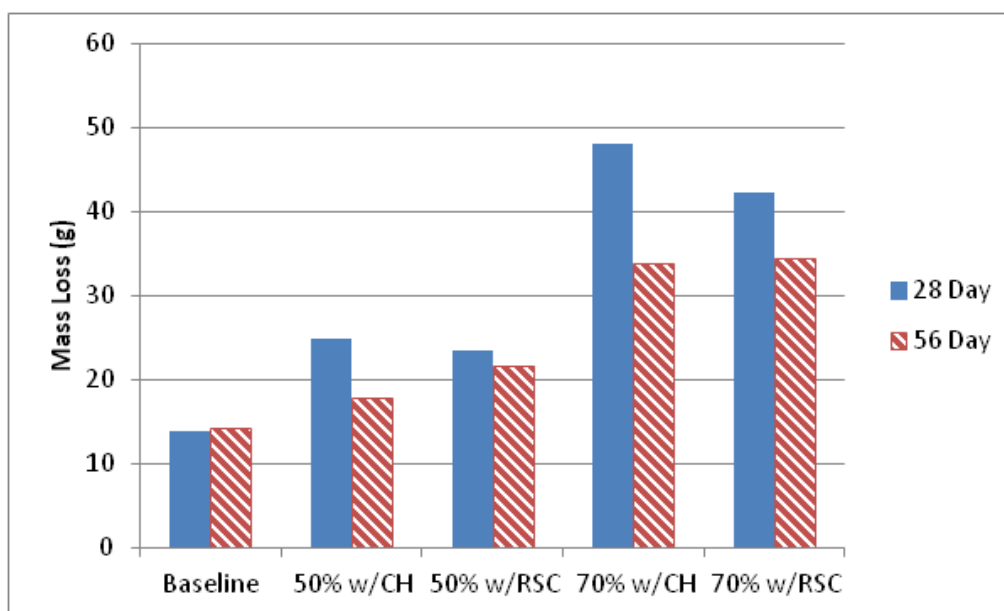
Figure 5.24 - Abrasion Resistance Mass Loss for 1-3

Figures 5.25 and **5.26** detail the depth of wear for each mix and show similar

results as the mass loss data. This data seems in agreement with research by Naik, Singh,

and Ramme on abrasion resistance of high volume Class C fly ash concretes: they noted

that replacement of cement with fly ash at low dosages (20% to 50%) fly ash seems to not greatly influence abrasion resistance of the concrete, while higher cement replacements show lowered resistance to abrasion. They also reported a gain in resistance with time. The authors also noted the significant effect of varying fly ash sources on abrasion resistance (Naik, et al, 2002).

Overall, the loss of abrasion resistance with increasing fly ash replacements is expected because of a similar effect on compressive strength, which correlates highly with abrasion resistance. This correlation between compressive strength and mass loss is illustrated in **Figure 5.27**, and between compressive strength and depth of wear in **Figure 5.28.**
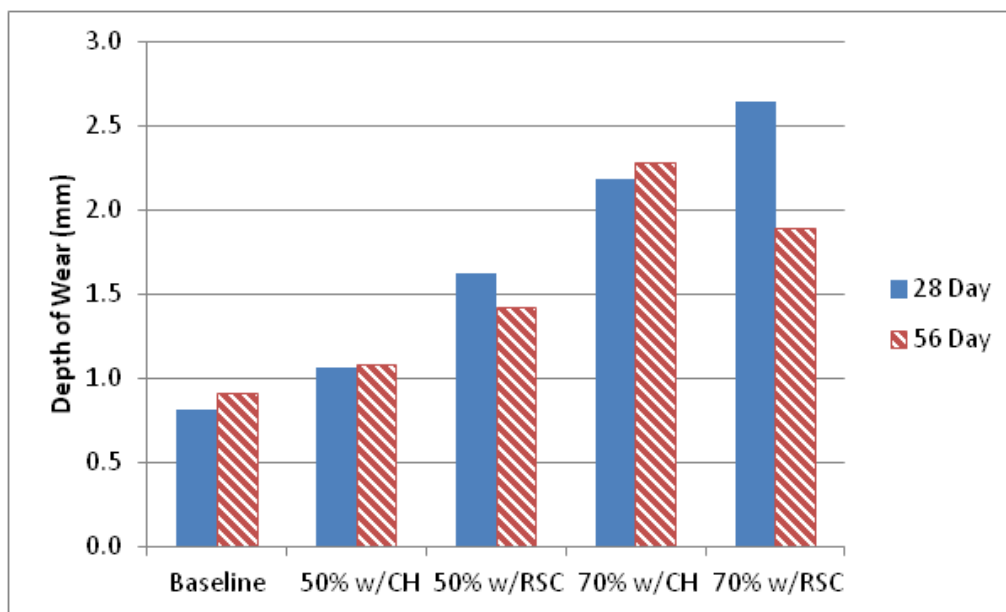
Figure 5.25 - Abrasion Resistance Depth of Wear for 4-1
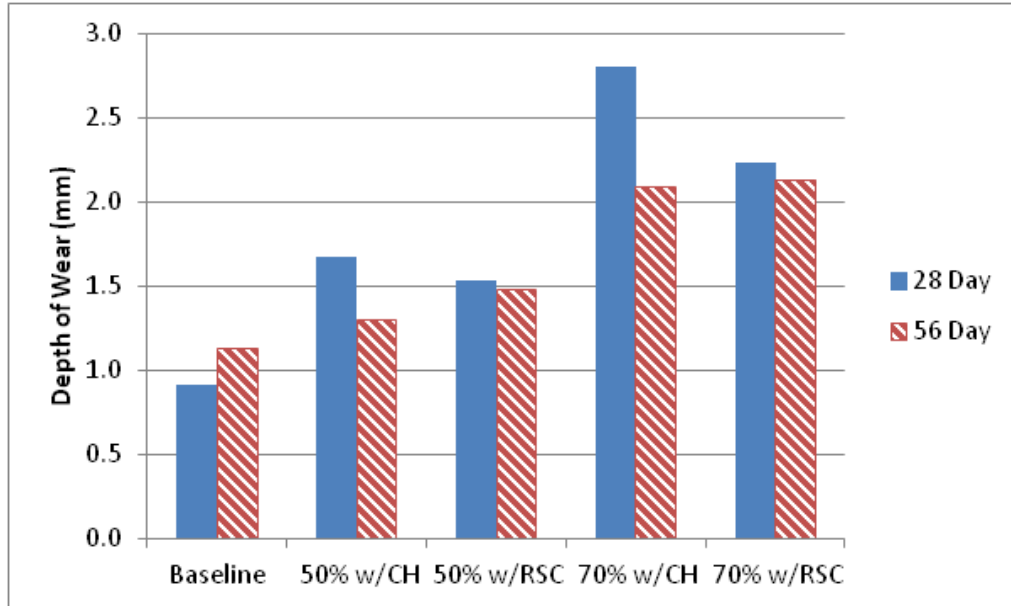
Figure 5.26 - Abrasion Resistance Depth of Wear for 1-3
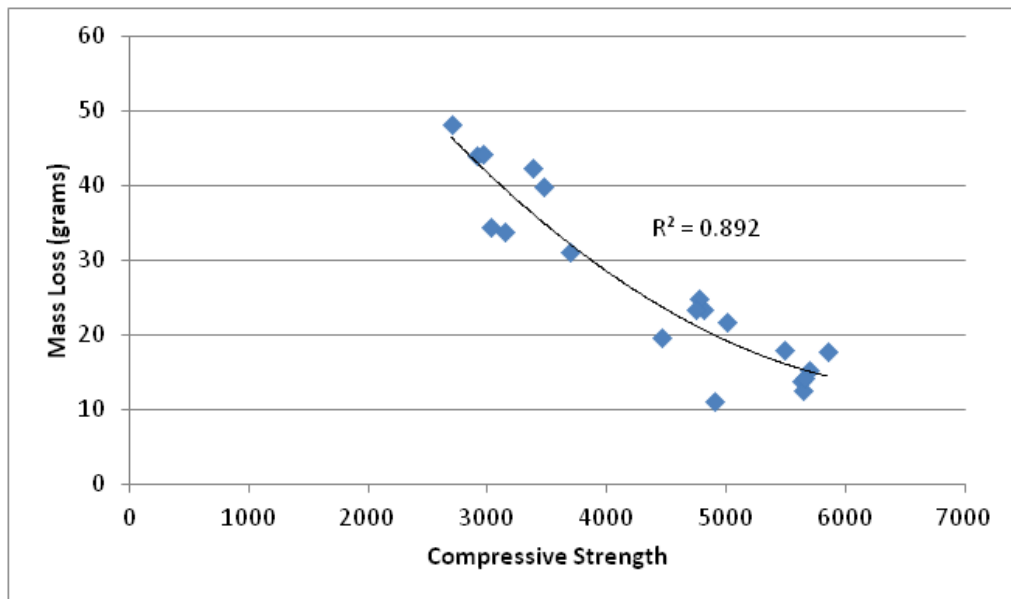
Figure 5.27 - Mass Loss versus Compressive Strength
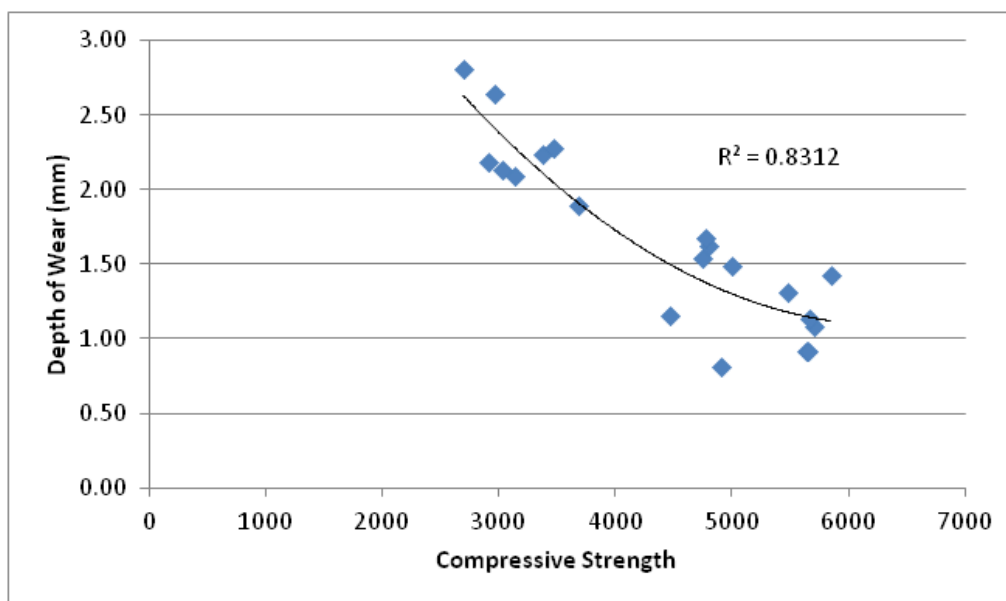
Figure 5.28 - Depth of Wear versus Compressive Strength

5.5.2.6. Drying Shrinkage. Linear shrinkage was measured on cylindrical specimens with two lines of DEMEC points applied at 180 degrees from each other. **Figure 5.29** below shows the shrinkage curves for combination 4-1, and **Figure 5.30** shows the shrinkage curves for combination 1-3. In all cases, fly ash mixes plotted below the baseline mix, meaning that these mixes incurred less shrinkage. The slopes of the lines parallel the baseline curve closely, making it unlikely that the fly ash mixes will cross the baseline curve and incur greater shrinkage. This lower shrinkage could be due to the decreased amount of water reducer needed in fly ash mixes, though this explanation is unlikely to explain the reduced shrinkage in combination 1-3, due to the need for increased water reducer dosages from the baseline in some cases. The lower shrinkage of high volume fly ash concrete mixes falls in line with results from Rivest, et al, suggesting that unhydrated cementitious material within the high volume fly ash mixes may be acting as aggregate and restraining the specimens from shrinkage. While

Rivest et al. used a lower *w/cm* for fly ash concretes and attributed the lower water content to decreased shrinkage of the HVFA mixes, it is clear that other factors are at work (Rivest, et al, 2004).
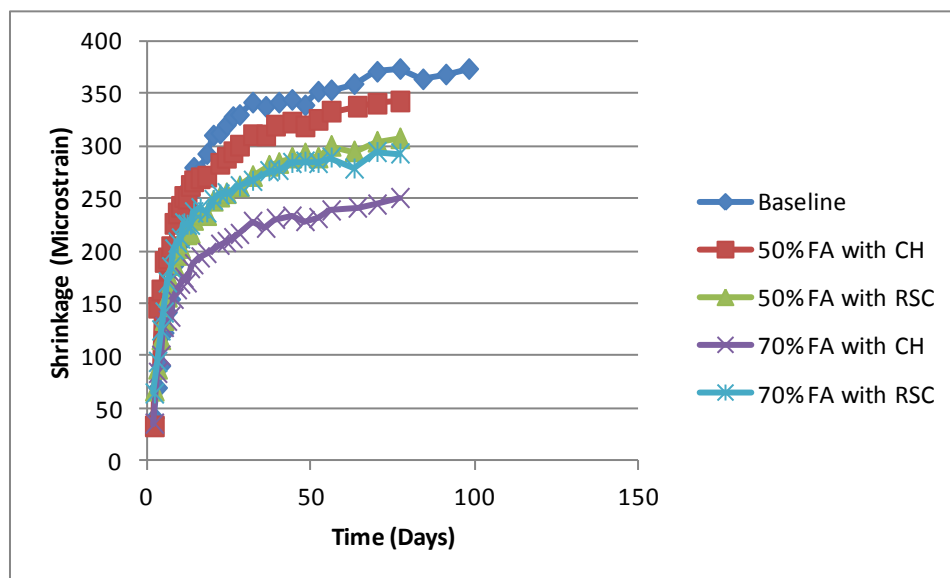
Figure 5.29 - Shrinkage Curves for Combination 4-1
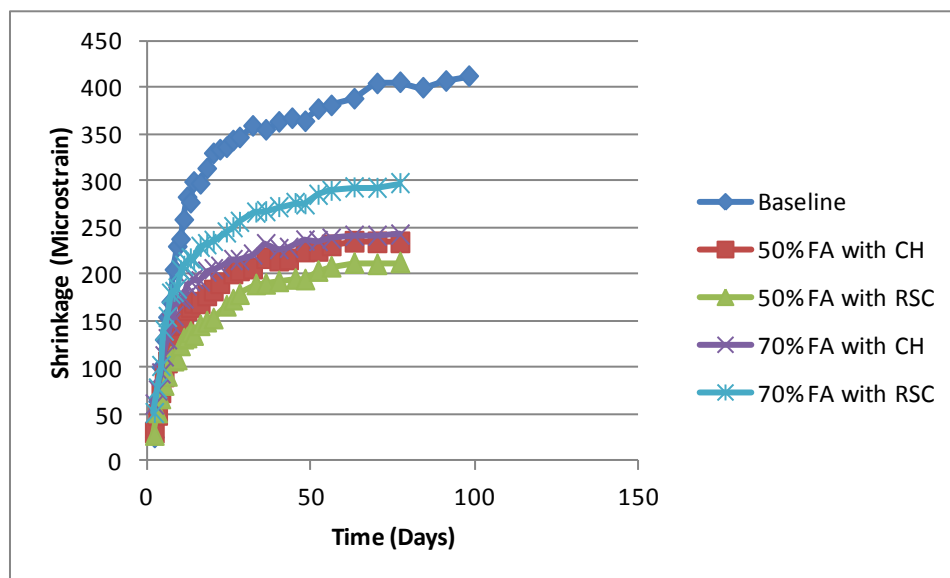
Figure 5.30 - Shrinkage Curves for Combination 1-3

5.5.2.7. Rapid Chloride Permeability. Outlier analyses of RCP test result to be an outlier—this was discarded. The rapid chloride permeability (RCP) test is a direct measure of electrical conductivity rather than an actual permeability test. However, this test shows good correlation with more intensive chloride ponding tests. This test was conducted on two cylinders for each concrete mix at 28 days of age. Two slices were taken of each cylinder, for a total of four measurements of charge passed. These four measurements were subject to an ASTM E 178 outlier analysis, and only one outlier was found. Permeability classes for each mix were determined in accordance with Table X1.1 from ASTM C 1202.

Figure 5.31 below shows the RCP test results for the most reactive combination, 4-1. At 50% replacement of cement with fly ash, both calcium hydroxide and rapid set cement mixes exhibited greatly decreased permeability, with an adjusted charge passed of less than half of that exhibited by the baseline mix. At 70% replacement, however, both calcium hydroxide and rapid set cement mixes proved to be more permeable than the baseline mix. It is important to note, however, that this test was conducted at 28 days, and as the 70% fly ash mixes approach 100% hydration, they may exhibit a more impermeable microstructure. In both cases, rapid set cement mixes had a more drastic effect on the permeability than calcium hydroxide.

Figure 5.32 shows the results of the RCP test on the least reactive combination, 1-3. Results for this combination are less clear cut, with 50% fly ash mixes exhibiting somewhat similar permeability to the baseline mix. The 50% fly ash mix utilizing rapid set cement as an activator decreased the permeability from the baseline mix by a slight amount, while the mix utilizing calcium hydroxide was more permeable than the baseline

mix. At 70%, both mixes exhibited high permeability, with the mix utilizing calcium hydroxide as an activator passing too high a charge to finish the test. Therefore, as the test could not run for the full 6 hours, no data for this test is provided. The compressive strength results are tabulated in Appendix J.
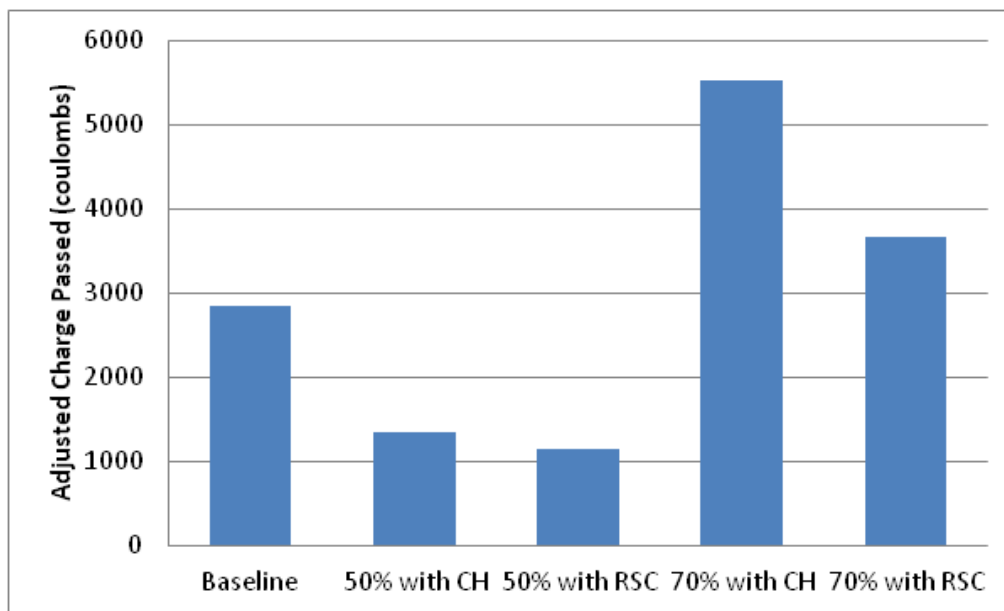
Figure 5.31 - Rapid Chloride Permeability Results for 4-1 Mixes
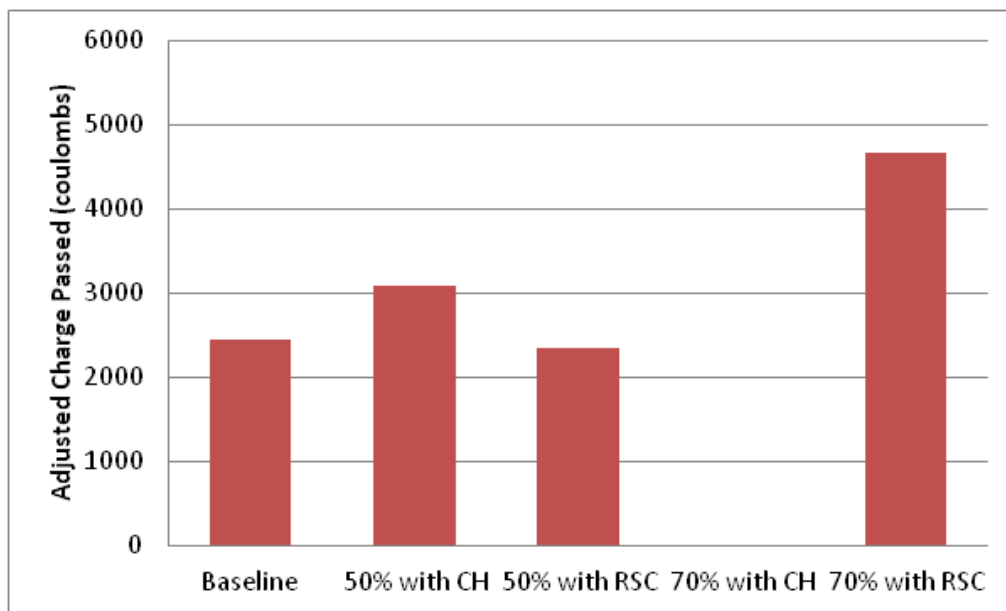
Figure 5.32 - Rapid Chloride Permeability Results for 1-3 Mixes

Previous research shows fly ash mixtures at 58% replacement exhibiting fairly low charges passed, with values falling off drastically at 91 days and 1 year (Bilodeau, et al. 1994; Gu, et al., 1999; Bouzoubaa et al., 2007). In the present study, the most reactive mix combination (4-1) shows similarly decreased chloride ion permeability at 50% fly ash content. Possible reasons for the higher charge passed at 70% for the 4-1 combination and for both 50% and 70% fly ash replacement of the 1-3 mix could be due to the test being conducted at the relatively early age of 28 days, when pozzolanic activity of the fly ash may not contribute significantly until 56 or 90 days of age, and therefore unreacted fly ash particles act as filler rather than hydration products, increasing the porosity of the paste microstructure.

5.5.2.8. Freeze-thaw Resistance. Three replicate beams were cast and tested for each mixture freeze-thaw resistance at 35 days of age; no outliers were found. Freeze-thaw resistance was measured by means of the durability factor (DF) in accordance with

ASTM C666, Method B. Freeze-thaw results for combinations 4-1 and 1-3 may be seen

in **Figure 5.33** and **Figure 5.34** below. All fly ash mixtures had DF's greater than 90.

The data suggests that the inclusion of fly ash, regardless of which powder activator is

used in the mix, significantly improves the durability factor from that of the baseline mix,

with 70% fly ash mixes in some cases showing a higher durability factor than those

containing 50% fly ash. The freeze-thaw results are tabulated in Appendix J.

While their concretes were not air entrained, this increased durability of high

volume fly ash concretes seems to be in line with previous work showing that higher

volume fly ash concretes resist freezing and thawing more than their cement-only

counterparts (Galeota, et al, 1995), and it shows high durability factors for fly ash mixes,

in line with other research which showed high volume fly ash mixes being able to

withstand severe freezing and thawing conditions, exhibiting high DF's (≥96) (Bilodeau,

et al, 1994).
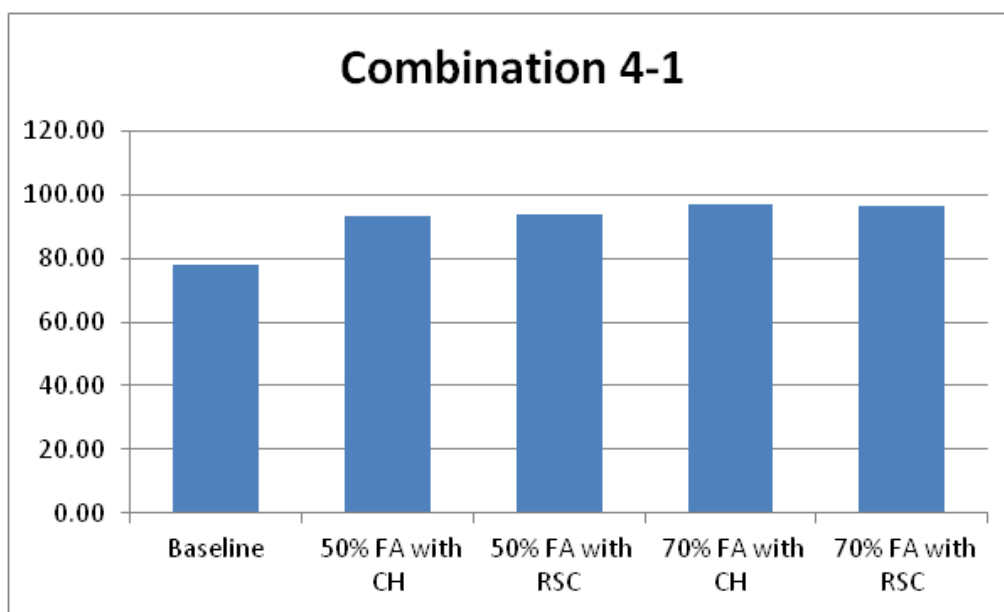
Figure 5.33 - Durability Factors of 4-1 Combinations
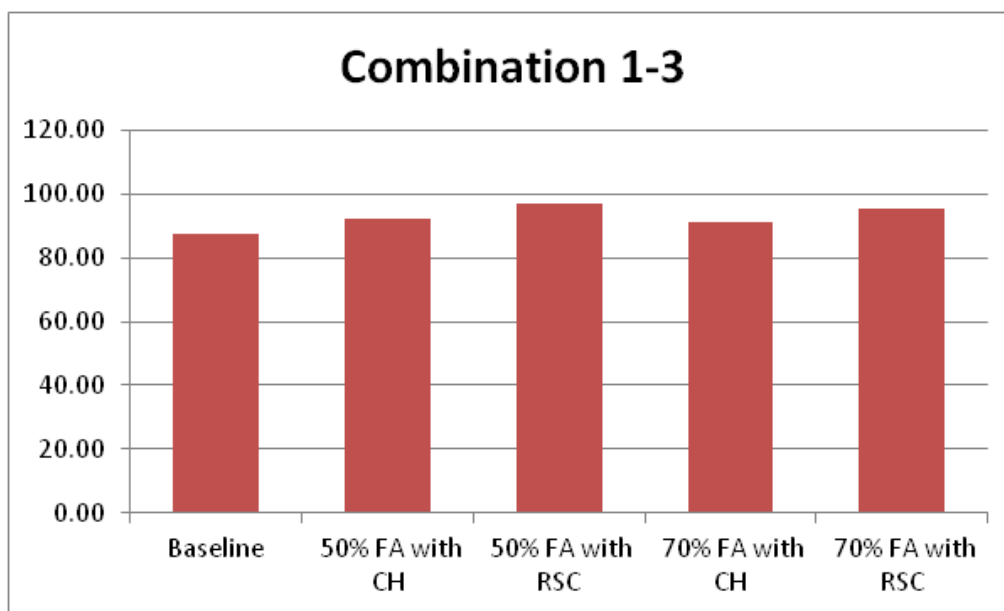
Figure 5.34 - Durability Factors of 1-3 Combinations

5.5.2.9. Salt Scaling Resistance. Three replicates of each mixture were tested for scaling resistance. Specimens were visually rated every five cycles, and rankings typically matched across all three replicate specimens. Small variations in finishing procedure may have led to differing rankings between specimens although most tests showed no variation between replicates. The results are shown in **Figure 5.35**. The baseline mixtures performed adequately (Scaling Scale ≤ 2), showing only very slight scaling (blend 4-1 rated 1 and blend 1-3 rated 2). This suggests that the molding and finishing procedures were adequate. Most fly ash mixtures showed severe scaling (rating = 5), defined by ASTM C 672 as coarse aggregate being visible over the entire surface of the specimen. Two mixtures (blend 1-3) fared slightly better: the 50% fly ash with RSC had a rating of 4, and the 70% fly ash with RSC was a 3. The mixtures containing 70% replacement of cement with fly ash show a much more rapid scaling than those containing 50%, albeit with the same end result. This tendency toward severe scaling

seems to mirror previous findings where eight different fly ashes with both high calcium

contents and low calcium contents (corresponding to Class C and Class F) were

examined. At 58% fly ash replacement, all 16 of the mixes showed severe scaling after

50 cycles according to ASTM C 672 (Bilodeau, et al., 1994). Results are tabulated in

Appendix J.
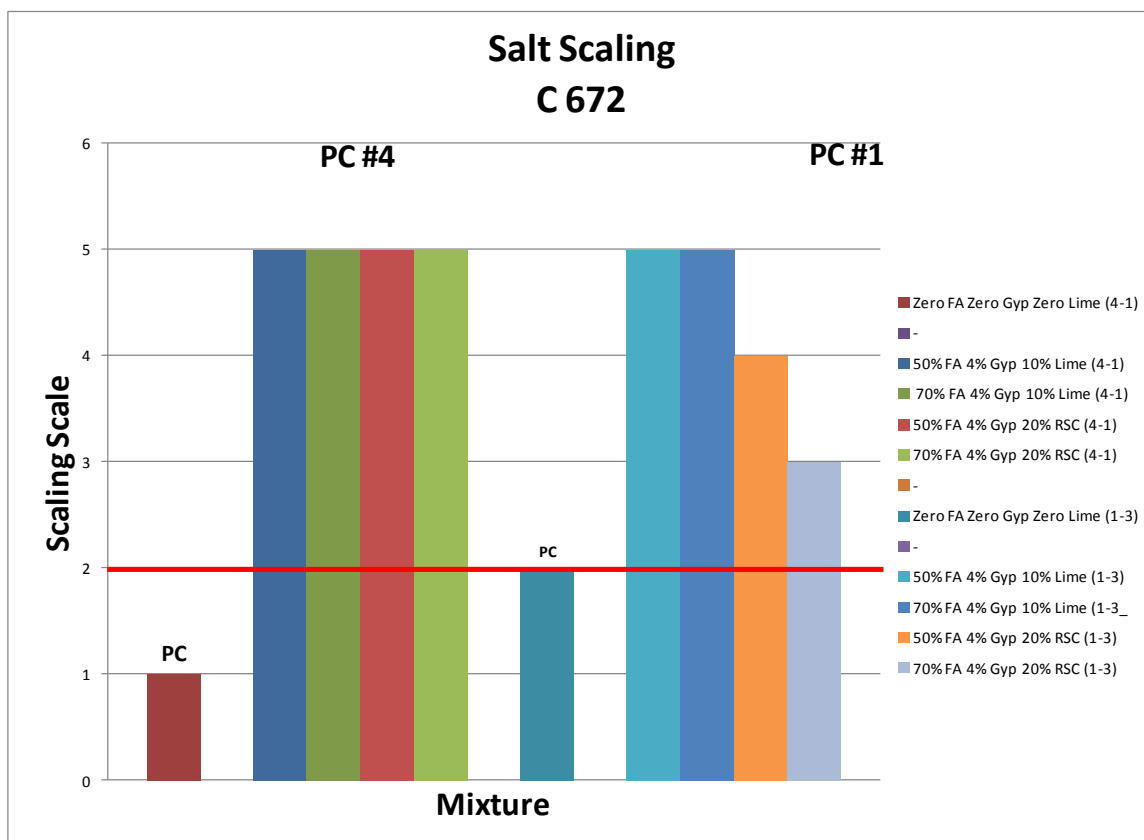
Figure 5.35 – Salt Scaling Results

6. SUMMARY AND CONCLUSIONS

In the Paste Screening Study, 25 combinations of five Type I/II portland cements and five Class C fly ashes in paste form with no chemical or powder additives were tested by semi-adiabatic calorimetry, Vicat setting time, miniature slump, and compressive strength at one and 28 days at room temperature. The two most reactive and least reactive combinations (defined by one day strengths) were further evaluated in the Main Effects Study.

In the Paste Main Effects Study, the effects of two levels each of WR/HRWR, gypsum, lime, RSC, and gypsum-lime, and gypsum-RSC were determined. Except for the WR/HRWR experiment, all other mixtures contained the low (2.75 fl oz/cwt) dosage. Except for the gypsum level experiment, all other mixtures contained 4% gypsum by mass of fly ash. The lime levels were 5 and 10% and the RSC levels were 10 and 20%, both by mass of fly ash.

The objective of the Concrete Properties Study was to scale up the most promising powder additive combinations from paste to concrete and evaluate the mixtures in terms of plastic and hardened properties. Thus the mixture matrix included OPC-fly ash blends at two levels ("4-1" and "1-3) and fly ash at three levels (zero, 50 and 70%). WR dosage (nominal 2.75 fl oz/cwt), gypsum content (4%), lime content (10%), and RSC content (20%) were held constant. The following are conclusions reached from the study of HVFA.

6.1. FLUIDITY

Increasing fly ash contents increased fluidity as evidenced by a greater spread of paste in the miniature slump test, and by decreasing required dosages of WR/HRWR to maintain fluidity in the concrete slump test. One exception to this was the 1-3 blend which required additional WR/HRWR. In all cases, the mixtures containing RSC need more WR/HRWR than their lime counterparts.

6.2. AIR ENTRAINMENT

As fly ash content increased, the required dosage to maintain 5% air decreased.

6.3. MICROWAVE WATER CONTENT

Within the confines of a limited use in this study, the microwave water content test method appears to have potential for field checking of the water content (and hence w/cm) of plastic concrete in the field.

6.4. REACTION TIME

Reaction time was evaluated by a combination of tests: semi-adiabatic calorimetry, Vicat setting time, and miniature slump early stiffening. Whether a given mixture behaved normally or was accelerated or retarded was a function of many variables, including the characteristics of the OPC and fly ash in conjunction with each other, type and level of powder additives used, dosage of WR/HRWR, and the type of test method used for evaluation.

At the 0.40 w/cm, the use of WR/HRWR was necessary to restore workability. The effect of WR/HRWR generally was to slow down reactions and their outcomes. Calorimeter curves were usually delayed and one day strengths were lower. However, the effect on setting times and early stiffening were mixed. Many times the setting time was accelerated, but sometimes retarded. Likewise, early stiffening was usually an issue, and but sometimes not. Beyond one day, strengths were usually increased. Overall, there was no clear advantage between the two dosage levels.

Fly ash effects on initial setting time were mixed. At 25%, retardation usually occurred. At 50%, both retardation and acceleration occurred. At 70%, many times acceleration occurred.

Gypsum addition generally usually delayed the calorimeter curves or was negligible. The higher dosage made a more pronounced effect. Setting time usually was retarded. Because in all four cases the setting time had been accelerated by the high fly ash substitution, retarding by gypsum was a positive benefit. Early stiffening tendencies were either improved or were negligibly affected.

The calorimeter curves were shifted to earlier times, with the 10% level earlier than the 5% level. The 10% lime mixture positions were almost restored back to where the zero fly ash curves were. Initial setting times had been accelerated by the replacement of fly ash. Upon addition of gypsum-lime, the 4-1 blend was retarded at both levels of fly ash, approaching the zero fly ash values (an improvement), but there was little effect on the 1-3 blend setting times. The tendency to early stiffen was alleviated somewhat by gypsum-lime in every blend but one, with the 10% level usually better.

In all cases of gypsum-RSC addition, the calorimeter curves were accelerated. In regard to initial setting time, all four blends had been accelerated by the fly ash replacement, three of the four severely so. Unfortunately, addition of gypsum-RSC made it worse in one blend, was negligible in two others, and helped (retarded) somewhat in the fourth blend. Also, in almost all mixtures, the early stiffening tendencies were significantly worsened. It should be noted that the combined SO3 content in some of these mixtures is somewhat high.

6.5 COMPRESSIVE STRENGTH

An increase in fly ash content decreased strength at all ages (one to 56 days). One day compressive strengths were greatly reduced by 50 fly ash replacement and even more so with 70% fly ash, even with the use of powder additives. In the paste study, one day compressive strengths were not enhanced much by gypsum, lime, or RSC by themselves, but gypsum-lime and gypsum-RSC did improve early strengths. In the concrete study, where gypsum was always present, the trend in strength loss was the same as in the paste. Effects of lime vs. RSC were not much different. That said, 12 combinations at 50% fly ash in the Screening Study met the 1200 psi (8.3 MPa) one day strength min. threshold with no powder additions, and in the concrete study, both 4-1 blends with lime or RSC met the 1000 psi (6.9 MPa) threshold. For concrete, all the 50% fly ash mixtures had reached 3000 psi (20.7 MPa) by day 7, with little advantage to lime vs. RSC. By day 28, all 50% mixtures had caught up with the OPC mixtures, and by 56 days, had exceeded the OPC strengths. The 70% mixtures lagged: however, they reached 3000 psi (20.7 MPa) by 28 days and about 3500 psi (24.1 MPa) at 56 days. For the most part, there was

no clear advantage of lime compared to RSC. Which one gave a little more strength

depended on the specific blend and fly ash level.

6.6. FLEXURAL STRENGTH

All tests were conducted at 28 days. Depending on the blend, the 50% fly ash

mixtures were about the same strength as the OPC mixture, or somewhat below, although

the weakest was still greater than 600 psi (4.1 MPa). At the 70% fly ash level, strengths

dropped below the 50% fly ash level. Only one mixture achieved 550 psi (3.8 MPa).

6.7. SPLITTING TENSILE STRENGTH

At the 50% fly ash level, the splitting tensile strengths either slightly exceeded or

were a bit below the OPC strengths. 70% fly ash level mixtures were weaker than 50%

fly ash mixtures.

6.8. MODULUS OF ELASTICITY

As a general rule, the 50% fly ash MOE values were close to, and in some cases

slightly greater than the OPC strengths. As expected, the 70 % mixtures were lower in

MOE.

6.9. ABRASION RESISTANCE

Abrasion resistance was measured in terms of both mass loss and depth of wear.

As expected, as fly ash level increased, abrasion resistance decreased significantly.

Results were mixed and not greatly different between lime and RSC. The abrasion

resistance at 56 days was greater than at 28 days, but with only the 50% mixtures

approaching the OPC levels of resistance.

6.10. DRYING SHRINKAGE

At the time of writing, the drying specimens were 80 to 100 days old. The fly ash

mixtures had lower shrinkage values than OPC mixtures. In the 4-1 blend case, the 70%

fly ash level mixtures had the lowest shrinkage, while the case of 1-3 blend, the 50% fly

ash level mixtures were lower.

6.11. RAPID CHLORIDE PERMEABILITY

RCP specimens were tested at 28 days. In three of the four of the cases, at 50%

fly ash, RCP was lower in the fly ash specimens than the OPC mixtures. However, all

mixtures at 70% fly ash had the greatest permeabilities, with RSC mixtures having lower

values than lime mixtures.

6.12. FREEZE-THAW RESISTANCE

Both 4-1 and 1-3 blends exhibited higher durability factors than their respective

OPC counterparts. Fly ash DF's were 93 or more.

6.13. SALT SCALING

OPC mixture specimens achieved scaling scores of 1 and 2 indicating adequate

scaling resistance. All fly ash mixtures fared worse, with the 70% mixtures deteriorating

more rapidly. Most fly ash mixtures reach a maximum level of 5; at the time of writing,

two mixtures are at 40 cycles and are already at scores of 3 and 4. However, several studies of actual pavements and sidewalks subjected to numerous freeze-thaw cycles and deicers have shown very good resistance to scaling, suggesting that the scaling test method is too severe (Bouzoubaa, et al.2001; Naik et al., 2003).

6.14. BOTTOM LINE

6.14.1 Compressive strength. At the 50% fly ash level, one day strengths were low no matter what powder additive was used, but 1000 psi (MPa) was reached in a number of OPC-fly ash blends, with and without powder additions. Good strengths can be achieved at 3 days. At the 70% fly ash level, concrete is weaker, but reasonable strengths can be reached at 28 days.

6.14.2. Abrasion Resistance. At 50% fly ash, resistance is somewhat lower. At 70% the effect is much worse.

6.14.3. Drying Shrinkage. It appears that HVFA mixtures shrink less than their OPC counterparts.

6.14.4. Rapid Chloride Permeability. In a comparison to OPC mixtures, RCP is lower for 50% fly ash mixtures, but 70% fly ash mixtures are more permeable.

6.14.5. Freeze-Thaw Resistance. All HVFA mixtures had greater DF's than the OPC mixtures.

6.14.6. Salt Scaling. All fly ash mixtures did poorly in regard to salt scaling.

6.14.7. Reaction Time. Reaction time (calorimeter curve time, setting time, stiffening time) varied as a function of characteristics of the OPC and fly ash in

conjunction with each other, type and level of powder additives used, dosage of

WR/HRWR, and the type of test method used for evaluation.

7. RECOMMENDATIONS

HVFA concrete at a 50% cement replacement level has been shown to be feasible under certain circumstances and applications, while use of a replacement at 70% level would be more restricted. In regard to 50% fly ash mixtures, it appears that although one day strengths may be low, certain blends of OPC and fly ash can reach minimum required strengths. Reasonable three day and later strengths can be achieved through use of certain powder activators, such as a combination of gypsum and lime or gypsum and rapid set cement. Delayed setting times may be problematic, thus construction operations would be impacted, especially during cool weather. However, certain blends of cement-fly ash-water reducers may actually accelerate hydration to the point of flash setting. Durability seems satisfactory in regard to permeability and freeze-thaw resistance. At this stage of development, use of HVFA for pavements, bridge decks, and other exterior slabs is not recommended because of salt scaling potential and possibly issues of excessive wear. The subject of plastic shrinkage cracking was not explored in this research project, but slabs with HVFA concrete may be prone to this problem.

Before HVFA is contemplated for use in a given project, it is absolutely imperative that the specific cement, fly ash, and admixtures be checked for incompatibilities through use of semi-adiabatic calorimetry, miniature slump, Vicat setting time, and the strength-type-of-interest at early, middle, and late ages, all at the temperature that will prevail during construction. Elevated temperatures are known to create additional incompatibilities with the cement, fly ash, and admixtures. Additionally, if the sulfate level will be adjusted (increased) through use of gypsum, RSC, or other source of sulfate, the mixture should be checked for excessive expansion characteristics.

REFERENCES

AASHTO. (2002). "Water content of freshly mixed concrete using microwave oven drying." *AASHTO T 318-02*, American Association of State Highway and Transportation Officials, Washington, D. C.

ACI. (1991). "Standard Practice for Selecting Proportions for Normal, Heavyweight, and Mass Concrete," *ACI 211.1-91*, American Concrete Institute, Farmington, MI.

ASTM. (2003). "Standard test method for scaling resistance of concrete surfaces exposed to deicing chemicals." *ASTM C 672/C 672M – 03*, ASTM International, West Conshohocken, PA.

ASTM. (2004). "Standard test method for materials finer than no. 200 sieve in mineral aggregates by washing." *ASTM C 117 – 12*, ASTM International, West Conshohocken, PA.

ASTM. (2005a). "Standard test method for heat of hydration of hydraulic cement." *ASTM C 186 – 05*, ASTM International, West Conshohocken, PA

ASTM. (2005b). "Standard test method for abrasion resistance of concrete or mortar surfaces   by the rotating-cutter method." *ASTM C 944/C 944M – 99*, ASTM International, West Conshohocken, PA.

ASTM. (2006a). "Standard practice for mechanical mixing of hydraulic cement pastes and mortars of plastic consistency." *ASTM C 305 – 06*, ASTM International, West Conshohocken, PA.

ASTM. (2006b). "Standard test method for sieve analysis of fine and coarse aggregates." *ASTM C 136 – 06*, ASTM International, West Conshohocken, PA.

ASTM. (2007). "Standard practice for making and curing concrete test specimens in the laboratory." *ASTM C 192/C 192M – 07*, ASTM International, West Conshohocken, PA.

ASTM. (2008a). "Standard test method for compressive strength of hydraulic cement mortars (using 2-in. or [50-mm] cube specimens." *ASTM C 109/C 109M – 08*, ASTM International, West Conshohocken, PA.

ASTM. (2008b). "Standard test method for time of setting of hydraulic cement by Vicat needle." *ASTM C 191 – 08*, ASTM International, West Conshohocken, PA.

ASTM. (2008c). "Standard test method for time of setting of concrete mixtures by penetration resistance." *ASTM C 403/C 403M – 08*, ASTM International, West Conshohocken, PA.

ASTM. (2008d). "Standard test method for length change of hardened hydraulic-cement mortar and concrete." *ASTM C 157/C 157 M – 03*, ASTM International, West Conshohocken, PA.

ASTM. (2008e). "Standard test method for resistance of concrete to rapid freezing and thawing." *ASTM C 666/C 666M – 03*, ASTM International, West Conshohocken, PA.

ASTM. (2009). "Standard practice for measuring the hydration kinetics of hydraulic cementitious mixtures using isothermal calorimetry." *ASTM C 1679 – 09*, ASTM International, West Conshohocken, PA.

ASTM. (2010a). "Standard test methods for slump of hydraulic cement concrete." *ASTM C 143/C 143M – 10a*, ASTM International, West Conshohocken, PA.

ASTM. (2010b). "Standard test method for normal consistency of hydraulic cement." *ASTM C 187 – 10*, ASTM International, West Conshohocken, PA.

ASTM. (2010c). "Standard test method for air content of freshly mixed concrete by the pressure method." *ASTM C 231/C 231M – 10*, ASTM International, West Conshohocken, PA.

ASTM. (2010d). "Standard test method for flexural strength of concrete (using simple beam with third-point loading)." *ASTM C 78/C 78M – 10*, ASTM International, West Conshohocken, PA.

ASTM. (2010e). "Standard test method for static modulus of elasticity and Poisson's ratio of concrete in compression." *ASTM C 469/C 469M – 10*, ASTM International, West Conshohocken, PA.

ASTM. (2011a). "Standard practice for evaluating hydration of hydraulic cementitious mixtures using thermal measurements (draft)." *ASTM WK23967*, ASTM International, West Conshohocken, PA.

ASTM. (2011b). "Standard test method for splitting tensile strength of cylindrical concrete specimens." *ASTM C 496/C 496M – 11*, ASTM International, West Conshohocken, PA.

ASTM. (2011c). "Standard test method for temperature of freshly mixed hydraulic-cement concrete." *ASTM C 1064/C 1064M – 11*, ASTM International, West Conshohocken, PA.

ASTM. (2012a). "Standard test method for density, relative density (specific gravity), and absorption of coarse aggregate." *ASTM C 127 – 12*, ASTM International, West Conshohocken, PA.

ASTM. (2012b). "Standard test method for density, relative density (specific gravity), and absorption of fine aggregate." *ASTM C 128 – 12*, ASTM International, West Conshohocken, PA.

ASTM. (2012c). "Standard test method for density (unit weight), yield, and air content (gravimetric) of concrete." *ASTM C 138/C 138M – 12*, ASTM International, West Conshohocken, PA.

ASTM. (2012d). "Standard test method for compressive strength of cylindrical concrete specimens." *ASTM C 39/C 39M – 12*, ASTM International, West Conshohocken, PA.

ASTM. (2012e). "Standard test method for electrical indication of concrete's ability to resist chloride ion penetration." *ASTM C 1202 – 12*, ASTM International, West Conshohocken, PA.

Bentz, D. P. (2010). "Powder additions to mitigate retardation in high-volume fly ash mixtures." *ACI Materials Journal*, 107(5), 508-514.

Bentz, D. P. and Ferraris, C. F. (2010). "Rheology and setting of high volume fly ash mixtures." *Cement & Concrete Composites*, 32, 265-270.

Bentz, D. P., Chiara, F. F., De La Varga, I., Peltz, M. A., & Winpigler, J. A. (2010). "Mixture Proportioning Options for Improving High Volume Fly Ash Concretes." *International Journal of Pavement Research and Technology, 3*(5), 234-240.

Bhattacharja, S. and Tang, F. J. (2001). "Rheology of cement paste in concrete with different mix designs and interlaboratory evaluation of the mini-slump cone test." *PCA R&D Serial No. 2412*, Portland Cement Association, Skokie, IL.

Bilodeau, A., Sivasundaram, V., Painter, K. E., and Malhotra, V. M. (1994). "Durability of concrete incorporating high volumes of fly ash from sources in the U.S." *ACI Materials Journal*, 91(1), 3-12.

Bouzoubaa, N., Bilodeau, A., Sivasundaram, V., & Chakraborty, A. (2007). "Mechanical Properties and Durability Characteristics of High Volume Fly Ash Concrete Made with Ordinary Portland Cement and Blended Portland Fly Ash Cement." *ACI Special Publication 242*, American Concrete Institute, Farmington Hills, MI, 303-320.

Bouzoubaa, N., Zhang, M. H., Malhotra, V. M., & Golden, D. M. (2001). "Mechanical Properties and Durability of Laboratory Produced High-Volume Fly Ash Blended Cements." *ACI Special Publication 199,* American Concrete Institute, Farmington Hills, MI, 55-82.

Calmetrix. (2010a). "Calcommander software v1.3 user manual." Calmetrix, Inc.

Calmetrix. (2010b). "F-cal 4000/8000 user manual." Calmetrix, Inc.

Cost, T. (2009). "Thermal measurements of hydrating concrete mixtures." *NRMCA Publication 2PE004*, National Ready Mixed Concrete Association, Silver Spring, MD.

Cost, V. T. and Knight, G. (2007). "Use of thermal measurements to detect incompatibilities of common concrete materials." *ACI Special Publication 241*, American Concrete Institute, Farmington Hills, MI, 39-58.

Detwiler, R. J., Bhatty, J. I., and Bhattacharja, S. (1996). "Supplementary cementing materials for use in blended cements." *Research and Development Bulletin RD112T*, Portland Cement Association, Skokie, IL.

Cabrera, J. G., & Atis, C. D. (1999). "Design and Properties of High Volume Fly Ash High-Performance Concrete." *ACI Special Publication 186,* American Concrete Institute, Farmington Hills, MI, 21-31

Galeota, D., Giammatteo, M., and Marino, R. (1995). "Structural concrete incorporating high volume of fly ash." *ACI Special Publication 153*, American Concrete Institute, Farmington Hills, MI, 25-42.

Gibbon, G. J., Ballim, Y., and Grieve, G. R. H. (1997). "A low-cost, computer-controlled adiabatic calorimeter for determining the heat of hydration of concrete." *Journal of Testing and Evaluation*, 25(2), 261-266

Gu, P., Beaudoin, J. J., Zhang, M.-H., & Malhotra, V. (1999). "Performance of Steel Reinforcement in Portland Cement and High-Volume Fly Ash Concretes Exposed to Chloride Solution. " *ACI Materials Journal, 96*(5), 551-558.

Hübert, C., Wieker, W., & Heideman, D. (2001). "Investigations of Hydration Products in High-Volume Fly Ash Binders. " *ACI Special Publication 199,* American Concrete Institute, Farmington Hills, MI, 83-97

Jiang, L., Lin, B., & Cai, Y. (1999). "Studies on Hydration in High-Volume Fly Ash Concrete Binders." *ACI Materials Journal, 96*(6), 703-706.

Kantro, D. L. (1980). "Influence of water-reducing admixtures on properties of cement paste – a miniature slump test." *Cement, Concrete, and Aggregates*, 2(2), 95-102.

Lerch, W. (1946). "The influence of gypsum on the hydration and properties of portland cement pastes." *Bulletin 12*, Portland Cement Association, Chicago, IL.

Marlay, K.M. (2011), "Hardened concrete properties and durability assessment of high volume fly ash concrete," M.S. Thesis, Missouri Univ. of Science and Technology, Rolla, MO.

Mehta, P., & Montiero, P. J. (1993). *Concrete Microstructure, Properties, and Materials.* McGraw-Hill.

Mindess, S., Young, J. F., and Darwin, D. (2003). "Concrete." Prentice Hall, Upper Saddle River, NJ.

MoDOT. (2011a), "Concrete, section 501, standard specifications." Jefferson City, MO.

MoDOT. (2011b), "Aggregate for concrete, section 501, standard specifications." Jefferson City, MO.

NCPTP. (2007), "Integrated materials and construction practices for concrete pavement: a state of the practice manual," National Concrete Pavement Technology Center, FHWA No. HIF-07-004, Washington, D.C.

Nagi, M. and Whiting, D. (1994). "Determination of water content of fresh concrete using a microwave oven." *Cement, Concrete, and Aggregates*, 16(2), 125-131.

Naik, T. R., Ramme, B. W., Kraus, R. N., & Siddique, R. (2003). "Long-Term Performance of High-Volume Fly Ash Concrete Pavements." *ACI Materials Journal, 100*(2), 150-155.

Naik, T. R., Ramme, B. W., and Tews, J. H. (1995). "Pavement construction with high-volume Class C and Class F fly ash concrete." *ACI Materials Journal*, 92(2), 200-210.

Naik, T. R., Singh, S. S., and Ramme B. W. (2002). "Effect of source of fly ash on abrasion resistance of concrete." *Journal of Materials in Civil Engineering*, 14(5), 417-426.

Rivest, M., Bouzoubaa, N., and Malhotra, V. (2004). "Strength development and temperature rise in high-volume fly ash and slag concretes in large experimental monoliths." *ACI Special Publication 221*, American Concrete Institute, Farmington Hills, MI, 859-878.

Roberts, L. R. and Taylor, P. C. (2007). "Understanding cement-SCM-admixture interaction issues." *Concrete International*, 29(1), 33-41.

Rosli, A., & Harnik, A. (1980). "Improving the Durability of Concrete to Freezing and Deicing Salts." *Durability of Building Materials and Components*, pp. 464-473.

Sandberg, J. P. and Liberman, S. (2007). "Monitoring and evaluation of cement hydration by semi-adiabatic field calorimetry." *ACI Special Publication 241*, American Concrete Institute, Farmington Hills, MI, 13-23.

Wang, K. (2006). "Monitoring heat evolution of concrete mixtures." *National Concrete Pavement Technology Center*

Wang, H. C., Qi, C., Farzam, H., & Turici, J. (2006). "Interaction of Materials Used in Concrete." *Concrete International, 28*(4), 47-52.

APPENDICES

APPENDIX A
Miniature Slump, Cement Cubes, and Calorimeter Combined Mixing
Procedure
(6-19-2012)

Procedure

1. Refer to Miniature Slump, Cement Cubes, and Calorimeter procedures for preparations needed prior to mixing cement paste.

2. Add all cementitious materials to the mixing bowl and follow the time schedule below. Refer to Miniature Slump, Cement Cubes, and Calorimeter procedures for more detail.

Elapsed Time (mm:ss)	Action
0:00	Add water to mixing bowl with cementitious materials Record time (Start Time)
0:10	Start mixing at Speed 2 (440 RPM)
0:30	Start mixing at Speed 6 (670 RPM)
1:30	Stop mixing Record temperature of paste Prepare mini-slump test
2:00	Lift mini-slump cone
4:00	Remix paste at Speed 2
4:30	Prepare mini-slump test
5:00	Lift mini-slump cone Prepare calorimeter specimens Insert calorimeter specimens in F-Cal 4000
10:00	Close and latch the lid of the F-Cal 4000
13:00	Remix paste at Speed 2
13:30	Prepare mini-slump test
15:00	Lift mini-slump cone

	Mold cement cubes
28:00	Remix paste at Speed 2
28:30	Prepare mini-slump test
30:00	Lift mini-slump cone
43:00	Remix paste at Speed 2
43:30	Prepare mini-slump test
45:00	Lift mini-slump cone
60:00	Measure and record mini-slump diameters

APPENDIX B

Using the F-Cal 4000 & CalCommander Software for Testing Cement Paste

(Calmetrix F-Cal 4000/8000 User Manual, CalCommander Software v1.3 User Manual, and ASTM C 305)

(Revised 6-19-2012)

Equipment and Materials

1. F-Cal 4000, USB cable, and CalCommander Software v1.3.
2. Black and Decker 250-Watt Hand Mixer (Model MX217) with egg beater paddles
3. 20-quart Hobart mixing bowl
4. Plastic ladle
5. Hamilton 1-mL Adjustable Volume SoftGrip Pipette (readable to 0.01 mL)
6. 3-quart or larger white plastic bowl with spout
7. Metal spoon
8. Small stainless steel spatula
9. Four, clean 4"x8" plastic cylinder molds and caps per mix
10. Sper Scientific Humidity/Temperature Monitor (Model 800016)
11. Analog thermometer with 5-inch probe
12. High silica sand obtained from U.S. Silica, Pacific, MO
13. 12-kg Denver Instrument balance
14. Space heater
15. Microsoft Excel and TableCurve 2D software

Procedure

1. At least 1 hour before inserting the first specimen: connect the F-Cal to the computer using the USB cable, open the CalCommander program, click

on the "F-Cal Logger" tab at the top of the window, and click on "Start Logging" at the right side of the window.

2. To enter information about the mix: click "Read Configuration from Logger", click on the tab in the bottom portion of the window which corresponds to the slot in which the specimen will be placed in the F-Cal; enter the Mix ID, Water/Cement Ratio, Cement Source, Cement Content (lbs/cy), and any SCMs (Type, Percent, and Source); and click "Update Configuration File" on the right side of the window. Also, make sure the Sensor Enabled box is checked.

3. Prepare a clean mold with a 1250 gram inert specimen. The inert specimen consists of high silica sand and deionized water. The proportion of water to oven-dried sand should reflect the proportion of water to cementitious materials used in the mixture being tested.

4. Verify that the air temperature is 23.0±3.0°C (68.0-78.8°F), mixing water temperature is 23.0±2°C (69.8-77.0°F), and that the relative humidity of the air is not less than 50%. Record these parameters.

5. To blend the dry constituents of the mix: Place about 1000 grams of the dry materials into a 4"x8" cylinder mold in the same proportions to be used in the paste mixture, hold the cylinder horizontally with one hand on each end of the cylinder, and then shake the cylinder 25 cycles using a 6" throw.

6. To dissolve admixtures into the mix water: Place all of the deionized water into the plastic bowl, use the 1-mL syringe to add the desired amount of admixture to the water, and use the small spatula to gently stir the water until all of the admixture is dissolved.

7. Add the pre-mixed cementitious materials to the mixing bowl, forming a donut shape.

8. Add all of the mix water to the mixing bowl, start the timer, and record the time (Start Time).

9. Wait 10 seconds to allow the cement to absorb the water.

10. Mix at Speed 2 (440 RPM) for 20 seconds. Rotate the bowl 90° every 5 seconds.

11. Mix at Speed 6 (670 RPM) for 60 seconds. Rotate the bowl 90° every 15 seconds and occasionally run the mixing paddles along the side of the bowl.

12. At the end of the initial mixing, record the temperature of the paste.

13. At 4 minutes, remix the paste at Speed 2 for 30 seconds.

14. After remixing, pour 1250 grams of paste into each of the three remaining 4"x8" cylinder molds. Tap each cylinder with an open hand 10 times to remove entrapped air.

15. Quickly cap the molds, ensure that the outsides of the molds are clear of paste or other debris, and place the molds into the appropriate slots in the F-Cal (including the mold with the control sand). This should be done within 10 minutes after the Start Time.

16. Enter the "Mix Date/Time" (noted in step #8) and "Mix Temperature" (noted in step #12) into the software under the mix information tabs and click "Update Configuration File".

17. Disconnect the USB cable from the computer and F-Cal, close and latch the F-Cal lid, and leave the specimens for at least 48 hours. Note: shorter logging times may be used depending on the amount of information desired and prior knowledge of the materials being tested. (CAUTION: DO NOT MOVE THE F-CAL WHILE TESTING IS IN PROGRESS)

18. After 48 hours, open the F-Cal lid, reconnect the USB cable, open the CalCommander software, click the "F-Cal Logger" tab, and click "Read Data from Logger" at the right side of the window. If it is decided that logging should cease, click "Stop Logging".

19. Save the log data by clicking "Read Data from Logger" and then selecting "Save Log Data to File".

20. Remove the specimens from the F-Cal.

21. To export data: click on "F-Cal Reports" at the top of the CalCommander software window, click "Add Logs" in the bottom right corner of the screen, select the appropriate file(s), select "Accept" in the "Add F-Cal/AdiaCal Logs" window, select the tab corresponding to the channel from which data is needed, click on "Save Selected Log as Text File" in the bottom right corner of the screen, input desired file name, and click "Save".

22. To import data into Microsoft Excel: Open Microsoft Excel, select "Data" at the top of the screen, go to "Import External Data", click "Import Data...", double-click on the desired text file, click the "Next >" button two times in the "Text Import Wizard" window, click "Finish", and then select "OK" in the "Import Data" window.

23. Record the Signal-to-Noise Ratio for each specimen. The Signal is the difference between the highest and lowest temperatures recorded for the sample being tested. The Noise is the difference between the highest and lowest temperatures recorded for the inert specimen. To calculate the Signal-to-Noise Ratios:

    a. Import the data for each specimen into Excel.

    b. Determine the difference between the time logging began and the time water was added to the cementitious materials (Start Time). This will be used to determine the log time that corresponds to the Start Time.

    c. For each specimen log, find the maximum temperature by using the MAX function for the range of specimen temperatures starting with the log time that corresponds to the Start Time and ending at the end of the logging period. To find the minimum temperature, follow a similar procedure using the MIN function for the same range.

    d. Calculate the Signal for each specimen by subtracting the minimum specimen temperature from the maximum specimen temperature.

    e. Calculate the Noise by subtracting the minimum temperature of the inert specimen from the maximum temperature of the inert specimen.

f. Divide the Signal for each specimen by the Noise to determine the Signal-to-Noise ratio for each specimen.

24. To estimate set times using the Percentage Method:

a. Import the data for each specimen into Excel.

b. Determine the difference between the time logging began and the time water was added to the cementitious materials (Start Time). This will be used to determine the log time that corresponds to the Start Time.

c. Remove all log data prior to the log time corresponding to the Start Time.

d. Find the average temperature log for the specimens by averaging the temperatures of the three specimens at every minute for the duration of the logging.

e. Subtract the inert specimen temperature log from the average temperature log to determine the corrected average temperature log.

f. Plot the corrected average hydration curve by plotting the corrected average temperatures against time.

g. Visually examine the curve to determine a time window that encompasses the dormant period and the peak of the hydration curve. There will be an initial rise in the temperature near time zero that indicates the initial rise in temperature of the thermistors from the ambient temperature to the specimen temperature. This area should not be considered to be part of the dormant period.

h. Use the MAX and MIN functions, within the time range chosen above, to determine the maximum and minimum temperatures (ΔT_{max} and ΔT_{min}) of the hydration curve.

i. Using the values from Step 25.h., calculate the main hydration response rise ($M = \Delta T_{max} - \Delta T_{min}$), twenty percent of the main hydration response rise ($M_{20\%} = 0.2M$), and fifty percent of the main hydration response rise ($M_{50\%} = 0.5M$).

j. Initial Set is taken as the time when 20% of the main hydration response rise ($M_{20\%} + \Delta T_{min}$) occurs.

k. Final Set is taken as the time when 50% of the main hydration response rise ($M_{50\%}+\Delta T_{min}$) occurs.

25. To estimate set times using the Derivatives Method:

a. Copy and paste the time log and corrected average temperature log from Step 25, above, into a new Excel file.

b. In TableCurve 2D, click "Import" in the upper left corner of the window and "Open" the Excel file.

c. In the "Select Columns for X-Y Data Table" window, select "(1)Sheet1!A" for the X Column, select "(1)Sheet1!B" for the Y Column, and then select "OK".

d. In the "Data Description and Variable Names" window, enter a title for the plot, enter titles for the axes, and select "OK".

e. Select "Data" at the top of the window, choose "Section Data...", select a time range from the dormant period to the peak of the main hydration curve, click the green checkmark box in the upper left corner, and select "Yes" in the "Update Data Table" window.

f. Select "Process" at the top of the window, choose "Curve-Fit All Equations", and select "Graph Start" after fitting has ceased. The curve-fit automatically applied has the highest R-squared value and should not be changed.

g. On the left side of the screen, select "Numeric". Look toward the bottom of the "Numeric Summary" screen to find the "1st Deriv max" and the "2nd Deriv max" with corresponding X-Values.

h. The time for Initial Set is the x-value corresponding to the maximum second derivative (2nd Deriv max).

i. The time for Final Set is the x-value corresponding to the maximum first derivative (1st Deriv max).

Calorimeter Data Sheet

High Volume Fly Ash Cement Paste Study

Date: _____

Technician: _____

Mix ID: _____

Cement: _____ %   Fly Ash: _____ %   Gypsum: _____ %

CH: _____ %   RS Cem: _____ %   Admix: _____   w/cm: _____

Cement Source: _____   Fly Ash Source: _____

Thermal Measurement Equip.: _____   Specimen Containers: _____

Material Type: _____

Inert Specimen Preparation	
Total Design Mass, $m_{i,T}$ (g):	
Proportion of Water to Sand, w/s [=w/cm]:	
Design Mass of Sand, $m_{i,S}$ (g) [=$(m_{i,T})/(1+w/s)$]:	
Design Mass of Water, $m_{i,W}$ (g) [=$m_{i,T} - m_{i,S}$]:	
Actual Mass of Sand (g):	
Actual Mass of Water (g):	
Total Actual Mass of Inert Specimen (g):	

Mixing and Sample Preparation	
Air Temperature (°F):	
Water Temperature (°F):	
Relative Humidity (%):	
Start Time:	
Admix Addition Time:	
Paste Temp. at End of Mixing (°F):	
Sample 1 Mass (g):	
Sample 2 Mass (g):	
Sample 3 Mass (g):	

Signal-to-Noise Ratios (Raw Data)	
Inert Specimen	
Max. Temperature of Inert Specimen, $T_{i,max}$ (°F):	
Min. Temperature of Inert Specimen, $T_{i,min}$ (°F):	
Sample 1	
Max. Temperature of Sample, $T_{s,max}$ (°F):	
Min. Temperature of Sample, $T_{s,min}$ (°F):	
Signal-to-Noise Ratio [=$(T_{s,max}-T_{s,min})/(T_{i,max}-T_{i,min})$]:	
Sample 2	
Max. Temperature of Sample, $T_{s,max}$ (°F):	
Min. Temperature of Sample, $T_{s,min}$ (°F):	
Signal-to-Noise Ratio [=$(T_{s,max}-T_{s,min})/(T_{i,max}-T_{i,min})$]:	
Sample 3	
Max. Temperature of Sample, $T_{s,max}$ (°F):	
Min. Temperature of Sample, $T_{s,min}$ (°F):	
Signal-to-Noise Ratio [=$(T_{s,max}-T_{s,min})/(T_{i,max}-T_{i,min})$]:	

Thermal Setting Times (Corrected Average Data)	
Percentage Method	
Max. Temp. of Main Hydration Curve, ΔT_{max} (°F):	
Time when ΔT_{max} Occurs (min):	
Min. Temp. During Dormant Period, ΔT_{min} (°F):	
Main Hydration Response Rise, M (°F) [=$\Delta T_{max} - \Delta T_{min}$]:	
20% of Main Hydration Response Rise, $M_{20\%}$ (°F) [=0.2M]:	
$M_{20\%}+\Delta T_{min}$ (°F):	
Initial Set (min) [=Time when $M_{20\%}+\Delta T_{min}$ First Occurs]:	
50% of Main Hydration Response Rise, $M_{50\%}$ (°F) [=0.5M]:	
$M_{50\%}+\Delta T_{min}$ (°F):	
Final Set (min) [=Time when $M_{50\%}+\Delta T_{min}$ First Occurs]:	
Derivatives Method	
Maximum 2nd Derivative (from Tablecurve):	
Initial Set (min) [=Time when Max. 2nd Derivative Occurs]:	
Maximum 1st Derivative (from Tablecurve):	
Final Set (min) [=Time when Max. 1st Derivative Occurs]:	

Notes/Deviations: _____

_____

APPENDIX C

Miniature Slump Cone

(Kantro (1980) and Bhattacharja & Tang (2001))

(Revised 6-19-2012)

Equipment

1. Black and Decker 250-Watt Hand Mixer (Model MX217) with egg beater paddles

2. 20-quart Hobart mixing bowl
3. Plastic ladle
4. Hamilton 1-mL Adjustable Volume SoftGrip Pipette, (readable to 0.01 mL)
5. 3-quart or larger white plastic bowl with spout
6. Metal spoon
7. Analog thermometer with 5-inch probe
8. Stopwatch
9. Small stainless steel spatula (0.625 in. wide and 4 in. long)

10. 2 mini-slump cones

11. Lucite sheet (0.2 inches thick). Label the area of the sheet where each test will be performed with the time the cone will be lifted (2, 5, 15, 30, 45 minutes)

12. Plastic wrap

13. 5 thin plastic discs (2 in. diameter) cut from Zip-lock bags

14. 12-kg Denver Instrument balance

15. Sper Scientific Humidity/Temperature Monitor (Model 800016)

Procedure

1. Place the 5 plastic discs on the board 8 inches apart on center and at least 3 inches away from any edge of the board.

2. Place each of the two mini-slump cones on a plastic disc.

3. Verify that the air temperature is 23.0±3.0°C (68.0-78.8°F), mixing water temperature is 23.0±2°C (69.8-77.0°F), and that the relative humidity of the air is not less than 50%. Record these parameters.

4. To blend the dry constituents of the mix: Place about 1000 grams of the dry materials into a plastic 4"x8" cylinder mold in the same proportions to

be used in the paste mixture, hold the cylinder horizontally with one hand on each end of the cylinder, and then shake the cylinder 25 cycles using a 6" throw.

5. To dissolve admixtures into the mix water: Place all of the deionized water into the plastic bowl, use the 1-mL syringe to add the desired amount of admixture to the water, and use the small spatula to gently stir the water until all of the admixture is dissolved.

6. Add all cementitious materials to the mixing bowl, forming a donut shape.

7. Add all of the water to the mixing bowl, start the timer, and record the time (Start Time).

8. Wait 10 seconds to allow the cement to absorb the water.

9. Mix at Speed 2 (440 RPM) for 20 seconds. Rotate the bowl 90° every 5 seconds.

10. Mix at Speed 6 (670 RPM) for 60 seconds. Rotate the bowl 90° every 15 seconds and occasionally run the mixing paddles along the side of the bowl.

11. Record the temperature of the paste.

12. At the completion of mixing (1.5 minutes after the Start Time), fill the first mini-slump cone until a slight hump is formed above the top of the cone.

13. Use the spatula with a rodding motion at a slight angle to remove entrapped air. The paste should be "rodded" 5 to 10 times.

14. If the paste is depressed below the top of the cone after removing the entrapped air, use paste spilled on the rim to fill the cone.

15. Use the spatula to strike off the top surface of the cone.

16. At 2 minutes after the Start Time, lift the cone within a few tenths of a second. The lifting motion should be rapid enough for the bottom of the cone to be free of the flowing paste, but slow enough to avoid imparting an upward momentum to the paste as it is flowing from the cone.

17. At 4 minutes after the Start Time, remix the paste remaining in the bowl at Speed 2 for 30 seconds.

18. Pour the paste into the second cone and remove entrapped air with the same procedure used above.

19. At 5 minutes after the Start Time, lift the cone.

20. Cover the remaining paste in the mixing bowl using plastic wrap.

21. At 13 minutes after the Start Time, uncover the paste and remix the paste at Speed 2 for 30 seconds.

22. Pour the paste into a clean, dry cone and remove entrapped air with the same procedure used above.

23. At 15 minutes after the Start Time, lift the cone.

24. Repeat the procedure in Steps 21-23 for slumps at 30 and 45 minutes after the Start Time. See the table, below, which summarizes the mixing, pausing, and testing times

25. At 1 hour after the Start Time, measure and record the diameter of each of the paste pats 4 times using digital calipers. The measurements should each be rotated 45°.

26. Calculate the average diameter of each pat and use the average diameter to calculate the area of the pat. Record this area in square inches.

Elapsed Time (mm:ss)	Action
0:00	Add water to mixing bowl with cementitious materials Record Time (Start Time)
0:10	Start mixing at Speed 2
0:30	Start mixing at Speed 6
1:30	Stop Mixing Record Temperature of Paste Prepare mini-slump test
2:00	Lift mini-slump cone
4:00	Remix paste at Speed 2
4:30	Prepare mini-slump test
5:00	Lift mini-slump cone
13:00	Remix paste at Speed 2
13:30	Prepare mini-slump test
15:00	Lift mini-slump cone
28:00	Remix paste at Speed 2
28:30	Prepare mini-slump test
30:00	Lift mini-slump cone
43:00	Remix paste at Speed 2
43:30	Prepare mini-slump test
45:00	Lift mini-slump cone
60:00	Measure and record mini-slump diameters

Miniature Slump Data Sheet

High Volume Fly Ash Cement Paste Study

Date: _____

Technician: _____

Mix ID: _____

Cement: _____ %   Fly Ash: _____ %   Gypsum: _____ %

CH: _____ %   RS Cem: _____ %   Admix: _____   w/cm: _____

Cement Source: _____   Fly Ash Source: _____

Air Temperature (°F): _____   Water Temperature (°F): _____   Relative Humidity (%): _____

Start Time: _____   Paste Temperature at Completion of Mixing (°F): _____

Test Time (min)	Diameter Measurements (in)				Average Diameter (in)	Area (in²)
2						
5						
15						
30						
45						

Notes/Deviations: _____

_____

_____

APPENDIX D

THERMAL CURVE PLOTS FROM THE SCREENING STUDY
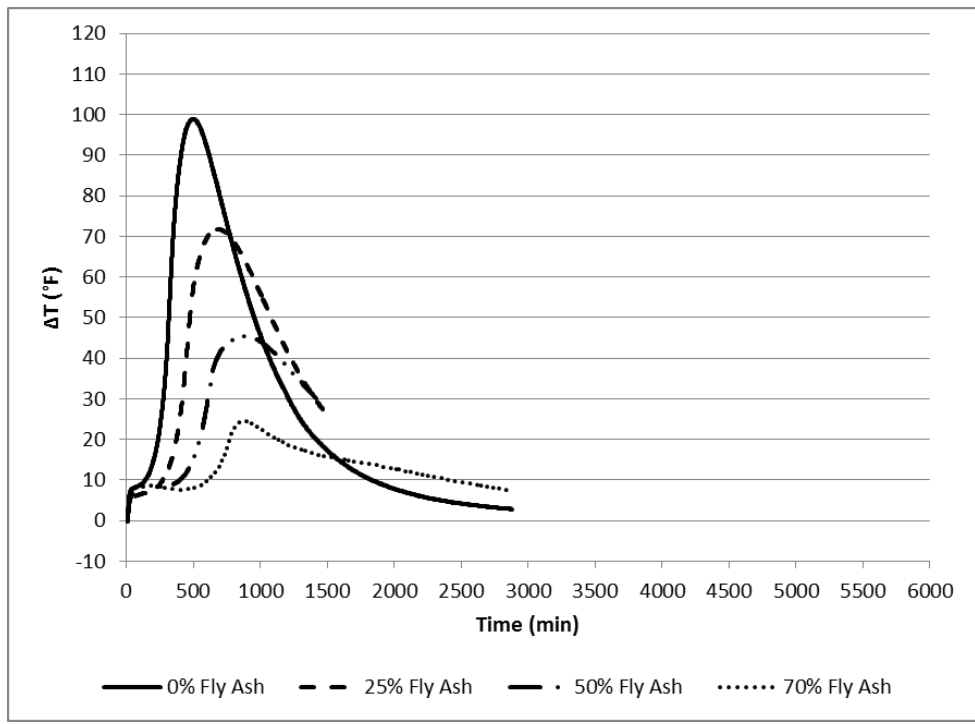
Figure D.1. Thermal Curve Plots for Combination 1-1
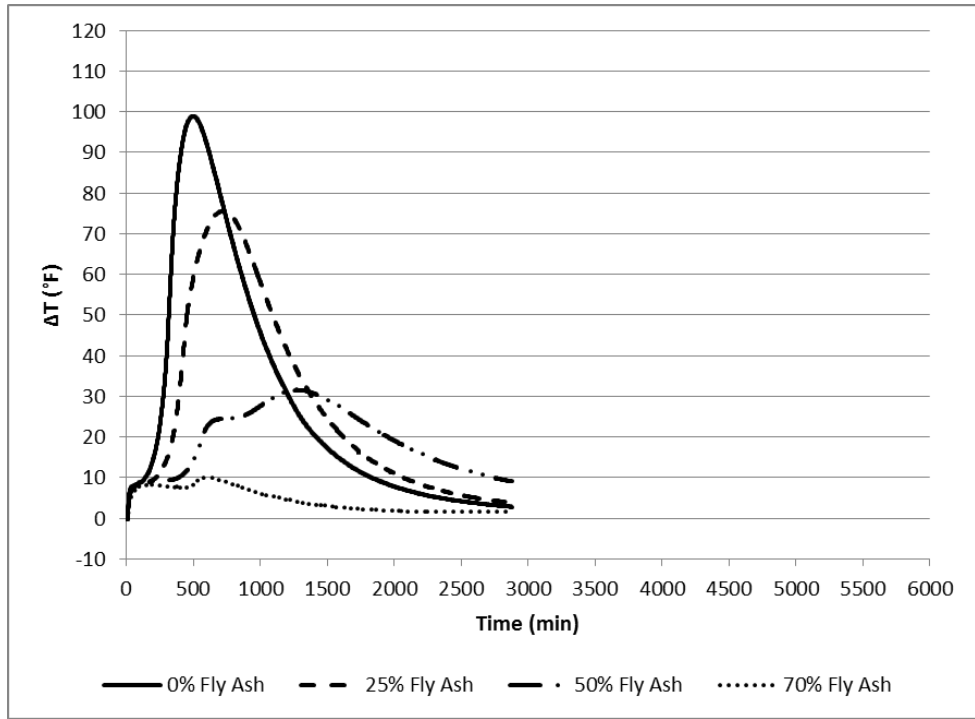
Figure D.2. Thermal Curve Plots for Combination 1-2
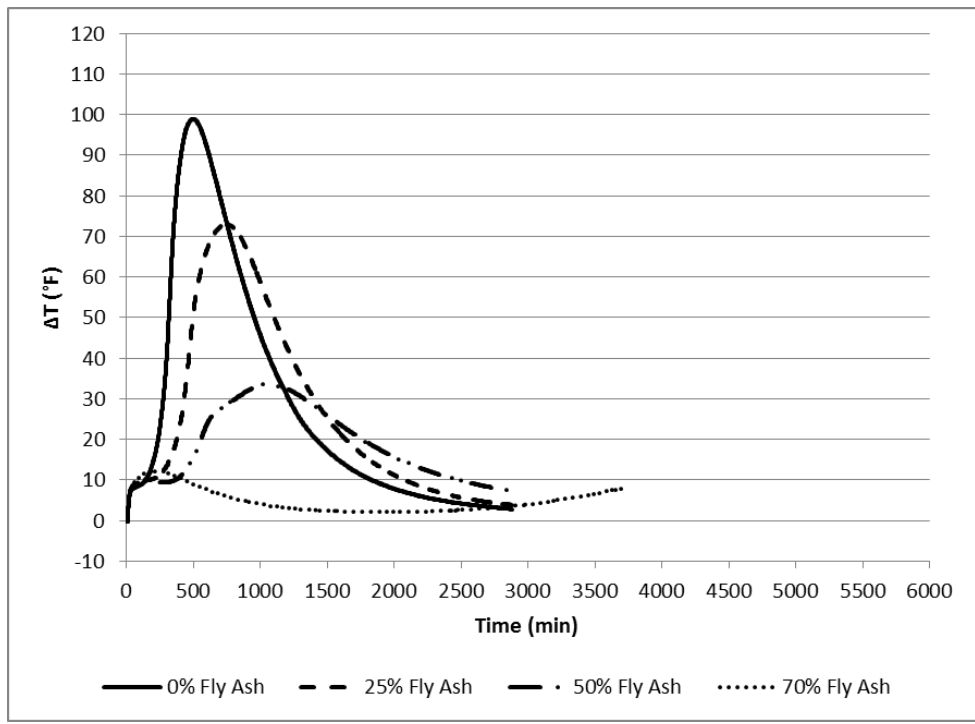
Figure D.3. Thermal Curve Plots for Combination 1-3
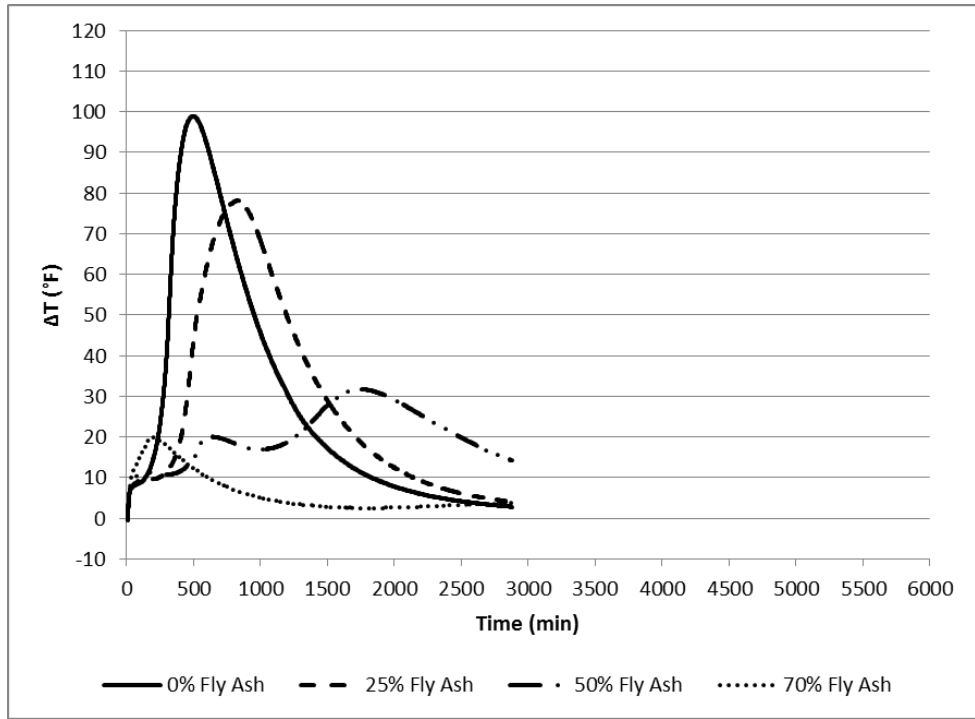
Figure D.4. Thermal Curve Plots for Combination 1-4
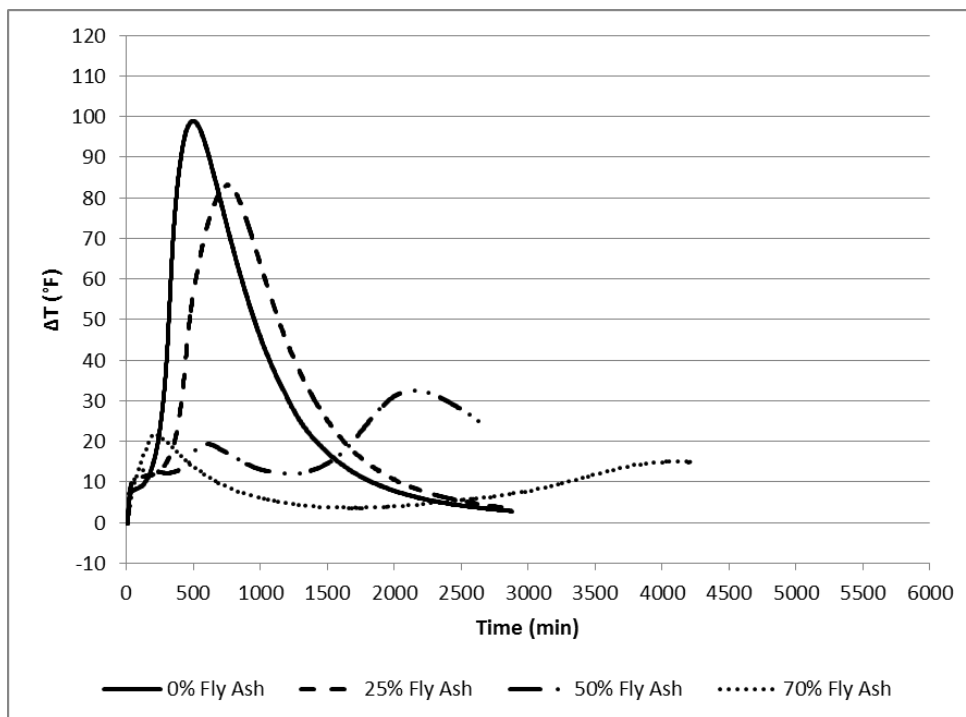
Figure D.5. Thermal Curve Plots for Combination 1-5
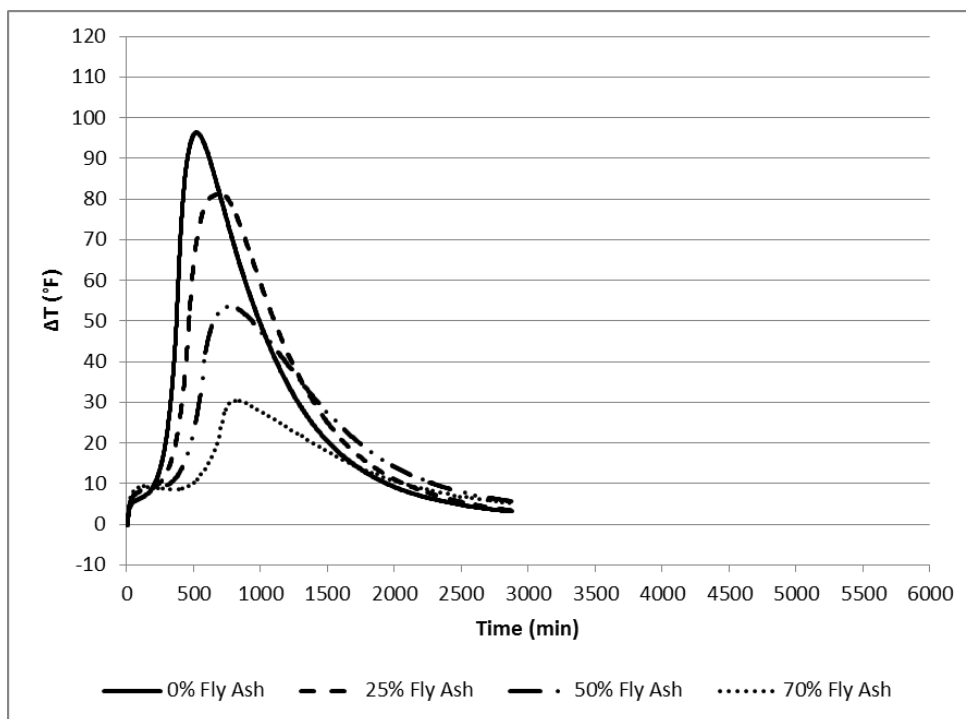
Figure D.6. Thermal Curve Plots for Combination 2-1
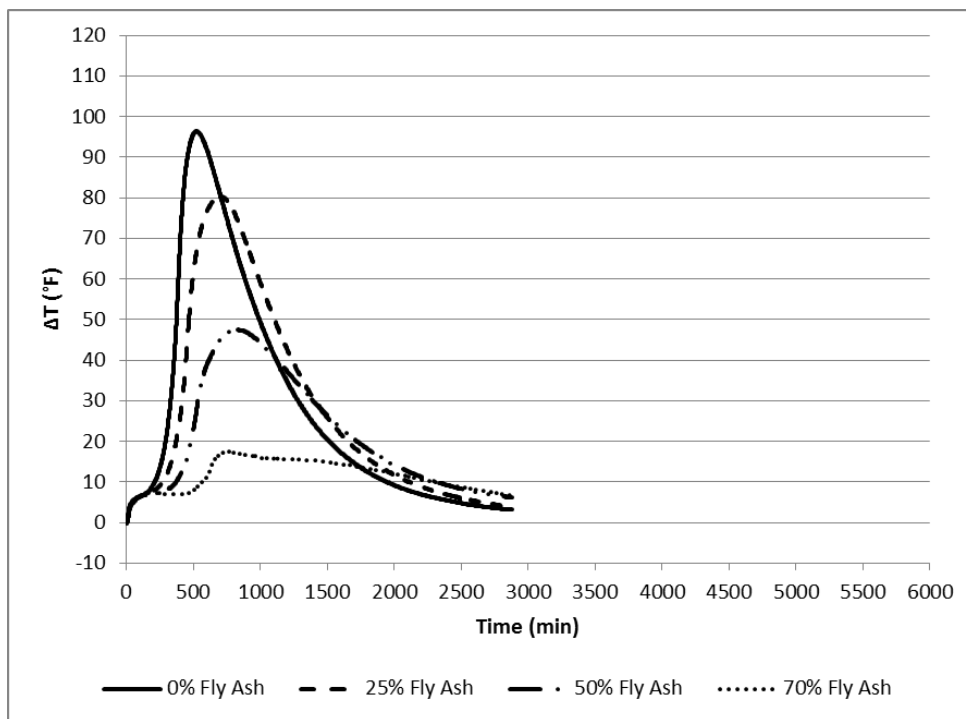
Figure D.7. Thermal Curve Plots for Combination 2-2
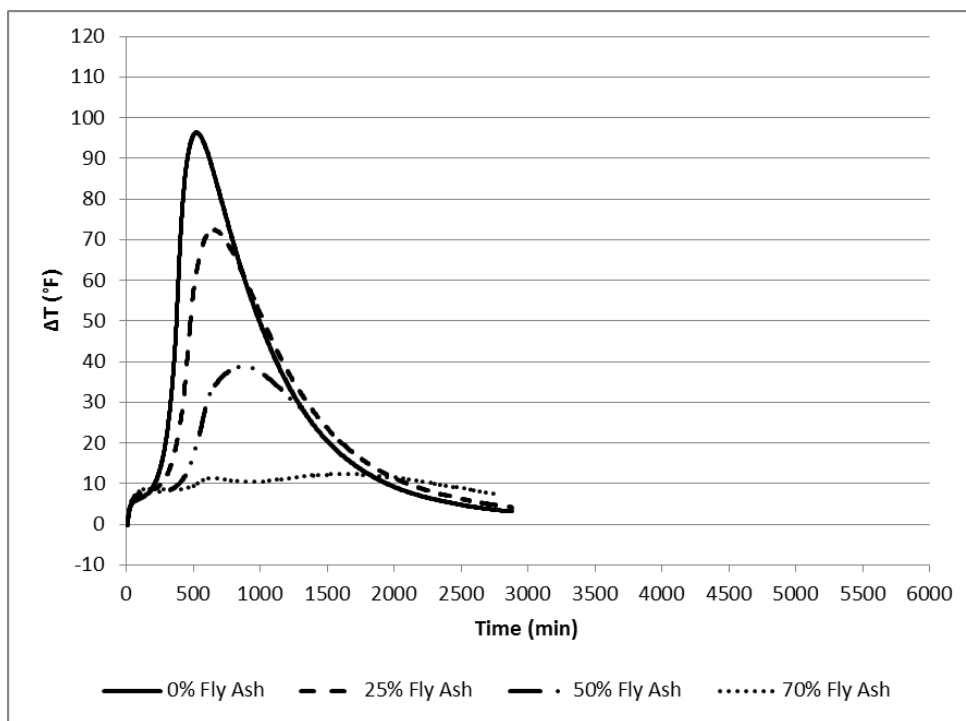
Figure D.8. Thermal Curve Plots for Combination 2-3
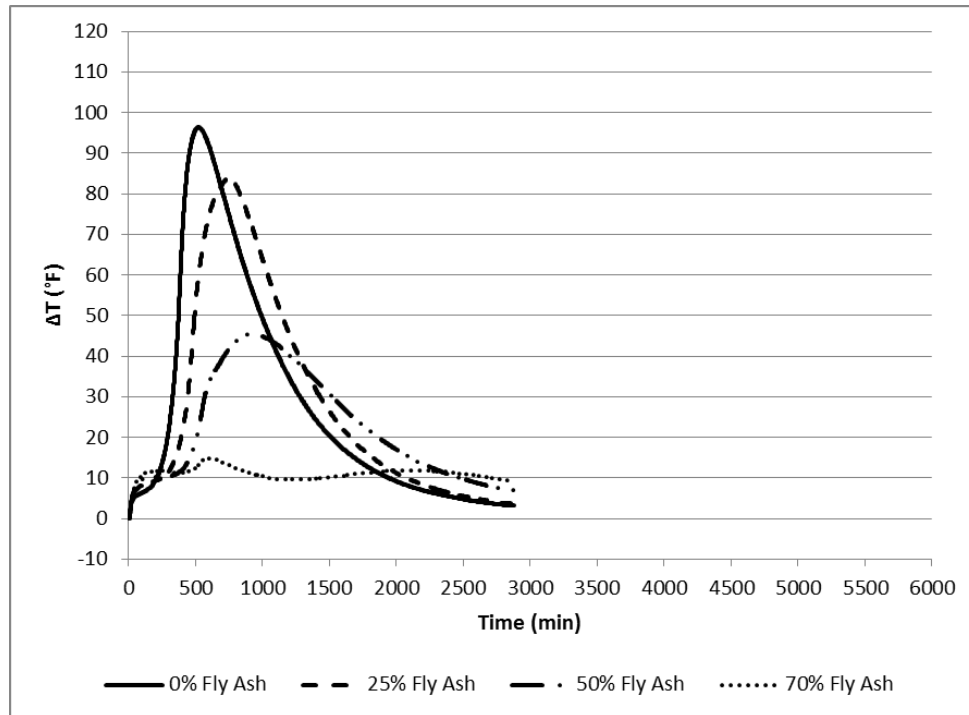
Figure D.9. Thermal Curve Plots for Combination 2-4
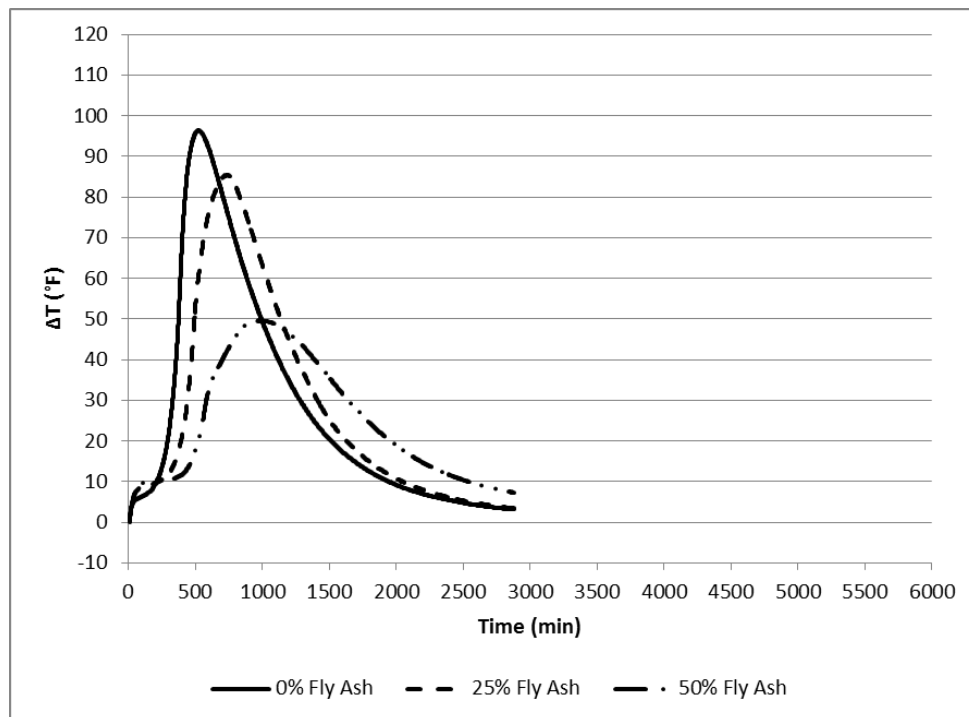
Figure D.10. Thermal Curve Plots for Combination 2-5
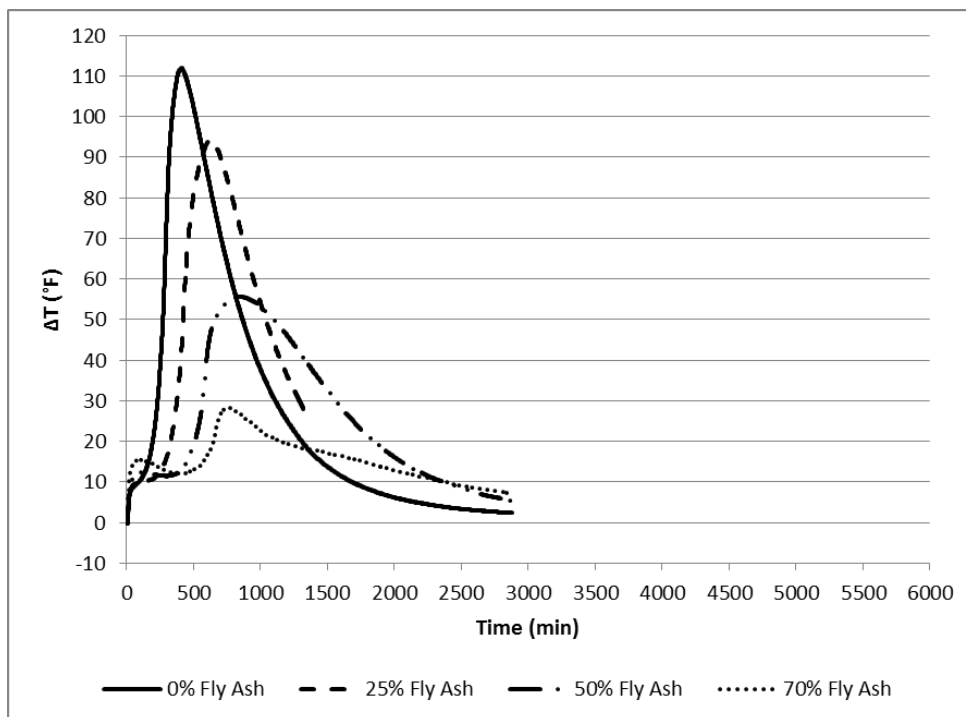
Figure D.11. Thermal Curve Plots for Combination 3-1
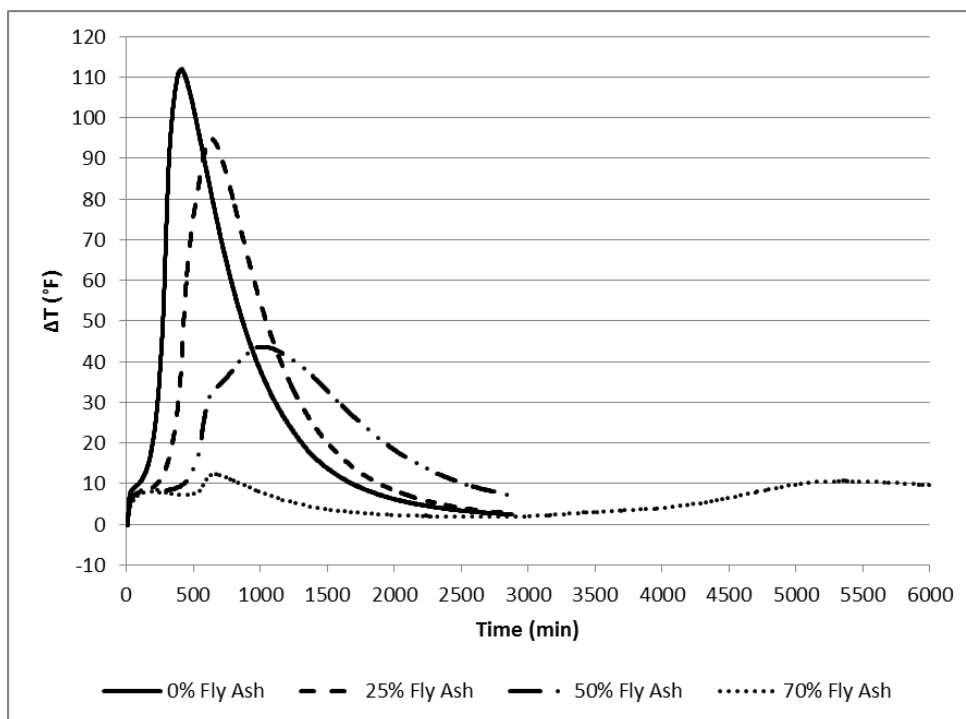
Figure D.12. Thermal Curve Plots for Combination 3-2
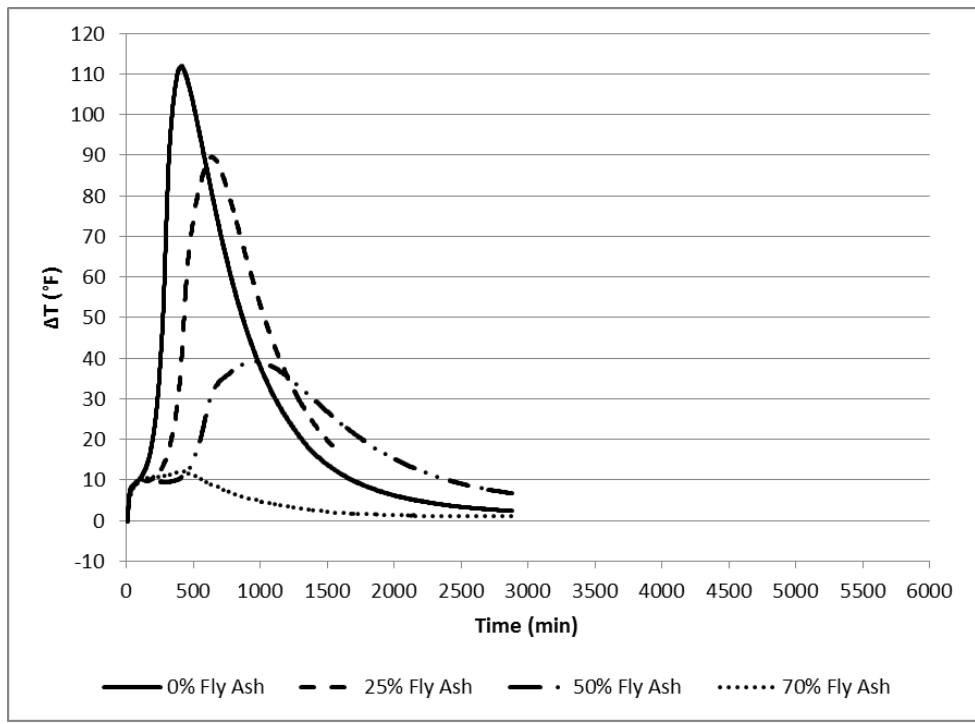
Figure D.13. Thermal Curve Plots for Combination 3-3
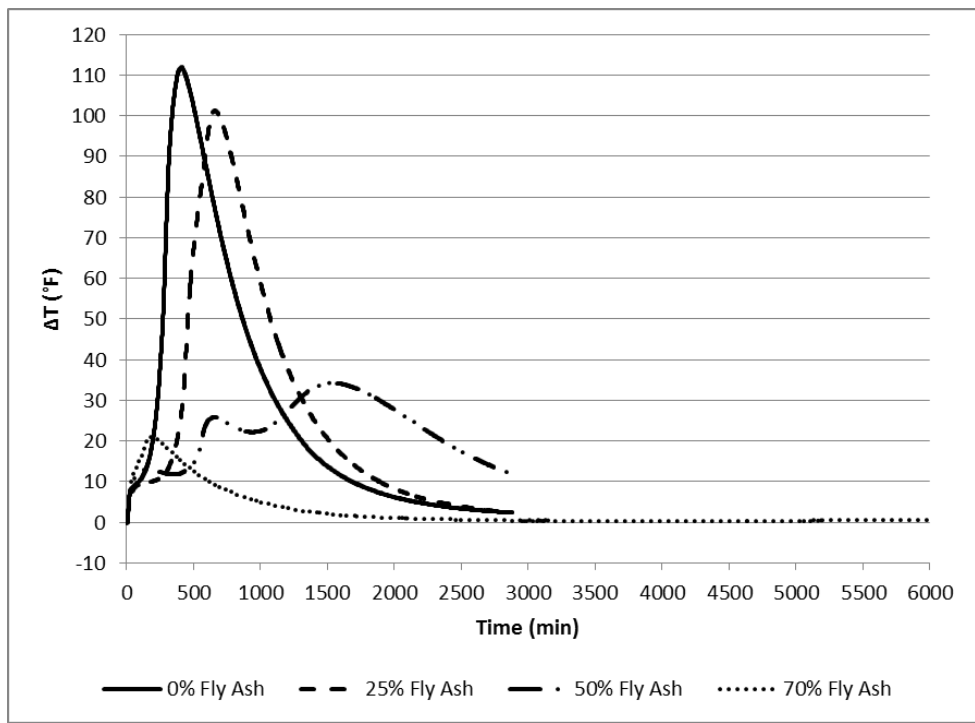
Figure D.14. Thermal Curve Plots for Combination 3-4
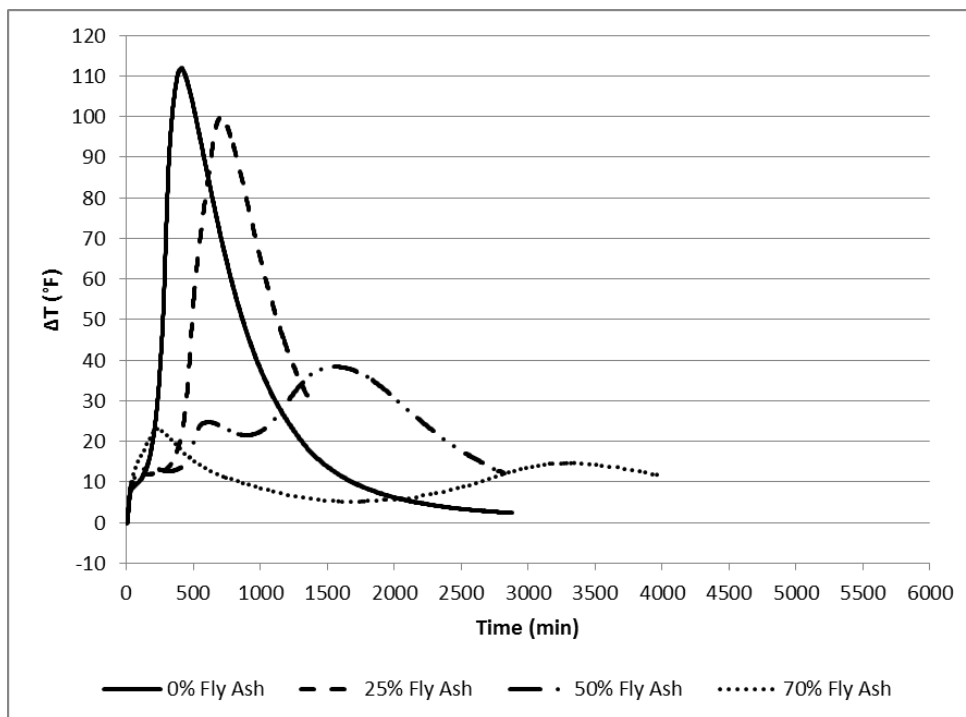
Figure D.15. Thermal Curve Plots for Combination 3-5
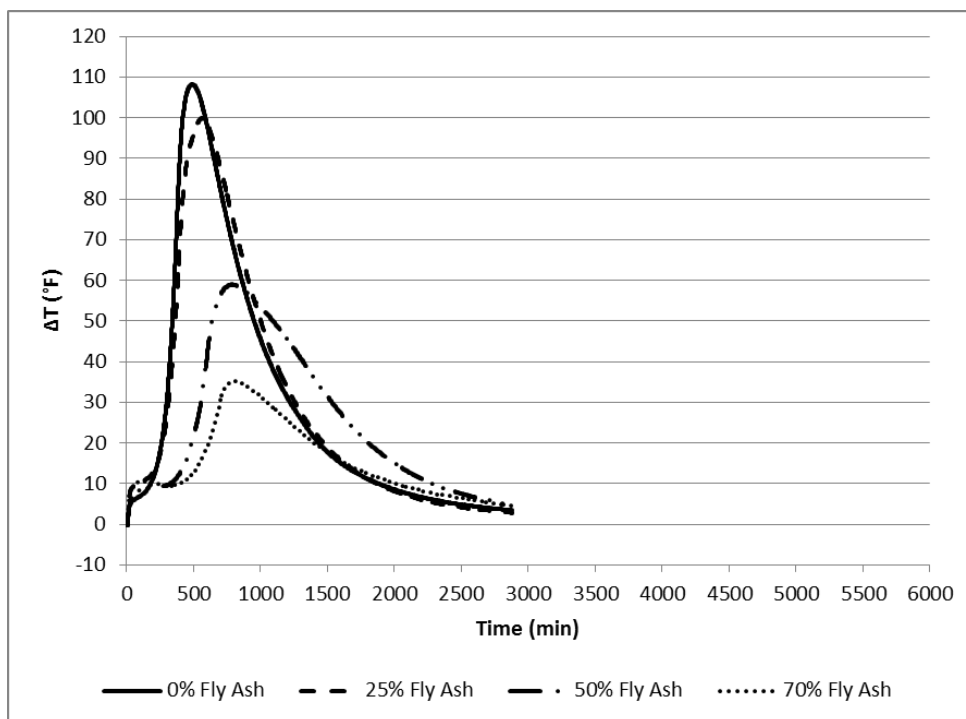
Figure D.16. Thermal Curve Plots for Combination 4-1
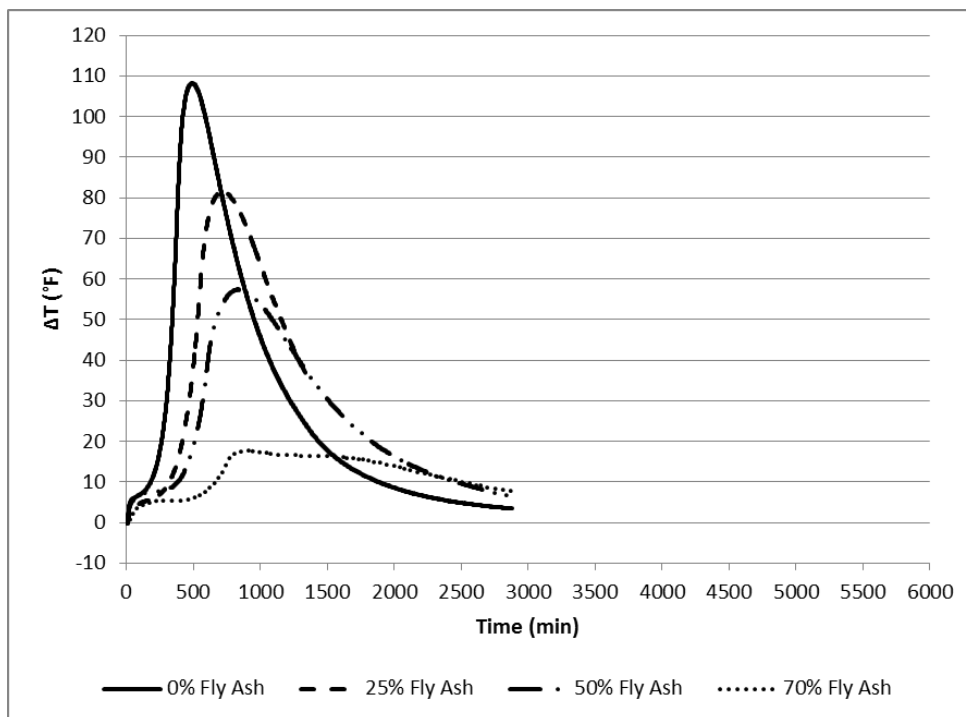
Figure D.17. Thermal Curve Plots for Combination 4-2
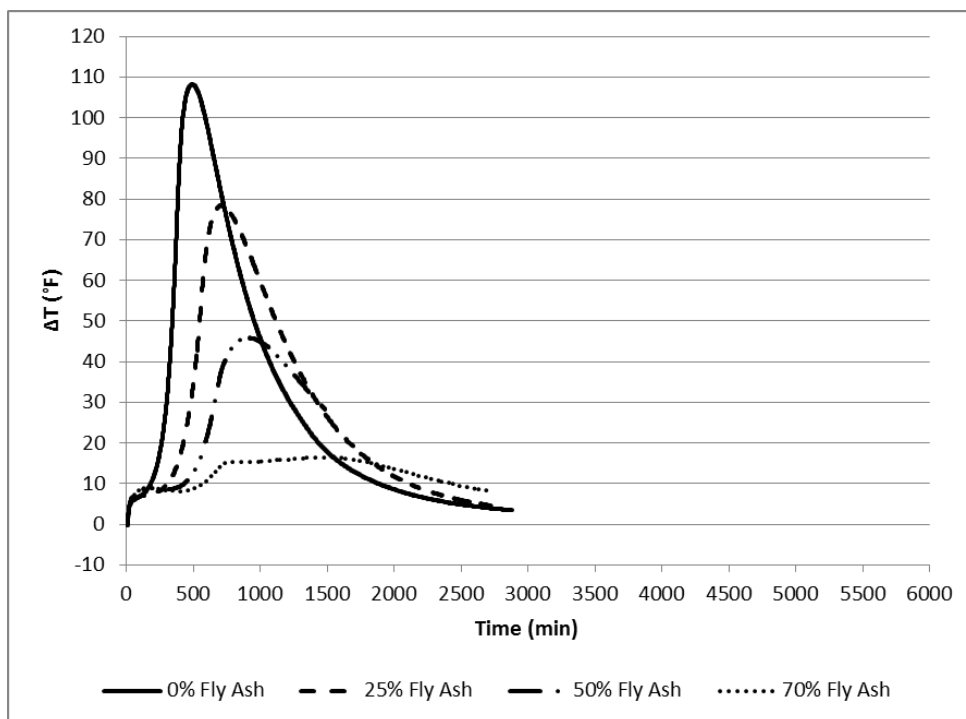
Figure D.18. Thermal Curve Plots for Combination 4-3

211
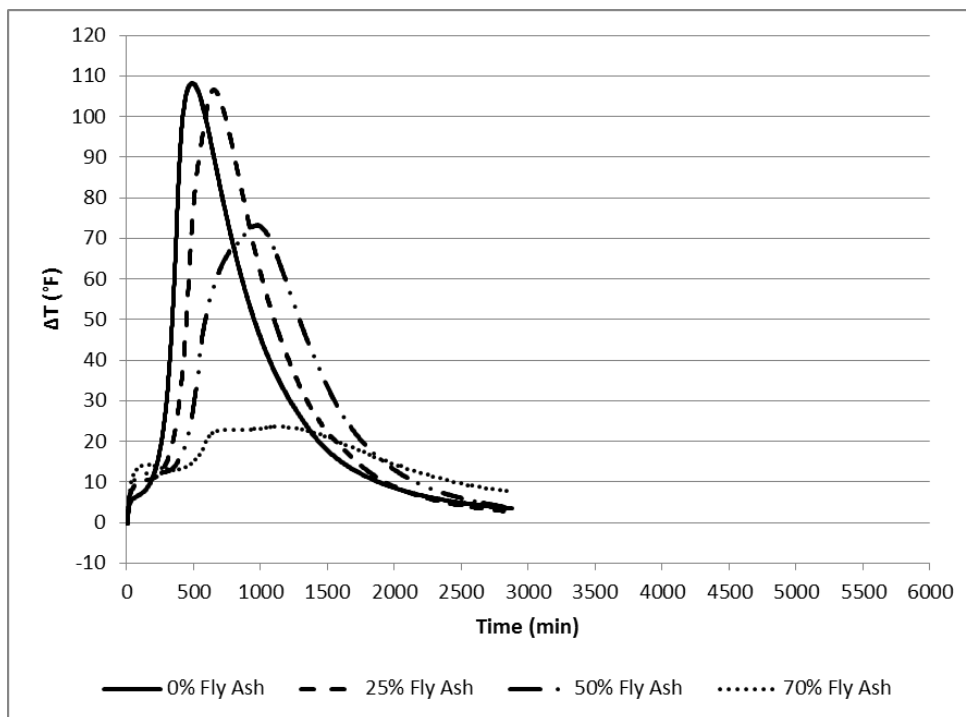
Figure D.19. Thermal Curve Plots for Combination 4-4
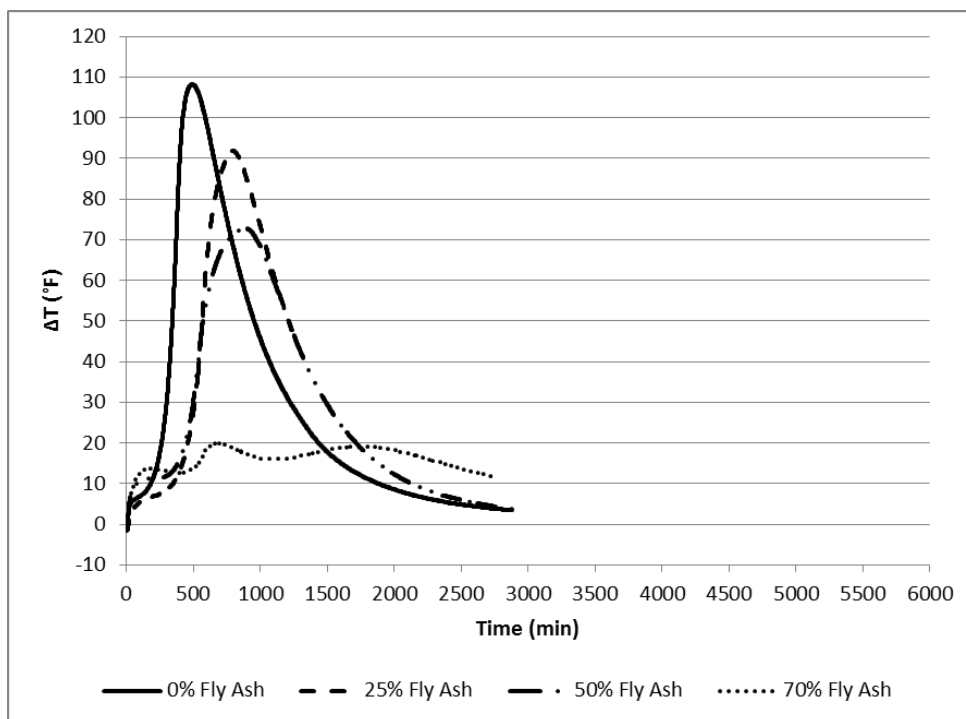
Figure D.20. Thermal Curve Plots for Combination 4-5
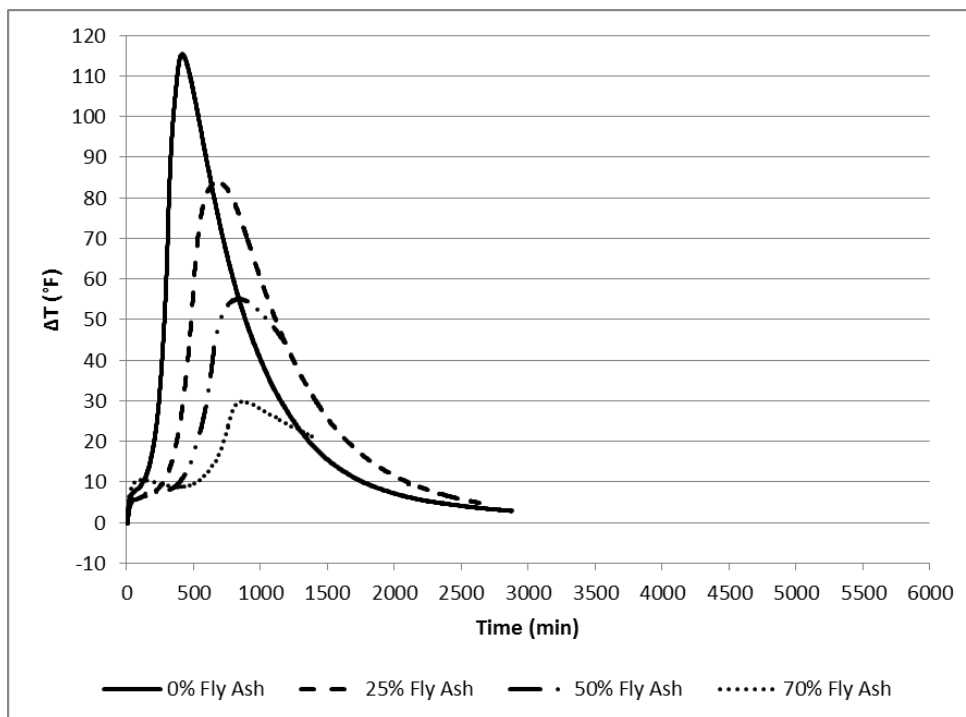
Figure D.21. Thermal Curve Plots for Combination 5-1
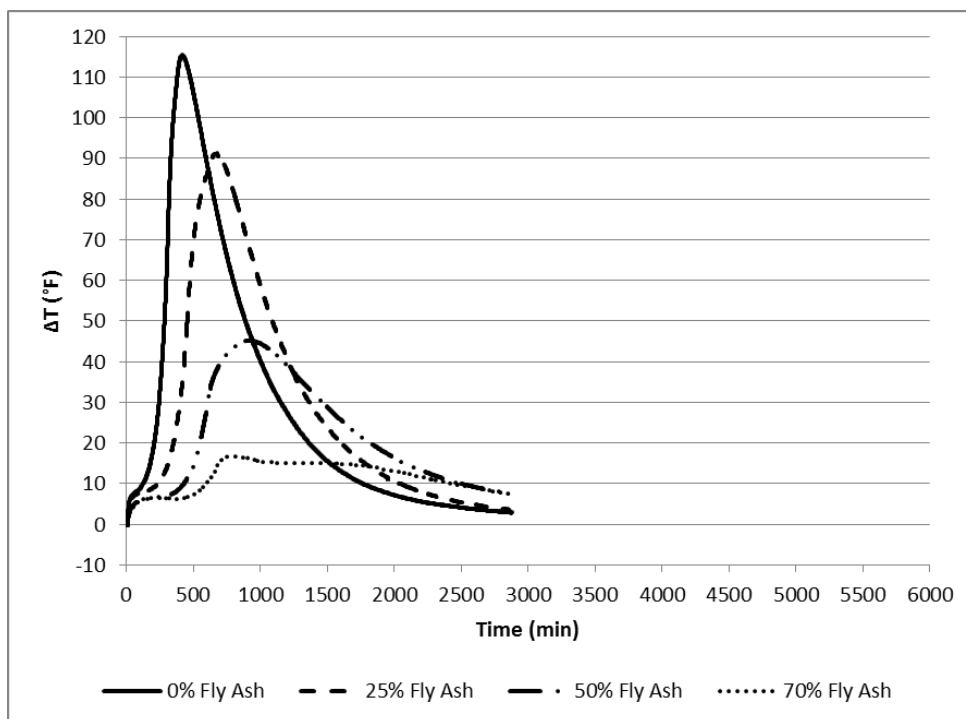
Figure D.22. Thermal Curve Plots for Combination 5-2
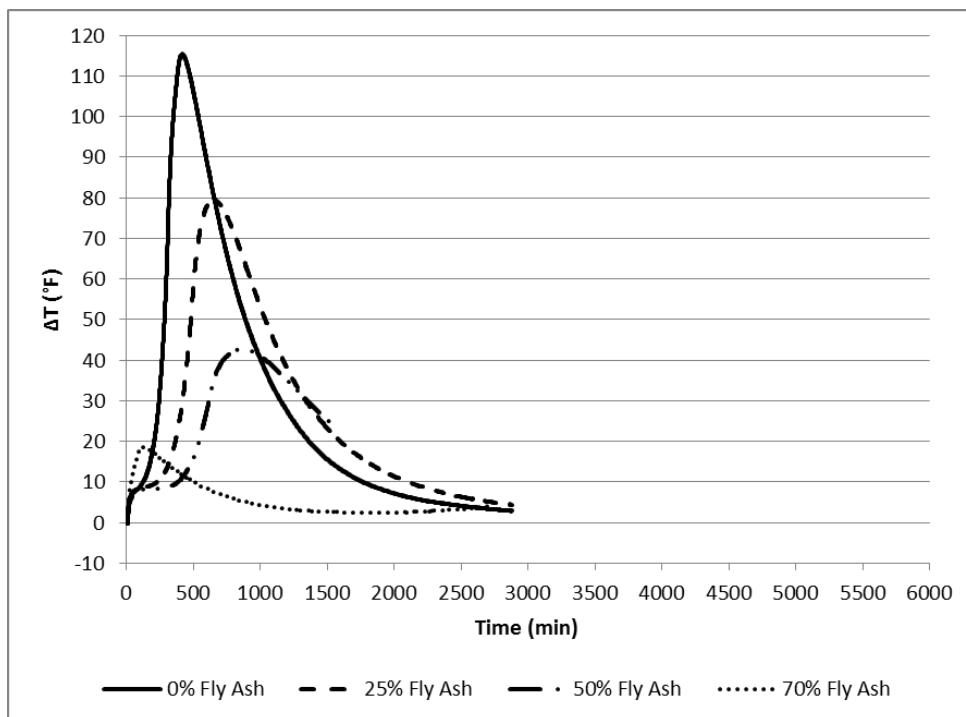
Figure D.23. Thermal Curve Plots for Combination 5-3
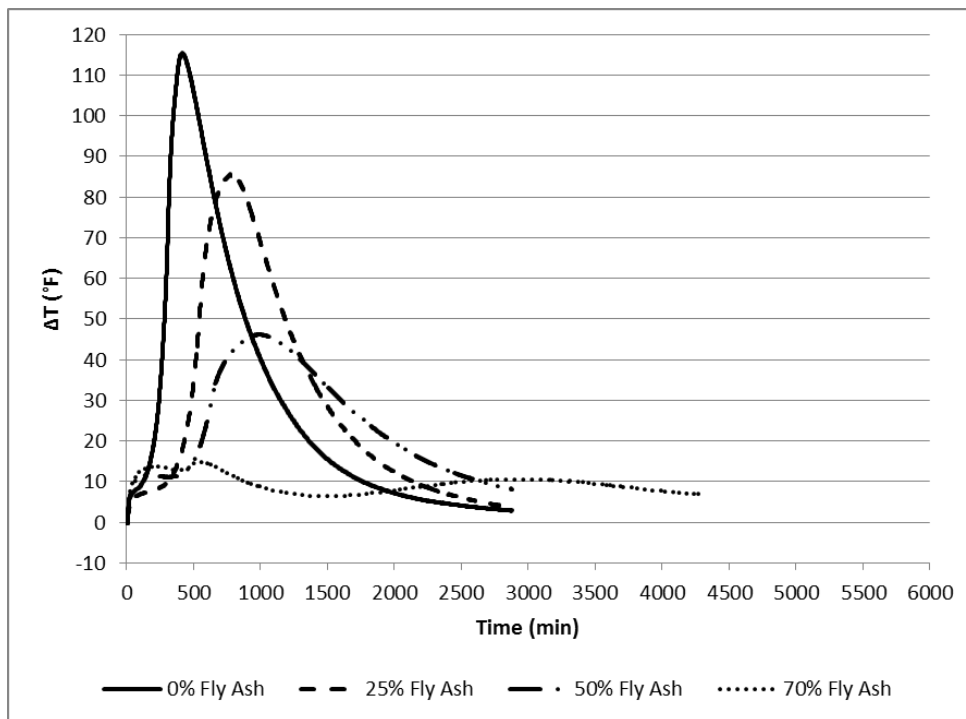
Figure D.24. Thermal Curve Plots for Combination 5-4
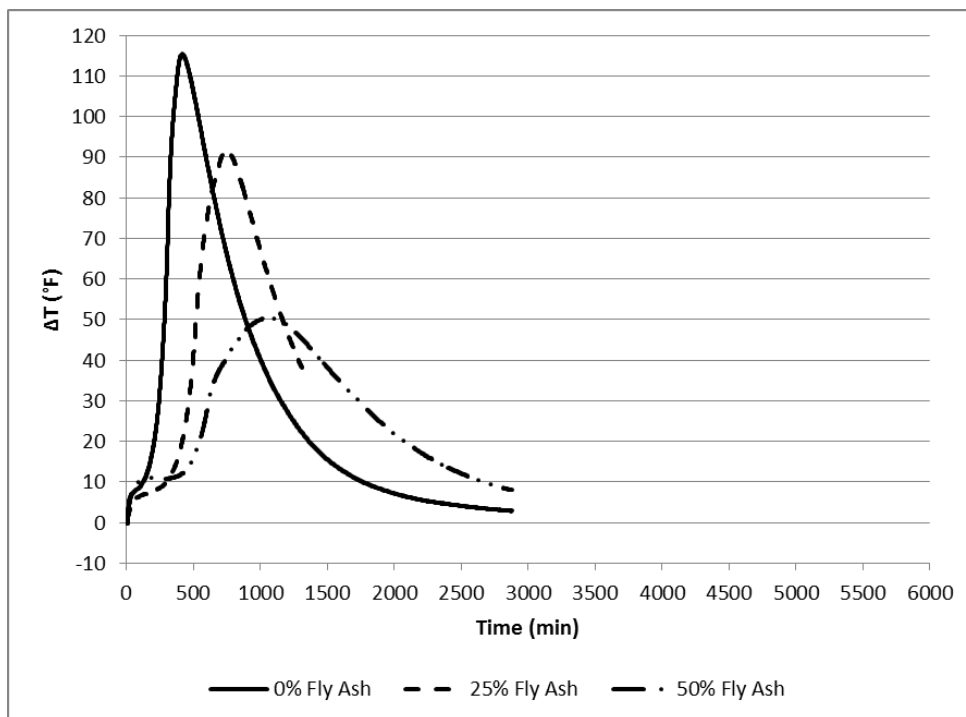
Figure D.25. Thermal Curve Plots for Combination 5-5

APPENDIX E

THERMAL CURVE PLOTS FROM THE MAIN EFFECTS PASTE STUDY
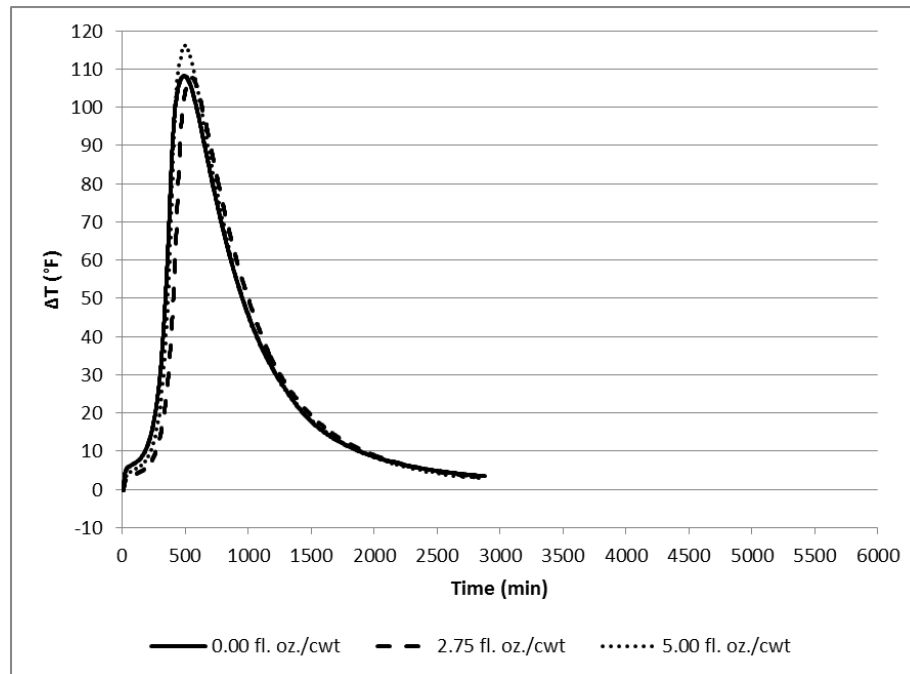
Figure E.1. Effect of Water Reducer on Combination 4-1 with 0% Fly Ash
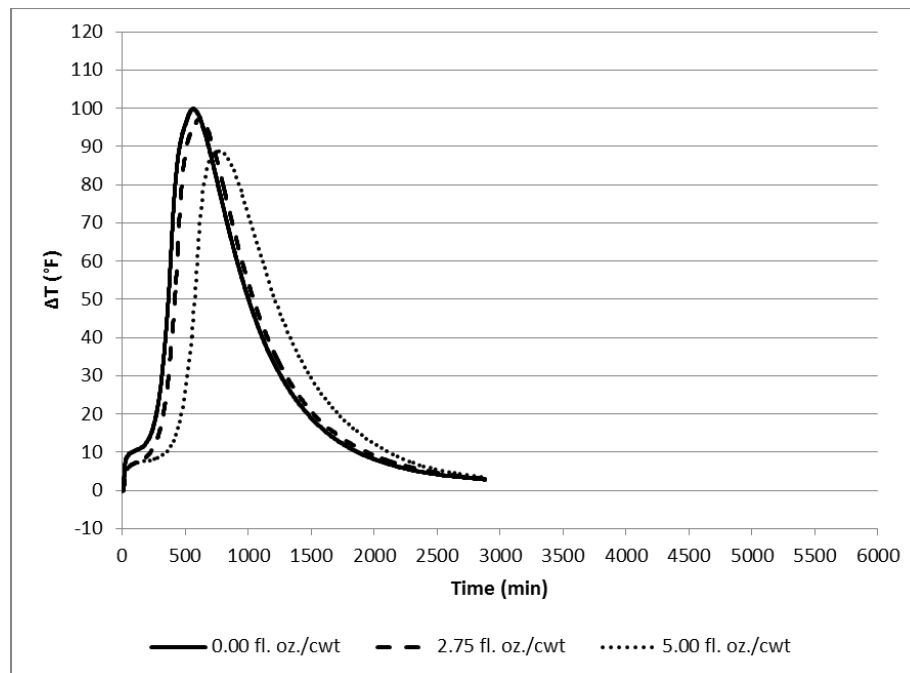
Figure E.2. Effect of Water Reducer on Combination 4-1 with 25% Fly Ash
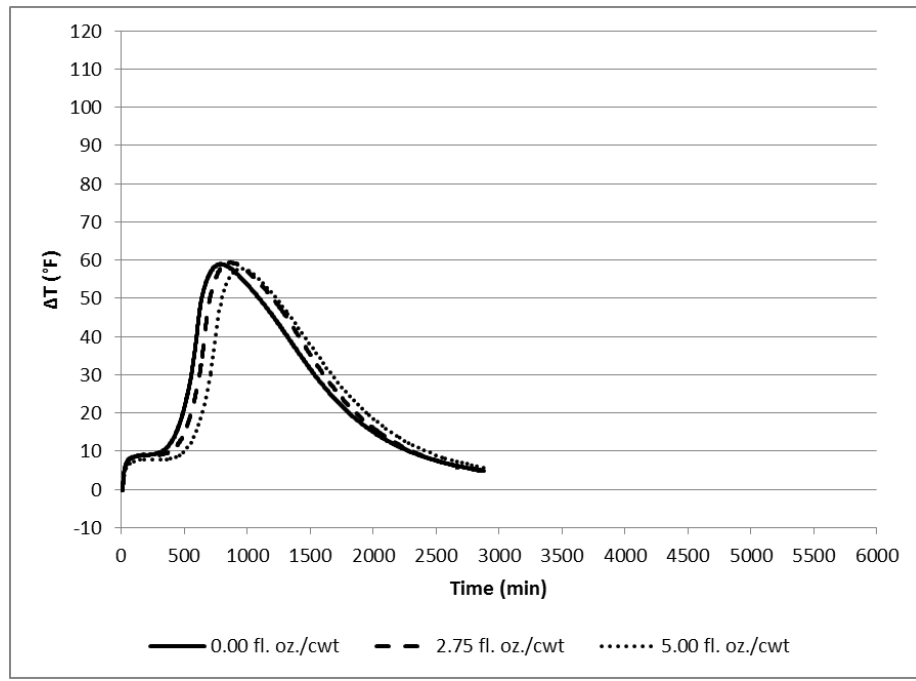
Figure E.3. Effect of Water Reducer on Combination 4-1 with 50% Fly Ash
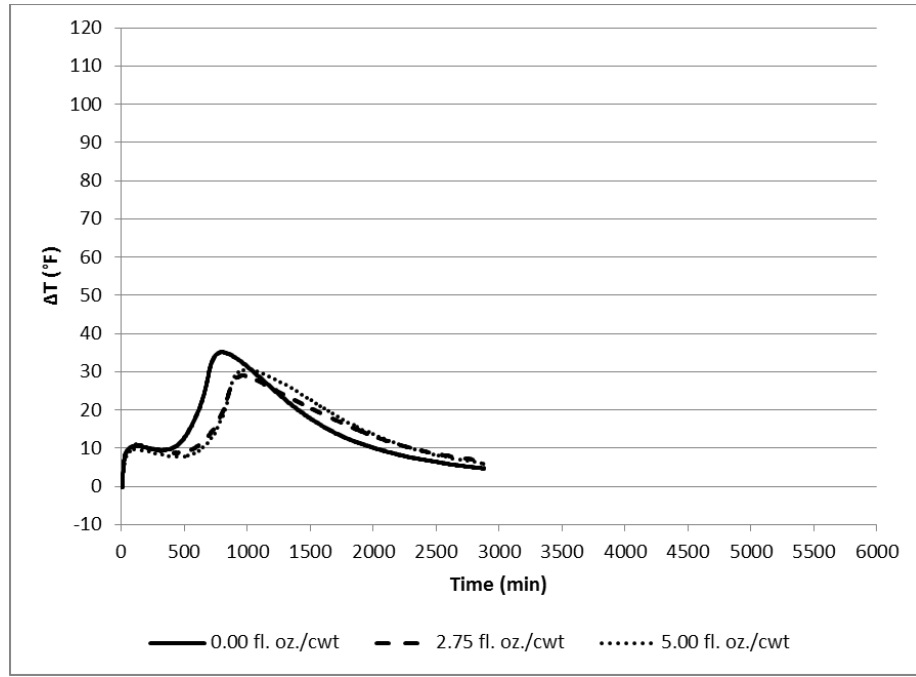
Figure E.4. Effect of Water Reducer on Combination 4-1 with 70% Fly Ash
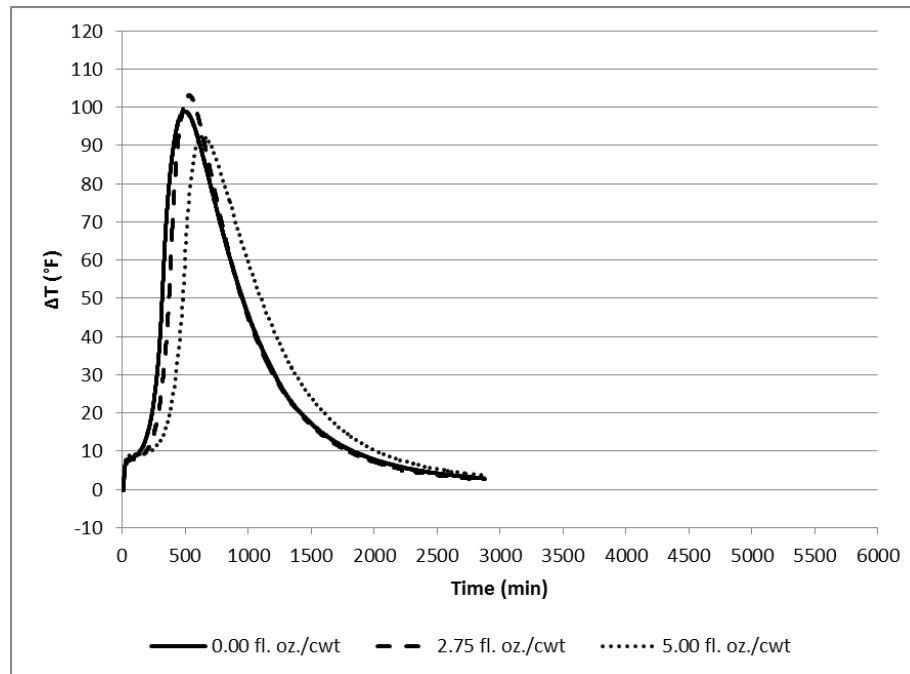
Figure E.5. Effect of Water Reducer on Combination 1-3 with 0% Fly Ash
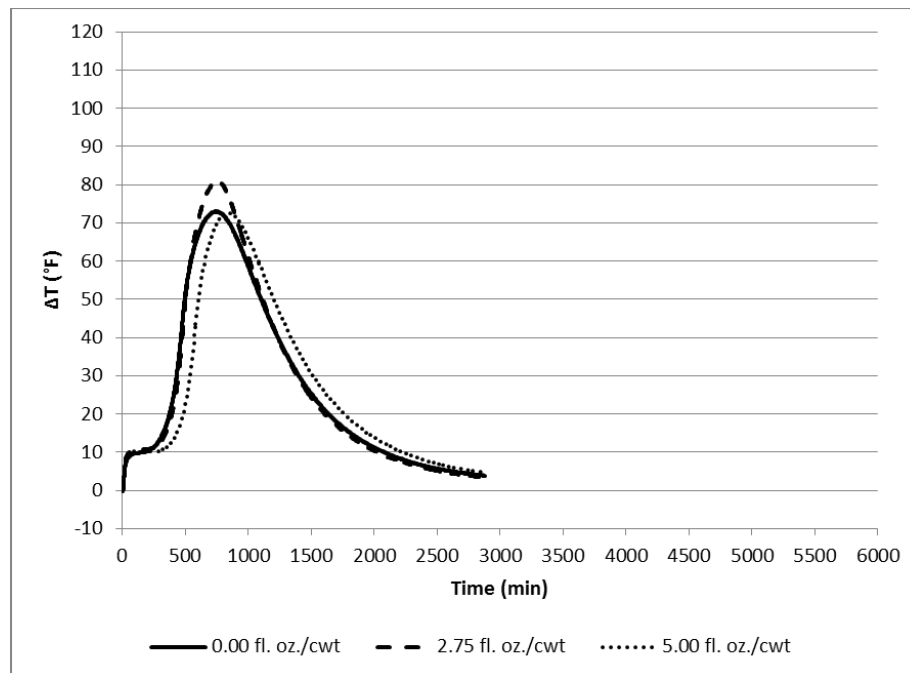
Figure E.6. Effect of Water Reducer on Combination 1-3 with 25% Fly Ash
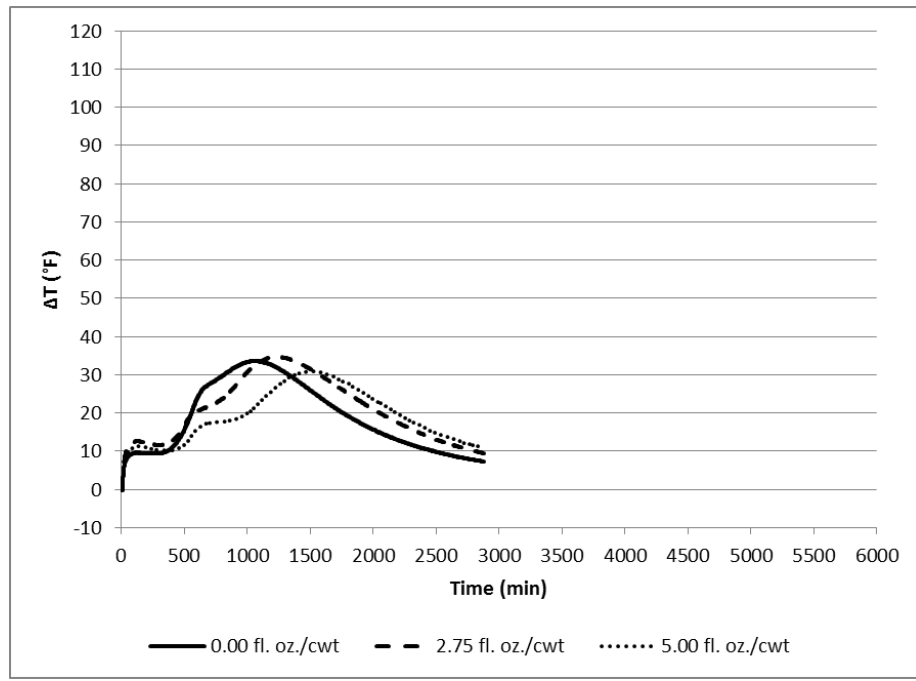
Figure E.7. Effect of Water Reducer on Combination 1-3 with 50% Fly Ash
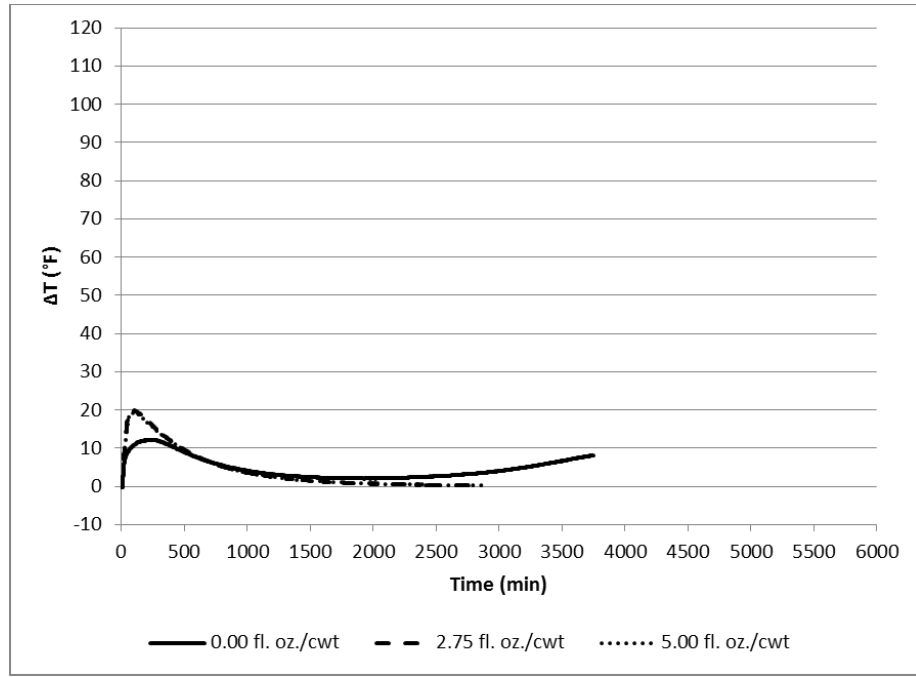
Figure E.8. Effect of Water Reducer on Combination 1-3 with 70% Fly Ash
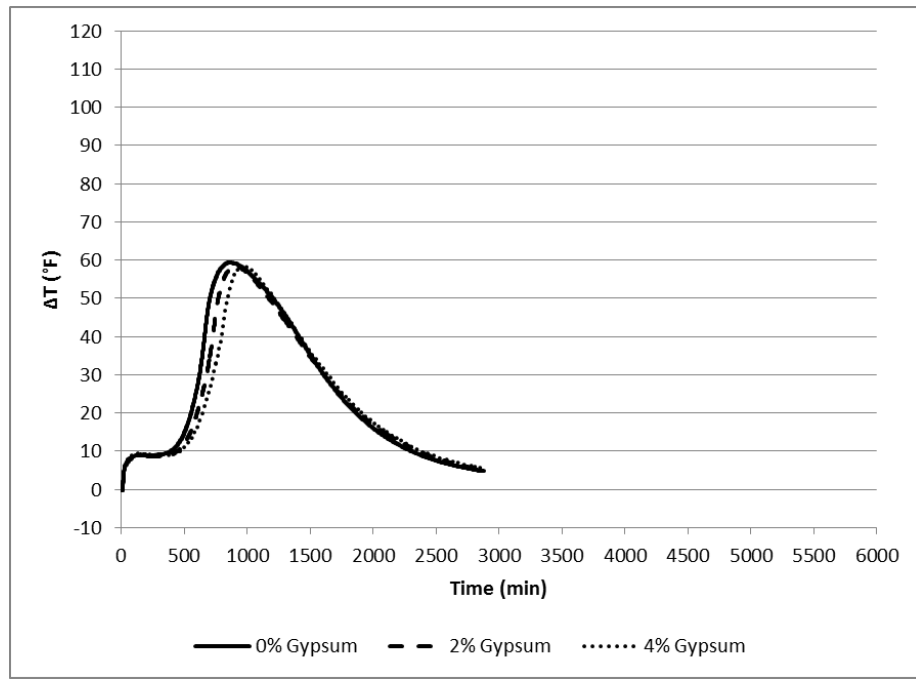
Figure E.9. Effects of Gypsum on Combination 4-1 with 50% Fly Ash and Low Dosage
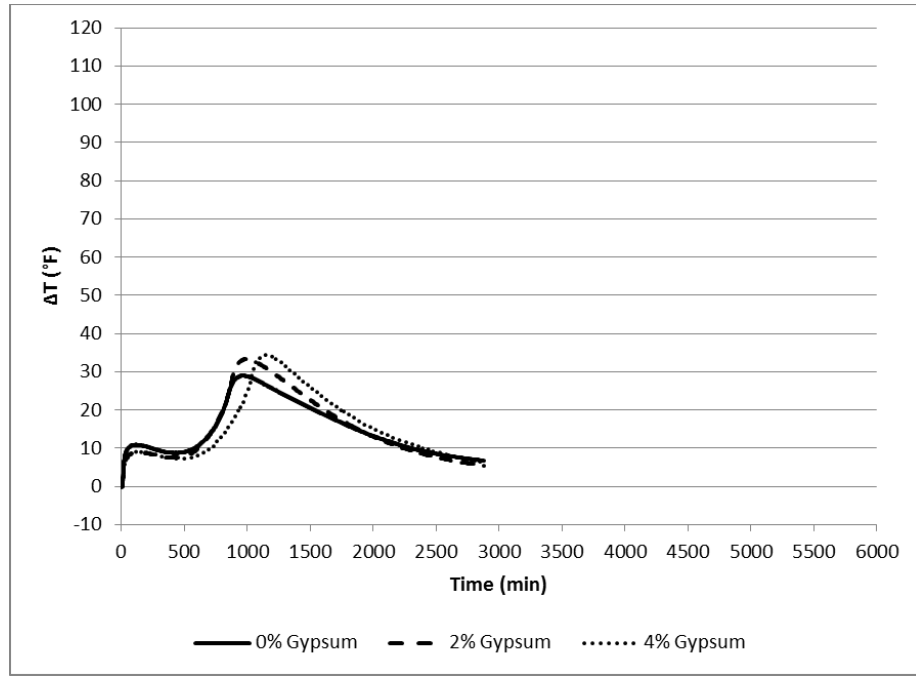
of Water Reducer

Figure E.10. Effects of Gypsum on Combination 4-1 with 70% Fly Ash and Low Dosage
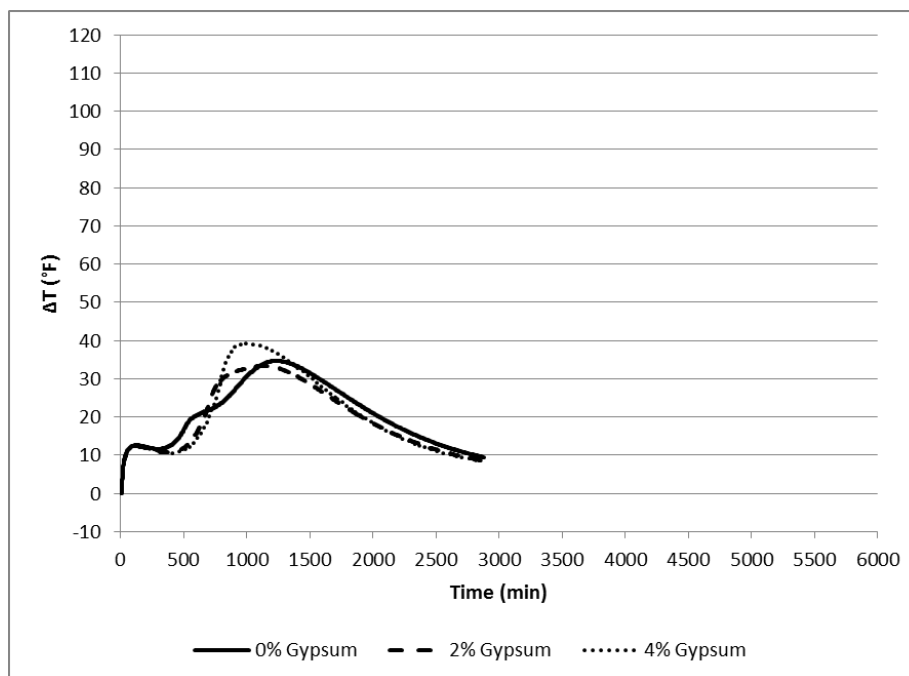
of Water Reducer

Figure E.11. Effects of Gypsum on Combination 1-3 with 50% Fly Ash and Low Dosage
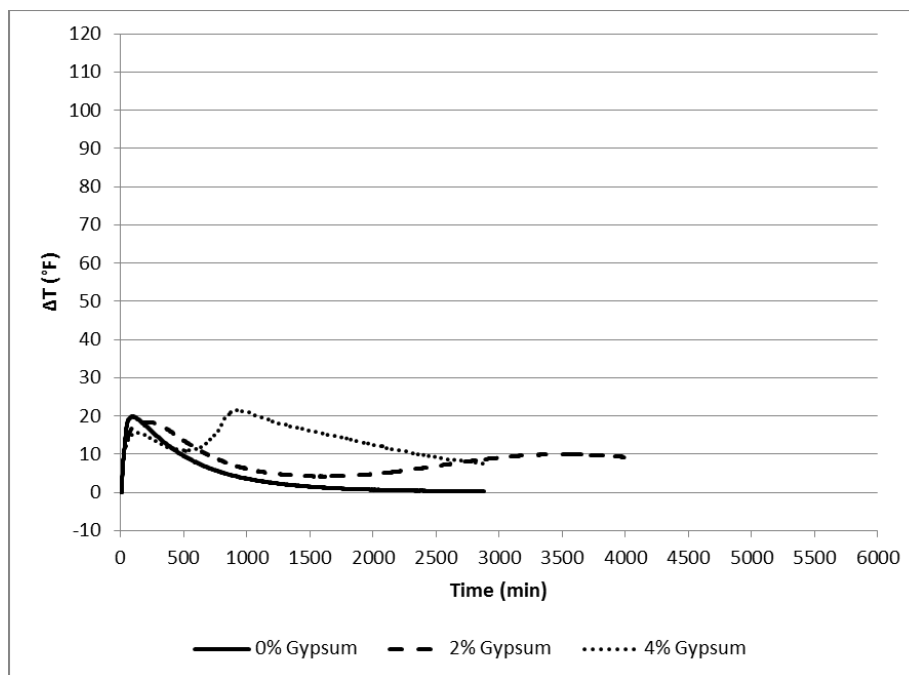
of Water Reducer

Figure E.12. Effects of Gypsum on Combination 1-3 with 70% Fly Ash and Low Dosage
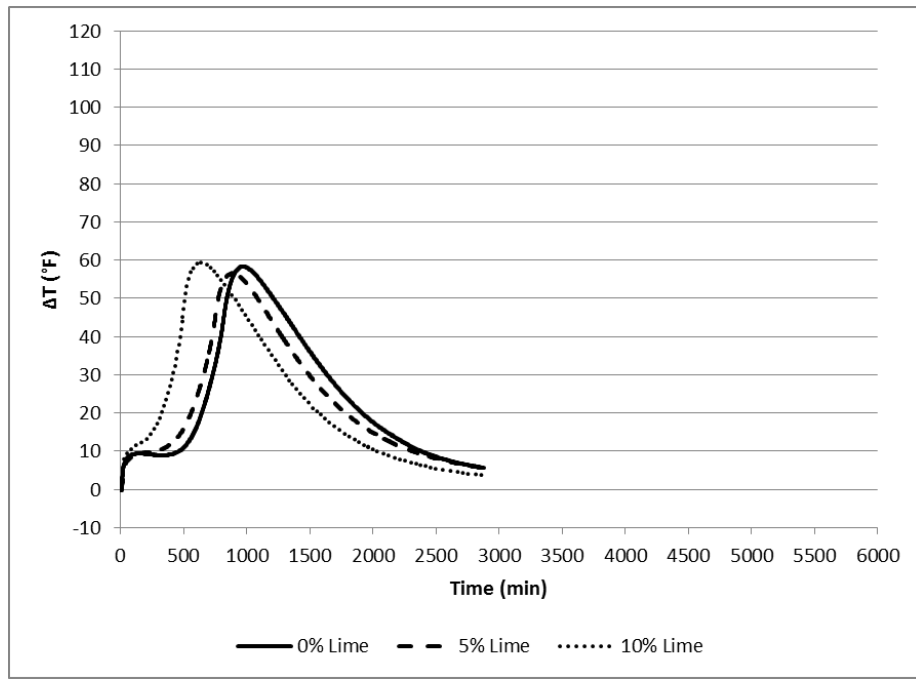
of Water Reducer

Figure E.13. Effects of Lime on Combination 4-1 with 50% Fly Ash, 4% Gypsum, and

Low Dosage of Water Reducer
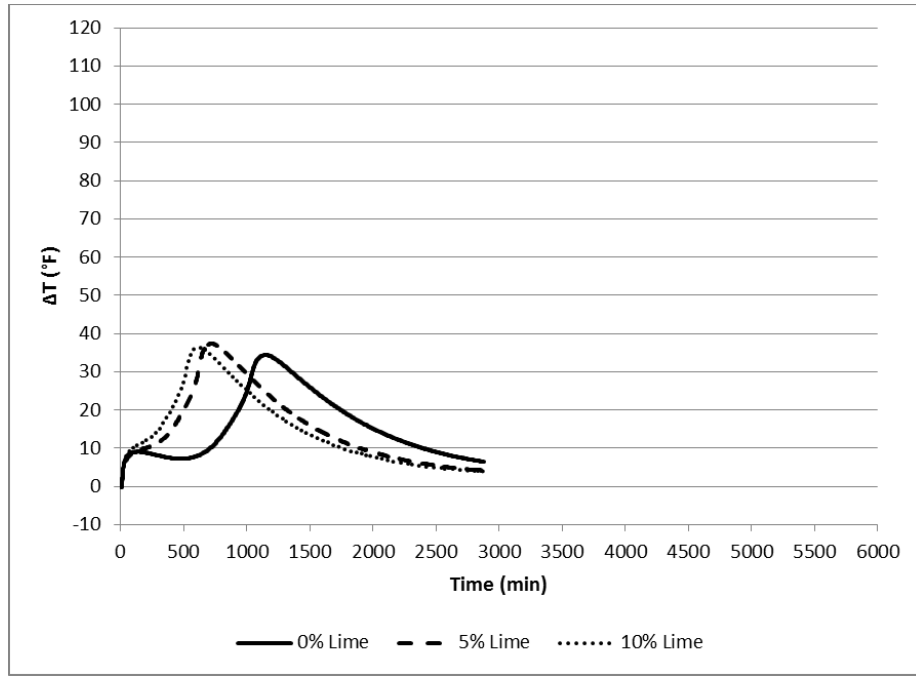
Figure E.14. Effects of Lime on Combination 4-1 with 70% Fly Ash, 4% Gypsum, and

Low Dosage of Water Reducer
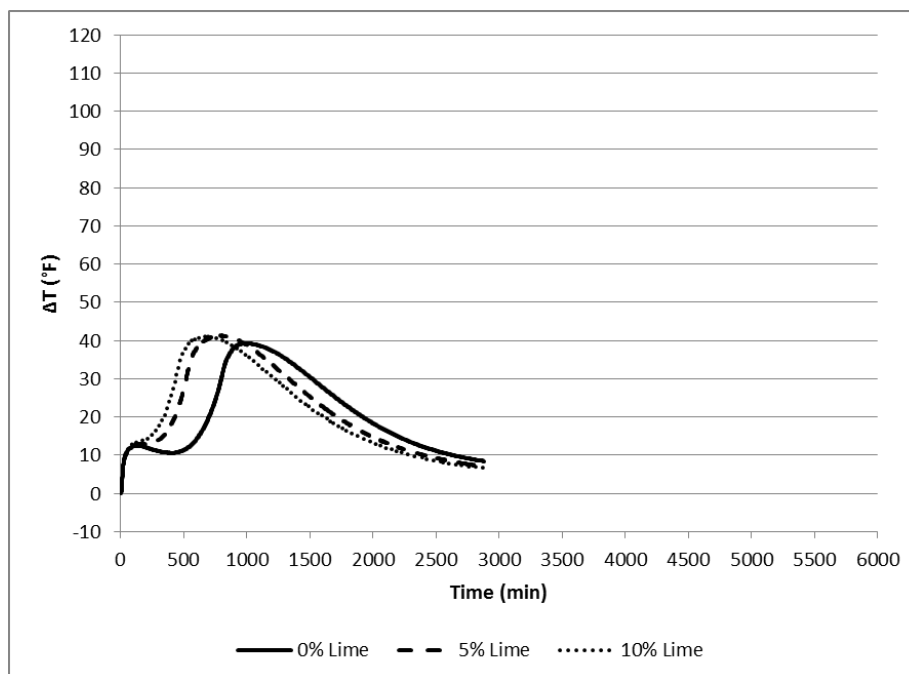
Figure E.15. Effects of Lime on Combination 1-3 with 50% Fly Ash, 4% Gypsum, and

Low Dosage of Water Reducer
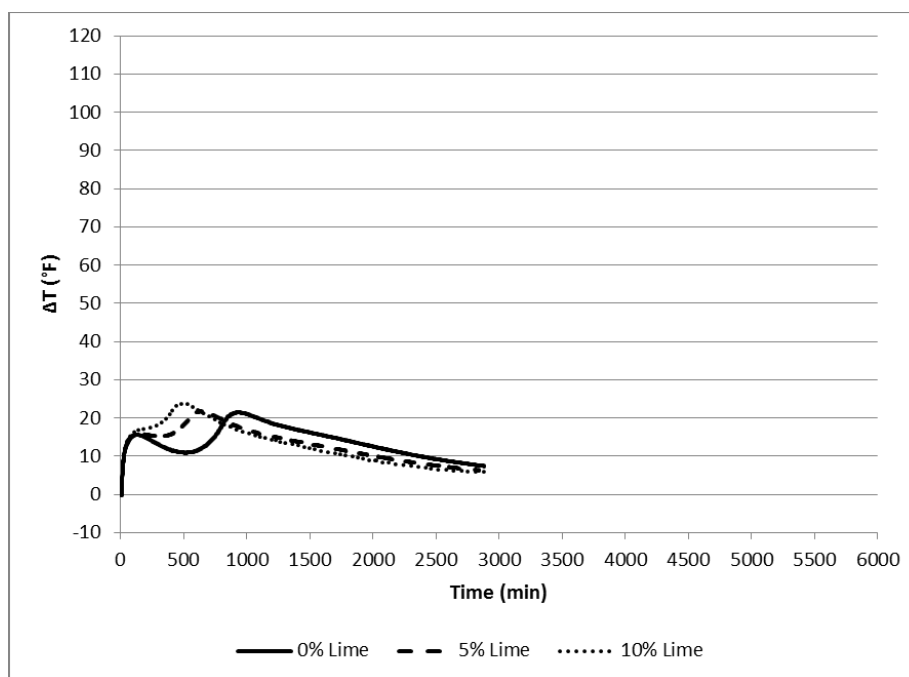
Figure E.16. Effects of Lime on Combination 1-3 with 70% Fly Ash, 4% Gypsum, and

Low Dosage of Water Reducer
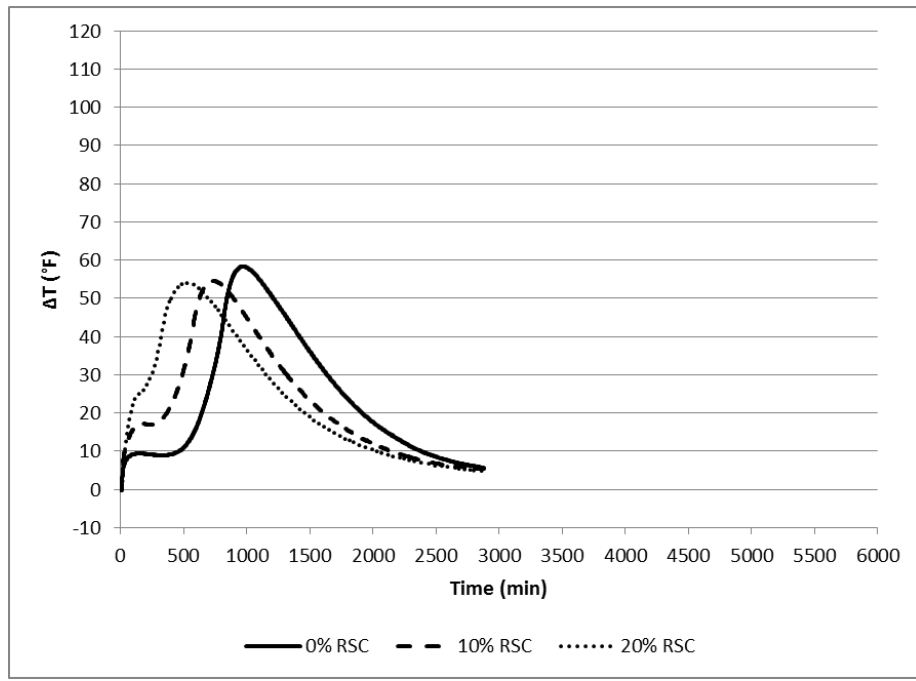
Figure E.17. Effects of Rapid Set Cement on Combination 4-1 with 50% Fly Ash, 4%

Gypsum, and Low Dosage of Water Reducer
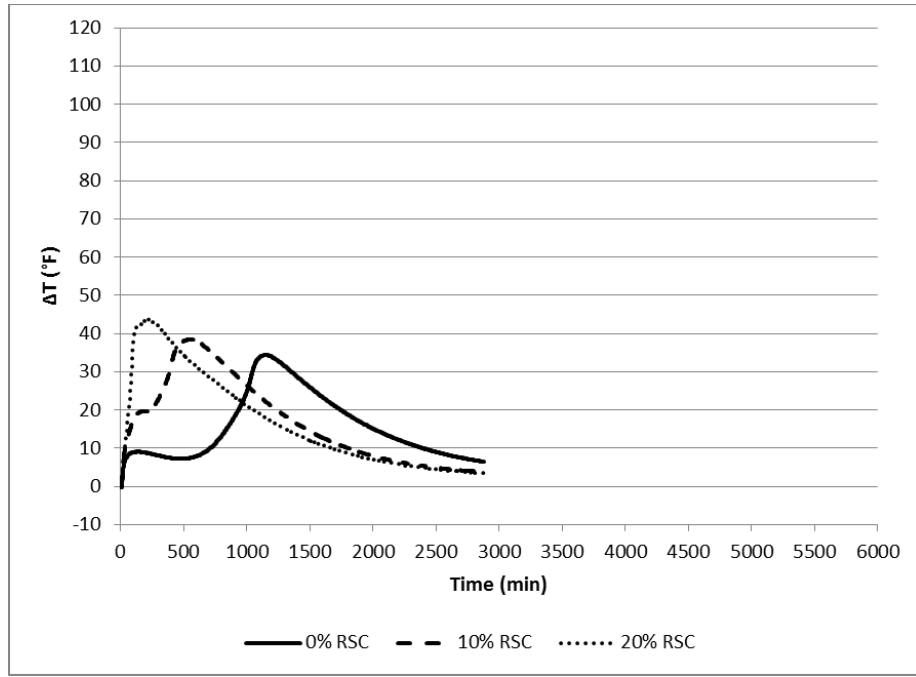
Figure E.18. Effects of Rapid Set Cement on Combination 4-1 with 70% Fly Ash, 4%

Gypsum, and Low Dosage of Water Reducer
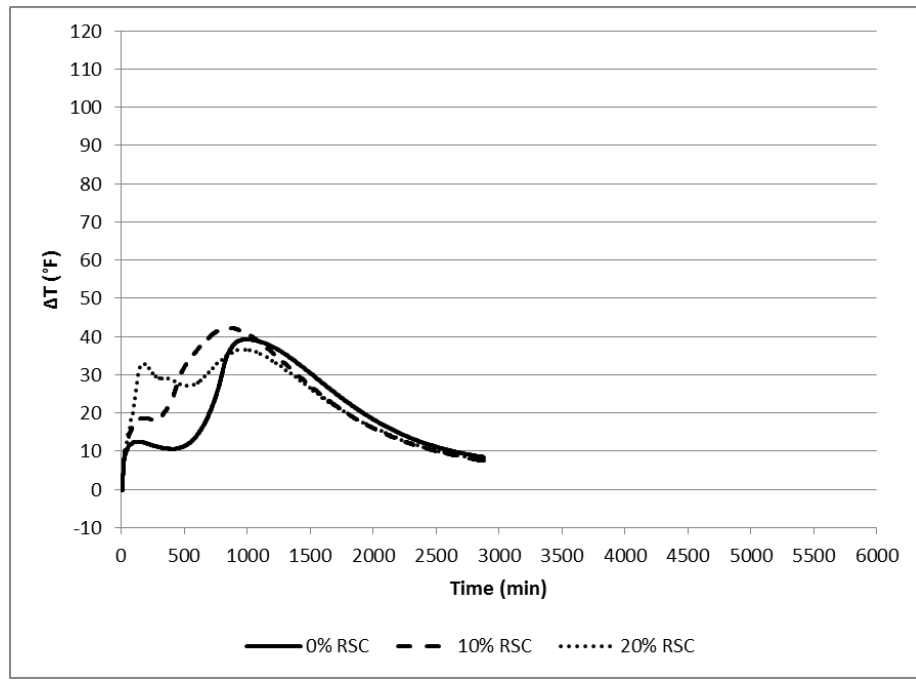
Figure E.19. Effects of Rapid Set Cement on Combination 1-3 with 50% Fly Ash, 4%

Gypsum, and Low Dosage of Water Reducer
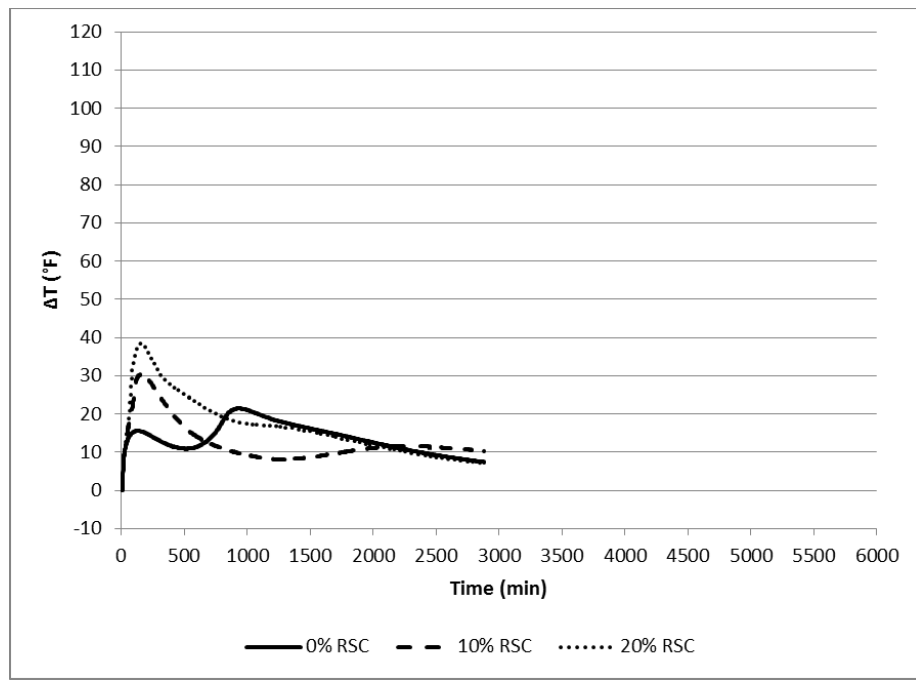
Figure E.20. Effects of Rapid Set Cement on Combination 1-3 with 70% Fly Ash, 4%

Gypsum, and Low Dosage of Water Reducer

APPENDIX F

SCREENING STUDY RESULTS

Vicat Setting Time

Combination	Proportions		Vicat Results		Combination	Proportions		Vicat Results	
	Cement (%)	Fly Ash (%)	Initial Set (min)	Final Set (min)		Cement (%)	Fly Ash (%)	Initial Set (min)	Final Set (min)
Baseline 1	100	0	110	210	Baseline 4	100	0	81	180
1-1	75	25	184	345	4-1	75	25	132	270
1-1	50	50	95	390	4-1	50	50	107	300
1-1	30	70	34	405	4-1	30	70	14	285
1-2	75	25	218	390	4-2	75	25	213	450
1-2	50	50	208	510	4-2	50	50	78	525
1-2	30	70	87	450	4-2	30	70	53	480
1-3	75	25	171	375	4-3	75	25	238	435
1-3	50	50	142	435	4-3	50	50	101	660
1-3	30	70	49	525	4-3	30	70	48	300
1-4	75	25	203	450	4-4	75	25	125	360
1-4	50	50	47	360	4-4	50	50	34	270
1-4	30	70	15	135	4-4	30	70	12	105
1-5	75	25	178	480	4-5	75	25	123	255
1-5	50	50	33	180	4-5	50	50	15	195
1-5	30	70	11	45	4-5	30	70	11	60
Baseline 2	100	0	158	255	Baseline 5	100	0	146	285
2-1	75	25	182	360	5-1	75	25	158	300
2-1	50	50	67	375	5-1	50	50	100	405
2-1	30	70	20	420	5-1	30	70	21	465
2-2	75	25	154	345	5-2	75	25	179	330
2-2	50	50	71	435	5-2	50	50	175	435
2-2	30	70	57	495	5-2	30	70	59	495
2-3	75	25	151	390	5-3	75	25	149	315
2-3	50	50	40	650	5-3	50	50	54	390
2-3	30	70	12	150	5-3	30	70	13	150
2-4	75	25	92	360	5-4	75	25	167	345
2-4	50	50	35	300	5-4	50	50	48	375
2-4	30	70	12	90	5-4	30	70	14	120
2-5	75	25	80	345	5-5	75	25	136	345
2-5	50	50	13	90	5-5	50	50	13	135
2-5	30	70	11	45	5-5	30	70	11	45
Baseline 3	100	0	78	180					
3-1	75	25	170	315					
3-1	50	50	85	360					
3-1	30	70	31	225					
3-2	75	25	146	315					
3-2	50	50	101	435					
3-2	30	70	59	435					
3-3	75	25	123	300					
3-3	50	50	96	450					
3-3	30	70	40	375					
3-4	75	25	172	375					
3-4	50	50	33	300					
3-4	30	70	12	60					
3-5	75	25	124	345					
3-5	50	50	12	75					
3-5	30	70	11	30					

Compressive Strength

Combination	Proportions Cement (%)	Proportions Fly Ash (%)	1-Day Cube Strength (psi)	28-Day Cube Strength (psi)	Combination	Proportions Cement (%)	Proportions Fly Ash (%)	1-Day Cube Strength (psi)	28-Day Cube Strength (psi)
Baseline 1	100	0	4693	11300	Baseline 4	100	0	4114	11261
1-1	75	25	2805	10992	4-1	75	25	3671	10535
1-1	50	50	1246	7912	4-1	50	50	1935	8500
1-1	30	70	332	4108	4-1	30	70	665	4144
1-2	75	25	2881	9925	4-2	75	25	3625	10053
1-2	50	50	610	7989	4-2	50	50	1302	8009
1-2	30	70	40	4084	4-2	30	70	277	3842
1-3	75	25	2774	10703	4-3	75	25	3230	9921
1-3	50	50	655	7874	4-3	50	50	1364	7849
1-3	30	70	16	2475	4-3	30	70	316	2897
1-4	75	25	2767	9889	4-4	75	25	3608	10698
1-4	50	50	335	8803	4-4	50	50	1483	8088
1-4	30	70	68	6037	4-4	30	70	332	4953
1-5	75	25	2924	11342	4-5	75	25	3783	10525
1-5	50	50	515	8323	4-5	50	50	1688	8148
1-5	30	70	100	5688	4-5	30	70	533	4926
Baseline 2	100	0	4562	11708	Baseline 5	100	0	4815	12207
2-1	75	25	2722	10107	5-1	75	25	3144	11087
2-1	50	50	1094	7241	5-1	50	50	1407	8005
2-1	30	70	407	3078	5-1	30	70	612	4321
2-2	75	25	2491	5916	5-2	75	25	3069	10911
2-2	50	50	934	4221	5-2	50	50	998	8001
2-2	30	70	178	2647	5-2	30	70	193	3730
2-3	75	25	2321	8888	5-3	75	25	2743	11481
2-3	50	50	837	6850	5-3	50	50	858	7703
2-3	30	70	62	2702	5-3	30	70	105	2412
2-4	75	25	2657	10426	5-4	75	25	2968	12079
2-4	50	50	1052	7906	5-4	50	50	1101	7625
2-4	30	70	90	4433	5-4	30	70	100	4019
2-5	75	25	2544	7915	5-5	75	25	3096	11674
2-5	50	50	1091	7828	5-5	50	50	1180	8725
2-5	30	70	285	4264	5-5	30	70	325	4309
Baseline 3	100	0	5182	11806					
3-1	75	25	3182	9886					
3-1	50	50	1271	6993					
3-1	30	70	308	4319					
3-2	75	25	3522	10514					
3-2	50	50	804	6718					
3-2	30	70	55	3818					
3-3	75	25	3154	9676					
3-3	50	50	917	6813					
3-3	30	70	22	2351					
3-4	75	25	3108	10421					
3-4	50	50	339	7692					
3-4	30	70	139	5353					
3-5	75	25	3329	8991					
3-5	50	50	926	6058					
3-5	30	70	137	5476					

Calorimeter Results

Combination	Cement (%)	Fly Ash (%)	ΔT_{max} (°F)	Time at ΔT_{max} (min)	Time at 20% ΔT_{max} (min)	Time at 50% ΔT_{max} (min)
Baseline 1	100	0	98.91	501	264	321
1-1	75	25	71.81	685	369	445
1-1	50	50	45.50	883	506	592
1-1	30	70	24.45	882	641	730
1-2	75	25	75.56	713	354	426
1-2	50	50	31.59	1256	488	571
1-2	30	70	10.05	599	493	519
1-3	75	25	72.96	749	392	469
1-3	50	50	33.58	1050	477	572
1-3	30	70	22.25	94	26	41
1-4	75	25	78.15	829	425	500
1-4	50	50	20.04	642	445	511
1-4	30	70	19.99	197	61	104
1-5	75	25	83.17	756	391	463
1-5	50	50	19.41	597	426	486
1-5	30	70	21.68	204	64	108
Baseline 2	100	0	96.40	521	305	374
2-1	75	25	81.29	705	380	455
2-1	50	50	53.69	763	455	548
2-1	30	70	30.52	819	573	671
2-2	75	25	80.25	714	374	452
2-2	50	50	47.50	822	438	520
2-2	30	70	17.39	757	541	612
2-3	75	25	72.43	644	376	452
2-3	50	50	38.92	861	462	552
2-3	30	70	11.41	627	471	526
2-4	75	25	83.87	744	413	484
2-4	50	50	45.47	927	481	556
2-4	30	70	14.71	588	471	512
2-5	75	25	85.44	738	414	486
2-5	50	50	49.62	977	508	581
2-5	30	70	----	----	----	----
Baseline 3	100	0	111.88	413	228	284
3-1	75	25	94.29	622	364	427
3-1	50	50	55.64	839	512	581
3-1	30	70	28.24	767	582	652
3-2	75	25	94.90	632	369	429
3-2	50	50	43.65	1010	521	582
3-2	30	70	12.26	664	546	576
3-3	75	25	89.61	635	364	428
3-3	50	50	39.26	966	506	583
3-3	30	70	12.15	400	179	316
3-4	75	25	101.17	664	413	469
3-4	50	50	25.77	660	500	550
3-4	30	70	20.99	185	38	86
3-5	75	25	99.82	703	446	505
3-5	50	50	24.73	607	452	493
3-5	30	70	23.04	232	62	116

Combination	Cement (%)	Fly Ash (%)	ΔT_{max} (°F)	Time at ΔT_{max} (min)	Time at 20% ΔT_{max} (min)	Time at 50% ΔT_{max} (min)
Baseline 4	100	0	108.25	486	288	353
4-1	75	25	99.92	567	306	374
4-1	50	50	58.97	785	475	573
4-1	30	70	35.17	794	537	640
4-2	75	25	81.61	713	412	513
4-2	50	50	57.41	837	483	578
4-2	30	70	17.74	885	591	696
4-3	75	25	78.41	705	431	526
4-3	50	50	45.85	917	545	642
4-3	30	70	16.53	1489	561	649
4-4	75	25	106.63	649	391	462
4-4	50	50	73.23	980	477	553
4-4	30	70	23.63	1150	503	570
4-5	75	25	91.93	791	474	563
4-5	50	50	72.94	881	463	541
4-5	30	70	19.85	681	512	562
Baseline 5	100	0	115.40	414	237	298
5-1	75	25	83.82	678	382	471
5-1	50	50	55.05	844	494	605
5-1	30	70	29.81	868	619	720
5-2	75	25	91.18	674	372	452
5-2	50	50	45.15	909	488	583
5-2	30	70	16.81	789	548	632
5-3	75	25	79.41	657	378	464
5-3	50	50	42.77	854	487	584
5-3	30	70	18.46	129	36	58
5-4	75	25	85.66	788	446	534
5-4	50	50	46.15	980	544	625
5-4	30	70	14.80	530	448	476
5-5	75	25	91.67	743	434	518
5-5	50	50	50.45	1063	533	617
5-5	30	70	----	----	----	----

Miniature Slump Results

Combination	Proportions Cement (%)	Proportions Fly Ash (%)	Early Stiffening Index (30-min/5-min)	Combination	Proportions Cement (%)	Proportions Fly Ash (%)	Early Stiffening Index (30-min/5-min)
Baseline 1	100	0	0.93	Baseline 4	100	0	0.92
1-1	75	25	1.02	4-1	75	25	0.91
1-1	50	50	0.84	4-1	50	50	0.72
1-1	30	70	0.69	4-1	30	70	0.64
1-2	75	25	0.87	4-2	75	25	1.08
1-2	50	50	0.79	4-2	50	50	0.73
1-2	30	70	0.55	4-2	30	70	0.54
1-3	75	25	0.95	4-3	75	25	0.88
1-3	50	50	0.83	4-3	50	50	0.71
1-3	30	70	0.59	4-3	30	70	0.57
1-4	75	25	0.89	4-4	75	25	0.77
1-4	50	50	0.59	4-4	50	50	0.65
1-4	30	70	0.50	4-4	30	70	0.57
1-5	75	25	0.87	4-5	75	25	0.64
1-5	50	50	0.68	4-5	50	50	0.55
1-5	30	70	0.36	4-5	30	70	0.35
Baseline 2	100	0	0.98	Baseline 5	100	0	0.77
2-1	75	25	0.95	5-1	75	25	0.85
2-1	50	50	0.75	5-1	50	50	0.71
2-1	30	70	0.49	5-1	30	70	0.56
2-2	75	25	0.78	5-2	75	25	0.77
2-2	50	50	0.66	5-2	50	50	0.69
2-2	30	70	0.50	5-2	30	70	0.51
2-3	75	25	0.76	5-3	75	25	0.77
2-3	50	50	0.58	5-3	50	50	0.74
2-3	30	70	0.49	5-3	30	70	0.58
2-4	75	25	0.72	5-4	75	25	0.71
2-4	50	50	0.49	5-4	50	50	0.58
2-4	30	70	0.30	5-4	30	70	0.48
2-5	75	25	0.75	5-5	75	25	0.72
2-5	50	50	0.46	5-5	50	50	0.57
2-5	30	70	0.27	5-5	30	70	0.26
Baseline 3	100	0	1.00				
3-1	75	25	0.90				
3-1	50	50	0.81				
3-1	30	70	0.63				
3-2	75	25	0.90				
3-2	50	50	0.83				
3-2	30	70	0.75				
3-3	75	25	0.96				
3-3	50	50	0.79				
3-3	30	70	0.61				
3-4	75	25	0.93				
3-4	50	50	0.79				
3-4	30	70	0.47				
3-5	75	25	0.86				
3-5	50	50	0.61				
3-5	30	70	0.50				

APPENDIX G

PASTE MAIN EFFECTS STUDY

Vicat Setting Time Results

Combination	Nominal Proportions						Vicat Results	
	Cement (%)	Fly Ash (%)	Gypsum (%)	Lime (%)	RSC (%)	WR (fl.oz./cwt)	Initial Set (min)	Final Set (min)
4-1	100	0	0	0	0	0.00	81	180
4-1	100	0	0	0	0	2.75	138	255
4-1	100	0	0	0	0	5.00	167	375
4-1	75	25	0	0	0	0.00	132	270
4-1	75	25	0	0	0	2.75	137	255
4-1	75	25	0	0	0	5.00	190	420
4-1	50	50	0	0	0	0.00	107	300
4-1	50	50	0	0	0	2.75	87	345
4-1	50	50	0	0	0	5.00	126	450
4-1	50	50	2	0	0	2.75	136	405
4-1	50	50	4	0	0	2.75	123	540
4-1	50	50	4	5	0	2.75	111	360
4-1	50	50	4	10	0	2.75	101	315
4-1	50	50	4	0	10	2.75	15	360
4-1	50	50	4	0	20	2.75	13	180
4-1	30	70	0	0	0	0.00	14	285
4-1	30	70	0	0	0	2.75	18	420
4-1	30	70	0	0	0	5.00	38	450
4-1	30	70	2	0	0	2.75	48	405
4-1	30	70	4	0	0	2.75	39	450
4-1	30	70	4	5	0	2.75	80	345
4-1	30	70	4	10	0	2.75	92	345
4-1	30	70	4	0	10	2.75	12	135
4-1	30	70	4	0	20	2.75	12	90
1-3	100	0	0	0	0	0.00	110	210
1-3	100	0	0	0	0	2.75	147	315
1-3	100	0	0	0	0	5.00	171	360
1-3	75	25	0	0	0	0.00	171	375
1-3	75	25	0	0	0	2.75	214	510
1-3	75	25	0	0	0	5.00	238	555
1-3	50	50	0	0	0	0.00	142	435
1-3	50	50	0	0	0	2.75	65	495
1-3	50	50	0	0	0	5.00	73	510
1-3	50	50	2	0	0	2.75	77	570
1-3	50	50	4	0	0	2.75	83	675
1-3	50	50	4	5	0	2.75	63	465
1-3	50	50	4	10	0	2.75	46	360
1-3	50	50	4	0	10	2.75	44	450
1-3	50	50	4	0	20	2.75	31	165
1-3	30	70	0	0	0	0.00	49	525
1-3	30	70	0	0	0	2.75	17	135
1-3	30	70	0	0	0	5.00	12	90
1-3	30	70	2	0	0	2.75	15	240
1-3	30	70	4	0	0	2.75	24	300
1-3	30	70	4	5	0	2.75	25	285
1-3	30	70	4	10	0	2.75	14	195
1-3	30	70	4	0	10	2.75	12	120
1-3	30	70	4	0	20	2.75	12	75

Compressive Strength Results

Combination	Nominal Proportions						Cube Compressive Strength (psi)				
	Cement (%)	Fly Ash (%)	Gypsum (%)	Lime (%)	RSC (%)	WR (fl.oz./cwt)	1-Day	3-Day	7-Day	28-Day	56-Day
4-1	100	0	0	0	0	0.00	4114	8111	9672	11261	12863
4-1	100	0	0	0	0	2.75	4199	8192	10232	11576	13625
4-1	100	0	0	0	0	5.00	5243	8808	10602	13116	13291
4-1	75	25	0	0	0	0.00	3671	6190	7842	10535	11125
4-1	75	25	0	0	0	2.75	3387	6779	7613	11015	12553
4-1	75	25	0	0	0	5.00	2857	6136	7513	10883	12989
4-1	50	50	0	0	0	0.00	1935	3535	4963	8500	8710
4-1	50	50	0	0	0	2.75	1381	3281	4855	6327	8071
4-1	50	50	0	0	0	5.00	1217	3580	4978	6574	8457
4-1	50	50	2	0	0	2.75	1284	3351	4811	6831	8169
4-1	50	50	4	0	0	2.75	710	3329	5118	6916	8364
4-1	50	50	4	5	0	2.75	622	3163	4871	6510	7204
4-1	50	50	4	10	0	2.75	1234	3134	4640	6160	7521
4-1	50	50	4	0	10	2.75	774	2940	5299	7191	8218
4-1	50	50	4	0	20	2.75	1202	3343	5311	7891	8186
4-1	30	70	0	0	0	0.00	665	1101	1740	4144	4125
4-1	30	70	0	0	0	2.75	309	1036	2056	3078	4360
4-1	30	70	0	0	0	5.00	369	1157	2075	3224	4422
4-1	30	70	2	0	0	2.75	462	1289	2088	3168	3626
4-1	30	70	4	0	0	2.75	212	1643	2441	3644	4267
4-1	30	70	4	5	0	2.75	557	1433	2157	3229	3405
4-1	30	70	4	10	0	2.75	544	1264	1992	2774	3256
4-1	30	70	4	0	10	2.75	675	1674	2793	3854	4641
4-1	30	70	4	0	20	2.75	802	1885	3067	4441	5207
1-3	100	0	0	0	0	0.00	4693	7892	8998	11300	11655
1-3	100	0	0	0	0	2.75	4176	7905	9015	12668	13979
1-3	100	0	0	0	0	5.00	3086	7790	9059	11673	13814
1-3	75	25	0	0	0	0.00	2774	4762	7034	10703	11838
1-3	75	25	0	0	0	2.75	2031	5387	7517	10577	11877
1-3	75	25	0	0	0	5.00	1642	4961	8276	11201	11913
1-3	50	50	0	0	0	0.00	655	2337	4218	7874	7480
1-3	50	50	0	0	0	2.75	239	2417	4289	5828	6915
1-3	50	50	0	0	0	5.00	135	2159	3932	6069	7232
1-3	50	50	2	0	0	2.75	348	2131	3971	5622	7354
1-3	50	50	4	0	0	2.75	315	2232	4193	5828	6986
1-3	50	50	4	5	0	2.75	656	2616	4399	5969	6393
1-3	50	50	4	10	0	2.75	697	2743	4185	5399	5972
1-3	50	50	4	0	10	2.75	660	2901	4587	6661	8249
1-3	50	50	4	0	20	2.75	606	2931	4785	7150	8480
1-3	30	70	0	0	0	0.00	16	75	93	2475	3168
1-3	30	70	0	0	0	2.75	58	71	103	2588	3867
1-3	30	70	0	0	0	5.00	59	76	98	2504	3414
1-3	30	70	2	0	0	2.75	64	457	1459	2831	3768
1-3	30	70	4	0	0	2.75	212	998	1696	2890	3750
1-3	30	70	4	5	0	2.75	244	913	1596	2669	3291
1-3	30	70	4	10	0	2.75	240	781	1432	2685	3118
1-3	30	70	4	0	10	2.75	275	1012	1875	3544	4331
1-3	30	70	4	0	20	2.75	443	567	2431	4362	5966

Calorimeter Results

Combination	\multicolumn{6}{c}{Nominal Proportions}	ΔT_{max} (°F)	Time at ΔT_{max} (min)	Time at 20% ΔT_{max} (min)	Time at 50% ΔT_{max} (min)
	Cement (%)	Fly Ash (%)	Gypsum (%)	Lime (%)	RSC (%)	WR (fl.oz./cwt)				
4-1	100	0	0	0	0	0.00	108.25	486	288	353
4-1	100	0	0	0	0	2.75	107.74	551	347	413
4-1	100	0	0	0	0	5.00	116.16	501	314	374
4-1	75	25	0	0	0	0.00	99.92	567	306	374
4-1	75	25	0	0	0	2.75	97.39	618	345	420
4-1	75	25	0	0	0	5.00	88.80	753	483	569
4-1	50	50	0	0	0	0.00	58.97	785	475	573
4-1	50	50	0	0	0	2.75	59.37	846	543	639
4-1	50	50	0	0	0	5.00	57.82	948	621	722
4-1	50	50	2	0	0	2.75	58.36	908	588	697
4-1	50	50	4	0	0	2.75	58.34	962	630	756
4-1	50	50	4	5	0	2.75	56.58	885	534	678
4-1	50	50	4	10	0	2.75	59.37	631	325	444
4-1	50	50	4	0	10	2.75	54.61	726	433	534
4-1	50	50	4	0	20	2.75	54.13	520	251	318
4-1	30	70	0	0	0	0.00	35.17	794	537	640
4-1	30	70	0	0	0	2.75	28.98	964	680	796
4-1	30	70	0	0	0	5.00	30.61	984	707	812
4-1	30	70	2	0	0	2.75	33.32	995	684	812
4-1	30	70	4	0	0	2.75	34.39	1148	787	947
4-1	30	70	4	5	0	2.75	37.37	720	394	547
4-1	30	70	4	10	0	2.75	36.38	613	286	441
4-1	30	70	4	0	10	2.75	38.50	544	303	378
4-1	30	70	4	0	20	2.75	43.67	210	56	81
1-3	100	0	0	0	0	0.00	98.91	501	264	321
1-3	100	0	0	0	0	2.75	103.14	532	314	378
1-3	100	0	0	0	0	5.00	92.43	636	407	481
1-3	75	25	0	0	0	0.00	72.96	749	392	469
1-3	75	25	0	0	0	2.75	80.95	757	423	490
1-3	75	25	0	0	0	5.00	72.64	836	502	577
1-3	50	50	0	0	0	0.00	33.58	1050	477	572
1-3	50	50	0	0	0	2.75	34.69	1245	493	778
1-3	50	50	0	0	0	5.00	30.88	1497	564	1020
1-3	50	50	2	0	0	2.75	33.35	1130	590	686
1-3	50	50	4	0	0	2.75	39.27	993	644	756
1-3	50	50	4	5	0	2.75	41.25	792	406	497
1-3	50	50	4	10	0	2.75	41.02	702	317	414
1-3	50	50	4	0	10	2.75	42.30	852	394	473
1-3	50	50	4	0	20	2.75	32.86	171	55	100
1-3	30	70	0	0	0	0.00	22.25	94	26	41
1-3	30	70	0	0	0	2.75	19.85	92	27	36
1-3	30	70	0	0	0	5.00	19.26	96	27	38
1-3	30	70	2	0	0	2.75	18.41	209	26	44
1-3	30	70	4	0	0	2.75	15.62	126	25	37
1-3	30	70	4	5	0	2.75	21.69	620	439	508
1-3	30	70	4	10	0	2.75	23.83	483	289	372
1-3	30	70	4	0	10	2.75	30.32	162	50	84
1-3	30	70	4	0	20	2.75	38.42	149	39	71

Miniature Slump Results

| Combination | Nominal Proportions | | | | | | Early Stiffening |
	Cement (%)	Fly Ash (%)	Gypsum (%)	Lime (%)	RSC (%)	WR (fl.oz./cwt)	Index (30-min/5-min)
4-1	100	0	0	0	0	0.00	0.92
4-1	100	0	0	0	0	2.75	0.83
4-1	100	0	0	0	0	5.00	1.14
4-1	75	25	0	0	0	0.00	0.91
4-1	75	25	0	0	0	2.75	0.73
4-1	75	25	0	0	0	5.00	1.01
4-1	50	50	0	0	0	0.00	0.72
4-1	50	50	0	0	0	2.75	0.76
4-1	50	50	0	0	0	5.00	0.94
4-1	50	50	2	0	0	2.75	0.71
4-1	50	50	4	0	0	2.75	0.72
4-1	50	50	4	5	0	2.75	0.84
4-1	50	50	4	10	0	2.75	0.61
4-1	50	50	4	0	10	2.75	0.59
4-1	50	50	4	0	20	2.75	0.42
4-1	30	70	0	0	0	0.00	0.64
4-1	30	70	0	0	0	2.75	0.48
4-1	30	70	0	0	0	5.00	0.81
4-1	30	70	2	0	0	2.75	0.46
4-1	30	70	4	0	0	2.75	0.61
4-1	30	70	4	5	0	2.75	0.53
4-1	30	70	4	10	0	2.75	0.62
4-1	30	70	4	0	10	2.75	0.29
4-1	30	70	4	0	20	2.75	0.20
1-3	100	0	0	0	0	0.00	0.93
1-3	100	0	0	0	0	2.75	1.35
1-3	100	0	0	0	0	5.00	1.65
1-3	75	25	0	0	0	0.00	0.95
1-3	75	25	0	0	0	2.75	0.84
1-3	75	25	0	0	0	5.00	1.17
1-3	50	50	0	0	0	0.00	0.83
1-3	50	50	0	0	0	2.75	0.47
1-3	50	50	0	0	0	5.00	0.80
1-3	50	50	2	0	0	2.75	0.53
1-3	50	50	4	0	0	2.75	0.56
1-3	50	50	4	5	0	2.75	0.59
1-3	50	50	4	10	0	2.75	0.59
1-3	50	50	4	0	10	2.75	0.42
1-3	50	50	4	0	20	2.75	0.37
1-3	30	70	0	0	0	0.00	0.59
1-3	30	70	0	0	0	2.75	-----
1-3	30	70	0	0	0	5.00	0.17
1-3	30	70	2	0	0	2.75	0.39
1-3	30	70	4	0	0	2.75	0.42
1-3	30	70	4	5	0	2.75	0.45
1-3	30	70	4	10	0	2.75	-----
1-3	30	70	4	0	10	2.75	0.38
1-3	30	70	4	0	20	2.75	-----

APPENDIX H

Abrasion Resistance of Concrete
ASTM C 944
7/3/12

Equipment

Equipment includes a drill press, an abrasion head conforming to ASTM C 944, a weight applied to the drill press arm conforming to a 44 pound double load, the 32 kg Ohaus balance, digital calipers, and a stopwatch.

Procedure

1. Remove the abrasion resistance test specimen from the moist room 15 minutes before testing, drying the surface with a cloth to remove free water.
2. Secure the abrasion head into the drill press and tighten down.
3. Check that the drill press is set for 300 RPM.
4. Set the drill press table to an appropriate height so that when the abrasion head is flush with the concrete surface, the drill press arm is parallel to the ground.
5. Record the time.
6. Obtain and record the initial weight of the sample.
7. Position the test specimen in the clamp on the drill press table so that there is adequate space to conduct the test. (IE, the specimen should be placed so that the abrasion head is grinding against the concrete specimen at all times during the test.)
8. Bring the head down into contact with the specimen. Hang the weight corresponding to a 44 pound double load from the arm of the drill press.

9. Turn the drill press on, and begin timing with the stop watch.

10. Turn the drill press off after two minutes of abrasion.

11. Carefully remove the test specimen from the clamp, taking care not to damage it. Remove dust from the surface with clean air.

12. Weigh the test specimen and record.

13. Replace the test specimen in the clamp, taking care to reposition it exactly beneath the abrasion head.

14. Bring the abrasion head down manually to check position. Do this at at least two degrees of rotation to ensure positioning.

15. Repeat steps 8 through 14 twice more, so that the test specimen has been abraded in the same location three times.

16. Using the digital calipers, check the depth of wear.

    a. An average depth of wear is calculated by checking the depth of wear at eight points.

    b. The eight points correspond to the 12 o'clock, 3 o'clock, 6 o'clock, and 9 o'clock positions on the test specimen at both the innermost and outermost abraded rings on the specimen.

17. Calculate mass loss for each of the abrasion periods.

18. Sum each mass loss and record a total mass loss for that replicate.

19. This abrasion procedure is conducted three times on the specimen, for a total of three replicate tests.

		28 Day	56 Day
Replicate 1	Start Time	3:30	2:57
	Initial Weight	13192.4	13456.4
	Weight 1	13169	13431.3
	Mass Loss 1	23.4	25.1
	Weight 2	13159	13422.1
	Mass Loss 2	10	9.2
	Weight 3	13150.5	13414.8
	Mass Loss 3	8.5	7.3
	Total Mass Loss	41.9	41.6
	Depth of wear	1.91	2.49
Replicate 2	Start Time	3:39	3:08
	Initial Weight	13150.5	13414.8
	Weight 1	13122.9	13392.4
	Mass Loss 1	27.6	22.4
	Weight 2	13112.6	13382.4
	Mass Loss 2	10.3	10
	Weight 3	13104.9	13375.5
	Mass Loss 3	7.7	6.9
	Total Mass Loss	45.6	39.3
	Depth of wear	2.29	2.31
Replicate 3	Start Time	3:48	3:20
	Initial Weight	13104.9	13374.1
	Weight 1	13077.1	13349.9
	Mass Loss 1	27.8	24.2
	Weight 2	13067.1	13342.6
	Mass Loss 2	10	7.3
	Weight 3	13060.1	13335.4
	Mass Loss 3	7	7.2
	Total Mass Loss	44.8	38.7
	Depth of wear	2.35	2.0425
Average Mass Loss		44.10	39.87
Average Depth of Wear		2.18	2.28

APPENDIX I
Testing Shrinkage Specimens
7/3/12

Equipment

Equipment includes DEMEC points, metal/concrete epoxy, and a DEMEC gauge with reference bar.

Procedure

20. 24 hours after casting, demold the specimens by use of a dremel tool with a cutting head.

21. Mark the shrinkage specimens with name and number with a black sharpie.

22. Using the DEMEC reference tool, mark the specimens with locations to place the DEMEC points, ensuring that they are placed in a vertical fashion. The first DEMEC point is placed 4 inches from the top of the specimen, and subsequent DEMEC points are placed the distance of the reference tool apart.

23. Apply a small amount of metal/concrete epoxy to the surface of the shrinkage specimen, where the DEMEC points are to be placed.

24. Press the DEMEC point into the epoxy.

25. Repeat steps 4 and 5 until all DEMEC points are applied to the specimen. For HVFA study, this is 10 DEMEC points, in lines of 5 at 180 degrees from each other.

26. Take initial readings as soon as possible after demolding and applying the DEMEC points.

Testing

1. Before taking readings, use the DEMEC gauge to take a length reading of the reference bar. Record this on the data sheet.

2. Record the temperature and relative humidity.

3. Record the time.

4. Fit the DEMEC gauge onto the points, rocking the gauge from side to side. The largest reading on the dial occurs when the gauge is perpendicular to the points, and this is the reading that should be recorded.

5. Readings should be taken on each specimen every day until 14 days of age, every 2 days until 28 days, every 4 days until 56 days, and every week thereafter.

Data

1. To obtain the shrinkage for each day, first subtract the reference bar reading from the day's length reading for each reading. These are the adjusted readings.

   a. *Example: Day 1 reading—1020. Day 2 reading—1018. Reference bar reads 800 for both days. Adjusted reading for Day 1 is 1020-800=220. Adjusted reading for Day 2 is 1018-800=218.*

2. The difference between two days (for instance, day 2 and day 1) provides the shrinkage for day 2 in dial reading increments.

   a. *Example: 220-218=2.*

3. Multiply the shrinkage in dial reading increments by the adjustment factor provided with the DEMEC gauge to convert to shrinkage in microstrain.

   a. *Example: 2*7.6 microstrain/dial reading = 15.2 microstrain.*

4. Average the microstrain for a given day.

   a. Each specimen will consist of 6 readings, averaged to determine an average strain.

5. Summing each day's strain, calculate the accumulative strain. Numbers will be negative due to calculation method.

6. Take the absolute value of these numbers to convert to a positive number, and plot accumulative strain versus age in days.

Cast Date
3-26-12

Read Date:	3-27-12	3-28-12	3-29-12	3-30-12	3-31-12	4-01-12	4-02-12	4-03-12	4-04-12	4-05-12	4-06-12	4-07-12
Time:	3:12	2:05	1:43	5:12	3:53	11:39	4:00	1:18	4:11	1:17	2:29	3:27
Temp:	72	70	70	72	72	72	72	72	72	72	72	78
Rel Humid:	55.00%	63.00%	61.00%	60.00%	60.00%	68.00%	60.00%	63.00%	70.00%	56.00%	36.00%	38.00%

Specimen	Reading	1	2	3	4	5	6	7	8	9	10	11	12
Refer Bar		806	806	807	807	807	807	806	807	807	806	807	808
Hbase 2	1--1	583	583	583	583	580	578	576	573	572	570	569	568
Hbase 2	1--2	976	975	973	970	968	965	961	958	955	954	953	948
Hbase 2	1--3	1070	1069	1065	1061	1058	1056	1052	1049	1048	1047	1042	1036
Hbase 2	2--1	470	466	463	457	456	454	451	449	448	447	444	443
Hbase 2	2--2	1268	1261	1258	1256	1251	1249	1246	1241	1238	1237	1236	1236
Hbase 2	2--3	706	697	689	682	677	675	674	671	668	668	669	663

Shrinkage Calcs:

Specimen	Reading Age	1	2	3	4	5	6	7	8	9	10	11	12
Hbase 2	1--1		0	-7.84	0	-23.52	-15.68	-7.84	-31.36	-7.84	-7.84	-15.68	-15.68
Hbase 2	1--2		-7.84	-23.52	-23.52	-15.68	-23.52	-23.52	-31.36	-23.52	0	-15.68	-47.04
Hbase 2	1--3		-7.84	-39.2	-31.36	-23.52	-15.68	-23.52	-31.36	-7.84	0	-47.04	-54.88
Hbase 2	2--1		-31.36	-31.36	-47.04	-7.84	-15.68	-15.68	-23.52	-7.84	0	-31.36	-15.68
Hbase 2	2--2		-54.88	-31.36	-15.68	-39.2	-15.68	-15.68	-47.04	-23.52	0	-15.68	-7.84
Hbase 2	2--3		-70.56	-70.56	-54.88	-39.2	-15.68	0	-31.36	-23.52	7.84	0	-54.88
Average			-28.7467	-33.9733	-28.7467	-24.8267	-16.9867	-14.3733	-32.6667	-15.68	0	-20.9067	-32.6667
Acc. Strain			-28.75	-62.72	-91.47	-116.29	-133.28	-147.65	-180.32	-196.00	-196.00	-216.91	-249.57
Plot			28.74667	62.72	91.46667	116.2933	133.28	147.6533	180.32	196	196	216.9067	249.5733

APPENDIX J
CONCRETE STUDY RESULTS

Table J.1 Concrete Setting Time

	Combination 4-1		Combination 1-3	
	Initial Set	Final Set	Initial Set	Final Set
Baseline	314	403	272	349
50% FA w/CH	461	579	556	733
50% FA w/RSC	388	566	582	797
70% FA w/CH	483	673	656	952
70% FA w/RSC	219	422	336	561

Table J.2 Concrete Compressive Strength (4-1)

	Combination 4-1				
Compressive Strength	Baseline	50% FA with CH	70% FA with CH	50% FA with RSC	70% FA with RSC
1 Day	2636	993	385	1063	548
7 Day	4440	3174	2017	3823	2045
28 Day	4909	4466	2916	4807	2962
56 Day	5651	5703	3470	5849	3686

Table J.3 Concrete Compressive Strength (1-3)

	Combination 1-3				
Compressive Strength	Baseline	50% FA with CH	70% FA with CH	50% FA with RSC	70% FA with RSC
1 Day	2586	624	158	525	264
7 Day	4750	3202	1304	3037	1748
28 Day	5634	4778	2696	4746	3376
56 Day	5663	5485	3139	5001	3033

Table J.4 Compressive Strength, MOR, Splitting tensile Strength, and MOE (4-1)

	Combination 4-1				
	Baseline	50% FA with CH	70% FA with CH	50% FA with RSC	70% FA with RSC
28 Day Comp. Str.	4909	4466	2916	4807	2962
Modulus of Rupture	727	695	460	698	546
Splitting Tensile	437	458	313	485	379
Modulus of Elasticity	4716461	5193245	4254350	5058505	4677422

Table J.5 Compressive Strength, MOR, Splitting tensile Strength, and MOE (1-3)

	Combination 1-3				
	Baseline	50% FA with CH	70% FA with CH	50% FA with RSC	70% FA with RSC
28 Day Comp. Str.	5634	4778	2696	4746	3376
Modulus of Rupture	796	637	395	622	455
Splitting Tensile	486	462	276	459	346
Modulus of Elasticity	5046413	4980308	3953000	5279370	4551751

Table J.6 Durability (4-1)

	4-1 Combinations				
	Baseline	50% FA with CH	70% FA with CH	50% FA with RSC	70% FA with RSC
RCP	2846	1339	5537	1139	3678
Durability Factor	78.16	92.97	96.66	93.47	96.49
Scaling @ 50 cycles	1	5	5	5*	5*

*Scaling @ 40 cycles

Table J.7 Durability (1-3)

	1-3 Combinations				
	Baseline	50% FA with CH	70% FA with CH	50% FA with RSC	70% FA with RSC
RCP	2438	3081	NA	2339	4669
Durability Factor	87.25	92.31	96.71	90.86	95.38
Scaling @ 50 cycles	2	5*	5*	4*	3*

*Scaling @ 40 cycles

Table J.8 Abrasion Resistance (4-1)

		Combination 4-1				
		Baseline	50% FA w/CH	50% FA w/RSC	70% FA w/CH	70% FA w/RSC
28 Day	Mass Loss	11.2	19.6	44.1	23.4	44.2
	Depth of Wear	0.8	1.2	2.2	1.6	2.6
56 Day	Mass Loss	12.7	15.4	39.9	17.8	31.2
	Depth of Wear	0.9	1.1	2.3	1.4	1.9

Table J.9 Abrasion Resistance (1-3)

		Combination 1-3				
		Baseline	50% FA w/CH	50% FA w/RSC	70% FA w/CH	70% FA w/RSC
28 Day	Mass Loss	13.8	24.9	48.2	23.5	42.3
	Depth of Wear	0.9	1.7	2.8	1.5	2.2
56 Day	Mass Loss	14.2	17.9	33.9	21.7	34.5
	Depth of Wear	1.1	1.3	2.1	1.5	2.1

Table J.10 Scaling Results

Blend	% Fly Ash	Additive	Rating
4-1	0	---	1
4-1	50	Lime	5
4-1	70	Lime	5
4-1	50	RSC	5
4-1	70	RSC	5
1-3	0	---	2
1-3	50	Lime	5
1-3	70	Lime	5
1-3	50	RSC	4 at 40 cycles
1-3	70	RSC	3 at 40 cycles

FINAL Report B

TRyy1110

**Project Title: Design and Evaluation of High-Volume
Fly Ash (HVFA) Concrete Mixes**

**Report B: Bond Behavior of Mild Reinforcing Steel in
HVFA Concrete**

ABSTRACT

The main objective of this study was to determine the effect on bond performance of high-volume fly ash (HVFA) concrete. The HVFA concrete test program consisted of comparing the bond performance of two concrete mix designs with 70% cement replacement with Class C fly ash relative to a Missouri Department of Transportation (MoDOT) standard mix design.

Two test methods were used for bond strength comparisons. The first was a direct pull-out test based on the RILEM 7-II-128 "RC6: Bond test for reinforcing steel. 1. Pull-out test" (RILEM, 1994). The direct pull-out tests were performed on specimens with #4 (#13) and #6 (#19) deformed reinforcing bars.

The second test method consisted of a full-scale beam splice test specimen subjected to a four-point loading until failure of the splice. This test method is a non-ASTM test procedure that is generally accepted as the most realistic test method for both development and splice length. The beam splice tests were performed on beams with #6 (#19) reinforcing bars spliced at midspan at a specific length to ensure bond failure occurred prior to shear or flexural failure.

Analysis of the HVFA concrete test data indicates that using greater than 50% replacement of cement with fly ash in concrete does not result in any increase in the required development length of mild reinforcing steel.

TABLE OF CONTENTS

LIST OF ILLUSTRATIONS

LIST OF TABLES

NOMENCLATURE

Symbol	Description
A_b	Area of reinforcing bar
c	Spacing or cover dimension
c_b, c_{min}	Smaller of the distance from center of a bar to nearest concrete surface or . one-half the center-to-center spacing of bars being developed
c_{max}	Larger of the distance from center of a bar to nearest concrete surface or one-half the center-to-center spacing of bars being developed
d_b	Nominal diameter of reinforcing bar
f'_c	Specified compression strength of concrete
f_y	Specified yield strength of reinforcement
K_{tr}	Transverse reinforcement index
l_d, l_{db}	Development length
α, φ_t	Reinforcement location modification factor
β, φ_e	Reinforcement coating modification factor
λ	Lightweight concrete modification factor
ω	$0.1\,(c_{max}/c_{min}) + 0.9 \leq 1.25$
φ_s	Reinforcement size modification factor

1. INTRODUCTION

1.1. BACKGROUND AND JUSTIFICATION FOR HIGH-VOLUME FLY ASH RESEARCH

1.1.1. General. Concrete is the world's most consumed man-made material. Unfortunately, the production of portland cement, the active ingredient in concrete, generates a significant amount of carbon dioxide. For each pound of cement produced, approximately one pound of carbon dioxide is released into the atmosphere. With cement production reaching nearly 6 billion tons per year worldwide, the sustainability of concrete is a very real concern. Since the 1930's, fly ash – a pozzolanic material – has been used as a partial replacement of portland cement in concrete to improve the material's strength and durability, while also limiting the amount of early heat generation (Volz and Myers, 2011).

1.1.2. Fly Ash. Fly ash is a siliceous material that has the capacity to create cementitious compounds when combined with water. However, due to differences in coals from different sources and designs of coal-fired boilers, not all fly ash produced is similar in composition. The chemical composition of fly ash could differ depending on where it was produced and by which company. Due to this variation in composition, standards were created to regulate the composition of fly ash used for specific purposes. For example, fly ash meant to be used as a replacement of portland cement in concrete must meet requirements set in ASTM C618-12, "Standard Specification for Coal Fly Ash and Raw or Calcined Natural Pozzolan for Use in Concrete." ASMT C618-12 defines two classes of fly ash, Class F and Class C, which are acceptable for use in concrete.

Class F fly ash is produced from the combustion of anthracite or bituminous coal and exhibits only pozzolanic properties. Class C fly ash is produced from the combustion of lignite or subbituminous coals and exhibits pozzolanic and cementitious properties (Federal Highway Administration, 2011).

1.1.3. Benefits of High-Volume Fly Ash Concrete. From an environmental perspective, replacing cement with fly ash reduces concrete's overall carbon footprint and diverts an industrial by-product from the solid waste stream. Traditional specifications limit the amount of fly ash to 25 or 30% cement replacement. Recent studies have shown that higher cement replacement percentages – even up to 70 % – can result in excellent concrete in terms of both strength (Wolfe, 2011) and durability (Marlay, 2011). Referred to as high-volume fly ash (HVFA) concrete, this material offers a viable alternative to traditional portland cement concrete and is significantly more sustainable (Volz and Myers, 2011).

1.1.4. Concerns with HVFA Concrete. At all replacement rates, fly ash generally slows down the setting time and hardening rates of concrete at early ages, especially under cold weather conditions, and when less reactive fly ashes are used. Furthermore, with industrial by-products, some variability in physical and chemical characteristics will normally occur, not only between power plants, but also within the same plant. Consequently, to achieve the benefits of HVFA concrete, guidelines are needed for its proper application in bridges, roadways, culverts, retaining walls, and other transportation-related infrastructure components (Volz and Myers, 2011).

1.2. OBJECTIES & SCOPE OF WORK

The main objective of this study was to determine the effect on bond performance of HVFA concrete. The HVFA concrete test program consisted of comparing the bond performance of two concrete mix designs with 70% cement replacement with Class C fly ash relative to a Missouri Department of Transportation (MoDOT) standard mix design at one strength level.

The following scope of work was implemented in an effort to attain these objectives: (1) review applicable literature; (2) develop a research plan; (3) design and construct test fixtures; (4) design and construct test specimens; (5) test specimens to failure and record applicable data; (6) analyze results and conduct comparisons between experimental and control mix designs; (7) develop conclusions and recommendations; (8) prepare this report in order to document the information obtained during this study.

1.3. RESEARCH PLAN

The research plan entailed determining the bond performance of HVFA concrete relative to MoDOT standard mix designs. For the HVFA concrete test program, two concrete mix designs with 70% replacement of cement with Class C fly ash, one with a relatively high cementitious material content and the other with a relative low cementitious material content, were used for comparison.

Two test methods were used for bond strength comparisons. The first was a direct pull-out test based on the RILEM 7-II-128 "RC6: Bond test for reinforcing steel. 1. Pull-out test" (RILEM, 1994). Although not directly related to the behavior of a reinforced concrete beam in flexure, the test does provide a realistic comparison of bond between

types of concrete. A total of 18 direct pull-out test specimens were constructed and tested to bond failure using this test method. The second test method consisted of a full-scale beam splice test specimen subjected to a four-point loading until failure of the splice. This test method is a non-ASTM test procedure that is generally accepted as the most realistic test method for both development and splice length. A total of 9 full-scale beam splice test specimens were constructed and tested to failure.

1.4. OUTLINE

This report consists of seven sections and six appendices. Section 1 briefly explains the characteristics, benefits, and concerns of HVFA concrete, as well as the study's objective and the manner in which the objective was attained.

Section 2 explains the mechanisms behind bond strength of deformed reinforcing bars embedded in concrete, common methods for testing bond strength, coal fly ash origins and uses, and past bond research conducted on HVFA concrete.

Section 3 details the mix designs used in this study and their associated fresh concrete properties as well as the mechanical and strength properties determined at the time of bond testing.

Section 4 details the direct pull-out and beam splice test specimen design, fabrication, and testing setup and procedure.

Sections 5 the test result normalization process, the recorded test program results, normalized test results, and the comparisons of HVFA concrete the control mix design.

Section 7 restates the findings that were established during the course of this study and presents conclusions and recommendations based on the test results obtained.

2. LITERATURE REVIEW

2.1. BOND CHARACTERISTICS

Due to its very low tensile strength, concrete, by itself, would be a poor structural material to use in members resisting anything but a concentric axial compressive load. The tensile strength of concrete is generally only 10% of its compressive strength. However, the addition of steel reinforcing bars in the areas of the cross section of the member experiencing tensile stresses has proven to be a suitable solution to overcoming the poor tensile strength of concrete. The high tensile strength of steel is able to withstand the tensile stresses upon failure of the concrete. In order to obtain complete composite behavior between the reinforcing steel and the concrete, the tensile stresses must be fully transferred to the steel from the concrete. This transfer of stresses is facilitated by an adequate bond between the steel reinforcing bars and concrete.

The three modes of stress transfer from concrete to deformed steel reinforcement are through chemical adhesion, friction along the steel-concrete interface, and bearing resistance of the ribs on the steel against the surrounding concrete, as shown in **Figure 2.1**. Chemical adhesion refers to the bonding of the steel to the concrete through chemical reactions between the two surfaces. Upon initial loading, the resistance through chemical adhesion is the first stress transfer mechanism to fail. Upon failure of the chemical adhesion, the slipping action of the bar initiates the transfer of stresses from friction and rib anchorage. Frictional forces developed along the smooth faces of the reinforcing bar are relatively small compared to the forces transferred through the ribs. As the bar slip

increases, stress transfer through friction decreases, to a point where most of the tensile stresses are transferred through anchorage of the ribs.
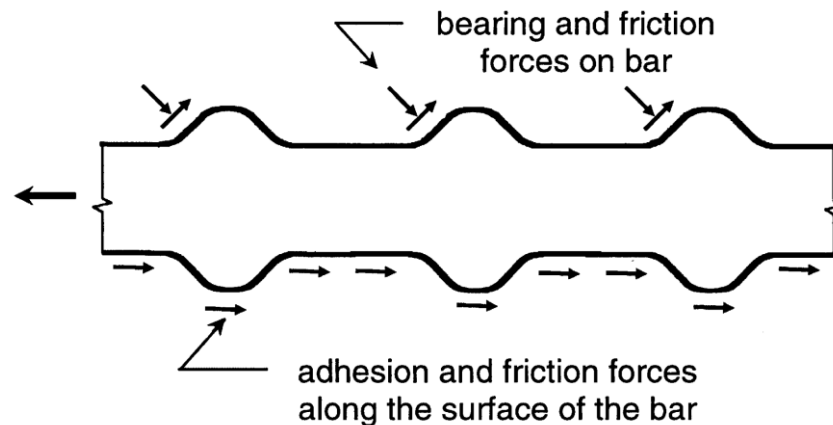
Figure 2.1 – Stress transfer between steel and surrounding concrete (ACI 408R, 2003)

As the load is increased, complete failure of the bond will occur by the concrete crushing against the ribs. One type of bond failure results when the bar is pulled directly out of the concrete, creating a shear plane along the outer edges of the steel ribs. This occurs when there is sufficient concrete cover and clear spacing between the reinforcing bars. Another type of bond failure is a splitting failure of the concrete cover. This occurs when there is insufficient concrete cover or insufficient clear spacing between the reinforcing bars (ACI 408R, 2003).

With adequate bond, tensile stresses can be transferred from the concrete to the reinforcing bar such that the bar will fail through yielding, and eventually fracture. The shortest length required to increase the stress of the bar from zero to the yield stress is called the development length of the bar. The development length of reinforcing steel is dependent on the bar diameter and yield stress, as well as the coefficient of friction on the

steel/concrete interface. The need for reinforcement splices is common in monolithic

construction of large members, such as columns extending multiple levels of a structure.

The allowable types of tension splices are lapped splices, mechanical splices, and welded

splices. Lap slices are the transfer of tensile stresses from one bar to the concrete, then

from the concrete to another bar by overlapping the two reinforcing bars. The

overlapping distance must be at least the development length of the bar. Mechanical

splices are achieved through the use of various steel devices that connect the ends of the

two bars being spliced. Welded splices consist of welding the two bars beings spliced

together (Wight and MacGregor, 2009).

The factors affecting the bond strength between reinforcing steel bars and

concrete are a function of the structural characteristics of the member, as well as

characteristics of the bar and concrete. One structural characteristic that plays a large role

in affecting the bond strength of steel and concrete is the concrete cover and spacing

between bars. As the concrete cover and bar spacing increase, the bond strength will also

increase. The increase in bond strength is attributed to the decreasing likelihood of

splitting failures with large spacing and cover. Another structural characteristic affecting

bond strength is the presence of transverse reinforcement. The presence of transverse

reinforcement surrounding the embedded bar slows the progressions of splitting cracks,

which effectively increases bond strength. Also, the location of the bar during casting of

the member affects the bond strength between the steel and concrete. Bars with a large

volume of concrete cast below them have lower bond strengths than bars cast at the

bottom of a member. This lower bond strength is caused by concrete settlement and the

presences of excess bleed water around top-cast bars (ACI 408R, 2003).

Reinforcing bar and concrete properties also play a role in affecting the bond strength of steel and concrete. Bar size and geometry can greatly alter bond strength. Larger bars with higher relative rib areas achieve higher total bond forces than small bars. Bar surface condition, such as cleanliness and coating, significantly affect bond strength. While bars with rust and mill scale do not adversely affect bond strength, surface contaminants such as mud, oil, and other nonmetallic coatings will decrease bond strength. Also, epoxy coated bars have a tendency to reduce bond strength. Concrete properties such as compressive and tensile strength, and fracture energy will also affect bond strength. Increasing compressive and tensile strengths, and fracture energy will subsequently increase bond strength. The addition of transverse reinforcement also increases the extent that the concrete compressive strength affects bond strength. Also, increasing the aggregate percentage in a concrete mix, as well as aggregate strength, will increase bond strength (ACI 408R, 2003).

2.2. COMMON BOND TESTS

There have been numerous test methods created to determine the bond strength between concrete and steel reinforcing bars. There are four common methods of bond testing. Two small-scale test methods are the direct pull-out test and the beam-end pullout test. Two large-scale test methods are the beam anchorage test and the beam splice test. The direct pull-out test specimen, shown in **Figure 2.2**, is the most common of the four tests listed above due to the ease of fabricating the test specimens and performing the test. This test is run by supporting the concrete and applying tension to the reinforcing bar

until failure, as shown in **Figure 2.2**. This bond test is the least accurate test for defining

the actual bond strength and is best used for comparison purposes only.
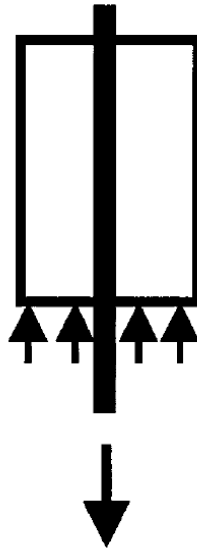
Figure 2.2 – Direct pull-out test specimen (ACI 408R, 2003)

The beam-end pull-out, also called the modified cantilever beam, test specimen is

shown in **Figure 2.3**. This test is relatively easy to construct and perform and gives an

accurate representation of how embedded reinforcing bars would behave in a full-scale

beam. The compressive force applied must be located at least the same distance as the

embedded length away from the end of the reinforcing bar. A length of reinforcing bar at

the contact surface is left unbounded in order to prevent a conical failure surface from

forming.
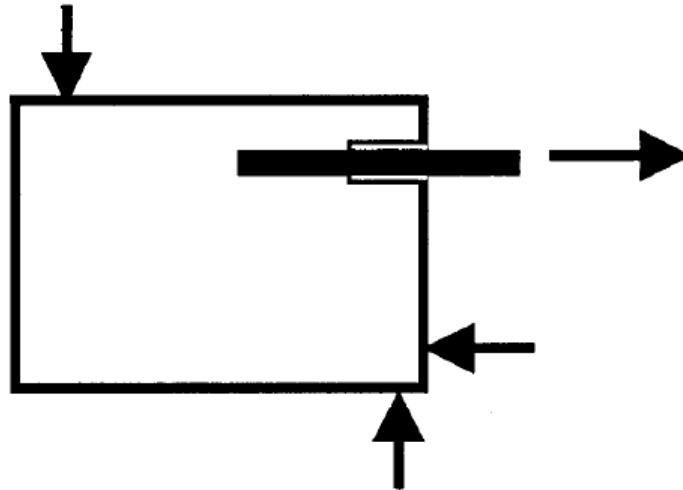
Figure 2.3 – Beam-end pull-out test specimen (ACI 408R, 2003)

The beam anchorage test specimen is shown in **Figure 2.4**. This test specimen is meant to represent a full-scale beam with a two cracked sections and a known length of bonded area. This test specimen is designed to measure development length of the reinforcing bar. **Figure 2.5** shows the beam splice test specimen. This test specimen is designed to measure the splice length of the reinforcing bar. The reinforcing bar splice placement and loading configuration is developed to subject the spliced region to a constant moment along the length of the splice. Current ACI 318-08 (ACI 318-08, 2008) design provisions for development length and splice length are based primarily on data from this type of test. Bond strengths determined from both test specimens are generally similar.
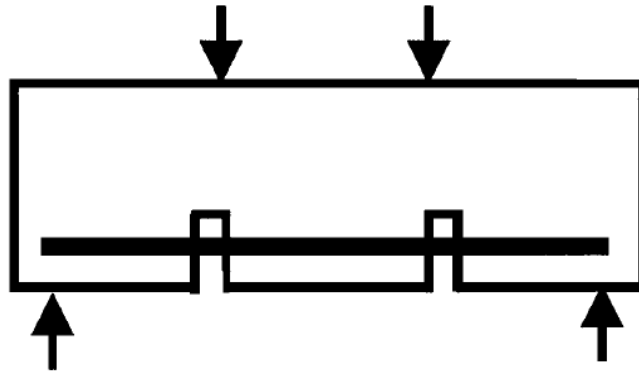
Figure 2.4 – Beam anchorage test specimen (ACI 408R, 2003)
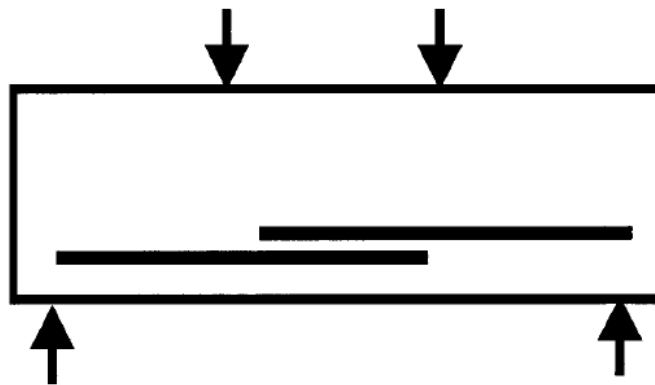
Figure 2.5 – Beam splice test specimen (ACI 408R, 2003)

2.3. COAL FLY ASH ORIGIN AND USES

Coal fly ash is one byproduct from the combustion of coal. The fly ash is a fine-grained, powdery particulate material that floats up the smoke stacks of typical electric producing facilities in flue gas. Current Environmental Protection Agency regulations require that the fly ash be collected before the combustion emissions are permitted to be released. Fly ash is usually collected from the flue gas by means of electrostatic precipitators, baghouses, or mechanical collection devices such as cyclones (Federal Highway Administration, 2011).

Fly ash is a versatile material with various potential applications due to its pozzolanic nature. It has been used as a substitute mineral filler in asphalt paving mixtures. Due to its chemical composition and fineness, fly ash generally meets the gradation, physical, and chemical requirements of mineral filler specifications. Fly ash can also be used as a fill or embankment material. Once compacted, fly ash at its optimum moisture content behaves similar to a well-compacted soil. Another beneficial use of fly ash is as a flowable fill, used as a substitute for compacted earth backfill. Depending on the pozzolanic properties of the specific fly ash, it can act as a fine aggregate, or as a cementitious material. No special processing of the fly ash is necessary for this application (Federal Highway Administration, 2011).

The single largest application of fly ash is as a replacement for portland cement in concrete. It is a siliceous material that has the capacity to create cementitious compounds when combined with water. However, due to differences in coals from different sources and designs of coal-fired boilers, not all fly ash produced is similar in composition. The chemical composition of fly ash could differ depending on where it was produced and by which company. Due to this variation in composition, standards were created to regulate the composition of fly ash used for specific purposes. For example, fly ash meant to be used as a replacement of portland cement in concrete must meet requirements set in ASTM C618-12, "Standard Specification for Coal Fly Ash and Raw or Calcined Natural Pozzolan for Use in Concrete." ASMT C618-12 defines two classes of fly ash, Class F and Class C, which are acceptable for used in concrete. Class F fly ash is produced from the combustion of anthracite or bituminous coal and exhibits only pozzolanic properties. Class C fly ash is produced from the combustion of lignite or subbituminous coals and

exhibits pozzolanic and cementitious properties (Federal Highway Administration, 2011).

Both classes of fly ash must conform to specific chemical compositions and physical

properties as shown in **Table 2.1** and **2.2**, respectively (ASTM C618-12, 2012).

Table 2.1 – Chemical composition requirements of fly ash (ASTM C618-12, 2012)

	Class F	Class C
SiO_2, plus Al_2O_3, plus Fe_2O_3 min.	70%	50%
SO_3 max.	5%	5%
Moisture content	3%	3%
Loss of ignition	6%	6%

Table 2.2 – Physical property requirements of fly ash (ASTM C618-12, 2012)

		Class F	Class C
Fineness:	Amount retained when wet-sieved on No. 325 (45 μm) sieve, max	34%	34%
Strength activity index:	With portland cement, at 7 days, min, percent of control	75%	75%
	With portland cement, at 28 days, min, percent of control	75%	75%
	Water requirement, max, percent of control	105%	105%
Soundness:	Autoclave expansion or contraction, max	0.8%	0.8%
Uniformity requirements:	Density, max variation from average	5%	5%
	Percent retained on No. 325 (45 μm), max variation from average	5%	5%

2.4. HIGH-VOLUME FLY ASH CONCRETE BOND RESEARCH

High-volume fly ash (HVFA) concrete differs from conventional concrete in that a large amount of portland cement is replaced with fly ash, generally 50% or more. Current standards limit the amount of fly ash replacement in concrete to a maximum of 35%. Fly ash is a pozzolan and reacts with the excess calcium hydroxide that is the byproduct of the cement hydration process (Headwaters Resources, 2011). However, activators such as gypsum and calcium hydroxide are necessary to accelerate the development of the binder calcium silicate hydrate. Gypsum is added in order to accelerate the onset of early-age strength gain. Calcium hydroxide is added to supplement what is released by cement hydration to better develop long term strength gain.

Various studies have been conducted to analyze the effect of large fly ash replacement of cement in conventional concrete mixes. However, very few studies focus on the bond characteristics of HVFA concrete. One of the first investigations focusing on the bond strength of fly ash concrete with 10, 20, and 30% replacement of cement with fly ash was conducted at the Center for By-Products Utilization in 1989 and was entitled "Concrete Compressive Strength, Shrinkage, and Bond Strength as Affected by Addition of Fly Ash and Temperature." The direct pull-out test specimens in this study were 6 in. (150 mm) diameter, 6 in. (150 mm) tall cylindrical concrete specimens with one reinforcing bar set vertically in the center. Each mix design was cured at a temperature of 73, 95, and 120 degrees Fahrenheit by keeping the specimens in temperature controlled rooms. The test results show that the ultimate bond stress increased with the addition of fly ash to a specific limit, and then decreased. The optimum fly ash replacement level

increased with the increase in testing temperature. The overall optimum fly ash replacement for cement was found to be 10 to 20% in this study (Naik *et al.*, 1989).

Another study focused on assessing the bond strength of HVFA concrete and was entitled "Structural Applications of 100 Percent Fly Ash Concrete" conducted at Montana State University (n.d.). The researchers conducted a series of direct pull-out tests for this study. The pull-out specimen consisted of a length of #4 (#13) reinforcing bar embedded at various lengths in 6 in. (152 mm) diameter, 12 in. (305 mm) tall cylinders of concrete. Six specimens were constructed for the conventional concrete mix design, as well as the 100% fly ash concrete mix design. Of those six specimens, the reinforcing bar was embedded 12 in. (305 mm) for three specimens, and 8 in. (203 mm) for the other three specimens. All the specimens were tested to failure. Failure for all the tested specimens consisted of splitting of the concrete section. This study indicated that the high-volume fly ash concrete mix had similar behavior as the conventional concrete mix (Cross, *et al*, n.d.).

Another study on the bond strength of high-volume fly ash concrete was conducted at the Structural Engineering Research Centre in India and is entitled "Demonstration of Utilizing High Volume Fly Ash Based Concrete for Structural Applications" (2005). This study focused on determining the bond strength of a concrete mix design with 50% replacement of cement with fly ash. The researchers conducted a series of direct pull-out tests for this study. The test specimens consisted of a length of 0.79 in (20 mm) mild steel bars embedded in 5.9 in. (150 mm) concrete cubes. The results of the direct pull-out tests indicated that the high-volume fly ash concrete mix design exhibited the same level of bond strength as the conventional concrete mix design

at 28 and 56 days, and higher bond strength at 90 days. Also, the load vs. slip plot indicates both concrete mix designs exhibited similar behavior (Gopalakrishnan, 2005). This study highlights the advantage of high-volume fly ash concrete in terms of later age bond strength.

Most recently, a study was conducted at the Missouri University of Science and Technology to determine the bond performance of concrete with 70% replacement of cement with Class C fly ash relative to conventional concrete and was entitled "Bond Strength of High-Volume Fly Ash Concrete" (Wolfe, 2011). This study focused on comparing bond strengths of deformed reinforcing bar in both direct pull-out test specimens, as well as full-scale beam splice specimens. The direct pull-out specimens were based on the RILEM 7-II-128 "RC6: Bond test for reinforcing steel. 1. Pull-out test" (RILEM, 1994). A length of #4 (#13) and #6 (#19) deformed reinforcing bars were embedded in a 12 in. (305 mm) diameter concrete cylinder. The bars were embedded 10 times the bar diameter into the concrete section, with half of the embedded length debonded using a polyvinyl chloride (PVC) sleeve. There were six specimens tested for each bar size, with three for the conventional concrete mix design and three for the HVFA concrete mix design. All direct pull-out specimens were tested to pull-out failure. The beam splice specimens were 14 ft. (4270 mm) in length, with a cross section of 12 in. x 18 in. (305 mm x 457 mm). The longitudinal reinforcement consisted of three #6 (#19) reinforcing bars that were spliced at midspan a length of 16.55 in. (420 mm). The beams were subjected to four-point loading to ensure the splice region was subjected to constant moment along its length. For beam specimens without confinement, the transverse reinforcement consisted of #3 (#10) closed stirrups spaced at 7 in. (178 mm) up until the

splice on either side. For beam specimens with confinement, the transverse reinforcement consisted of #3 (#10) closed stirrups spaced at 7 in. (178 mm) along the entire length of the beam. Six beams were tested for each mix design, of which three contained a confined splice and three an unconfined splice. All beam splice specimens were tested to failure of the splice. The author concluded that 70% replacement of cement with Class C fly ash is not only feasible in terms of bond, but is superior in some cases (Wolfe, 2011).

3. MIX DESIGNS AND CONCRETE PROPERTIES

3.1. INTRODUCTION

The following chapter contains the mix designs for the high-volume fly ash (HVFA) concretes evaluated in this study, as well as the control mix design used for comparison. Also included in this chapter are the methods and results of the testing done to determine the fresh and hardened properties of each mix.

3.2. CONCRETE PROPERTIES

3.2.1. Fresh Concrete Properties. Various tests were conducted on the fresh concrete prior to casting the test specimens. The type of fresh concrete test was dependent on the type of concrete being tested. A slump test was performed on all the concrete mixes upon arrival of the concrete mixing truck in accordance with ASTM C143/C143M "Standard Test Method for Slump of Hydraulic-Cement Concrete" (ASTM C143/C143M, 2010). A standard mold for the slump test was dampened and placed on a metal slump pan. Then the mold was filled to one-third of its volume with the fresh concrete. The concrete was then rodded 25 times uniformly over the crossed section with a standard tamping rod. This process was repeated for the subsequent two layers. Upon finishing the last layer, the top of the concrete was smoothed using the tamping rod and any excess concrete was removed from around the base of the mold. The mold was then lifted vertically slowly in accordance with the ASTM. The length that the top of the fresh concrete slumped upon removal of the mold was recorded as the slump of the concrete. The slump test is shown in **Figure 3.1.**

Figure 3.1 – Slump test

The unit weight and air content were also determined. The unit weight of the fresh

concrete was determined in accordance with ASTM C138/C138M "Standard Test

Method for Density (Unit Weight), Yield, and Air Content (Gravimetric) of Concrete"

(ASTM C138/C138M, 2010). A steel cylindrical container was used as the measure for

this test. The inside of the measure was first dampened, and then it was weighed and

measured to determine its empty weight and volume, respectively. Then fresh concrete

was added to the measure to one-third of its volume. The concrete was then rodded 25

times with a standard tamping rod and the measure was struck with a rubber mallet 15

times around its outside perimeter. This step was repeated for the second and third level

of concrete. Upon filling the measure, the concrete was finished with a strike-off place

and any excess concrete was removed from the rim of the measure using a sponge. The

measure was then weighed to determine its weight and the weight of the concrete it

contained. The weight of the measure was then subtracted from the combined weight of

the measure and the concrete to determine the weight of the concrete. The weight of the

concrete was then divided by the volume of the measure to determine the unit weight of

the concrete.

The air content of the concrete was determined in accordance with ASTM

C231/C231M "Standard Test Method for Air Content of Freshly Mixed Concrete by the

Pressure Method" (ASTM C231/C231M, 2010). A standard type-B meter was used for

this test. The same steel container and filling procedure used for determining the unit

weight were used for the air content test. After completing the filling process, the flange

of the cover assembly was thoroughly cleaned and clamped onto the steel container. Both

petcocks were opened and water was added to one petcock until the water emerged from

the other petcock to remove any excess air in the steel container. The air bleeder valve

was then closed and air was pumped into the container until the gauge hand was on the

initial pressure line. Both petcocks were then closed and the main air valve was opened

while simultaneously tapping the container smartly with a rubber mallet. The air content

shown on the gauge was then recorded as the air content of the concrete.

3.2.2. Compressive Strength of Concrete. The concrete compressive strength

was determined in accordance with ASTM C39/39M "Standard Test Method for

Compressive Strength of Cylindrical Concrete Specimens" (ASTM C39/C39M, 2011).

The specimens consisted of 4 in. (102 mm) diameter, 8 in. (203 mm) tall cylinders for

each mix design. **Figure 3.2** displays the cylinders being cast. Prior to testing, the

cylinders were capped in order to eliminate the effect of point stresses caused by an

uneven surface. The capped cylinders were then subjected to a compressive axial load

across their entire circular cross section until failure, applied at a rate appropriate for the

testing apparatus and in conformance with ASTM C39/C39M. The test setup is shown in

Figure 3.3.

Figure 3.2 – Casting compressive strength cylinders

Figure 3.3 – Compressive strength test setup

3.2.3. Modulus of Rupture of Concrete. The modulus of rupture was determined in accordance with ASTM C78/C78M "Standard Test Method for Flexural Strength of Concrete (Using Simple Beam Third-Point Loading) (ASTM C78/C78M, 2010). The test consists of subjecting a 6 in. x 6 in. x 24 in. (152 mm x 152 mm x 610 mm) concrete beam to a four-point load until failure. **Eq. 3.1** was used to determine the modulus of rupture from each beam test result.

$$R = \frac{PL}{bd^2} \tag{3.1}$$

Where R is the modulus of rupture, P is the maximum applied load, L is the span length, b is the average width of the specimens at the fractured surface, and d is the average depth of the specimen at the fractured surface. The test specimens are shown in **Figure 3.4** and the test setup is shown in **Figure 3.5**.

Figure 3.4 – Modulus of rupture test specimens

Figure 3.5 – Modulus of rupture test setup

3.2.4. Splitting Tensile Strength of Concrete. The splitting tensile strength was determined in accordance with ASTM C496/C496M "Standard Test Method for Splitting Tensile Strength of Cylindrical Concrete Specimens" (ASTM C496/C496M, 2011). The specimens consisted of 6 in. (152 mm) diameter, 12 in. (305 mm) tall cylinders for each mix design, which were tested upon reaching the appropriate concrete compressive strength. **Eq. 3.2** was used to determine the splitting tensile strength of each cylinder test result.

$$T = \frac{2P}{\pi l d}$$
(3.2)

Where T is the splitting tensile strength, P is the maximum applied load, l is the length of the specimen, and d is the diameter of the specimen. The splitting tensile strength test setup is shown in **Figure 3.6**.

Figure 3.6 – Splitting tensile strength test setup

3.3. HIGH-VOLUME FLY ASH (HVFA) CONCRETE MIX DESIGNS

There were three concrete mix designs evaluated in the HVFA concrete test program. Two HVFA concrete mix designs were compared to a standard Missouri Department of Transportation (MoDOT) mix design in this study. All three mix designs had a target air content of 6% and a target slump of 4 to 5 in. (100 to 130 mm). The air entraining admixture consisted of MB-AE-90, and the water reducing admixture consisted of Glenium 7500, both manufactured by BASF and both approved for use in MoDOT projects. Gypsum and lime were added to the HVFA concrete mixes to increase early-age strength gain. The gypsum prevents sulfate depletion, and the lime provides the byproduct normally produced during cement hydration and necessary for the pozzolanic reaction of the fly ash.

3.3.1. HVFA Control Mix Design and Concrete Properties. The HVFA control mix design was designated HVFA-C and is shown in **Table 3.1**.

The slump, air content, and unit weight of the concrete used for the fabrication of test specimens was determined upon arrival of the concrete mixing truck. The slump measured 5 in. (127 mm), the air content measured 6.5%, and the unit weight measured 143.6 lb./ft^3 (2300 kg/m^3).

Test specimens for determining the compressive strength and modulus of rupture of the concrete were fabricated along with the bond test specimens. The compressive strength results are shown in **Table 3.2** and plotted in **Figure 3.7**. The splitting tensile strength results are shown in **Table 3.3**. The modulus of rupture test results are shown in **Table 3.4**.

Table 3.1 – HVFA-C mix proportions

Ingredient	Weight (lb./yd^3)
w/cm	0.40
Cement (Type 1)	564
Coarse Aggregate	1,860
Fine Aggregate	1,240
MB-AE-90	0.625 oz./cwt.
Glenium 7500	2.5 oz./cwt.

Conversion: 1 lb./yd^3 = 0.59 kg/m^3
1 oz. = 29.6 ml
1 lb. = 0.45 kg

Table 3.2 – Compressive strength data of HVFA-C

Day	Average Strength (psi)
1	2,850
3	4,050
6	4,480

Conversion: 1 psi = 6.9 kPa
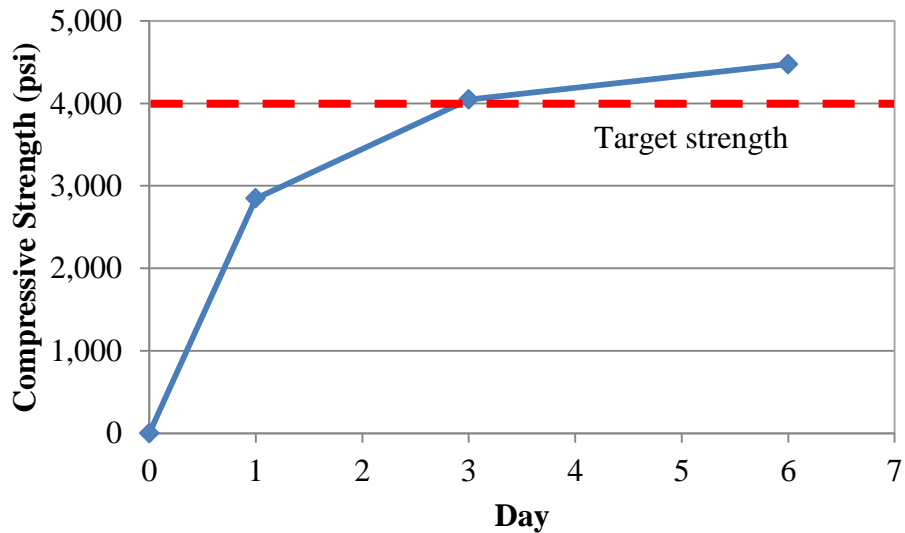
Figure 3.7 – Plot of HVFA-C compressive strength
Conversion: 1 psi = 6.9 kPa

Table 3.3 – Splitting tensile strength test results for HVFA-C

Specimen	Peak Load (lb.)	Splitting Tensile Strength (psi)
HVFA-C1	41,620	365
HVFA-C2	36,520	320
HVFA-C3	35,410	310
Average:		330

Conversion: 1 lb. = 4.45 N

1 psi = 6.9 kPa

Table 3.4 – Modulus of rupture test results for HVFA-C

Specimen	Peak Load (lb.)	Modulus of Rupture (psi)
HVFA-C1	4,560	380
HVFA-C2	4,720	390
HVFA-C3	5,495	460
HVFA-C4	5,450	430
Average:		415

Conversion: 1 lb. = 4.45 N

1 psi = 6.9 kPa

3.3.2. HVFA 70% Replacement, High Cementitious Material Mix Design and Concrete Properties. The HVFA 70% replacement, high cementitious material mix design was designated HVFA-70H and is shown in **Table 3.5**.

The slump and unit weight of the concrete used for the fabrication of test specimens was determined upon arrival of the concrete mixing truck. The slump measured 4.5 in. (114 mm) and the unit weight measured 142.5 lb./ft^3 (2280 kg/m^3).

Table 3.5 – HVFA-70H mix proportions

Ingredient	Weight (lb./yd^3)
w/cm	0.40
Cement (Type 1)	230
Coarse Aggregate	1,754
Fine Aggregate	1,016
Fly Ash (Class C)	537
Gypsum	24
Calcium Hydroxide	60
Glenium 7500	2.5 oz./cwt.

Conversion: 1 lb./ yd^3 = 0.59 kg/m^3

1 oz. = 29.6 ml

1 lb. = 0.45 kg

Test specimens for determining the compressive strength, splitting tensile strength, and modulus of rupture of the concrete were fabricated along with the bond test specimens. The concrete compressive strength results are shown in **Table 3.6** and plotted in **Figure 3.8**. The splitting tensile strength test results are shown in **Table 3.7**. The modulus of rupture results are shown in **Table 3.8**.

Table 3.6 – Compressive strength data of HVFA-70H

Day	Average Strength (psi)
1	710
3	1,505
7	2,400
14	2,955
28	3,100
56	3,420

Conversion 1 psi = 6.9 kPa
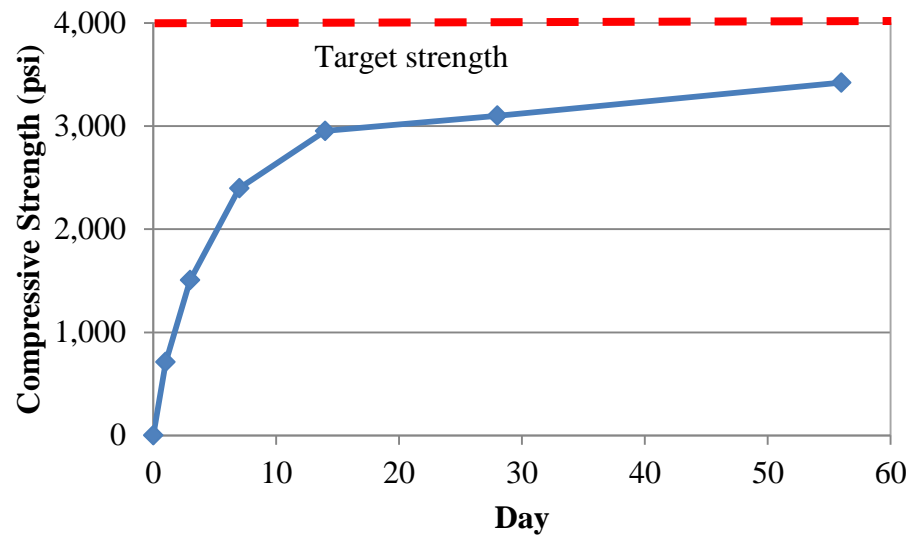
Figure 3.8 – Plot of HVFA-70H compressive strength
Note: 1 psi = 6.9 kPa

Table 3.7 – Splitting tensile strength test results for HVFA-70H

Specimen	Peak Load (lb.)	Splitting Tensile Strength (psi)
HVFA-70H1	31,635	280
HVFA-70H2	26,550	235
HVFA-70H3	32,865	290
	Average:	300

Note: 1 lb. = 4.45 N
1 psi = 6.9 kPa

Table 3.8 – Modulus of rupture test results for HVFA-70H

Specimen	Peak Load (lb.)	Modulus of Rupture (psi)
HVFA-70H1	4,315	350
HVFA-70H2	4,120	345
HVFA-70H3	4,085	340
HVFA-70H4	4,515	365
Average:		350

Conversion: 1 lb. = 4.45 N

1 psi = 6.9 kPa

3.3.3. HVFA 70% Replacement, Low Cementitious Material Mix Design and Concrete Properties. The HVFA 70% replacement, low cementitious material mix design was designated HVFA-70L and is shown in **Table 3.9**.

The slump and unit weight of the concrete used for the fabrication of test specimens was determined upon arrival of the concrete mixing truck. The slump measured 4.5 in. (114 mm) and the unit weight measured 149.6 lb./ft^3 (2400 kg/m^3).

Table 3.9 – HVFA-70L mix proportions

Ingredient	Weight (lb./yd^3)
w/cm	0.40
Cement (Type 1)	155
Coarse Aggregate	1,860
Fine Aggregate	1,240
Fly Ash (Class C)	360
Gypsum	18
Calcium Hydroxide	49
Glenium 7500	4 oz./cwt.

Conversion: 1 lb./ yd^3 = 0.59 kg/m^3

1 oz. = 29.6 ml

1 lb. = 0.45 kg

Test specimens for determining the compressive strength, splitting tensile strength, and modulus of rupture of the concrete were fabricated along with the bond test specimens. The concrete compressive strength test results are shown in **Table 3.10** and plotted in **Figure 3.9**. The splitting tensile strength results are shown in **Table 3.11**. The modulus of rupture test results are shown in **Table 3.12**.

Table 3.10 – Compressive strength data of HVFA-70L

Day	Average Strength (psi)
1	820
3	1,815
7	2,750
14	3,235
28	3,480
33	3,450

Conversion: 1 psi = 6.9 kPa
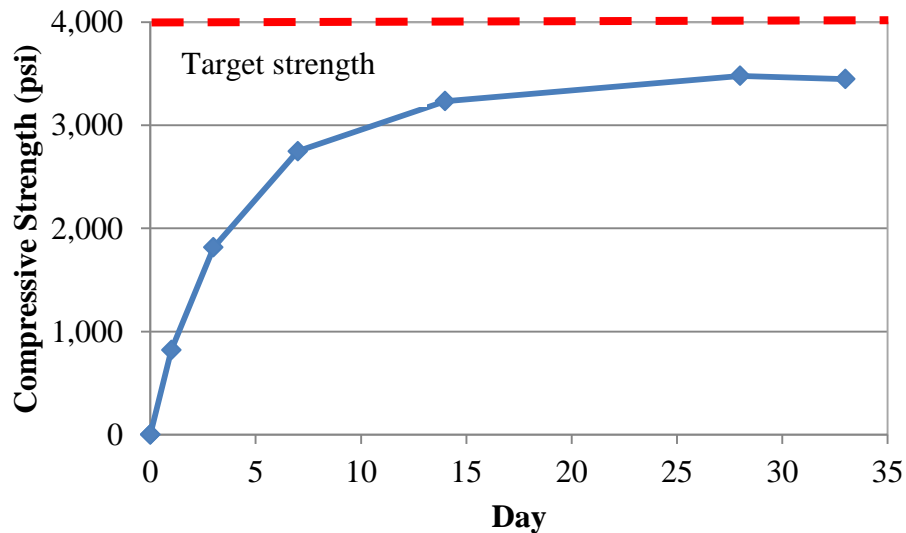
Figure 3.9 – Plot of HVFA-70L compressive strength
Conversion: 1 psi = 6.9 kPa

Table 3.11 – Splitting tensile strength test results for HVFA-70L

Specimen	Peak Load (lb.)	Splitting Tensile Strength (psi)
HVFA-70L1	34,530	305
HVFA-70L2	35,235	310
HVFA-70L3	33,075	290
Average:		300

Conversion: 1 lb. = 4.45 N

1 psi = 6.9 kPa

Table 3.12 – Modulus of rupture test results for HVFA-70L

Specimen	Peak Load (lb.)	Modulus of Rupture (psi)
HVFA-70L1	5,290	420
HVFA-70L2	5,570	460
HVFA-70L3	5,140	425
HVFA-70L4	5,080	425
Average:		430

Conversion: 1 lb. = 4.45 N

1 psi = 6.9 kPa

4. EXPERIMENTAL PROGRAM

4.1. INTRODUCTION

The experimental program included both direct pull-out tests, as well as well as full-scale beam splice specimen tests. The direct pull-out specimens were based on RILEM 7-II-128 "RC6: Bond test for reinforcing steel. 1. Pull-out test" (RILEM, 1994). The beam splice specimen tests were based on recommendations in ACI 408R-03 "Bond and Development of Straight Reinforcing Bars in Tension" (ACI 408R-03, 2003). The following is a discussion of the design, setup, instrumentation, and procedures for both testing methods.

4.2. DIRECT PULL-OUT TEST

4.2.1. Direct Pull-out Specimen Design. The direct pull-out specimen tests were based on the RILEM 7-II-128 "RC6: Bond test for reinforcing steel. 1. Pull-out test" (RILEM, 1994). Several changes were made to the recommended test specimen based on results from previous research (Wolfe, 2011). The test involves casting a length of reinforcing bar within a concrete cylinder and applying a direct tension force on the bar until the bonded length fails. Although not directly related to the behavior of a reinforced concrete beam in flexure, the test does provide a realistic comparison of bond between types of concrete.

The RILEM standard states that the reinforcing bar will be embedded in the concrete a total length of 15 times the bar diameter to be tested. A bond breaker a length of 7.5 times the bar diameter is to be placed so that the bar is unbonded from the bottom

surface to halfway in the concrete, leaving a bonded length of 7.5 times the bar diameter. The unbounded length at the bottom of the concrete segment is to reduce restraint stresses caused by friction with the loading head. Previous testing showed this bonded length to be too long and yielding of the bar occurred prior to failure in some instances (Wolfe, 2011). To ensure the bond failed before the bar yielded, the total concrete depth was reduced to 10 times the bar diameter with a bonded length of 5 times the bar diameter.

The RILEM standard specifies a square concrete cross section with sides having a length of 8.75 in. (222 mm). For this test program, a circular concrete cross section with a diameter of 12 in. (305 mm) was used instead. This change eliminated the potential for a splitting failure (side cover failure) and also maintained a constant cover for the reinforcing bar.

The protocol for the direct pull-out tests included two bar sizes – #4 (#13) and #6 (#19) – in order to evaluate the bond performance over a range of reinforcing sizes. The total length of each bar was 40 in (1016 mm). A length of 3/8 in. (10 mm) was left exposed at the top of the specimen to measure bar slip using a Linear Voltage Differential Transformer (LVDT). **Figures 4.1** and **4.2** are schematic diagrams of the specimen dimensions for the #4 (#13) and #6 (#19) bars, respectively.
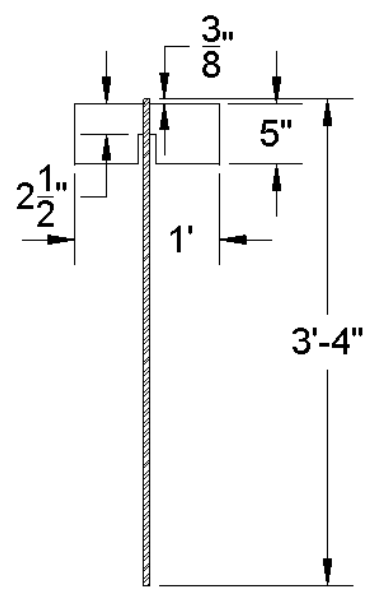
Figure 4.1 – Pull-out specimen with dimensions for #4 (#13) reinforcing bars
Conversion: 1 in. = 25.4 mm
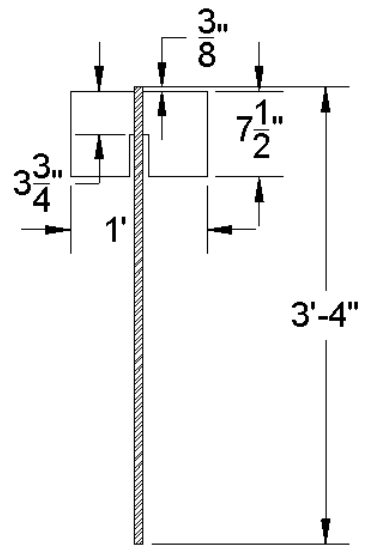
Figure 4.2 – Pull-out specimen with dimensions for #6 (#19) reinforcing bars
Conversion: 1 in. = 25.4 mm

4.2.2. Direct Pull-out Specimen Fabrication. The formwork base for the direct pull-out test specimen was constructed with a 14-in.-square (356 mm), 3/8-in.-thick (10 mm) section of plywood. A hole that was 1/16 in. (0.16 mm) larger than the bar diameter being tested was drilled through the center of the plywood squares. Cardboard tubing (Quick-Tube) was then cut to the required length, depending on the bar size being tested. Waterproof silicone adhesive caulk was then used to bind the cardboard tubing to the plywood squares.

The reinforcing bar for each specimen was sectioned into 40 in. (1016 mm) lengths. Polyvinyl chloride (PVC) tubing was used to form the bond breaker. For the #4 (#13) bar, the PVC had an inside diameter of 3/4 in. (19 mm) and was sectioned into lengths of 2.5 in. (64 mm). For the #6 (#19) bar, the PVC had an insider diameter of 1 in. (25 mm) and was sectioned into 2.75 in. (70 mm) lengths. A mark was made on each bar to facilitate the placement of the PVC bond breaker. The PVC was slid onto the reinforcing bar and shims of cardboard were used to center the bar in the PVC. The PVC was then adhered to the reinforcing bar using waterproof silicone adhesive caulk and was carefully finished to ensure there were no gaps in the caulk for the concrete paste to get between the bar and the PVC.

The top of the formwork was also a 14-in.-square (356 mm) of 3/8-in.-thick (10 mm) plywood with a hole drilled through its center. To ensure that the bars were plumb within the concrete encasement, prior to constructing the specimens, the reinforcing bars were placed in the completed forms and leveled. Upon leveling the bars, an outline of the cylindrical form was drawn on the underside of the top plywood square. Wood spacers were then screwed into the plywood square along the outline of the cardboard tubing.

The specimens were cast by first placing the reinforcing bar through the hole in the base of the formwork. Concrete was then placed in the cylindrical formwork and consolidated as necessary. After proper placement of the concrete, the exposed surface was finished. The top of the formwork was then carefully slid down the reinforcing bar and the wood spacers were fit snugly over the cylindrical forms. The reinforcing bar was checked to ensure it was plumb and then the sides of the cylindrical forms were lightly vibrated. The pull-out and companion material property specimens were allowed to cure until the concrete reached its specified strength prior to testing. The cardboard tubing was removed on the day of testing. Construction of the pull-out specimens is shown in **Figure 4.3**, with complete specimens shown in **Figure 4.4**.

Figure 4.3 – Pull-out specimen construction

Figure 4.4 – Completed specimens

4.2.3. Direct Pull-out Test Setup. Testing of the direct pull-out specimens was completed using a 200,000-lb-capacity (890 kN) testing machine manufactured by Tinius Olson. The test setup is shown in **Figures 4.5** and **4.6**. The cylindrical forms were removed immediately prior to testing. A neoprene pad with a hole in its center was placed on the top platform of the test machine to ensure uniform bearing of the concrete. The specimens were flipped upside down and the reinforcing bar was then threaded through the hole in the neoprene pad on the top platform and placed between the grips installed on the middle platform. An LVDT was then clamped to a stand, and the stand was placed on top of the concrete section of the specimen. The needle of the LVDT was placed on top of the 3/8 in. (10 mm) length of exposed reinforcing bar to measure slip.
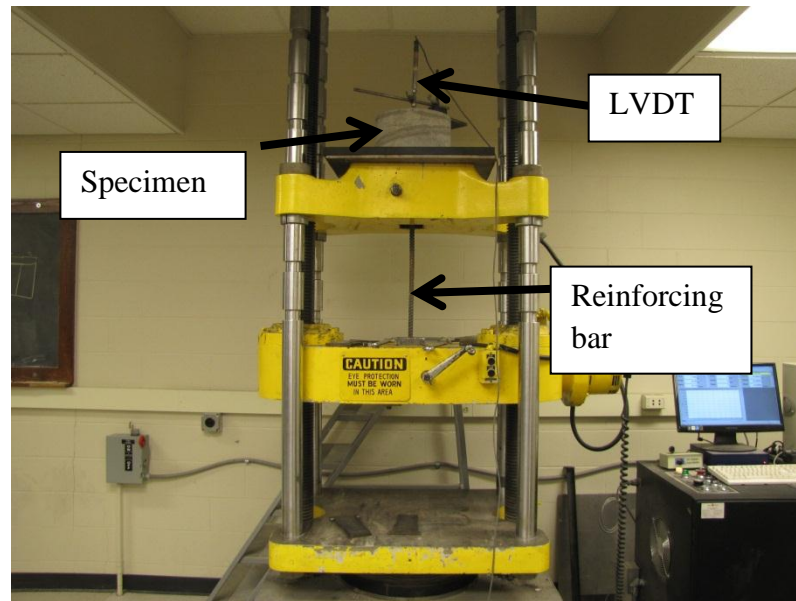
Figure 4.5 – Direct pull-out test setup
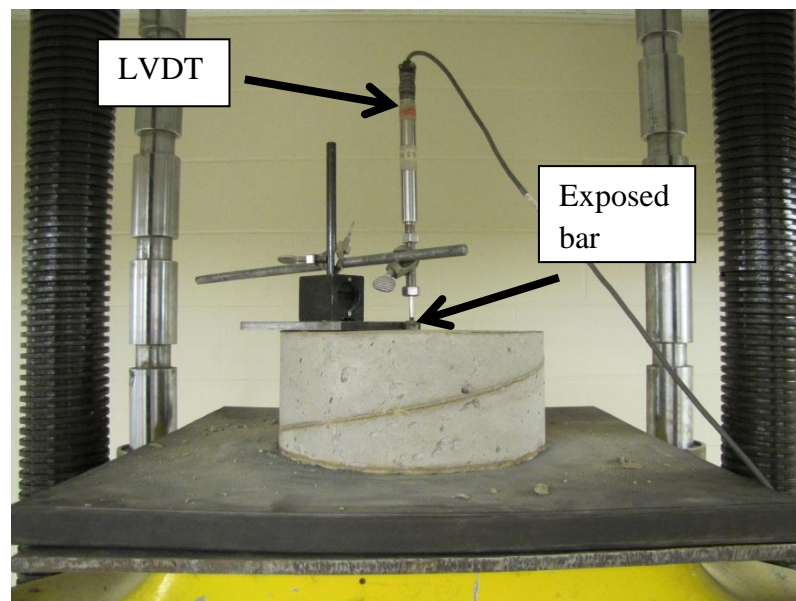
Figure 4.6 – LVDT installation to measure bar slip

4.2.4. Direct Pull-out Test Procedure. The middle platform was manually

positioned to allow for the reinforcing bar to be clamped. The equipment controlling the

Tinius Olson was programed to apply a displacement controlled load rate of 0.1 in. (3 mm) per minute. Upon initiating a new test, the LVDT data collection platform was started and the clamps were closed around the reinforcing bar while the middle platform was simultaneously lowered. This step was done to seat the test specimen and apply an initial load sufficient to maintain a proper grip on the reinforcing bar during testing. The test program was then initiated and allowed to run until a distinct peak was observed in the applied load vs. bar slip plot. This step was done to ensure there was no residual load carrying capacity in the bonded region and that the proper failure load was determined. At that point, the test program and LVDT data collection platform were both stopped and the test specimen was removed.

4.3. BEAM SPLICE TEST

4.3.1. Beam Splice Specimen Design. The beam splice test specimens were designed following a non-ASTM test procedure that is generally accepted as the most realistic test method for both development and splice length. This test consists of applying a full-scale beam specimen to a four-point loading until failure of the splice occurs. The splice is located in the region of the beam subjected to a constant moment, and thus constant stress. The realistic stress-state in the area of the reinforcing bars makes for an accurate representation of the bond strength of the tested member (ACI 408R-03, 2003).

Details of the beam splice specimens used in this current study are shown in **Figures 4.7** and **4.8**. The beams measured 10 ft. (3050 mm) in length, with a cross section of 12 in. x 18 in. (305 mm x 457 mm) and contained a splice centered at midspan.

Transvers steel consisting of #3 (#10), ASTM A615-09, Grade 60, U-shaped stirrups

were used for shear reinforcement. A stirrup spacing less than the ACI 318-08 maximum

stirrup spacing was used to ensure that bond failure occurred prior to shear failure. The

stirrups were terminated at approximately 5 in. (127 mm) from each end of the splice to

eliminate the effects of confinement within the splice region. The longitudinal

reinforcement consisted of three, ASTM A615-09, Grade 60, #6 (#19) bars spliced at

midspan of the beam. The splice length was based on a percentage of the development

length of the longitudinal reinforcing bars calculated in accordance with ACI 318-08

"Building Code Requirements for Structural Concrete" (ACI 318-08, 2008) (**Eq. 4.1**).

$$l_d = \left(\frac{3}{40} \frac{f_y}{\lambda \sqrt{f'_c}} \frac{\Psi_t \Psi_e \Psi_s}{\left(\frac{c_b + K_{tr}}{d_b} \right)} \right) d_b \tag{4.1}$$

Where l_d is the development length, f_y is the specified yield strength of reinforcement, λ

is the lightweight concrete modification factor, f'_c is the specified compressive strength

of concrete, Ψ_t is the reinforcement location modification factor, Ψ_e is the reinforcement

coating modification factor, Ψ_s is the reinforcement size modification factor, c_b is the

smaller of the distance from center of a bar to nearest concrete surface and one-half the

center-to-center spacing of bars being developed, K_{tr} is the transverse reinforcement

index, and d_b is the nominal diameter of the reinforcing bar.
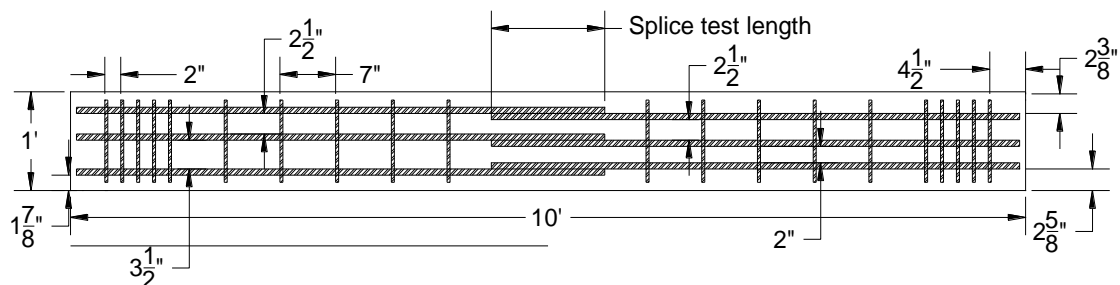
Figure 4.7 – Beam splice specimen reinforcing layout
Conversion: 1 in. = 25.4 mm
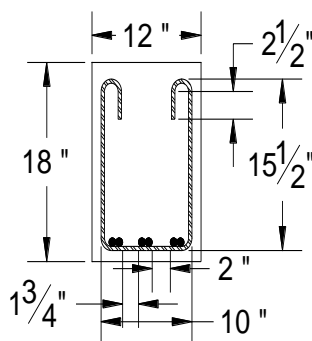
Figure 4.8 – Beam splice specimen cross section
Conversion: 1 in. = 25.4 mm

To ensure bond failure before yielding of the reinforcing bar, a splice length less than the code required development length was used in the test specimen. Prior researchers used one-half of a Class B splice as the lap length (Wolfe, 2011). However, several test specimens in that study exhibited signs of yielding in the reinforcement prior to bond failure. Therefore, for this current study, the splice length was limited to 70% of the development length.

4.3.2. Beam Splice Specimen Fabrication. The concrete formwork consisted of five removable and reusable pieces constructed from steel and wood. The pieces were connected through the use of steel keys and wire ties were used to hold the keys in place. The original beam forms were 14 ft. (4267 mm) in length. Consequently, 4 ft. (1219 mm)

wooden bulkheads were constructed to reduce the length of the beam forms to 10 ft. (3048 mm).

The #3 (#10) reinforcing bars were then sectioned to the appropriate length and bent to form the U-stirrups. The longitudinal reinforcement was sectioned to the appropriate length to obtain the proper splice length, as well as create a standard hook at the opposite end for proper development. All rust and mill scale was removed from the spliced region of each bar using a wire brush cup attached to an electric grinder. This step was done to ensure the bond strength was not affected in any way by the existence of rust and mill scale, thus maintaining conformity between the splice in each specimen. The longitudinal bars were then placed on saw-horses, aligned to obtain the appropriate splice length, and the stirrups were secured to the longitudinal bars using steel wire tires. A strain gauge was attached to the longitudinal bars at one end of each splice to monitor the strain during testing. Then, to ensure the stirrups stayed aligned vertically within the forms, two #4 (#13) bars were tied to the top bend of the stirrups and the end stirrups were tied to the hooked ends of the longitudinal bars. A finished reinforcing bar cage is shown in **Figure 4.9**.

Figure 4.9 – Finished reinforcing bar cage

Two of the cages were then lowered into the beam forms using 1 in. (25 mm) steel chairs on the bottom and sides to maintain 1 in. (25 mm) of clear cover to the outside edge of the stirrups. The third cage was turned upside down and 1.5 in. (38 mm) chairs were attached to the bottom of the cage to maintain clear cover to the splice at the top of the beam. Then, 1 in. (25 mm) chairs were also attached to the side of the stirrups to maintain 1 in. (25 mm) clear cover to the stirrups. Steel crossties were attached to the tops of the beam forms to maintain the proper beam width along the depth of the beam. Hooks were then tied to the crossties to facilitate transportation of the specimen after curing. **Figure 4.10** shows a picture of the spliced region in the beam forms, and **Figure 4.11** displays the three cages in their respective forms.
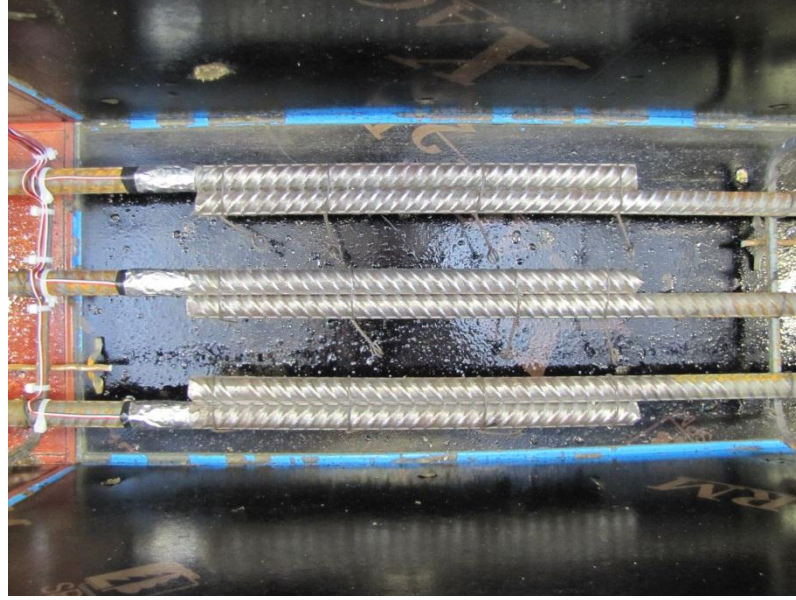
Figure 4.10 – Spliced longitudinal bars for normal strength concrete

Figure 4.11 – Reinforcing bar cages in beam forms

The concreted used to construct the specimens was delivered from a local ready-mix facility, Rolla Ready Mix (RRM). The mix design was supplied to RRM although

some of the water was held in abeyance in order to adjust the water content at the lab.

Once the concrete truck arrived at the lab, the slump was measured and the reserve water

was added as necessary to arrive at the required water-to-cementitious material ratio. At

that point, all necessary activators and admixtures were added to the concrete truck,

which was then mixed at high speed for 10 minutes to obtain the final material. At this

point, the fresh concrete was loaded into a concrete bucket as shown in **Figure 4.12**. The

bucket was then positioned with the overhead crane to facilitate placement of the

concrete into the formwork as shown in **Figure 4.13**. The concrete was then consolidated

as required for the particular concrete mix. This process was repeated until the beam

forms were filled. The tops of the beams were then finished using trowels as shown in

Figure 4.14.

Figure 4.12 – Concrete bucket being filled with fresh concrete

Figure 4.13 – Placement of concrete into beam forms

Figure 4.14 – Finished beams in forms

Once the concrete reached initial set, the beam specimens and companion material

property specimens were covered with wet burlap and plastic. The specimens were

allowed to cure until the concrete compressive strength reached a minimum of 1500 psi

(10.3 MPa), at which point they were removed from the forms and remained within the

temperature-controlled High Bay Lab. The beams were then tested upon reaching their

respective design compressive strengths.

     4.3.3. Beam Splice Specimen Test Setup. A schematic and photograph of the

test setup are shown in **Figures 4.15** and **4.16**, respectively. The test consists of

subjecting the beam splice specimen to four-point loading, ensuring that the region

containing the splice is located in a constant moment region. The beam was then placed

onto the supports. Two steel rollers were placed on the top surface of the beam specimen

and steel spreader beams were used to transfer the applied load from two 140-kip-

capacity (623 kN) hydraulic actuators.
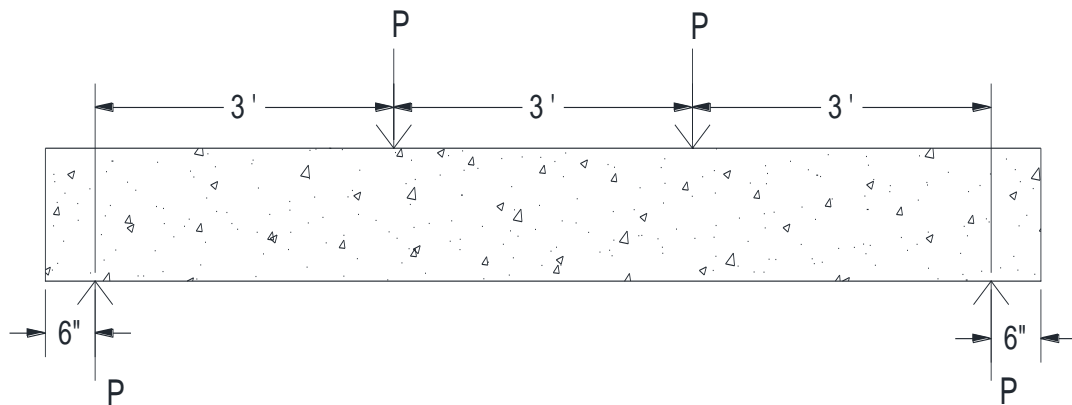
Figure 4.15 – Beam loading schematic
Conversion: 1 in. = 25.4 mm

     The process of installing the beams into the test setup started with marking the

center point, load points, and spreader beam outline onto each specimen. The strain gauge

wires were then attached to a strain gauge converter box for subsequent attachment to the

data acquisition system. At this point, the overhead crane was used to transport the beams

to a location adjacent to the test setup. The beams were then lowered onto steel rollers to

facilitate placement into the test setup. The beam was then rolled into a position where

the center point mark was directly below the center web stiffener on the spreader beam.

One end was lined up with the spreader beam, lifted off of the steel roller with a

hydraulic jack, and then lowered onto the support. This process was then repeated for the

other support to line the beam up properly in the test frame. Once the beam was

positioned within the test frame, metal plates were installed at the load point marks and

the transfer beam was lowered into place. **Figure 4.16** shows the beam in the load frame

located at the Missouri S&T High-Bay Structures Laboratory. A segment of aluminum

angle was attached to the midpoint of the beam and an LVDT was placed on the

aluminum to measure the deflection at midspan during testing as shown in **Figure 4.17**.

The strain gauge wire converter box was then attached to the data acquisition system.

Figure 4.16 – Beam positioned within load frame

Figure 4.17 – LVDT installation

4.3.4. Beam Splice Test Procedure. Prior to beginning the test, the data acquisition system was initiated to record applied load, LVDT data, and strain gauge data. The load was then applied by the two 140-kip-capacity (623 kN) hydraulic actuators acting through the spreader beams. Each test was performed under displacement control, and the load was applied in a series of loading steps of 0.02 in. (0.5 mm), which corresponded to a load of approximately 3 kips (13 kN), until failure. Electronic measurements of strain and deformation were recorded throughout the entire loading history of the specimens. The crack patterns in the concrete were marked at every other load step to track propagation as the load was increased. Loading of the beams continued until a very prominent failure occurred, which was usually signaled both audibly and by a significant drop in the load-deflection behavior of the specimen.

5. HVFA TEST RESULTS AND EVALUATION

5.1. DIRECT PULL-OUT TEST RESULTS

The direct pull-out test specimens were constructed to evaluate the bond performance of HVFA concrete. The MoDOT standard mix design was used as a baseline for test result comparisons. A total of 18 direct pull-out test specimens were constructed for the HVFA concrete test program. There were six test specimens constructed for each of the HVFA concrete mix designs, as well as for the control mix design. Of the six specimens constructed for each mix design, three specimens contained a #4 (#13) reinforcing bar and three specimens contained a #6 (#19) reinforcing bar. The test matrix for the HVFA concrete direct pull-out test program is shown in **Table 5.1**.

Table 5.1 – HVFA concrete direct pull-out test matrix

Mix I.D.	Bar Size	No. of Specimens
HVFA-C	#4 (#13)	3
	#6 (#19)	3
HVFA-70H	#4 (#13)	3
	#6 (#19)	3
HVFA-70L	#4 (#13)	3
	#6 (#19)	3

Due to the limitations of the local ready mix concrete plant, it was necessary to add the appropriate amount of powder activators (gypsum and calcium hydroxide) specified in each HVFA concrete mix design upon arrival of the mixing truck. The addition of calcium hydroxide can be seen in **Figure 5.1**.

Figure 5.1 – Adding calcium hydroxide to the mixing truck

The applied load and corresponding slip of each reinforcing bar through the surrounding concrete were recorded for each test. Once compiled, the maximum applied load (peak load) for each test specimen was determined and used for bond strength comparisons. **Table 5.2** displays the peak load for each of the test specimens in the HVFA concrete test program, as well as the average coefficient of variation (COV) for each group of data. The first number in the specimen name represents the bar size, the following PO designates that specimen as a pull-out specimen, and the final number is the number of the specimen. Plots of the peak load for the HVFA-C, HVFA-70H, and HVFA-70L specimens are shown in **Figures 5.2**, **5.3**, and **5.4**, respectively. The plots indicate that results from tests having the same parameters are relatively similar. This facet is also demonstrated by the relatively small COV within a group of test results, with the highest being 7%. The consistent results between tests with the same parameters lend

confidence in the ability of this test to accurately compare the bond strength between mix

designs.

Table 5.2 – HVFA concrete pull-out test results

Mix	Bar Size	Specimen	Max Applied Load (lb.)	Average Applied Load (lb.)	COV (%)
HVFA-C	#4 (#13)	4PO1	10,002	10,270	6.8
		4PO2	11,058		
		4PO3	9,749		
	#6 (#19)	6PO1	24,289	24,784	3.6
		6PO2	24,234		
		6PO3	25,829		
HVFA-70H	#4 (#13)	4PO1	8,604	8,912	3.0
		4PO2	9,091		
		4PO3	9,042		
	#6 (#19)	6PO1	24,770	24,264	4.1
		6PO2	24,902		
		6PO3	23,120		
HVFA-70L	#4 (#13)	4PO1	9,989	9,243	7.1
		4PO2	8,750		
		4PO3	8,992		
	#6 (#19)	6PO1	23,120	23,817	4.7
		6PO2	25,108		
		6PO3	23,222		

Conversion: 1 lb. = 4.45 N
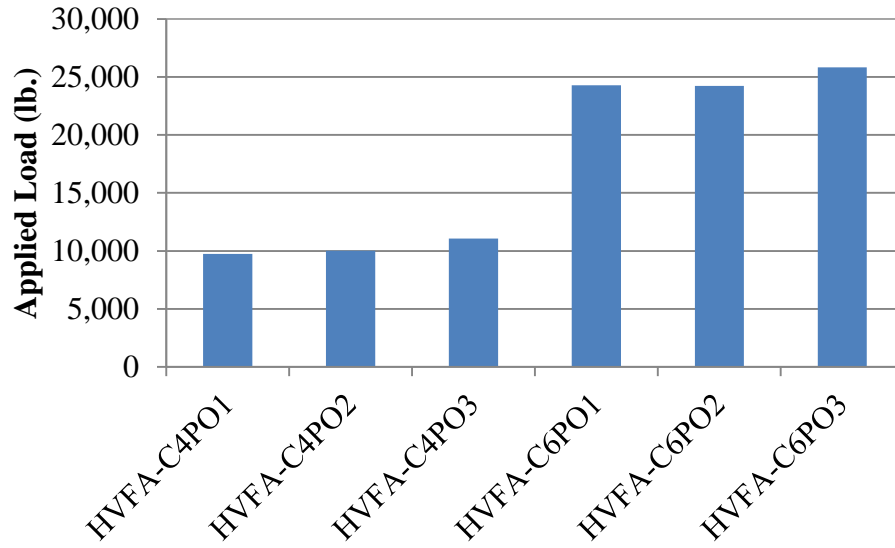
Figure 5.2 – HVFA-C pull-out test results
Conversion: 1 lb. = 4.45 N
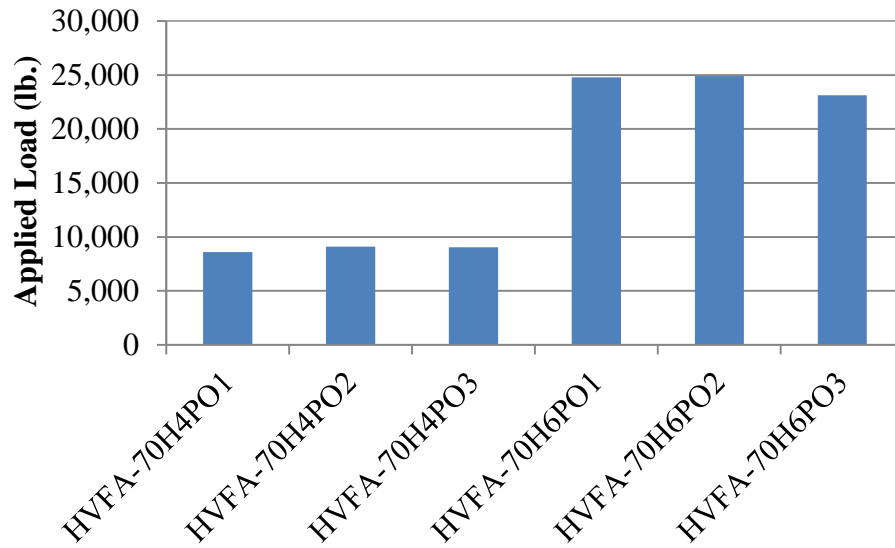
Figure 5.3 – HVFA-70H pull-out test results
Conversion: 1 lb. = 4.45 N
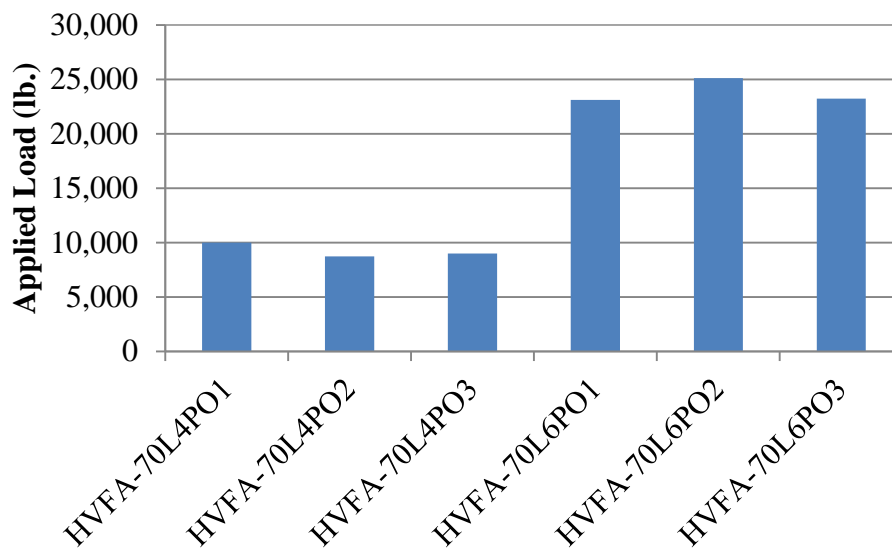
Figure 5.4 – HVFA-70L pull-out test results
Conversion: 1 lb. = 4.45 N

The load and bar slip data were also plotted for comparison. An example of a load

vs. slip plot is shown in **Figure 5.5**. All other load vs. slip plots have a similar shape and

only differ in the magnitude of the values plotted, with one exception. The most

consistent mode of failure of the pull-out test specimens consisted of the reinforcing bar

slipping through the concrete section. However, the test specimen HVFA-C6PO3 failed

by splitting of the concrete section, as shown in **Figure 5.6**. This mode of failure was due

to the reinforcing bar being noticeably out of plumb. The load vs. slip plot for HVFA-

C6PO3 is shown in **Figure 5.7**. Appendix B contains the load vs. slip plots for all 18

pull-out specimens.
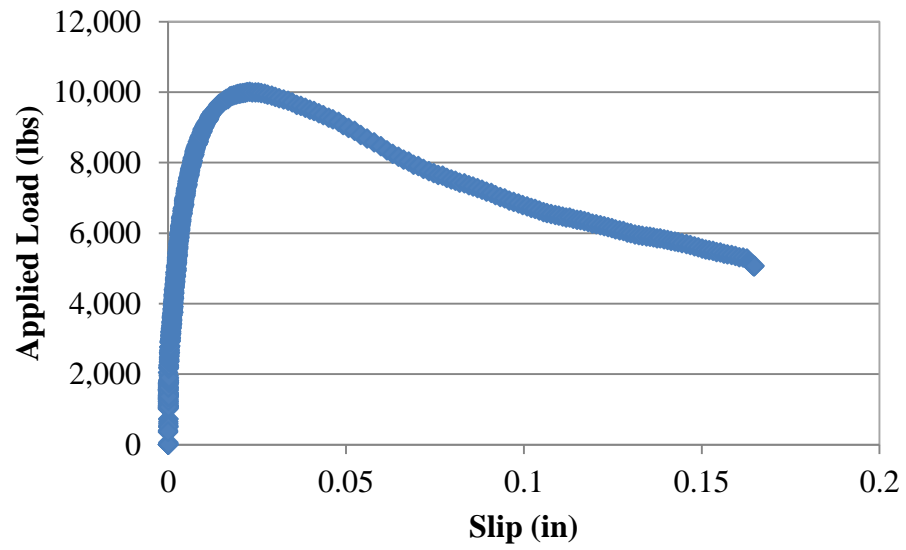
Figure 5.5 – Example applied load vs. slip plot
Conversion: 1 in. = 25.4 mm
1 lb. = 4.45 N
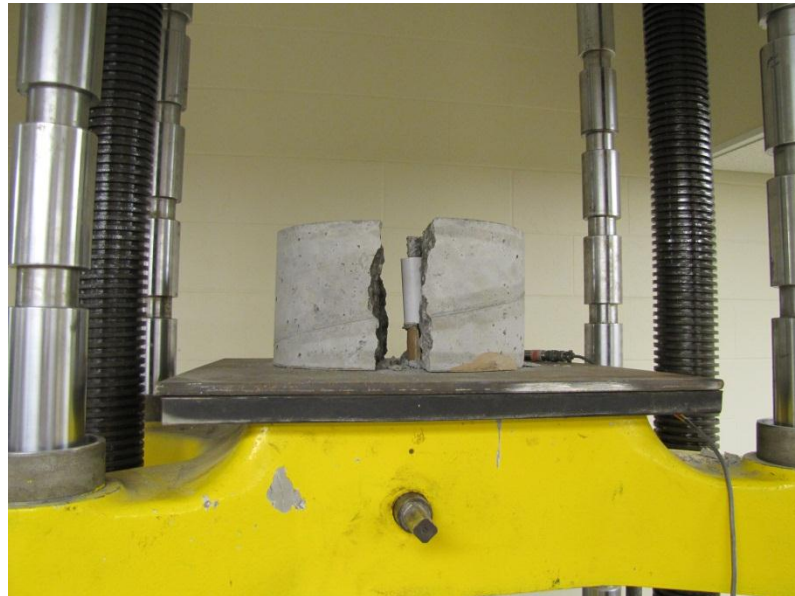
Figure 5.6 – HVFA-C6PO3 failed specimen
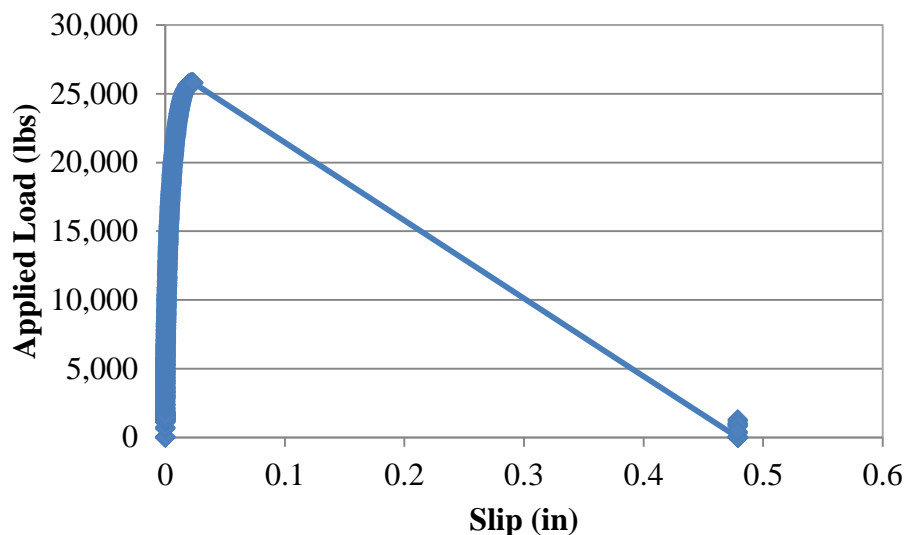
Figure 5.7 – HVFA-C6PO3 applied load vs. slip plot
Conversion: 1 in. = 25.4 mm
1 lb. = 4.45 N

5.2. BEAM SPLICE TEST RESULTS

The beam splice test specimens were constructed to evaluate the bond

performance of HVFA concrete under more realistic loading conditions. The MoDOT

standard mix design was used as a baseline for test result comparisons. A total of nine

test specimens with 3#6 (#19) longitudinal reinforcing bars spliced at midspan were

constructed for the HVFA concrete test program. There were three test specimens

constructed for each of the two HVFA concrete mix designs to be evaluated, as well as

for the control mix design. Of the three test specimens, two specimens were constructed

with the spliced reinforcing bar located at the bottom of the beam cross section and one

specimen was constructed with the splice at the top of the beam cross section to evaluate

the top-bar effect. The test matrix for the HVFA concrete beam splice test program is

shown in **Table 5.3**. A splice length of 14.34 in. (364 mm) was used for each test

specimen.

Table 5.3 – HVFA concrete beam splice test matrix

Mix I.D.	Bar Size	Splice Location	No. of Specimens
HVFA-C	#6 (#19)	Bottom	2
		Top	1
HVFA-70H	#6 (#19)	Bottom	2
		Top	1
HVFA-70L	#6 (#19)	Bottom	2
		Top	1

The applied load, corresponding midspan deflection, and corresponding strain at the end of each bar splice were recorded for each test. The peak load and peak stress were collected for each test specimen and are shown in **Table 5.4**. The bottom splice specimens are denoted with the abbreviation BB and the top splice specimens are denoted with the abbreviation TB. Steel stress recorded at failure of the specimen was determined by averaging the strain readings from each strain gage in a member and finding the peak strain that occurred during loading. This peak strain was then multiplied by the average modulus of elasticity of the steel determined from the tension test to determine the peak stress. The peak loads for the HVFA-C, HVFA-70H, and HVFA-70L specimens are plotted in **Figures 5.8**, **5.9**, and **5.10**, respectively.

Table 5.4 – Peak load and reinforcing bar stresses

Mix	Specimen	Steel Stress Recorded at Failure (ksi)	Peak Load (kips)
HVFA-C	**BB1**	54.6	53.3
	BB2	48.6	49.7
	TB	48.1	49.5
HVFA-70H	**BB1**	62.4	55.9
	BB2	55.1	56.1
	TB	62.8	60.2
HVFA-70L	**BB1**	54.0	55.2
	BB2	49.9	51.1
	TB	51.7	55.1

Conversion: 1 ksi = 6.9 MPa
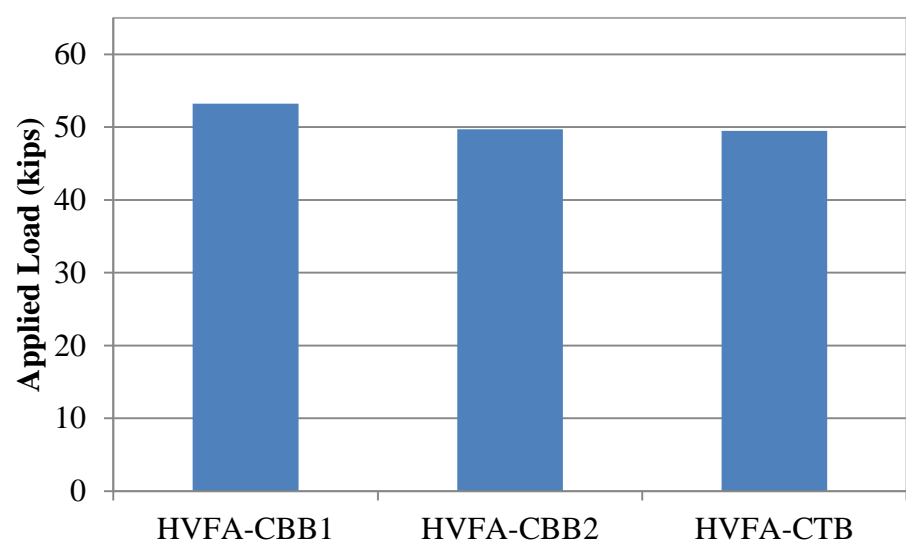
Figure 5.8 – HVFA-C peak load plot
Conversion: 1 kip = 4.45 kN
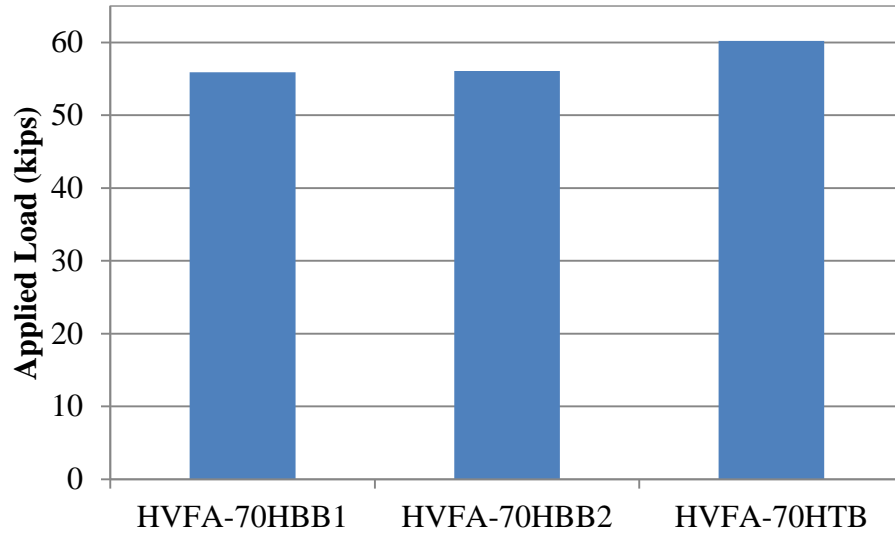
Figure 5.9 – HVFA-70H peak load plot
Conversion: 1 kip = 4.45 kN
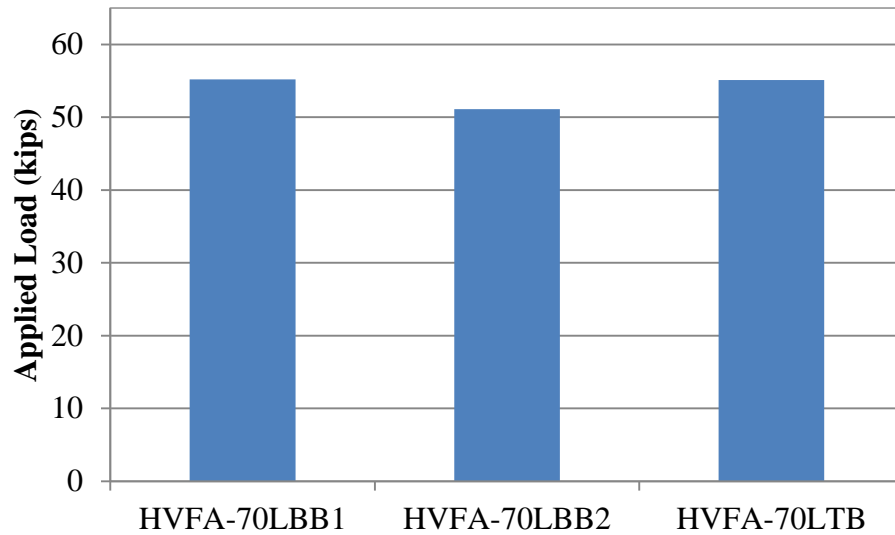
Figure 5.10 – HVFA-70L peak load plot
Conversion: 1 kip = 4.45 kN

The deflection and strain data were also plotted with the load data to observe the

response of the specimens during testing. A typical load vs. displacement at midspan plot

is shown in **Figure 5.11**. A typical load vs. strain plot is shown in **Figure 5.12**. The plots

shown are from the HVFA-CBB1 specimen. Both plots indicate that the beam began to develop flexural cracks at a load of approximately 12 kips (53 kN). At the failure load, all specimens exhibited visible and audible signs of complete bond failure, having never yielded the reinforcing bars. Evidence of this is shown in the linear behavior indicated in both the load vs. deflection plot and the load vs. strain plot. Appendix B contains the load vs. slip plots for all nine beam splice specimens.

The cracking patterns in the beam splice specimens also revealed a bond failure. For example, **Figures 5.13**, **5.14**, and **5.15** display the failed beam specimen designated HVFA-70HBB2. **Figures 5.14** and **5.15** in particular display longitudinal cracking along the bars within the splice zone, which is indicative of a bond-splitting failure. Appendix A contains the photographs of the nine beam splice specimens after failure.
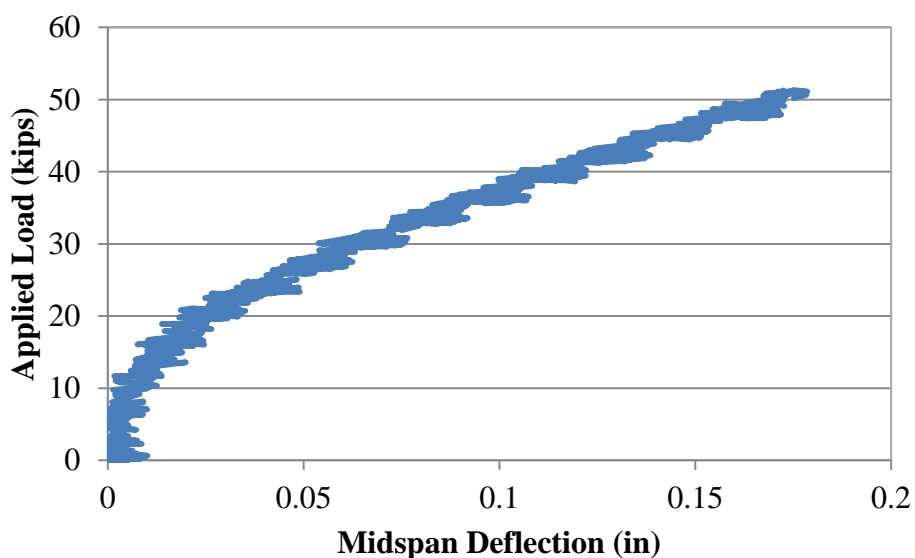
Figure 5.11 – Typical load vs. deflection plot
Conversion: 1 in. = 25.4 mm
1 kip = 4.45 kN
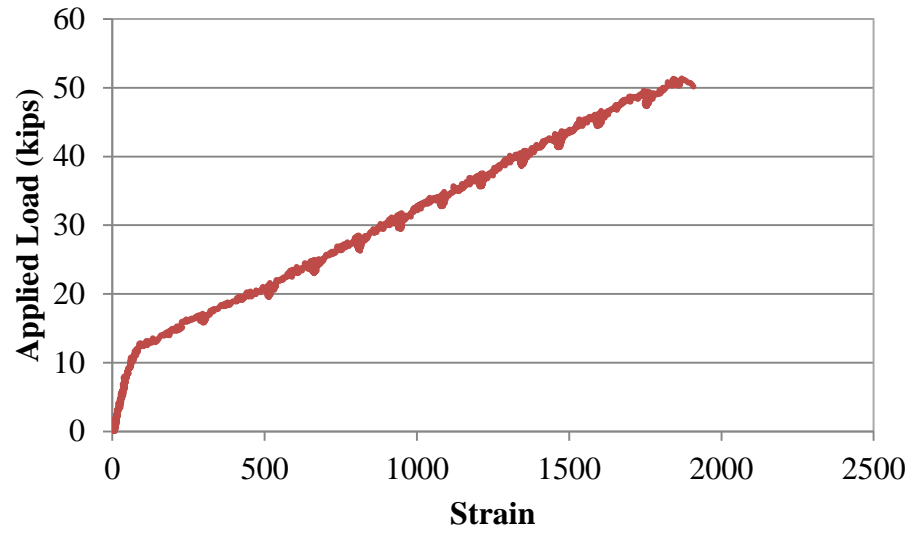
Figure 5.12 – Typical load vs. strain plot
Conversion: 1 kip = 4.45 kN
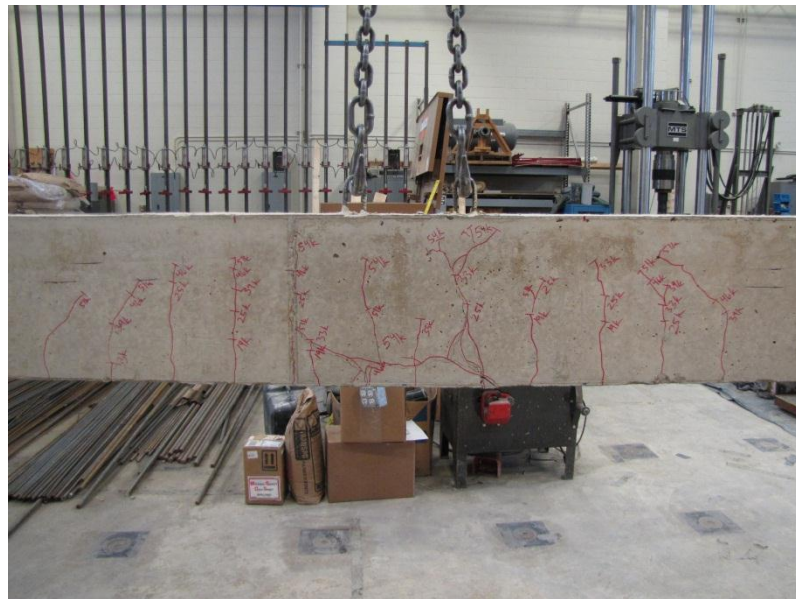
Figure 5.13 – Cracked length of HVFA-70HBB2
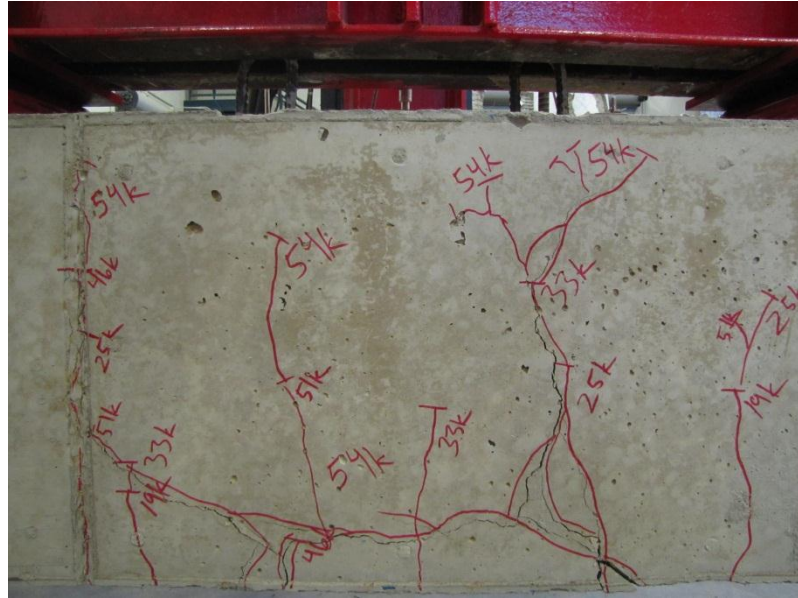
Figure 5.14 – Failed splice region of HVFA-70HBB2

Figure 5.15 – Bottom of splice region of HVFA-70HBB2

5.3. REINFORCING BAR DIRECT TENSION TEST

A tension test was performed on the #6 (#19) longitudinal reinforcing bars used in each beam specimen following ASTM E8-09, "Standard Test Methods for Tension Testing of Metallic Materials" (ASTM E9-09). Three 30 in. (762 mm) lengths of reinforcing bar were clamped at each end in a 200,000 lb. (890 kN) Tinius Olson testing machine and load was applied until the bar fractured. The strain and applied load were recorded during testing. The strain with a 0.5% offset was recorded and used to determine the yield strength of each bar. The modulus of elasticity was also determined for each bar. The average yield stress of the test was used as a comparison tool to check that the reinforcing bars within the splice region of each beam specimen did not reach yield. **Table 5.5** displays the results of the tension test performed.

Table 5.5 – #6 (#19) reinforcing bar tension test results

Specimen	Yield Stress (ksi)	Average Yield Stress (ksi)	Initial Tangent Modulus (ksi)	Average Modulus (ksi)
1	81.1		33,130	
2	81.3	81.1	26,510	30,310
3	81.0		31,295	

Conversion: 1 ksi = 6.9 MPa

5.4. ANALYSIS OF RESULTS

5.4.1. Methodology. Direct comparison between test results is not possible due to the fact that the test day concrete strength varies for each mix. Therefore, normalization of the value of interest was completed to facilitate direct comparison of test results. Two separate normalization formulas were used in this study. The first normalization formula

is based on the development length equations in ACI 318-08 (ACI 318-08, 2008) and

AASHTO LRFD-07 (AASHTO, 2007), shown as **Eq. 5.1** and **5.2**, respectively. Both

equations express the development length of a reinforcing bar in tension as a function of

the inverse square root of the compressive strength. Therefore, the first normalization of

the test results was based on multiplying values by the square root of the ratio of the

specified design strength and the test day compressive strength, shown in **Eq. 5.3**.

$$l_d = \left(\frac{3}{40} \frac{f_y}{\lambda \sqrt{f'_c}} \frac{\Psi_t \Psi_e \Psi_s}{\left(\frac{c_b + K_{tr}}{d_b} \right)} \right) d_b \qquad (5.1)$$

Where l_d is the development length, f_y is the specified yield strength of reinforcement, λ

is the lightweight concrete modification factor, f'_c is the specified compressive strength

of concrete, Ψ_t is the reinforcement location modification factor, Ψ_e is the reinforcement

coating modification factor, Ψ_s is the reinforcement size modification factor, c_b is the

smaller of the distance from center of a bar to nearest concrete surface or one-half the

center-to-center spacing of bars being developed, K_{tr} is the transverse reinforcement

index, and d_b is the nominal diameter of reinforcing bar.

$$l_{db} = \frac{1.25 \, A_b \, f_y}{\sqrt{f'_c}} \geq 0.4 \, d_b \, f_y \qquad (5.2)$$

Where l_{db} is the tension development length, f_y is the specified yield strength of

reinforcement, A_b is the area of reinforcing bar, f'_c is the specified compressive strength

of concrete, and d_b is the reinforcing bar diameter.

$$Normalizied\ Load = Failure\ load \sqrt{\frac{Design\ strength}{Strength\ at\ testing}} \tag{5.3}$$

The second normalization formula is based on the development length equation in ACI 408R-04 (2003), as shown in **Eq. 5.4**. The development length of a reinforcing bar in tension in this equation is a function of the inverse fourth root of the compressive strength. Therefore, the normalization of the test results was based on the fourth root of the ratio of the specified design strength and the test day compressive strength, as shown in **Eq. 5.5**.

$$l_d = \left(\frac{\left(\frac{f_y}{f'_c{}^{1/4}} - 1970\ \omega \right) \alpha\ \beta\ \lambda}{62 \left(\frac{c\ \omega + K_{tr}}{d_b} \right)} \right) d_b \tag{5.4}$$

Where l_d is the development length, f_y is the specified yield strength of reinforcement, λ is the lightweight concrete modification factor, f'_c is the specified compressive strength of concrete, α is the reinforcement location modification factor, β is the reinforcement coating modification factor, ω is equal to 0.1 $(c_{max}/c_{min}) + 0.9 \leq 1.25$, c is the spacing or cover dimension, d_b is the nominal diameter of reinforcing bar, and K_{tr} is the transverse reinforcement index.

$$Normalizied\ Load = Failure\ load \left(\frac{Design\ strenght}{Strength\ at\ testing} \right)^{1/4} \tag{5.5}$$

The design strength for the HVFA concrete test program was 4,000 psi (27.6

MPa) and the strengths at testing for each mix design can be seen in **Table 5.6**.

Table 5.6 – Test day compressive strengths for test specimens

	Test Day Strength (psi)				
	Cylinder 1	**Cylinder 2**	**Cylinder 3**	**Average**	**COV (%)**
HVFA-C	4560	4390	4480	4475	1.9
HVFA-70H	3300	3480	3560	3450	3.8
HVFA-70L	3530	3320	3415	3420	3.1

Conversion: 1 psi = 6.9 kPa

5.4.2. Analysis and Interpretation – Direct Pull-out Test Results. Table 5.7

contains the peak load, concrete strength at time of testing, and normalized peak load for

each specimen. **Figure 5.16** is a plot of the square root normalized peak load for each of

the mix designs and bar sizes. The error bars indicate the range of test data collected. For

the #4 (#13), all three mix designs performed at essentially the same level. The HVFA-

70H normalized peak load average was 131 lb. (0.6 kN) lower, and the HVFA-70L

normalized peak load average was 286 lb. (1.3 kN) higher than that of the control, which

represents differences of 1.4 and 3%, respectively. The closeness of these results

indicates that both fly ash mix designs have the same level of bond strength as the control

for #4 (#13) reinforcing bars, particularly given the expected variation in results. Slightly

more variability occurred for the #6 (#19) bars. The HVFA-70H and HVFA-70L

normalized peak load averages were 2,645 lb. (11.8 kN) and 2,321 lb. (10.3 kN) higher

than that of the control, representing differences of 11.3 and 9.9%, respectively.

However, paired t-tests indicate that there is no statistically significant difference

between the results for each mix design, indicating that the HVFA concrete has essentially the same bond strength as conventional concrete.
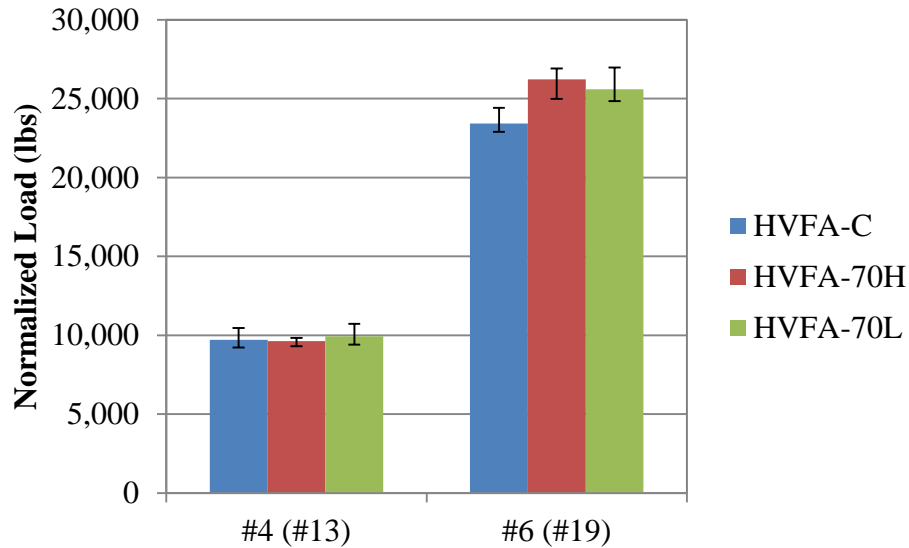
Figure 5.16 – Plot of normalized average peak load for each HVFA concrete mix design
Conversion: 1 lb. = 4.45 N

Figure 5.17 displays a representative normalized load vs. slip plot of the #4 (#13) pull-out specimens, and **Figure 5.18** displays the same plot for the #6 (#19) pull-out specimens. The plots indicate that bar slip occurred around the same load for each test specimen. More importantly, the overall behavior was very similar between all three mix designs. This behavior, combined with a forensic investigation of the failed specimens, indicates that the concrete surrounding the bar crushed around the same load for both fly ash mixes and the control mix.

Table 5.7 – Normalized HVFA concrete pull-out test results

Mix	Bar Size	Specimen	Peak Load (lb.)	Concrete Compressive Strength (psi)	Normalized Load (lb.)				COV (%)
					Square Root Adjustment	Fourth Root Adjustment	Average of Square Root Adjustment	Average of Fourth Root Adjustment	
HVFA-C	#4 (#13)	4PO1	10,002	4,476	9,455	9,725	9,708	9,985	6.8
		4PO2	11,058		10,453	10,752			
		4PO3	9,749		9,216	9,479			
	#6 (#19)	6PO1	24,289		22,961	23,616	23,429	24,097	3.6
		6PO2	24,234		22,909	23,562			
		6PO3	25,829		24,417	25,113			
HVFA-70H	#4 (#13)	4PO1	8,604	3,464	9,246	8,919	9,577	9,239	3.0
		4PO2	9,091		9,769	9,424			
		4PO3	9,042		9,716	9,373			
	#6 (#19)	6PO1	24,770		26,617	25,677	26,074	25,153	4.1
		6PO2	24,902		26,759	25,814			
		6PO3	23,120		24,845	23,967			
HVFA-70L	#4 (#13)	4PO1	9,989	3,422	10,799	10,386	9,994	9,611	7.1
		4PO2	8,750		9,460	9,098			
		4PO3	8,992		9,722	9,350			
	#6 (#19)	6PO1	23,120		24,997	24,040	25,750	24,765	4.7
		6PO2	25,108		27,146	26,107			
		6PO3	23,222		25,107	24,146			

Conversion: 1 in. = 25.4 mm
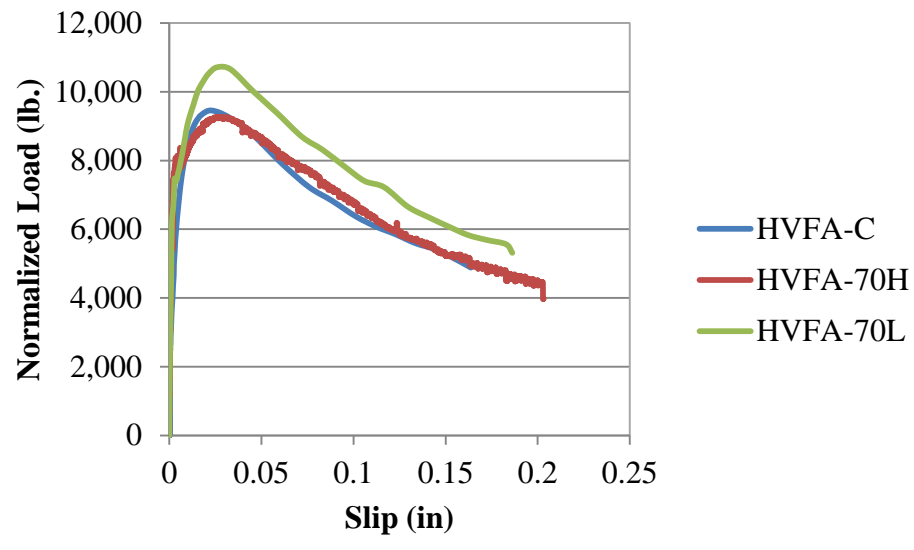
Figure 5.17 – Normalized load vs. slip plot for #4 (#13) reinforcing bars
Conversion: 1 in. = 25.4 mm
1 lb. = 4.45 N
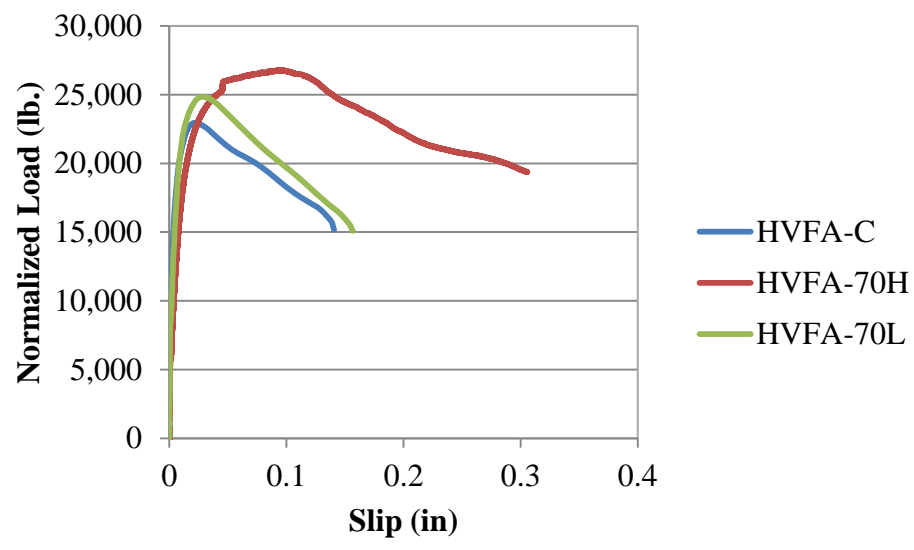
Figure 5.18 – Load vs. slip plot for #6 (#19) reinforcing bars
Conversion: 1 in. = 25.4 mm
1 lb. = 4.45 N

5.4.3. Analysis and Interpretation – Beam Splice Test Results. Table 5.8

contains the peak load, concrete strength at time of testing, and normalized peak load of each specimen tested. The square root normalized peak loads are plotted in **Figure 5.19**. **Table 5.9** contains the measured steel stress at failure, concrete strength at time of testing, and normalized measured steel stress at failure. The square root normalized steel stresses are shown plotted in **Figure 5.20**. The error bars indicate the range of test data collected. The normalized steel stresses were compared to the theoretical stress calculated using the moment-curvature program Response-2000 (Bentz, 2000) and are shown in **Table 5.10**. The moment at midspan of the specimen used when calculating the theoretical stress was a combination of both applied load moment and dead load moment. The applied load moment includes the weight of the spreader beams used to distribute the load from the actuators. The design concrete strength of 4,000 psi (27.6 MPa) was used when calculating the theoretical steel stress.

The data collected indicates that both fly ash mix designs exhibited improved bond performance compared to the control mix design. The average longitudinal bar stress for the HVFA-70H and HVFA-70L bottom splice beam specimens was 14.4 ksi (99 MPa) and 7.4 ksi (51 MPa) higher than that of the control bottom splice specimens, which represents a difference of 29 and 15%, respectively. The top splice beam specimens showed a similar trend, with the HVFA-70H and HVFA-70L bar stress being 22.1 ksi (152 MPa) and 10.5 ksi (72 MPa) higher than the control specimen, which represents a difference of 49 and 23%, respectively. The peak load data shows the same trend. These results indicate that the HVFA concrete mix designs have higher bond strength than that of the control mix design.

Table 5.8 – Normalized peak loads for each specimen

Mix	Specimen	Max Applied Load (kips)	Concrete Compressive Strength (psi)	Normalized Load (kips)			
				Square Root Adjustment	Fourth Root Adjustment	Average of Square Root Adjustment	Average of Fourth Root Adjustment
HVFA-C	BB1	53.3	4476	50.4	51.8	48.7	50.1
	BB2	49.7		47.0	48.3		
	TB	49.5		46.8	48.1	N/A	N/A
HVFA-70H	BB1	55.9	3464	60.1	57.9	60.2	58.1
	BB2	56.1		60.3	58.2		
	TB	60.2		64.7	62.4	N/A	N/A
HVFA-70L	BB1	55.2	3422	59.7	57.4	57.5	55.3
	BB2	51.1		55.2	53.1		
	TB	55.1		59.6	57.3	N/A	N/A

Conversion: 1 kip = 4.45 kN
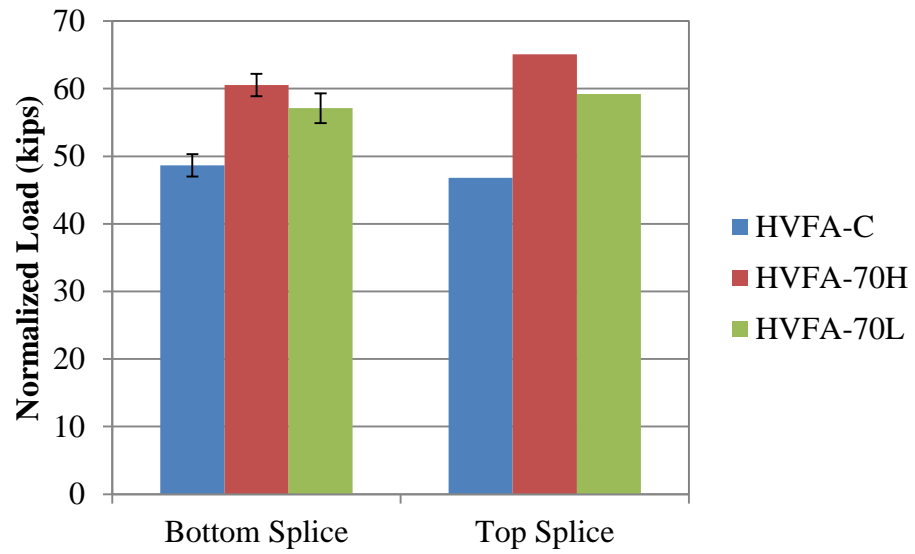
Figure 5.19 – Normalized peak load
Conversion: 1 kip = 4.45 kN
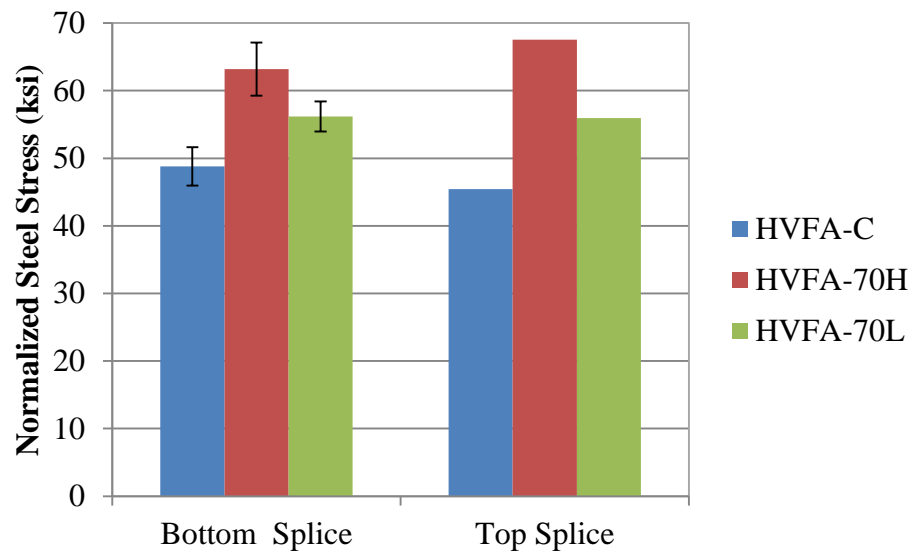
Figure 5.20 – Normalized steel stress at failure load
Conversion: 1 kip = 4.45 kN

Table 5.9 – Normalized steel stress at failure for each specimen

Mix	Specimen	Steel Stress Measured at Failure (ksi)	Concrete Compressive Strength (psi)	Normalized Steel Stress (ksi)	
				Square Root Adjustment	Fourth Root Adjustment
HVFA-C	BB1	54.6	4476	51.6	53.1
	BB2	48.6		46.0	47.3
	TB	48.1		45.4	46.7
HVFA-70H	BB1	62.4	3464	67.1	64.7
	BB2	55.1		59.2	57.2
	TB	62.8		67.5	65.1
HVFA-70L	BB1	54.0	3422	58.4	56.2
	BB2	49.9		53.9	51.9
	TB	51.7		55.9	53.8

Conversion: 1 ksi = 6.9 MPa

Table 5.10 – Normalized steel stress compared to theoretical steel stress at failure

Mix	Specimen	Normalized Steel Stress (ksi)		Calculated Stress at Failure Load (ksi)	Measured/Calculated Stress	
		Square Root Adjustment	Fourth Root Adjustment		Square Root Adjustment	Fourth Root Adjustment
HVFA-C	BB1	51.6	53.1	51.0	0.99	1.04
	BB2	46.0	47.3	47.6	1.04	0.99
	TB	45.4	46.7	47.5	1.05	0.98
HVFA-70H	BB1	67.1	64.7	53.4	0.80	1.21
	BB2	59.2	57.2	53.6	0.90	1.07
	TB	67.5	65.1	57.5	0.85	1.13
HVFA-70L	BB1	58.4	56.2	52.8	0.90	1.06
	BB2	53.9	51.9	49.0	0.91	1.06
	TB	55.9	53.8	52.7	0.94	1.02

Conversion: 1 ksi = 6.9 MPa

The difference in bond strength between the high and low cementitious material fly ash mix designs can be attributed to the difference in paste content of each mix. The higher paste content can facilitate consolidation of the concrete and allow for a more thorough coating of concrete around the perimeter of the reinforcing bar, thus increasing bonded area.

Normalized load vs. strain of the longitudinal reinforcing bar was also plotted for comparison. A typical plot of the average bottom splice strain for a specimen of each mix design is shown in **Figure 5.21**. As seen in the plot, all three specimens have two distinct linear sections. The first represents pre-flexural cracking behavior and the second represents post-flexural cracking behavior. The HVFA-70H specimen had a much lower cracking load than either mix. This was typical behavior of all HVFA-70H beam specimens. Most importantly, all load-strain plots indicated linear behavior up to failure. In other words, the reinforcing bars failed in bond, having never reached yield.
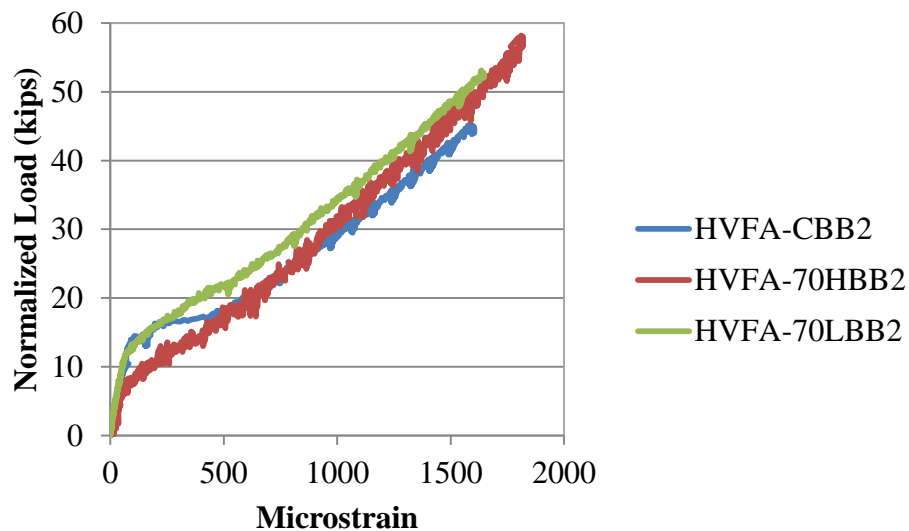
Figure 5.21 – Typical normalized load vs. strain plot
Conversion: 1 kip = 4.45 kN

5.5. FINDINGS AND CONCLUSIONS

Based on an analysis of the test results, the following conclusions are presented:

1. The average peak load for the #4 (#13), HVFA-70H and HVFA-70L pull-out specimens was 0.7% lower and 2.3% higher than that of the control, respectively. The average peak load for the #6 (#19), HVFA-70H and HVFA-70L pull-out specimens was 12% and 9.2% higher than that of the control, respectively. This data indicates that both HVFA mix designs have comparable bond strengths to the control mix design with #4 (#13) bars and higher bond strength with #6 (#19) bars. However, statistical analysis indicates that all three mix designs performed equally.

2. The average peak bar stress for the HVFA-70H and HVFA-70L bottom splice beam specimens was 29% and 15% higher than that of the control specimens, respectively. The peak bar stress for the HVFA-70H and HVFA-70L top splice beam specimens was 49% and 23% higher than that of the control specimens, respectively. This data indicates that both HVFA mix designs exhibited improved bond performance under realistic stress states than the control mix design.

6. FINDINGS, CONCLUSIONS, AND RECOMMENDATIONS

The main objective of this study was to determine the effect on bond performance of high-volume fly ash (HVFA) concrete. The HVFA concrete test program consisted of comparing the bond performance of two concrete mix designs with 70% cement replacement with Class C fly ash relative to a Missouri Department of Transportation (MoDOT) standard mix design at one strength level.

Two test methods were used for bond strength comparisons. The first was a direct pull-out test based on the RILEM 7-II-128 "RC6: Bond test for reinforcing steel. 1. Pull-out test" (RILEM, 1994). Although not directly related to the behavior of a reinforced concrete beam in flexure, the test does provide a realistic comparison of bond between types of concrete. The second test method consisted of a full-scale beam splice test specimen subjected to a four-point loading until failure of the splice. This test method is a non-ASTM test procedure that is generally accepted as the most realistic test method for both development and splice length.

This section contains the findings of both test programs, as well as conclusions based on these findings and recommendations for future research.

6.1. FINDINGS

6.1.1. Direct Pull-out Testing. A total of 18 direct pull-out test specimens were constructed for the HVFA concrete test program. There were six test specimens constructed for each of the HVFA concrete mix designs, as well as for the control mix design. Of the six specimens constructed for each mix design, three specimens contained

a #4 (#13) reinforcing bar and three specimens contained a #6 (#19) reinforcing bar. Each specimen was tested until failure. The average peak load for the #4 (#13), HVFA-70H and HVFA-70L pull-out specimens was 0.7% lower and 2.3% higher than that of the control, respectively. The average peak load for the #6 (#19), HVFA-70H and HVFA-70L pull-out specimens was 11.3% and 9.9% higher than that of the control, respectively.

6.1.2. Beam Splice Testing. A total of nine test specimens with 3#6 (#19) longitudinal reinforcing bars spliced at midspan were constructed for the HVFA concrete test program. There were three test specimens constructed for each of the two HVFA concrete mix designs to be evaluated, as well as for the control mix design. Of the three test specimens, two specimens were constructed with the spliced reinforcing bar located at the bottom of the beam cross section and one specimen was constructed with the splice at the top of the beam cross section to evaluate the top-bar effect. Each specimen was tested to bond failure. The average peak bar stress for the HVFA-70H and HVFA-70L bottom splice beam specimens was 29.5% and 15.2% higher than that of the control specimens, respectively. The peak bar stress for the HVFA-70H and HVFA-70L top splice beam specimens was 48.7% and 23.1% higher than that of the control specimens, respectively.

6.2. CONCLUSIONS

6.2.1. Direct Pull-out Testing. Analysis of the data indicates that both HVFA concrete mix designs have comparable bond strengths to the control mix design with #4 (#13) bars and higher bond strength with #6 (#19) bars. However, statistical analysis indicates that all three mix designs performed comparably.

6.2.2. Beam Splice Testing. Analysis of the data indicates that both HVFA concrete mix designs exhibited improved bond performance under realistic stress states than the control mix design. These findings, along with the findings from the direct pull-out tests, indicate that using greater than 50% replacement of cement with fly ash in concrete is feasible in terms of bond and development of reinforcing steel.

6.3. RECOMMENDATIONS

Future research in bond behavior of HVFA concrete is necessary due to the limited number of studies conducted on the subject. Much more research must be completed in order to create a more sizeable database that can eventually be used for comparison as well as for future ACI design code changes. Also important for design would be to explore whether or not certain ACI code distinctions, such as confinement, bar size, or bar coating factors, used for conventional concrete designs also apply to HVFA concrete, or if they need to be developed specifically for HVFA concrete. Below is a list of recommendations for testable variables related to HVFA concrete bond behavior:

- Perform tests with a larger variation in bar sizes based on ACI 318 code distinctions for bar size effect on development length

- Test pull-out specimens designed to fail by splitting rather than pull-out of the reinforcing bar

- Conduct direct tension on reinforcing bar embedded in HVFA concrete to determine development length and compare to the current ACI code provisions

- Perform studies with fly ash from different sources

- Perform studies with aggregates form different sources

- Perform bond tests on more specimen types mentioned in ACI 408

APPENDIX A

HVFA TEST PROGRAM BEAM SPLICE FAILURE PHOTOGRAPHS

(a) Bottom view
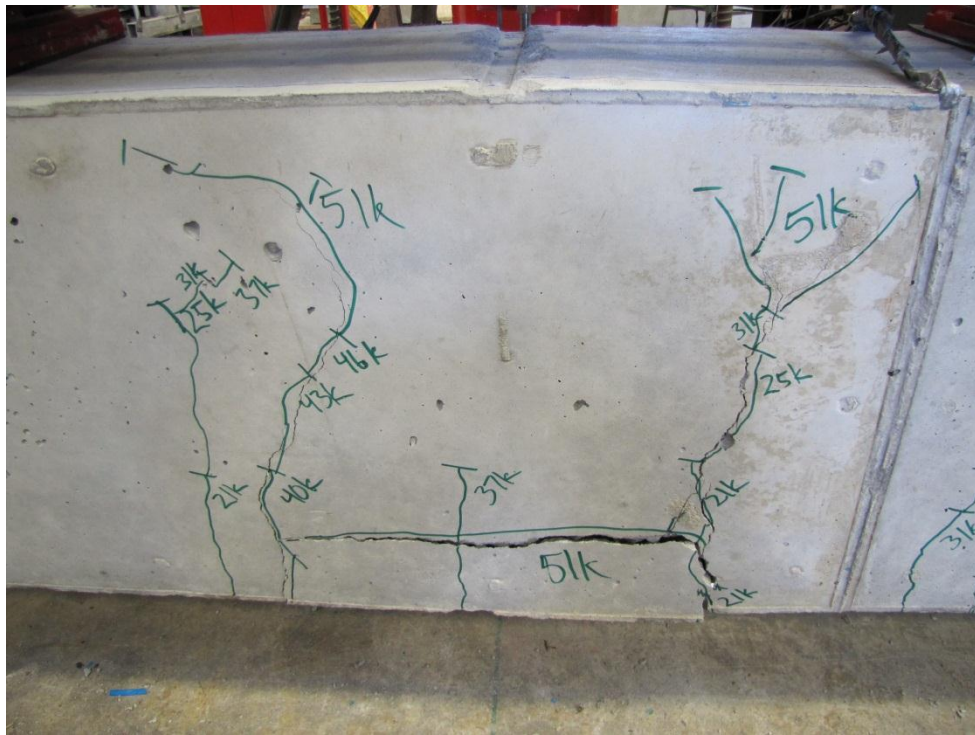
(b) Side view

Figure A.1 – HVFA-CBB1

(a) Bottom View

(b) Side View

Figure A.2 – HVFA-CBB2

(a) Bottom View
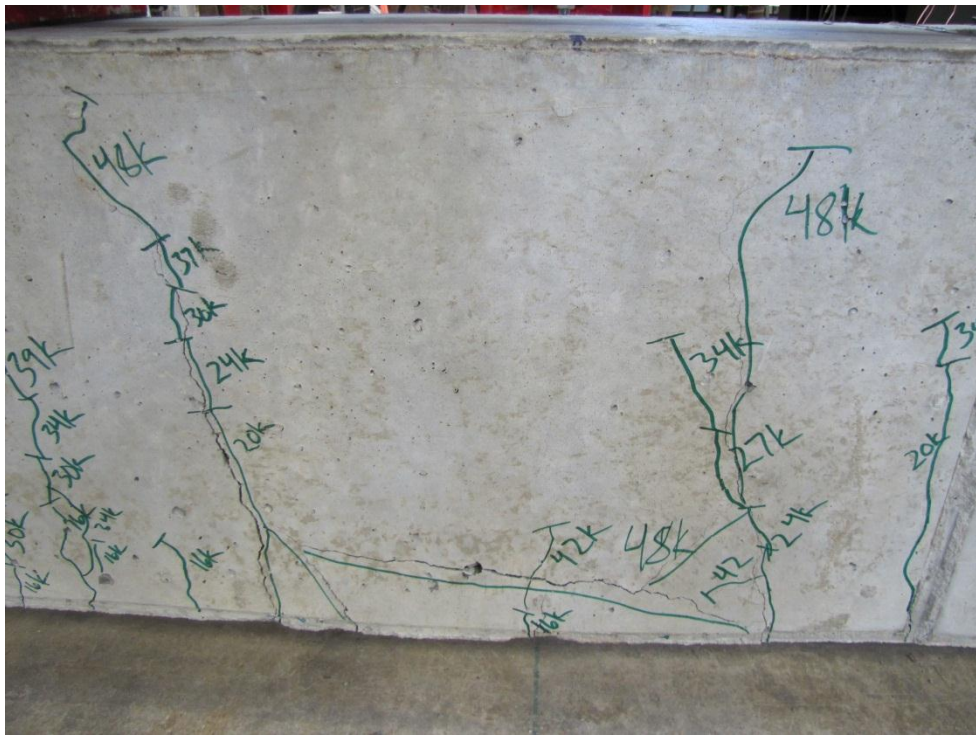
(b) Side View

Figure A.3 – HVFA-CTB

(a) Bottom View

(b) Side View

Figure A.4 – HVFA-70HBB1

(a) Bottom View
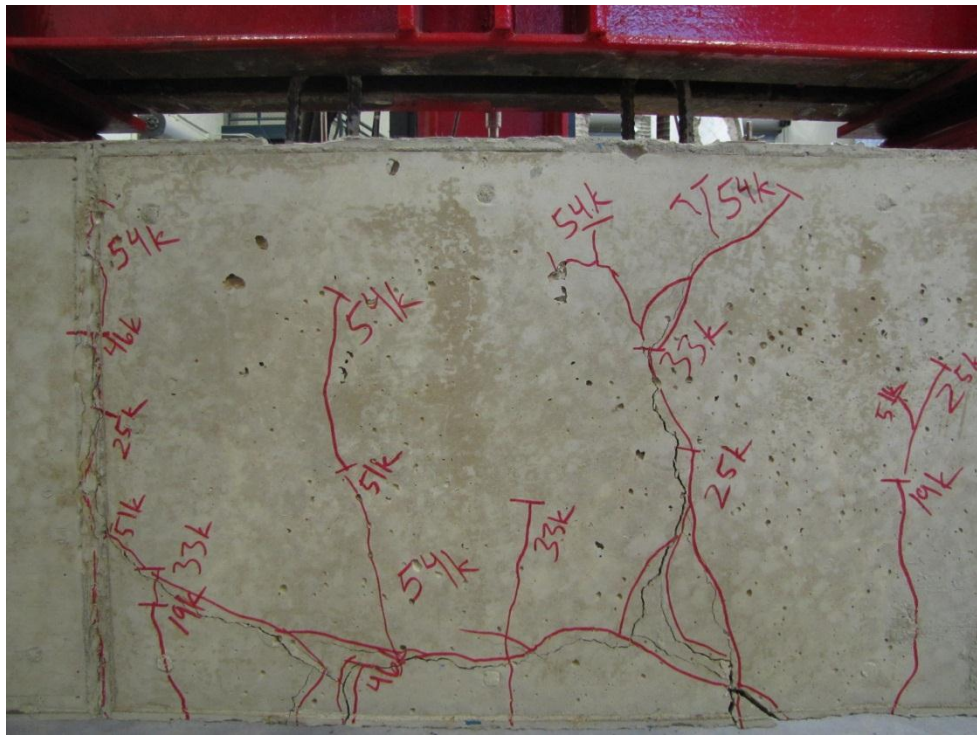
(b) Side View

Figure A.5 – HVFA-70HBB2

(a) Bottom View

(b) Side View

Figure A.6 – HVFA-70HTB

(a) Bottom View
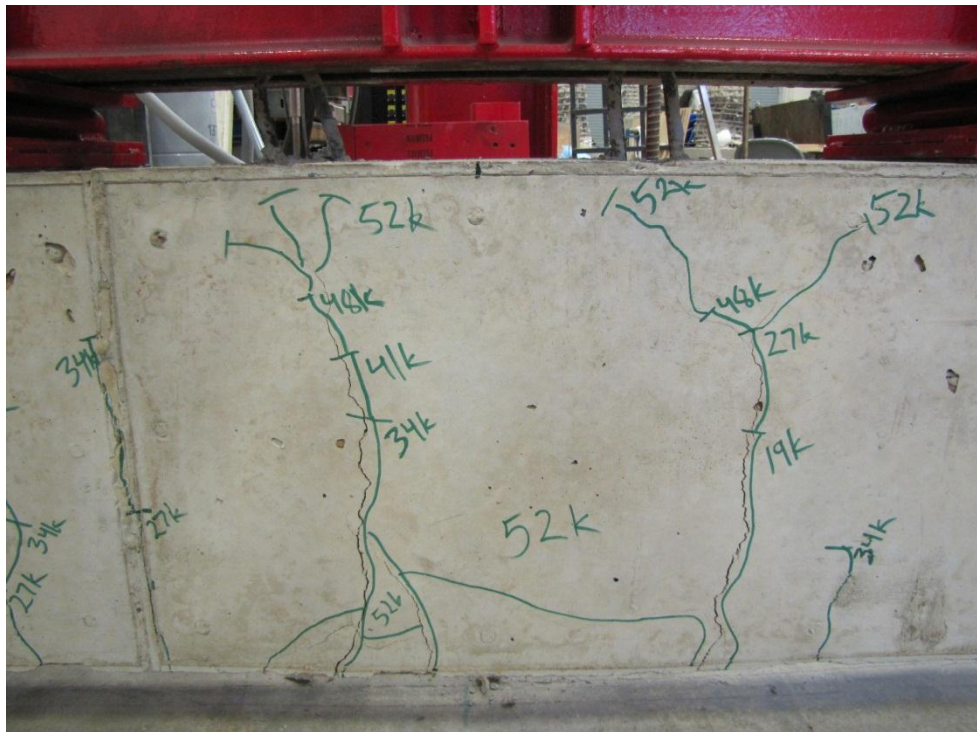
(b) Side View

Figure A.7 – HVFA-70LBB1

(a) Bottom View
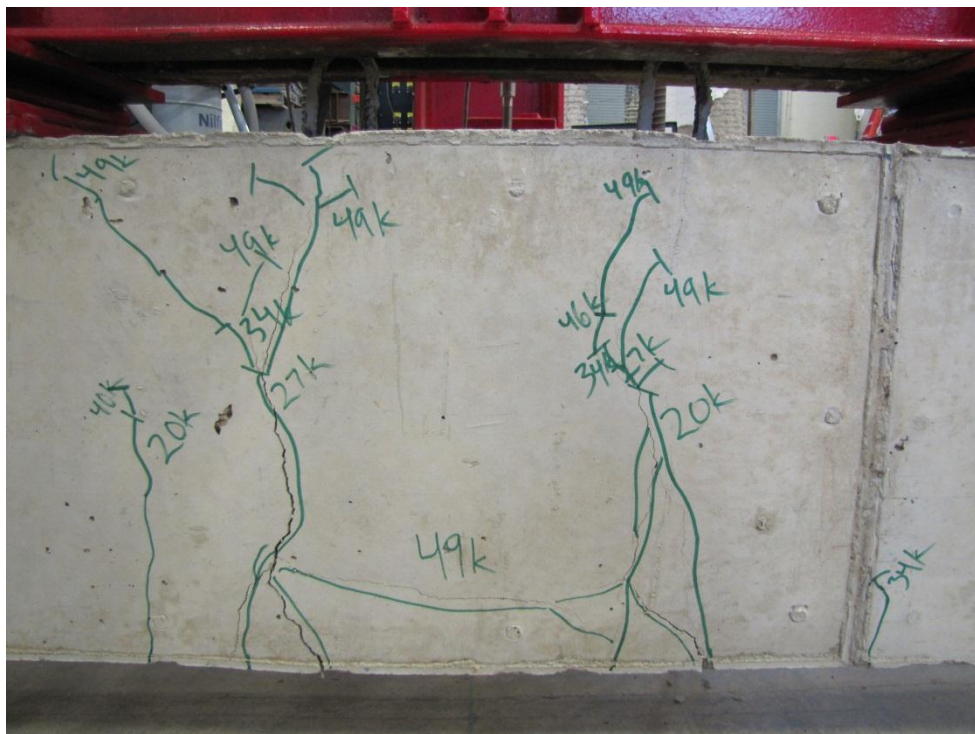
(b) Side View

Figure A.8 – HVFA-70LBB2
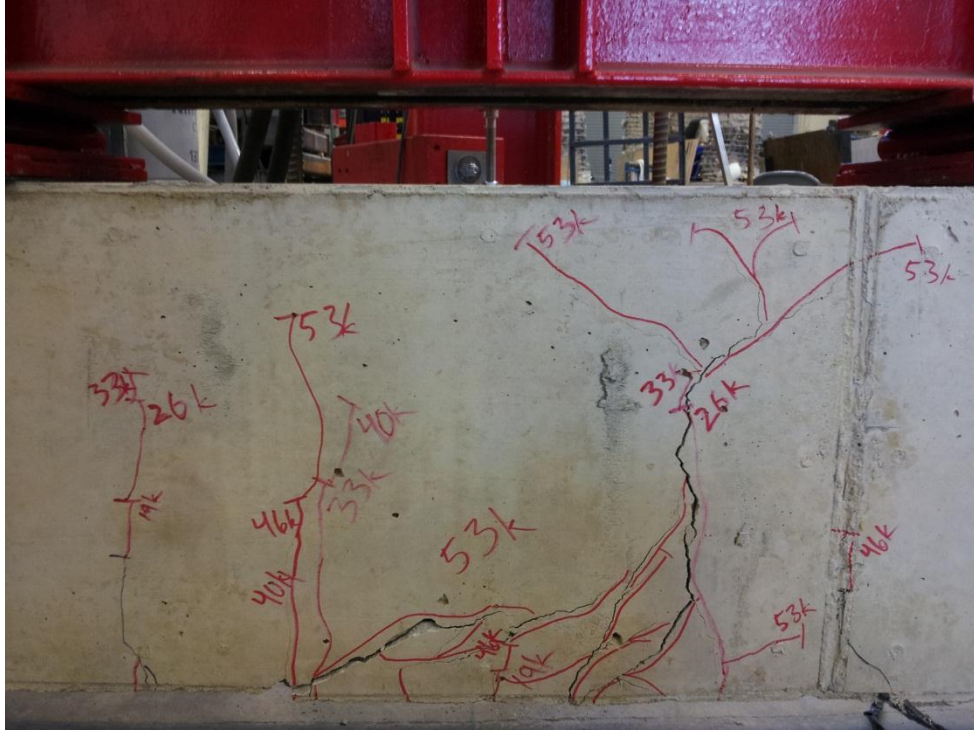
Figure A.9 – HVFA-70LTB side view

APPENDIX B

HVFA TEST PROGRAM TEST DATA PLOTS
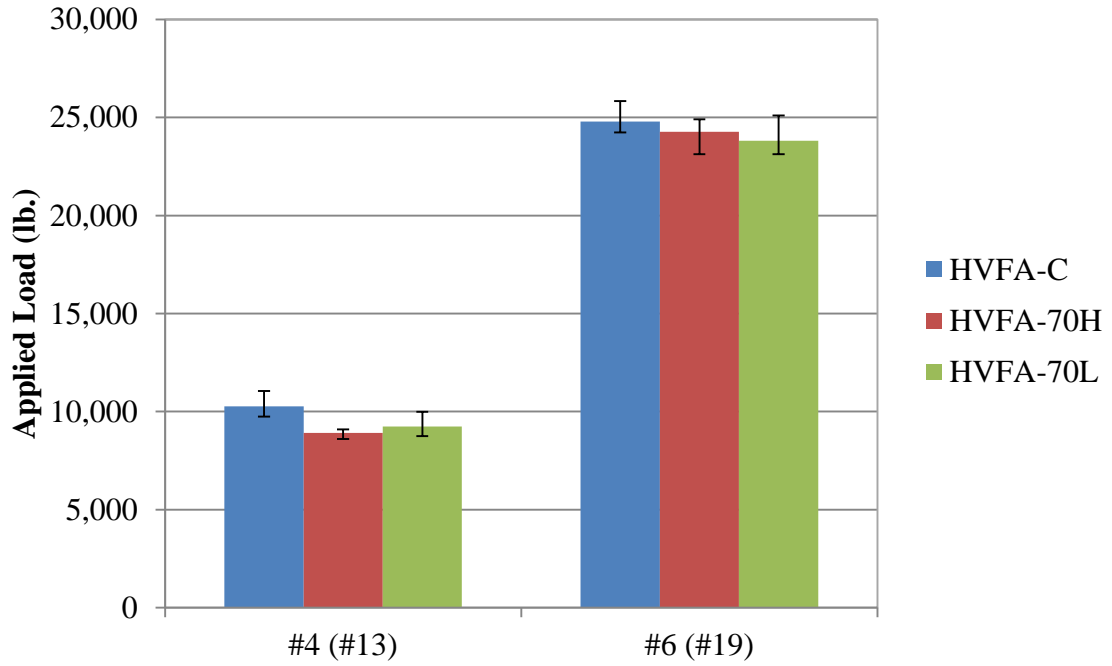
Figure B.1 – Direct pull-out applied load comparisons
Conversion: 1 lb. = 4.45 N
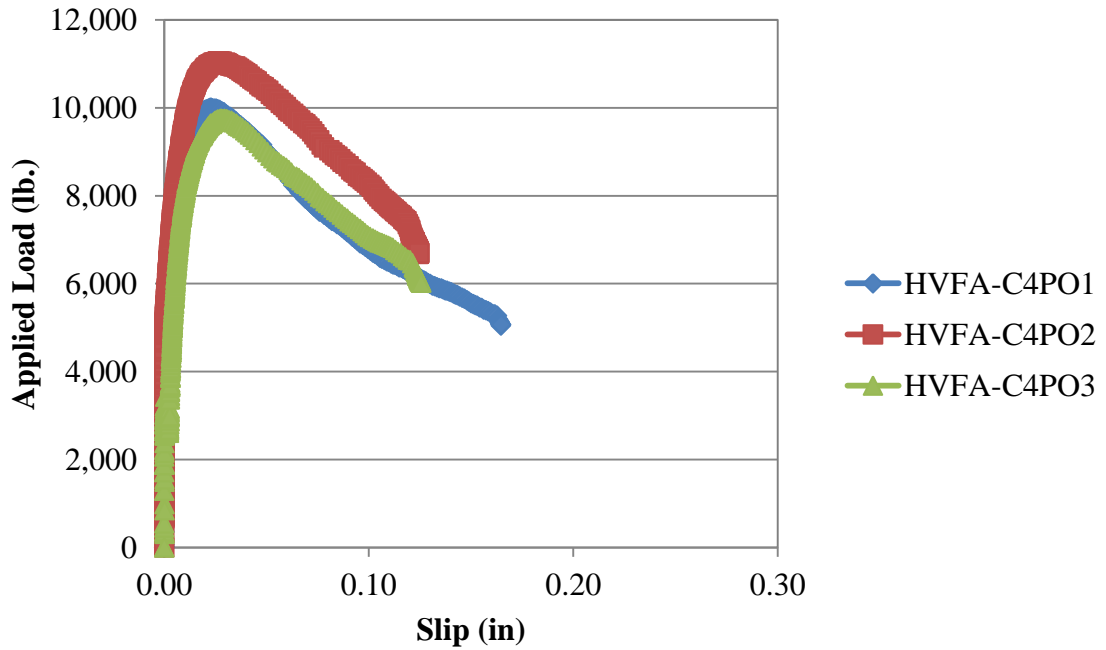
Figure B.3 – Applied load vs. slip plot for #4 (#13) HVFA-C
Conversion: 1 in. = 25.4 mm
1 lb. = 4.45 N
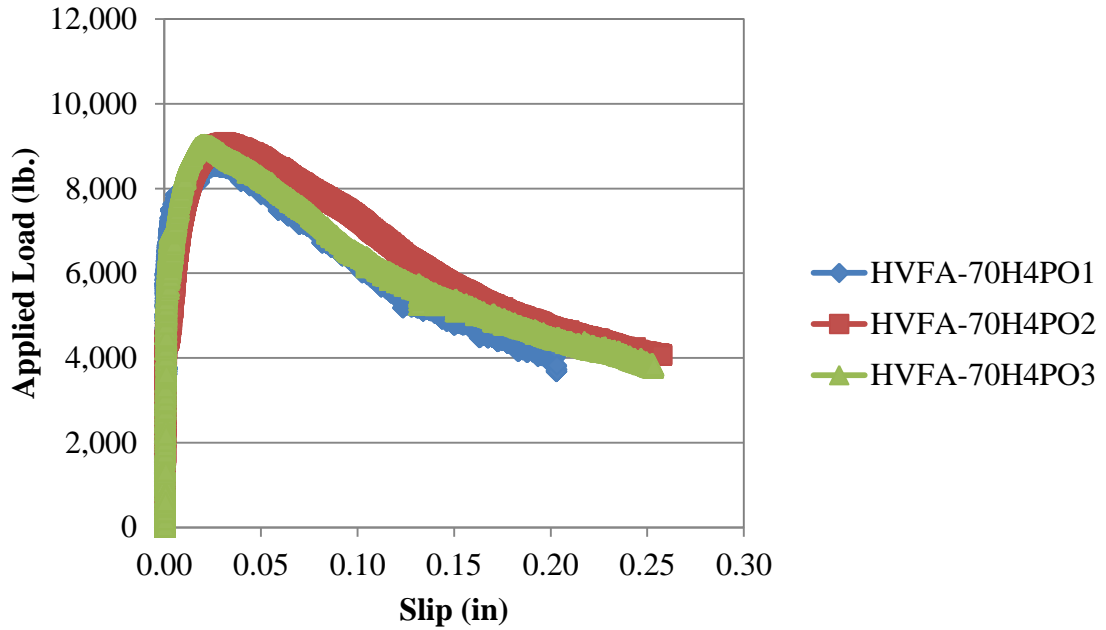
Figure B.4 – Applied load vs. slip plot for #4 (#13) HVFA-70H
Conversion: 1 in. = 25.4 mm
1 lb. = 4.45 N
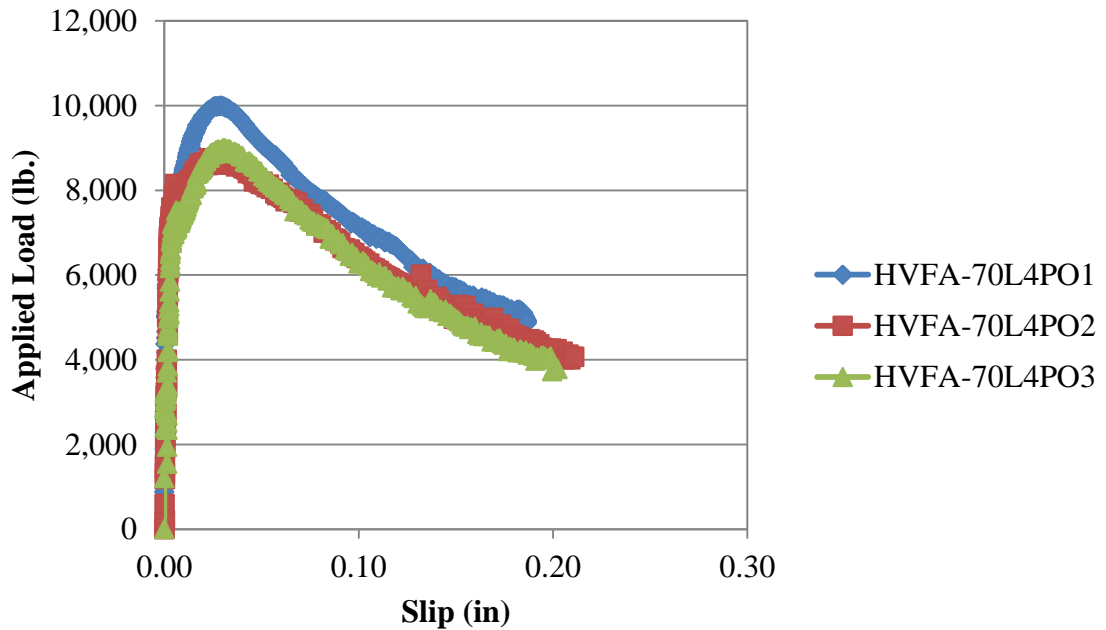
Figure B.5 – Applied load vs. slip plot for #4 (#13) HVFA-70L
Conversion: 1 in. = 25.4 mm
1 lb. = 4.45 N
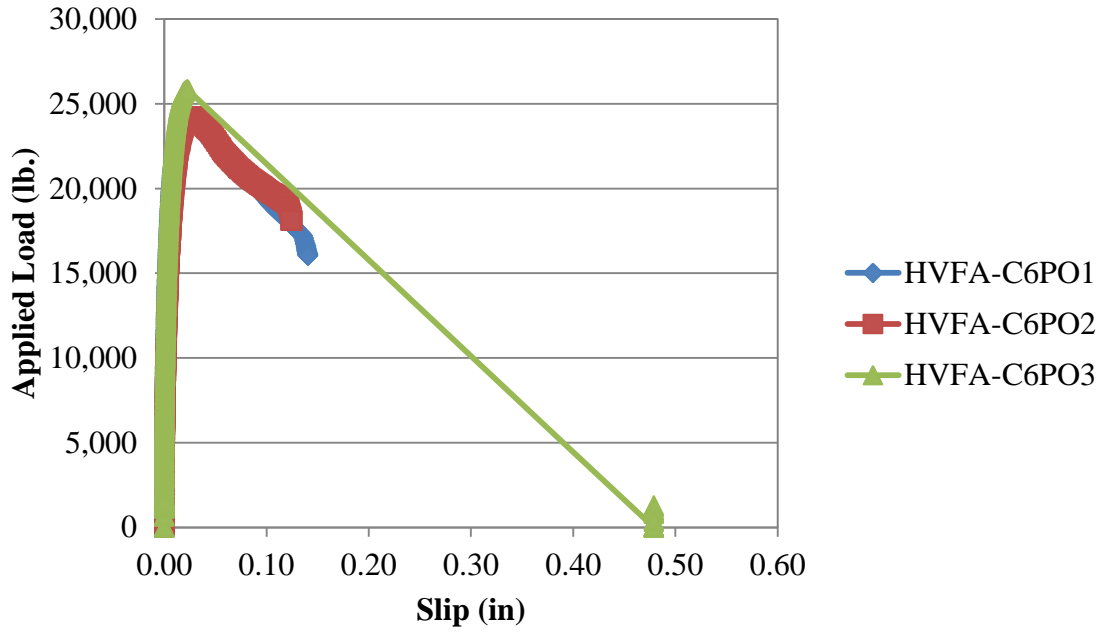
Figure B.6 – Applied load vs. slip plot for #6 (#19) HVFA-C
Conversion: 1 in. = 25.4 mm
1 lb. = 4.45 N
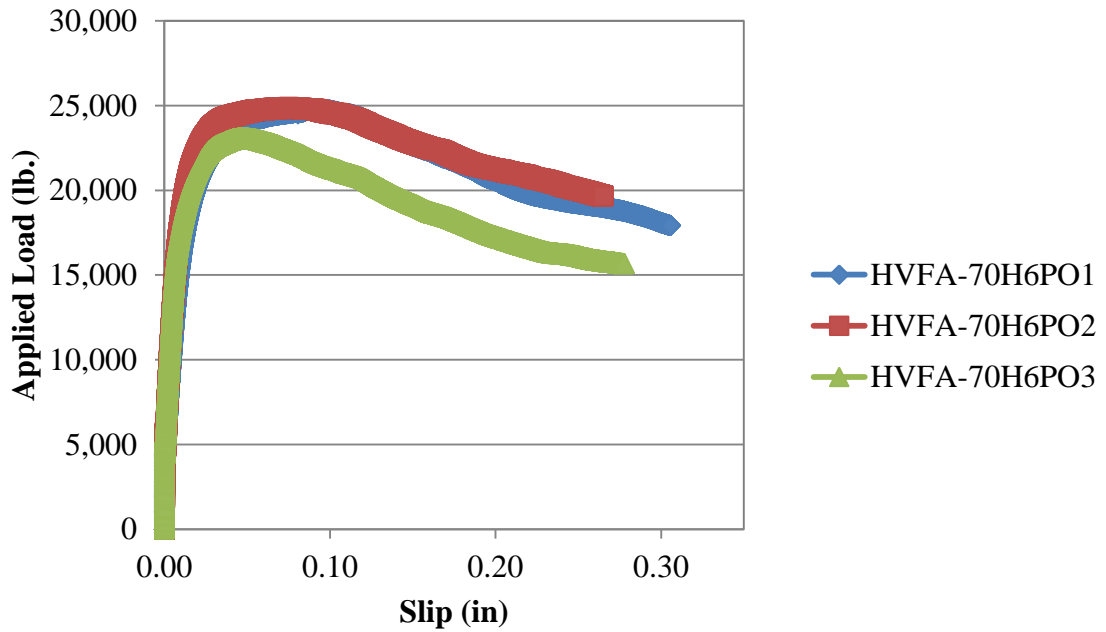
Figure B.7 – Applied load vs. slip plot for #6 (#19) HVFA-70H
Conversion: 1 in. = 25.4 mm
1 lb. = 4.45 N
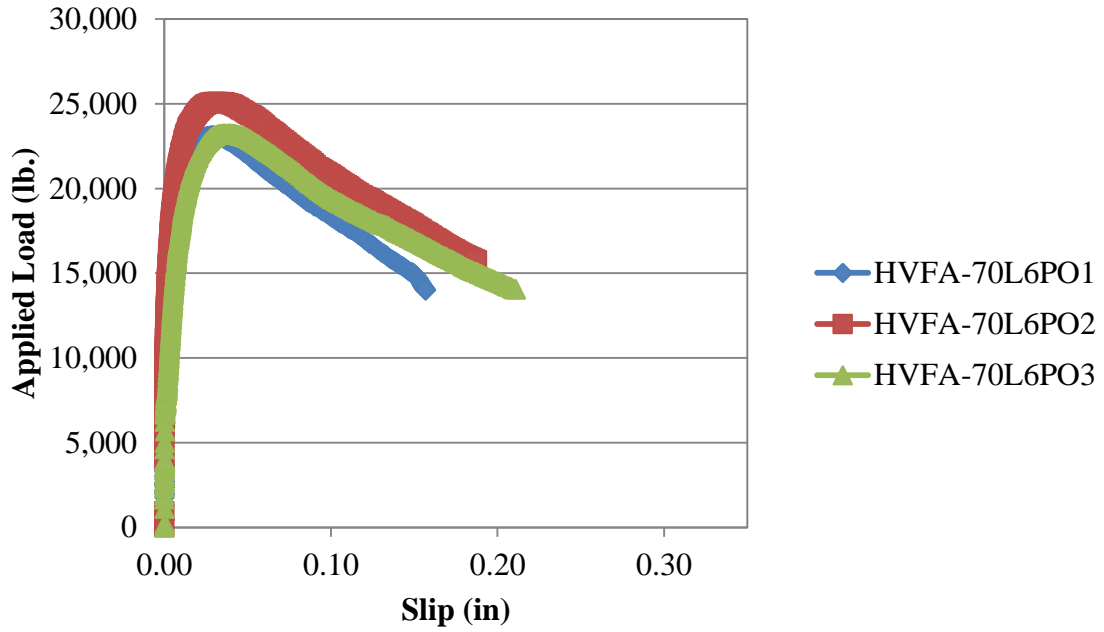
Figure B.8 – Applied load vs. slip plot for #6 (#19) HVFA-70L
Conversion: 1 in. = 25.4 mm
1 lb. = 4.45 N
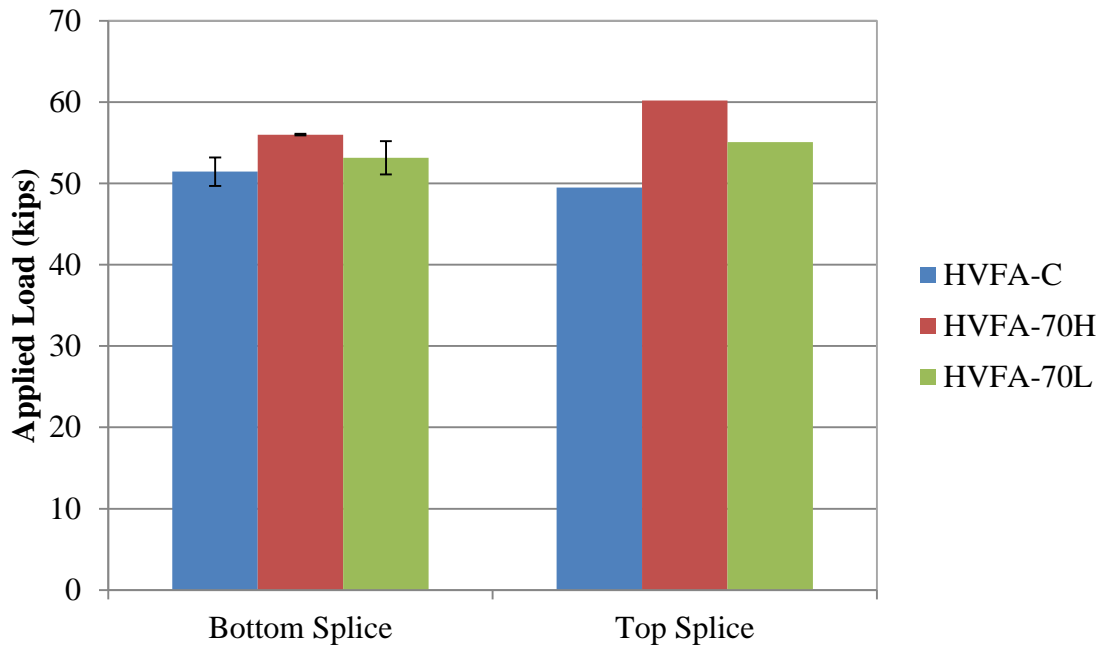
Figure B.11 – Beam splice applied load comparisons
Conversion: 1 kip = 4.45 kN
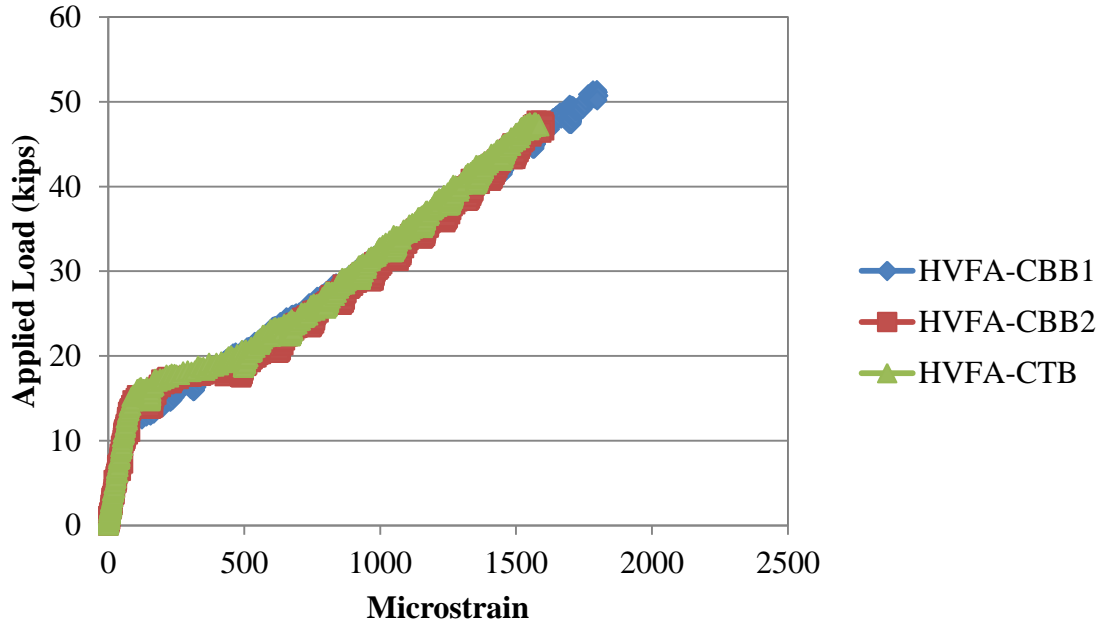
**Figure B.13 – Applied load vs. strain (average of all gages per specimen)
for HVFA-C**
Conversion: 1 kip = 4.45 kN
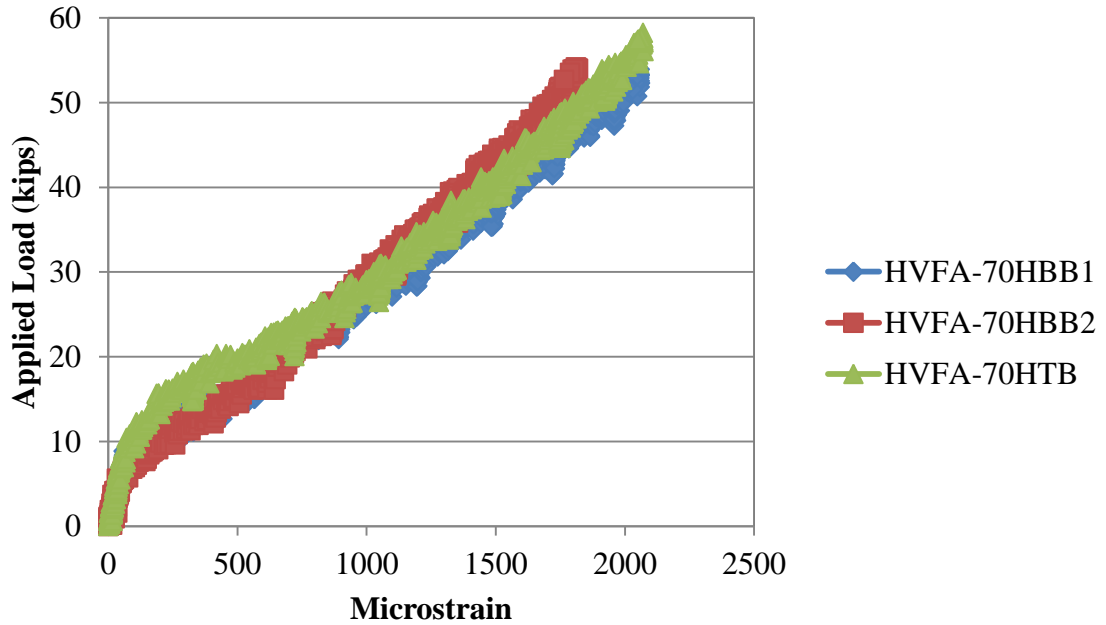
**Figure B.14 – Applied load vs. strain (average of all gages per specimen)
for HVFA-70H**
Conversion: 1 kip = 4.45 kN
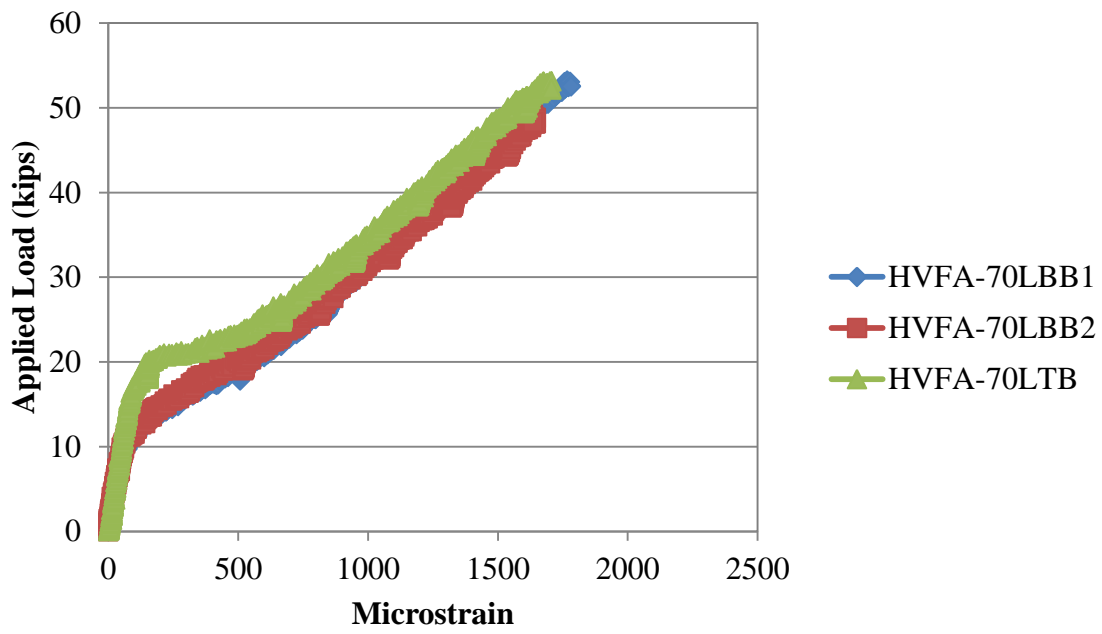
Figure B.15 – Applied load vs. strain (average of all gages per specimen) for HVFA-70L

Conversion: 1 kip = 4.45 kN
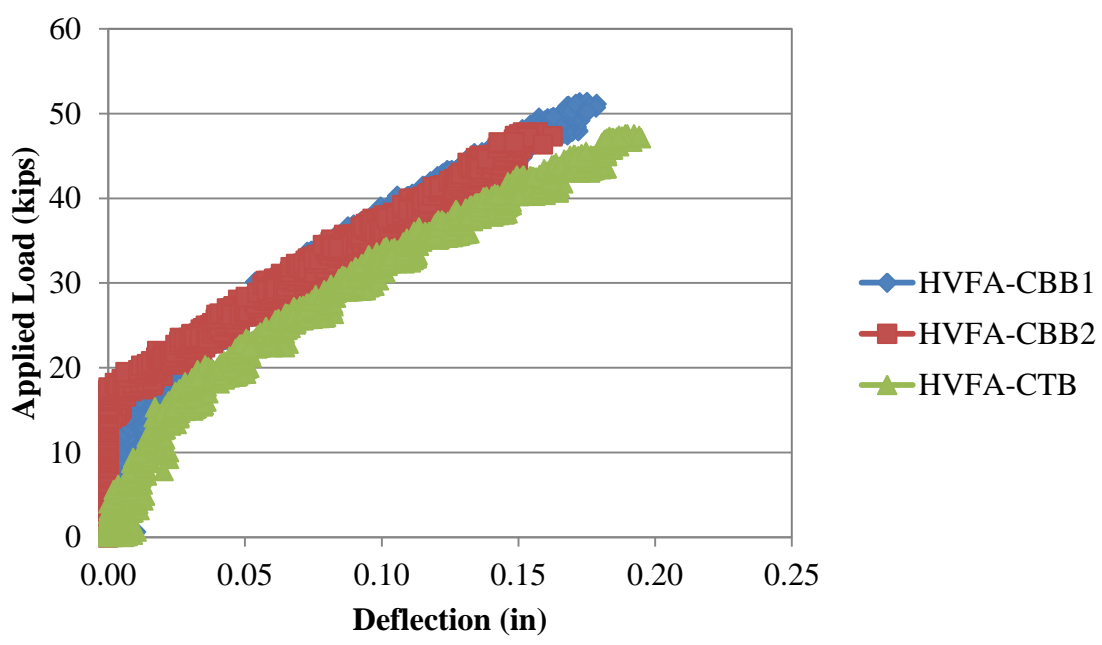
Figure B.16 – Applied load vs. displacement for HVFA-C

Conversion: 1 in. = 25.4 mm
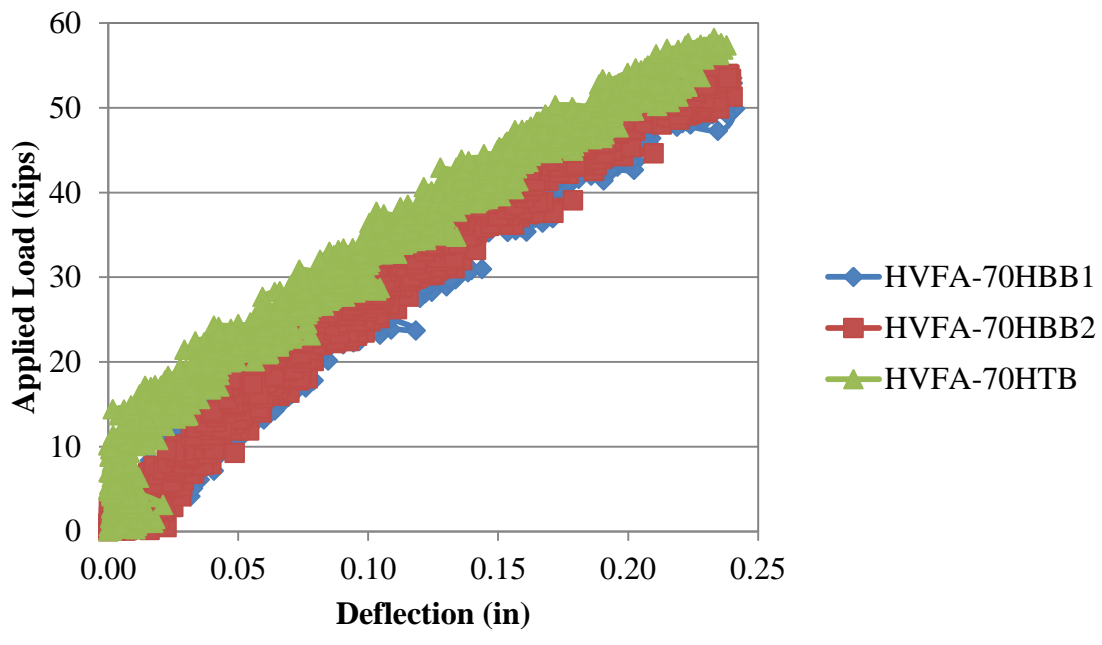
1 kip. = 4.45 kN

Figure B.17 – Applied load vs. displacement for HVFA-70H
Conversion: 1 in. = 25.4 mm
1 kip. = 4.45 kN
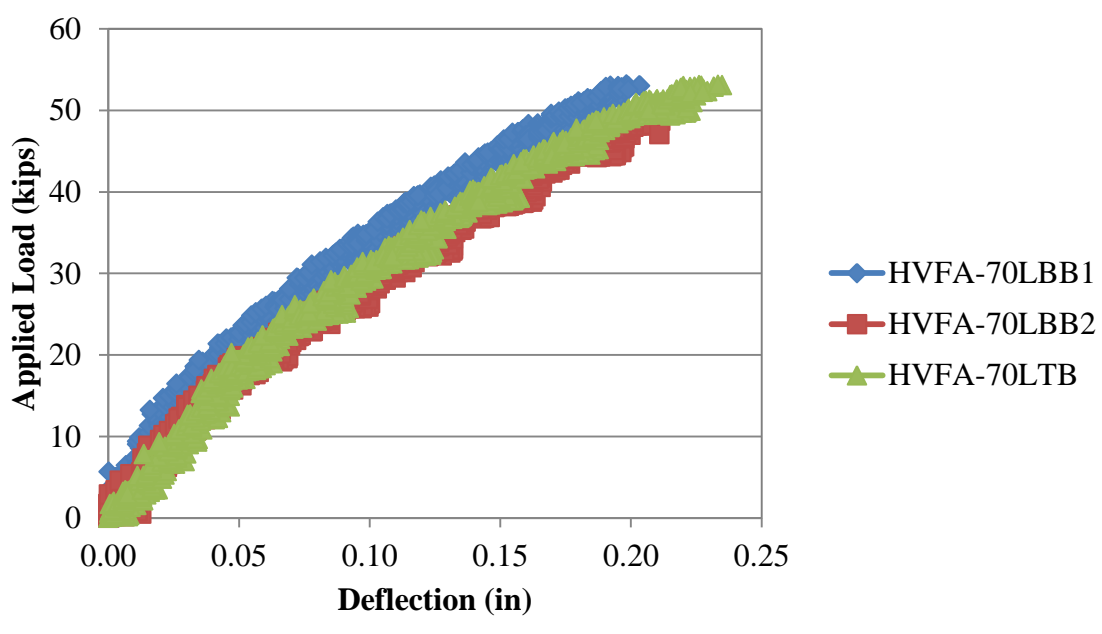
Figure B.18 – Applied load vs. displacement for HVFA-70L
Conversion: 1 in. = 25.4 mm
1 kip. = 4.45 kN

APPENDIX C

HVFA TEST PROGRAM STATISTICAL ANALYSIS

**Table C.1 – t-test for #4 (#13) HVFA-C and HVFA-70H
direct pull-out specimen average comparison**

	Variable 1	*Variable 2*
Mean	9708.257886	9635.442595
Variance	430834.9717	84064.43405
Observations	3	3
Pearson Correlation	0.576305254	
Hypothesized Mean Difference	0	
df	2	
t Stat	0.231990714	
P(T<=t) one-tail	0.419060699	
t Critical one-tail	2.91998558	
P(T<=t) two-tail	0.838121398	
t Critical two-tail	4.30265273	

**Table C.2 – t-test for #4 (#13) HVFA-C and HVFA-70L
direct pull-out specimen average comparison**

	Variable 1	*Variable 2*
Mean	9708.257886	9932.861212
Variance	430834.9717	497843.3526
Observations	3	3
Pearson Correlation	-0.497953779	
Hypothesized Mean Difference	0	
df	2	
t Stat	-0.329976631	
P(T<=t) one-tail	0.386387326	
t Critical one-tail	2.91998558	
P(T<=t) two-tail	0.772774651	
t Critical two-tail	4.30265273	

**Table C.3 – t-test for #6 (#19) HVFA-C and HVFA-70H
direct pull-out specimen average comparison**

	Variable 1	*Variable 2*
Mean	23429.14052	26233.26766
Variance	732596.0679	1151632.636
Observations	3	3
	-	
Pearson Correlation	0.999346127	
Hypothesized Mean Difference	0	
df	2	
	-	
t Stat	2.518156716	
P(T<=t) one-tail	0.064045916	
t Critical one-tail	2.91998558	
P(T<=t) two-tail	0.128091832	
t Critical two-tail	4.30265273	

**Table C.4 – t-test for #6 (#19) HVFA-C and HVFA-70L
direct pull-out specimen average comparison**

	Variable 1	*Variable 2*
Mean	23429.14052	26233.26766
Variance	732596.0679	1151632.636
Observations	3	3
	-	
Pearson Correlation	0.999346127	
Hypothesized Mean Difference	0	
df	2	
	-	
t Stat	2.518156716	
P(T<=t) one-tail	0.064045916	
t Critical one-tail	2.91998558	
P(T<=t) two-tail	0.128091832	
t Critical two-tail	4.30265273	

Table C.5 – t-test for HVFA-C and HVFA-70H beam splice average comparison

	Variable 1	Variable 2
Mean	47.68025213	64.6223856
Variance	11.79358493	21.70748414
Observations	3	3
Pearson Correlation	0.392158818	
Hypothesized Mean Difference	0	
df	2	
t Stat	-6.410891402	
P(T<=t) one-tail	0.011738856	
t Critical one-tail	2.91998558	
P(T<=t) two-tail	0.023477711	
t Critical two-tail	4.30265273	

Table C.6 – t-test for HVFA-C and HVFA-70L beam splice average comparison

	Variable 1	Variable 2
Mean	47.68025213	56.09310113
Variance	11.79358493	4.983445281
Observations	3	3
Pearson Correlation	0.85801692	
Hypothesized Mean Difference	0	
df	2	
t Stat	-7.657183005	
P(T<=t) one-tail	0.008315558	
t Critical one-tail	2.91998558	
P(T<=t) two-tail	0.016631115	
t Critical two-tail	4.30265273	

BIBLIOGRAPHY

AASHTO (2007). AASHTO LRFD Bridge Design Specification. Fourth Edition, Washington, D.C.

ACI 318 (2008). Building Code Requirements for Structural Concrete (ACI 318-08) and Commentary. American Concrete Institute, Farminton Hills, MI.

ACI 408R (2003). Bond and Development of Straight Reinforcing Bars in Tension. American Concrete Institute, Farminton Hills, MI

ASTM C 39 (2011). Standard Test Method for Compressive Strength of Cylindrical Concrete Specimens. *American Society for Testing and Materials*. West Conshohocken, PA.

ASTM C 78 (2010). Standard Test Method for Flexural Strength of Concrete (Using Simple Beam with Third-Point Loading). *American Society for Testing and Materials*. West Conshohocken, PA.

ASTM C 138 (2010). Standard Test Method for Density (Unit Weight), Yield, and Air Content (Gravimetric) of Concrete. *American Society for Testing and Materials*. West Conshohocken, PA.

ASTM C 143 (2010). Standard Test Methods for Slump of Hydraulic Cement Concrete. *American Society for Testing and Materials*. West Conshohocken, PA.

ASTM C 231 (2010). Standard Test Method for Air Content of Freshly Mixed Concrete by the Pressure Method. *American Society for Testing and Materials*. West Conshohocken, PA.

ASTM C 496 (2011). Standard Test Method for Splitting Tensile Strength of Cylindrical Concrete Specimens. *American Society for Testing and Materials*. West Conshohocken, PA.

ASTM C 618 (2012). Standard Specification for Coal Fly Ash and Raw or Calcined Natural Pozzolan for Use in Concrete. *American Society for Testing and Materials*. West Conshohocken, PA.

ASTM E 8 (2009). Standard Test Methods for Tension Testing of Metallic Materials. *American Society for Testing and Materials*. West Conshohocken, PA.

Bentz, E., Collins, M. (2000). Response-2000 Reinforced Concrete Sectional Analysis. Version 1.0.5. Toronto, Canada.

Cross, D., Stephens, J., and Vollmer, J. (n.d.). "Structural Applications of 100 Percent Fly Ash Concrete." Montana State University, Bozeman, MT.

Federal Highway Administration (2011). Coal Fly Ash – Material Description. <http://www.tfhrc.gov/hnr20/recycle/waste/cfa51.htm>

Gopalakrishnan, S. (2005). "Demonstration of Utilising High Volume Fly Ash Based Concrete for Structural Applications." Structural Engineering Research Centre, Chennai India.

Headwaters Resources (2011). Fly Ash for Concrete. <http://www.flyash.com/data/upimages/press/fly%20ash%20for%20concrete.pdf>

Marlay, K. (2011). "Hardened Concrete Properties and Durability Assessment of High-Volume Fly Ash Concrete." Thesis. Missouri S&T, Rolla, MO.

Naik, T.R., Singh, S. S., Sivasundaram, V. (1989). "Concrete Compressives Strength, Shrinkage and Bond Strength As Affected by Addition of Fly Ash and Temperature." The University of Wisconsin – Milwaukee, Milwaukee, WI.

RILEM 7-II-28. (1994). "Bond Test for Reinforcing Steel. 2. Pull-out test." E & FN Spon, London.

Volz, J., Myers, J. J. (2011) "Design and Evaluation of High-Volume Fly Ash Concrete Mixes." Missouri University of Science and Technology, Rolla, MO.

Wight, J., MacGregor, J., "Reinforced Concrete Mechanics and Design." Fifth Edition. Upper Saddle River, NJ: Pearson Education, Inc., 2009. 360-406.

Wolfe, M. (2011). "Bond Strength of High-Volume Fly Ash Concrete." M.S. Thesis, Missouri University of Science and Technology, Rolla, MO.

FINAL Report C

TRyy1110

**Project Title: Design and Evaluation of High-Volume
Fly Ash (HVFA) Concrete Mixes**

Report C: Shear Behavior of HVFA Reinforced Concrete

ABSTRACT

Concrete is the most widely used man-made material on the planet. Unfortunately, producing Portland cement generates carbon dioxide (a greenhouse gas) at roughly a pound for pound ratio. High-volume fly ash (HVFA) concrete – concrete with at least 50% of the cement replaced with fly ash – offers a potential "green" solution. However, because it is still relatively new and has some disadvantages, there are still many questions that need to be answered.

Most research to date has consisted only of the evaluation of the strength and durability of HVFA concrete mixtures, while only a limited number of studies have implemented full-scale testing of specimens constructed with HVFA concrete to determine its potential use in the industry. For this research, a laboratory testing program was developed to investigate the shear performance of reinforced concrete (RC) beams constructed with HVFA concrete. The experimental program consisted of 32 tests performed on full-scale RC beams. The principal parameters investigated were: (1) concrete type (HVFA concrete or conventional concrete (CC)), (2) amount of total cementitious material, (3) amount of shear reinforcement, and (4) amount of longitudinal (flexural) reinforcement. The full-scale test results were compared to the theoretical results using design approaches contained in several codes common to North America. The results indicate that existing design code provisions for conventional concrete are equally applicable to the design of HVFA concrete.

TABLE OF CONTENTS

LIST OF ILLUSTRATIONS

LIST OF TABLES

NOMENCLATURE

Symbol	Description
A	Angular coefficient of linear regression plot (Equation 3-34)
A_c	Area of concrete on flexural tension side
A_p	Area of prestressing steel
A_{ps}	Area of prestressing steel
A_s	Area of longitudinal reinforcement
A'_s	Area of compression reinforcement
A_{sl}	Area of longitudinal reinforcement
A_{sw}	Steel vertical reinforcement area
A_v	Steel vertical reinforcement area
A_{vi}	Cross-sectional area in the ith stirrup crossing the critical crack
$A_{v,min}$	Minimum shear reinforcement area
a	Aggregate size (Equation 3-18)
a	Depth of equivalent rectangular stress block
a	Shear span
$\underline{a}$	Critical crack length
a/d	Shear span-to-depth ratio
a_0	Notch depth
a_0/d	Notch depth-to-depth ratio
a_c	Critical position of diagonal crack
a_g	Aggregate size (AASHTO LRFD, 2004)

a_s Shear span

B Coefficient obtained through linear regression plot (Equation 3-27)

B Width of cross-section

b Width of cross-section

b_v Effective width of cross-section

b_w Width of cross-section

C_i Measured initial compliance

C_u Unloading compliance

c Distance from extreme compression fiber to the neutral axis

c_v Concrete cover for transverse reinforcement

c_x Concrete cover for longitudinal reinforcement

D Diameter of the cylinder

D_{max} Aggregate size

d Characteristic dimension of structure (Equation 3-28)

d Effective depth of cross-section

d' Distance from extreme compression fiber to centroid of

longitudinal compression reinforcement

d_0 Coefficient determined experimentally (Bazant and Pfeiffer, 1987)

d_{agg} Aggregate size

d_{bv} Diameter of transverse steel reinforcement

d_{bx} Diameter of longitudinal steel reinforcement

d_v Effective shear depth (AASHTO LRFD, 2004)

E Modulus of elasticity of the concrete (Equation 3-34)

E_c	Modulus of elasticity of the concrete
E_p	Modulus of elasticity of the prestressing steel
E_s	Modulus of elasticity of the steel
F_c	Concrete compressive force
F_s	Longitudinal reinforcement force
f_1	Principal tensile stress of the concrete
f_2	Principal compressive stress of the concrete
$f_{2,max}$	Maximum principal compressive stress of the concrete
f'_c	Compressive strength of the concrete
f_{ci}	Compressive stress on crack surface
f_{cr}	Concrete stress at cracking
f_{ct}	Tensile strength of the concrete
f_{cx}	Horizontal concrete stress
f_{cy}	Vertical concrete stress
f_{p0}	Parameter to account for level of prestressing (AASHTO LRFD, 2004)
f_t	Splitting tensile strength of the concrete
f'_t	Tensile strength of the concrete
f_v	Tensile stress in the stirrups
f_{vi}	Stress in the ith stirrup crossing the critical crack
f_y	Yield stress of steel
f_{yt}	Yield stress of transverse steel reinforcement
G	Fracture energy consumption (Equation 3-36)

G_F Fracture energy (Work-of-fracture method)

G_f Fracture energy (Size effect method)

G_f Fracture energy (Two parameter method)

G_s Shear modulus of steel

$g_f(\alpha_0)$ Non-dimensional energy release rate (Equation 3-34)

H Height of cross-section

H_0 Thickness of clip gauge holder

h Height of cross-section

jd Distance between resultants of internal compressive and tensile

forces on a cross-section

K_{Ic} Stress intensity factor

k Parameter to reflect size effect (Equation 3-27)

k_1 Coefficient that characterizes bond properties of bars (Equations 3-

20)

k_3 Empirical coefficient (Equation 3-49)

L Length of the beam

M_{exp} Experimentally determined total moment applied to specimen

M_f Factored shear moment

M_n Nominal moment capacity

M_u Factored shear moment

MOR Modulus of rupture of the concrete

N_h Tensile force in longitudinal reinforcement

N_u Factored axial force

n	Curve-fitting factor (Collins and Mitchell, 1997)
n	Number of data points
P	Maximum load at failure (Equation 6-23)
P_{max}	Measured peak load
S	Specimen loading span
s	Center-to-center spacing of steel stirrups
s	Shear crack sliding
s	Standard deviation
s_{mv}	Average spacing of cracks perpendicular to transverse reinforcement
s_{mx}	Average spacing of cracks perpendicular to longitudinal reinforcement
s_x	Crack spacing parameter (AASHTO LRFD, 2004)
s_x	Spacing of longitudinal steel reinforcement
s_{xe}	Effective crack spacing
s_z	Crack spacing parameter (CSA A23.3, 2004)
s_{ze}	Effective crack spacing
s_θ	Crack spacing
$T_{n,1}$	Test criterion (ASTM E178 [2008])
V	External shear force
V_c	Concrete contribution to shear strength
V_{cr}	Ultimate shear force
V_{cz}	Uncracked concrete force

V_d	Longitudinal reinforcement dowel force
V_f	Factored shear force
V_i	Interlock forces
V_n	Nominal shear strength
$V_{n,exp}$	Experimentally determined total resistance
$V_{n,max}$	Maximum nominal shear strength
V_p	Vertical component of prestressing force
V_r	Nominal shear resistance
V_s	Steel contribution to shear strength
V_{test}	Experimentally determined total shear resistance
V_u	Factored shear force
v	Shear stress
v_{ci}	Shear transferred by aggregate interlock
$v_{ci,max}$	Maximum shear transferred by aggregate interlock
v_{cxy}	Shear stress on concrete layer face
W	Depth of cross-section (Equation 6-10)
W	Total energy dissipated (Equation 3-26)
W_{ext}	Work of external force (Equation 3-36)
w	Average crack width (Equation 3-18)
w	Crack opening (Einsfeld and Velasco, 2006)
w	Unit weight of the concrete (Equation 6-28)
w	Width of idealized prismatic strut
w/c	Water-to-cement ratio

w/cm	Water-to-cementitious material ratio
$\bar{x}$	Arithmetic average
y	Diagonal crack extent (Equation 3-38)
z	Inner level arm
α_0	Aggregate shape factor (Equation 3-51)
α_0	Relative notch length (Equation 3-35)
α_1	Coefficient for bond characteristics of reinforcement (Vecchio and Collins, 1993)
α_2	Coefficient for type of loading (Vecchio and Collins, 1993)
β	Brittleness number (Equation 3-27)
β	Concrete softening coefficient (Equation 3-14)
β	Deviation angle (Equation 7-32)
β	Shear retention factor (AASHTO LRFD, 2004)
γ_{xy}	Shear strain
δ_e	Variation of unbounded length
δ_s	Unbounded length of reinforcement
ε_0	Concrete strain at peak stress
ε_1	Principal tensile strain in concrete
$\bar{\varepsilon}_1$	Uniaxial tensile strain in the perpendicular direction
ε_2	Principal compressive strain in concrete
ε_c	Compressive strain in the concrete
ε'_c	Compressive strain in the concrete
ε_{cr}	Crack strain in concrete

ε_s — Measured longitudinal strain at the center of gravity at the bottom steel reinforcement

ε_s — Strain in the tension reinforcement

ε'_s — Measured longitudinal strain at the top steel reinforcement

ε'_s — Strain in the compression reinforcement

ε_{sm} — Measured longitudinal strain at the bottom steel reinforcement

ε_{td} — Transverse strain

ε_x — Longitudinal strain (AASHTO LRFD, 2004)

ε_x — Strain in the x-direction

ε_{xx} — Horizontal strain

ε_{xy} — Shear strain

ε_y — Strain in the y-direction

ε_{yield} — Yield strain of steel

ε_{yy} — Vertical strain

$\boldsymbol{\theta}$ — Shear crack angle

$\boldsymbol{\theta_c}$ — Shear crack angle

ξ — Concrete softening coefficient

$\xi f'_c$ — Concrete peak softened stress

$\xi \varepsilon_0$ — Concrete softened compressive strain

$\boldsymbol{\rho_L}$ — Longitudinal reinforcement ratio

$\boldsymbol{\rho_s}$ — Longitudinal reinforcement ratio

$\boldsymbol{\rho_v}$ — Transverse reinforcement ratio

$\boldsymbol{\rho_w}$ — Longitudinal reinforcement ratio

$\boldsymbol{\rho_x}$	Longitudinal reinforcement ratio
σ_N	Nominal stress at failure (Equation 3-27)
Σ_s	Reduced cross section of rebar (Equation 3-38)
$\emptyset$	Capacity reduction factor
$\emptyset_c$	Capacity reduction factor
$\emptyset_s$	Capacity reduction factor
Γ	Fracture energy per unit length of splitting crack extension

1. INTRODUCTION

1.1. BACKGROUND

Fly ash is one of the by-products of the combustion of coal in electric power generating plants. For over 75 years, fly ash has been widely used as a supplementary cementitious material for the production of concrete in the United States and other countries. Typically, fly ash replacement levels for the production of concrete have been limited to roughly 35% by weight of the total cementitious materials due to concerns about in-place performance and constructability.

Concrete, which is the most widely used construction material on the planet, is a composite of coarse and fine aggregates, Portland cement, and potable water. However, Portland cement production poses challenges of excessive energy usage and depletion of natural resources. Additional to this, there is an abundance of coal combustion products (CCPs), such as fly ash, that are disposed of in landfills that could instead be utilized positively in the production of concrete. Portland cement is chemically manufactured from calcium, silicates, and aluminates in a process that releases carbon dioxide as a by-product into the atmosphere and reduces the mineral resources of our planet. In 2007, the world production of cement was approximately 2.6 billion metric tons, with 127 million produced and consumed within the United States. However, when a ton of fly ash is used in place of Portland cement, 55 gallons of oil required to produce the Portland cement is saved and an equal amount of carbon dioxide that would be produced by the manufacturing process is prevented from entering the Earth's atmosphere, hence making a significant positive impact on the environment and preservation of natural resources (ACAA, 2009).

Portland cement is the most expensive material used in the production of concrete. The cost of one ton of fly ash is typically half the price of one ton of Portland cement. Therefore, the production cost for concrete can also be reduced by replacing a portion of the cement with less expensive cementitious materials. High-volume fly ash (HVFA) concrete may be produced with significant cost savings when compared to conventional Portland-cement concrete.

In an attempt to improve the environment and enhance the concrete industry, it is essential to provide more sustainable and green options as solutions and better alternatives to existing products. Extensive research has been done in an attempt to make concrete products more sustainable and cost effective, and HVFA concrete is one potential option.

In addition to the economic and environmental advantages presented above, HVFA concrete has shown better performance characteristics when compared to conventional Portland-cement concrete. Fly ash is now used in concrete for many reasons, including: improvements in workability of fresh concrete, reduction in temperature rise during initial hydration, improved resistance to sulfates, reduced expansion due to alkali-silica reaction, and increased durability and strength of hardened concrete (ACI 232.2R, 2003).

The two most common classes of fly ash used in concrete are Class C and Class F as defined by ASTM C618 [2008] "Standard Specification for Coal Fly Ash and Raw or Calcined Natural Pozzolan for Use in Concrete". Both classes are pozzolanic, meaning they react with excess calcium hydroxide (CH) in concrete, formed from cement hydration, to form calcium silicate hydrate (CSH), but Class C fly ash also contains

higher levels of calcium which makes it more desirable for higher replacement percentages.

In conclusion, HVFA concrete could offer a solution to the problem of meeting the increasing demands for concrete in the future in a sustainable manner and at reduced or no additional cost, and at the same time reducing the environmental impact of two industries that are essential to economic development, the Portland cement industry and the coal-fired power industry. The use of high volumes of fly ash in concrete generates a direct link between durability and resource productivity, thus increasing the use of HVFA concrete will help to improve the sustainability of the concrete industry.

The main problem with using HVFA concrete in construction is the increased setting time. Retarded set time delays form removal, which increases time of construction (Marotta et al., 2011). Since labor is the primary cost contributing factor in construction, the setting time of high-volume fly ash concrete must be accelerated. Previous research has proven that the addition of chemical admixtures or activators, such as calcium hydroxide and gypsum, assist in initiating the hydration process allowing for a shorter curing period, while still gaining sufficient strength.

1.2. OBJECTIVE AND SCOPE OF WORK

The main *objective* of this research study was to evaluate the shear behavior and response of HVFA concrete through material, component, and full-scale testing. This objective included a study and evaluation of current analytical models used to predict the shear response of conventional Portland-cement concrete as applied to HVFA concrete, including recommended modifications.

The following *scope of work* was implemented in order to achieve the objective of the research study:

- Perform a literature review;

- Develop a research plan;

- Develop mix designs for both conventional and HVFA concrete;

- Evaluate the fresh and hardened properties of several HVFA concrete and CC mixes;

- Design and construct small and full-scale specimens;

- Test specimens to failure;

- Record and analyze data from tests;

- Compare test results to current guidelines and previous research findings;

- Provide greater insight into the shear resistance mechanisms and quantify their effect;

- Evaluate the applicability of current analytical models to predict the shear behavior and response of HVFA concrete;

- Develop conclusions and recommendations; and

- Prepare this report to document the details, results, findings, conclusions, and recommendations of this study.

1.3. RESEARCH METHODOLOGY

The proposed research methodology included six (6) tasks necessary to successfully complete the study. They are as follows:

Task #1: Perform a literature review. The goal of the literature review was to become familiarized with testing methods and results from previous studies. This knowledge was used for a better understanding of the behavior of the specimens, to avoid mistakes, as well as to provide support for comparisons.

Task #2: Develop HVFA concrete and CC mix designs. The purpose of this task was to develop HVFA concrete mix designs that maximized the percentage of fly ash, but that still fulfilled typical construction needs, such as early strength development. Conventional concrete mix designs served as controls during this study. ACI 211.1-91 formed the basis for developing the mix designs.

Task #3: Perform material and component testing. A number of hardened concrete property tests were completed to evaluate the performance of the HVFA concrete mix and determine the validity of using these tests to predict the performance of concretes containing high volumes of fly ash.

Task #4: Perform full-scale testing. This task was critical as current shear design provisions for reinforced concrete are largely empirical. This task involved the construction and testing of full-scale specimens to confirm the potential of HVFA concrete. The full-scale specimens included beam specimens for shear testing only. These specimens were constructed with materials from the local Ready Mix Concrete plant to validate the ability of transferring the mix designs from the laboratory to the field. In order to compare the shear strength of conventional and HVFA concrete, full-scale beams were tested in a third point loading configuration. These beams were designed to fail in shear by increasing the flexural reinforcement. Different longitudinal reinforcement ratios and stirrup designs were also considered. Strain gauges were applied to the stirrups and to

the flexural reinforcement, and the maximum load applied to the beam was also recorded and used to calculate the strength of the beams and the different shear components.

Task #5: Analyze test data. The material, component, and full-scale test results were analyzed to evaluate the shear behavior and response of HVFA concrete compared to conventional Portland-cement concrete. The test data included: concrete compressive and tensile strength, modulus of elasticity (MOE), modulus of rupture (MOR), shear force-deflection plots, crack formation and propagation, and reinforcement strains.

Task #6: Develop findings, conclusions, and recommendations. This task synthesized the results of the previous tasks into findings, conclusions, and recommendations on the shear behavior and response of HVFA concrete.

1.4. REPORT OUTLINE

This report includes six chapters. This section will discuss the information that will be presented in more detail throughout this document.

Chapter 1 acts as an introduction to the report. This introduction contains a brief background of fly ash as a material, fly ash as a mineral admixture to concrete, and the environmental concerns regarding Portland cement production. It also discusses the research objective, scope of work, and research plan.

Chapter 2 includes information from previous research performed on the characterization of fly ash and its applications as a concrete binder.

Chapter 3 presents information from previous research performed on shear design including the different methods and approaches formulated to address this phenomenon. Four different approaches are presented: truss model, Strut and Tie Model (STM),

Modified Compression Field Theory (MCFT), and fracture mechanics approach. A collection of three design code philosophies that can be found in North America are also presented in this chapter.

Chapter 4 includes information about the experimental program. The experimental program consisted of 32 tests performed on full-scale reinforced concrete beams as well as material and component testing to determine hardened concrete properties such as compressive strength, splitting tensile strength, flexural strength, and modulus of elasticity. This chapter also describes the fabrication process, test set-up, and instrumentation for the full-scale testing.

Chapter 5 presents the test results and the different analyses used to investigate the shear resistance mechanisms. The overall behavior of the specimens is described first, with a focus on crack patterns, failure modes, and shear strength.

Chapter 6 concludes this document, summarizing the findings and conclusions of this study and proposing recommendations and future research.

2. LITERATURE REVIEW ON FLY ASH

2.1. GENERAL

Conventional Portland-cement concrete is produced more than any other material in the world. It is used in every civil engineering field for applications such as pavements, dams, bridges, and buildings because of its versatility, strength, and durability. In this chapter, a brief review is presented of the research performed on concrete mixtures containing high levels of fly ash by weight of the cementitious materials. Mechanisms are discussed by which the incorporation of high volumes of fly ash in concrete reduces the water demand, improves the workability and finishing aspects of the concrete, minimizes cracking due to thermal and drying shrinkage, and enhances durability to reinforcement corrosion, sulfate attack, and alkali-silica expansion.

Fly ash incorporated in concrete has shown results of increased strength and durability of the concrete. Its utilization in the US stretches back to the 1930s when it was first used on construction of the Hoover Dam. Fly ash from coal-burning electric power plants became readily available as early as the 1930s with the first study published by Davis et al. in 1937.

Concrete with high volumes of fly ash can be produced to achieve desired strengths at various ages, with a given water-cementitious ratio, aggregate size, air content, and slump as it is done for conventional concrete. In some instances 100% fly ash (Class C) concrete has been produced and has been found to meet acceptable concrete standards. However, its use has not yet found much acceptance in the construction industry due to its low early strength.

Concrete with fly ash has been widely used in the highway industry. Fly ash has been used in several engineering applications such as structural fill, waste stabilization and solidification, soil stabilization, aggregate and filler material, road sub-base, raw feed for cement clinkers, mine reclamation, grout, and of course, as partial replacement of Portland cement. However, considering that concrete containing fly ash has been acknowledged as a green product, the amount of fly ash produced is still much greater than the amount of fly ash that is put to beneficial use.

A brief description of two of the major cementitious materials used in concrete, Portland cement and fly ash, is given in this chapter as well as a summary of previous studies on the characterization of fly ash and its applications as a concrete binder.

2.2. USE OF FLY ASH AS SUPPLEMENTARY CEMENTITIOUS MATERIAL

2.2.1. Background. The United States consumes over 108 million tons of Portland cement each year, roughly 25% of which is imported (Butalia and Bargaheiser, 2004). The use of Portland cement is expected to continue to grow throughout the world. Unfortunately, the challenge is that for every ton of cement produced, approximately one ton of carbon dioxide (CO_2) is released into the atmosphere, and carbon dioxide is the primary greenhouse gas (GHG) attributed to global warming and climate change. However, concrete, of which Portland cement is the active ingredient, is an extremely versatile construction material and is, in fact, the second most consumed product in the world, just below water. Current U.S. production of Portland cement contributes over 75 million tons of CO_2 to the earth's atmosphere annually. Governmental regulations and growing concerns over GHG emissions are stimulating the cement industry to examine the increased use of supplementary binder materials in order to reduce CO_2 emissions.

The increased interest in sustainable design and construction has created an interest in Coal Combustion Products (CCPs) or Coal Combustion Residuals (CCRs). According to the United States Geological Survey, CCPs rank third as the most abundant non-fuel mineral resource in the U.S., with its annual production just below crushed stone, sand, and gravel. Seventy percent of all energy in the U.S. is produced by approximately 720 coal-fired power plants in 45 states. When burning coal at these power plants, two main types of ash are produced, fly ash and bottom ash. Fly ash is the very fine material carried in the flue gas, typically collected by a baghouse, and stored in silos as shown in **Figure 2.1**. Bottom ash is the larger/heavier particles that fall to the bottom of the boiler after combustion. The 720 coal-fired power plants produce approximately 63 million tons of fly ash annually. About 31 million tons are disposed of in landfills. Only approximately 12 million tons are recycled and put to beneficial reuse in the concrete industry. The remaining 20 million tons are used for a range of other applications including soil stabilization, roller compacted concrete, road base stabilization, etc.

Figure 2.1- Fly Ash Production
(**http://www.tradeindia.com/fp426361/Ammonia-Flue-Gas-Conditioning-Systems.html**)

2.2.2. General remarks on Portland cement. The manufacture of Portland cement requires raw materials that contain lime, silica, alumina, and iron. After the materials are acquired, the limestone is reduced to an approximately 5 in. size in the primary crusher and further reduced to ¾ in. in the secondary crusher. For a better understanding, **Figure 2.2** presents a flow chart of the manufacture of Portland cement. All raw materials are stored in the bins and proportioned prior to delivery to the grinding mill. There are two processes, the wet process that results in a slurry, which is mixed and pumped to storage bins, and the dry process that produces a fine ground powder which is also stored in bins (Marotta et al., 2011). Both processes feed the rotary kilns where the chemical changes take place. Once the raw feed has been ground and blended, it is fed into the kiln, and as the kiln rotates, the material passes slowly from the upper to the lower end at a rate controlled by the slope and speed of rotation of the kiln. Four distinct processes take place in the kiln: evaporation, calcination, clinkering, and cooling (Mindess et al., 2002). In the evaporation zone, the feed is heated to calcination temperatures to remove free water. In the calcination zone, the feed is transformed into a reactive mixture of oxides that can enter into new chemical combinations. As the material passes through the kiln, its temperature is raised to the point of clinkering. In the clinkering zone, the final chemical combination occurs to form the calcium silicates. Depending on the raw material, this temperature varies between 2400°F and 2700°F. Finally, as the material moves past the flame, it rapidly drops off in temperature in the cooling zone. Here the liquid phase solidifies to produce the hard nodules called clinker. Clinker is the final state of the material as it emerges from the kiln. The clinker produced is black or greenish black in color and rough in texture. The material is then transported

to final grinding where gypsum is added to control the setting time of the Portland
cement when it is mixed with water. If gypsum is not added, flash setting of the clinker
could occur.
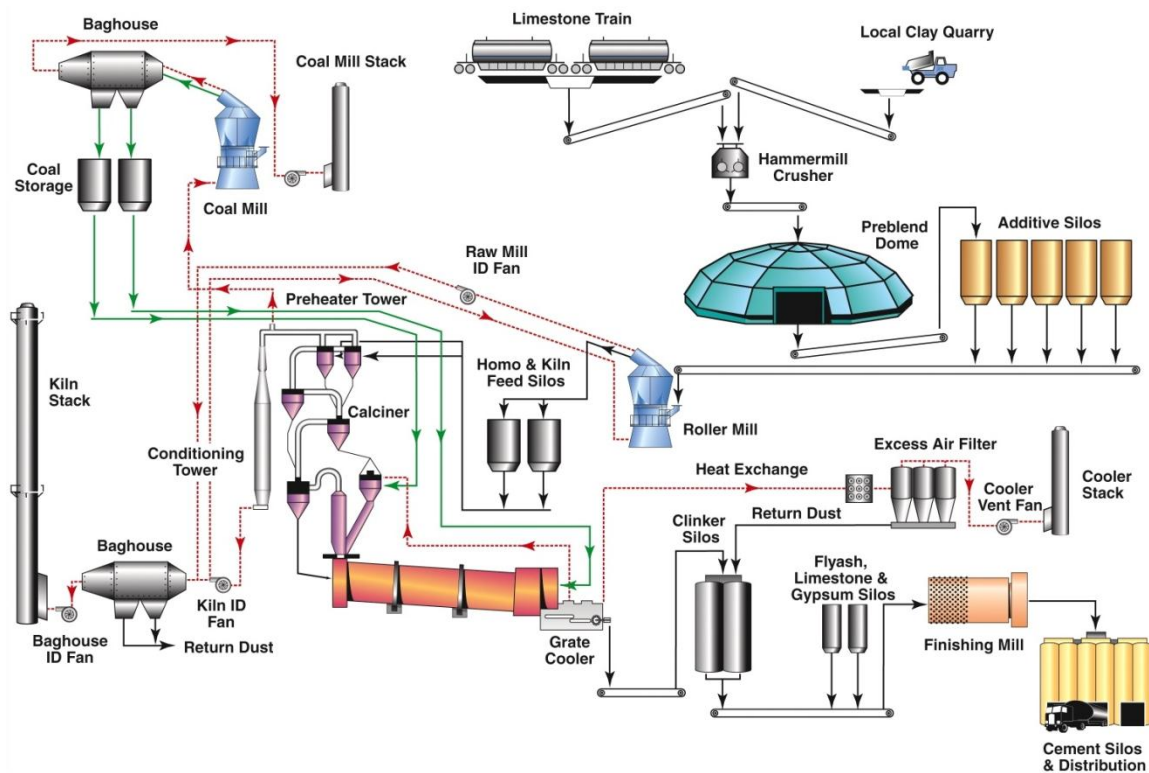
Figure 2.2- Flow Chart of Manufacture of Portland Cement
(http://www.4us2be.com/technology/cement-manufacturing-process/)

Portland cements are typically composed of four basic chemical compounds
summarized in **Table 2.1** with their names, chemical formulas and abbreviations, and
approximate weight percent for an ordinary Portland cement. Each of these compounds
exhibits a particular behavior. The tricalcium silicate hardens rapidly and is largely
responsible for initial set and early strength. The dicalcium silicate hardens slowly and its
effect on strength increases occurs at ages beyond one week. The tricalcium aluminate

contributes to strength development in the first few days because it is the first compound to hydrate. However, the tricalcium aluminate is the least desirable compound due to its high heat generation and reactiveness with soils and water with moderate-to-high sulfate concentration. The tetracalcium aluminoferrite aids in the manufacture of Portland cement by allowing lower clinkering temperature. The presence of gypsum slows the early rate of hydration of the tricalcium aluminate.

Table 2.1- Typical Composition of an Ordinary Portland Cement (Mindess et al., 2002)

Chemical name	Chemical formula	Abbreviation	Weight (%)
Tricalcium silicate	$3CaO \cdot SiO_2$	C_3S	55
Dicalcium silicate	$2CaO \cdot SiO_2$	C_2S	18
Tricalcium aluminate	$3CaO \cdot Al_2O_3$	C_3A	10
Tetracalcium aluminoferrite	$3CaO \cdot Al_2O_3 \cdot Fe_2O_3$	C_4AF	8
Calcium sulfate dihydrate (gypsum)	$CaSO_4 \cdot 2H_2O$	$C\bar{S}H_2$	6

Hydration is the chemical reaction that takes place when Portland cement and water are mixed together. The hydration reaction is considered complete at 28 days. The process when cement is mixed with water to form a paste is called setting. Most Portland cements exhibit initial set in about 3 hours and final set in about 7 hours (Marotta et al., 2011). The hydration reaction of Portland cement is exothermic. Thus, the concrete is being continually warmed by internal heat during the hardening process.

There are two possible problems of early stiffening on cement paste. The first one is termed false set, which refers to the rapid development of rigidity in cement paste with little evidence of significant heat generation. The plasticity can be regained by further mixing with no addition of water. And the second one is termed flash set, which refers to

the rapid development of rigidity in cement paste with the release of considerable heat. This phenomenon cannot be overcome and the plasticity cannot be regained.

2.2.3. General remarks on fly ash. Fly ash is a coal ash recovered in an electrostatic precipitator (ESP) at coal-fired thermal power plants and contains small amounts of iron, magnesium, and calcium as well as the main elements of silica and aluminum. Most thermal power plants use furnaces fired with pulverized coal. As the coal travels through the high-temperature zone in the furnace, the volatile matter and carbon are burnt off whereas most of the mineral impurities are carried away by the flue gas in the form of ash (Malhotra and Mehta, 2008). These ash particles become fused in the combustion zone of the furnace but once they leave the combustion zone, the molten ash is cooled rapidly and solidifies as spherical, glassy particles.

The ASTM C618 [2008] "Standard Specification for Coal Fly Ash and Raw or Calcined Natural Pozzolan for Use in Concrete" uses the bulk chemical composition to subdivide fly ashes into two classes, C and F, which reflect the composition of the inorganic fractions. However, this standard does not address the nature or reactivity of the particles. Class F fly ashes are produced from either anthracite bituminous or sub-bituminous coals. Class C fly ashes derive from sub-bituminous or lignitic coals. In other words, the two classes of fly ash are distinguished by the silica oxide content of the type of coal burned. Fly ash can be cementitious or pozzolanic, or both. Class F fly ash is pozzolanic while Class C fly ash is cementitious and pozzolanic. Cementitious fly ash hardens when wetted while pozzolanic fly ash requires a reaction with lime before hardening. This is why Class C fly ash has a higher potential for use in high-volume fly ash (HVFA) concrete. **Table 2.2** summarizes the average bulk composition of both class

C and F fly ashes based on 97 and 45 analyses, respectively, developed by Scheetz et al. (1997).

Fly ash consists of heterogeneous combinations of amorphous (glassy) and crystalline phases (ACI 232.2R, 2003). The largest fraction of fly ash consists of glassy spheres of two types, solid and hollow, that usually represent 60 to 90% of the total mass of the fly ash, with the remaining fraction made up of a variety of crystalline phases. This union of phases makes fly ash a complex material to classify and characterize in specific terms.

Low calcium fly ashes (Class F) contain chemically inactive crystalline phases: quartz, mullite, ferrite spinel, and hematite class. High calcium fly ashes (Class C) contain the previously mentioned phases but may also contain additional crystalline phases such as anhydrite, alkali sulfate, dicalcium silicate, tricalcium aluminate, lime, melilite, merwinite, periclase, and sodalite (ACI 232.2R, 2003). These additional phases found in the Class C fly ash are reactive, and this is why Class C fly ash exhibits both cementitious and pozzolanic properties.

Fly ash looks very similar to cement in appearance. However, when magnified, fly ash will appear as spherical particles, similar to ball bearings, whereas cement appears angular, more like crushed rock as shown in **Figure 2.3**. The small size of the fly ash particles is the key to producing smooth cement paste, allowing better bonding between aggregate and cement, and resulting in a more durable concrete. The round shape of the particles increases the concrete workability without adding extra water.

The use of fly ash (Class C and Class F) in concrete offers several significant advantages such as:

- Improved freeze-thaw durability.

- Improved long-term strength of the concrete.

- Increased workability (plasticity) of the concrete.

- Increased flexural and compressive strength of the concrete.

- Increased pumpability.

- Reduced permeability.

- Reduced water-to-cementitious materials ratio ($^w/_{cm}$).

- Reduced concrete segregation.

- Reduced heat of hydration.

- Reduced bleeding of the concrete.

- Reduced corrosion damage.

- Reduced cost of the concrete.

- Reduced volume changes (dry shrinkage).

However, the use of fly ash requires some considerations. Although certain fly ashes exhibit some cementitious properties, the main contribution to the hardened concrete properties results from the pozzolanic reaction of the fly ash with the calcium hydroxide ($Ca(OH)_2$) released by the Portland cement during hydration. The pozzolanic reaction typically occurs more slowly than cement hydration reactions and consequently concrete containing fly ash requires more curing during early ages. **Figure 2.4** presents a graphic description of the pozzolanic reaction (Headwaters Resources Tech Bulletin, 2008).

Table 2.2- Average Bulk Composition of Class C and F Fly Ashes

Oxide	Weight % / STD	
	Class C	Class F
SiO_2	36.9 ± 4.7	52.5 ± 9.6
Al_2O_3	17.6 ± 2.7	22.8 ± 5.4
Fe_2O_3	6.2 ± 1.1	7.5 ± 4.3
CaO	25.2 ± 2.8	4.9 ± 2.9
MgO	5.1 ± 1.0	1.3 ± 0.7
Na_2O	1.7 ± 1.2	1.0 ± 1.0
K_2O	0.6 ± 0.6	1.3 ± 0.8
SO_3	2.9 ± 1.8	0.6 ± 0.5
$Moisture$	0.06 ± 0.06	0.11 ± 0.14
LOI	0.33 ± 0.35	2.6 ± 2.4
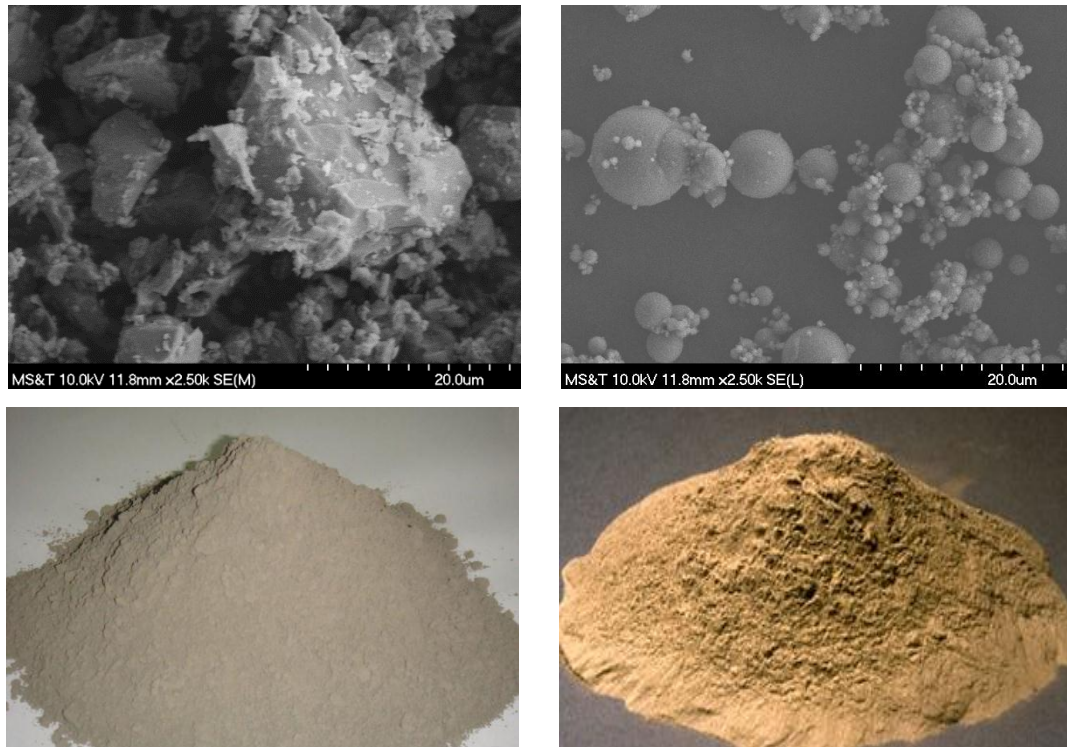
Figure 2.3- Comparison Between Portland Cement (left) and Fly Ash (right) Shapes
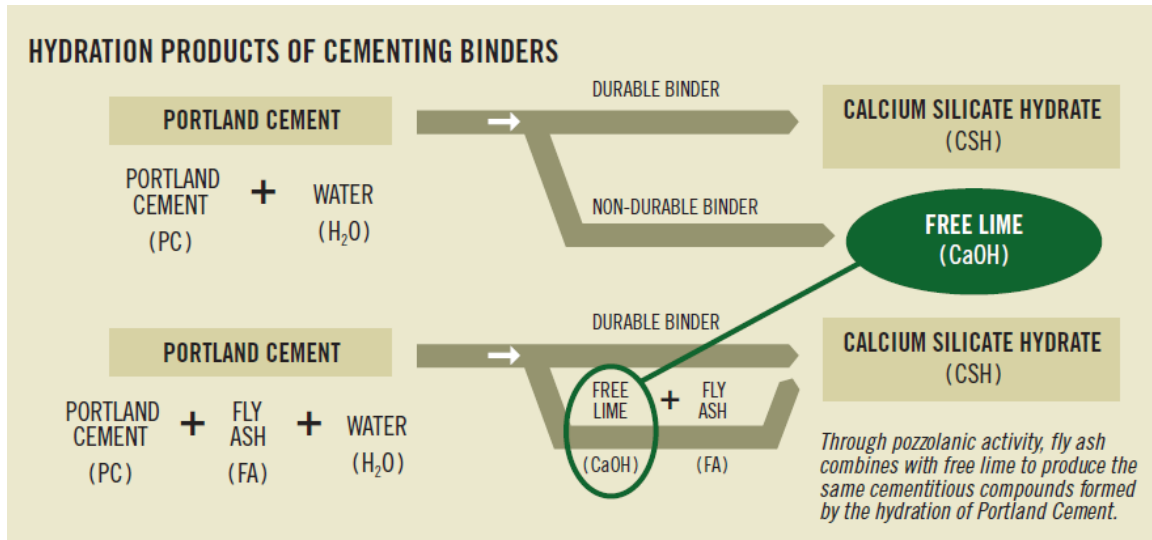
Figure 2.4- Pozzolanic Reaction

2.3. HIGH-VOLUME FLY ASH (HVFA) CONCRETE

Currently in the U.S., traditional specifications limit the amount of fly ash to 25 to 35% replacement by weight of the Portland cement in the concrete. Recent studies have shown that higher cement replacement percentages (up to 70%) can result in excellent concrete in terms of both strength and durability. Referred to as high-volume fly ash (HVFA) concrete, this type of concrete offers a viable alternative to traditional Portland-cement concrete (referred to as conventional concrete) and is significantly more sustainable. HVFA concrete is typically defined as concrete having a fly ash content of 50% or greater by weight of cementitious materials. As sustainability concerns continue to increase in both the construction industry and society as a whole, greater emphasis is being placed on producing concrete mixtures with increased volume fractions of supplementary cementitious materials, such as fly ash.

However, HVFA concrete can be susceptible to long delays in finishing and may sometimes lack necessary early age strength development. At all replacement rates, fly

ash generally slows down the setting time and hardening rates of concrete at early ages. Powder additions examined in previous research (Bentz, 2010) showed that the addition of 5% calcium hydroxide by mass of the total solids provides a significant reduction in the retardation measured in mixtures based on either class of fly ash.

2.4. PREVIOUS STUDIES RELATED TO HVFA CONCRETE

In 1937, Davis et al. conducted a study to determine the effect of using fly ash as a replacement for Portland cement upon the properties of mortars and concretes. This study included fly ashes from 15 different sources and Portland cements of seven compositions. In this study, fly ashes in percentages up to 50% were blended with the Portland cements. The properties investigated included strength, elasticity, volume change, plastic flow, heat of hydration, and durability as indicated by resistance to freezing and thawing, and by resistance to the action of sodium sulfate. The authors concluded that fly ashes of moderately low carbon content and moderately high fineness exhibit a high degree of pozzolanic activity as compared with most natural pozzolans. They reported that when such fly ashes are used in moderate percentages (between 30% and 50%) as replacement of Portland cement, it is possible to produce concretes with the same quality and sometimes superior than those concretes made of Portland cement only. In fact, Davis et al. reported that concrete mixes containing fly ash had lower compressive strengths at early ages but substantially higher compressive strengths at later ages, as well as lower heat of hydration and greater resistance to sulfate attack.

In 1985, the Canada Center for Mineral and Energy Technology (CANMET) developed HVFA concrete incorporating high volumes of low-calcium fly ash (Class F).

Numerous investigations performed at CANMET showed that HVFA concrete has excellent mechanical properties and durability characteristics.

In 1989, Langley et al. investigated concrete incorporating high volumes of Class F fly ash. These concrete mixtures contained 56% replacement of fly ash by weight of the total cementitious materials. The concretes investigated presented several different water-to-cementitious materials ratios. Because of the very low water contents used in this study, a high-range water reducer (HRWR) admixture was used to achieve high slumps. The authors concluded that the use of high volumes of Class F fly ash in concrete provide an economical material for strengths on the order of 9,000 psi at 120 days. They also reported that the extensive laboratory data showed that the optimum percentage of fly ash should be in the range of 55% to 60% of the total cementitious materials content. In terms of significant conclusions, they reported that the test data on strength properties, modulus of elasticity, drying shrinkage, creep, and freeze-thaw durability showed that concrete incorporating low Portland cement contents and high volumes of fly ash compared favorably to conventional Portland-cement concrete.

In 1990, CANMET carried out a project to develop an engineering data base on HVFA concrete incorporating selected fly ashes and cements from the U.S. This investigation was performed by the Electric Power Research Institute (EPRI) in Palo Alto, CA. Eight fly ashes, covering a wide range of mineralogical and chemical compositions, and two ASTM Type I Portland cements from two different sources were used in this study. A total of 16 air-entrained concrete mixtures were considered. The water-to-cementitious materials ratio was maintained at a constant value of 0.33 for all mixtures. The proportion of fly ash in the total cementitious materials content was 58%

by weight. Bilodeau et al. (1994) concluded that regardless of the type of fly ash and the

ASTM Type I brand of cement used, all air-entrained, HVFA concretes exhibited

excellent durability characteristics to freezing and thawing cycling, resistance to chloride-

ion penetration, and water permeability tests. However, they reported that the

performance of HVFA concrete in deicing salt-scaling tests was unsatisfactory.

In 1993, Carette et al. studied the properties of fresh and hardened HVFA

concretes. The properties of fresh concrete investigated included workability, bleeding,

setting time, and autogenous temperature rise. The properties of hardened concrete

investigated were compressive, flexural, and splitting-tensile strengths, modulus of

elasticity, creep, and drying shrinkage. The authors concluded that a high-performance,

air-entrained HVFA concrete can be produced with the eight fly ashes (produced in the

U.S.) and two Portland cements used in this study. The HVFA concrete produced

presented low bleeding, satisfactory slump and setting characteristics, and low

autogenous temperature rise. The authors also reported that these concretes also presented

excellent mechanical properties with compressive strengths reaching as high as 7,000 psi

and modulus of elasticity of 6,000 ksi at 91 days. In terms of significant findings, they

reported that using Portland cement with a high C_3A alkali content resulted in

considerably higher strength values at early ages than those obtained with the use of a

Portland cement with low C_3A alkali content.

In 1994, Berry et al. examined the hydration chemistry and microstructure of a

paste prepared incorporating 58% of a typical Class F fly ash and a Portland cement from

U.S. sources, and a paste with Portland cement only. The authors performed thermal

analysis, x-ray diffraction, pore fluid extraction, and scanning electron microscopy to

study cement and cement-fly ash pastes cured up to 180 days. They observed extensive participation by the fly ash in hydration and cementation reactions. They concluded that cement pastes in which 58% of the mass of Portland cement was replaced by fly ash appeared to hydrate and gain strength by the following mechanisms: (a) the hydration of Portland cement by normal chemical reaction, (b) the improved densification through particle packing, aided by the use of superplasticizers and the spherical shape of the fly ash, (c) the reactions of fly ash particles that produced insoluble silicate and aluminate hydrates at particle boundary regions at late ages, and (d) the hydration of individual fly ash particles that remained physically intact and largely unchanged in morphology, capable of filling in void space (paste densification).

In 1995, Galeota et al. studied the mechanical and durability properties of HVFA concretes for structural applications. They used four different concrete mixtures with fly ash from an Italian source, varying from 0% to 50% replacement by weight of the total cementitious materials. They evaluated the compressive, flexural and splitting-tensile strength, modulus of elasticity, fracture parameters, concrete-steel bond properties, drying shrinkage, and durability properties. The authors reported that concretes containing 30% and 40% replacement of Portland cement with fly ash showed adequate early age compressive strength at 3 days for structural applications (approximately 3,500 psi). They also found that the modulus of elasticity in all the HVFA concretes of this study was a little lower (approximately 10% lower) than that of the conventional mix; however, it was still considered adequate for structural applications. One of the most significant findings the authors reported was that after 28 days there was a high bond

strength gain (up to 60%) between the HVFA concrete and steel as compared to the conventional concrete.

In 1998, Swamy and Hung developed a high performance, HVFA concrete incorporating a small amount of silica fume (SF) and partial replacement of both Portland cement and fine aggregate with fly ash. They studied the engineering properties such as strength, modulus of elasticity, and drying shrinkage of this HVFA concrete. The mixtures were designed to give 4,000 to 6,000 psi cube strengths at 28 days. In each mixture, a 60% replacement of Portland cement with fly ash was considered. Some mixtures contained a 6% replacement of cementitious materials with silica fume and some others a 25% replacement of fine aggregate with fly ash. The authors concluded that the total binder content had little effect on the strength and drying shrinkage, but had a significant effect on the modulus of elasticity, implying a clear densification of the microstructure by the fly ash and silica fume. They also found that 7 days of curing were not enough to reach the full strength potential of the HVFA concrete. In terms of significant findings, the authors reported that a HVFA concrete with replacement of Portland cement and fine aggregate with both silica fume and fly ash showed the best overall performance based on the tests carried out in this study. They recommend HVFA concrete for use in structural and mass concrete applications because the engineering properties found in this study showed good potential and were comparable to those of a conventional Portland-cement concrete.

In 1999, Cabrera and Atis developed a new method for the determination of the optimum water-to-cementitious materials ratio for maximum compaction of no slump concrete made with high volumes of fly ash. This research explored the effect of the fly

ash fineness and, in particular, the carbon content on the compressive strength of the mixtures made with 50% and 70% replacement or Portland cement with fly ash. The authors concluded that the compactability of no slump HFVA concrete can be effectively controlled using the vibrating slump test. Based on this test, the optimum water-to-cementitious materials ratio for maximum compaction can be determined. They also concluded that the compressive strength of HVFA concrete with or without the superplasticizer places these mixtures in the class of high-strength concrete (HSC). Finally, they reported that the fatigue resistance of the HVFA concrete presented better performance results than those of the conventional mix.

In 1999, Jiang et al. tested different pastes made with different fly ash contents, water-to-cementitious materials ratios, and admixtures, such as high-range water reducers (HRWR), for a period up to 90 days. They studied the hydration progress, the hydration product, and the microstructure of the pastes employing strength development tests, thermal analysis, silicate polymerization analysis, pore structure analysis, x-ray diffraction analysis, and scanning electron microscopy. The authors concluded that the HRWR affects the progress of hydration, and activator admixtures accelerate the hydration of HVFA concrete binders. They also observed that the total porosity increases with the increment of the fly ash content, and decreases with time. Other significant findings reported by the authors were that the presence of fly ash can improve the pore size distribution and that the fly ash in HVFA systems cannot be fully hydrated. They recommended that the fly ash content in HVFA concrete should be lower than 70%.

In 2004, Li performed a laboratory study on the properties of high-volume fly ash, high-strength concrete incorporating nano-SiO_2 (SHFAC). The author compared the

results with those of regular Portland-cement concrete and high-volume fly ash, high-strength concrete (HFAC). Assessment of these concrete mixes was based on short- and long-term performance. The author evaluated the compressive strength and pore size distribution, reporting strength increments of about 81% at early ages (3 days) in the SHFAC compared to the HFAC. Some improvements in the pore size distribution of SHFAC were also reported. One of the most significant findings was that the addition of fly ash leads to higher porosity at short curing time, while nano-SiO_2 acting as an accelerating additive leads to more compact structures, even at short curing times.

In 2005, Cross et al. investigated a concrete mixture in which the Portland cement was replaced completely by Class C fly ash for the binder. The authors investigated the engineering properties required for structural design and the behavior and performance of beams and columns made of a 100% fly ash admixture. The engineering properties investigated included the modulus of elasticity, the splitting tensile strength, the tensile flexural strength, the shrinkage properties, and the reinforcing bar bond behavior. The authors evaluated the effectiveness of the empirical equations available to estimate some of these properties for conventional Portland-cement concrete concluding that with a few exceptions, the equations available were found to apply to fly ash concrete. The tensile strength was found to be 15% to 30% lower than would be expected based on the compressive strength. With respect to anchorage and development length, the results were inconclusive because at an embedment length of 12 in., bars embedded in fly ash concrete behaved as expected based on equations for conventional concrete, but in shorter lengths, the results were significantly different. Cross et al. also conducted tests on simple beam and column elements to observe the performance of the fly ash concrete.

Three beams singly reinforced in accordance with the ACI code were tested to failure using a four-point load test setup. The beams were simply supported with a cross section of 6 in. × 10 in. Shear reinforcement was provided at 4 in. spacing. All beams were designed to fail in flexure and they performed satisfactorily. There was no evidence of any anchorage problems with the flexural or shear reinforcement during the tests. The beam behavior observed during the tests matched the predicted behavior using the same theoretical approach as that for a conventional concrete RC beam. All of the beams presented adequate shear resistance. In the column elements, the specimens matched the same behavior expected of a conventional concrete column. The columns measured 6 in. in diameter with a length of 18 in. They were tested in uniaxial compression to failure. As a final conclusion, the authors reported that existing flexural design procedures can be employed on fly ash concrete elements with the exception of the embedment length calculations.

In 2007, Bouzoubaâ et al. investigated HVFA concrete using fly ash with ordinary Portland cement and Portland-pozzola cement. A total of 7 mixtures with three different target compressive strengths (3,000, 6,000, and 9,000 psi) were used. For the ordinary Portland cement, four mixes including a control mix were used incorporating 30%, 40%, and 50% replacement of Portland cement with fly ash. For the Portland-pozzola cement, three mixes including a control mix were used incorporating 40% and 50% replacement of this cement with fly ash. For each concrete mixture, the authors measured the compressive strength at 1, 3, 7, 28, 56, and 91 days, the splitting-tensile strength, flexural strength, and resistance to chloride-ion penetration at 28 and 91 days. They concluded that for similar target compressive strength, slump range, and cementitious materials

content, the water required decreased with the increment of fly ash content. They reported that it was possible to design concrete incorporating up to 50% replacement with fly ash that meets the strength requirements of the target compressive strengths. In terms of significant findings, the HVFA concrete considered in this study was found to develop acceptable early-age strength, higher later-age strength, and lower chloride-ion penetrability when compared to the conventional concrete made with ordinary Portland cement.

In 2008, Koyama et al. investigated the ultimate mechanical behavior and deformability of RC beams containing large quantities of fly ash. Eleven test beams were fabricated and tested under monotonic bending and shear. The experimental variables included the shear span-to-depth ratio, the amount of transverse reinforcement, and the amount of fly ash. The shear span-to-depth ratios studied in this program included values of 1.0, 1.5, and 2.0 that represent specimens with a deep beam behavior. In this study, the amount of Portland cement was held constant as well as the water-to-cementitious materials ratio, and the fly ash was used as a replacement of the fine aggregate. The cross section of the beams measured 9.8 in. $\times$ 15.7 in. The authors tested three beams under pure bending while the other eight beams were subjected to monotonic shear. Five of the shear specimens were constructed without shear reinforcement. All of the beams were simply supported using a three-point load test setup. The authors concluded that the specimens constructed using a 50% replacement of the fine aggregate with fly ash presented a higher shear strength and a steeper crack angle. They also concluded that it is possible to change the failure mode of the beams from a shear failure to a flexural failure by incorporating large quantities of fly ash in the mix.

In 2009, Namagga and Atadero studied the benefits of using high lime fly ash in concrete as a replacement for large proportions of cement. They focused on testing the compressive strength, durability, and bond strength properties of concrete. They varied the amounts of fly ash as partial replacements of the Portland cement and fine aggregate. The authors compared the results with conventional concrete to indicate whether the use of fly ash can improve strength so that fly ash can be accepted as a cost effective solution. Their findings included that the replacement of high lime fly ash in concrete generally increases the ultimate strength. They also reported that a 25% to 35% fly ash replacement provides the most optimal strength results, because beyond 35% fly ash replacement, the rate of gain of compressive strength decreases but still maintains a strength value above the desired strength.

In 2010, Bentz conducted isothermal calorimetry studies to examine excessive retardation in HVFA mixtures based on both Class C and Class F fly ashes. In order to quantify the retardation, the author used the calorimetric curves to evaluate the performance of mitigation strategies based on various powder additions. He examined powder additions including aluminum trihydroxide, calcium hydroxide, cement kiln dust, condensed silica fume, limestone, and rapid-set cement. He reported that using an addition of either 5% calcium hydroxide or 10% rapid-set cement by mass of total cementitious materials provides a significant reduction in the retardation measured in mixtures based on either class of fly ash for the material combinations examined in his study. Bentz concluded that these two powder additions provide viable solutions to mitigate excessive retardation, extending the use of HVFA mixtures in practice.

In 2011, Mohan Rao et al. conducted a study on the shear resistance of RC beams without web reinforcement using a high volume fly ash concrete mix with a 50% replacement by mass of the Portland cement. The authors used a water-to-cementitious material ratio of 0.32. The shear specimens presented a constant shear span-to-depth ratio of 2.50. The beams were simply supported with a cross section of 3.9 in. × 7.9 in. Various longitudinal reinforcement ratios were considered such as 0.58%, 1.0%, 2.0%, and 2.95%. Mechanical properties including compressive strength and split tensile strength were also studied. All the beams were loaded symmetrically under a four point load test setup. The authors compared the results of the HVFA specimens with others obtained from a conventional mix. Comparison with codes of practice and other empirical models was also carried out. As remarkable finding, the authors reported that the experimental results were very close to the theoretical values obtained using the CEB-FIP model code.

The ACI 232.2R (2003) document on fly ash mentions the wide range of applications of fly ash materials in the concrete industry. Fly ash can be used in ready-mixed concrete, concrete pavements, mass concrete, roller-compacted concrete (RCC), self-consolidated concrete (SCC), high-volume fly ash (HVFA) concrete, high-performance concrete (HSC), concrete masonry units, concrete pipes, precast/prestressed products, no-slump extruded hollow-core slabs, grouts and mortars, controlled low-strength materials, soil cements, sulfur concrete, cellular concrete, shotcrete, blended cements, oil-well cementing, and finally as a filler.

Table 2.3 summarizes all the variables addressed in previous research such as the percentage replacements of Portland cement with fly ash, the properties investigated, and the presence of full-scale testing.

Table 2.3- Summary of Studies in HVFA Concrete

Researcher (s)	Year	Fly ash addition			Properties investigated								Full-scale testing
		50%-59%	60% -69%	70% - 100%	Strength	Modulus of elasticity	Bond properties	Durability	Heat of hydration	Plastic flow	Dry shrinkage	Creep	
Davis et al.	1937	X			X	X		X	X	X			
Langley et al.	1989				X			X			X	X	
Carette et al.	1993		X		X			X				X	
Berry et al.	1994	X							X				
Bilodeau et al.	1994	X						X					
Galeota et al.	1995	X			X	X		X			X		
Swamy and Hung	1998		X		X	X					X		
Cabrera and Atis	1999	X	X		X					X			
Jiang et al.	1999		X						X				
Li	2004	X			X				X				
Cross et al.	2005			X	X		X				X		X
Bouzoubaâ et al.	2007	X			X			X					
Koyama et al.	2008	X			X								X
Namagga and Atadero	2009				X			X	X				
Bentz	2010	X			X				X				
Mohan Rao et al.	2011	X			X								X

2.5. CONCLUDING REMARKS

The literature review reported that incorporating fly ash in concrete reduces the compressive strength at early ages but there is a valuable increase in the compressive strength at later ages. It was found that the early age strength is reduced further if the percentage of replacement is increased. However, on the other hand, when the percentage of replacement is increased, the water-to-cementitious materials ratio can be reduced,

therefore increasing the later age compressive strength. Properly cured HVFA concrete products are very homogenous in microstructure and highly durable. Several studies showed that HVFA concrete presents lower heat of hydration and higher resistance to chloride-ion penetration. Several researchers recommended that the fly ash content in HVFA concrete should be lower than 70%. In conclusion, HVFA concrete could offer a solution to the problem of meeting the increasing demands for concrete in the future in a sustainable manner and at reduced or no additional cost, and at the same time reducing the environmental impact of two industries that are essential to economic development, the Portland cement industry and the coal-fired power industry. The use of high volumes of fly ash in concrete generates a direct link between durability and resource productivity, thus increasing the use of HVFA concrete will help to improve the sustainability of the concrete industry.

3. LITERATURE REVIEW ON SHEAR

3.1. GENERAL

The main subject of this document is the shear behavior of reinforced concrete (RC) beams composed of high-volume fly ash (HVFA) concrete. The current shear design methods and guidelines are presented in this chapter. Four different approaches are presented: truss model, Strut and Tie Model (STM), Modified Compression Field Theory (MCFT), and fracture mechanics approach. A collection of three design code philosophies that can be found in North America will also be used in the evaluation of the shear strength. Some of these guidelines rely on empirical formulas, such as the ACI 318-08, while others, such as the AASHTO LRFD and CSA A23.3-04, rely more on concrete models such as the MCFT.

3.2. FACTORS AFFECTING SHEAR BEHAVIOR

Shear strength is controlled by the presence of web reinforcement, longitudinal reinforcement, coarse aggregate size, presence of axial loads, depth of the member, tensile strength of the concrete, and shear span to depth ratio (a/d). Some of these parameters are included in design equations and others are not.

Web reinforcement, typically called stirrups, is used to increase the shear strength of concrete beams and to ensure flexural failure. This is necessary due to the explosive and sudden nature of shear failures, compared with flexural failures which tend to be more ductile. Web reinforcement is normally provided as vertical stirrups and is spaced at varying intervals along a beam depending on the shear requirements. Alternatively, this reinforcement may be provided as inclined longitudinal bars. In general, small sized bars

such as #3 and #4 are used in a U-shaped configuration that may be open or closed, or used as multiple legs.

Shear reinforcement has very little effect prior to the formation of diagonal cracks. However after cracking, the web reinforcement enhances the beam in the following ways (Nilson et al., 2004):

- The stirrups crossing the crack help in resisting the shear force.

- The stirrups restrict the growth of the cracks and reduce their penetration further into the compression zone.

- The stirrups oppose widening of the cracks, which helps to maintain aggregate interlock within the concrete.

- The presence of stirrups provides extra restraint against the splitting of concrete along the longitudinal bars due to their confinement effect.

The longitudinal reinforcement ratio (ρ_L) affects the extent and the width of the flexural cracks. If this ratio is small, the flexural cracks extend higher into the beam and open wider. When the crack width increases, the components of shear decrease, because they are transferred either by dowel action or by shear stresses on the crack surfaces.

The coarse aggregate type and size noticeably affect the shear capacity, especially for beams without stirrups. Lightweight aggregate has a lower tensile strength than normal aggregate. The shear capacity of a concrete beam with no stirrups is directly related to the tensile strength, therefore, the failure due to mortar cracking, which is more desirable, could be preceded by aggregate failure instead. The aggregate size also affects the amount of shear stresses transferred across the cracks. Large diameter aggregate

increases the roughness of the crack surfaces, allowing higher shear stresses to be transferred (Wight and MacGregor, 2009).

Researchers have concluded that axial compression serves to increase the shear capacity of a beam while axial tension greatly decreases the strength. As the axial compressive force is increased, the onset of flexural cracking is delayed, and the flexural cracks do not penetrate as far as into the beam (Wight and MacGregor, 2009).

The size of the beam affects the shear capacity at failure. If the overall depth of a beam is increased, it could result in a smaller shear force at failure. The reasoning is that when the overall depth of a beam increases, so do the crack width and crack spacing, causing loss of aggregate interlock. This condition is known as a size effect.

The tensile strength of the concrete (f_{ct}) also affects the shear strength. Because of the low tensile strength of the concrete, diagonal cracking develops along planes perpendicular to the planes of principal tensile stress. The shear strength of an RC beam increases as the concrete material strength increases. The tensile strength of the concrete is known to have a great influence on the shear strength, but the concrete compressive strength (f'_c) is used instead in most shear strength formulas. This approach is used because tensile tests are more difficult to conduct and usually show greater scatter than compression tests.

The shear span to depth ratio (a/d) does not considerably affect the diagonal cracking for values larger than 2.5. The shear capacity increases as the shear span to depth ratio decreases. This phenomenon is quite significant in deep beams ($a/d \leq 2.5$) because a portion of shear is transmitted directly to the support by an inclined strut or

arch action. For deep beams, the initial diagonal cracking develops suddenly along almost the entire length of the test region (Wight and MacGregor, 2009).

3.3. BASIC SHEAR TRANSFER MECHANISMS

The 1973 ASCE-ACI Committee 426 Report concluded that shear is transferred by the following four mechanisms: shear stress in the uncracked concrete, interface shear transfer, dowel action, and arch action. In a RC beam, after the development of flexural cracks, a certain amount of shear is carried by the concrete in the compression zone. The shear force carried by the uncracked concrete in the compression zone can be represented by the compressive strength of concrete and the longitudinal reinforcement ratio. Shear may continue to be transferred across a crack in the concrete by interface shear transfer, also known as aggregate interlock. Since the flexural crack width is approximately proportional to the strain of the tension reinforcement, the crack width at failure becomes smaller as the longitudinal reinforcement ratio is increased. It is also expected that the interlocking force will be increased when the compressive strength of the concrete is high. If longitudinal reinforcing bars cross a crack, dowel forces in the bars will resist shear displacement. The dowel force induces tension in the surrounding concrete that may produce splitting cracks along the longitudinal reinforcement. Although there is some contribution in dowel action by the number and arrangement of longitudinal bars, spacing of flexural cracks, and the concrete cover, the main factors influencing this mechanism are the flexural rigidity of the longitudinal bars and the strength of the surrounding concrete. Arch action occurs where shear flow cannot be transmitted. Arch action is dominant in deep beams. For this mechanism to be developed, a tie is required

to restrain the thrust developed as a result of the arch. For deep beams, failure is often due to anchorage failure of the bars restraining this thrust.

Shear can be carried through beam action, arch action or any combination of the two. When shear is carried through beam action, the tensile force in the reinforcement varies through bond stresses and plane sections remain plane. These are the normal assumptions of elastic beam theory.

The 1998 ASCE-ACI Committee 445 Report highlights a new mechanism, residual tensile stresses, which are transmitted directly across cracks. The basic explanation of residual tensile stresses is that when concrete first cracks, small pieces of concrete bridge the crack and continue to transmit tensile force as long as cracks do not exceed 0.00197-0.0059 in. in width. The application of fracture mechanics to shear design is based on the premise that residual tensile stress is the primary mechanism of shear transfer.

3.4. SHEAR DESIGN PRINCIPLES

3.4.1. Truss model. The truss method of analysis has for some time been accepted as an appropriate method for the design of structural concrete members comprising both reinforced and prestressed concrete elements, and now forms the basis of many design standard recommendations. The truss model was presented by the Swiss engineer Ritter (1899) to explain the flow of forces in cracked reinforced concrete. The principle of the truss model is based on the following assumptions: (1) the longitudinal tension reinforcement acts as a tension chord of the truss while the flexural compressive zone of the beam acts as the compression chord, and (2) the diagonal compressive

stresses (green lines in **Figure 3.1**) act as diagonal members, and the stirrups (blue lines in **Figure 3.1**) are considered as vertical tension members.

Mörsch (1902), a German engineer, pointed out that the compression diagonals do not need to extend from the top of one stirrup to the bottom of the next stirrup, and that the stirrups represent a continuous field of stresses rather than discrete diagonal compressive struts. Mörsch and Ritter neglected the tensile stress in cracked concrete assuming that only after cracking the diagonal compression stresses would remain at 45 degrees. Mörsch also proposed truss models to explain the behavior of beams detailed with bent-up longitudinal reinforcing bars. He also used the principal stress trajectories as an indication of how tensile reinforcement should be proportioned and detailed in a region where the internal stress flow is complex. **Figure 3.2** presents the model proposed by Mörsch.
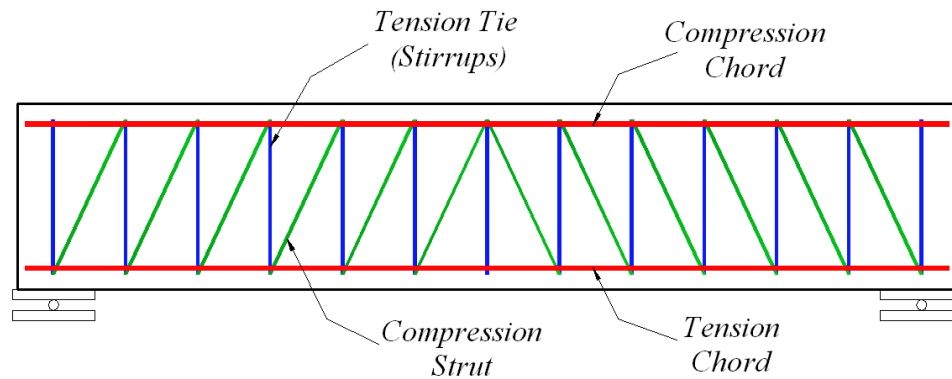
Figure 3.1- Ritter's Truss Analogy for Shear
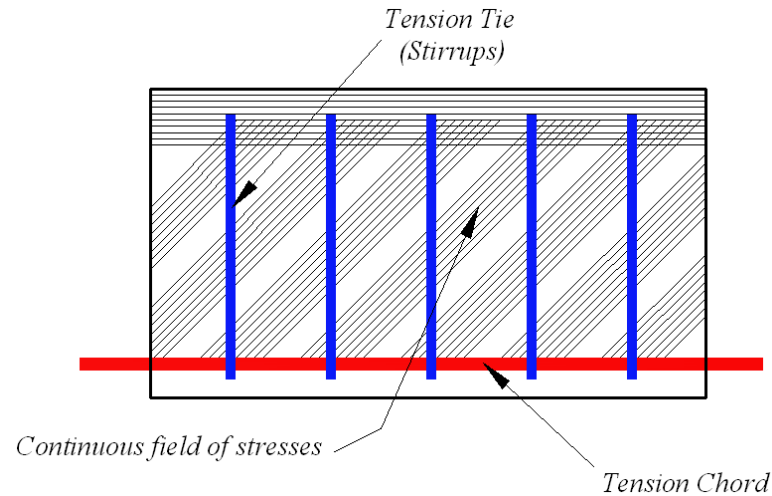
Figure 3.2- Truss Model for Beams Postulated by Mörsch

The truss model is derived using the equilibrium condition between the external and internal forces as presented in **Figure 3.3**. The shear stresses are assumed to be uniformly distributed over an effective shear area b_w wide and d deep. Between the external shear force V, and the total diagonal compressive force, **Equation 3-1** can be written, from which the principal compressive stress (f_2) can be determined assuming a crack angle of 45 degrees.

The longitudinal component of the diagonal compressive force is considered equal to the external shear force. The tensile stress in stirrups is determined considering **Equation 3-2**. Allowing only the use of the 45 degrees crack angle the method is robust and gives conservative results, and it is widely used by designers because of its simplicity.
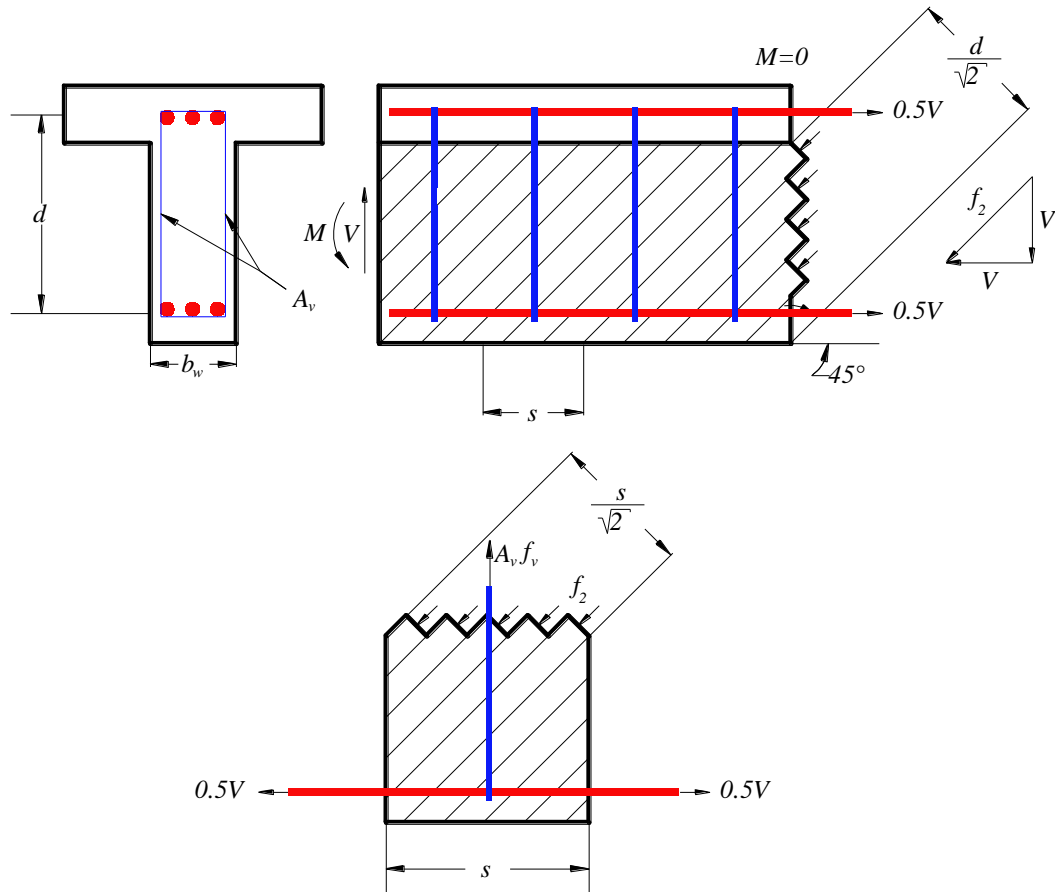
Figure 3.3- Equilibrium Conditions for the Truss Model (Collins and Mitchell, 1991)

$$\frac{f_2 b_w d}{\sqrt{2}} = \sqrt{2}V \tag{3-1}$$

$$\frac{A_v f_v}{s} = \frac{V}{d} \tag{3-2}$$

The variable-angle truss model is derived from the Mörsch truss model. This model adds a concrete contribution to shear strength to compensate for the conservative nature of the model based on a variable angle of the crack (θ). The principle is very similar to the one presented in **Figure 3.3**. In this model, the required magnitude of the principal compressive stress (f_2) is determined from the equality between the resultant of the diagonal stresses and the projection of the shear force, as stated in **Equation 3-3**. The tensile force in the longitudinal reinforcement (N_h) due to shear will be equal to the

horizontal projection of the shear force, as stated in **Equation 3-4**. The tensile stress in

the stirrups is multiplied by the factor $\tan\theta$, as stated in **Equation 3-5**.

$$f_2 = \frac{V}{b_w d}(\tan\theta + \cos\theta) \tag{3-3}$$

$$N_h = V\cos\theta \tag{3-4}$$

$$\frac{A_v f_v}{s} = \frac{V}{d}\tan\theta \tag{3-5}$$

Since there are only three equations of equilibrium (**Equations 3-3**, **3-4**, and **3-5**),

and there are four unknowns (f_2, N_h, f_v, and θ), the stresses in a beam caused by a given

shear force cannot be explicitly determined. For design considerations, the shear force

can be predicted assuming the crack angle at 45 degrees and the tensile stress in the

stirrups as the tensile strength of steel (f_y). Another approach could be assuming the

compressive stress in the concrete to determine the crack angle (**Equation 3-3**) and the

shear force (**Equation 3-5**). Other approaches to solving the variable angle truss model

have been developed based on subsequent test data. For instance, it has been suggested

that the effective compressive strength should be taken as $0.6f'_c$, and that the factor $\tan\theta$

should be less than 0.5 (Collins and Mitchell, 1991).

Proportioning and detailing of the transverse reinforcement in members with a

complex flow of internal stresses was a main aspect of structural concrete research in

central Europe during the 1960s and 1970s. Leonhardt, from the University of Stuttgart in

Germany, and Thürlimann and Müeller, from the Swiss Federal Institute of Technology

in Zürich, were instrumental in the development of analysis and design methods for

structural concrete regions with complex internal stress flows. Leonhardt focused mainly

on the analysis and design of deep beams and anchorage end regions in post-tensioned beams. In most of his work, the detailing of the reinforcing steel closely followed the principal tensile stress trajectories found from an elastic analysis of a homogeneous isotropic element. Thürlimann focused mainly on the application of the theory of plasticity in reinforced and prestressed concrete, with practical applications to the design for shear and torsion.

In the mid-1970s, Park and Paulay, from the University of Canterbury, extended many of the analytical and design concepts developed by Leonhardt to include, for the first time, the detailing of regions having a complex flow of stresses and subjected to cyclic load reversals caused by earthquake excitation (Park and Paulay, 1975). One of these regions is the joint between the beam and column in a moment resisting frame. In the analysis and design of beam-column joints, Park and Paulay deviated from Leonhardt's method by proposing a simple mechanism of shear transfer that did not follow the principal tensile stress trajectories shown by an elastic analysis. This model requires vertical and horizontal reinforcement to sustain the diagonal compressive field introduced into the joint as a result of bond forces from the outermost longitudinal column and beam bars.

The truss model is also the starting point of the shear friction model, also known as Loov's theory (1998), in which the shear forces are carried by stirrups and shear friction across the concrete crack. The method comprises the calculation of the shear capacity from all possible crack angles by identifying the weakest plane of failure. The force that holds the two surfaces together is equal to the yield stress multiplied by the cross-sectional area of any steel crossing the crack for bars perpendicular to the failure

plane. In addition to the friction of the failure plane surface, the model accounts for shearing of the reinforcement and the dowel action that they generate. The main drawback to the use of the shear friction models for beam shear is that the critical failure plane is typically unknown, so an interactive approach must be conducted to find the weakest or most critical failure plane.

    3.4.2. Strut and tie model. The Strut and Tie Model (STM) was developed in the late 1980s. It was formalized and popularized by Schlaich et al. in a comprehensive paper published in 1987. Reinforced concrete theory hinges on various assumptions of simple beam theory such as plane sections remaining plane. However, regions near a discontinuity do not satisfy this assumption and are called D-regions, which stands for disturbed regions that do not follow simple beam theory. These regions extend approximately a distance h away from the discontinuity which may include concentrated loads, openings, or changes in the cross section. Entire beams consisting of a D-region are called deep beams. Regions in between these areas are subjected to typical beam behavior and are called B-regions. **Figure 3.4** shows the distribution of D- and B-regions, where D stands for discontinuity or disturbed, and B stands for beam or Bernoulli. The STM was developed based on the truss model to account for these D-regions. They consist of struts, ties, and nodal zones. **Figure 3.5** shows how each are combined within a beam.
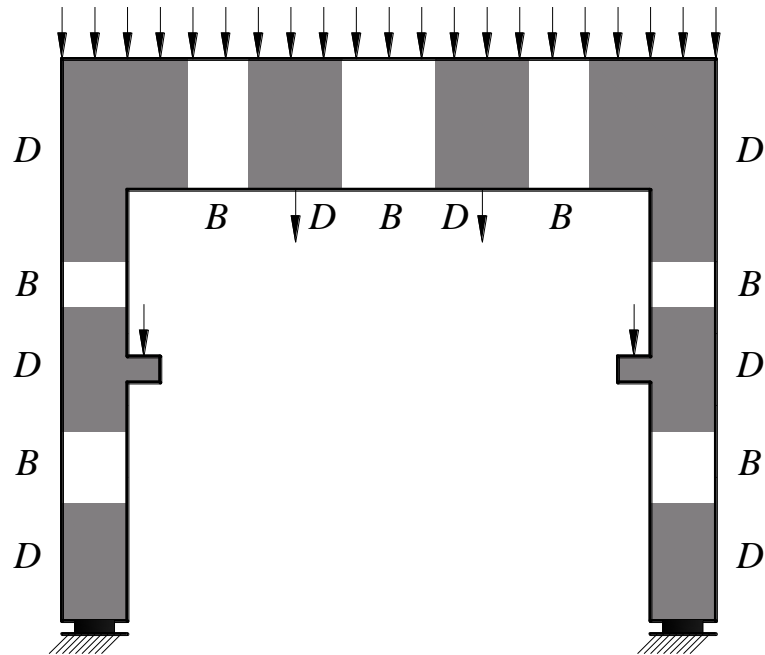
Figure 3.4- B-Regions and D-Regions (Schlaich et al., 1987)

Struts are internal concrete compression members which may be rectangular or bottle-shaped. Bottle-shaped struts swell throughout their depth, and are wider at the center than at the ends. The STM shown in **Figure 3.5** features a rectangular strut, but the bottle-shaped strut is depicted with dashed lines. Ties are tension members within the model and consist of steel reinforcement, plus the portion of concrete surrounding the steel. However, the model assumes that the steel carries all of the tension force. Nodal zones are regions where struts, ties, and concentrated loads meet. Nodes are classified by the types of forces passing into them, which create four types: (a) C-C-C, (b) C-C-T, (c) C-T-T, and (d) T-T-T, where C represents compression and T represents tension. **Figure 3.6** presents each node type.

The following procedure is used to develop a STM:

- Defining of the D-region; borders and forces within these boundaries.

- Drawing a STM based on the assumed node geometry.

- Solving for the truss member forces.

- Calculating the reinforcement layout providing the required tied capacity and enough anchorage length for the bars to ensure the correct behavior at the nodes.

- Dimensioning nodes using truss member forces obtained previously.

- Repeating analysis for the new geometry in order to find a converged solution.

The STM method is not always trouble-free and has many uncertainties. There are four major problems in developing STM, and these are:

- Uncertainties in obtaining dimensions, stiffness, and effective strength of strut, ties, and nodes for the truss models.

- Need to select the optimal STM and iteratively adjust and refine the truss geometry.

- Need to combine different load cases.

- Multiple potential solutions for statically indeterminate models.
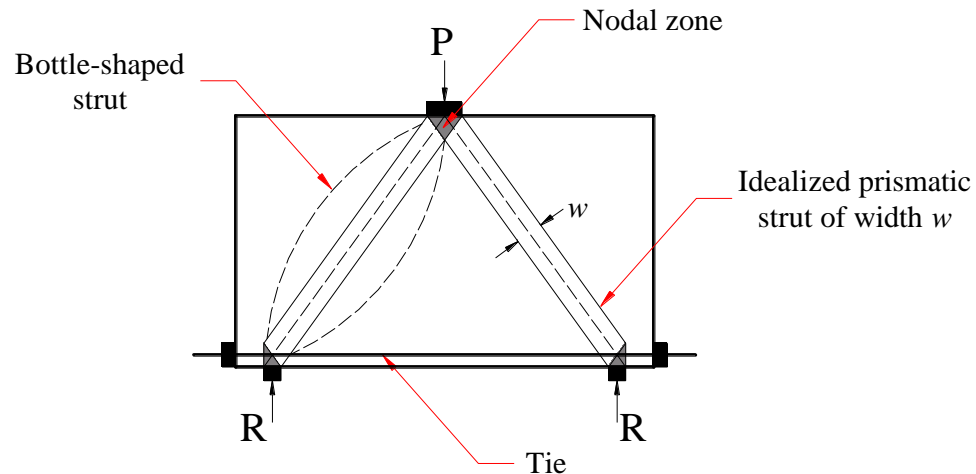
Figure 3.5- Strut and Tie Model (Nilson et al., 2004)

(a) C-C-C   (b) C-C-T   (c) C-T-T   (d) T-T-T
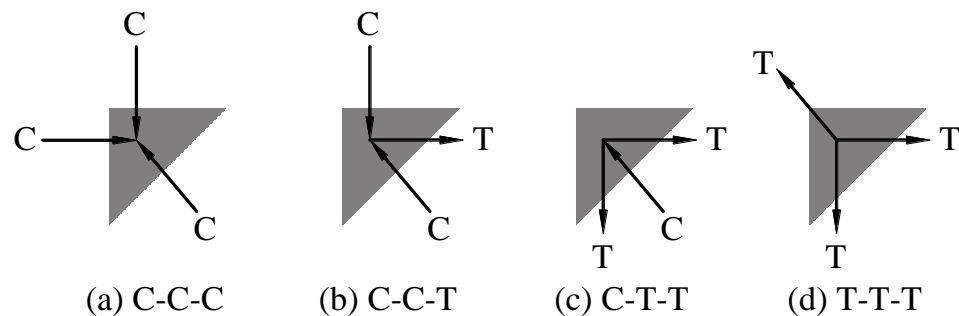
Figure 3.6- Nodal Zones (Nilson et al., 2004)

The creation of the strut and tie model offers no unique solution, and more than one admissible model may be valid for a given problem. The STM must be statically admissible, thus, in equilibrium with the external loads, reactions and nodes. Design takes place by selecting the amount of steel for the tension ties, effective width of the strut, and shape of the nodal zone such that the strength is adequate.

Previous researchers (Kani, 1967) have found that beams with shear span-to-depth ratios greater than 2.5 are governed by conditions away from the disturbed regions adjacent to the support and the loads. In this range, the strength of the beam is not influenced by details such as the size of the bearing plates, and the strength decreases by

only a small amount as the shear span increases. Collins and Mitchell (1997) presented an example of the use of the strut and tie model illustrated in **Figure 3.7**, which shows how the shear strength of a simply supported reinforced concrete beam loaded with two point loads changes as the shear span changes. This study shows that a beam can resist a higher shear force if the shear is produced by a load that is closer to the support. This series of beams was tested by Kani (1967), and based on the observation of the results, it was concluded that the shear strength was reduced by a factor of about 6 as the shear span-to-depth ratio decreased from 1 to 7 (Collins and Mitchell, 1997). This result can be explained by the fact that deep beams carry the load by strut-and-tie action, and as the applied load moves closer to the support, the angle of the compression strut increases, reducing the force (stress) in the strut, and thus increasing the capacity of a given cross section. Typical failure mode of these beams involves crushing of the concrete strut.
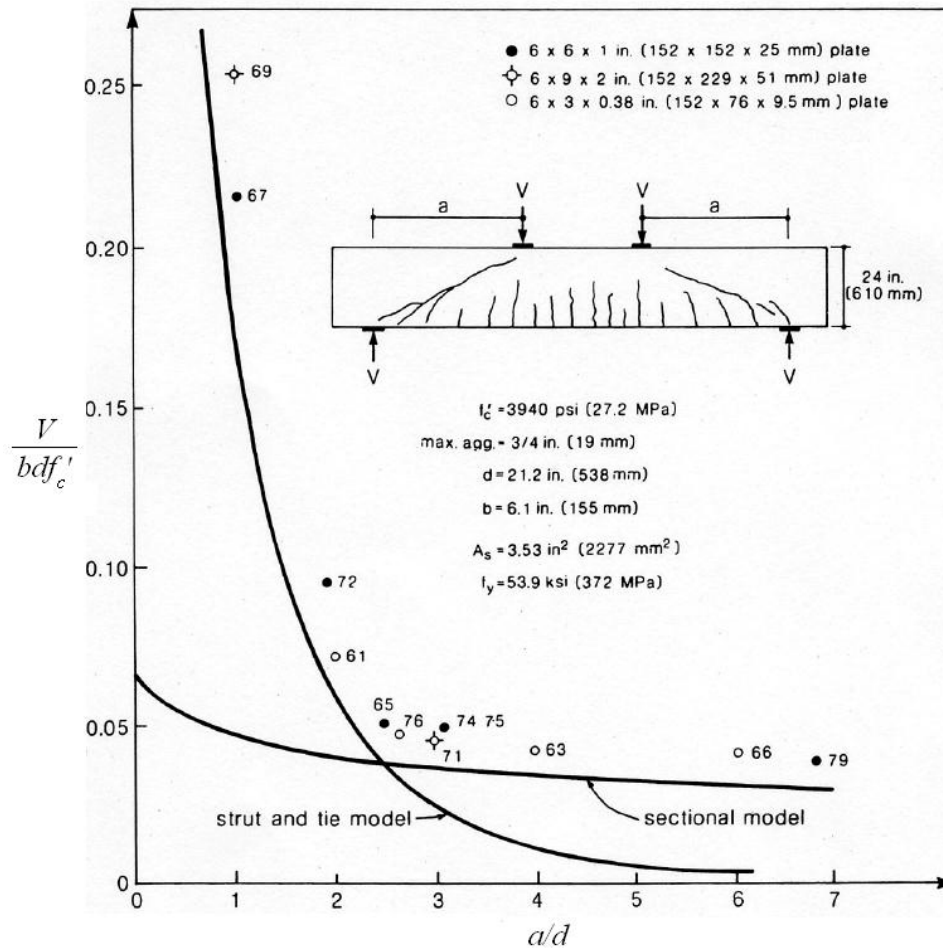
Figure 3.7- Predicted and Observed Strengths of a Series of RC Beams Tested by Kani (Collins and Mitchell, 1997)

The STM approach is rapidly gaining popularity for the analysis and design of

deep beams, and has been adopted in several North American codes, such as the

American Concrete Institute (ACI) Building Code Requirements for Structural Concrete

(ACI 318-08) and the Canadian Standard Association (CSA) Design of Concrete

Structures (CSA A23.3-04). Appendix A of ACI 318-08 provides guidance for sizing

struts, nodes, and ties. The code addresses the performance of highly stressed

compression zones that may be adjacent to or crossed by cracks in a member, the effect

of stresses in nodal zones, and the requirements for bond and anchorage of ties. However,

ACI 318-08 provides no clear guidance to indicate when a strut should be considered as rectangular or bottle-shaped.

Furthermore, as shown in **Figure 3.8**, structural elements may consist of B-regions, D-regions, or a combination of both depending on several factors. ACI 318-08 states that if there is a B-region located between D-regions in a shear span, as shown in **Figure 3.8(b)**, the strength of the shear span is governed by the strength of the B-region if the B- and D-regions have similar geometry and reinforcement. This is because the shear strength of a B-region is less than the shear strength of a comparable D-region. Shear spans containing B-regions are designed for shear using traditional truss model approaches.

Figure 3.9 presents the layout and dimensions of the beam specimens tested in the current study. Based on the previous discussion, the presence of B-regions within the shear span precludes the application of a STM approach in determining the capacity of this section. Instead, these beams are governed by the traditional truss model approach.

3.4.3. Modified compression field theory. The Modified Compression Field Theory (MCFT) was developed by Vecchio and Collins in 1986, and is a further development of the Compression Field Theory (CFT) derived by Collins and Mitchell in 1980. In the CFT it is assumed that the principal tensile stress (f_1) is zero after the concrete has cracked while in the MCFT the effect of the residual stress in the concrete between the cracks is taken into account. Tensile stresses across the diagonal struts increase from zero at the cracks to a maximum in the middle of the strut as shown in **Figure 3.10**.
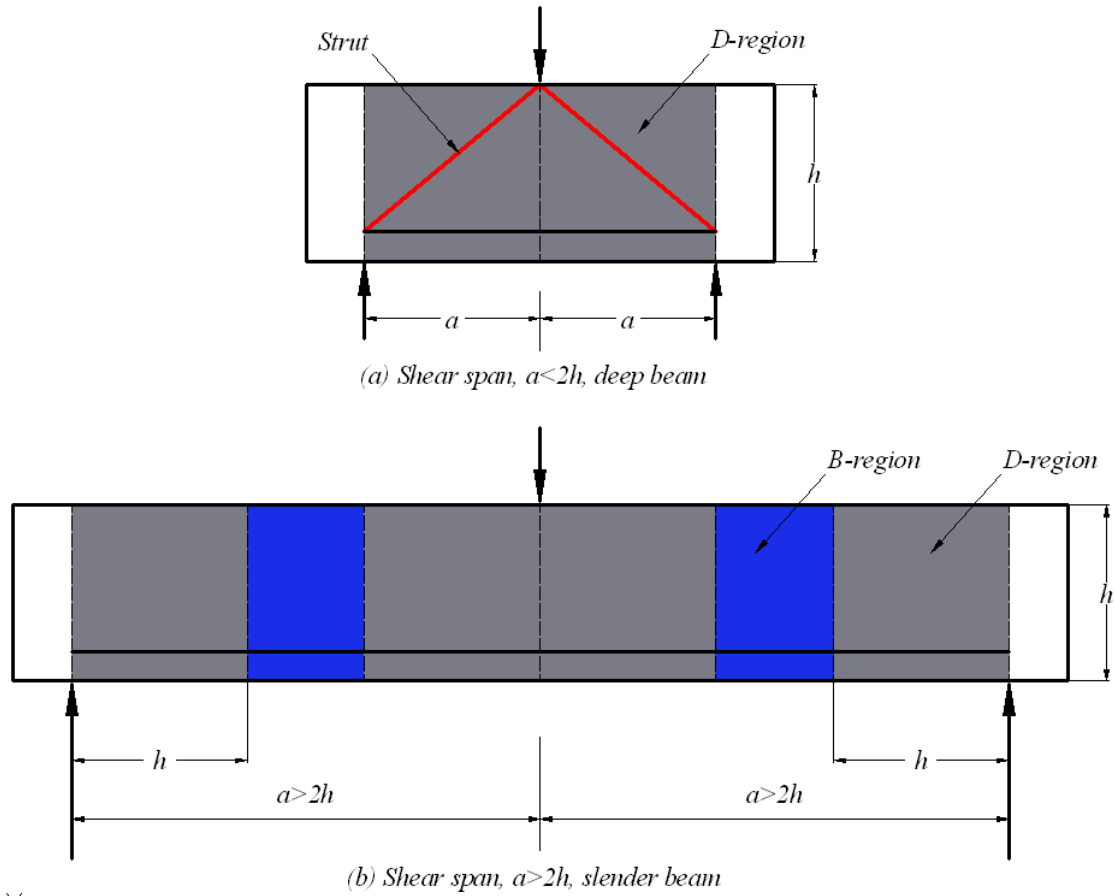
Figure 3.8- Description of Deep and Slender Beams (ACI 318-08)
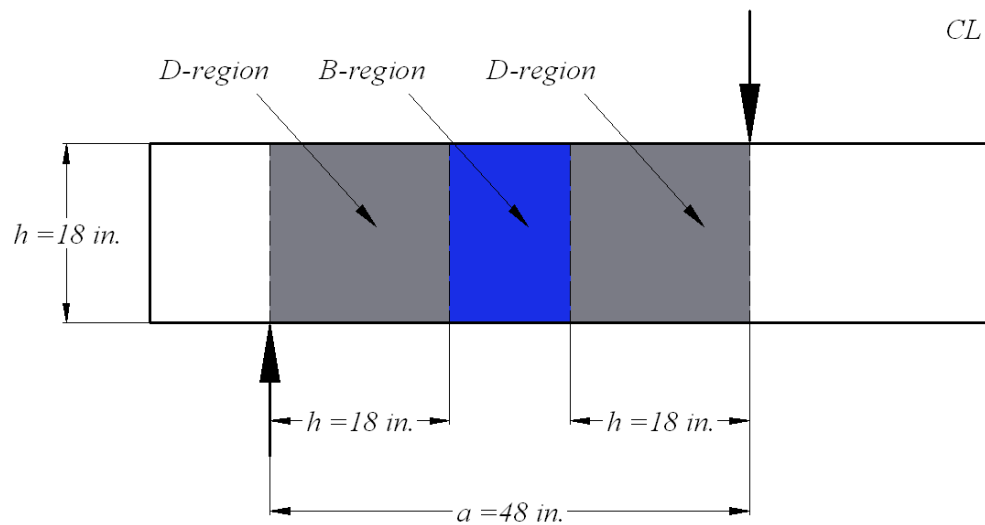
Figure 3.9- Slender Beams Used in This Study

The MCFT model consists of strain compatibility and equilibrium equations which can be used to predict the complete shear deformation response. All the compatibility equations are expressed in terms of average strains measured over base lengths long enough to include several cracks. The compatibility equations for both the CFT and the MCFT are given in **Equations 3-6**, **3-7**, and **3-8**, which are obtained from the Mohr's circle shown in **Figure 3.11**.
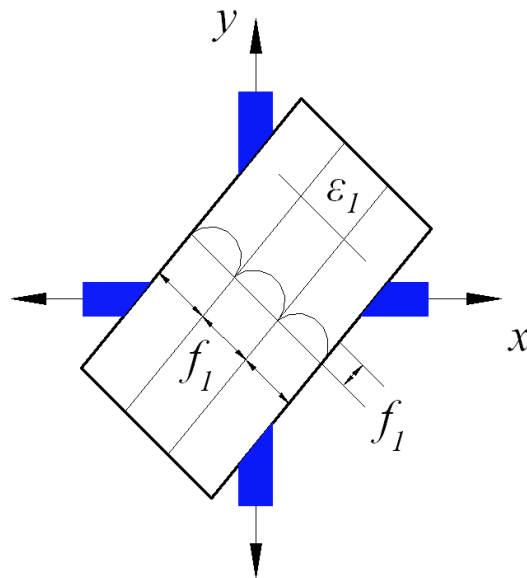
Figure 3.10- Tensile Stress Along a Cracked Strut (Vecchio and Collins, 1986)

$$\gamma_{xy} = \frac{2(\varepsilon_x - \varepsilon_2)}{\tan\theta} \tag{3-6}$$

$$\varepsilon_1 + \varepsilon_2 = \varepsilon_x + \varepsilon_y \tag{3-7}$$

$$tan^2\theta = \frac{\varepsilon_x - \varepsilon_2}{\varepsilon_y - \varepsilon_2} = \frac{\varepsilon_1 - \varepsilon_y}{\varepsilon_1 - \varepsilon_x} \tag{3-8}$$

where γ_{xy} is the shear strain, ε_x is the strain in the x-direction, ε_y is the strain in the y-direction, ε_1 is the principal tensile strain in concrete (positive value), and ε_2 is the principal compressive strain in concrete (negative value).
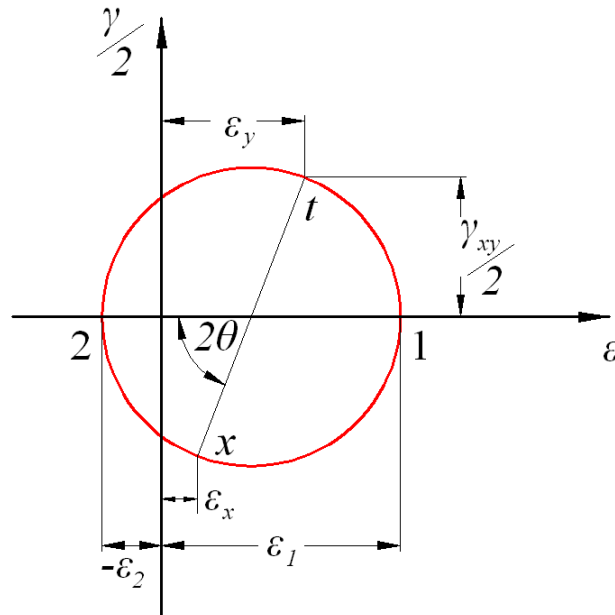
Figure 3.11- Mohr's Circle for Average Strains

The concrete element shown in **Figure 3.12** will resist concrete shear forces (v_{cxy}), horizontal concrete stresses (f_{cx}), and vertical concrete stresses (f_{cy}). All three forces combine to form the principal tensile stress (f_1), and the principal compressive stress (f_2). Converting these stresses into a Mohr's circle of stress, as shown in **Figure 3.13**, the equilibrium **Equations 3-9** and **3-10** can be derived.
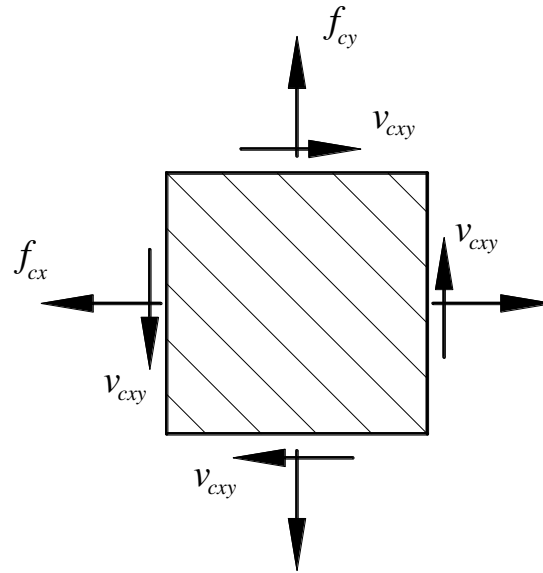
Figure 3.12- Average Concrete Stress in a Cracked Element (Vecchio and Collins, 1986)
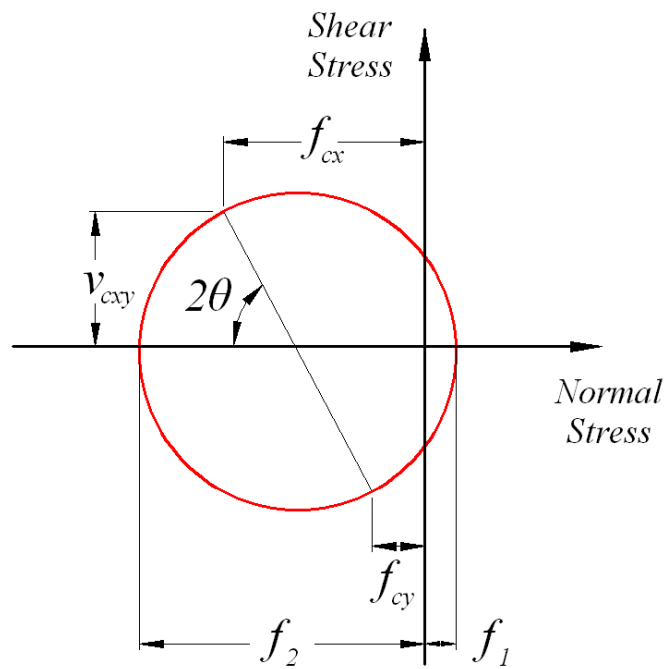
Figure 3.13- Mohr Stress Circle for Average Concrete Stresses

$$f_{cx} = f_1 - \frac{v_{cxy}}{\tan \theta} \qquad (3\text{-}9)$$

$$f_{cy} = f_1 - v_{cxy} \tan \theta \qquad (3\text{-}10)$$

The Mohr's circle can also be used to derive an equation for relating the principal compressive stress (f_2) and tensile stresses as shown in **Equation 3-11**.

$$f_2 = (\tan\theta + \cot\theta)v - f_1 \qquad (3\text{-}11)$$

where, $v = \dfrac{V}{b_w jd}$ and jd is the distance between the resultants of the internal compressive and tensile forces on a cross section.

The equilibrium conditions for a symmetrical cross section subjected to pure shear are shown in **Figure 3.14**. These conditions can be expressed as shown in **Equation 3-12**.
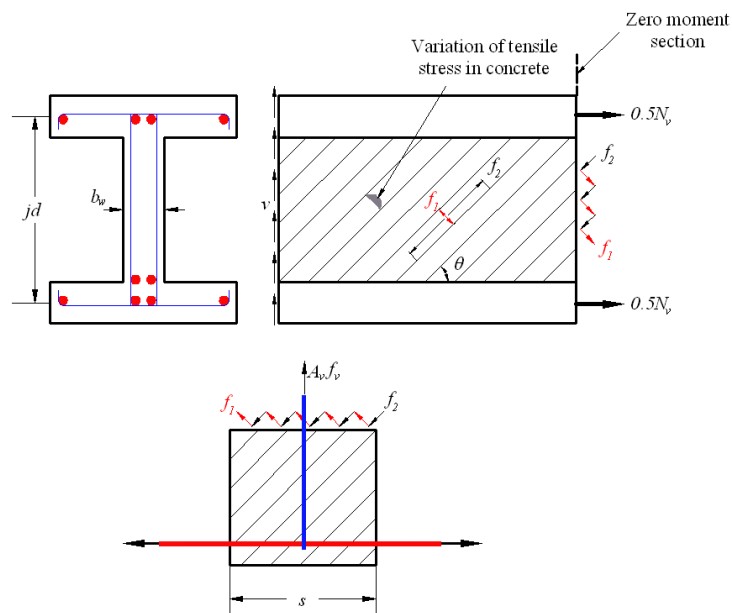
Figure 3.14- Cross Section, Principal Stresses, and Tension in Web Reinforcement (Collins and Mitchell, 1991)

$$A_v f_v = (f_2 sin^2\theta - f_1 cos^2\theta)b_w s \tag{3-12}$$

where A_v is the steel vertical reinforcement area and f_v is the stress in the stirrups.

Substituting **Equation 3-11** into **3-12** generates the expression in **Equation 3-13**.

$$V = f_1 b_w jd \cot\theta + \frac{A_v f_v}{s} jd \cot\theta \tag{3-13}$$

Collins and Mitchell (1991) noted that **Equation 3-13** expresses shear resistance in terms of the sum of the concrete and steel contributions, as the traditional or classical method. The concrete contribution depends on the average tensile stresses in the concrete, and the steel contribution depends on the tensile stresses in the stirrups. It must be clarified that although the MCFT and the truss model approaches might seem to be similar, the concrete contribution from the concrete suggested by the MCFT is not constant as assumed in the classical truss model. The shear contribution of the concrete (V_c) in the MCFT is not equal to the shear strength of a similar member without shear reinforcement. According to the MCFT, the contribution of the concrete is a function primarily of the crack width. Increasing the number of stirrups reduces the crack spacing, this decreases the crack width and thus increases the concrete contribution (Cladera, 2002).

One of the most important features of the MCFT is the average strain-stress relationships derived from the tests of reinforced panels subjected to pure shear (Vecchio and Collins, 1986). The concrete compressive strength is reduced to take into account softening due to transverse tensile strain (ε_1). Initially, a parabolic relationship for

cracked concrete in compression subjected to high tensile strains in the direction normal to the compression was suggested, as shown in **Equation 3-14**.

$$f_2 = f_{2,max} \left[2 \left(\frac{\varepsilon_2}{\varepsilon'_c} \right) - \left(\frac{\varepsilon_2}{\varepsilon'_c} \right)^2 \right] \tag{3-14}$$

where ε'_c is the strain in the concrete, and for the MCFT, $\beta = \frac{f_{2,max}}{f'_c} = \frac{1}{0.8 - 0.34 \frac{\varepsilon_1}{\varepsilon'_c}} \leq 1.0$

This relationship for the concrete softening (β) was derived for the MCFT in which the crack slip is not taken into account. According to Vecchio and Collins (1993), concrete strength can also have an influence in concrete softening. Moreover, size effects can also have an effect. For concrete in tension, the curve proposed in Vecchio and Collins (1986) is given by **Equations 3-15** and **3-16**.

$$\text{If } \varepsilon_1 \leq \varepsilon_{cr} \text{ then } f_1 = E_c \varepsilon_1 \tag{3-15}$$

$$\text{If } \varepsilon_1 > \varepsilon_{cr} \text{ then } f_1 = \frac{f_{cr}}{1 + \sqrt{200 \varepsilon_1}} \tag{3-16}$$

where ε_{cr} is the crack strain, E_c is the modulus of elasticity of the concrete, and f_{cr} is the stress in the concrete at cracking.

Equation 3-16 was updated by Vecchio and Collins (1993) to include two new parameters (α_1 and α_2) to account for the bond characteristics of the reinforcement and the type of loading. The updated equation is presented in **Equation 3-17**.

$$f_1 = \frac{\alpha_1 \alpha_2 f_{cr}}{1+\sqrt{500\varepsilon_1}} \tag{3-17}$$

where, $f_{cr} = 0.33\sqrt{f'_c}$

The stress and strain formulations adopted in the MCFT use average values, so local variations are not considered. In this methodology, a check must be done to ensure that the reinforcement can take the increment in tensile stress at the crack. In order to make this check, a value of the stress along the crack must be assumed. The shear transfer at the cracks by aggregate interlock action is estimated using the relationship in **Equation 3-18**. This equation was developed based on Walraven's (1980) experiments.

The MCFT can provide accurate predictions of shear strength and deformation. The first and most important assumption made in the MCFT is that of a rotating crack model in which previous cracks are assumed to be inactive. The MCFT assumes that the angles of the axes for the principal strains and principal stresses coincide (θ). The crack in which all the checks are performed is assumed to be oriented at the same angle, θ, as the compressive stress field.

$$v_{ci} = 0.18v_{ci,max} + 1.64f_{ci} - 0.82\frac{f_{ci}^2}{v_{ci,max}} \tag{3-18}$$

where, $v_{ci,max} = \frac{\sqrt{f'_c}}{0.31+\frac{24w}{a+16}}$

In the expression above, a is the maximum aggregate size in millimeters, and w is the average crack width over the crack surface which is estimated as the product of the

principal tensile strain (ε_1) and the crack spacing (s_θ). The spacing of shear cracks is

considered to be dependent on the crack spacing in the longitudinal and transverse

reinforcement directions. The crack spacing can be calculated by using **Equation 3-19**. In

this equation s_{mx} is the average spacing of cracks perpendicular to the longitudinal

reinforcement, and s_{mv} is the average spacing of cracks perpendicular to the transverse

reinforcement. Finally, s_{mx} and s_{mv} are estimated using the formulas given by

Equations 3-20 and **3-21**.

$$s_\theta = \frac{1}{\frac{\sin\theta}{s_{mx}} + \frac{\cos\theta}{s_{mv}}} \tag{3-19}$$

$$s_{mx} = 2\left(c_x + \frac{s_x}{10}\right) + 0.25k_1\frac{d_{bx}}{\rho_x} \tag{3-20}$$

$$s_{mv} = 2\left(c_y + \frac{s}{10}\right) + 0.25k_1\frac{d_{bv}}{\rho_v} \tag{3-21}$$

where c_x and c_y are the concrete covers for the longitudinal and transverse

reinforcement respectively; s_x and s are the spacing of the longitudinal and transverse

reinforcement respectively; d_{bx} and d_{bv} are the bar diameters of the longitudinal and

transverse reinforcement respectively; ρ_x and ρ_v are the ratios for the longitudinal and

transverse reinforcement respectively; and k_1 equals 0.4 for deformed bars and 0.8 for

plain bars.

The MCFT has been criticized from a practical perspective since it requires the

use of a computer in order to solve the system of equations. This problem was addressed

by Bentz and Collins by providing two free software packages, called RESPONSE 2000 and MEMBRANE 2000, to solve these equations.

Bentz et al. (2006) developed simplified versions of the MCFT which can be used in order to predict the maximum shear capacity rather than the complete load-deformation response. **Equations 3-22** and **3-23** present these expressions that are also incorporated in the Canadian Code CSA A23.3 (2004).

$$V_r = V_c + V_s \leq 0.25 \emptyset_c f'_c b_w d \qquad (3\text{-}22)$$

$$V_r = \emptyset_c \beta \sqrt{f'_c} b_w d + \emptyset_s \frac{A_{sw}}{s} f_y d \cot \theta \qquad (3\text{-}23)$$

where $\emptyset_c$ and $\emptyset_s$ are the capacity reduction factors, b_w is the width of the web, d is the effective shear depth ($d_v = 0.9d$), A_s is the area of longitudinal reinforcement on the flexural tension side. The parameter β represents the shear retention factor that can be defined as the ability of cracked concrete to transmit shear by means of aggregate interlock, while θ is the angle of inclination of the strut. These two parameters are estimated in terms of the longitudinal strain at the mid-depth of the section using **Equations 3-24** and **3-25**.

$$\beta = \frac{0.40}{1 + 1500\varepsilon_x} \cdot \frac{1300}{1000 + s_{xe}} \qquad (3\text{-}24)$$

$$\theta = 29 + 7000\varepsilon_x \qquad (3\text{-}25)$$

where, $\varepsilon_x = \dfrac{\frac{M_f}{d}+V_f}{2E_sA_{sl}}$

The parameters V_f and M_f are the factored shear force and moment at the section. The effective crack spacing (s_{xe}) is taken as 11.8 in. for members with at least minimum stirrups and for members without stirrups, $s_{xe} = \dfrac{35s_x}{15+a_g} \geq 0.85s_x$. The crack spacing parameter (s_x) is the longitudinal spacing between cracks, measured at mid-depth of the member. For members without horizontal reinforcement at the web, s_x is usually taken as d_v.

3.4.4. Fracture mechanics approach. Although fracture mechanics was developed by Griffith in 1920, for half a century, it was considered inappropriate for concrete. The reason that it took so long to apply this method to concrete is that the traditional fracture mechanics approach was developed for homogeneous materials, such as steel. However, the existence of a size effect observed in experimental results obtained during previous research (Bazant and Kim, 1984) prompted several researchers to apply fracture mechanics to shear failures. The use of fracture mechanics in design could increase the safety and reliability of concrete structures. Numerous analytical and numerical tools have been developed to simulate the fracture behavior of concrete structures, and in connection with these developments, researchers are focused on designing experimental methods to measure the different parameters required for these models. The ACI 446.1R (1999) document highlights five compelling reasons to use a fracture mechanics approach. The first one is the energy required for crack formation. This reason states that the actual formation of cracks requires energy, called fracture energy, which represents the surface energy of a solid. The second one is the objectivity

of the calculations. Any physical theory must be objective and the result of the calculations must not depend on subjective aspects such as choice of coordinates, mesh, etc. Objectivity should come ahead of experimental verification. The third reason is the lack of yield plateau. Based on load-deflection diagrams, there are two distinguishable basic types of structural failure, plastic and brittle. Plastic failures typically develop a single-degree-of-freedom mechanism such that the failure proceeds simultaneously in various parts of the structure. These failures are characterized by the presence of a long yield plateau on the load-deflection diagram. If this diagram does not have such a plateau, the failure is brittle or brittle-ductile. The fourth reason is capability to absorb energy, as related to ductility. The area under the complete load-deflection diagram represents the energy which the structure will absorb during failure, and this energy must be supplied by the loads. The current plastic limit analysis cannot give information on the post-peak decline of the load and energy dissipated in this process. The fifth and most compelling reason for using fracture mechanics is the size effect. ACI 446.1R (1999) defines the size effect through a comparison of geometrically similar structures of different sizes, characterized in terms of the nominal stress at maximum ultimate load. When this nominal stress does not change its value for geometrically similar structures of different sizes, it can be said that there is no size effect.

The study of fracture mechanics of concrete started in 1961 with Kaplan. Later, in 1972, Kesler et al. concluded that the classical linear elastic fracture mechanics (LEFM) approach with only one fracture parameter, either the fracture energy or the fracture toughness, was not applicable to concrete. Kesler et al. suggested at least two fracture parameters.

The simplest model that describes the progressive fracture process is the cohesive crack model (Hillerborg et al., 1976). Hillerborg et al. proposed the cohesive crack model for simulation of plain concrete, in which concrete fracture energy characterized the softening response of a cohesive crack that could develop anywhere in a concrete structure. The softening curve is the main feature of the cohesive crack model. This curve presents an initial portion with a steep descending slope, followed by a smooth drop when the stress reaches a value approximately equal to 1/3 of the nominal tensile strength (f'_t), and a long tail asymptotic to the horizontal axis (crack opening, w) as shown in **Figure 3.15**. Geometrically, the area under the complete curve represents the fracture energy. The fracture energy is defined as the amount of energy necessary to create a crack of unit surface area projected in a plane parallel to the crack direction.

Hillerborg (1985) provided a theoretical basis for a concrete fracture energy testing procedure, often referred to as the work-of-fracture method (WFM), in which the fracture energy per unit area of concrete is computed as the area under the experimental load-deflection response curve for a notched concrete beam subjected to three-point bending, divided by the area of fracture concrete.
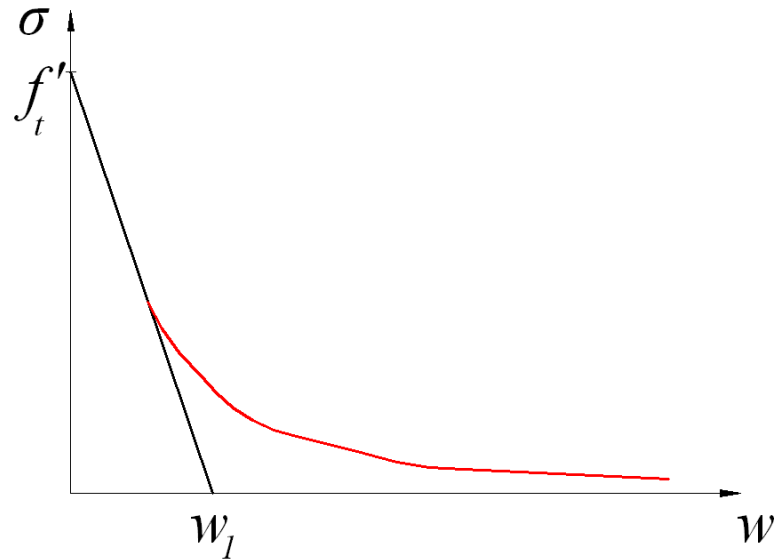
**Figure 3.15- Softening Function and Initial Tangent for Cohesive Crack
Model (Einsfeld and Velasco, 2006)**

For example, when conducting three-point bending tests on notched beams, as the
beam splits into two halves, the fracture energy (G_F) can be determined by dividing the
total dissipated energy by the total surface area of the crack as shown in **Equation 3-26**.

$$G_F = \frac{W}{b(d-a_0)}$$ (3-26)

where W is the total energy dissipated in the test, and b, d, and a_0 are the
thickness, height and notch depth of the beam, respectively.

Several additional test methods have been proposed in recent years to determine
concrete fracture properties from which fracture energy may be computed.

In 1987, Bazant and Pfeiffer concluded that the cohesive crack model results in
fracture characteristics that are ambiguous and size-dependent. As a consequence,
different values for the fracture energy could be obtained for specimens of different sizes.

Bazant and Pfeiffer proposed a method where the fracture energy is calculated based on the size effect law. In this approach, the fracture energy is independent of the size of the specimens. This asymptotic approach is known as the size effect method (SEM). Bazant and Pfeiffer suggested the following relationship shown in **Equation 3-27**.

$$\sigma_N = B(1 + \beta^k)^{\frac{1}{2k}} \qquad (3\text{-}27)$$

where σ_N is the nominal stress at failure, B is the coefficient obtained through the linear regression plot of the results, β is the brittleness number, and k is a parameter to reflect the size effect.

The brittleness number indicates whether the behavior of any structure is related to either the limit state analysis or to LEFM analysis. Bazant and Pfeiffer proposed **Equation 3-28** for the brittleness number.

$$\beta = \frac{d}{d_0} \qquad (3\text{-}28)$$

where d is the characteristic dimension of the structure (for their study, the specimen height), and d_0 is a coefficient determined experimentally. The coefficients B and d_0 are determined by linear regression. In this approach, specimens of different sizes but geometrically similar can be rearranged in a linear regression plot as shown in **Equation 3-29**. **Equations 3-30** to **3-33** present the different relationships for the parameters contained in **Equation 3-29**.

Rupture of a structure of infinite size follows the LEFM theory, since the plastic region around the concrete fracture zone is relatively small. In this case, the fracture energy can be calculated using **Equation 3-34**.

$$y = Ax + C \tag{3-29}$$

$$y = \left(\frac{1}{\sigma_N}\right)^2 \tag{3-30}$$

$$x = d \tag{3-31}$$

$$d_0 = \frac{C}{A} \tag{3-32}$$

$$B = \frac{1}{\sqrt{C}} \tag{3-33}$$

$$G_f = \frac{g_f(\alpha_0)}{AE} \tag{3-34}$$

where E is the modulus of elasticity of the concrete, A is the angular coefficient of the linear regression plot, $g_f(\alpha_0)$ is the non-dimensional energy release rate calculated according to LEFM, and α_0 is the relative notch length defined in **Equation 3-35**.

$$\alpha_0 = \frac{a_0}{d} \tag{3-35}$$

The fracture energy normally associated with WFM is different from the one calculated through SEM. They are usually differentiated as G_F for values calculated with WFM, and G_f for values calculated using SEM. The values obtained with WFM are

sensitive to the specimen size and shape. On the other hand, values obtained with SEM are independent of the structure size as well as geometry (Einsfeld and Velasco, 2006).

While G_F corresponds to the area under the complete softening stress-separation curve of the cohesive crack model, G_f corresponds to the area under the initial tangent of the stress-separation curve as shown in **Figure 3.16**.

Bazant and Kim (1984) and Bazant and Sun (1987) developed a set of equations to describe the dependence of the diagonal shear strength on the size, shape, and longitudinal reinforcement ratio of beams failing in diagonal shear. The shear strength in this model is assumed to result from the combination of the arching action and the composite beam action. The summation of the two components resulted on an expression similar to that of the ACI building code. However, this expression failed to explain the structural behavior.
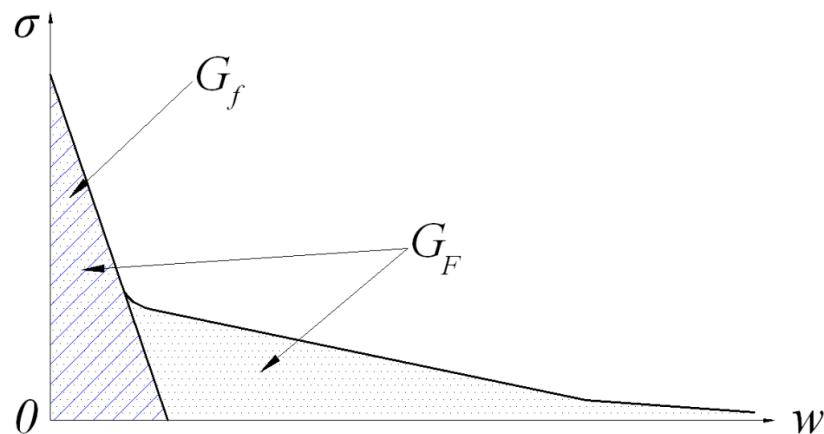
Figure 3.16- Softening Stress-Separation Curve of Cohesive Crack Model (Bazant and Becq-Giraudon, 2002)

Gustafsson and Hillerborg in 1988 investigated the diagonal shear strength of members without stirrups using the cohesive crack concept, with the objective to show that a size effect can be predicted theoretically. This model assumes that a single

polygonal cohesive crack with linear softening is formed, while the bulk of the concrete remains linear elastic. The behavior of the steel is assumed to be linear elastic. The failure criterion adopted is crushing of the concrete. Using this approach Gustafsson and Hillerborg analyzed the influence of the size, longitudinal reinforcement ratio, and the shear span-to-depth ratio.

Jenq and Shah (1989) adopted a more physical approach applying a two-parameter nonlinear fracture mechanics model to the shear failure. In this model, the ultimate shear capacity is assumed to be the summation of the contributions from the reinforcement and the concrete. The concrete contribution is derived using the fracture mechanics model. The steel contribution is estimated by considering the average ultimate bond stress, which is assumed to be proportional to the embedded length.

In 1993, So and Karihaloo criticized Jenq and Shah's approach pointing out that their approach was oversimplified and ignored the influence of the reinforcement on the fracture behavior of the concrete. Large discrepancy between the predicted and measured capacity confirmed their criticism. Khariloo introduced a failure criterion for longitudinal splitting using Van der Veen's model (Van der Veen, 1990) to derive the maximum bond stress. Finally, Karihaloo concluded that the bond-slip relationship, the dowel action, and the aggregate interlock must be taken into account to accurately predict the shear capacity using Jenq and Shah's approach. The only weak point of Karihaloo's model is the significant use of empirical equations.

In 2001, Gastebled and May proposed a fracture mechanics model for the flexural-shear failure of reinforced concrete beams without stirrups. This model was developed assuming that the ultimate shear load is reached when the splitting crack starts

to propagate. The critical load is calculated considering the energy balance of the system during splitting crack propagation. The position of the critical diagonal crack is obtained using Kim and White's semi-empirical formula proposed in 1991. Gastebled and May used the empirical formula for the assessment of the fracture energy proposed by the CEB-FIP Model Code.

The formulation of this model is based on the fundamental relation of LEFM presented in **Equation 3-36**, where G is the fracture energy consumption and W_{ext} is the work of the external force. The external load is produced by the rotation under constant load about the tip of the diagonal crack. In order to calculate the energy release, the rotational stiffness of the beam must be determined. This stiffness depends on the axial and dowel stiffness of the longitudinal reinforcement. The stiffness is calculated based on the free body diagram (FBD) presented in **Figure 3.17**.

$$\delta G = \frac{1}{2}\delta W_{ext} \tag{3-36}$$
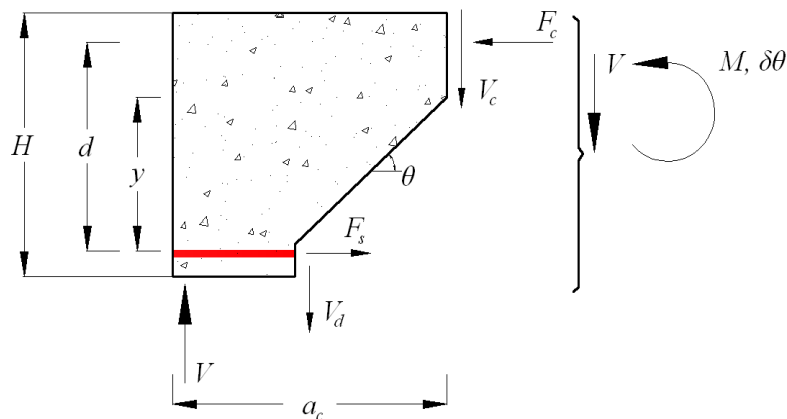
Figure 3.17- Free Body Diagram and Notation Definition (Gastebled and May, 2001)

The axial and shear force in the steel bar crossing the diagonal crack were linked to the angle of rotation (θ) using the elastic properties of the bar and the geometry of the deformation mechanism as shown in **Equation 3-37**. The beam bending theory for a circular cross section is also used to derive the dowel force as shown in **Equation 3-38**.

$$F_S = \frac{E_S A_S}{\delta_s} y\theta \tag{3-37}$$

$$V_d = \frac{G_S \Sigma_S}{\delta_s} y\theta = \frac{9}{26} \cdot \frac{E_S A_S}{\delta_s} y\theta \tag{3-38}$$

where F_s is the longitudinal reinforcement force, δ_s is the unbounded length of the reinforcement, y is the diagonal crack extent, θ is the rotation, V_d is the longitudinal reinforcement dowel force, G_s is the shear modulus of steel, and Σ_s is the reduced cross section of the bar (taken as $0.9A_s$).

The equilibrium of the FBD presented in **Figure 3.17** is reached when the following relationships shown in **Equations 3-39** to **3-41** are maintained (horizontal, vertical, and moment equilibrium, respectively). Assuming that the diagonal crack extent and the internal moment arm (jd) are proportional to the height of the beam as shown in **Equations 3-42** and **3-43**, **Equation 3-41** can be rewritten and is presented in **Equation 3-44**. **Equation 3-44** provides the rotational stiffness.

$$F_s = F_c \tag{3-39}$$

$$V_c + V_d = V \tag{3-40}$$

$$F_s jd + V_d y = V a_c \tag{3-41}$$

$$y = \beta H \tag{3-42}$$

$$jd = \gamma H \tag{3-43}$$

$$\beta \left(\frac{9}{26} \beta + \gamma \right) \frac{E_s A_s}{\delta_s} H^2 \theta = V a_c \tag{3-44}$$

After differentiating **Equation 3-44** and using the fundamental relation of fracture mechanics as a criterion for splitting failure as shown in **Equation 3-36**, **Equations 3-45** and **3-46** are derived to obtain the expression for the critical shear load.

$$a_c V_{cr} \delta \theta = 2 \Gamma \delta_e \tag{3-45}$$

$$V_{cr} = \sqrt{\frac{9}{13} + 2 \frac{\gamma}{\beta}} \cdot \frac{\beta H}{a_c} \cdot \sqrt{\Gamma A_s E_s} \tag{3-46}$$

where δ_e is the variation of the unbonded length, and Γ is the fracture energy necessary to extend the splitting crack by a unit length. For simplicity of calculations and based on experimental observations, γ and β can be taken as 0.9 and 0.8 respectively. The units for this model have been set as follows: V_{cr} in kN, Γ in kN-m/m, A_s in mm^2, and E_s in GPa.

This model uses the equation given by the CEB-FIP Model Code for the assessment of the fracture energy and is presented in **Equation 3-47**. The maximum aggregate size (d_{agg}) is assumed in Gastebled and May's model as 0.75 in. Based on all

the previous assumptions and assuming a dynamic mode of failure, **Equation 3-46** can be simplified and is presented in **Equation 3-48**.

$$G_f = \left(0.0469 d_{agg}^2 - 0.5 d_{agg} + 26\right)\left(\frac{f'_c}{10}\right)^{0.7} \qquad (3\text{-}47)$$

$$V_{cr} = 4.517 \cdot \frac{H}{a_c} \cdot (f'_c)^{0.35}\sqrt{A_s E_s b} \qquad (3\text{-}48)$$

The units for this model have been set as follows: V_{cr} in kN, f'_c in MPa, A_s in m^2, and E_s in GPa, and b in mm.

The only problem in this model is the determination of the location of the critical diagonal crack. Kim and White (1991) postulated the same failure mechanism and adopted a mixed approach, partly physical and partly empirical, to predict the flexural-shear cracking and the position of the critical diagonal crack. **Equation 3-49** presents the model to calculate the location of the critical diagonal crack.

$$a_c = k_3 a_s \left(\frac{\rho_s\left(\frac{d}{a_s}\right)^2}{\left(1-\sqrt{\rho_s}\right)^2}\right)^{\frac{1}{3}} \qquad (3\text{-}49)$$

where k_3 is an empirical coefficient determined through statistical analysis and has a value of 3.3, a_s is the shear span, ρ_s is the geometrical reinforcement ratio, and d is the effective depth of the beam. Limited experimental data was available to check the position of the critical diagonal crack, however, Kim and White found 14 experimental results to perform the statistical analysis and determine a value for the coefficient k_3. Significant scatter was reported by the authors.

The final expression is obtained by substituting **Equation 3-49** into **Equation 3-48** and is shown in **Equation 3-50**. In this expression, the first term corresponds to the size effect, the second term takes into account the slenderness of the beam, the third and fourth terms reflect the reinforcement ratio influence, and the fifth term corresponds to the influence of the concrete strength.

$$V_{cr} = \frac{1.109}{\sqrt{H}} \cdot \left(\frac{H}{a_s}\right)^{\frac{1}{3}} \cdot \left(1 - \sqrt{\rho_s}\right)^{\frac{2}{3}} \cdot \rho_s^{\frac{1}{6}} \cdot f'^{0.35}_c \cdot \sqrt{E_s} \cdot bH \qquad (3\text{-}50)$$

where H is the height of the beam, a_s is the shear span, ρ_s is the geometrical reinforcement ratio, f'_c is the concrete compressive strength, E_s is the steel modulus of elasticity, and b is the width of the beam.

Bazant and Becq-Giraudon (2002) formulated the empirical expression shown in **Equation 3-51** to compute fracture energy for specimens with rounded aggregate. This equation was calibrated using 161 RILEM work-of-fracture tests whereas the equation proposed by CEB-FIP was calibrated using much less data. Bazant and Becq-Giraudon also reported that G_F data computed from work-of-fracture testing have significantly more scatter than G_f data computed using other test methods and suggested that this scatter was due to errors in measurement of the tail of the load-displacement response curve.

$$G_f = 0.0143\alpha_0 \left(\frac{f'_c}{8.41}\right)^{0.40} \left(1 + \frac{D_{max}}{0.0763}\right)^{0.43} \left(\frac{w}{c}\right)^{-0.18} \qquad (3\text{-}51)$$

where α_0 is an aggregate shape factor ($\alpha_0 = 1$ for rounded aggregate, and $\alpha_0 = 1.12$ for angular aggregate), f'_c is the compressive strength of the concrete, D_{max}

is the maximum aggregate size, and $\frac{w}{c}$ is the water-to-cement ratio of the concrete. The

units of this model have been set as follows: f'_c in psi, and D_{max} in inches.

3.4.5. Truss model and modified compression field theory comparison. The

MCFT can be explained as a truss model in which the shear strength is the sum of the

steel and concrete contributions. The main difference from a classic truss model with

concrete contribution is that the concrete contribution in the MCFT is the vertical

component of the shear stress transferred across the crack (v_{ci}) and not the diagonal

cracking strength.

Cladera (2002) highlighted the main differences between the truss model and the

MCFT concrete contributions:

- The truss model concrete contribution is considered equal to the

shear strength of a similar beam without shear reinforcement. The MCFT takes

into account a concrete contribution based on the actual collapse mechanism of a

RC beam.

- The truss model concrete contribution does not vary with the

amount of the transverse reinforcement. The MCFT concrete contribution

depends on the crack width. The more shear reinforcement, the lesser the crack

width, and the greater the concrete contribution.

3.4.6. Summary of shear design. Shear design in structural concrete has been a

challenging topic for many years. The truss analogy first proposed by Ritter (1899) and

then improved by Mörsch (1902) has been a powerful tool up in understanding the shear

transfer mechanism in a RC beam. However, progress has been made since those early

truss models. Three different groups of approaches have been developed: (1) 45 degrees

truss model, (2) compression field theories, and (3) fracture mechanics approach. Predictions of the shear provided by these approaches have improved considerably from early formulations, which were based on empirical results. As reported by Collins et al. (2008), early design equations for shear have been proven to be unsafe since the experimental data used in calibrating the models corresponded to rather small specimens. The MCFT offers a rational approach in which the shear transmitted along the crack is limited according to the crack width and aggregate size. The STM which was developed by Schaich et al. (1987) is often claimed as a transparent method for designing and detailing discontinuity regions. It has been highlighted that the method requires several simplifications regarding geometry assumed for the truss elements or the effective strength of the struts. Finally, it is clear that several difficulties can be faced in developing a STM, such as uniqueness of the model, combinations with other load cases or dealing with statically indeterminate systems.

3.5. DESIGN CODES REVIEW

There are a variety of design code philosophies that can be found around the world for shear design. Some of these rely on empirical formulas for estimating the shear strength, such as the ACI 318-08 (2008), while others such as the AASHTO LRFD (2004) rely more on concrete models such as the MCFT. This section will detail three selected design codes.

3.5.1. American Concrete Institute, ACI 318-08. The ACI 318-08 method is most commonly used for shear design in the United States, and is based on a 45 degree truss model. The shear strength is based on an average shear stress distribution across the

entire cross section, and is composed of a concrete component (V_c) and a steel component (V_s). The basic equations for normal-weight, non-prestressed reinforced concrete are listed in **Equations 3-52** to **3-56**.

$$V_u \leq V_n = V_c + V_s \tag{3-52}$$

$$V_c = \left(1.9\sqrt{f'_c} + 2500\rho_w \frac{V_u d}{M_u}\right) b_w d \leq 3.5\sqrt{f'_c} b_w d \tag{3-53}$$

$$\text{Simplified version: } V_c = 2\sqrt{f'_c} b_w d \tag{3-54}$$

$$A_{v,min} = 0.75\sqrt{f'_c}\frac{b_w s}{f_{yt}} \geq 50\frac{b_w s}{f_{yt}} \tag{3-55}$$

$$V_s = \frac{A_v f_{yt} d}{s} \tag{3-56}$$

where, V_u is the factored shear force on the section, $\emptyset$ is the strength reduction factor equal to 0.75 and not shown in **Equation 3-52**, V_n is the nominal shear strength, $\rho_w = \frac{A_s}{b_w d}$, A_s is the area of longitudinal reinforcement, b_w is the width of the web, d is the distance from the extreme compression fiber to the center of gravity of the steel, M_u is the factored moment at the section, f'_c is the concrete compressive strength (psi), f_{yt} is the yield strength of the transverse reinforcement (psi), s is the spacing of the transverse reinforcement, and A_v is the area of shear reinforcement. The following condition must be maintained $\frac{V_u d}{M_u} \leq 1.0$

The ACI 318-08 presents a procedure for calculating the failure shear strength for concrete beams without shear reinforcement. The simplified method is presented in

Equation 3-54. Some research data indicate that **Equation 3-53** overestimates the

influence of f'_c and underestimates the influence of ρ_w and $\frac{V_u d}{M_u}$. This is why, for most

designs, it is convenient to assume that the second term of this equation equals to $0.1\sqrt{f'_c}$

and use **Equation 3-54** to calculate the shear contribution of the concrete.

3.5.2. AASHTO LRFD Bridge Design Specifications. The AASHTO LRFD

(2007) method is known as the Sectional Design Model, and is based on the MCFT. The

nominal shear resistance (V_n) can be computed by **Equations 3-57** to **3-61**.

$$V_n = V_c + V_s + V_p \tag{3-57}$$

$$V_{n,max} = 0.25 f'_c b_v d_v + V_p \tag{3-58}$$

$$V_c = 0.0316\beta\sqrt{f'_c}b_v d_v \tag{3-59}$$

$$V_s = \frac{A_v f_y d_v \cot\theta}{s} \tag{3-60}$$

$$A_{v,min} \geq 0.0316\sqrt{f'_c}\frac{b_v s}{f_y} \tag{3-61}$$

where, V_p is the vertical component of the prestressing force, b_v is the effective

width of the web taken as the minimum web width within the depth, d_v is the effective

shear depth taken as the greater of $0.9d$ or $0.72h$, β is the factor indicating the ability of

diagonal cracked concrete to transmit tension, θ is the angle of inclination of the diagonal

compressive struts, f'_c is the concrete compressive strength (ksi), and f_y is the yield

strength of the transverse reinforcement (ksi).

For sections containing at least the minimum amount of transverse reinforcement, the values of β and θ may be found using **Table 3.1**. The designer selects the row corresponding to the shear design stress ratio $\frac{v}{f'_c} = \frac{V_u}{b_v d_v f'_c}$, and selects the column corresponding to the longitudinal strain (ε_x) at mid-depth. The longitudinal strain may be computed using **Equation 3-62**.

Table 3.1- Values of θ and β for Sections With Transverse Reinforcement
(AASHTO LRFD, 2004)

$\frac{V_u}{f'_c}$		$\leq$ -0.20	$\leq$ -0.10	$\leq$ -0.05	≤ 0	≤ 0.125	≤ 0.25	≤ 0.50	≤ 0.75	≤ 1.00	≤ 1.50	≤ 2.00
							$\varepsilon_x \times 1000$					
≤ 0.075	θ	22.3°	20.4°	21.0°	21.8°	24.3°	26.6°	30.5°	33.7°	36.4°	40.8°	43.9°
	β	6.32	4.75	4.10	3.75	3.24	2.94	2.59	2.38	2.23	1.95	1.67
≤ 0.100	θ	18.1°	20.4°	21.4°	22.5°	24.9°	27.1°	30.8°	34.0°	36.7°	40.8°	43.1°
	β	3.79	3.38	3.24	3.14	2.91	2.75	2.50	2.32	2.18	1.93	1.69
≤ 0.125	θ	19.9°	21.9°	22.8°	23.7°	25.9°	27.9°	31.4°	34.4°	37.0°	41.0°	43.2°
	β	3.18	2.99	2.94	2.87	2.74	2.62	2.42	2.26	2.13	1.90	1.67
≤ 0.150	θ	21.6°	23.3°	24.2°	25.0°	26.9°	28.8°	32.1°	34.9°	37.3°	40.5°	42.8°
	β	2.88	2.79	2.78	2.72	2.60	2.52	2.36	2.21	2.08	1.82	1.61
≤ 0.175	θ	23.2°	24.7°	25.5°	26.2°	28.0°	29.7°	32.7°	35.2°	36.8°	39.7°	42.2°
	β	2.73	2.66	2.65	2.60	2.52	2.44	2.28	2.14	1.96	1.71	1.54
≤ 0.200	θ	24.7°	26.1°	26.7°	27.4°	29.0°	30.6°	32.8°	34.5°	36.1°	39.2°	41.7°
	β	2.63	2.59	2.52	2.51	2.43	2.37	2.14	1.94	1.79	1.61	1.47
≤ 0.225	θ	26.1°	27.3°	27.9°	28.5°	30.0°	30.8°	32.3°	34.0°	35.7°	38.8°	41.4°
	β	2.53	2.45	2.42	2.40	2.34	2.14	1.86	1.73	1.64	1.51	1.39
≤ 0.250	θ	27.5°	28.6°	29.1°	29.7°	30.6°	31.3°	32.8°	34.3°	35.8°	38.6°	41.2°
	β	2.39	2.39	2.33	2.33	2.12	1.93	1.70	1.58	1.50	1.38	1.29

$$\varepsilon_x = \frac{\frac{M_u}{d_v}+0.5N_u+0.5(V_u-V_p)\cot\theta-A_{ps}f_{po}}{2(E_sA_s+E_pA_p)} \tag{3-62}$$

For sections containing less than the minimum amount of transverse reinforcement, the values of β and θ may be found using **Table 3.2**. The designer selects the row corresponding to an equivalent spacing parameter (s_{xe}), and selects the column

corresponding to the longitudinal strain at mid-depth. The equivalent spacing may be computed using **Equation 3-63**. The longitudinal strain for this case may be computed using **Equation 3-64**.

Table 3.2- Values of θ and β for Sections With Less Than Minimum Transverse Reinforcement (AASHTO LRFD, 2004)

s_{xe} (in.)		$\varepsilon_x \times 1000$										
		≤ -0.20	≤ -0.10	≤ -0.05	≤0	≤0.125	≤0.25	≤0.50	≤0.75	≤1.00	≤1.50	≤2.00
≤ 5	θ	25.4°	25.5°	25.9°	26.4°	27.7°	28.9°	30.9°	32.4°	33.7°	35.6°	37.2°
	β	6.36	6.06	5.56	5.15	4.41	3.91	3.26	2.86	2.58	2.21	1.96
≤ 10	θ	27.6°	27.6°	28.3°	29.3°	31.6°	33.5°	36.3°	38.4°	40.1°	42.7°	44.7°
	β	5.78	5.78	5.38	4.89	4.05	3.52	2.88	2.50	2.23	1.88	1.65
≤ 15	θ	29.5°	29.5°	29.7°	31.1°	34.1°	36.5°	39.9°	42.4°	44.4°	47.4°	49.7°
	β	5.34	5.34	5.27	4.73	3.82	3.28	2.64	2.26	2.01	1.68	1.46
≤ 20	θ	31.2°	31.2°	31.2°	32.3°	36.0°	38.8°	42.7°	45.5°	47.6°	50.9°	53.4°
	β	4.99	4.99	4.99	4.61	3.65	3.09	2.46	2.09	1.85	1.52	1.31
≤ 30	θ	34.1°	34.1°	34.1°	34.2°	38.9°	42.3°	46.9°	50.1°	52.6°	56.3°	59.0°
	β	4.46	4.46	4.46	4.43	3.39	2.82	2.19	1.84	1.60	1.30	1.10
≤ 40	θ	36.6°	36.6°	36.6°	36.6°	41.2°	45.0°	50.2°	53.7°	56.3°	60.2°	63.0°
	β	4.06	4.06	4.06	4.06	3.20	2.62	2.00	1.66	1.43	1.14	0.95
≤ 60	θ	40.8°	40.8°	40.8°	40.8°	44.5°	49.2°	55.1°	58.9°	61.8°	65.8°	68.6°
	β	3.50	3.50	3.50	3.50	2.92	2.32	1.72	1.40	1.18	0.92	0.75
≤ 80	θ	44.3°	44.3°	44.3°	44.3°	47.1°	52.3°	58.7°	62.8°	65.7°	69.7°	72.4°
	β	3.10	3.10	3.10	3.10	2.71	2.11	1.52	1.21	1.01	0.76	0.62

$$S_{xe} = \frac{1.38 s_x}{a_g + 0.63} \tag{3-63}$$

$$\varepsilon_x = \frac{\frac{M_u}{d_v} + 0.5 N_u + 0.5 (V_u - V_p) \cot\theta - A_{ps} f_{po}}{E_s A_s + E_p A_p} \tag{3-64}$$

If either value computed for ε_x is negative, the user should use **Equation 3-65** to compute the longitudinal steel strain instead.

$$\varepsilon_x = \frac{\frac{M_u}{d_v}+0.5N_u+0.5(V_u-V_p)\cot\theta-A_{ps}f_{po}}{2(E_cA_c+E_sA_s+E_pA_p)} \qquad (3\text{-}65)$$

where, A_c is the area of concrete on the flexural tension side, A_p is the area of

prestressing steel on the flexural tension side, A_s is the area of non-prestressed steel on

the flexural tension side, f_{po} is computed by the modulus of elasticity of the prestressing

tendons (E_p) times the locked difference in strain at ultimate load between the

prestressing tendons and the surrounding concrete, N_u is the factored axial force, s_x is the

crack spacing parameter, and a_g is the maximum aggregate size in inches.

A simplified procedure is presented in the AASHTO LRFD (2007) where the

values of β and θ can be calculated using the following expressions shown in **Equations**

3-66 and **3.67**. The parameter s_{xe} can be calculated using **Equation 3-63**.

$$\beta = \frac{4.8}{1+750\varepsilon_x} \cdot \frac{51}{39+s_{xe}} \qquad (3\text{-}66)$$

$$\theta = 29 + 3500\varepsilon_x \qquad (3\text{-}67)$$

3.5.3. Canadian Standards Association, CSA A23.3-04. The Canadian

Standards Association method, also based on MCFT, gives the following **Equations 3-68**

to **3-76** to calculate the shear strength of a section using their general method. Note that

the equations are given in psi and in. units, with the same notation defined in previous

sections.

$$V_n = V_c + V_s + V_p \qquad (3\text{-}68)$$

$$V_{n,max} = 0.25f'_cb_vd_v + V_p \qquad (3\text{-}69)$$

$$V_c = \beta \sqrt{f'_c} b_v d_v \qquad (3\text{-}70)$$

$$\beta = \frac{0.40}{1+1500\varepsilon_x} \cdot \frac{1300}{1000+s_{ze}} \qquad (3\text{-}71)$$

$$s_{ze} = \frac{35s_z}{15+a_g} \qquad (3\text{-}72)$$

The term a_g should be taken as zero if f'_c exceeds 10,150 psi. The crack spacing parameter s_z can be taken as d_v or as the maximum distance between layers of distributed longitudinal reinforcement, whichever is less. Each layer of reinforcement must have an area at least equal to $0.003b_v s_z$. However, $s_{ze} \geq 0.85s_z$.

$$\varepsilon_x = \frac{\frac{M_u}{d_v}+0.5N_u+V_u-V_p-A_{ps}f_{po}}{2(E_s A_s+E_p A_p)} \qquad (3\text{-}73)$$

$$V_s = \frac{A_v f_y d_v \cot\theta}{s} \qquad (3\text{-}74)$$

$$\theta = 29 + 7000\varepsilon_x \qquad (3\text{-}75)$$

$$A_{v,min} \geq 0.06\sqrt{f'_c}\frac{b_v s}{f_y} \qquad (3\text{-}76)$$

4. EXPERIMENTAL PROGRAM

4.1. GENERAL

The objective of this study was to investigate the shear performance of reinforced concrete (RC) beams composed of high-volume fly ash (HVFA) concrete. The experimental program consisted of 32 tests performed on full-scale RC beams. The principal parameters investigated were:

(1) concrete type – HVFA concrete or conventional concrete (CC),

(2) total amount of cementitious material – with one mix having a relatively high total cementitious content and the other mix having a relatively low total cementitious content,

(3) amount of longitudinal reinforcement, and

(4) amount of shear reinforcement.

Also, as part of this study, small scale testing was performed to determine hardened concrete properties such as compressive strength, flexural strength, splitting tensile strength, and modulus of elasticity.

4.2. TEST BEAMS

The reinforcement for the beams was designed in accordance with the AASHTO LRFD Bridge Design Specifications (AASHTO LRFD, 2007). Each beam measured 14 ft. in length with a cross section of 12 in. x 18 in. The cross section was selected to maintain a slender beam with a shear span-to-depth ratio larger than 3.0, thus avoiding any deep beam effects. The longitudinal reinforcement was selected to ensure a shear failure prior to a flexural failure yet still remain below the maximum amount allowed by

code. Each beam had two test regions, with each region measuring approximately 4 ft. in length. All of the specimens had #3 stirrups spaced at 2 in. within the bearing area to prevent premature failure as well as #3 stirrups spaced at 7 in. within the middle region to support the reinforcing cage and prevent any premature failure outside of the shear test regions. For the shear specimens with transverse reinforcement, the shear reinforcing consisted of #3 stirrups spaced at 7 in.

Table 4.1 summarizes the test matrix used in this study. The beam designation included a combination of letters and numbers: NS and S stand for no stirrups and stirrups, respectively, within the test region. The numbers 4, 5, 6, and 8 indicate the number of #7 longitudinal reinforcement bars within the tension area of the beam section. For example, NS-6 indicates a beam with no stirrups and 6 #7 bars within the bottom of the beam. Two beams were constructed and tested for each combination of variables shown in **Table 4.1**. The cross sections for these specimens are shown in **Figure 4.1**. **Figure 4.2** shows the load pattern and location of strain gauges on the test beams.

Table 4.1- Shear Beam Test Matrix

Cementitious Content	Section	Bottom reinforcement	Top reinforcement	ρ	Stirrups
High	NS-5	5#7	4#4	0.0159	-
	NS-6	6#7	4#4	0.0203	-
	NS-8	8#7	4#4	0.0271	-
	S-8	8#7	4#4	0.0271	#3@7 in.
Low	NS-4	4#7	2#4	0.0127	-
	NS-6	6#7	2#4	0.0203	-
	NS-8	8#7	2#7	0.0271	-
	S-8	8#7	2#7	0.0271	#3@7 in.

4#4   4#4   4#4

5#7   6#7   8#7

NS-5   NS-6   NS-8 & S-8
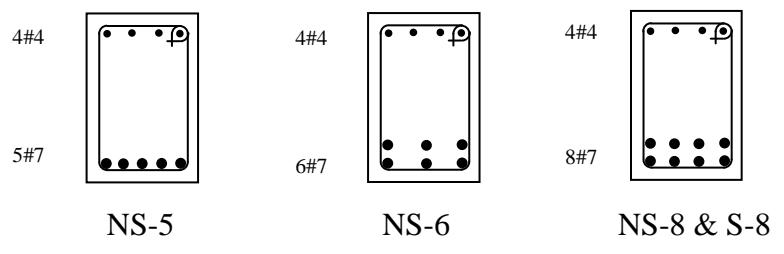
a) Sections used for High Cementitious Content Mix

2#4   2#4   2#4

4#7   6#7   8#7

-8
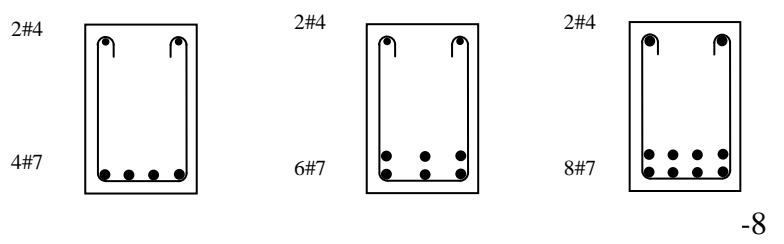
b) Sections used for Low Cementitious Content Mix

Figure 4.1- Cross Sections and Reinforcement Layout of the Beams

a) Without stirrups in test region

b) With stirrups in test region
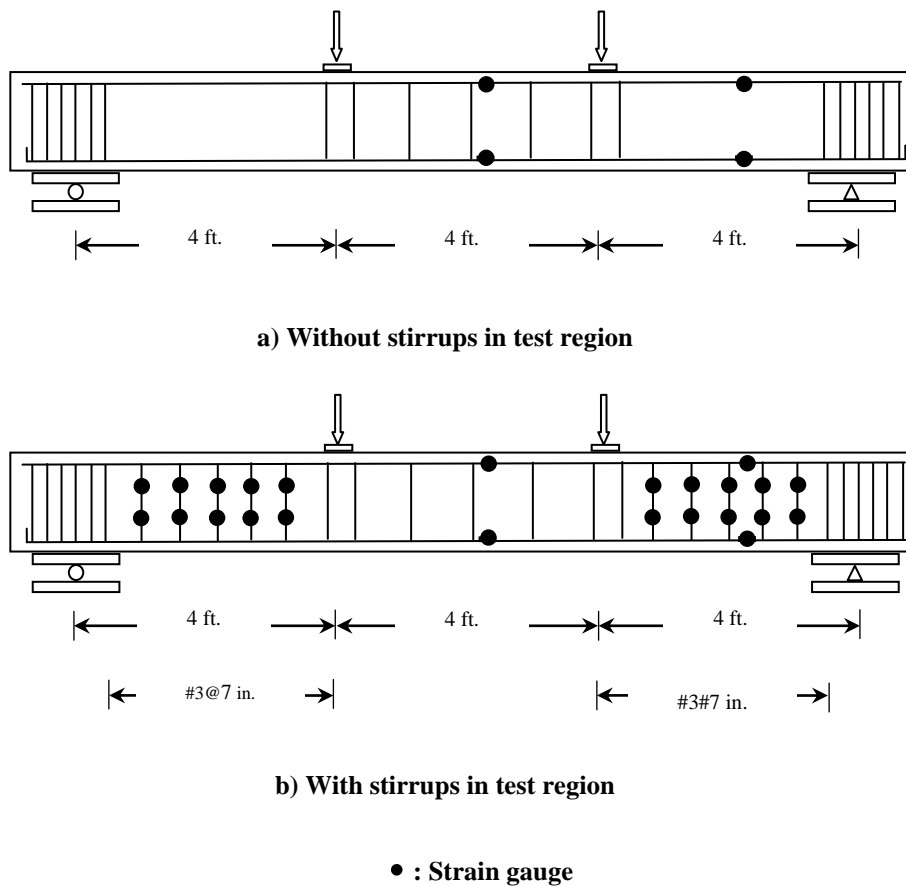
● **: Strain gauge**

Figure 4.2 – Load Pattern and Location of Strain Gauges on the Test Beams

4.3. MATERIALS

4.3.1. Concrete. The concrete mixtures with a target compressive strength of 4000 psi were delivered by a local ready-mix concrete supplier (Rolla, MO). The purpose of using the ready-mix supplier was to validate the HVFA concrete concept in actual production runs. The mixture proportions are given in **Table 4.2**. The design of the mixes was based on significant input from MoDOT as well as results of previous research conducted at Missouri S&T. The HVFA concrete mixes used a 70% replacement of cement with fly ash – with one mix containing a relatively high total cementitious content

(756 lb/yd^3) and the other mix containing a relatively low total cementitious content (564

lb/yd^3). In addition to the HVFA concrete mix designs, two conventional concrete (CC)

mix designs were used for comparison, which were identical to the HVFA concrete mixes

except they used 100% Portland cement for the binder. The notation for the mix designs

consisted of CC-H and HVFA-70H for the high cementitious content conventional and

HVFA concrete mixes, respectively, and CC-L and HVFA-70L for the low cementitious

content conventional and HVFA concrete mixes, respectively.

Table 4.2- Mix Designs per Cubic Yard

	CC-H	HVFA-70H	CC-L	HVFA-70L
Cement (Type I) (lb)	756	219	564	155
Fly Ash (lb)	0	511	0	360
w/cm	0.45	0.40	0.40	0.40
Coarse Aggregate (lb)	1750	1754	1860	1860
Fine Aggregate (lb)	1110	1080	1240	1240
HRWR (fl. oz)	0	0	16.9	15.5
CaOH (lb)	0	51	0	39
Gypsum (lb)	0	21	0	16

For the HVFA concrete mixes, the gypsum was used to maintain the initial

hydration stage by preventing sulfate depletion, while the calcium hydroxide ensured a

more complete hydration of the fly ash with the low content of Portland cement in the

mix. The drums were charged at the ready-mix facility with the required amounts of

cement, fly ash, sand, coarse aggregate, and water, while the powder activators (gypsum

and lime) were added when the truck arrived at the lab, approximately 5 minutes later, as

shown in **Figure 4.3**. After the gypsum and lime were added, the HVFA concrete was

mixed at high speed for 10 minutes. For the CC mixes, all of the constituents were added

at the ready-mix facility. **Table 4.3** presents representative fresh and hardened strength

properties of the CC and HVFA concrete mixes.

Table 4.3- Typical Fresh and Hardened Concrete Properties for CC and HVFA Concrete Mixes

Property	CC-H	HVFA-70H	CC-L	HVFA-70L
Slump (in.)	4.5	5	4.5	5.5
Air content (%)	1.5	1.5	2.5	2.5
Unit weight (lb/ft^3)	149	146	144	147
Split cylinder strength (psi)	480	380	420	410
Compressive strength (psi)	5010	3540	4200	4450

(a) Adding gypsum

(b) Adding calcium hydroxide

(c) Concrete placement

Figure 4.3- HVFA Concrete Mixing Procedures

4.3.2. Steel reinforcement. Shear reinforcement for the test specimens consisted of A615, Grade 60 #3 reinforcing bars. Longitudinal reinforcement for the test specimens consisted of A615, Grade 60 #4 and #7reinforcing bars. All the steel reinforcement was tested in accordance with ASTM A370 (2011) "Standard Test Methods and Definitions for Mechanical Testing of Steel Products" to obtain the mechanical properties, which are summarized in **Table 4.4**. These results are the average of three replicate specimens.

4.4. BEAM FABRICATION

All the test beams were fabricated in the Structural Engineering High-Bay Research Laboratory (SERL) at Missouri S&T. Steel formwork was used to cast the beams. The steel cage was assembled from reinforcement that was bent in the laboratory to the desired geometry. Due to the dimension of the beams, it was possible to cast three beams at a time. After casting, the top surface of the beams was covered with burlap and plastic sheeting, and a wet surface was maintained for three days to retain moisture for proper curing. Cylinders were cured in the same environment as the test beams by placing them next to the beams. The sheeting and burlap were then removed, and the beams were allowed to air cure in the lab environment. Photographs showing the reinforcing cages and the construction process are shown in **Figures 4.4** and **4.5**.

Table 4.4- Mechanical Properties of Steel Reinforcement

Bar size	Yield strength (psi)
#3	67,740
#4	67,970
#7	69,380
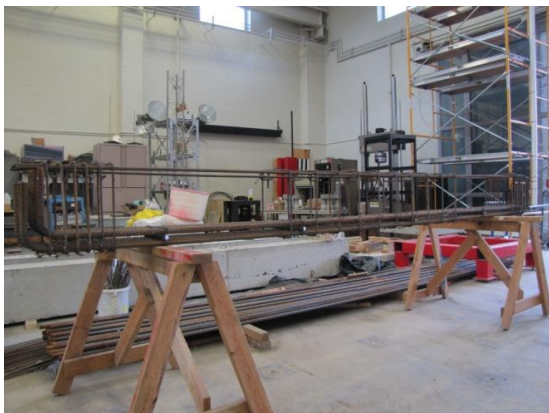
(a) Beams with no stirrups in test region

(b) Beams with no stirrups in test region

(c) Beams with stirrups in test region

(d) Beams with stirrups in test region

Figure 4.4- Reinforcing Cage Assembly

(a) Formwork

(b) Concrete placement
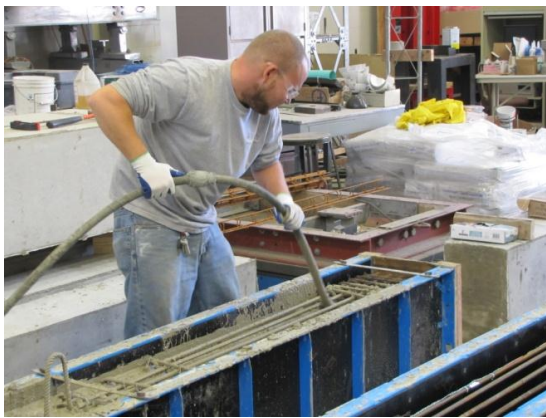
(c) Concrete consolidation

(d) Concrete finishing

Figure 4.5- Beam Construction Process

4.5. TEST SET-UP

All the specimens were tested as simply supported and subjected to a four-point loading. The maximum compression capacity of the actuators available in SERL, when working individually, were insufficient to cause specimen failure. Therefore, the test set-up required the simultaneous action of two actuators as shown in **Figure 4.6**.
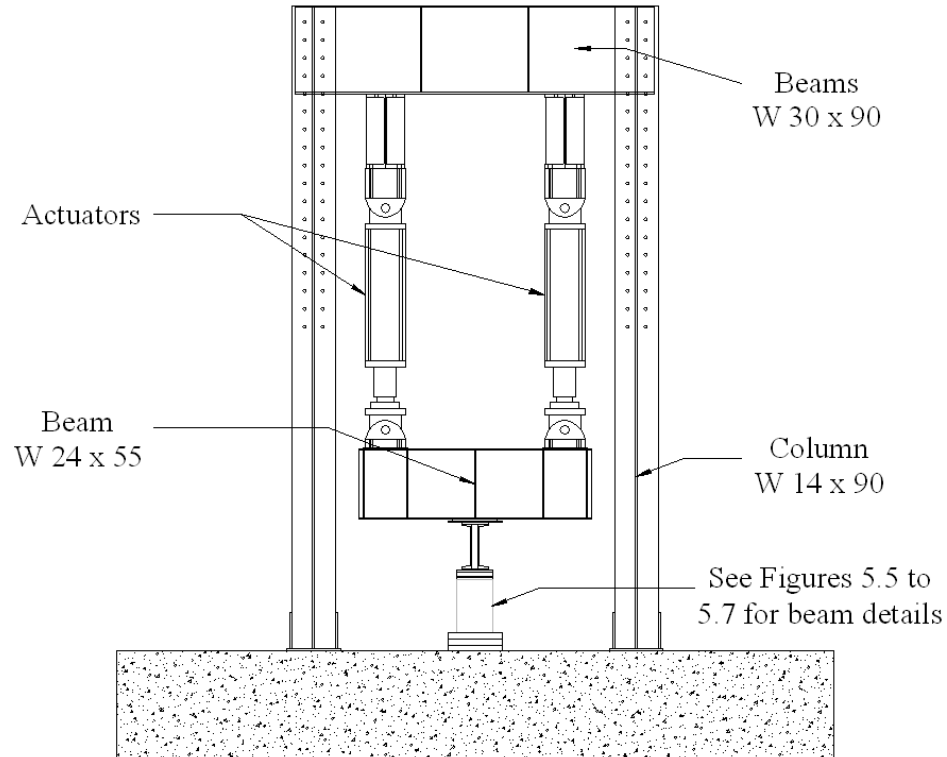
Figure 4.6- Details of Test Set-Up (1)

Two actuators, each with a 140-kip compressive capacity, were used to apply load to the beam specimens, as shown in **Figure 4.7**. The actuators applied load by pushing the steel beam downward to distribute the load onto two points of the test specimen. The loading frame assembly was designed to withstand at least two times the anticipated maximum load applied to fail the beams. Each test was performed under displacement control, and the load was applied in a series of loading steps of 0.05 in., which corresponded to a load of approximately 8 kips, until failure. Electronic measurements of strain and deformation were recorded throughout the entire loading history of the specimens, while hand measurements of strain and crack pattern formations were taken at the end of each load step while the load was paused. Each beam consisted of two test regions. The total beam length was 14 ft, with a simply supported span length of 12 ft.

The load was applied at 4 ft from each support, representing a shear span-to-depth ratio between 3.00 and 3.30 depending on the specimen, as measured from center of support to center of load. **Figure 4.8** shows a photograph of the test set-up.
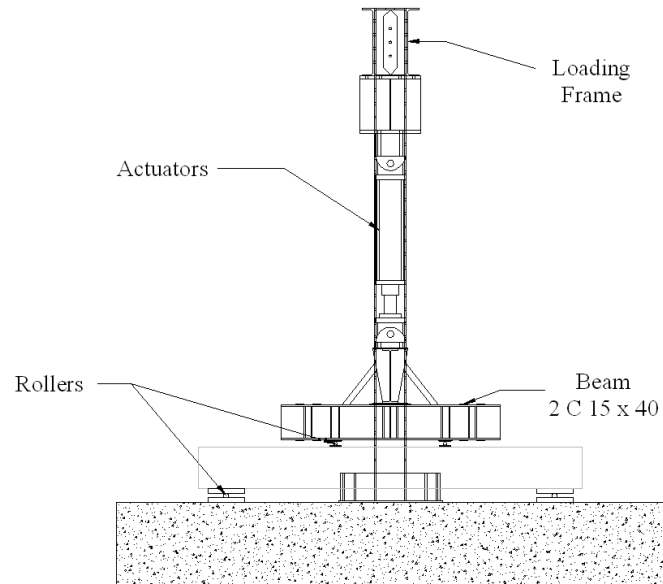
Figure 4.7- Details of Test Set-Up (2)
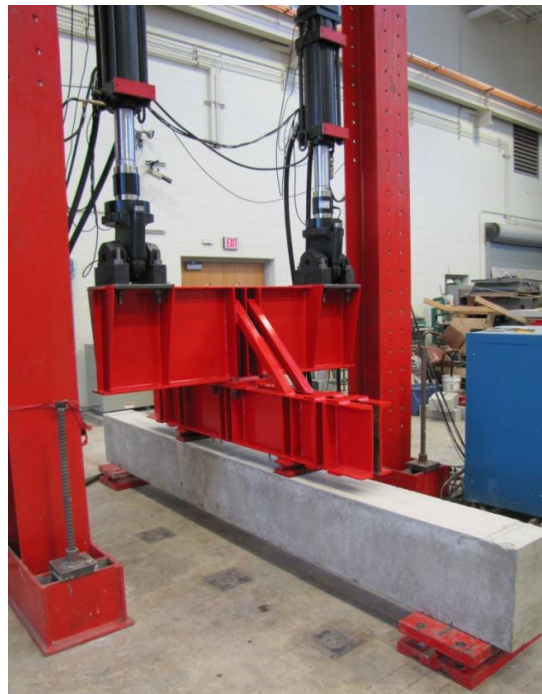
Figure 4.8- Test Set-Up

4.6. INSTRUMENTATION

      The specimens were instrumented with several measurement devices in order to monitor global and local deformations and strains. The load was directly measured from the load cell of the actuators. All devices were connected to a data acquisition system capable of reading up to 120 channels and all the data was recorded as shown in **Figure 4.9.**

Figure 4.9- Data Acquisition System

      4.6.1. Local deformations and strains. Electric resistance gauges were used to monitor local strains in the stirrups of the test region. The strain gauges were purchased from Vishay Precision Group. They were made of constantan foil with 120 ohm resistance and had a linear pattern (uniaxial) with a gauge length of ¼ in. Two strain

gauges were installed on each stirrup in the test region as shown in **Figure 4.2.** The strain

values obtained from the strain gauges are localized measurements at the point where the

gauge is installed. The location of the strain gauges in the transverse reinforcement was

chosen to account for the unpredictability of the crack formation. The strain gauge pattern

was designed to better capture measurements along the cracks. In addition, strain gauges

were placed at various locations along the longitudinal tension and compression

reinforcement so that the strain distribution diagrams could be constructed along the

height of the cross section at various locations. The first one was located at the midpoint

of the shear test region, while the second was located at mid-span.

     4.6.2. Global deformations. One Linear Variable Displacement Transducer

(LVDT) was used to monitor vertical deflection of the test specimen. The LVDT was

located at the midpoint of the test specimen, 3 in. from the top of the beam as shown in

Figures 4.10 and **4.11**.
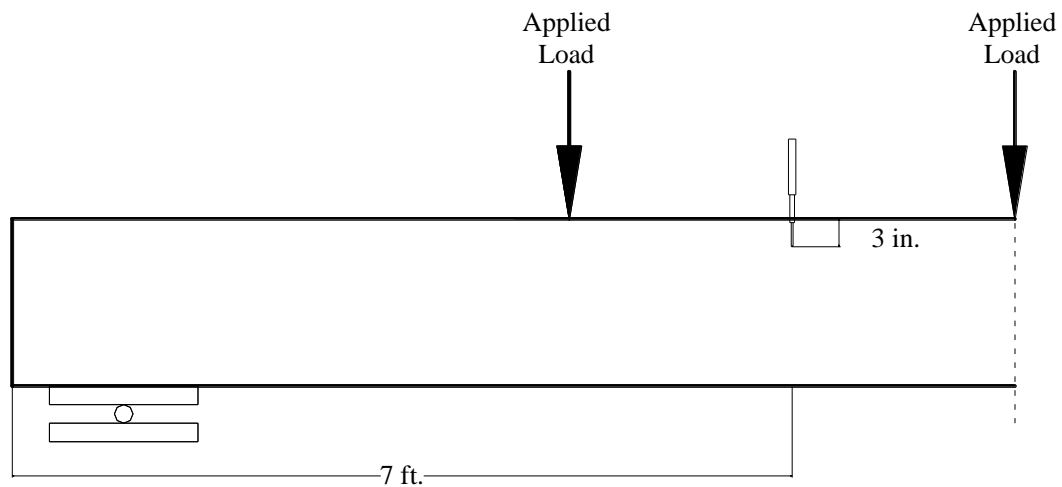
Figure 4.10- Location of LVDT to Measure Deflection

Figure 4.11- Detail of LVDT for Deflection Measurement

5. TEST RESULTS, BEHAVIOR & ANALYSIS

5.1. GENERAL

The purpose of this study was to evaluate the shear behavior of full-scale reinforced concrete (RC) beams constructed from high-volume fly ash (HVFA) concrete, which has not been fully investigated in previous research studies. The objectives of this section are to: (1) discuss the overall behavior of the specimens, (2) discuss the crack morphology and progression, (3) discuss the load-deflection response, (4) evaluate the failure mechanism including critical crack angle and reinforcement strains, (5) compare the test results with predicted capacities based on applicable design standards, (6) compare the HVFA concrete test results with the control specimen results, and (7) compare the test results with a shear test database of conventional concrete specimens.

5.2. TEST RESULTS & BEHAVIOR OF FULL-SCALE SPECIMENS

Table 5.1 summarizes the compressive strength at time of testing, shear force at failure, V_{test}, average shear stress at failure, $V_{test}/b_w d$, ratio of the average shear stress to compressive strength, and ratio of the average shear stress to square root of the compressive strength, $v_{test}/\sqrt{f'c}$. The average shear stress of the CC beams varies from 3.4% to 5.6% of the compressive strength for the low cementitious mix and from 3.4% to 4.8% of the compressive strength for the high cementitious mix. However, for the HVFA concrete beams, the average shear stress increased to 4.4% to 6.8% of the compressive strength for the low cementitious mix and 3.6% to 8.5% of the compressive strength for the high cementitious mix. Another useful comparison is to compare the last column in

Table 5.1 with ACI 318 (2008) Equation 11-3, rewritten in terms of average shear stress for normal weight concrete and shown as **Equation 5-1**. The ratio of experimental shear stress to square root of compressive strength for the beams without stirrups exceeded the ACI coefficient of 2 for all of the beams tested, both CC and HVFA concrete, even at low longitudinal reinforcement ratios.

$$v_c = 2\sqrt{f_c'} \tag{5-1}$$

In addition to studying the behavior of the specimens, the crack patterns experienced by the beams were also evaluated. During testing, cracks within the test region were marked using a permanent marker after each load step. Typical crack pattern progressions are shown in **Figures 5.1** and **5.2** for specimens without and with transverse reinforcement, respectively. Furthermore **Figures 5.3** and **5.4** show the crack pattern for the CC and HVFA concrete beams with different percentages of longitudinal reinforcement, respectively. For both cases, cracks typically began on the tension face of the beam near the loading points. As the loading progressed, the flexural cracks in the shear test region formed inclined flexure-shear cracks. For the specimens with transverse reinforcement, it was observed that at failure, the cracks were typically spaced approximately the same distance as the stirrups, and failure occurred on one side of the beam. For the specimens without transverse reinforcement, the formation of the inclined flexure-shear crack did not result in immediate failure, and additional load was required prior to failure. In general, the failure crack typically extended from the beam support to the loading point on the top side of the beam.

Table 5.1- Test results summary

Mix Design	Section		f_c' psi	V^*_{test} kips	$v_{test}=V_{test}/b_w d$ psi	v_{test}/f_c' %	$v_{test}/\sqrt{f_c'}$
CC-H	NS-5	1	5010	31.6	167.8	3.4	2.4
		2	4640	31.0	164.5	3.6	2.4
	NS-6	1	5010	39.1	220.1	4.4	3.1
		2	4640	32.3	182.5	3.9	2.7
	NS-8	1	5010	49.3	278.5	5.6	3.9
		2	4640	33.0	186.4	4.0	2.7
	S-8	1	5020	82.7	467.2	-	-
		2	5020	79.2	447.5	-	-
HVFA-70H	NS-5	1	3190	31.6	167.7	4.8	3.0
		2	3130	25.8	136.9	4.4	2.4
	NS-6	1	3190	29.7	167.8	5.2	3.0
		2	3130	27.3	154.2	4.9	2.8
	NS-8	1	3190	38.4	216.9	6.8	3.8
		2	3130	36.6	206.8	6.6	3.7
	S-8	1	3540	73.9	417.5	-	-
		2	3540	74.8	422.6	-	-
CC-L	NS-4	1	4200	26.9	142.8	3.4	2.2
		2	3840	25.6	135.9	3.5	2.2
	NS-6	1	4200	34.5	194.9	4.6	3.0
		2	3840	32.5	183.6	4.8	3.0
	NS-8	1	4200	33.2	187.5	4.5	2.9
		2	3840	32.3	182.5	4.8	2.9
	S-8	1	4400	67.4	380.8	-	-
		2	4400	71.9	406.2	-	-
HVFA-70L	NS-4	1	4450	30.2	160.3	3.6	2.4
		2	3000	27.6	146.5	4.9	2.7
	NS-6	1	4450	33.8	191.0	4.3	2.9
		2	3000	37.8	213.6	7.1	3.9
	NS-8	1	4450	36.5	206.2	4.6	3.1
		2	3000	45.3	255.9	8.5	4.7
	S-8	1	5030	73.9	417.5	-	-
		2	5030	75.8	428.2	-	-

[*]: Includes part of the load frame not registered by the load cells and also the beam self weight at a distance d from the interior face of the support plate.
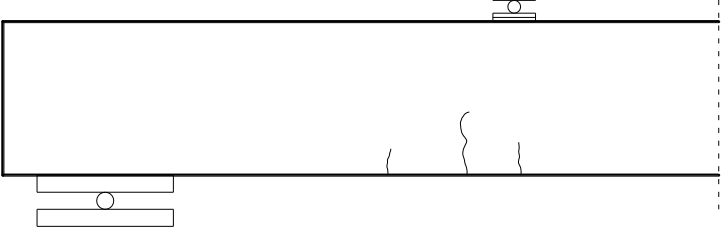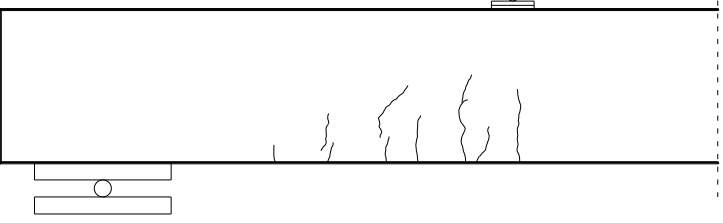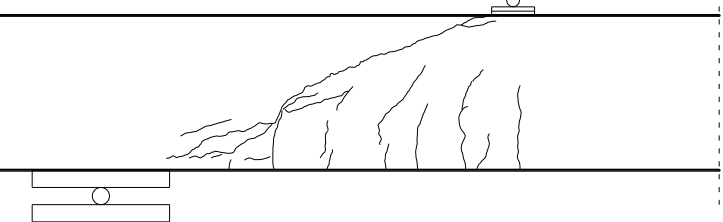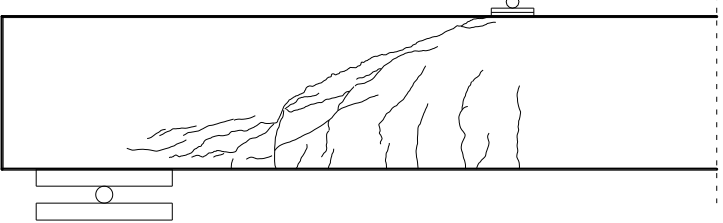
Shear force (kips)	Crack development
15.5	
24.0	
31.0	
36.6 (*Failure*)	

Figure 5.1- Crack progression for HVFA-70H-NS-8-2
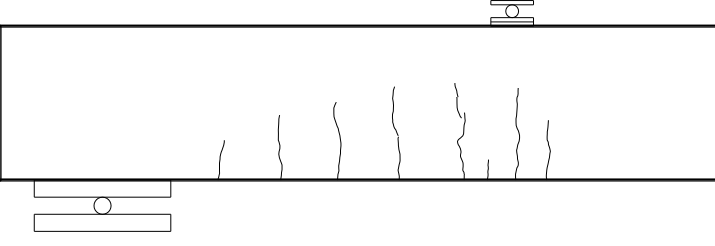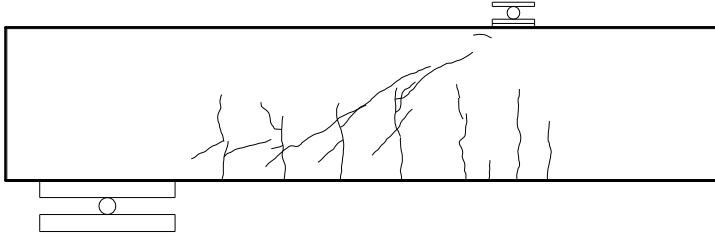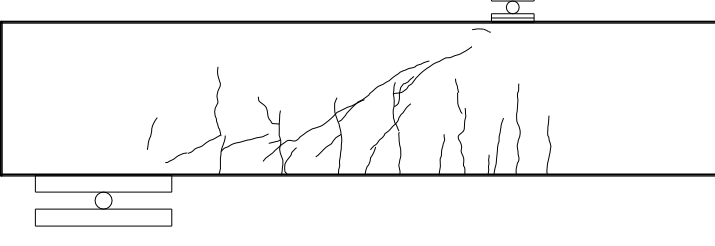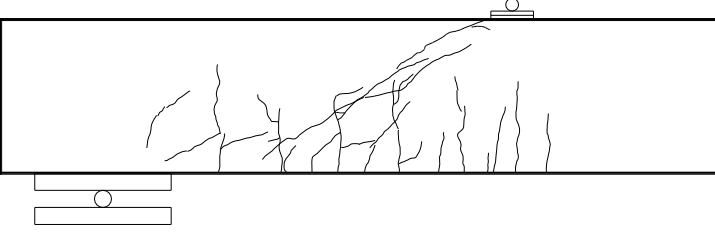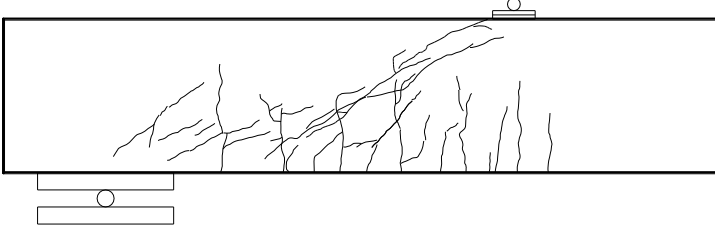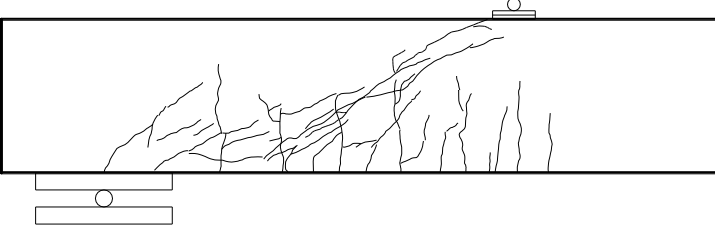
Shear force (kips)	Crack development
26.0	
37.5	
45.5	
53.0	
64.0	
73.9 (*Failure*)	

Figure 5.2- Crack progression for HVFA-70H-S-8-1

CC-H-NS-5

HVFA-70H-NS-5

CC-H-NS-6

HVFA-70H-NS-6

CC-H-NS-8

HVFA-70H-NS-8

CC-H-S-8

HVFA-70H-S-8
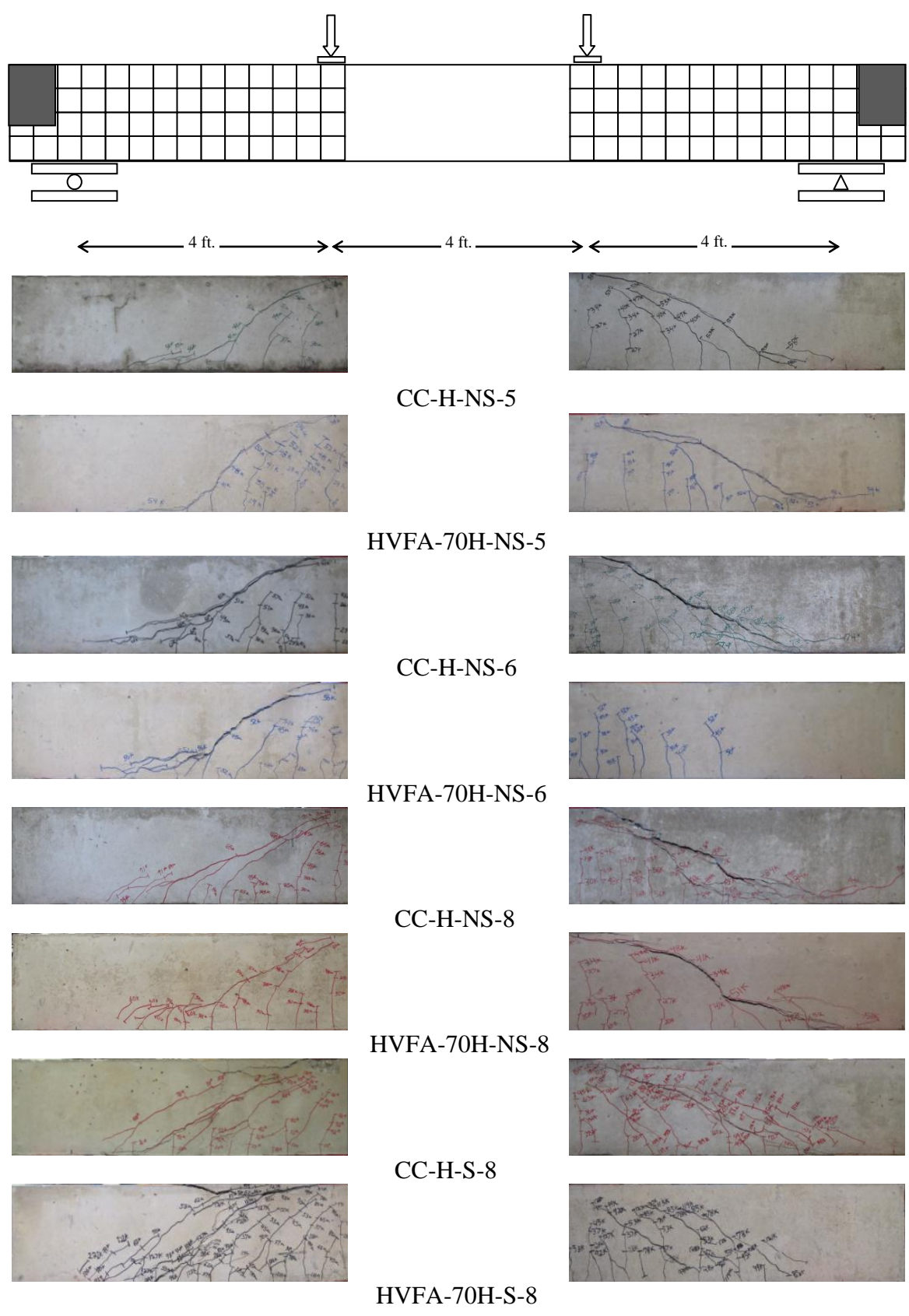
Figure 5.3- Crack Pattern at Failure for CC-H Beams (High cementitious mix)
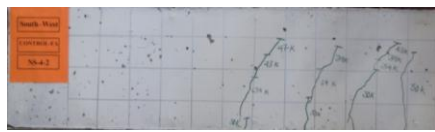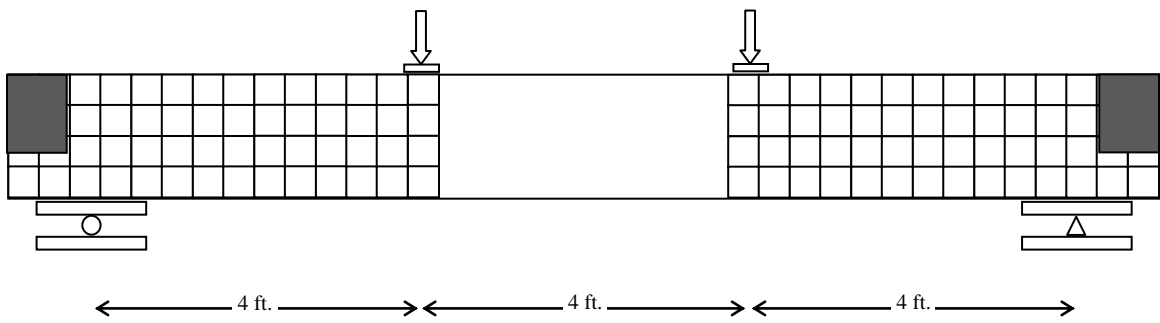
CC-L-NS-4
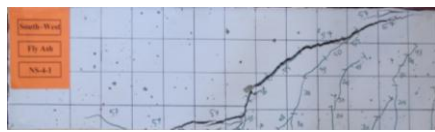
HVFA-L70-NS-4
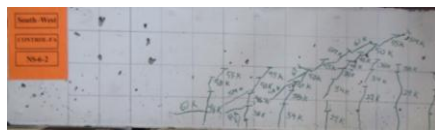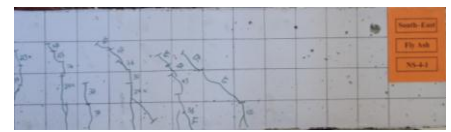
CC-L-NS-6
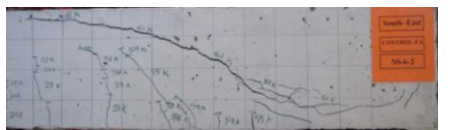
HVFA-L70-NS-6
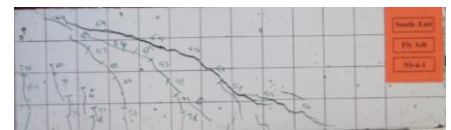
CC-L-NS-8
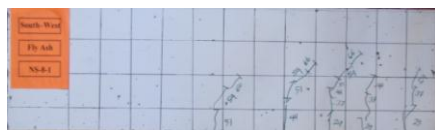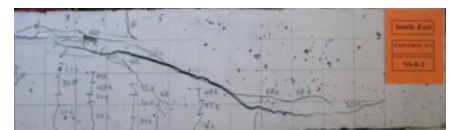
HVFA-L70-NS-8

CC-L-S-8
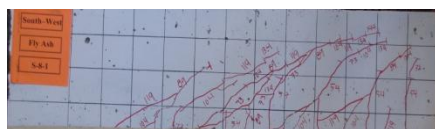
HVFA-L70-S-8
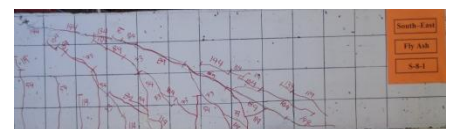
Figure 5.4- Crack pattern of the beams at shear failure (Low cementitious mix)

Figures 5.5 and **5.6** show the load-deflection behavior for the beams with different longitudinal reinforcement ratios (the deflection was measured at midspan) for the high and low cementitious mixes, respectively. Before the first flexural cracks occurred (point A), all of the beams displayed a steep linear elastic behavior. After additional application of load, the beams eventually developed the critical flexure-shear crack, which resulted in a drop in load and redistribution of the internal shear (point B for example). After this redistribution, the beams were able to support additional load until reaching failure. As expected, sections with a higher percentage of longitudinal reinforcement had a higher shear capacity, which can be attributed to a combination of additional dowel action (Taylor 1972, 1974), tighter shear cracks and thus an increase in aggregate interlock, and a larger concrete compression zone due to a downward shift of the neutral axis.
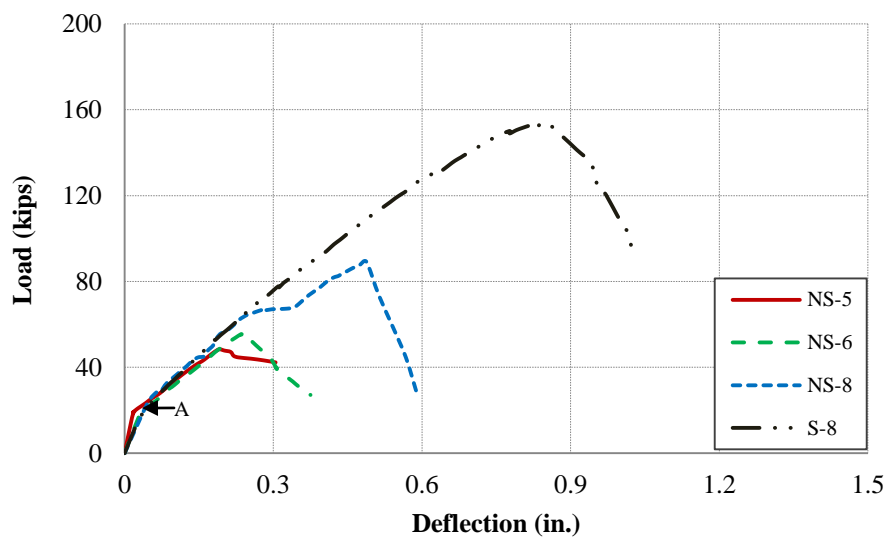
a) CC-H Beams
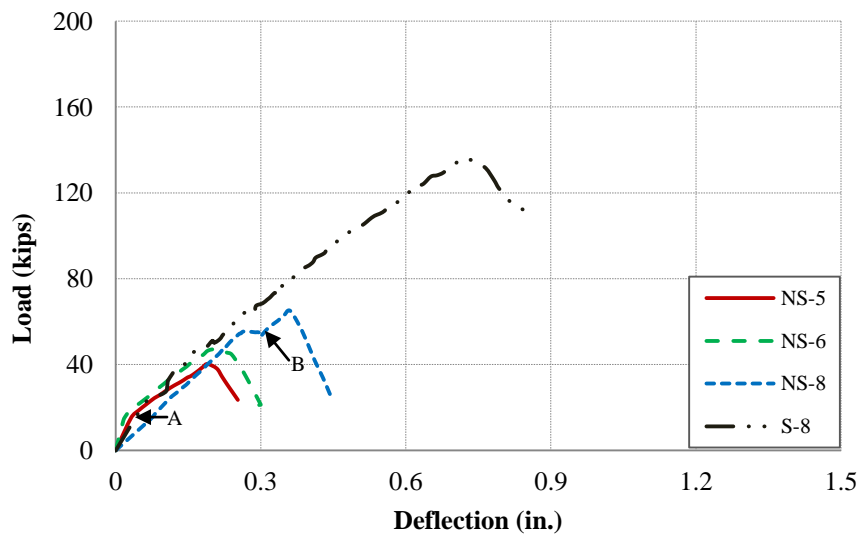
b) HVFA-70H Beams

Figure 5.5- Load-deflection of the Beams (High cementitious content)
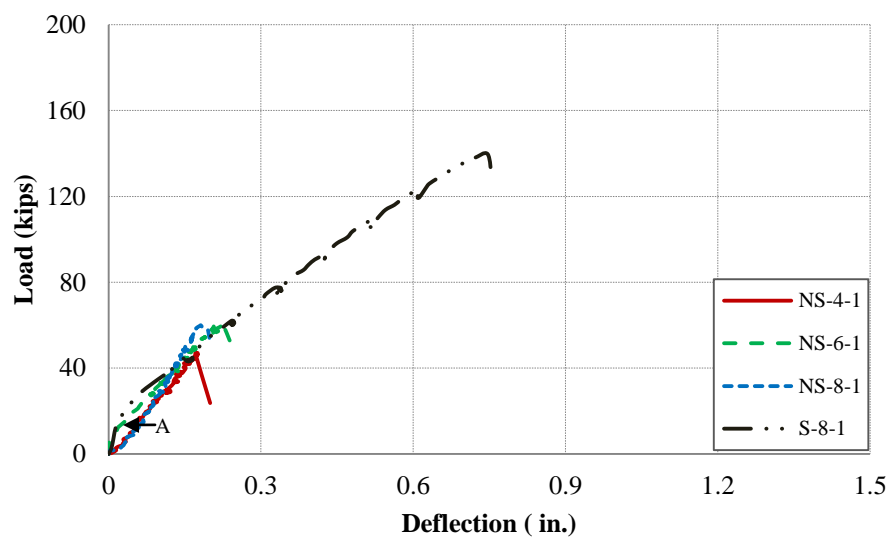
a) CC-L Beams
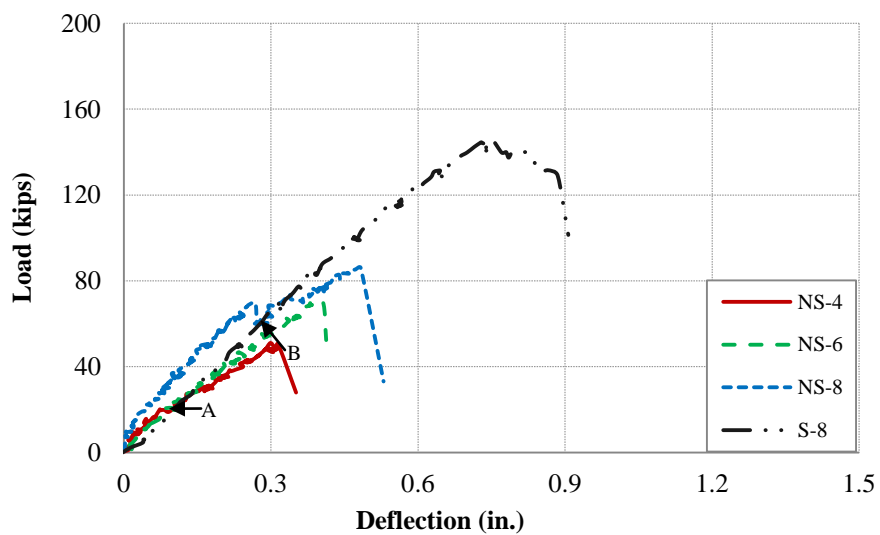
b) HVFA-70L Beams

Figure 5.6- Load-deflection of the Beams (Low cementitious content)

5.3. CRITICAL SHEAR CRACK ANGLE

The angle of the critical shear crack (θ_c) is an important design parameter in the

AASHTO LRFD (2007) sectional design method. Although it is difficult to determine

precisely as it is open to interpretation, the measurement is valuable in studying the

behavior of RC beams subjected to shear failure. The procedure used to determine this

angle consisted of measuring the angle of a portion of the critical shear crack between

two reference points, with the points corresponding to right after crossing the alignment

of the longitudinal reinforcement and before entering the compression zone, as shown in

Figure 5.7.

Table 5.2 compares measured critical crack angles from test specimens with the

calculated angle from the AASHTO LRFD (2007) equation. As it can be seen from

Table 5.2, the AASHTO LRFD (2007) equation slightly overestimated the critical crack

angles for the high cementitious mix, but it very accurately predicted the critical crack

angles for the low cementitious mix.
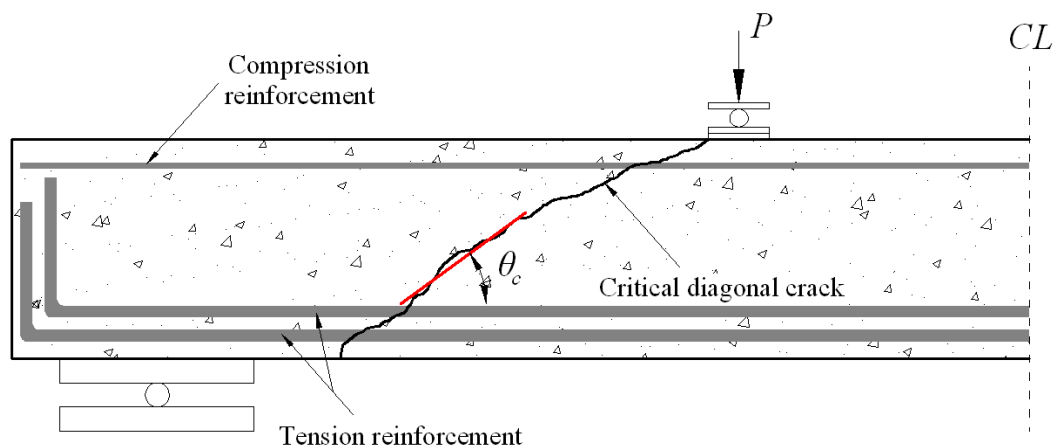
Figure 5.7- Crack angle measurement

Table 5.2- Critical Crack angle

Mix Design	Section		θ_{TEST}	θ_{AASHTO}	$\dfrac{\theta_{AASHTO}}{\theta_{TEST}}$
CC-H	NS-5	1	35	35.7	1.0
		2	29	35.6	1.2
	NS-6	1	26	34.8	1.3
		2	30	33.8	1.1
	NS-8	1	27	34.5	1.3
		2	29	32.7	1.1
	S-8	1	33	38.2	1.2
		2	34	37.8	1.1
Ave.					**1.2**
HVFA-70H	NS-5	1	28	35.1	1.3
		2	34	34.4	1.0
	NS-6	1	29	33.4	1.2
		2	33	33.0	1.0
	NS-8	1	31	33.3	1.1
		2	24	33.1	1.4
	S-8	1	38	37.2	1.0
		2	32	37.3	1.2
Ave.					**1.1**
CC-L	NS-4	1	40	34.7	0.9
		2	34	34.4	1.0
	NS-6	1	41	34.1	0.8
		2	35	33.8	1.0
	NS-8	1	40	32.7	0.8
		2	29	32.6	1.1
	S-8	1	27	36.5	1.4
		2	33	37.0	1.1
Ave.					**1.0**
HVFA-70L	NS-4	1	36	35.4	1.0
		2	45	34.8	0.8
	NS-6	1	35	34.0	1.0
		2	35	34.6	1.0
	NS-8	1	35	33.0	0.9
		2	34	34.0	1.0
	S-8	1	27	37.2	1.4
		2	28	37.4	1.3
Ave.					**1.0**

5.4. COMPARISON OF REINFORCEMENT STRAINS FROM EXPERIMENT AND AASHTO LRFD (2007)

According to the AASHTO LRFD standard (2007), strain in the longitudinal tension reinforcement can be determined by

$$\varepsilon_s = \frac{\left(\dfrac{|M_u|}{d_v} + |V_u|\right)}{E_s A_s} \tag{5-2}$$

Table 5.3 presents the tensile strain in the longitudinal tension reinforcement at the quarter-point of the span (middle of the shear test region) obtained from both the experiments (strain gauges) and the AASHTO LRFD (2007) equation. The AASHTO LRFD equation estimates the strain for both the HVFA concrete and CC beams very well for low and medium reinforcement ratios (NS-4 and NS-6), but it underestimates the strain for the sections with higher reinforcement ratios (NS-8 and S-8). Most importantly, the ratios of analytical-to-experimental strain are relatively consistent between the HVFA concrete and CC specimens.

**Table 5.3- Comparison of reinforcement strain from experiment and
AASHTO LRFD (2007) equation**

Mix	Section		CC			HVFA concrete		
			ε_{s} quarter-point Equation	ε_{s} quarter-point Experiment	$\dfrac{\varepsilon_{s-Eq.}}{\varepsilon_{s-Ex.}}$	ε_{s} quarter-point Equation	ε_{s} quarter-point Experiment	$\dfrac{\varepsilon_{s-Eq.}}{\varepsilon_{s-Ex.}}$
High cementitious	NS-5	1	1179	*		1077	*	
		2	1159	*		962	*	
	NS-6	1	1013	1004	1.01	766	591	1.30
		2	837	692	1.21	706	661	1.07
	NS-8	1	1457	1526	0.95	745	974	0.76
		2	573	641	0.89	709	737	0.96
	S-8	1	1602	2098	0.76	1430	1658	0.86
		2	1536	2038	0.75	1448	1866	0.78
Ave.					0.93			0.96
COV (%)					18.53			21.27
Low cementitious	NS-4	1	1004.0	*		1127.0	1211	0.93
		2	954.0	844	1.13	1029.0	730	1.41
	NS-6	1	892.0	989	0.90	875.0	943	0.93
		2	840.0	906	0.93	977.0	1148	0.85
	NS-8	1	645.0	726	0.89	707.0	780	0.91
		2	626.0	818	0.77	878.0	1483	0.59
	S-8	1	1305.0	1648	0.79	1431.0	1700	0.84
		2	1392.0	1791	0.78	1468.0	1847	0.79
Ave.					0.88			0.91
COV (%)					14.39			25.45

*: No usable data

5.5. STATISTICAL DATA ANALYSIS

Statistical tests were used to evaluate whether there is any statistically significant difference between the normalized shear strength of the HVFA concrete and the CC beams. Both parametric and nonparametric statistical tests were performed.

5.5.1. Parametric Test. The paired t-test is a statistical technique used to compare two population means. This test assumes that the differences between pairs are normally distributed. If this assumption is violated, the paired t-test may not be the most powerful test. The hypothesis for the paired t-test is as follows:

H_o: The means of the normalized shear capacity of the HVFA-70H/70L is higher than the CC-H/L beams.

H_a: Not H_o.

The statistical computer program Minitab 15 was employed to perform these statistical tests. Both Kolmogorov-Smirnov and Anderson-Darling tests showed the data, the differences between the shear capacities of the HVFA concrete and the CC beams, follows a normal distribution. Therefore, the paired t-tests could be performed. The result of the paired t-test showed that the p-values were 0.88 and 0.963 (>0.05) for the high and low cementitious mixes, respectively. This confirms the null hypothesis at the 0.05 significance level. In other words, the means of the normalized shear capacity of the HVFA concrete was statistically higher than the CC beams.

5.5.2. Nonparametric Test. Unlike the parametric tests, nonparametric tests are referred to as distribution-free tests. These tests have the advantage of requiring no assumption of normality, and they usually compare medians rather than means. The Wilcoxon signed-rank test is usually identified as a nonparametric alternative to the paired t-test. The hypothesis for this test is the same as those for the paired t-test. The Wilcoxon signed rank test assumes that the distribution of the difference of pairs is symmetrical. This assumption can be checked; if the distribution is normal, it is also symmetrical. As mentioned earlier, the data follows normal distribution and the

Wilcoxon signed ranks test can be used. The p-values for the Wilcoxon signed rank were

0.78 and 0.995 (>0.05) for the high and low cementitious mixes, respectively. That

confirmed the null hypothesis at the 0.05 significance level. Interestingly, the p-values for

both the paired t-tests (parametric test) and the Wilcoxon signed rank test (nonparametric

test) are very close to each other.

Overall, results of the statistical data analyses showed that the HVFA concrete

beams (both the high and low cementitious) had higher normalized shear capacity than

the CC beams.

5.6. COMPARISON OF TEST RESULTS WITH SHEAR PROVISIONS OF SELECTED STANDARDS

In the following section, the experimental shear strengths of the beams are

compared with the shear provisions of the following standards: AASHTO LRFD (2007),

ACI 318 (2008), and CSA (2004). For this comparison, all of the safety factors of the

standards were set equal to one and all ultimate moments and shear forces were

calculated without load factors.

Table 5.4 presents the ratio of experimental-to-code predicted capacity

(V_{test}/V_{code}) for the selected design standards for all the beams. In comparing the two

mixes, the ratios are very similar, particularly given the wide scatter normally associated

with shear testing of reinforced concrete. Most importantly, the ratio for most of the

beams in all the selected standards is greater than one. This result indicates that existing

code provisions conservatively predict the shear strength of HVFA concrete beams.

For the CC beams without stirrups, the ratios range from 0.96 to 1.48 for the low cementitious mix and 0.91 to 1.41 for the high cementitious mix. For the HVFA concrete beams without stirrups, the ratios range from 1.01 to 1.92 for the low cementitious mix and 1.06 to 1.85 for the high cementitious mix. On average, the ratios for the HVFA concrete beams were higher than those for the CC beams, indicating that the HVFA concrete beams exceeded the code predicted strengths by a larger margin. For the beams with stirrups, the ratios were in much closer agreement between the two concrete types, most likely due to the greater predictability of the stirrup capacity portion of the shear strength, with ratios ranging from 1.16 to 1.60 for the CC and 1.24 to 1.60 for the HVFA concrete. For both mixes and both concrete types, the AASHTO LRFD and CSA offered the closest agreement between experimental and code predicted strengths.

Table 5.4- Comparison of shear strength of experiment and codes

Mix			High Cementitious Mix			Low Cementitious Mix		
Section			AASHTO	ACI	CSA	AASHTO	ACI	CSA
CC	NS-5	1	1.08	1.12	1.09	0.93	1.04	0.94
		2	1.09	1.14	1.10	0.91	1.02	0.91
	NS-6	1	1.31	1.48	1.31	1.19	1.41	1.20
		2	1.04	1.26	1.04	1.15	1.38	1.15
	NS-8	1	1.61	1.86	1.62	1.02	1.33	1.03
		2	0.96	1.26	0.97	1.03	1.34	1.03
	Ave		1.18	1.35	1.19	1.04	1.25	1.04
	COV		20.19	20.57	20.19	10.87	14.02	10.86
	S-8	1	1.55	1.58	1.44	1.20	1.32	1.13
		2	1.46	1.51	1.37	1.31	1.41	1.23
	Ave		1.51	1.54	1.41	1.25	1.36	1.18
	COV		4.22	3.08	3.99	6.30	4.70	6.00
HVFA concrete	NS-5	1	1.18	1.36	1.19	1.07	1.14	1.08
		2	1.01	1.22	1.02	1.14	1.25	1.15
	NS-6	1	1.11	1.48	1.11	1.13	1.34	1.13
		2	1.00	1.38	1.01	1.60	1.82	1.61
	NS-8	1	1.42	1.92	1.43	1.12	1.43	1.13
		2	1.34	1.85	1.35	1.84	2.15	1.85
	Ave		1.18	1.54	1.19	1.32	1.52	1.33
	COV		14.69	18.53	14.65	24.49	25.36	24.42
	S-8	1	1.42	1.58	1.33	1.32	1.40	1.24
		2	1.45	1.60	1.35	1.37	1.44	1.28
	Ave		1.44	1.59	1.34	1.35	1.42	1.26
	COV		1.48	0.89	1.06	2.63	1.99	2.24

5.7. COMPARISON OF TEST RESULTS WITH SHEAR TEST DATABASE

Figure 5.8 presents the normalized shear strength versus longitudinal reinforcement ratio for the beams of this study as well as the wealth of shear test data available in the literature (Reineck 2003). Given the significant scatter of the database of previous shear test results, it is somewhat difficult to draw definitive conclusions on the current test values. Nonetheless, visually, **Figure 5.8** seems to indicate that the CC and HVFA concrete test results fall within the central portion of the data and follow the same general trend of increasing shear strength as a function of the longitudinal reinforcement ratio. Furthermore, statistical analysis of the data indicates that the CC and HVFA concrete test results fall within a 95% confidence interval of a nonlinear regression curve fit of the database. Furthermore, a significant majority of the HVFA concrete test results fall at or above the nonlinear regression curve fit. This result indicates that the test values are very consistent with the wealth of shear test data available in the literature and that, in general, the HVFA concrete test results tend to be greater than CC.

Since span-to-depth ratio plays a significant role in the shear strength of beams (Taylor 1972, 1974), **Figure 5.9** shows the normalized shear strength for the beams of this study with the portion of the database that had similar span-to-depth ratios of the current study (span-to-depth ratio$\pm$ 5% [2.9-3.4]). It can be seen from **Figure 5.9** that the test results of this current study are within a 95% confidence interval of a nonlinear regression curve fit of this subset of the shear database. As a result, it would appear that the shear strength of HVFA concrete is higher than CC for the beams tested in this investigation.
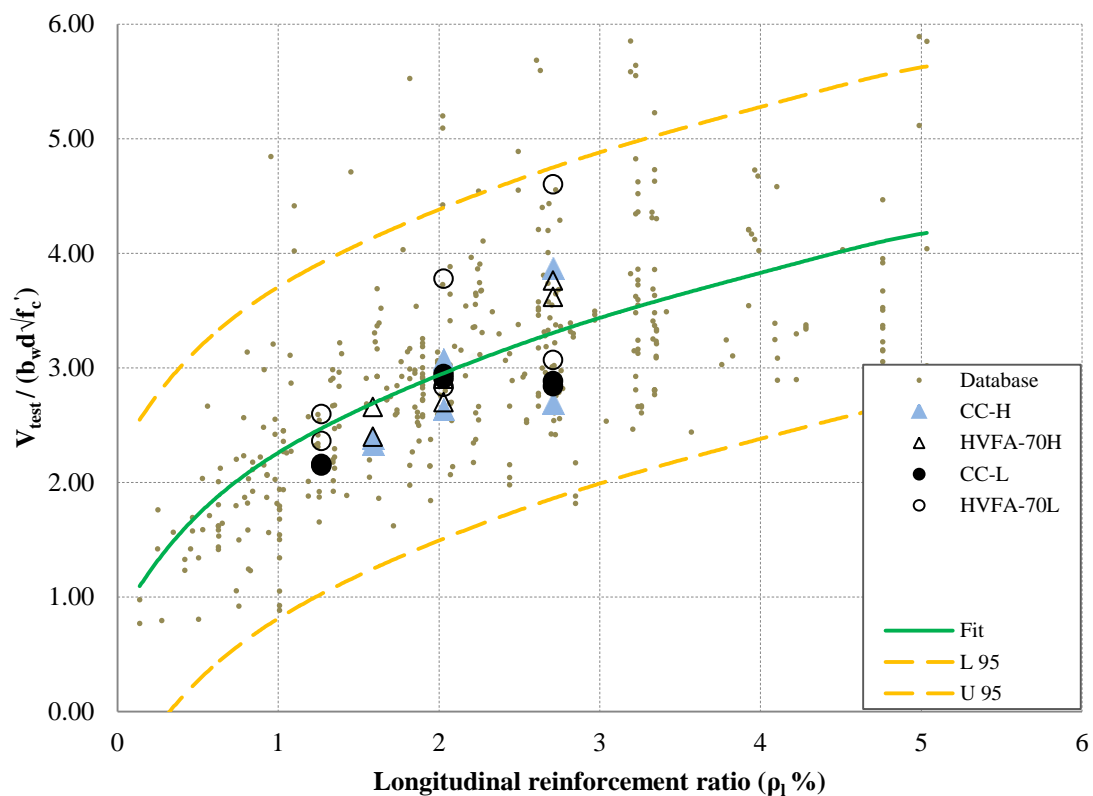
Figure 5.8- Shear strength vs. longitudinal reinforcement ratio; results from Reineck (2003) and test results of this study
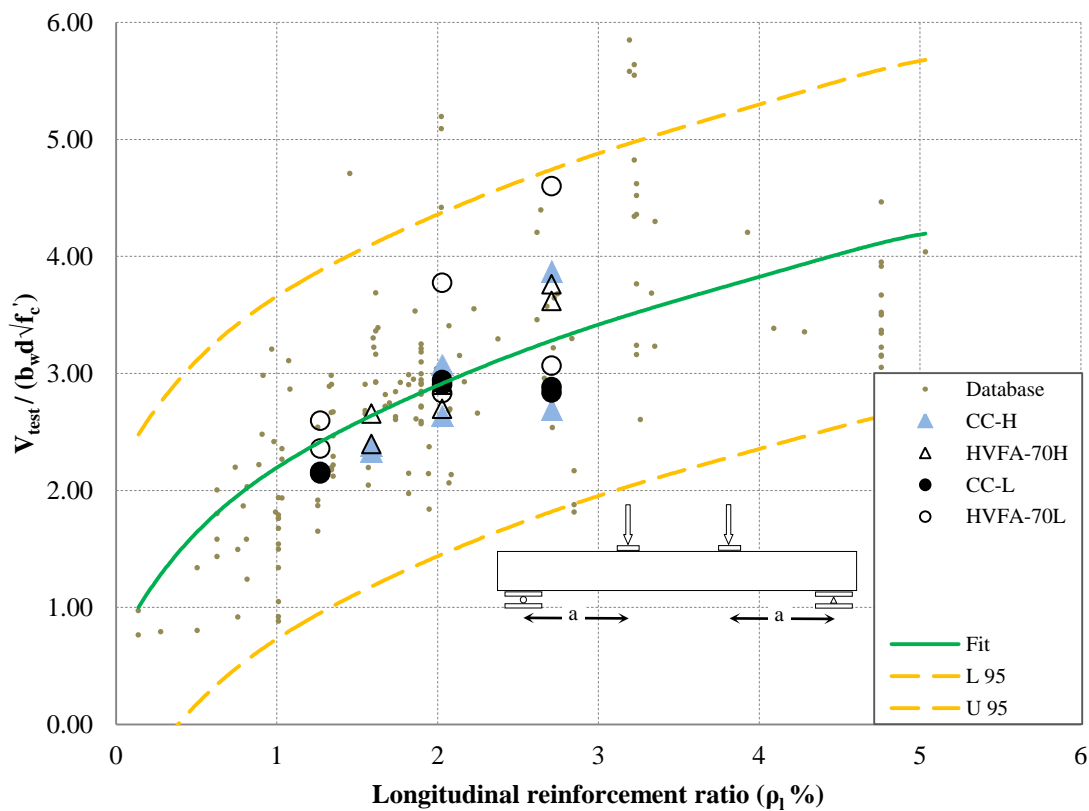
Figure 5.9- Shear strength vs. longitudinal reinforcement ratio; results from (Reineck et al. 2003) ($2.9 \leq \frac{a}{d} \leq 3.4$) and test results of this study

6. FINDINGS, CONCLUSIONS, AND RECOMMENDATIONS

The main objective of this research study was to evaluate the shear behavior and response of high-volume fly ash (HVFA) concrete through material, component, and full-scale testing. The main feature of the experimental program consisted of 32 tests performed on full-scale reinforced concrete beams. The principal parameters investigated were: (1) concrete type – HVFA concrete or conventional concrete (CC), (2) amount of total cementitious material, (3) amount of shear reinforcement, and (4) amount of longitudinal (flexural) reinforcement. The behavior of the HVFA concrete was examined in terms of crack morphology and progression, load-deflection response, failure mechanism including critical crack angle and reinforcement strains, comparison with predicted strengths from design standards, comparison with identical CC test specimens (including statistical analyses), and comparison with a shear test database of CC specimens. This section contains the findings of the test program as well as conclusions and recommendations.

6.1. FINDINGS AND CONCLUSIONS

Based on the results of this research study, the following findings and conclusions are presented:

- In terms of crack morphology, crack progression, and load-deflection response, the behavior of the HVFA concrete and CC beams was virtually identical.

- The AASHTO LRFD equation slightly overestimated the critical crack angles for the high total cementitious content mix but very accurately predicted the

critical crack angles for the low total cementitious content mix. Most importantly, the critical crack angles for the HVFA concrete beams were very consistent with those of the CC beams.

- The AASHTO LRFD equation estimates the reinforcement strain for both the HVFA concrete and CC beams very well for low and medium reinforcement ratios, but it underestimates the strain for sections with higher reinforcement ratios.

- Statistical data analyses – both parametric and nonparametric – showed that the HVFA concrete beams had higher normalized shear capacity than the CC beams.

- Existing design standards (AASHTO, ACI, CSA) conservatively predicted the shear capacity of the HVFA concrete beams.

- In general, the HVFA concrete beams exceeded the code predicted shear strengths by a larger margin than the CC beams.

- The total cementitious content had little effect on the shear behavior of the HVFA concrete beams.

- The HVFA concrete and CC test results fall within a 95% confidence interval of a nonlinear regression curve fit of the CC shear test database.

- A significant majority of the HVFA concrete test results fall at or above the nonlinear regression curve fit of the CC shear test database.

6.2. RECOMMENDATIONS

Based on the findings and conclusions discussed previously, the following recommendations are presented:

- Although the normalized HVFA concrete shear test results exceeded the CC shear test results, due to the inherent scatter associated with shear testing of reinforced concrete, the investigators recommend using existing design equations for HVFA concrete.

- Additional testing is required to determine whether HVFA concrete has increased shear capacity compared to CC. This testing should investigate additional mix design variations, aggregate type and content, cross section aspect ratio, and type of loading. This database will then provide a basis for modifications to existing design standards.

BIBLIOGRAPHY

AASHTO LRFD, (2007). Bridge Design Specifications and Commentary (4th Ed.). American Association of State and Highway Transportation Officials. Washington, DC.

AASHTO T 318 (2002). Water Content of Freshly Mixed Concrete Using Microwave Oven Drying. American Association of State Highway and Transportation Officials, Washington D.C.

American Coal Ash Association (ACAA). (2009). Facts About Coal Ash. Access online at www.coalashfacts.org

ACI Committee 211, (1991). Standard Practice for Selecting Proportions for Normal, Heavyweight, and Mass Concrete (ACI 211.1-91). American Concrete Institute, Farmington Hills, MI.

ACI Committee 232, (2003). Use of Fly Ash in Concrete (ACI 232.2R-03). American Concrete Institute, Farmington Hills, MI.

ACI Committee 318, (2008). Building Code Requirements for Structural Concrete and Commentary (ACI 318-08). American Concrete Institute, Farmington Hills, MI.

ACI Committee 445, (2009). Recent Approaches to Shear Design of Structural Concrete (ACI 445R-99). American Concrete Institute, Farmington Hills, MI.

ACI Committee 446, (1999). Fracture Mechanics of Concrete: Concepts, Models and Determination of Material Properties (ACI 446.1R). American Concrete Institute, Farmington Hills, MI.

ASCE-ACI Task Committee 426, (1973). The Shear Strength of Reinforced Concrete Members. ASCE Journal of the Structural Division, Vol. 99, No. 6, pp. 1091-1187.

ASCE-ACI Task Committee 445, (1998). Recent Approaches to Shear Design of Structural Concrete. ASCE Journal of Structural Engineering, Vol. 124, No. 12, pp. 1375-1417.

ASTM A370, (2011). Standard Test Methods and Definitions for Mechanical Testing of Steel Products. American Society for Testing Materials (ASTM International).

ASTM C109, (2008). Standard Test Method for Compressive Strength of Hydraulic Cement Mortars. American Society for Testing Materials (ASTM International).

ASTM C127, (2007). Standard Test Method for Density, Relative Density (Specific Gravity), and Absorption of Coarse Aggregate. American Society for Testing Materials (ASTM International).

ASTM C128, (2007). Standard Test Method for Density, Relative Density (Specific Gravity), and Absorption of Fine Aggregate. American Society for Testing Materials (ASTM International).

ASTM C138, (2010). Standard Test Method for Density (Unit Weight), Yield, and Air Content (Gravimetric) of Concrete. American Society for Testing Materials (ASTM International).

ASTM C192, (2007). Standard Practice for Making and Curing Concrete Test Specimens in the Laboratory. American Society for Testing Materials (ASTM International).

ASTM C231, (2010). Standard Test Method for Air Content of Freshly Mixed Concrete by the Pressure Method. American Society for Testing Materials (ASTM International).

ASTM C39/C39M, (2011). Standard Test Method for Compressive Strength of Cylindrical Concrete Specimens. American Society for Testing Materials (ASTM International).

ASTM C469, (2002). Standard Test Method for Static Modulus of Elasticity and Poisson's Ratio of Concrete in Compression. American Society for Testing Materials (ASTM International).

ASTM C496, (2004). Standard Test Method for Splitting Tensile Strength of Cylindrical Concrete Specimens. American Society for Testing Materials (ASTM International).

ASTM C566, (1997). Standard Test Method for Total Evaporable Moisture Content of Aggregate by Drying. American Society for Testing Materials (ASTM International).

ASTM C617, (2009). Standard Practice for Capping Cylindrical Concrete Specimens. American Society for Testing Materials (ASTM International).

ASTM C618, (2008). Standard Specification for Coal Fly Ash and Raw or Calcined Natural Pozzolan for Use in Concrete. American Society for Testing Materials (ASTM International).

ASTM C78, (2009). Standard Test Method for Flexural Strength of Concrete (Using Simple Beam with Third-Point Loading). American Society for Testing Materials (ASTM International).

ASTM E178, (2008). Standard Practice for Dealing with Outlying Observations. American Society for Testing Materials (ASTM International).

Bazant, Z.P., and Becq-Giraudon, E., (2002), Statistical prediction of fracture parameters of concrete and implications for choice of testing standards. Cement and Concrete Research Journal, Vol. 32, No. 4, pp. 529-556.

Bazant, Z.P., and Kim, J.K., (1984). Size Effect in Shear Failure of Longitudinally Reinforced Beams. ACI Journal Proceedings, Vol. 81, pp. 456-468.

Bazant, Z.P., and Pfeiffer, P.A., (1987). Determination of Fracture Energy from Size Effect and Brittleness Number. ACI Materials Journal, Vol. 84, No. 6, pp. 463-480.

Bazant, Z.P., and Sun, H.H., (1987). Size Effect in Diagonal Shear Failure: Influence of Aggregate Size and Stirrups. ACI Journal Proceedings, Vol. 84, pp. 259-272.

Bentz, D.P., (2010). Powder Additions to Mitigate Retardation in High-Volume Fly Ash Mixtures. ACI Materials Journal, Vol. 107, No. 5, pp. 508-514.

Bentz, E.C., Vecchio, F.J, and Collins, M.P., (2006). Simplified Modified Compression Field Theory for Calculating Shear Strength of Reinforced Concrete Elements. ACI Structural Journal, Vol. 103, No. 4, pp. 614-624.

Berry, E.E., Hemmings, R.T., Zhang, M., Cornelius, B.J., and Golden, D.M., (1994). Hydration in High-Volume Fly Ash Concrete Binders. ACI Materials Journal, Vol. 91, No. 4, pp. 382-389.

Bilodeau, A., Sivasundaram, V., Painter, K.E., and Malhotra, V.M., (1994). Durability of Concrete Incorporating High Volumes of Fly Ash from Sources in the U.S. ACI Materials Journal, Vol. 91, No. 1, pp. 3-12.

Boresi, A.P., and Schmidt, R.J., (2003). Advanced Mechanics of Materials (6th Ed.). John Wiley & Sons.

Bouzoubaâ, N., Bilodeau, A., Sivasundaram, V., and Chakraborty, A.K., (2007). Mechanical Properties and Durability Characteristics of High-Volume Fly Ash Concrete Made with Ordinary Portland Cement and Blended Portland Fly Ash Cement. ACI Special Publication, Vol. 242, pp. 303-320.

Brooks, J.J., and Sikharulidze, Z.D., (1992). Strength and Fracture Energy of Concrete with and without Fly Ash Cured in Water at Different Constant Temperatures. ACI Special Publication, Vol. 132, pp. 299-317.

Butalia, T.S, and Bargaheiser, K., (2004). Corrosion in Concrete and the Role of Fly Ash in its Mitigation. Energeia, Vol. 15, No. 4, University of Kentucky, Center for Applied Energy Research.

Cabrera, J.G., and Atis, C.D., (1999). Design and Properties of High-Volume Fly Ash High- Performance Concrete. ACI Special Publication, Vol. 186, pp. 21-38.

Carette, G., Bilodeau, A., Chevrier, R.L., and Malhotra, V.M., (1993). Mechanical Properties of Concrete Incorporating High Volumes of Fly Ash from Sources in the U.S. ACI Materials Journal, Vol. 90, No. 6, pp. 535-544.

Cladera, A., (2002). Shear Design of Reinforced High-Strength Concrete Beams. PhD Thesis. Universitat Politécnica de Catalunya. Barcelona, Spain.

Collins, M.P., and Mitchell, D., (1991). Prestressed Concrete Structures. Response Publications.

Collins, M.P., Bentz, E.C., and Sherwood, E.G., (2008). Where is Shear Reinforcement Required? Review of Research Results and Design Procedures. ACI Structural Journal, Vol. 105, No. 5, pp. 590-600.

Collins, M.P., Mitchell, D., and Bentz, E.C., (2008). Shear Design of Concrete Structures. The Structural Engineer, Vol. 86, No. 10, pp. 32-39.

Comite Euro-International du Beton, (1990). CEB-FIP Model Code 1990, Redwood Books, Wiltshire, England.

Coronado, C., (2006). Characterization, Modeling and Size Effect of Concrete-Epoxy Interfaces. PhD Thesis. Pennsylvania State University. United States of America.

Cross, D., Stephens, J., and Vollmer, J., (2005). Structural Applications of 100 Percent Fly Ash Concrete. 2005 World of Coal Ash Conference. Lexington, KY, United States of America.

CSA Committee A23.3, (2004). Design of Concrete Structures (CSA A23.3-04). Canadian Standards Association. Rexdale, ON, Canada.

Dahl, H., and Brincker, R., (1989). Fracture Energy of High-Strength Concrete in Compression. International Conference on Fracture of Concrete and Rock: Cardiff. Elsevier Science, pp. 523-536.

Davis, R.E., Carlson, R.W., Kelly, J.W., and Davis, H.E., (1937). Properties of Cements and Concretes Containing Fly Ash. ACI Journal Proceedings, Vol. 33, No. 5, pp. 577-612.

Duthinh, D., (1999). Sensitivity of Shear Strength of Reinforced Concrete and Prestressed Concrete Beams to Shear Friction and Concrete Softening According to Modified Compression Field Theory. ACI Structural Journal, Vol. 96, No. 4, pp. 495-508.

Einsfeld, R.A., and Velasco, M.S.L., (2006). Measurement of the Ratio G_F/G_f for Numerical Analysis of Concrete Structures. Latin American Journal of Solids and Structures, Vol. 3, pp. 361-376.

Eurocode 2, (2004). Design of Concrete Structures − Part 1.1: General Rules and Rules for Buildings. EN 1992-1-1. Brussels. Belgium.

Galeota, D., Giammatteo, M.M., and Marino, R., (1995). Structural Concrete Incorporating High Volume of Fly Ash. ACI Special Publication, Vol. 153, pp. 25-42.

Gastebled, O.J., and May, I.M., (2001). Fracture Mechanics Model Applied to Shear Failure of Reinforced Concrete Beams without Stirrups. ACI Structural Journal, Vol. 98, No. 2, pp. 184-190.

Ghaemmaghami, A., and Ghaemian, M., (2004). Specific Fracture Energy Approximation of Dam Concrete. 13th World Conference on Earthquake Engineering. Paper No. 69. Vancouver, BC. Canada.

Griffith, A.A., (1920). The Phenomena of Rupture and Flow in Solids. Philosophical Transactions, Series A, Vol. 221, pp. 163-198.

Guinea, G.V., Planas, J., and Elices, M., (1992). Measurement of the Fracture Energy Using Three-Point Bend Tests: Part 1 − Influence of Experimental Procedures. Materials and Structures. Materials and Structures, Vol. 25, pp. 212-218.

Gustafsson, P.J., and Hillerborg, A., (1988). Sensitivity in Shear Strength of Longitudinally Reinforced Concrete Beams to Fracture Energy of Concrete. ACI Journal Proceedings, Vol. 85, pp. 286-294.

Headwaters Resources, (2008). Fly Ash for Concrete. Brochure. http://www.flyash.com/data/upimages/press/fly%20ash%20for%20concrete.pdf

Hillerborg, A., (1985). Theoretical Basis of a Method to Determine the Fracture Energy G_F of Concrete. Materials and Structures, Vol. 18, No. 106, pp. 291-296.

Hillerborg, A., Modeer, M., and Petersson, P.E., (1976). Analysis of Crack Formation and Crack Growth in Concrete by Means of Fracture Mechanics and Finite Elements. Cement and Concrete Research Journal, Vol. 6, pp. 773-782.

Hsu, T.T.C., (1993). Unified Theory of Reinforced Concrete. CRC Press.

Hsu, T.T.C., and Mo, Y.L., (2010). Unified Theory of Concrete Structures. John Wiley & Sons.

http://www.4us2be.com/technology/cement-manufacturing-process/. December, 2011.

http://www.tradeindia.com/fp426361/Ammonia-Flue-Gas-Conditioning-Systems.html. December, 2011.

Irwin, G.R., Kies, J.A., and Smith, H.L., (1958). Fracture Strength Relative to Onset and Arrest of Crack Propagation. Proceedings ASTM, Vol. 58, pp. 640-657.

Jenq, Y.S., and Shah, S.P., (1989). Shear Resistance of Reinforced Concrete Beams − A Fracture Mechanics Approach. ACI Special Publication, Vol. 118, pp. 237-258.

Jiang, L., Lin, B., and Cai, Y., (1999). Studies on Hydration in High-Volume Fly Ash Concrete Binders. ACI Materials Journal, Vol. 96, No. 6, pp. 703-706.

Kaplan, M.F., (1961). Crack Propagation and the Fracture of Concrete. ACI Journal Proceedings, Vol. 58, pp. 591-610.

Kellermann, W.F., (1933). Effect of Size of Specimen, Size of Aggregate and Method of Loading upon the Uniformity of Flexural Strength Results. Public Roads, Vol. 13, No. 11, pp. 177-184.

Kesler, C.E., Naus, D.J., and Lott, J.L., (1972). Fracture Mechanics − Its Applicability to Concrete. Proceedings of the International Conference on the Mechanical Behavior of Materials, Vol. IV, pp. 113-124, Kyoto, Japan.

Kim, J.K., and Park, Y.D., (1996). Prediction of Shear Strength of Reinforced Concrete Beams without Web Reinforcement. ACI Materials Journal, Vol. 93, No. 3, pp. 213-222.

Kim, W., and White, R.N., (1991). Initiation of Shear Cracking in Reinforced Concrete Beams with No Web Reinforcement. ACI Structural Journal, Vol. 88, No. 3, pp. 301-308.

Koyama, T., Sun, Y.P., Fujinaga, T., Koyamada, H., and Ogata, F., (2008). Mechanical Properties of Concrete Beam Made of Large Amount of Fine Fly Ash. The 14th World Conference on Earthquake Engineering. Beijing, China.

Kuchma, D., (2009). Contribution of Stirrups to Shear Resistance. Structures Congress 2009: Don't Mess with Structural Engineers, ASCE, pp. 1587-1594.

Langley, W.S., Carette, G.G., and Malhotra, V.M., (1989). Structural Concrete Incorporating High Volumes of ASTM Class F Fly Ash. ACI Materials Journal, Vol. 86, No. 5, pp. 507-514.

Laskar, A., Hsu, T.T.C., and Mo, Y.L.C., (2010). Shear Strengths of Prestressed Concrete Beams Part 1: Experiments and Shear Design Equations. ACI Structural Journal, Vol. 107, No. 3, pp. 330-339.

Leonhardt, F., and Mönnig, E., (1975). Vorlesungen über Massivbau. Berlin/Heidelberg, Germany.

Li, G., (2004). Properties of High-Volume Fly Ash Concrete Incorporating Nano- SiO_2. Cement and Concrete Research Journal, Vol. 34, pp. 1043-1049.

Loov, R.E., (1998). Review of A23.3-94 Simplified Method of Shear Design and Comparison with Results using Shear Friction. Canadian Journal of Civil Engineering, Vol. 25, No. 3, pp. 437-450.

Malhotra, V.M., and Mehta, P.K., (2008). High-Performance, High-Volume Fly Ash Concrete for Building Sustainable and Durable Structures (3rd Ed.). Supplementary Cementing Materials for Sustainable Development Inc. Ottawa, Canada.

Marotta, T.W., Coffey, J.C., LaFleur, C.B., and LaPlante, C., (2011). Basic Construction Materials (8th Ed.). Pearson-Prentice Hall.

Martin, J., Stanton, J., Mitra, N., and Lowes, L.N., (2007). Experimental Testing to Determine Concrete Fracture Energy Using Simple Laboratory Test Setup. ACI Materials Journal, Vol. 104, No. 6, pp. 575-584.

Mehta, P.K., (2004). High-Performance, High-Volume Fly Ash Concrete for Sustainable Development. Proceedings of the International Workshop on Sustainable Development and Concrete Technology, Center for Transportation Research and Education, Iowa State University. United States of America.

Mindess, S., Young, J.F., and Darwin, D., (2003). Concrete (2nd Ed.). Prentice Hall.

Mohan Rao, R, Mohan, S., and Sekar, S.K., (2011). Shear Resistance of High Volume Fly Ash Reinforced Concrete Beams without Web Reinforcement. International Journal of Civil and Structural Engineering, Vol. 1, No. 4, pp. 986-993.

Mörsch, E., (1902). Der Eisenbetonbau, Seine Theorie und Anwendung. Stuggart, Germany.

Namagga, C., and Atadero, R.A., (2009). Optimization of Fly Ash in Concrete: High Lime Fly Ash as a Replacement for Cement and Filler Material. 2009 World of Coal Ash Conference. Lexington, KY, United States of America.

Neville, A.M., (1997). Properties of Concrete (4th Ed.). John Wiley & Sons.

Nielsen, K.E.C., (1954). Effect of Various Factors on the Flexural Strength of Concrete Tests Beams. Magazine of Concrete Research, No. 15, pp. 105-114.

Nilson, A.H., Darwin, D., and Dolan, C.W., (2004). Design of Concrete Structures (13th Ed.). McGraw Hill.

Padevet, P., and Zobal, O., (2011). Fracture Energy of Cement Paste with Addition of the Fly Ash. 4th International Conference Modelling of Mechanical and Mechatronic Systems 2011, Technical University of Kosice. Kosice. Slovakia.

Park, R., and Paulay, T., (1975). Reinforced Concrete Structures. John Wiley & Sons.

Rangan, B.V., (1991). Web Crushing Strength of Reinforced and Prestressed Concrete Beams. ACI Structural Journal, Vol. 88, No. 1, pp. 12-16.

Reineck, KH, Kuchma, DA, Kim, KS; and Marx, S., (2003). "Shear Database for Reinforced Concrete Members without Shear Reinforcement," ACI Structural Journal, V. 100, No. 2, pp. 240-249.

Raphael, J.M., (1984). Tensile Strength of Concrete. Concrete International, Vol. 81, No. 2, pp. 158-165.

RILEM TC 89-FMT Fracture Mechanics of Concrete-Test Methods, (1990). Determination of Fracture Parameters (K_{IC} and $CTOD_C$) of Plain Concrete Using Three-Point Bend Tests. Materials and Structures, Vol. 23, pp. 457-460.

RILEM TC 89-FMT Fracture Mechanics of Concrete-Test Methods, (1990). Size Effect Method for Determining Fracture Energy and Process Zone Size of Concrete. Materials and Structures, Vol. 23, pp. 461-465.

Ritter, W., (1899). Die Bauweise Hennebique. Schweizerische Bauzeitung. Zurich, Switzerland.

Scheetz, B.E., Menghini, M.J., Hornberger, R.J., Owens, T.D., and Schueck, J., (1997). Beneficial Use of Coal Ash in Anthracite and Bituminous Mine Reclamation and Mine Drainage Pollution Abatement in Pennsylvania. Proceedings of the Air & Waste Management Association. Toronto, ON, Canada.

Schlaich, J., Schäfer, K., and Jennewein, M., (1987). Towards a Consistent Design of Structural Concrete. PCI Journal, Vol. 32, No. 3, pp. 74-150.

Shah, S.G., Bhasya, V., and Chandra Kishen, J.M., (2011). Tension-Softening Properties for Concrete-Concrete Interfaces. ACI Structural Journal, Vol. 108, No. 6, pp. 725-734.

Shah, S.P., and Carpinteri, A., (1991). Fracture Mechanics Test Methods for Concrete: Report of Technical Committee 89-FMT (1st Ed.). Chapman and Hall.

So, K.O., and Karihaloo, B.L., (1993). Shear Capacity of Longitudinally Reinforced Beams – A Fracture Mechanics Approach. ACI Structural Journal, Vol. 90, No. 6, pp. 591-600.

Swamy, R.N., and Hung, H.H., (1998). Engineering Properties of High Volume Fly Ash Concrete. ACI Special Publication, Vol. 178, pp. 331–359.

Taylor, HPJ. (1972). "Shear Strength of Large Beams," Journal of the Structural Division, ASCE, V. 98, No. ST11, Nov., pp. 2473-2489.

Taylor, HPJ. (1974). "The Fundamental Behavior of Reinforced Concrete Beams in Bending and Shear," American Concrete Institute, Shear in Reinforced Concrete, SP-42, pp. 43-77.

Thomas, M., (2007). Optimizing the Use of Fly Ash in Concrete. Portland Cement Association. Skokie, Illinois. United States of America.

Tureyen, A.K., (2001). Influence of Longitudinal Reinforcement Type on the Shear Strength of Reinforced Concrete Beams without Transverse Reinforcement. PhD Thesis. Purdue University. United States of America.

Tureyen, A.K, and Frosch, R.J., (2003). Concrete Shear Strength: Another Perspective. ACI Structural Journal, Vol. 100, No. 5, pp. 609-615.

van der Veen, C., (1990). Cryogenic Bond Stress-Slip Relationship. MS Thesis. Delft University. Delft, Netherlands.

Vecchio, F.J., and Collins, M.P., (1986). The Modified Compression Field Theory for Reinforced Concrete Elements Subjected to Shear. ACI Journal Proceedings, Vol. 83, No. 2, pp. 219-231.

Vecchio, F.J., and Collins, M.P., (1993). Compression Response of Cracked Reinforced Concrete. Journal of Structural Engineering, Vol. 119, No. 12, pp. 3590-3610.

Walraven, J.C., (1980). Aggregate Interlock: a Theoretical and Experimental Analysis. PhD Thesis. Delft University of Technology. Delft, Netherlands.

Whitney, C.S., (1937). Design of Reinforced Concrete Members Under Flexure or Combined Flexure and Direct Compression. ACI Journal Proceedings, Vol. 33, No. 3, pp. 483-498.

Wight, J.K., and MacGregor, J.G., (2009). Reinforced Concrete Mechanics and Design (5th Ed.). Pearson-Prentice Hall.

Wright, P.J.F, (1955). Comments on an Indirect Tensile Test on Concrete Cylinders. Magazine of Concrete Research, Vol. 7, No. 20, pp. 87-96.

Zakaria, M., Ueda, T., Wu, Z., and Meng, L., (2009). Experimental Investigation on Shear Cracking Behavior in Reinforced Concrete Beams with Shear Reinforcement. Journal of Advanced Concrete Technology, Vol. 7, No. 1, pp. 79-96.

FINAL Report D

TRyy1110

**Project Title: Design and Evaluation of High-Volume
Fly Ash (HVFA) Concrete Mixes**

**Report D: Creep, Shrinkage, and Abrasion Resistance of
HVFA Concrete**

ABSTRACT

The main objective of this study was to determine the effect on shrinkage, creep, and abrasion resistance of high-volume fly ash (HVFA) concrete. The HVFA concrete test program consisted of comparing the shrinkage, creep, and abrasion performance of two concrete mix designs with 70% cement replacement with Class C fly ash relative to a Missouri Department of Transportation (MoDOT) standard mix design.

Modified versions of standard test methods were used for the shrinkage and creep portions of the study. Shrinkage was measured through a modified version of ASTM C157 "Standard Test Method for Length Change of Hardened Hydraulic-Cement Mortar and Concrete," while creep was measured through a modified version of ASTM C512 "Standard Test Method for Creep of Concrete in Compression." Abrasion resistance was measured in accordance with ASTM C944 "Standard Test Method for Abrasion Resistance of Concrete or Mortar Surfaces by Rotating-Cutter Method."

In addition to comparisons between the three mix designs, the results were also compared to existing prediction models and previous research results on HVFA concrete. Both HVFA concrete mixes showed a significant decrease in shrinkage strain relative to the control concrete, which was very consistent with previous research. With regard to creep, both HVFA concrete mixes also showed improved performance over the control mix, again confirming previous research results. However, the control concrete exhibited improved abrasion resistance relative to the two HVFA concrete mixes, which coincided with the higher strength of the control mix. At later ages, the abrasion resistance of the HVFA concrete improved due to late age strength gain characteristic of this material.

TABLE OF CONTENTS

LIST OF ILLUSTRATIONS

LIST OF TABLES

NOMENCLATURE

Symbol	Description
A	Cement type correction factor (NCHRP 628)
A_c	Cross-section area (mm^2) (CEB-FIP 90)
c	Cement content (lb/yd^3) (ACI 209R-92)
D	Effective cross-section thickness (Model B3)
D_0	Datum reading on the reference bar
D_i	Subsequent reading on the reference bar
f	Size effects factor (ACI 209R-92)
f'_c	Tested compressive strength of concrete (psi, ksi, MPa)
f'_{ci}	Specified compressive strength of concrete (ksi) (NCHRP 496)
f_{cm}	Tested compressive strength of concrete at 28 days age (psi, ksi, MPa) (CEB-FIP 90)
G	Gauge factor
H	Relative humidity (% or decimal)
K	Cement type correction factor (GL 2000)
k_f	Concrete strength factor (NCHRP 496)
k_{hc}	Humidity factor (NCHRP 496)
k_{hs}	Humidity factor (NCHRP 496 and NCHRP 628)
k_{la}	Loading factor (NCHRP 496)
k_s	Size factor (NCHRP 496 and NCHRP 628) or Cross-section shape factor (Model B3)
k_{td}	Time development factor (NCHRP 496)

R_0	Datum reading on tested material
RH	Relative humidity (%) (CEB-FIP 90)
R_i	Subsequent reading on tested material
s	Slump of fresh concrete (in)
S(t)	Time dependence factor (Model B3)
t	Age of concrete (days)
t_0	Age of concrete when drying begins (days) (Model B3)
	or Age at which creep specimen is loaded (days) (ACI 209R-92
	and CEB FIP 90)
t_c	Age of concrete when drying begins (days) (ACI 209R-92
	and GL 2000)
t_i	Age at which creep specimen is loaded (days) (NCHRP 496)
t_s	Age of concrete at the beginning of shrinkage (days) (CEB-FIP 90)
u	Perimeter in contact with the atmosphere (mm) (CEB-FIP 90)
V/S	Volume to Surface area ratio (in or mm)
w	Water content of concrete (lb/ft^3)
α	Concrete air content (%)
$α_1$	Cement type correction factor (Model B3)
$α_2$	Curing condition correction factor
β(h)	Humidity correction factor (GL 2000)
β(t)	Time effect correction factor (GL 2000)
$β_c$	Coefficient to describe the development of creep with time after loading
	(CEB FIP 90)

β_{RH}	Relative humidity correction factor (CEB-FIP 90)
β_s	Coefficient to describe the development of shrinkage with time (CEB-FIP 90)
β_{sc}	Concrete type correction factor (CEB-FIP 90)
$\gamma_{c,RH}$	Humidity correction factor (ACI 209R-92)
$\gamma_{c,s}$	Slump correction factor (ACI 209R-92)
$\gamma_{c,t0}$	Curing condition correction factor (ACI 209R-92)
$\gamma_{c,vs}$	Size correction factor (ACI 209R-92)
$\gamma_{c,\alpha}$	Air content correction factor (ACI 209R-92)
$\gamma_{c,\psi}$	Fine aggregate correction factor (ACI 209R-92)
$\gamma_{sh,c}$	Cement content correction factor (ACI 209R-92)
$\gamma_{sh,RH}$	Relative humidity correction factor (ACI 209R-92)
$\gamma_{sh,s}$	Slump correction factor (ACI 209R-92)
$\gamma_{sh,tc}$	Initial moist cure duration correction factor (ACI 209R-92)
$_{sh,vs}$	Volume/surface area correction factor (ACI 209R-92)
$\gamma_{sh,\alpha}$	Air content correction factor (ACI 209R-92)
$\gamma_{sh,\psi}$	Fine aggregate correction factor (ACI 209R-92)
$\Delta_{\varepsilon c}$	Change in creep strain from one reading to the next
$\Delta_{\varepsilon s}$	Change in shrinkage strain from one reading to the next
ε_{cso}	Notional shrinkage coefficient (CEB-FIP 90)
$\varepsilon_{es(t,ts)}$	Calculated ultimate shrinkage strain ($\mu\varepsilon$) (CEB-FIP 90)
ε_i	Measured strain due to initial loading of creep specimen
$\varepsilon_{es(t,t0)}$	Calculated shrinkage strain at a given age ($\mu\varepsilon$) (Model B3)

ε_{sh}	Calculated shrinkage strain at a given age ($\mu\varepsilon$) (NCHRP 496, GL 2000, and NCHRP 628)
$\varepsilon_{sh(t,tc)}$	Calculated shrinkage strain at a given age ($\mu\varepsilon$) (ACI 209R-92)
ε_{shu}	Calculated ultimate shrinkage strain ($\mu\varepsilon$) (ACI 209R-92) or Notional ultimate shrinkage strain (GL 2000)
$\varepsilon_{sh\infty}$	Calculated ultimate shrinkage strain ($\mu\varepsilon$) (Model B3)
ε_t	Measured creep strain at a given age
λ_Δ	Multiplier for additional deflection due to long-term effects (ACI 318-08)
ξ	Time dependant factor for sustained load (ACI 318-08)
ρ'	Compression reinforcement ratio (ACI 318-08)
τ_{sh}	Size dependence factor (Model B3)
$\Phi_{(t,t0)}$	Calculated creep coefficient at a given age (ACI 209R-92 and CEB FIP 90) or Measured creep coefficient at a given age
Φ_0	Notional creep coefficient (CEB FIP 90)
Φ_{28}	Calculated creep coefficient at a given age (GL 2000)
$\Phi_{(tc)}$	Factor that takes into account drying before loading (GL 2000)
Φ_u	Calculated ultimate creep coefficient (ACI 209R-92)
Ψ	Ratio of fine aggregate to total aggregate by weight (%)
$\Psi_{(t,ti)}$	Calculated creep coefficient at a given age (NCHRP 496 and NCHRP 628)

1. LITERATURE REVIEW

1.1. HIGH VOLUME FLY ASH CONCRETE (HVFA)

1.1.1. Fly Ash. Fly ash is defined by ACI 116R-00 as "the finely divided residue that results from the combustion of ground or powdered coal and that is transported by flue gases from the combustion zone to the particle removal system." Fly ash is often collected in this manner from coal burning electric power plants and is considered a waste product of the power plant. As reported by the American Coal Ash Association's 2010 Coal Combustion Product Production & Use Survey Report, there were 67,700,000 tons (61,400,000,000 kg) of fly ash produced, of which 11,000,000 tons (9,990,000,000 kg) (16.3%) were used in concrete, concrete products, or grout.

1.1.2. Definition of HFVA. Concretes containing 15% - 35% fly ash replacement by mass of total cementitious material are typically used. High volume concrete is concrete that contains a much higher percentage of fly ash replacement than the typical fly ash concrete mix. The exact definition of high volume fly ash concrete varies depending on the source. ACI 232.2R-03 states "HVFA concrete may be defined as having a fly ash content of 50% or greater by mass of cementitious materials." ACI also cites research from Haque, Langan, and Ward (1984) and Ramme and Tharaniyil (2000) which define high volume fly ash concrete as concrete with fly ash replacement of 40% and 37% respectively. The report concludes that "HVFA concrete can be considered to represent concrete containing higher percentages of fly ash than normal for the intended application of the concrete." (ACI 232.2R-11)

1.1.3. Advantages of HVFA. The advantages of using fly ash as a replacement

for Portland cement in concrete production include economic benefits, environmental

benefits, as well as some advantageous material properties. Fly ash is generally cheaper

to purchase than Portland cement, however this is dependent on local availability and

transportation costs. Since fly ash is otherwise considered a waste product, which is

either disposed of in landfills or released into the atmosphere, its use as a recycled

material is considered very environmentally advantageous. The use of HVFA concrete

can contribute to LEED certification by the U.S. Green Building Council, applicable to

MR credit 4-recycled content (USGBC). Use of fly ash also has beneficial effects on the

properties of the concrete in which it is used. Because fly ash has a lower specific gravity

than cement, its replacement by mass will increase the paste volume of the concrete,

allowing for an increase in workability. Fly ash also contributes to less bleeding in fresh

concrete. HVFA concrete also retards setting time and strength gain, which can be

beneficial in mass concrete projects. Research has also shown that fly ash concrete

reaches a higher ultimate strength than conventional concrete.

1.2. SHRINKAGE OF CONCRETE

1.2.1. Definition of Shrinkage. Shrinkage of concrete is the decrease in

volume of hardened concrete with time. Shrinkage is expressed as the strain measured on

a load-free specimen, most often as the dimensionless unit microstrain (strain x10^{-6}).

Concrete experiences shrinkage in three ways, drying shrinkage, autogenous (chemical)

shrinkage, and carbonation shrinkage. Autogenous shrinkage is due strictly to the

hydration reactions of the cement. Drying shrinkage is the strain imposed on a specimen

exposed to the atmosphere and allowed to dry. Carbonation shrinkage is caused by the reaction of calcium hydroxide with cement with carbon dioxide in the atmosphere. The magnitude and rate of shrinkage is dependent on a number of factors. These factors are accounted for and described in the various industry models and research projects in the following sections.

1.2.2. Factors Affecting Shrinkage (ACI 209.1R-05). Shrinkage of concrete is closely related to shrinkage of paste. Therefore the amount of paste in the mix significantly affects the level of concrete shrinkage. Paste volume is determined by the quantity, size, and gradation of aggregate. Because paste volume is largely dependent on aggregate properties, the most important factor in determining a concrete's shrinkage level is the aggregate used in the mix. Similarly, the water content, cement content, and slump will affect the shrinkage of concrete. These three factors are indications of the paste volume and therefore can be used to determine the shrinkage potential of a mix. Aggregate acts as a restraining force to shrinkage, therefore an aggregate with a higher modulus of elasticity (MOE) will better restrain against shrinkage than an aggregate with a lower MOE. The characteristics of the cement itself are other significant indicators of shrinkage potential. Research has shown cements with low sulfate content, high alumina content, and cements that are finely ground exhibit increased shrinkage.

The environment which the concrete is exposed to can also influence shrinkage. The biggest environmental factor is the relative humidity of the surrounding air. As shown by **Eq. 2.1**, as relative humidity increases, shrinkage decreases due to the decrease in potential moisture loss. It has also been shown that an increase in temperature increases the ultimate shrinkage of concrete.

$$\text{shrinkage} \propto 1 - \left(\frac{h}{100}\right)^b \tag{1.1}$$

Where: h is relative humidity in percent, and b is a constant that ranges from 1 to 4.

Finally, the design and construction of concrete specimens can influence shrinkage. The curing conditions experienced by the concrete have a significant effect on shrinkage. Generally, the longer the specimen is allowed to moist cure, the less it will shrink. However, research conducted by Perenchio (1997), **Figure 1.1**, shows that there may not be a simple relationship between moist cure time and shrinkage.
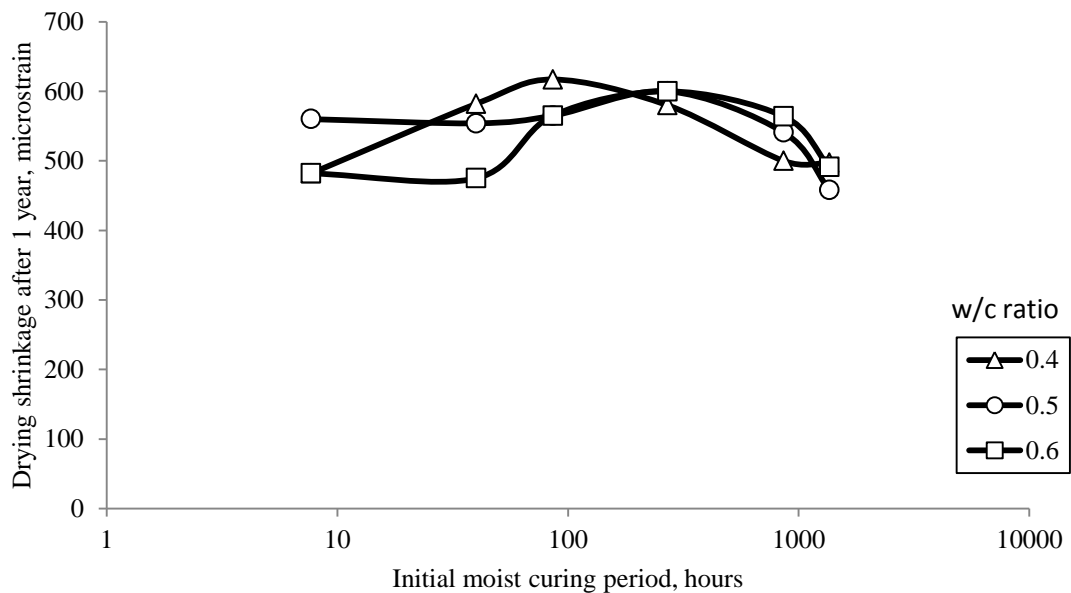
Figure 1.1 - Relationship Between Moist Cure Time and Shrinkage Strain (adapted from Perenchio 1997)

Larger members tend to dry slower, so the ratio of volume to surface area is a significant factor in shrinkage of concrete.

$$\text{shrinkage} \propto \frac{1}{(\frac{V}{S})^2} \qquad (1.2)$$

Where: V/S is the volume to surface area ratio in inches.

1.3. SHRINKAGE MODELS.

The ability to accurately predict the shrinkage of a concrete structure is extremely important. An accurate model for shrinkage will allow the engineer to predict long term serviceability, durability, and stability of a given structure. As mentioned above, there are many different factors that affect a concrete's susceptibility to shrinkage. Because of these factors, accurate prediction of shrinkage is very difficult. The models described below take into account many of the factors described above in their attempt to predict concrete shrinkage (Bazant and Baweja, 2000).

1.3.1. ACI 209R-92. This model, developed by Branson and Christiason (1971) and modified by ACI committee 209, predicts shrinkage strain of concrete at a given age under standard conditions. The original model by Branson and Christiason was developed based on a best fit from a sample of 95 shrinkage specimens and using an ultimate shrinkage strain of 800×10^{-6} in./in. (mm/mm). However, subsequent research by Branson and Chen, based on a sample of 356 shrinkage data points, concluded that the ultimate shrinkage strain should be 780×10^{-6} in./in. (mm/mm). The prediction model, **Eq. 1.3 – 1.5**, apply only to the standard conditions as shown in **Table 1.1**.

$$\varepsilon_{sh}(t, t_c) = \frac{(t-t_c)^\alpha}{f+(t-t_c)^\alpha} \epsilon_{shu} \quad (\mu\varepsilon) \tag{1.3}$$

$$\varepsilon_{shu} = 780 \times 10^{-6} \quad (\mu\varepsilon) \tag{1.4}$$

$$f = 26.0e^{\{0.36(V/S)\}} \tag{1.5}$$

Where: f is 35 (moist cure) or 55 (steam cure), or by **Eq. 1.5** if size effects are to be considered, α is assumed to be 1, t is the age of concrete it days, and t_c is the age of concrete when drying begins in days.

Table 1.1 - Standard Conditions as Defined by ACI 209R-92

Factors			Variables	Standard
Concrete	Concrete Composition	Cement Paste Content	Type of Cement	Type I or III
		W/C	Slump	2.7 in (70mm)
		Mix Proportions	Air Content	≤ 6%
		Aggregate Characteristics	Fine Aggregate %	50%
		Degree of Compaction	Cement Content	470 to 752 lb/yd^3 (279 to 446 kg/m^3)
	Initial Curing	Length of Initial Curing	Moist Cured	7 days
			Steam Cured	1 - 3 days
		Curing Temperature	Moist Cured	73.4 ± 4°F (23 ± 2°C)
			Steam Cured	≤212°F (≤100°C)
		Curing Humidity	Relative Humidity	≥95%
Member Geometry & Environment	Environment	Concrete Temperature	Concrete Temperate	73.4°F ± 4°F (23 ± 2°C)
		Concrete Water Content	Ambient Relative Humidity	40%
	Geometry	Size and Shape	Volume-Surface Ratio (V/S)	V/S = 1.5 in (38mm)
			Minimum Thickness	6 in (150mm)

When concrete is not subject to any or all of the standard conditions, correction factors shall be applied, as shown in **Eq. 1.6 – 1.16**.

$$\varepsilon_{sh}(t, t_c) = \frac{(t-t_c)^\alpha}{f+(t-t_c)^\alpha} \times \varepsilon_{shu} \quad (\mu\varepsilon) \tag{1.6}$$

$$f = 26.0 e^{\{0.36(V/S)\}} \tag{1.7}$$

$$\varepsilon_{shu} = 780\gamma_{sh} \times 10^{-6} \quad (\mu\varepsilon) \tag{1.8}$$

$$\gamma_{sh} = \gamma_{sh,tc}\gamma_{sh,RH}\gamma_{sh,vs}\gamma_{sh,s}\gamma_{sh,\psi}\gamma_{sh,c}\gamma_{sh,\alpha} \tag{1.9}$$

$$\gamma_{sh,tc} = 1.202 - .2337\log(t_c) \tag{1.10}$$

$$\gamma_{sh,RH} = \begin{array}{ll} 1.40 - 1.02h & \text{for } 0.40 \leq h \leq 0.80 \\ 3.00 - 3.0h & \text{for } 0.80 \leq h \leq 1 \end{array} \tag{1.11}$$

$$\gamma_{sh,vs} = 1.2e^{\{-0.12(V/S)\}} \tag{1.12}$$

$$\gamma_{sh,s} = 0.89 + 0.041s \tag{1.13}$$

$$\gamma_{sh,\psi} = \begin{array}{ll} 0.30 + 0.014\psi & \text{for } \psi \leq 50\% \\ 0.90 + 0.002\psi & \text{for } \psi > 50\% \end{array} \tag{1.14}$$

$$\gamma_{sh,c} = 0.75 + 0.00036c \tag{1.15}$$

$$\gamma_{sh,\alpha} = 0.95 + 0.008\alpha \geq 1 \tag{1.16}$$

Where: $\varepsilon_{sh}(t,t_c)$ is the calculated shrinkage strain at a given age, ε_{shu} is the calculated ultimate shrinkage strain, $\gamma_{sh,tc}$ is the initial moist cure duration correction factor, t is the age of concrete in days, t_c is the age of concrete when drying starts in days, $\gamma_{sh,RH}$ is the relative humidity correction factor, h is humidity in decimals, $\gamma_{sh,vs}$ is the volume/surface

area correction factor, where V/S is the volume to surface area ratio in inches, $\gamma_{sh,s}$ is the slump correction factor, s is slump in inches, $\gamma_{sh,\psi}$ is the fine aggregate correction factor, ψ is the ratio of fine aggregate to total aggregate by weight expressed as percentage, $\gamma_{sh,c}$ is the cement content correction factor, c is the cement content in lb/yd^3, $\gamma_{sh,\alpha}$ is the air content correction factor, and α is the air content in percent. In **Eq 1.6**, the value of α can be assumed to be equal to 1, with f assumed to be equal to 35 for concrete that is moist cured for seven days or 55 for concrete subject to 1-3 days of steam curing. In order to totally consider shape and size effects, α is still assumed to be equal to 1, with f given by **Eq. 1.7**.

   1.3.2. NCHRP Report 496 (2003). The National Cooperative Highway Research Program (NCHRP) conducted research on shrinkage of high strength concrete in the states of Nebraska, New Hampshire, Texas, and Washington. This research project was sponsored by the American Association of State Highway and Transportation Officials (AASHTO) and the results adopted into the 2007 AASHTO LRFD Bridge Design Specifications. Laboratory shrinkage data was obtained from three 4 in. (101.6 mm) by 4 in. (101.6 mm) by 24 in. (609.6 mm) specimens per mix, with a total of 48 specimens tested including both normal and high strength concrete. Field specimens were also made and cured in the same condition as corresponding bridge girders in each of the four participating states. The field program consisted of a set of three 4 in. (101.6 mm) by 4 in. (101.6 mm) by 24 in. (609.6 mm) shrinkage specimens at each location with measurements taken for 3 months. The data showed that an ultimate shrinkage strain of 480×10^{-6} in./in. (mm/mm) should be assumed. The modification factors in the model

account for the effects of high strength concrete. **Eq. 1.17 – 1.22** present the proposed

shrinkage formula as proposed in this study.

$$\varepsilon_{sh} = 480 \times 10^{-6} \gamma_{sh} \ (\mu\varepsilon) \tag{1.17}$$

$$\gamma_{sh} = k_{td} k_s k_{hs} k_f \tag{1.18}$$

$$k_{td} = \frac{t}{61 - 4f'_{ci} + t} \tag{1.19}$$

$$k_{hs} = 2.00 - 0.0143H \tag{1.20}$$

$$k_s = \frac{1064 - 94^V/_S}{735} \tag{1.21}$$

$$k_f = \frac{5}{1 + f'_{ci}} \tag{1.22}$$

Where: ε_{sh} is the calculated shrinkage strain at a given age, k_{td} is the time development

factor, t is the age of the concrete in days, k_{hs} is the humidity factor, H is the average

ambient relative humidity in percent, k_s is the size factor, V/S is the volume to surface

area ratio in inches, k_f is the concrete strength factor, and f'_{ci} is the specified compressive

strength of concrete in ksi.

1.3.3. Model B3. Model B3 (Bazant and Baweja) is the third update of

shrinkage predictions developed at Northwestern University, based on BP model β3 and

BP-KX model β4. This model is simpler than previous versions and is validated by a

larger set of test data. **Eq. 1.23 – 1.32** present the B3 shrinkage prediction model.

$$\varepsilon_{sh}(t, t_0) = -\varepsilon_{sh\infty} k_h S(t) \ (\mu\varepsilon) \tag{1.23}$$

$$S(t) = \tanh \sqrt{\frac{t - t_0}{\tau_{sh}}} \tag{1.24}$$

$$k_h = \begin{array}{ll} 1 - h^3 & \text{for} \quad h \le 0.98 \\ -0.2 & \text{for } h = 1 (\text{swelling in water}) \\ \text{linear} \\ \text{interpolation} & \text{for} \quad 0.98 \le h \le 1 \end{array} \tag{1.25}$$

$$\tau_{sh} = k_t (k_s D)^2 \tag{1.26}$$

$$k_t = 190.8 t_0^{-0.08} f'_c{}^{-1/4} \tag{1.27}$$

$$D = {2V}/{S} \ (\text{in.}) \tag{1.28}$$

$$k_s = \begin{array}{ll} 1.00 & \text{for} \quad \text{an infinite slab} \\ 1.15 & \text{for} \quad \text{an infinite cylinder} \\ 1.25 & \text{for} \quad \text{an infinite square prism} \\ 1.30 & \text{for} \quad \text{a sphere} \\ 1.55 & \text{for} \quad \text{a cube} \end{array} \tag{1.29}$$

$$\varepsilon_{sh\infty} = -\alpha_1\alpha_2\left[26w^{2.1}f'_c{}^{-0.28} + 270\right] \ (\mu\varepsilon) \tag{1.30}$$

$$\alpha_1 = \begin{array}{ll} 1.0 & \text{for type I cement} \\ 0.85 & \text{for type II cement} \\ 1.1 & \text{for type III cement} \end{array} \tag{1.31}$$

$$\alpha_2 = \begin{array}{ll} 0.75 & \text{for steam} - \text{curing} \\ 1.2 & \begin{array}{l}\text{for sealed or normal curing in air} \\ \text{with initial protection against drying}\end{array} \\ 1.0 & \text{for curing in water or at 100\% relative humidity} \end{array} \tag{1.32}$$

Where: $\varepsilon_{shu}(t,t_0)$ is the calculated shrinkage strain at a given age, $S(t)$ is the time dependence factor, t is the age of concrete in days, t_0 is the age of concrete at which drying begins, τ_{sh} is the size dependence factor, $f'c$ is the cylinder compressive strength in psi, D is the effective cross-section thickness, V/S is the volume to surface area ratio in inches, k_s is the cross-section shape factor, $\varepsilon_{sh\infty}$ is the calculated ultimate shrinkage strain, α_1 is the cement type correction factor, α_2 is the curing condition correction factor, and w is the water content of the concrete in lb/ft^3.

1.3.4. CEB-FIP 90. This model, developed jointly by Euro-International Concrete Committee (CEB – Comité Euro-International du Béton) and the International Federation for Prestressing (FIP – Fédération Internationale de la Précontrainte) is found in the CEB-FIP Model Code 1990. It is stated that due to its international character, the code is more general than most and does not apply to any particular structure type. **Eq. 1.33 – 1.38** present this model for calculating shrinkage strain.

$$\varepsilon_{es}(t, t_s) = \varepsilon_{cso}\beta_s(t - t_s) \ (\mu\varepsilon) \tag{1.33}$$

$$\varepsilon_{cso} = \varepsilon_s(f_{cm})(\beta_{RH}) \tag{1.34}$$

$$\beta_s(t - t_s) = \sqrt{\frac{(t-t_s)}{350(\frac{2A_c}{100u})^2+(t-t_s)}} \tag{1.35}$$

$$\varepsilon_s(f_{cm}) = [160 + 10\beta_{sc}(9 - 0.1f_{cm})] \times 10^{-6} \tag{1.36}$$

$$\beta_{RH} = -1.55[1 - (^{RH}/_{100})^3] \tag{1.37}$$

$$\beta_{sc} = \begin{array}{ll} 4 & \text{for slowly hardening cements} \\ 5 & \text{for normal or rapid hardening cements} \\ 8 & \text{for rapid hardening high strength cements} \end{array} \tag{1.38}$$

Where: $\varepsilon_{es}(t,t_s)$ is the calculated ultimate shrinkage strain, ε_{cso} is the notional shrinkage coefficient, β_s is the coefficient to describe the development of shrinkage with time, t is the age of concrete in days, t_s is the age of concrete at the beginning of shrinkage in days, A_c is the cross section area in mm^2, u is the perimeter in contact with the atmosphere in mm, f_{cm} is the compressive strength of concrete at age of 28 days in MPa, β_{RH} is the relative humidity correction factor, RH is the relative humidity in percent, and β_{sc} is the concrete type correction factor.

1.3.5. GL 2000. This model, developed by Gardener and Lockman was published in the ACI materials journal under the title "Design provisions for drying shrinkage and Creep of Normal-Strength Concrete." The model developed is shown in **Eq. 1.39 – 1.43**.

$$\varepsilon_{sh} = \varepsilon_{shu}\beta(h)\beta(t) \ (\mu\varepsilon) \tag{1.39}$$

$$\varepsilon_{shu} = 1000K\sqrt{\frac{30}{f'_c}} \times 10^{-6} \ (\mu\varepsilon) \tag{1.40}$$

$$\beta(h) = 1 - 1.18h^4 \tag{1.41}$$

$$\beta(t) = \sqrt{\frac{t-t_c}{t-t_c+0.15(V/S)^2}} \tag{1.42}$$

$$K = \begin{array}{ll} 1 & \text{for type I cement} \\ 0.75 & \text{for type II cement} \\ 1.15 & \text{for type III cement} \end{array} \tag{1.43}$$

Where: ε_{sh} is the calculated shrinkage strain at a given age, ε_{shu} is the notional ultimate shrinkage strain, $\beta(h)$ is the humidity correction factor, h is humidity in decimals, $\beta(t)$ is the correction factor for the effect of time on shrinkage, t_c is the age that drying has commenced in days, t is age of concrete in days, V/S is the volume to surface area ratio, and K is the cement type correction factor.

1.4. HVFA SHRINKAGE RESEARCH

Shrinkage of concrete containing fly ash has been researched extensively. The sections below present the data collected and results compiled from research programs into shrinkage of HVFA concrete.

1.4.1. Atis. Six concrete mixes were tested for shrinkage strain at ages up to

6 months. Two mixes were conventional concrete, two had a fly ash replacement of 70%

by mass of cement, and the final two mixes had a fly ash replacement of 50% by mass of

cement. The mix designs used in this project are shown in **Table 1.2**. Each pair of mixes

(OPC, 70%, and 50%) had one mix which was considered roller compacted concrete

(RCC) and had a slump of zero. The other mix contained superplasticizer which produced

a mix which was practically flowable. At every age of testing and for each type of mix,

RCC and flowable, except at 14 days for the flowable mixes, the measured shrinkage

strain decreased as the fly ash replacement percentage increased. The results show that

concrete made with superplasticizer showed higher shrinkage strains than concrete made

without superplasticizer. It was also concluded that, because of HVFA concrete's lower

shrinkage strain, the number of joints in concrete pavement construction could be

reduced by the use of HVFA concrete. The experimental results are shown in **Table 1.3**.

Table 1.2 - Mix Designs (Atis 2003) (kg per cubic meter)

Mix	M1	M2	M3	M4	M5	M6
Cement (kg)	400	400	120	120	200	200
Fly ash (kg)	---	---	280	280	200	200
Sand (kg)	600	600	600	600	600	600
Gravel (kg)	1200	1200	1200	1200	1200	1200
Water (L)	136	128	112	116	132	120
Optimum W/C ratio	0.32	0.32	0.29	0.29	0.30	0.30
Actual W/C ratio	0.34	0.32	0.28	0.29	0.33	0.30
Superplasticizer	5.6	---	5.6	---	5.6	---
Flow table (mm)	560	0	570	0	600	0

Conversion: 1 kg/m^3 = 1.686 lb/yd^3

Table 1.3 - Experimental Shrinkage Results (Atis 2003) (microstrain)

Drying Time	M1	M2	M3	M4	M5	M6
1 day	86	72	56	34	63	38
3 days	134	122	94	69	109	88
7 days	172	148	144	100	153	113
14 days	225	190	164	141	192	125
28 days	347	265	231	163	256	169
56 days	390	296	294	200	319	213
3 months	488	334	350	225	363	256
6 months	554	385	394	263	413	294

1.4.2. Termkhajornkit, et. al. One ordinary Portland cement mix and three different kinds of fly ash mixes were tested to determine autogenous shrinkage of each mix. Fly ash replacement of 25% and 50% were used for two of the mixes, while the third had only a 50% replacement mix. In order to isolate autogenous shrinkage, the specimens were cast in molds and sealed to avoid evaporation. Strain was measured using a strain gauge placed in the center of the mold with concrete cast around it. The samples were kept in a controlled chamber with constant humidity and temperature. For the two mixes where the fly ash replacement was varied, the higher level (50% replacement) mix showed a significant reduction in measured shrinkage strain. Interestingly, all three mixes with 50% replacement outperformed the conventional mixes, while both 25% replacement mixes underperformed the conventional mixes.

1.4.3. Gao, et. al. RCC concrete typical to dam and pavement construction was tested for shrinkage strain. Shrinkage data was recorded for one baseline mix and one equivalent mix with a 50% cement replacement with fly ash. It was concluded that, at 150 days, the shrinkage strains of the 50% replacement mix was approximately 33% less than that of the specimen without fly ash.

1.4.4. Nath and Sarker. Two different concrete series, labeled as series A and B in this study, were tested for drying shrinkage up to 180 days. Both series had one mix with no fly ash replacement, one mix with 30% replacement, and one mix with 40% replacement. Series A was designed in a way that all three mixes attained similar 28 day compressive strengths. Series B was designed so that all three mixes had an identical water to total binder content ratio (w/b) of 0.29. The results of series A show that, with varying w/b and similar strength, fly ash concretes show less shrinkage as the replacement is increased. Series B shows that with an increase in total cementitious material at a constant w/b, the shrinkage strains shown at 180 days of fly ash mixes are very similar to the control mix. Results are shown in **Figures 1.2 – 1.3**.
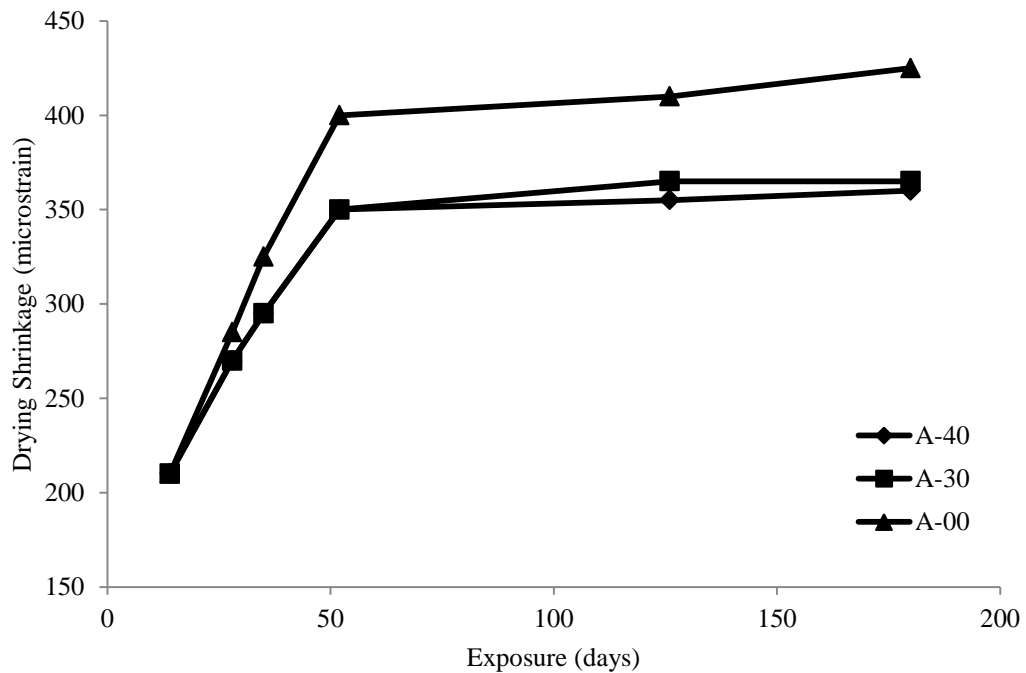
Figure 1.2 - Series A Shrinkage Results (adapted from Nath and Sarker)
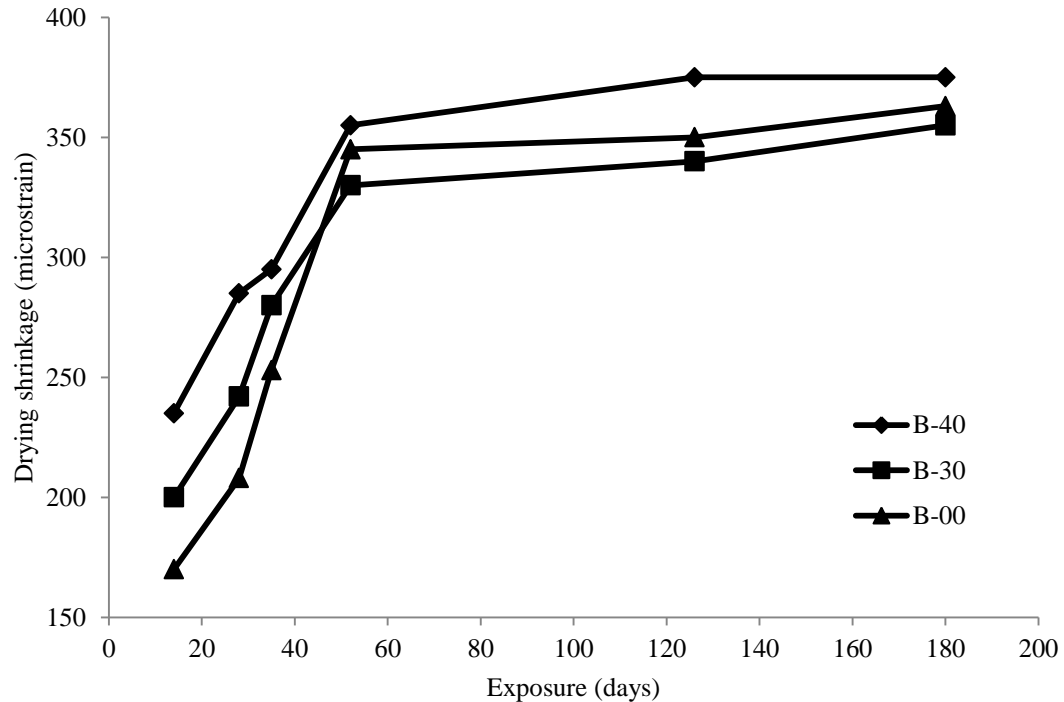
Figure 1.3 - Series B Shrinkage Results (adapted from Nath and Sarker)

1.5. CREEP OF CONCRETE

1.5.1. Definition of Creep. Creep of concrete is defined as "the time-dependent increase in strain under sustained constant load taking place after the initial strain at loading" (ACI 209.1R-05). Initial strain is the short term strain at the moment of loading. Initial strain is difficult to determine as it is very dependent on the duration and rate of initial load and there is no clear distinction between initial strain and creep strain. Creep strain can be broken up into two parts, basic creep and drying creep. Basic creep is "the increase in strain under sustained constant load of a concrete specimen in which moisture losses or gains are prevented." Even after 30 years of measurement on sealed concrete specimens, it had yet to be determined if basic creep approaches an ultimate value. Drying creep is the additional creep occurring in a specimen exposed to the environment and allowed to dry. The effects of creep can be expressed in three ways. The first is

similar to that of shrinkage, where creep strain is simply expressed in terms of microstrain (strain $x10^{-6}$). The second way is called the creep coefficient. The creep coefficient is the ratio of creep strain to the initial strain at loading. The third is specific creep. Specific creep is the ratio of microstrain to applied load (psi).

1.5.2. Factors Affecting Creep. Like shrinkage, creep is affected by numerous material, mix design, environmental, and construction related factors. Similar to shrinkage, the amount, size, gradation, and properties of the aggregate are very influential on creep of concrete. An increase in aggregate volume will decrease creep. Aggregate gradation is believed to influence creep of concrete because of its relation to changes in overall aggregate volume. The size of aggregate affects bond between paste and aggregate, which controls stress concentration and microcracking. Unlike shrinkage, which is primarily affected by properties of the paste, creep is very dependent on the elastic properties of the aggregate. Concretes with aggregate that have a lower modulus of elasticity generally have higher creep. The primary environmental factor in creep is relative humidity. As relative humidity increases, drying creep significantly decreases. Specimens in environments where drying cannot occur may have only one quarter of the creep of concrete which is allowed to dry. The effects of construction and design on creep are slightly different than shrinkage. One similarity is that increased curing time will decrease creep strain. Unlike shrinkage, basic creep is not affected by the size and shape of the member. The factor that most affects creep is the load applied to the specimen. The magnitude of the load, and the age at which the load is first applied are very important. Loads up to $0.40f'_c$ are considered to be linearly related to creep. Finally, concrete loaded at later ages has lower creep.

1.6. CREEP MODELS

As with shrinkage, considerable research has been done and models developed to predict the creep potential of concrete. The following sections will present various models for calculating creep.

1.6.1. ACI 209R-92. This model is based on the same research as the ACI 209 shrinkage model. The standard conditions as shown in **Table 1.1** apply to creep as well. **Eq. 1.44 – 1.46** represent the general model for concrete meeting the standard conditions. If standard conditions are met, γ_c is taken to be equal to 1. Like the shrinkage model, if any or all of the standard conditions are not met, the model modification factors must be used as shown in **Eq. 1.47 – 1.53**.

$$\Phi(t, t_0) = \frac{(t-t_0)^\Psi}{d+(t-t_0)^\Psi} \Phi_u \tag{1.44}$$

$$\Phi_u = 2.35\gamma_c \tag{1.45}$$

$$d = 26.0e^{\{0.36(V/S)\}} \tag{1.46}$$

$$\gamma_c = \gamma_{c,to}\gamma_{c,RH}\gamma_{c,vs}\gamma_{c,s}\gamma_{c,\psi}\gamma_{c,\alpha} \tag{1.47}$$

$$\gamma_{c,to} = \begin{array}{ll} 1.25t_0^{-0.118} & \text{for moist curing} \\ 1.13t_0^{-0.094} & \text{for steam curing} \end{array} \tag{1.48}$$

$$\gamma_{c,RH} = 1.27 - 0.67h \tag{1.49}$$

$$\gamma_{c,vs} = \frac{2}{3}(1 + 1.13e^{\{-0.54(V/S)\}}) \tag{1.50}$$

$$\gamma_{c,s} = 0.82 + 0.067s \tag{1.51}$$

$$\gamma_{c,\psi} = 0.88 + 0.0024\psi \tag{1.52}$$

$$\gamma_{c,\alpha} = 0.46 + 0.09\alpha \geq 1 \tag{1.53}$$

Where: $\Phi(t,t_0)$ is the calculated creep coefficient at a given age, Φ_u is the calculated ultimate creep coefficient, t is the age of the specimen in days, $\gamma_{c,to}$ is the curing condition correction factor, t_0 is the age at which the specimen is loaded in days, $\gamma_{c,RH}$ is the humidity correction factor, h is relative humidity in decimals, $\gamma_{c,VS}$ is the size correction factor, V/S is the volume to surface area ratio, $\gamma_{c,s}$ is the slump correction factor, s is slump in inches, $\gamma_{c,\psi}$ is the fine aggregate correction factor, ψ is the ratio of fine aggregate to total aggregate by weight expressed as percentage, $\gamma_{c,\alpha}$ is the air content correction factor, and α is the air content in percent. For shape and size effects to be totally considered, d is to be determined using **Eq. 1.46** and ψ assumed to be equal to 1.0. Otherwise, average values of d=10 and ψ=0.6 are to be assumed.

 1.6.2. NCHRP Report 496. This proposed creep model was developed in a similar manner to that of the NCHRP Report 496 shrinkage model. The correction factors that are identical to those used in the corresponding shrinkage model have already been defined in Section 1.3.2 The model is shown in **Eq. 1.54 – 1.60**.

$$\psi(t, t_i) = 1.90\gamma_{cr} \tag{1.54}$$

$$\gamma_{cr} = k_{td}k_{la}k_sk_{hc}k_f \tag{1.55}$$

$$k_{td} = \frac{t}{61 - 4f'_{ci} + t} \tag{1.56}$$

$$k_{la} = t_i^{-0.118} \tag{1.57}$$

$$k_s = \frac{1064 - 94 V/S}{735} \tag{1.58}$$

$$k_{hc} = 1.56 - 0.008H \tag{1.59}$$

$$k_f = \frac{5}{1 + f'_{ci}} \tag{1.60}$$

Where: $\psi(t,t_i)$ is the calculated creep coefficient at a given age, k_{td} is the time development factor, t is the age of the concrete in days, k_{la} is the loading factor, t_i is the age at which creep specimen is loaded in days, k_s is the size factor, V/S is the volume to surface area ratio, k_{hc} is the humidity factor, H is the average ambient relative humidity in percent, k_f is the concrete strength factor, and f'_{ci} is the specified compressive strength of concete in ksi.

1.6.3. CEB-FIP 90. The following equations apply to the creep model as

developed jointly by CEB and FIP as presented in the CEB-FIP Model Code 1990.

$$\Phi(t, t_0) = \Phi_0 \beta_c(t - t_0) \tag{1.61}$$

$$\Phi_0 = \Phi_{RH} \beta(f_{cm}) \beta(t_0) \tag{1.62}$$

$$\Phi_{RH} = 1 + \frac{1 - RH}{0.46(\frac{2A_c}{100u})^{1/3}} \tag{1.63}$$

$$\beta(f_{cm}) = \frac{5.3}{(f_{cm}/10)^{0.5}} \tag{1.64}$$

$$\beta(t_0) = \frac{1}{0.1 + t_0^{0.2}} \tag{1.65}$$

$$\beta_c(t - t_0) = \left[\frac{(t - t_0)}{\beta_H + (t - t_0)}\right]^{0.3} \tag{1.66}$$

$$\beta_H = 150\{1 + (1.2RH)^{18}\}(\frac{2A_c}{100u}) + 250 \leq 1500 \tag{1.67}$$

Where: $\Phi(t, t_0)$ is the calculated creep coefficient at a given age, Φ_0 is the notional creep

coefficient, β_c is the coefficient to describe the development of creep with time after

loading, t is the age of concrete in days, t_0 is the age of concrete at loading in days, RH is

the relative humidity in decimals, Ac is the cross section area in mm^2, u is the perimeter

in contact with the atmosphere in mm, and f_{cm} is the mean compressive strength of concrete at the age of 28 days in MPa.

1.6.4. GL 2000. As with the GL 2000 shrinkage model, the following creep model was published in the ACI materials journal under the title "Design Provisions for Drying Shrinkage and Creep of Normal-Strength Concrete".

$$\Phi_{28} = \Phi(t_c)\left[2\left(\frac{(t-t_c)^{0.3}}{(t-t_c)^{0.3}+14}\right) + \left(\frac{7}{t_0}\right)^{0.5}\left(\frac{t-t_c}{t-t_c+7}\right)^{0.5}\right.$$

$$\left. +2.5(1-1.086h^2)\left(\frac{t-t_0}{t-t_0+97(V/S)^2}\right)^{0.5}\right] \qquad (1.68)$$

$$\Phi(t_c) = \left[1 - \left(\frac{t-t_c}{t-t_c+97(V/S)^2}\right)^{0.5}\right]^{0.5} \qquad (1.69)$$

Where: Φ_{28} is the calculated creep coefficient at a given age, $\Phi(t_c)$ is a factor that takes into account drying before loading, t is age of concrete in days, t_c is the age of concrete when drying begins, t_0 is the age the concrete was loaded, h is humidity in decimals, and V/S is the volume to surface area ratio in mm.

1.7. HVFA CREEP RESEARCH

Research has shown that the replacement of Portland cement with fly ash produces concrete which exhibits lower long term creep. Suggested reasons why this is true are discussed in the following sections.

1.7.1. ACI 232.2R-03. The ACI 232.2R committee report cites several sources that have researched creep of fly ash concrete. Lane and Best showed that, when formulated to have the same compressive strength at the age of testing, fly ash concretes

display lower shrinkage. It is suggested that this is due to the higher late age strength of fly ash concrete.

1.7.2. Alexander, et. al. Concrete with 25% fly ash replacement was tested for creep up to the age of 6 years. The specimens were tested at loads of 25% and 40% of 28 day compressive strength. A control conventional concrete mix was also tested simultaneously. All specimens tested had a strength of 4000 psi (27.58 MPa) at 28 days. The results show that concrete without fly ash showed 50% higher creep than concrete which had 25% fly ash replacement. These results were recorded at two years of age, and remained unchanged up to six years.

1.8. APPLICATION OF SHRINKAGE AND CREEP

1.8.1. Prestress Loss. Prestress loss is "the loss of compressive force acting on the concrete component of a prestressed concrete section" (NCHRP 426). The ability to accurately predict the prestress loss in beams is very dependent on the ability to predict the beam's shortening due to shrinkage and creep. Shortening of the beam reduces the tensile force in the prestressed reinforcement and must be accounted for in design. NCHRP 426 names three components which significantly affect the prestress loss in pretensioned concrete members which directly relate to shrinkage and creep. These components are:

1. Instantaneous prestress loss due to elastic shortening at transfer of force from prestressed reinforcement to concrete.

2. Long-term prestress loss due to shrinkage and creep of concrete and relaxation of prestressing strands between the time of transfer and deck placement.

3.   Long-term prestress loss between the time of deck placement to the final service

life of the structure due to shrinkage and creep of the girder.

Figure 1.4 shows the prestress loss over the life cycle of a pretensioned concrete

girder. The loss between points D and E represent the loss due to creep, shrinkage, and

relaxation of prestressing strands.
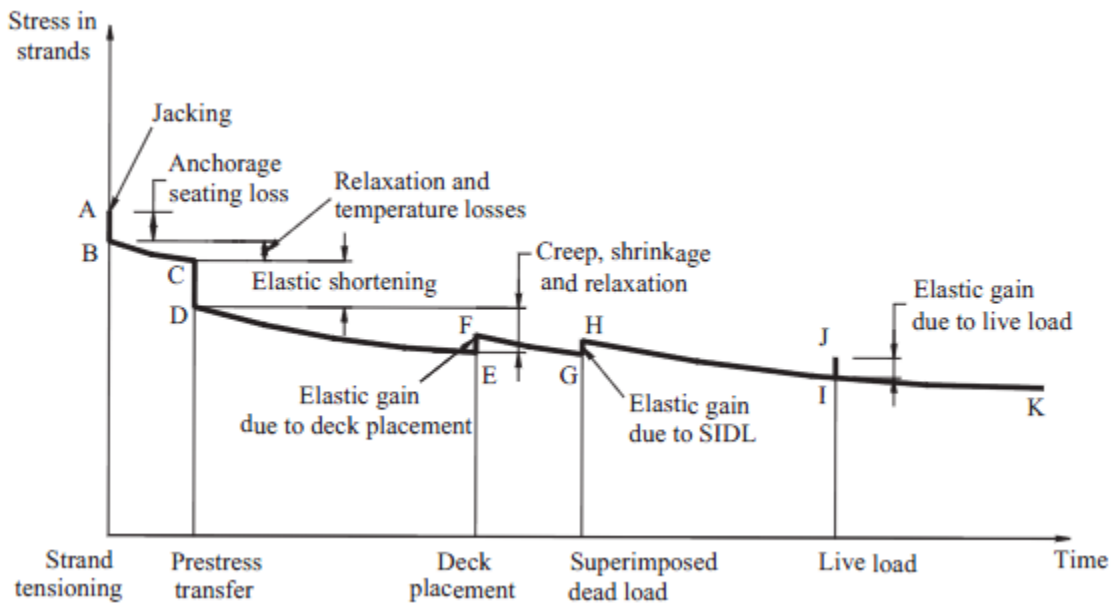
Figure 1.4 - Stress vs. Time for Prestressed Bridge Girder (Tadros et. al. 2003)

1.8.2. Load Effects. The procedures in "Design of Continuous Highway

Bridges with Precast, Prestressed Concrete Girders" published by the Portland Cement

Association (PCA) take into account additional moments due to shrinkage and creep

when determining loads for design. In this method, fixed end moments due to creep and

end driving moments due to shrinkage are calculated. These applied moments result from

a continuity connection being made at supports by the placement of the bridge deck. The

placement restricts free rotation of the beams and therefore produces moment in the

connection. The moments calculated by this method are then added to all other load

effects at all sections for determination of the ultimate design load. The shrinkage driving

moment calculation is done by first calculating theoretical ultimate shrinkage values for

the beam and the slab. The differential shrinkage between the beam and slab are then

used to determine an applied moment due to shrinkage. The applied moment due to creep

results from prestressed creep and dead load creep. Theoretical creep coefficients are

calculated for the time before and after deck placement. The creep that occurs after deck

placement is what contributes to the applied moment.

1.8.3. Beam Deflection. Shrinkage and creep must also be accounted for

when calculating long term deflection of flexural members. Eq. 9-11 of ACI 318-08,

shown here as **Eq. 1.70**, accounts for long term sustained loads. This factor is multiplied

by the immediate deflection caused by the load considered.

$$\lambda_\Delta = \frac{\xi}{1+50\rho'} \qquad (1.70)$$

Where: λ_Δ is the multiplier for additional deflection due to long-term effects, ξ is the time

dependent factor for sustained load, and ρ' is compression reinforcement ratio.

1.9. CONCRETE ABRASION

1.9.1. Definition of Concrete Abrasion. Abrasion is the physical wearing

down of a material. The most common sources of abrasion of concrete structures are by

the friction between vehicle tires and concrete pavement road surfaces, and by water

flows over exposed dam or bridge footings. Concrete abrasion leads to a decrease in member thickness which can lead to cracking or failure of the structure (Atis).

1.9.2. Factors Affecting Concrete Abrasion. Several material properties and construction factors can affect the abrasion resistance of concrete. The concrete strength is the most influential property in regards to abrasion resistance. The properties of the aggregate are also very important in a concrete's resistance to abrasion. The surface finish and whether or not a hardener or topping is used effects abrasion resistance as well (Naik et. al.).

1.10. HVFA ABRASION RESEARCH

There is considerable data available on the abrasion resistance of HVFA concrete. The motivation for research of HVFA concrete abrasion resistance is that HVFA concrete has been proposed as a possible material for paving.

1.10.1. Naik, et. al. The objective of this testing program was to determine the abrasion resistance of HVFA concrete mixes. Three sources of fly ash were used. Mixes containing 40%, 50%, and 60% fly ash were tested according to a modified version of ASTM C944 for each source along with one convention concrete mix. In this study, depth of wear was used as the measure of value. Results show that above 50%, abrasion resistance of fly ash mixes is slightly lower than that of the reference mix. Results also show that, above all, the concrete's strength was the most influential factor in abrasion resistance.

1.10.2. Atis. The objective of this program was to determine the abrasion resistance of HVFA concrete for use as a pavement material. Five different mixes were tested. One baseline mix, two 50% HVFA mixes, and two 70% HVFA mixes were tested in accordance to BSI 1993 – British Standards Institute "Method for determination of aggregate abrasion value (AAV)." This test method is similar to ASTM C944, which was followed during testing of specimens in this report. Mass loss was the measure of value in this test. Again, results show that abrasion resistance is primarily dependent on the concrete's strength rather than fly ash content. However results also suggest that at higher strengths, the 70% fly ash mix showed higher resistance than the 50% mix and conventional mix, but at lower strengths the opposite is true.

2. RESEARCH PROGRAM

2.1. MIX DESIGNS

2.1.1. HVFA. The HVFA concrete testing program consisted of three mixes. The first mix tested was a conventional concrete baseline mix (HVFA-C), based on a MoDOT standard mix design. The other two were HVFA concrete mixes. Both HVFA concrete mixes had 70% Class C fly ash replacement, one with a relatively high amount of total cementitious material (HVFA-H) and the other with a relatively low amount of total cementitious material (HVFA-L). The HVFA-H mix design was based on research done by Ortega (2010) at Missouri S&T. The HVFA-L mix design was a modification of the control baseline mix. Both HVFA concrete mixes were batched with the assistance of a local ready mix concrete supplier (Rolla Ready Mix). A partial mix was delivered, with the gypsum, calcium hydroxide, and HRWR added upon arrival. The mix designs tested can be found in **Table 2.1** along with the measured 28 day compressive strength (f'c) and modulus of elasticity (MOE). All aggregate weights found in **Table 2.1** are based on SSD conditions.

Table 2.1 - HVFA Test Program Mix Designs and mechanical properties

	Amount (per cubic yard)		
Material	HVFA-C	HVFA-H	HVFA-L
Water	226 lb.	321 lb.	226 lb.
Cement (Type I)	564 lb.	219 lb.	155 lb.
Coarse Aggregate (3/4" JC Dolomite)	1860 lb.	1754 lb.	1754 lb.
Fine Aggregate (Missouri River Sand)	1240 lb.	1080 lb.	1080 lb.
Fly Ash	N/A	511 lb.	360 lb.
Gypsum	N/A	20.4 lb	14.4 lb.
Calcium Hydroxide	N/A	51.1 lb.	36 lb.
BASF Glenium 7500 (HRWR)	3.0 fl oz/cwt	N/A	3.0 fl oz/cwt
f'c (psi)	5,400	3,100	3,500
MOE (psi)	3,386,000	3,475,000	3,163,000

Conversion: $1 \text{ kg/m}^3 = 1.686 \text{ lb/yd}^3$

1 fl oz = 26.57 mL

1 psi = 6.89 kPa

2.2. SHRINKAGE AND CREEP SPECIMEN CONSTRUCTION

2.2.1. Shrinkage and Creep Specimens. Both shrinkage and creep testing were done using identical specimens. Although only four specimens per mix were necessary for testing (two each for shrinkage and creep), six specimens per mix were cast in case any specimens were damaged during de-molding. These specimens were fabricated and prepared as described below.

2.2.2. Shrinkage and Creep Molds. The molds for the shrinkage and creep specimens were 4 in. diameter PVC pipe adhered to a plywood base. The PVC was cut into 24 in. sections with care being taken to ensure all cuts were made so that the mold would sit flush and orthogonal to the base. The PVC was also notched on opposite sides. The notches made de-molding much easier and significantly reduced the possibility of damaging the specimens during de-molding. Once prepared the PVC was adhered to a 1

ft. (304.8 mm) by 1 ft. (304.8 mm) plywood base using a waterproof silicon sealant. The

completed molds were allowed to sit for at least 24 hours before use to allow for the

sealant to fully set up. **Figure 2.1** shows a completed shrinkage and creep mold.

Figure 2.1 - Shrinkage and Creep Form

2.2.3. Shrinkage and Creep Specimen Casting. Specimens were consolidated

in a manner similar to that prescribed in ASTM C31 "Standard Practice for Making and

Curing Concrete Test Specimens in the Field" for a 6 in. diameter cylinder. Consolidation

and vibration were performed when necessary. The specimens were cast in three layers of

approximately equal depth and were rodded 25 times per layer. External vibration was

also performed after each layer was rodded using an electric handheld concrete vibrator as needed. Specimens were moist cured until de-molded and prepared.

2.2.4. Shrinkage and Creep De-Molding and Preparation. All specimens were de-molded within 24 hours of their initial set time. De-molding was done by first cutting through the notched section with a utility knife. A hammer and chisel were then used to split the mold and remove it from the concrete. Creep specimens were sulfur capped on both ends in preparation for loading at 28 days. Shrinkage specimens were sulfur capped on only the bottom end, allowing for stability and more accurate readings.

2.2.5. Shrinkage and Creep Data Acquisition. A demountable mechanical strain gauge (DEMEC) was used to measure strain in the concrete. DEMEC points, small pre-drilled stainless steel discs, were adhered to the surface of the specimen. They were arranged in three vertical lines of five points, 120º apart, as shown in **Fig. 2.2**. This arrangement allowed for 9 readings to be taken per specimen. The average of all readings taken per specimen was taken as the value to be used for strain calculation. The points in one line per specimen were adhered using gel control super glue. The instant hardening allowed for initial readings to be made on each specimen as soon as possible. The remaining points were adhered using concrete/metal epoxy, which took up to 24 hours to fully harden for accurate reading to be taken. The points adhered with super glue were later protected using the epoxy.
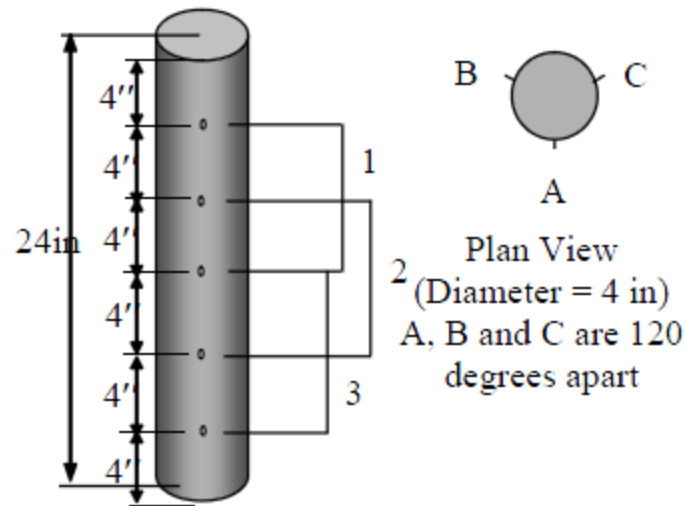
Figure 2.2 – Shrinkage and Creep Specimens and DEMEC Point Arrangement (Myers and Yang, 2005)

2.3. ABRASION SPECIMEN CONSTRUCTION

One specimen per mix was cast for abrasion test. Each specimen was large enough so that three replicate abrasion tests could be done for each mix. Abrasion specimens measured 6 in. (152.4 mm) by 16 in. (406.4 mm) by 3.5 in. (88.9 mm) and were cast in a mold made from wooden 2x4 sections and attached to a plywood base. The baseline and HVFA concrete mixes were consolidated similar to that prescribed in ASTM C31 "Standard Practice for Making and Curing Concrete Test Specimens in the Field" for a 6 in. (152.4 mm) wide beam. External vibration was used as necessary. To ensure that abrasion tests on all specimens were consistent, every specimen tested was finished by the same individual using a hand trowel. Specimens were moist cured until tested. All testing was performed on the top finished surface of the specimen.

2.4. TESTING PROCEDURES

      2.4.1. Shrinkage Testing Procedures. A modified version of ASTM C157

"Standard Test Method for Length Change of Hardened Hydraulic-Cement Mortar and

Concrete" was used to determine the shrinkage of the concrete specimens. Until the age

of loading for creep, four specimens were used for shrinkage determination. At 28 days,

two of these specimens were transferred to creep frames, leaving two remaining

specimens to be tested for long term shrinkage. Nine strain readings could be taken per

specimen, with the average of all readings taken as the value to be used for shrinkage

calculation. Strain was determined using the DEMEC readings and calculated by **Eq. 2.1**

as found in "Simplified Instructions for Using a Digital DEMEC Gauge". An example of

a DEMEC reading being taken on a specimen is in **Figure 2.1**. Readings were normalized

by taking a reading on the reference bar, shown in **Figure 2.2** with a reading taken on the

reference bar shown in **Figure 2.3**. Shrinkage strain experienced during the first day after

demolding was estimated based on linear interpolation of subsequent strain values, as

calculated by **Eq. 2.1**

$$\Delta\varepsilon_s = G((R_i - R_0) - (D_i - D_0)) \ (\mu\varepsilon) \tag{2.1}$$

Where: $\Delta\varepsilon_s$ is the change in strain from one reading to the next, G is the gauge factor

shown in **Figure 2.3**, 0.400×10^{-5} strain per division (4 microstrain), D_0 is the datum

reading on the reference bar, D_i is the subsequent reading on the reference bar, R_0 is the

datum reading on the tested material, and R_i is the subsequent reading on the tested

material. Gauge units are the digital gauge reading without the decimal point. For

example, **Figure 2.4** shows a reading of 2.523 which equates to 2523 gauge units.

Figure 2.3 – DEMEC Reading Taken on Specimen

Figure 2.4 - Reference Bar

Figure 2.5 - Reading Taken on Reference Bar

Figure 2.6 - Gauge Factor Used for Shrinkage and Creep Calculations

Figure 2.7 - Example DEMEC Gauge Reading

2.4.2. Creep Testing Procedures. A modified version of ASTM C512 "Standard

Test Method for Creep of Concrete in Compression" was used to determine the creep of

the concrete specimens tested. Until the age of loading, creep specimens acted as

shrinkage specimens. This is a modification of ASTM C512, as the specimens were not

moist cured beyond the time of de-molding. Additionally, humidity was not controlled

however it was recorded.

At 28 days, representative specimens were tested according to ASTM C39

"Standard Test Method for Compressive Strength of Cylindrical Concrete Specimens"

and ASTM C469 "Standard Test Method for Static Modulus of Elasticity and Poisson's

Ratio of Concrete in Compression." Creep specimens were then loaded to 40% of their

measured 28 day compressive strength in the creep frames shown in **Figures 2.8 – 2.9**.

The design of the creep frames was based on research done by Myers and Yang (2005).
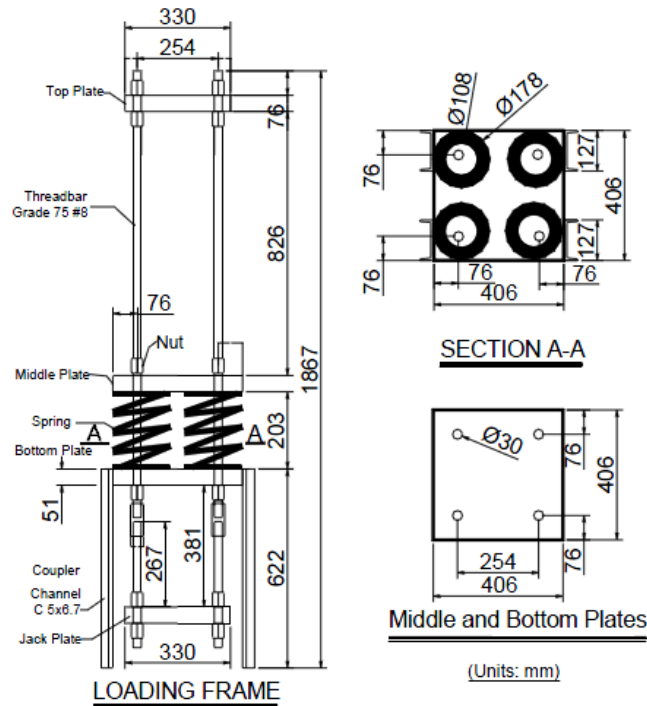
Figure 2.8 - Schematic of Creep Loading Frame (Myers and Yang, 2005)
(1 in = 25.4 mm)

Figure 2.9 - Creep Loading Frame with Specimen

Measurements taken on creep specimens were done in the exact way as with the shrinkage specimens. **Eq. 2.2** was used to determine the change in strain between one creep reading to the next. Using the calculated creep strain, the coefficient of creep could be determined by **Eq. 2.3**. Creep and shrinkage readings for like specimens were taken at the same interval. Readings were also taken immediately before and after loading to determine initial elastic strain due to loading. **Figure 2.10** shows a reading being taken on a creep specimen.

$$\Delta\varepsilon_c = G((R_i - R_0) - (D_i - D_0)) - \Delta\varepsilon_s \ (\mu\varepsilon)$$ (2.2)

Where: $\Delta\varepsilon_c$ is the change in creep strain between readings.

$$\Phi(t, t_0) = \varepsilon_t / \varepsilon_i$$ (2.3)

Where: $\Phi(t,t_0)$ is the measured creep coefficient at a given age, ε_i is the measured strain due to initial loading of the specimen, ε_t is the measured creep strain at a given age.

Figure 2.10 - Reading Taken on Creep Specimen

2.4.3. Abrasion Resistance Testing Procedures. ASTM C944 "Standard Test Method for Abrasion Resistance of Concrete or Mortar Surfaces by the Rotating-Cutter Method" was used to determine abrasion resistance. A schematic of the rotating cutter used is shown in **Figure 2.11** , which is taken from ASTM C944. The actual rotating cutter is shown in **Figure 2.12**. Abrasion specimens were moist cured until testing at 28 days age. The two HVFA concrete mixes were also tested after an additional 10 weeks of moist cure to further investigate how the late age strength gain of HVFA concrete affected abrasion resistance. One specimen per mix was constructed, which allowed for three abrasion tests. One abrasion test consisted of three abrasion cycles. Each cycle lasted two minutes. A load of 44lb, defined as a double load in ASTM C944, was applied at a rate of 300 rpm using a drill press as shown in **Figure 2.13**. After each cycle, mass loss (mg) was recorded by subtracting the final weight from the initial weight. Each cycle per test was done on the same spot. After completion of each abrasion test, the average depth of wear (mm) was measured using digital calipers. The average depth of wear was calculated from a total of eight depth measurements relative to the adjacent untested surface, four taken on the outer perimeter of the tested surface and four taken around the inner perimeter, at the points indicated in **Figure 2.14**. The measurements were made using a digital caliper. On the day of testing, the specimen was removed from moist cure and surface dried by blotting with paper towels. This was done to avoid any mass loss due to moisture loss. A completed specimen after all three abrasion tests is shown in **Figure 2.15**.

Note: Washers shall have a smaller outside diameter than the dressing wheel before and after the test period.

ROD END BEARING

WALL TUBING

9.5 mm-0.6 [3/8 in.-16]   JAM NUTS

9.5 mm-0.6 [3/8 in.-16] THREADED ROD

DRESSING WHEELS

WASHERS

PLAIN WASHERS
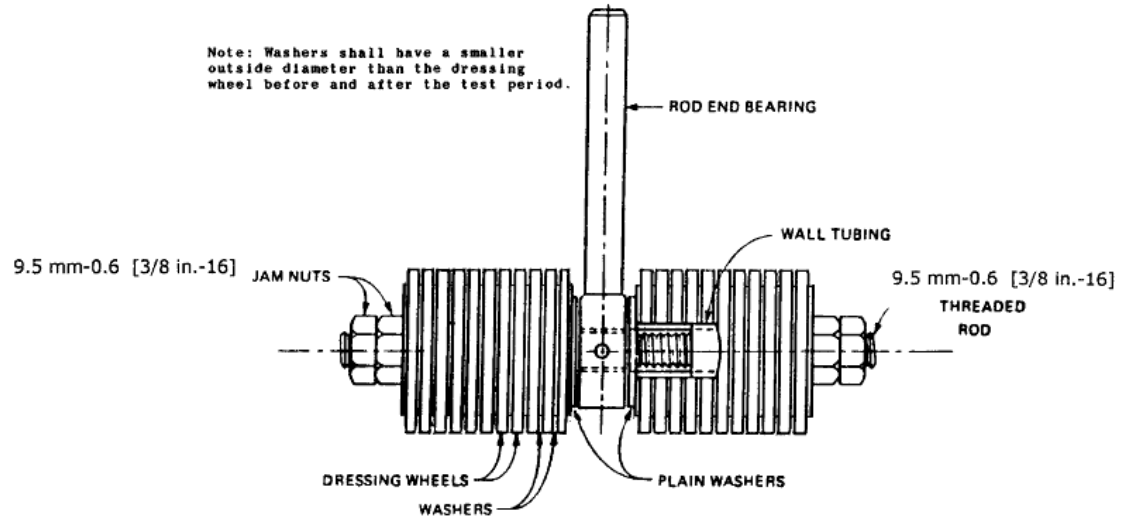
Figure 2.11 - Schematic of Abrasion Rotating Cutter (ASTM C944)
(1 in = 25.4 mm)

Figure 2.12 - Rotating Cutter

Figure 2.13 - Abrasion Resistance Test in Progress

Figure 2.14 - Depth of Wear Measurement Points
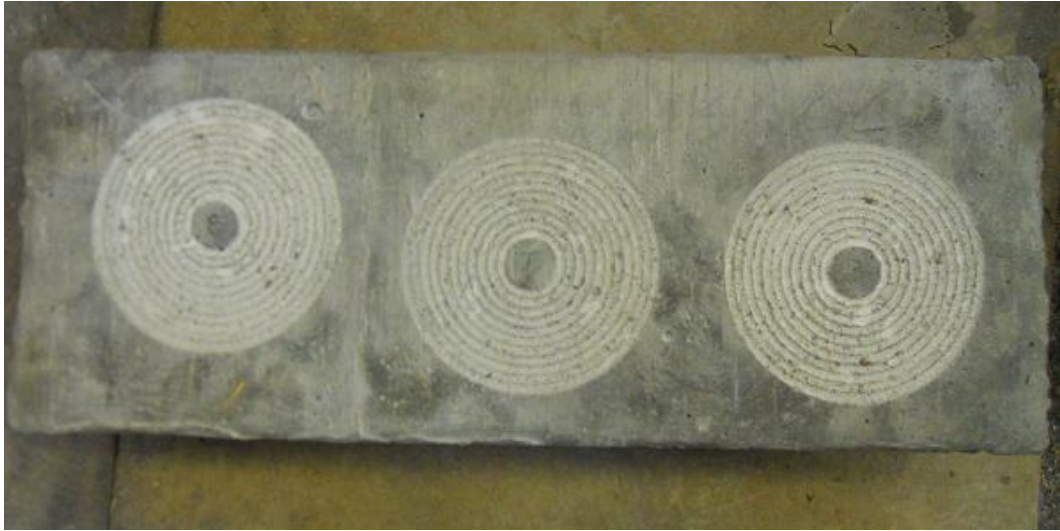
Figure 2.15 - Abrasion Resistance Specimen after Testing

3. HVFA RESULTS AND DISCUSSION

3.1. SHRINKAGE

3.1.1. Results. **Figures 3.1 – 3.3** show the experimental data obtained from shrinkage tests of the HVFA concrete plotted with the various prediction models discussed in Section 1. **Figure 3.4** shows the experimental results of all four mixes plotted with one another. In figures where different data sources are together, the source of the data can be found in parentheses after the data label in the legend of its respective figure. For all specimens tested for this study, the notation (S&T) will be used.

3.1.2. Conclusions and Discussion. For both HVFA concrete mixes, results were very consistent with data from numerous previous research projects described in sections 1.4.1-1.4.4. It was expected that the two HVFA concrete mixes would experience a decrease in shrinkage strain relative to the conventional mix. It was also expected that HVFA-L, due to the lower level of cementitious material, would experience a further decrease in shrinkage strains.

Both HVFA-H and HVFA-L showed a significant decrease in shrinkage strain relative to HVFA-C. Therefore, for use in practice when shrinkage is a design concern, both HVFA mixes are superior to their equivalent conventional concrete mix.

When comparing results to previous studies, both HVFA-H and HVFA-L performed as expected. **Figures 3.5 – 3.6** show the results of HVFA-H and HVFA-L plotted against shrinkage results from Marlay (2011) and Atis (2003) both of which tested HVFA concrete specimens with 70% replacement of Portland cement with fly ash, in addition to two mixes with 50% replacement for comparison. The results from Marlay and Atis validate the relatively low shrinkage strains experienced by HVFA-H and

HVFA-L compared to conventional concrete. Both databases together with experimental results are shown in **Figure 3.7**.
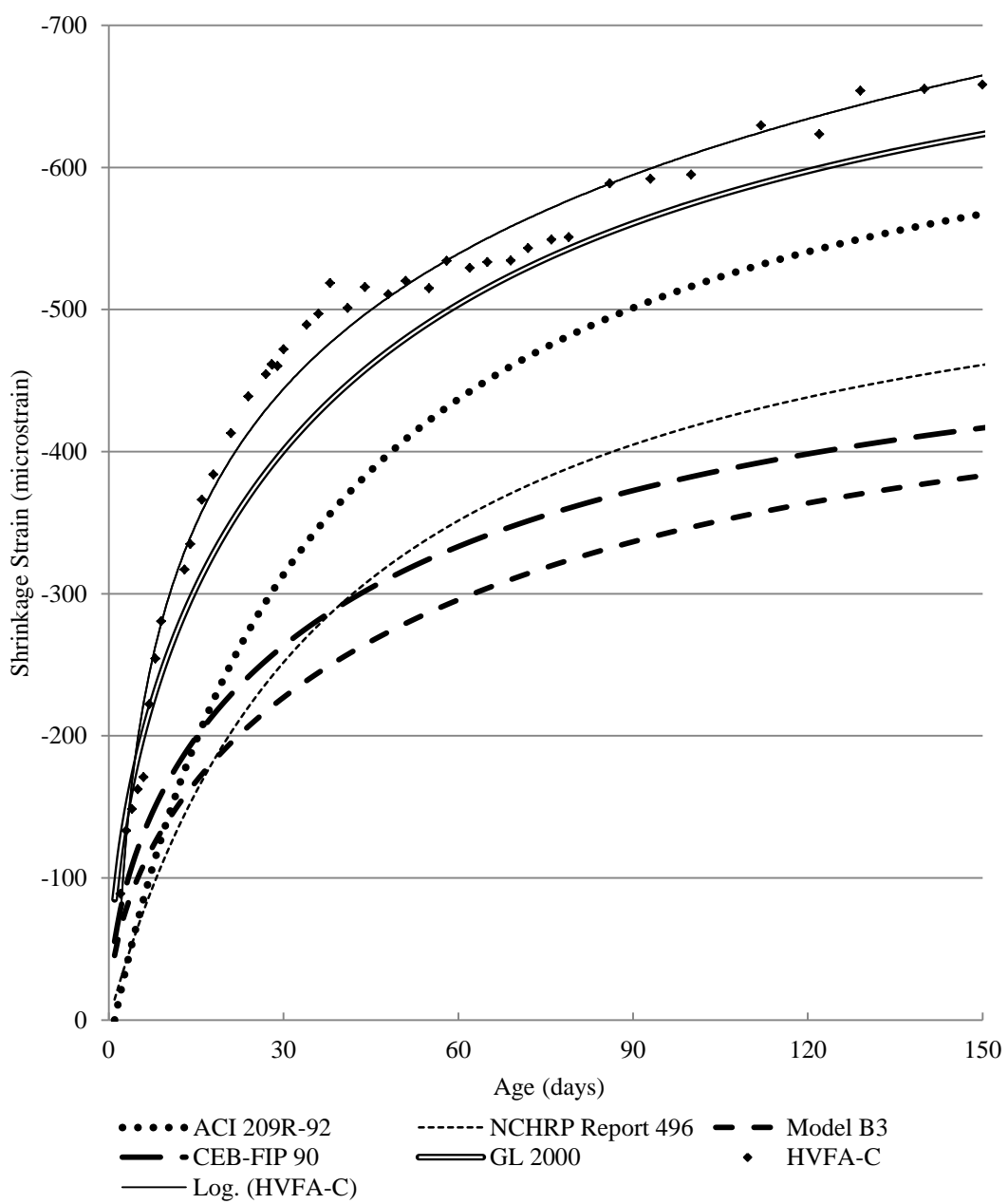
Figure 3.1 - HVFA-C Shrinkage Results and Prediction Models
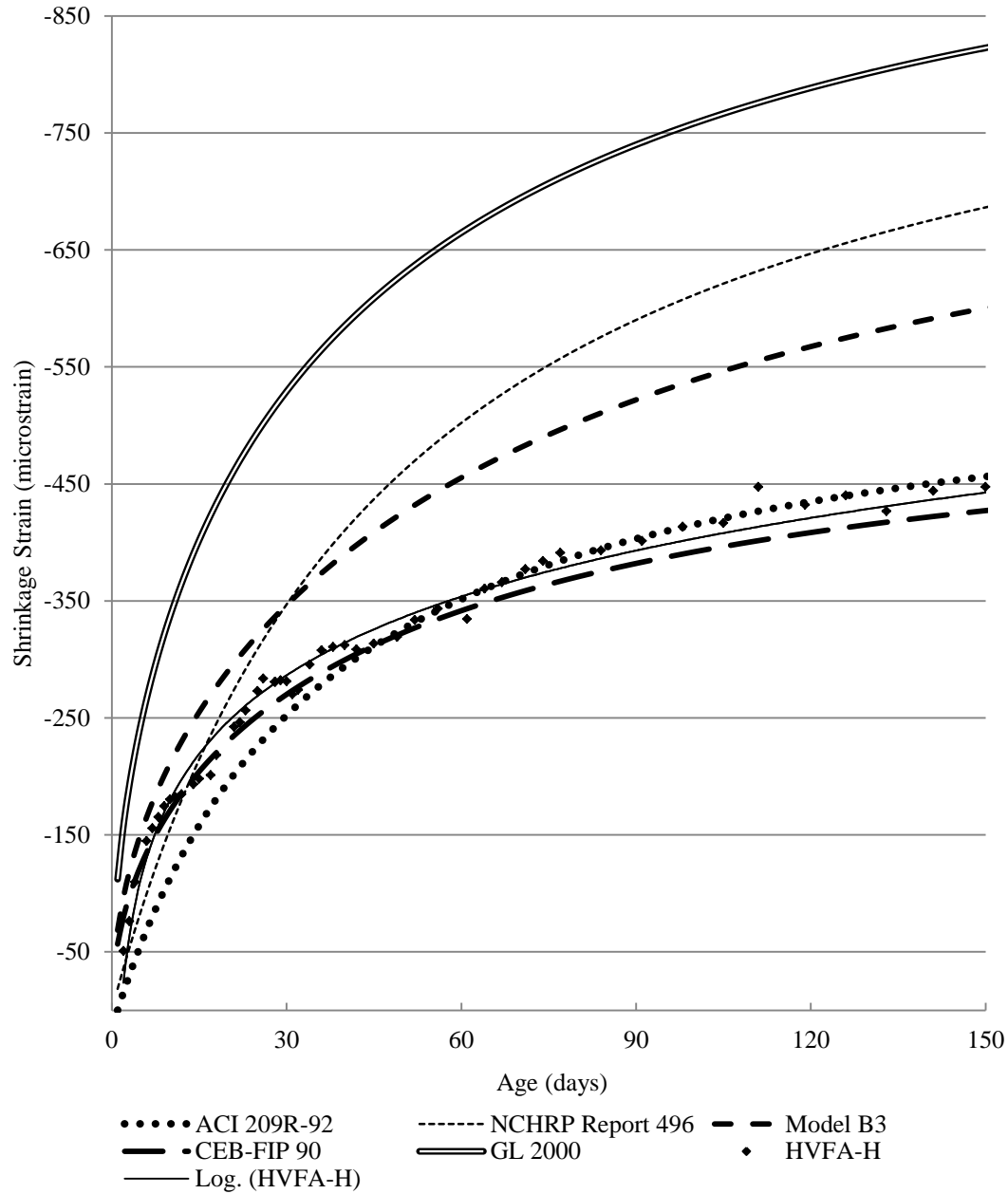
Figure 3.2 - HVFA-H Shrinkage Results and Prediction Models
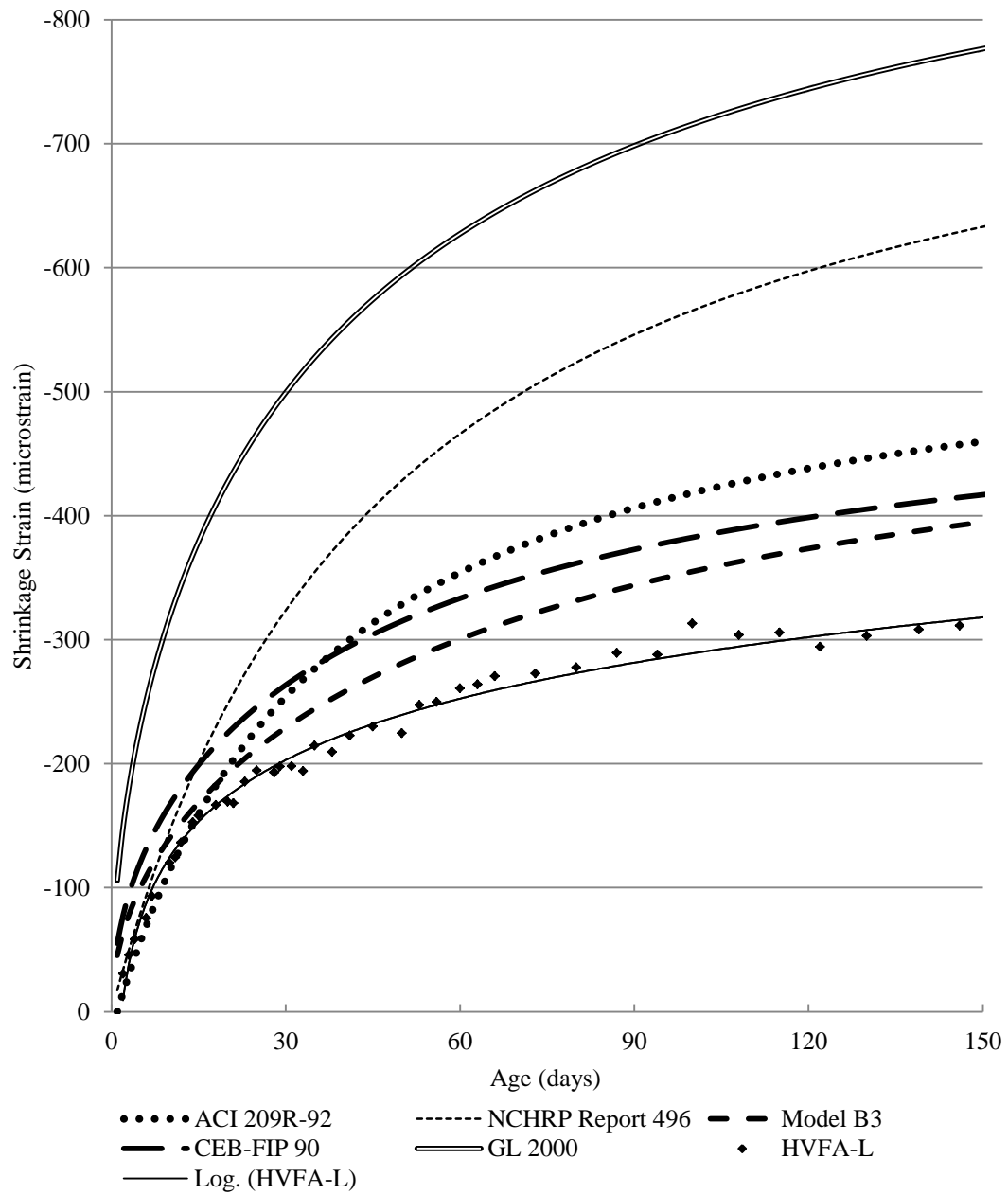
Figure 3.3 - HVFA-L Shrinkage Results and Prediction Models
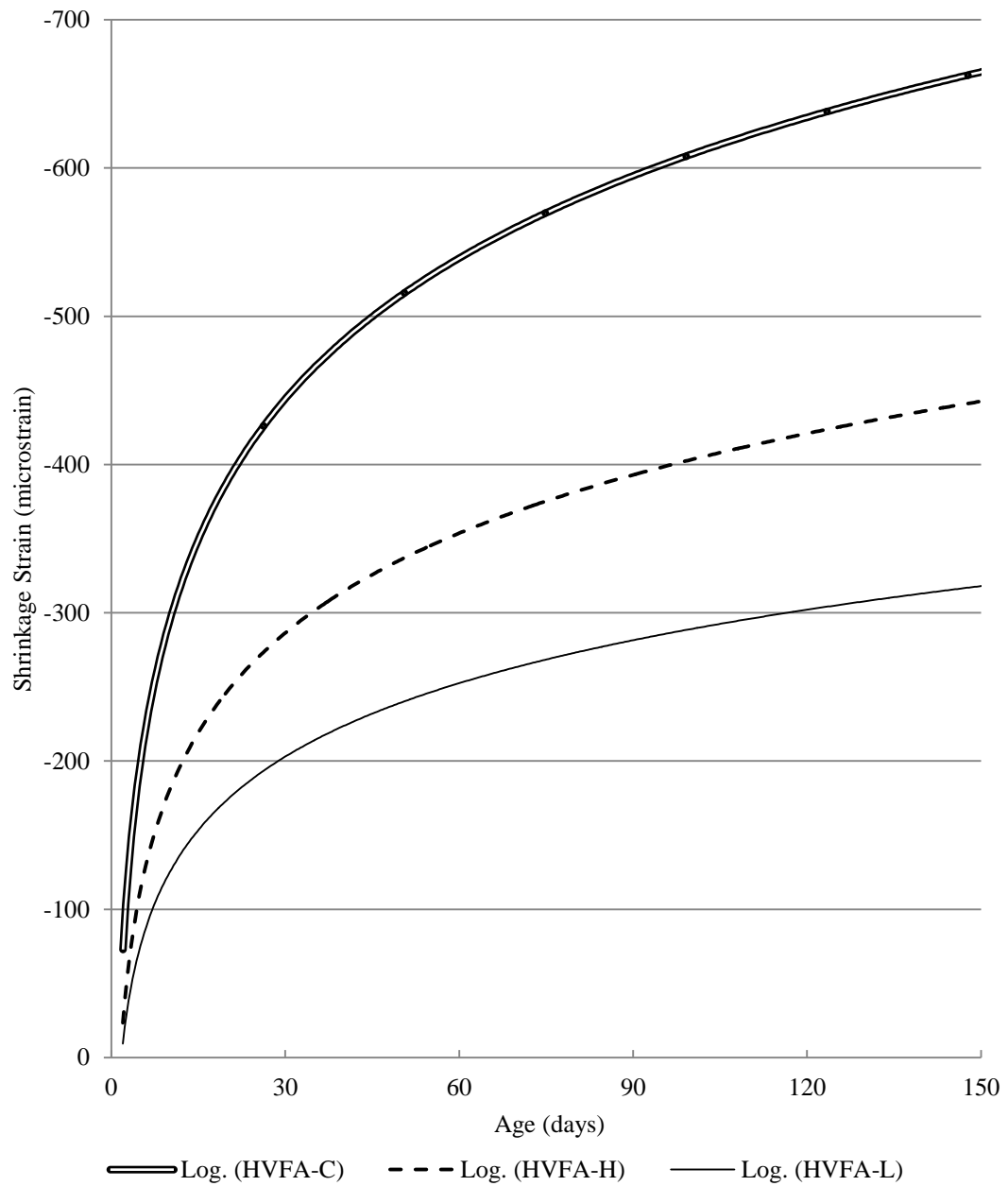
Figure 3.4 – HVFA Shrinkage Results (Best fit Logarithmic)
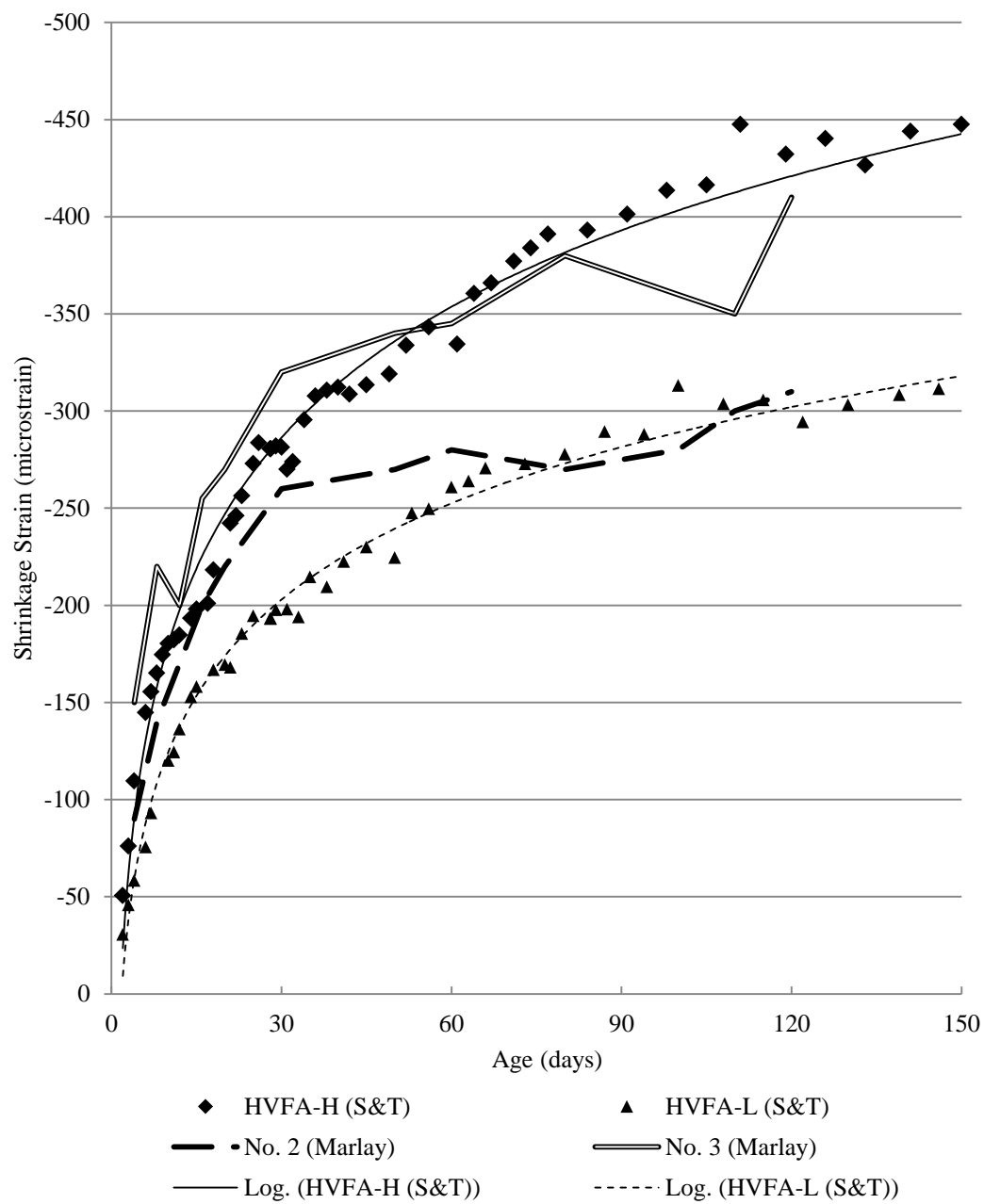
Figure 3.5 – HVFA Shrinkage Results Compared to Marlay (2011)
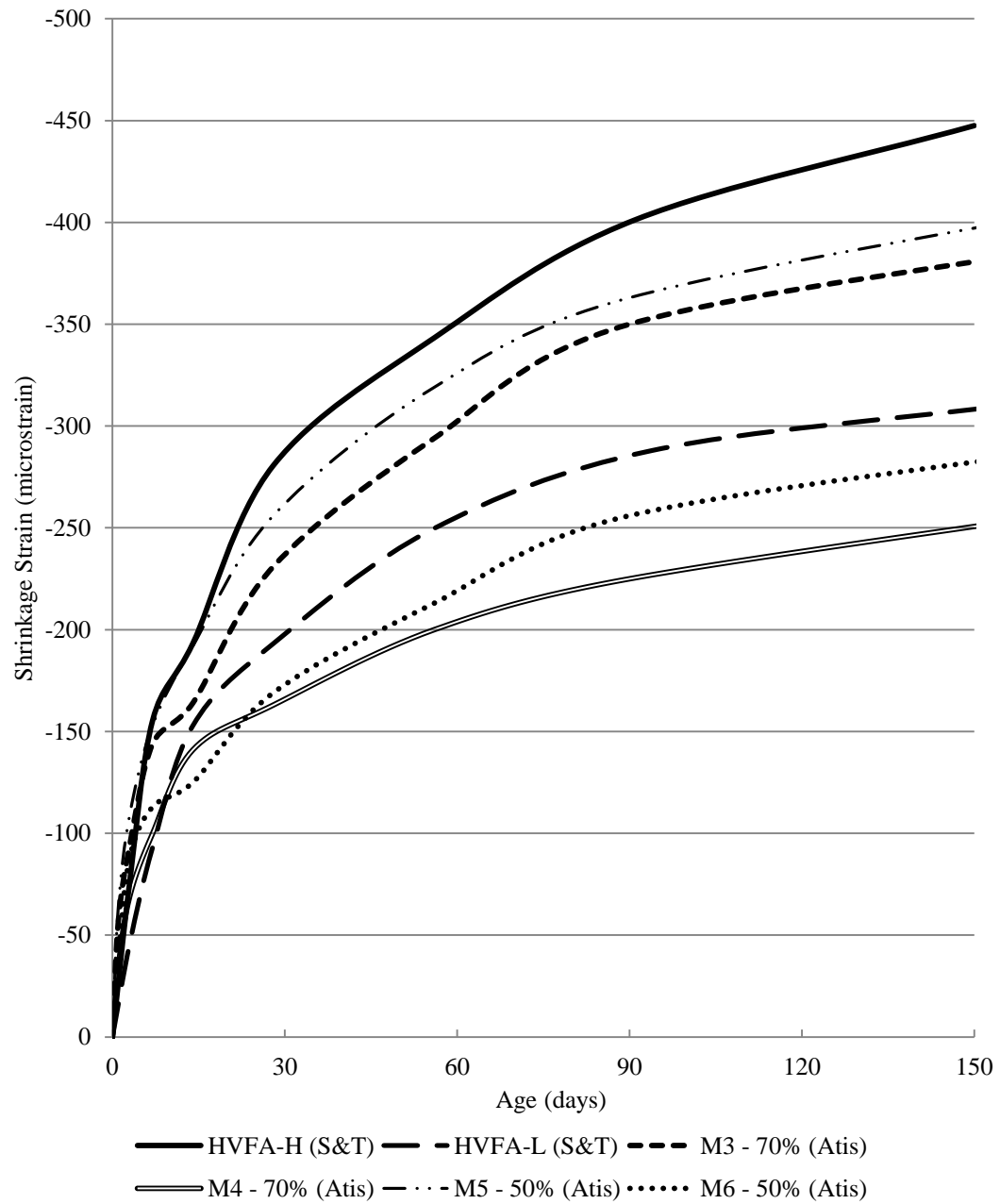
Figure 3.6 – HVFA Shrinkage Results Compared to Atis (2003)
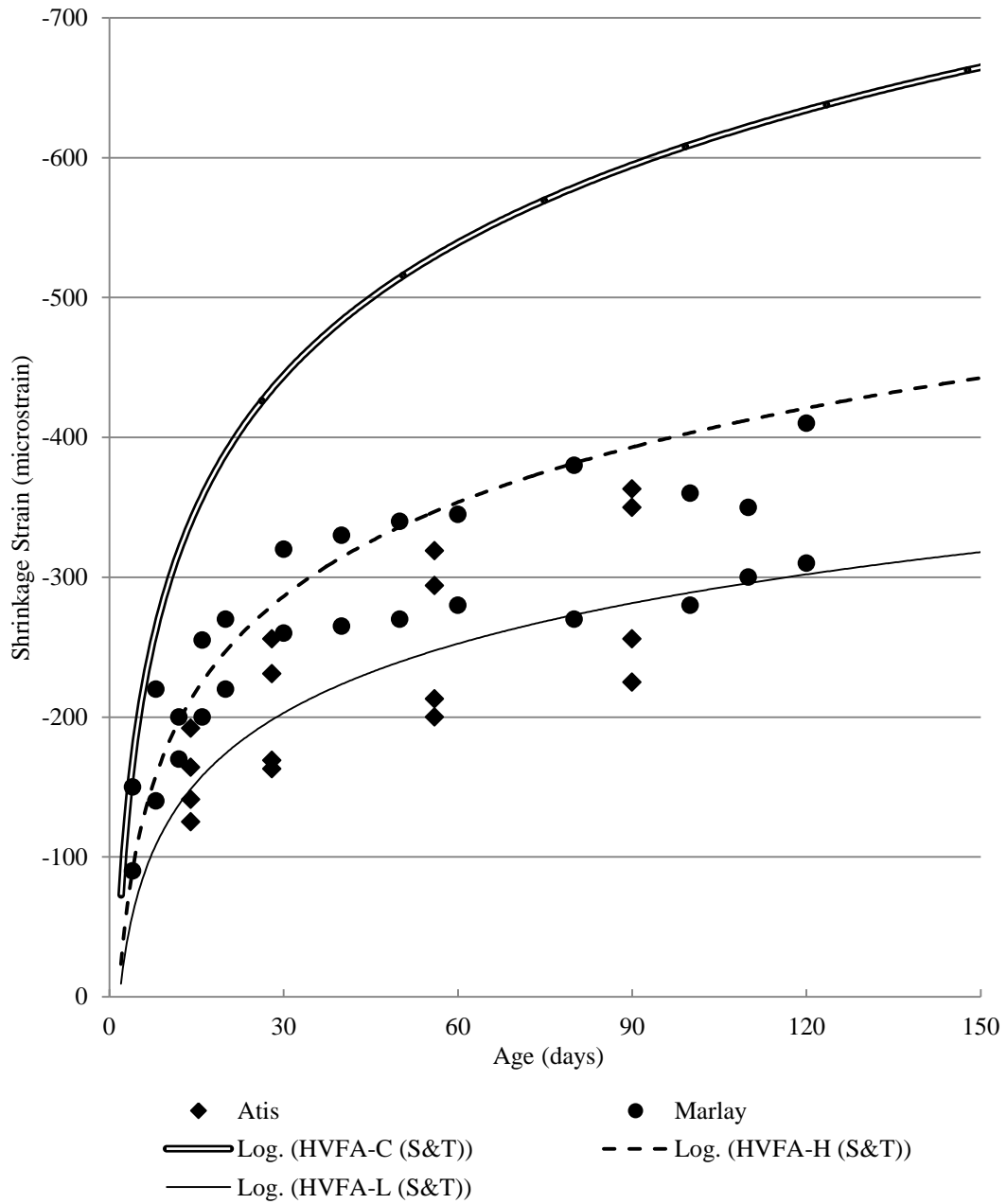
Figure 3.7 – HVFA Results with Shrinkage Databases

3.2. CREEP

3.2.1. Results. Creep Results are shown in **Table 3.1.**

Table 3.1 - Summary of HVFA Creep Results

Creep Strain (microstrain)				
Specimen	Days After Loading			
	7	14	56	126
HVFA-C	296	397	707	1070
HVFA-H	256	333	596	791
HVFA-L	178	225	377	489
Percentage of 126 Day Creep				
HVFA-C	28	37	66	100
HVFA-H	32	42	75	100
HVFA-L	36	46	77	100
Measured Creep Coefficient				
HVFA-C	0.464	0.622	1.12	1.68
HVFA-H	0.463	0.603	1.08	1.43
HVFA-L	0.421	0.533	0.893	1.16
Specific Creep ($\mu\varepsilon$/psi)				
HVFA-C	0.137	0.184	0.327	0.496
HVFA-H	0.206	0.269	0.481	0.638
HVFA-L	0.128	0.162	0.271	0.351

Conversion: 1 MPa = 145.04 psi

3.2.2. Discussion and Conclusions. With the exception of HVFA-H in terms of specific creep, both HVFA concrete specimens outperformed the conventional concrete specimens in creep testing. Both HVFA concrete specimens experienced significantly less creep strain at 126 days after loading than the conventional concrete mix. Creep strain data may be misleading due to the fact that HVFA specimens were loaded at lower levels than conventional concrete due to their decreased compressive strengths at the time of loading. To normalize results, specific creep can be examined. As mentioned above, HVFA-H performed poorly in creep when taken in terms of specific creep. As the specimens got older, however, specific creep of HVFA-H got closer to that of HVFA-C.

At early ages, all three mixes tested showed similar behavior under load, however as the specimens got older, the advantage of HVFA concrete over conventional concrete became more clear. This is demonstrated best by the percentage of 126 day creep. The data shows that during the first two weeks of loading, the HVFA concrete specimens experienced a greater percentage of their ultimate creep strain than did the conventional concrete specimens. However, due to the tendency of HVFA concrete to gain strength at later ages, creep performance improved as the specimens got older.

This late age improvement in creep behavior is exactly what was discovered by Lane and Best, as summarized in ACI 232.2R-03. It was determined that since HVFA concrete had a lower strength at time of loading with increase in strength gain as it aged, its creep behavior would be superior to that of conventional concrete. Additionally, it was shown that concrete with fly ash which had the same strength as conventional concrete still produced less creep at all ages. These properties of creep of HVFA concrete were again confirmed by the results gained in this study.

3.3. ABRASION RESISTANCE

The following sections contain all measured data resulting from abrasion resistance testing along with discussions and conclusions.

3.3.1. Results. Figures 3.8 – 3.10 show the mass losses recorded after each abrasion cycle for each mix tested. **Figures 3.11 – 3.12** show the relative abrasion resistance of each HVFA concrete specimen by age. **Figures 3.13 -3.14** show the results of all specimens tested together. **Table 3.2** shows a summary of all results along with measured 28 day compressive strength.
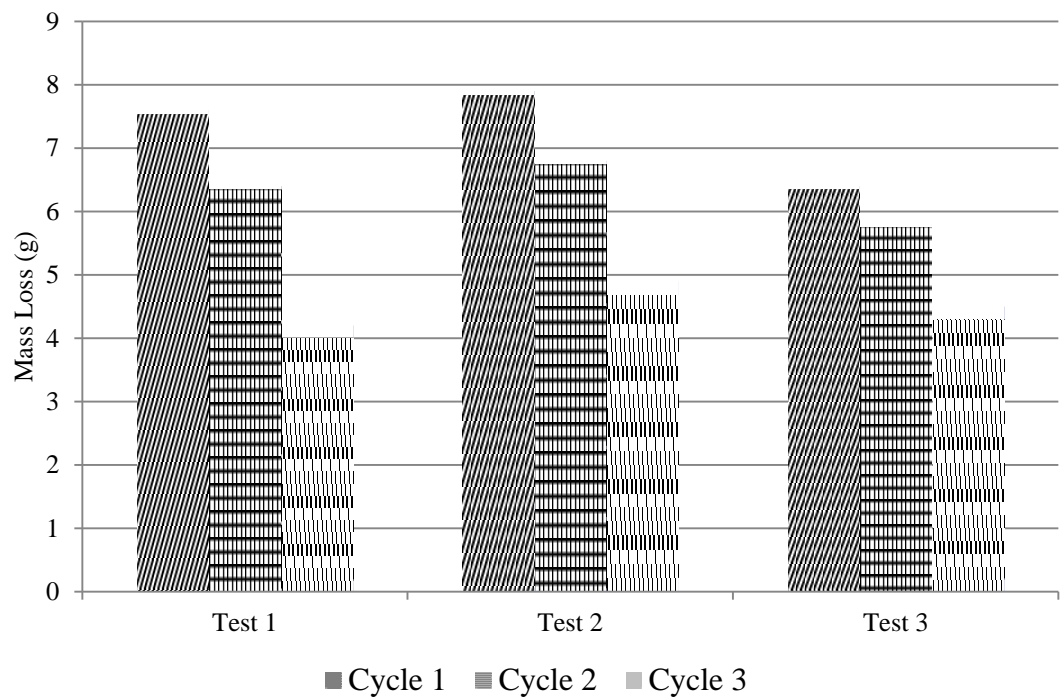
Figure 3.8 - HVFA-C Mass Loss Results
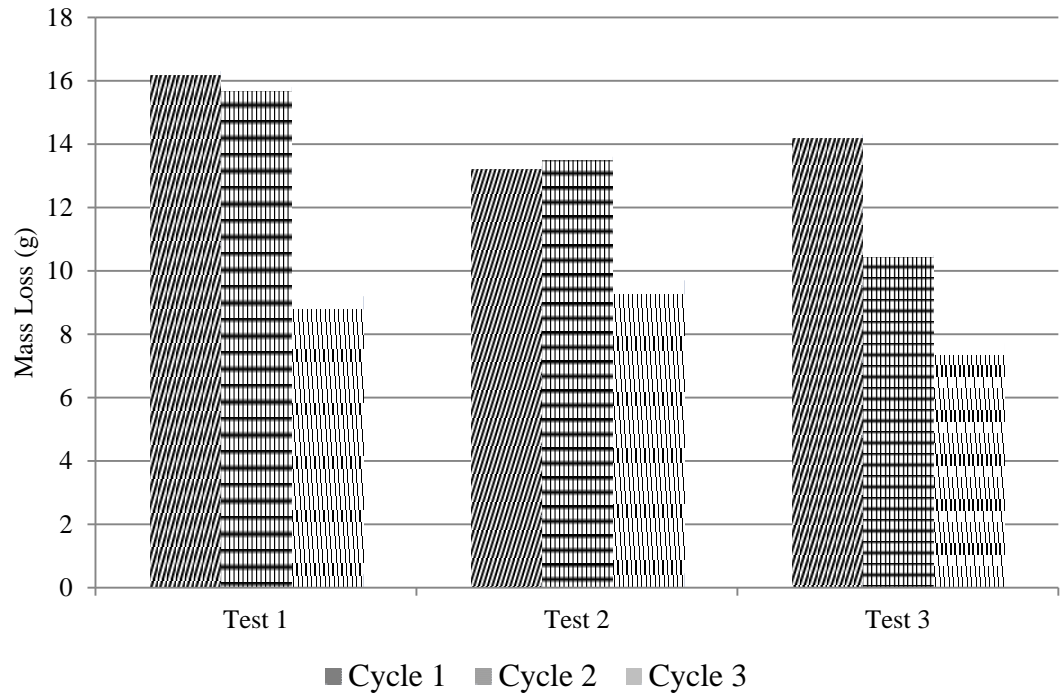
Figure 3.9 - HVFA-H Mass Loss Results
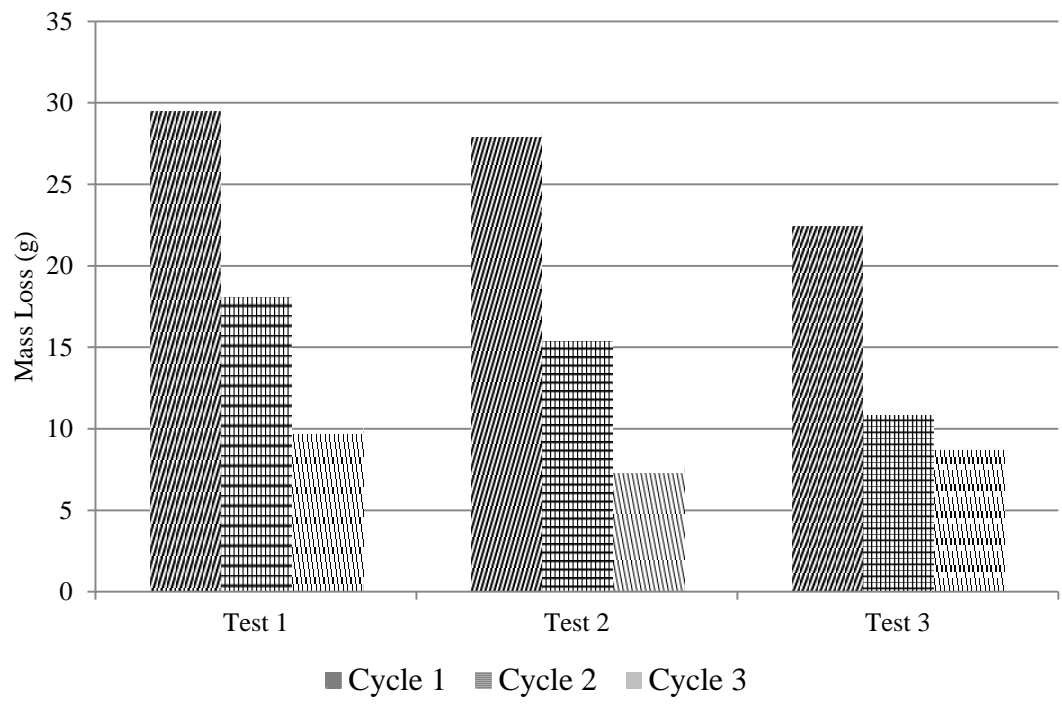
Figure 3.10 - HVFA-L Mass Loss Results
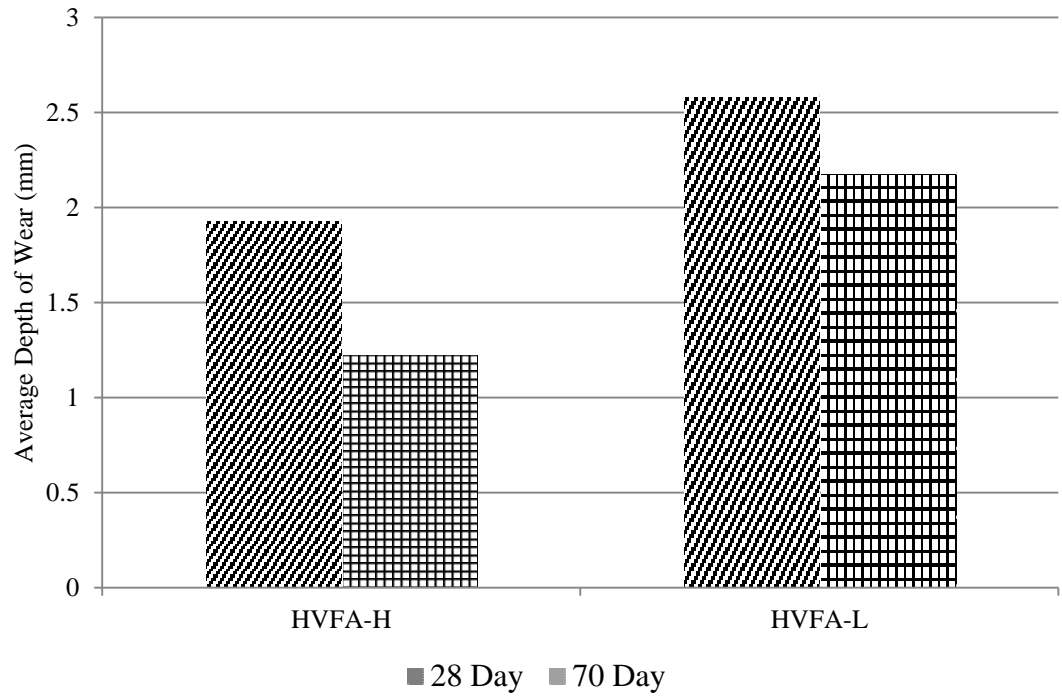
Figure 3.11 - HVFA Average Depth of Wear by Age
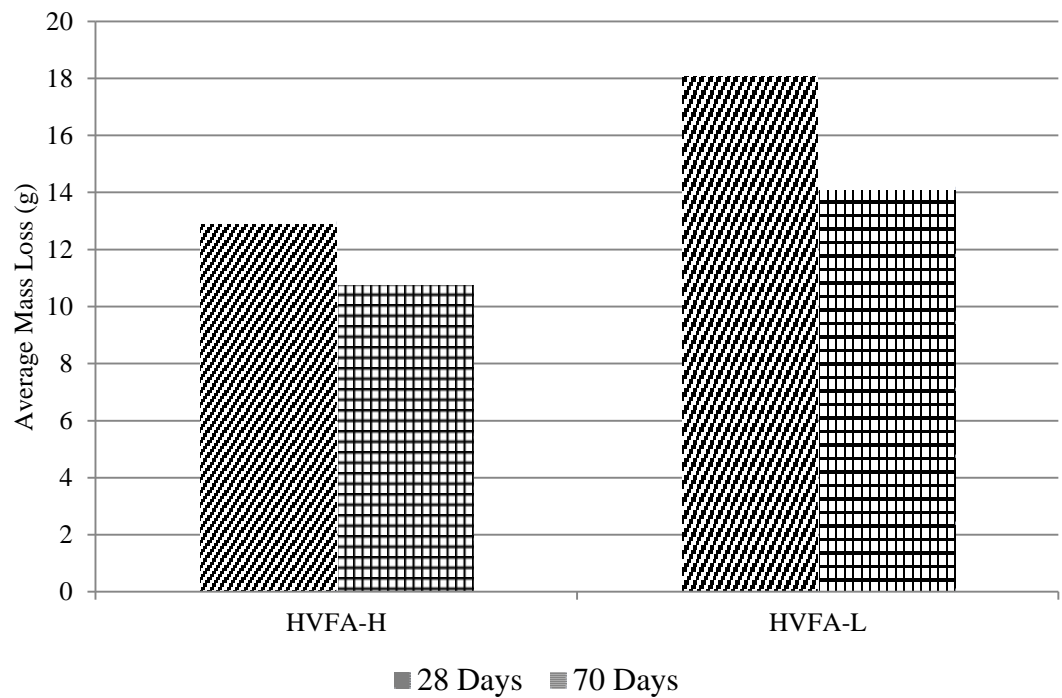
Figure 3.12 - HVFA Average Mass Loss by Age
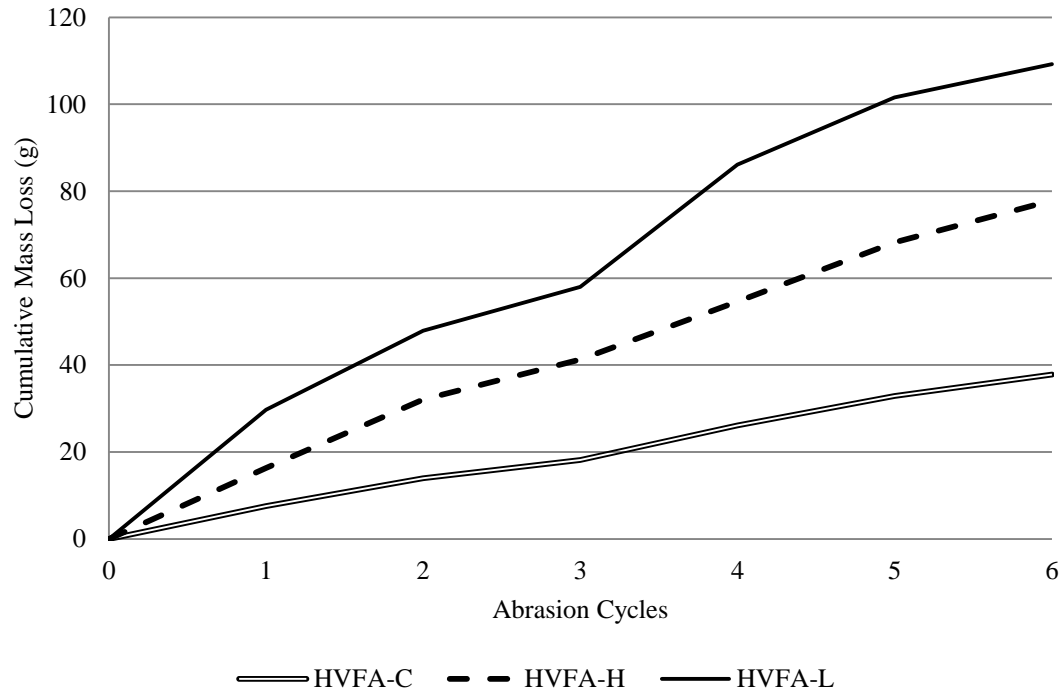
Figure 3.13 - HVFA Mass Loss Results
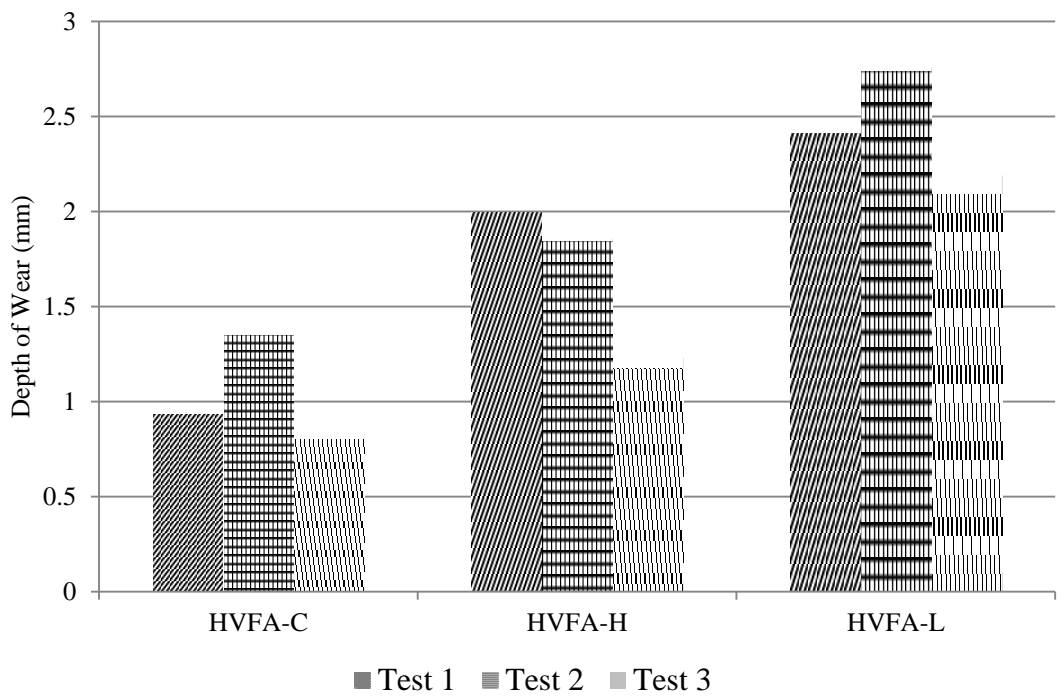
Figure 3.14 - HVFA Depth of Wear Results

Table 3.2 - Average Mass Loss Shown with 28 Day Compressive Strength

	HVFA-C	HVFA-H		HVFA-L	
28 Day Compressive Strength (psi)	5,400	3,100		3,500	
Age (days)	28	28	70	28	70
Avg. Mass Loss (g)	6.06	12.98	10.83	18.2	14.2
Avg. Depth of Wear (mm)	1.05	1.94	1.23	2.60	2.19

Conversion: 1 MPa = 145.04 psi
1 lb. = 453.59 g
1 in. = 25.4 mm

3.3.2. Discussion and Conclusions. Results are very consistent with

findings by both Naik and Atis. The compressive strength of the concrete seems to have

the most influence on its abrasion resistance. The two HVFA concrete mixes showed

significantly less resistance to abrasion than HVFA-C. This can be attributed to the lower compressive strengths of the HVFA concrete relative to the control. When comparing the two HVFA concrete mixes to each other, however, compressive strength does not seem to be as indicative of abrasion resistance. The results suggest that at identical levels of fly ash replacement, abrasion resistance is more affected by volume of cementitious material rather than compressive strength, however more testing is warranted to confirm this conclusion. Because the lower relative resistance to abrasion of HVFA concrete is most likely due to its strength, and not necessarily the fly ash replacement level, it is difficult to make conclusive findings on the effect of fly ash replacement on abrasion resistance without a larger scale investigation. As shown in **Figures 3.10 -3.11**, the abrasion resistance of both HVFA concrete mixes did increase with age. This suggests that, at later ages when HVFA concrete reaches improved strength, its abrasion resistance could be similar to that of conventional concrete, although further testing would be needed.

APPENDIX A

SHRINKAGE DATA WITH RELATIVE HUMIDITY DATA
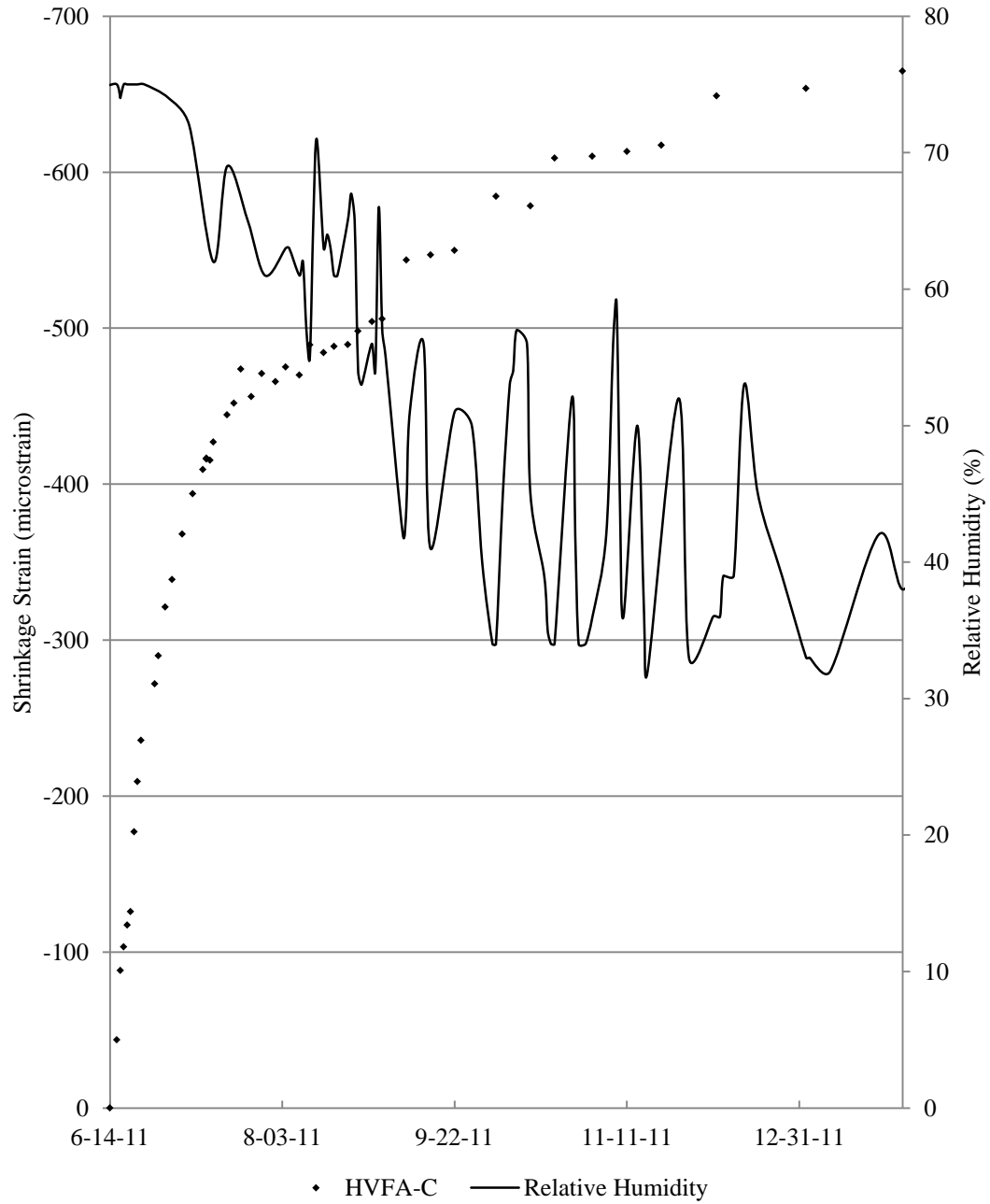
Figure A.1 – HVFA-C shrinkage data shown with recorded relative humidity
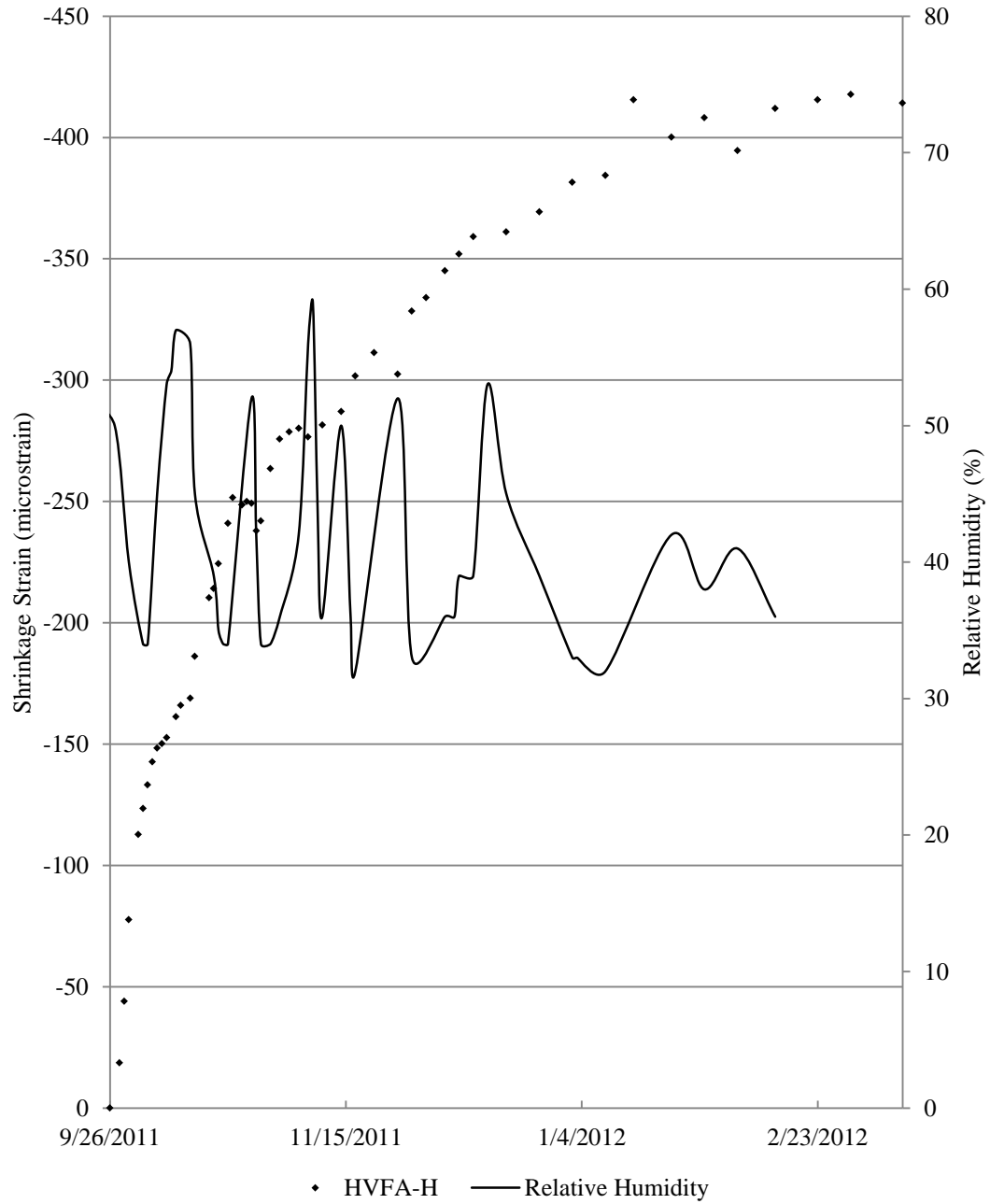
Figure A.2 – HVFA-H shrinkage data shown with recorded relative humidity
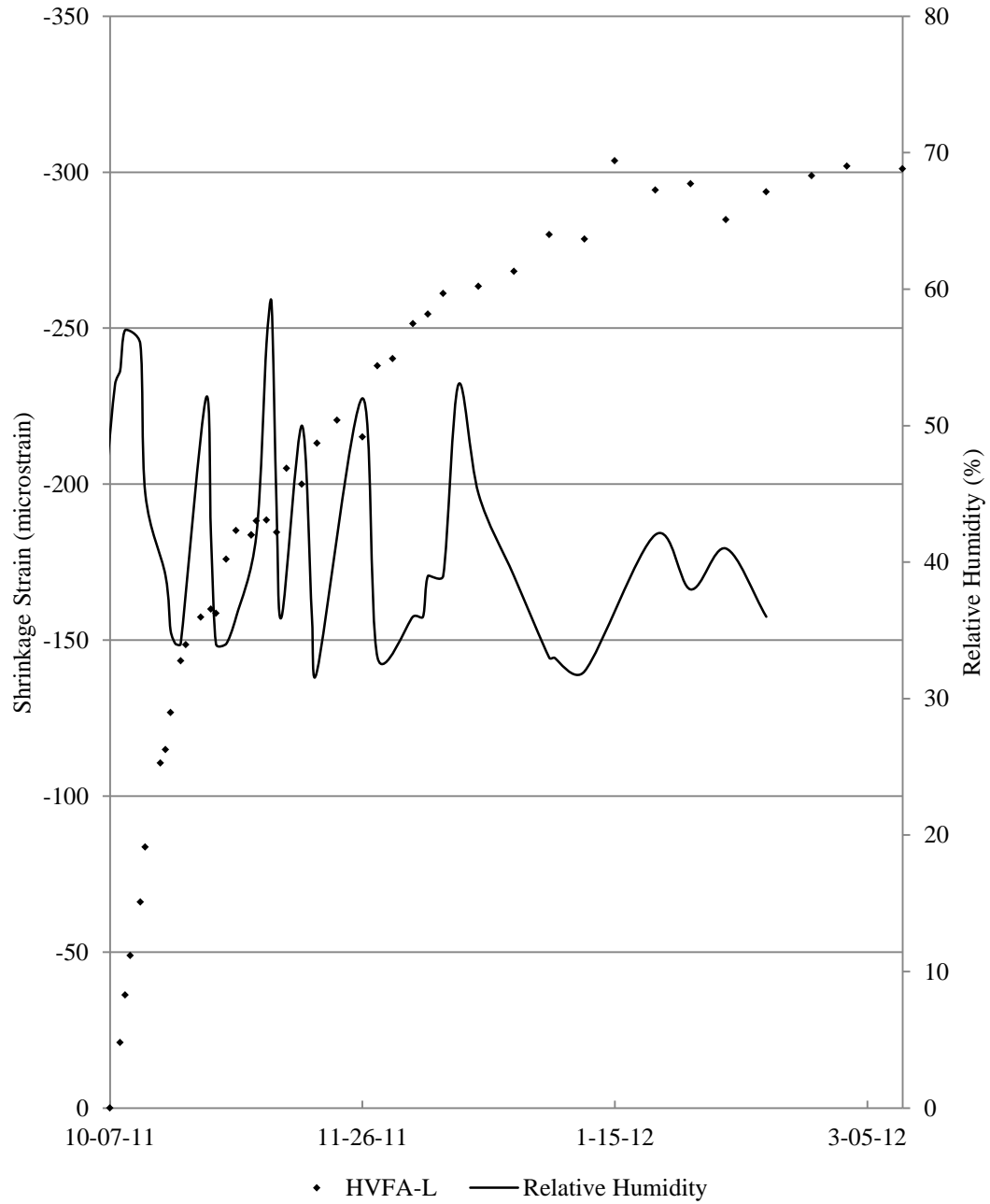
Figure A.3 – HVFA-L shrinkage data shown with recorded relative humidity

APPENDIX B

EXAMPLE STRAIN CALCULATIONS

	A	B	C	D	E	F	G
1			Example Shrinkage and Creep Calculation				
2							
3		G=	0.40	x 10^-5 (mm/mm)			
4		G=	4.00	x 10^-6 (mm/mm)			
5							
6					Measured Data		
7		Specimen		Reading			
8		Refer Bar			2525	2524	2525
9		C6-58L SH1		1--1	2130	2111	2106
10		C6-58L SH1		1--2	3633	3615	3611
11		C6-58L SH1		1--3	4018	4002	3998
12		C6-58L SH1		2--1	2549	2531	2529
13		C6-58L SH1		2--2	3179	3162	3162
14		C6-58L SH1		2--3	3230	3213	3210
15		C6-58L SH1		3--1	5867	5846	5846
16		C6-58L SH1		3--2	1980	1962	1960
17		C6-58L SH1		3--3	2182	2166	2165
18							
19							
20					Calculated Strain		
21							
22		C6-58L SH1		1--1		-72	-24
23		C6-58L SH1		1--2		-68	-20
24		C6-58L SH1		1--3		-60	-20
25		C6-58L SH1		2--1		-68	-12
26		C6-58L SH1		2--2		-64	-4
27		C6-58L SH1		2--3		-64	-16
28		C6-58L SH1		3--1		-80	-4
29		C6-58L SH1		3--2		-68	-12
30		C6-58L SH1		3--3		-60	-8
31							
32			Average Shrinkage			-67.1	-13.3
33			Cumulative Shrinkage			-67.1	-80.4
34							

Figure B.1 – Example shrinkage and creep strain calculation

	A	B	C	D	E	F	G
1				Example Shrinkage and Creep Calculation			
2							
3		G=	0.4	x 10^-5 (mm/mm)			
4		G=	4	x 10^-6 (mm/mm)			
5							
6						Measured Data	
7			Specimen	Reading			
8			Refer Bar		2525	2524	2525
9			C6-58L SH1	1--1	2130	2111	2106
10			C6-58L SH1	1--2	3633	3615	3611
11			C6-58L SH1	1--3	4018	4002	3998
12			C6-58L SH1	2--1	2549	2531	2529
13			C6-58L SH1	2--2	3179	3162	3162
14			C6-58L SH1	2--3	3230	3213	3210
15			C6-58L SH1	3--1	5867	5846	5846
16			C6-58L SH1	3--2	1980	1962	1960
17			C6-58L SH1	3--3	2182	2166	2165
18							
19							
20						Calculated Strain	
21							
22			C6-58L SH1	1--1		=$B$4*((F9-E9)-(F$8-E$8))	=$B$4*((G9-F9)-(G$8-F$8))
23			C6-58L SH1	1--2		=$B$4*((F10-E10)-(F$8-E$8))	=$B$4*((G10-F10)-(G$8-F$8))
24			C6-58L SH1	1--3		=$B$4*((F11-E11)-(F$8-E$8))	=$B$4*((G11-F11)-(G$8-F$8))
25			C6-58L SH1	2--1		=$B$4*((F12-E12)-(F$8-E$8))	=$B$4*((G12-F12)-(G$8-F$8))
26			C6-58L SH1	2--2		=$B$4*((F13-E13)-(F$8-E$8))	=$B$4*((G13-F13)-(G$8-F$8))
27			C6-58L SH1	2--3		=$B$4*((F14-E14)-(F$8-E$8))	=$B$4*((G14-F14)-(G$8-F$8))
28			C6-58L SH1	3--1		=$B$4*((F15-E15)-(F$8-E$8))	=$B$4*((G15-F15)-(G$8-F$8))
29			C6-58L SH1	3--2		=$B$4*((F16-E16)-(F$8-E$8))	=$B$4*((G16-F16)-(G$8-F$8))
30			C6-58L SH1	3--3		=$B$4*((F17-E17)-(F$8-E$8))	=$B$4*((G17-F17)-(G$8-F$8))
31							
32			Average Shrinkage			=AVERAGE(F22:F30)	=AVERAGE(G22:G30)
33			Cumulative Shrinkage			=F32	=F33+G32
34							
35							

Figure B.2 – Example shrinkage and creep strain calculations with equations shown

APPENDIX C
COEFFICIENT OF VARIATION DATA

HVFA-C Shrinkage

Age (days)	2	3	4	5	6	7	8	9	13	14	16	18	21	24	27
COV	0.14	0.20	0.57	0.41	1.66	0.34	0.33	0.34	0.31	0.38	0.22	0.20	0.17	0.21	0.51

	28	29	30	34	36	38	41	44	48	51	55	58	62	65	69
	0.57	0.44	0.41	0.37	0.32	0.30	0.52	0.32	0.47	0.31	0.49	0.21	0.61	7.27	3.11

	72	76	79	86	93	100	112	122	129	140	150
	0.34	0.34	0.36	1.48	1.69	0.20	0.13	0.43	0.10	0.36	0.36

Creep

Age (days after loading)	1	2	6	8	10	13	16	20	23	27	30	34
COV	0.44	0.41	0.37	0.32	0.30	0.52	0.32	0.47	0.31	0.49	0.21	0.61

37	41	44	48	51	58	65	72	84	94	101	112	122
7.27	3.11	0.34	0.34	0.36	1.48	1.69	0.20	0.13	0.43	0.10	0.36	0.36

HVFA-H Shrinkage

Age (days)	2	3	4	6	7	8	9	10	11	12	14	15	17	18	21
COV	0.46	0.22	0.15	0.19	0.37	0.39	0.42	0.54	1.29	1.13	0.42	0.60	1.07	0.16	0.20

22	23	25	26	28	29	30	31	32	34	36	38	40	42	45
1.03	0.38	0.47	0.60	1.17	3.09	4.24	0.14	1.50	0.23	0.24	1.04	2.36	0.94	0.77

49	52	56	61	64	67	71	74	77	84	91	98	105	111	119
0.75	0.21	0.36	0.40	0.23	1.08	0.26	0.33	0.36	1.97	0.49	0.31	1.63	0.16	0.24

126	133	141	150
0.34	0.15	0.27	1.01

Creep

Age (days after loading)	1	2	3	4	6	8	10	12	14	17	21	24
COV	0.49	0.81	0.90	0.31	0.25	0.22	0.51	1.31	0.67	0.33	0.37	0.30

28	33	36	39	43	46	49	56	63	70	77	83	91	98	105
0.21	0.66	0.21	0.35	0.16	0.25	0.30	0.36	0.26	0.19	0.21	0.10	1.59	1.08	5.28

113	122
0.21	0.24

Figure C.1 – HVFA-C and HVFA-H COV Data

HVFA-L   Shrinkage

Age (days)	2	3	4	6	7	10	11	12	14	15	18	20	21	23	25
COV	0.25	0.27	0.35	0.29	0.16	0.15	0.57	0.26	0.22	0.67	0.42	0.83	2.88	0.19	0.36

28	29	31	33	35	38	41	45	50	53	56	60	63	66	73
1.70	0.47	10.22	0.78	0.13	0.36	0.37	0.47	0.37	0.24	2.45	0.25	0.54	0.39	1.64

80	87	94	100	108	115	122	130	139	146	157
0.66	0.25	2.09	0.24	0.81	1.52	0.19	0.26	0.48	0.54	1.99

Creep

Age (days after loading)	1	3	5	7	10	13	17	22	25	28	32	35
COV	0.56	0.37	0.37	0.28	0.66	0.24	0.21	0.47	0.37	0.40	0.17	0.55

38	45	52	59	66	72	80	87	94	102	111	118	129
0.55	0.30	0.19	0.24	0.34	0.15	1.87	0.53	6.72	0.22	2.53	5.17	1.43

Figure C.2 – HVFA-L COV Data

BIBLIOGRAPHY

Alexander, K.M., Wardlaw, J., and Ivanusec, I. (1986). "A 4:1 Range in Concrete Creep When Cement SO_3 Content, Curing Temperature and Fly Ash Content are Varied." Cement and Concrete Research, Vol. 16, 173-180.

American Coal Ash Association (ACAA) (2010). "2010 Coal Combustion Product (CCP) Production & Use Survey Report." ACAA, Aurora, Colorado.

American Concrete Institute (ACI 116R-00) (2000), "Cement and Concrete Terminology." American Concrete Institute, Detroit, Michigan.

American Concrete Institute (ACI 209R-92) (1997), "Prediction of Creep, Shrinkage, and Temperature Effects in Concrete Structures." American Concrete Institute, Detroit, Michigan.

American Concrete Institute (ACI 209.1R-05) (2005), "Report on Factors Affecting Shinkage and Creep of Hardened Concrete." American Concrete Institute, Detroit, Michigan.

American Concrete Institute (ACI 232.2R-03) (2003), "Use of Fly Ash in Concrete." American Concrete Institute, Detroit, Michigan.

American Concrete Institute (ACI 318-08) (2008), "Buiding Code Requirements for Structural Concrete and Commentary." American Concrete Institute, Detroit, Michigan.

ASTM C31/C31 M-09 (2009). "Standard Practice for Making and Curing Concrete Test Specimens in the Field." American Society for Testing and Materials, West Conshohocken, Pennsylvania.

ASTM C39/C39 M-05 (2005). "Standard Test Method for Compressive Strength of Cylindrical Concrete Specimens." American Society for Testing and Materials, West Conshohocken, Pennsylvania.

ASTM C157/C157 M-08 (2008). "Standard Practice for Length Change of Hardened Hydraulic-Cement Mortar and Concrete." American Society for Testing and Materials, West Conshohocken, Pennsylvania.

ASTM C3512/C512 M-10 (2010). "Standard Practice for Creep of Concrete in Compression." American Society for Testing and Materials, West Conshohocken, Pennsylvania.

ASTM C944/C944 M-99 (2005). "Standard Practice for Abrasion Resistance of Concrete of Mortar Surfaces by the Rotating-Cutter Method." American Society for Testing and Materials, West Conshohocken, Pennsylvania.

Atis, C.D. (2002). "High Volume Fly Ash Abrasion Resistant Concrete." Journal of Materials in Civil Engineering, May/June 2002, 274-277.

Atis, C.D. (2003). "High-Volume Fly Ash Concrete with High Strength and Low Drying Shrinkage." Journal of Materials in Civil Engineering, March/April 2003, 153-156.

Bazant, Z. P. and Baweja, S. (2000). "Creep and Shrinkage Prediction Model for Analysis and Design of Concrete Structures: Model B3" Adam Neville Symposium: Creep and Shrinkage—Structural Design Effects, ACI SP–194, A.Al-Manaseer, ed., Am. Concrete Institute, Farmington Hills, Michigan, 2000, 1–83.

Comite Euro – International Du Beton (CEB) (1990), "CEB-FIP Model Code 1990" Thomas Telford, 1990-1993, 53-58.

Freyermuth, C.L. (1969). "Design of Continuous Highway Bridges with Precast, Prestressed Concrete Girders." Journal of the Prestressed Concrete Institute, Vol. 14, No. 2, 14-39.

Gao, P., et. al. (2006). "Effect of Fly Ash on Deformation of Roller-Compacted Concrete." ACI Materials Journal, October 2006, 336-339.

Gardner, N.J., and Lockman, M.J. (2001), "Design Provisions for Drying Shrinkage and Creep of Normal-Strength Concrete" ACI Materials Journal, 159-167.

Marlay, K.M., (2011). "Hardened Concrete Properties and Durability Assessment of High Volume Fly Ash Concrete." M.S. Thesis, Missouri University of Science and Technology, Rolla, MO.

Myers, J.J., Carrasquillo, R.L. (1999). "The Production and Quality Control of High Performance Concrete in Texas Bridge Structures," Center for Transportation Research, Report Number 580-589-1, November 1999, pp 564.

Myers, J.J. and Yang, Y. "High Performance Concrete for Bridge A6130-Route 421 Pemiscot County, MO." UTC R39.

Naik, T.R.., Singh, S.S., and Ramme, B.W. (2002). "Effect of Source of Fly Ash on Abrasion Resistance of Concrete." Journal of Materials in Civil Engineering, September/October 2002, 417-426.

Nath, P. and Sarker, P. (2011). "Effect of Fly Ash on the Durability Properties of High Strength Concrete." Procedia Engineering, 14 (2011), 1149-1156.

Ortega, C.A., (2012). "Shear and Fracture Behavior of High-Volume Fly Ash Reinforced Concrete for Sustainable Construction." PhD Dissertation, Missouri University of Science and Technology, Rolla, MO.

Perenchio, W.F., (1997). "The Drying Shrinkage Dilemma-Some Observations and Questions About Drying Shrinkageand its Consequence," *Concrete Construction*, V. 42, No. 4,pp. 379-383.

Tadros, M.K., Al-Omaishi, N., Seguirant, S.J., and Gallt, J.G. (2003). "Prestress Losses in Pretensioned High-Strength Concrete Bridge Girders." National Cooperative Highway Research Program Report 496, Transportation Research Board, National Research Council, Washington, D.C.

Termkhajornkit, P., et.al. (2005). "Effect of Fly Ash on Autogenous Shrinkage." Cement and Concrete Research, 35 (2005), 473-482.

U.S. Green Building Council (USGBC) (2009). "LEED Reference Guide for Green Building and Construction." USGBC, Washington, D.C.,369-377.

FINAL Report E

TRyy1110

**Project Title: Design and Evaluation of High-Volume
Fly Ash (HVFA) Concrete Mixes**

**Report E: Hardened Mechanical Properties and Durability
Performance of HVFA Concrete**

Prepared for
Missouri Department of Transportation
Construction and Materials

Missouri University of Science and Technology, Rolla, Missouri

October 2012

ABSTRACT

A rising concern in today's construction industry is environmental responsibility. The addition of fly ash is a leading innovation in sustainable design of concrete. Fly ash, a waste by-product of coal burning power plants, can be used to replace a portion of the Portland cement in concrete. Investigators are pushing for higher and higher total replacement levels in what is known as high-volume fly ash (HVFA) concrete. However, minor issues observed with lower fly ash replacement levels may be exacerbated as the levels increase.

Before the implementation of any new and innovative concrete, a new mix must be subjected to a series of tests and then compared to a conventional concrete mix that was subjected to the same test. In this investigation HVFA concrete was subjected to mechanical property tests such as compressive strength and modulus of elasticity as well as durability tests such resistance to freeze-thaw and chloride penetration. After being subjected to these tests, the HVFA concrete was found to be comparable to conventional concrete except for salt scaling.

TABLE OF CONTENTS

LIST OF ILLUSTRATIONS

LIST OF TABLES

1. INTRODUCTION

1.1. BACKGROUND, PROBLEM, & JUSTIFICATION

Concrete is one of the most widely used materials in the world. It is used in a variety of applications and produced in massive quantities. With this mass production of concrete comes the negative side effect of large amounts of carbon dioxide emissions, a greenhouse gas. These emissions are created from the production of Portland cement, a major component of concrete. Any material that would be able to partially replace Portland cement as a supplementary cementitious material might help lower emissions and be beneficial to the overall environmental impact of concrete applications.

In the 1930's, an inorganic noncombustible by-product of coal burning electric power plants known as fly ash became readily available. Researchers began testing the use of fly ash in concrete applications. The earliest study on concrete containing fly ash was published in 1937 [Davis et al., 1937]. Since this initial study, significant strides have been made to standardize the use of fly ash in concrete. Most commonly, the concrete industry uses fly ash replacement in small percentages, usually limiting the quantity to 35 percent or less of the total cementitious material. Due to growing environmental concerns over greenhouse gases, researchers have begun to evaluate whether higher replacement percentages – even up to 75 percent – are feasible in terms of concrete production, placement, and structural behavior. Referred to as high-volume fly ash (HVFA) concrete, this material offers a viable alternative to traditional Portland cement concrete and is significantly more sustainable.

Aside from its environmental impact, fly ash has been shown to improve some of the characteristics of concrete, both fresh and hardened. The physical structure of fly ash

can be described as "tiny ball bearings". This spherical shape increased the workability of concrete while maintaining cohesiveness. Also, fly ash has a relatively low reactivity relative to Portland cement and therefore shows very low heat of hydration. This property can be useful in some concrete applications, particularly mass concrete where heat control is a major concern. However, this low reactivity of fly ash has raised concerns over its usage. Adequate early strength gains of concrete containing high amounts of fly ash can negatively impact construction schedules. Also, while concrete containing fly ash has shown comparable durability performance, some reports suggest that HVFA concrete may have poor scaling resistance. While the increased usage of fly ash in concrete would solve many environmental concerns, there are still many questions to be answered as the limits are raised on the amount of fly ash in concrete. Negative issues observed in concrete containing lower volumes of fly ash may only be magnified with an increase in fly ash. Further testing on the hardened properties and durability performance on HVFA concrete is required.

1.2. OBJECTIVES & SCOPE OF WORK

The main objective of this study is to investigate the mechanical properties and durability performance of HVFA concrete in comparison to conventional concrete.

The following scope of work was implanted in an effort to attain this objective: (1) review applicable and relevant literature; (2) develop a research plan; (3) evaluate the mechanical properties and durability of several HVFA concrete mixes; (4) compare the HVFA concrete mixes with conventional concrete mixes; (5) verify the validity of using current hardened property tests on HVFA concrete; (6) analyze the information gathered

throughout the testing to develop findings, conclusions, and recommendations; and
(7) prepare this report in order to document the information obtained during this
investigation.

1.3. RESEARCH PLAN

The research plan entailed the development of several concrete mixes that
contained 70% fly ash by total mass of cementitious material. These mixes varied in the
amount of total cementitious material used and are described in Section 3. Several
standard hardened property tests were selected to evaluate the performance of the HVFA
mixes in comparison to conventional concrete, including compressive strength, modulus
of elasticity, modulus of rupture, and splitting-tensile strength. These tests were also used
to determine their validity in predicting the performance of HVFA concrete.

Specimens were also fabricated in order to evaluate the durability performance of
HVFA concrete. The tests performed on the mixes consisted of chloride penetration by
electrical indication and ponding methods, freeze-thaw resistance, concrete resistivity,
and scaling resistance. Both the conventional and HVFA mixes were subjected to these
durability tests in order to compare their performance.

1.4. OUTLINE

This report consists of seven sections and one appendix. Section 1 briefly explains
the history and benefits of using fly ash in concrete. Also within Section 1 are the
objectives, scope of work, and research plan.

Section 2 summarizes how fly ash is produced as well as the chemical composition and difference among types of fly ash. The mechanical property tests are also discussed in further detail. Lastly, the durability tests as well as the mechanisms behind the durability issues are discussed.

Section 3 explains the development of the HVFA concrete mix designs including the selection of chemical admixtures. This section includes typical fresh properties measured during this investigation. Also, the mechanical property tests are discussed in more detail as well as equations used to estimate the behavior of concrete.

Section 4 consists of discussing the tests used to evaluate the durability performance in further detail.

Section 5 presents the results of both the mechanical property tests as well as the durability tests. Also presented in this section are the normalized results of the mechanical property tests in comparison to traditional relationships used to estimate the behavior of concrete.

Section 6 outlines the results of the investigation and evaluates the data based on a statistical analysis. Also, the results of the investigation are discussed to propose a theory on the outcome of the tests in order to recommend how to successfully implement HVFA concrete.

Section 7 consists of the conclusion of the investigation as well as any recommendations based on the findings from the mechanical tests as well as the durability performance of the HVFA concrete mixes in comparison to conventional concrete.

The appendix contains additional test data associated with the durability tests of the HVFA mixes.

2. LITERATURE REVIEW

2.1. HIGH-VOLUME FLY ASH CONCRETE

The use of fly ash in concrete has been in practice for nearly 100 years. In recent years, the use of fly ash has grown considerably and it is estimated that over 6 million tons are used in concrete each year. The American Concrete Institute (ACI) has limited the amount of fly ash used in concrete applications to a maximum of 25 percent by mass of total cementitious content [ACI 318-08, 2008]. Researchers are investigating the possibility of increasing the limit of the amount of fly ash that can be incorporated into concrete. It has been suggested that concrete with a minimum of 50 percent by mass of total cementitious material is considered a high-volume fly ash (HVFA) concrete [Hopkins, 2003]. It has been found that when the total amount of fly ash used crosses this 50 percent limit, the characteristic of the concrete begin to differ from concrete containing only Portland cement and may require special consideration.

Fly ash is the incombustible, inorganic, by-product of burning pulverized coal in electricity-generating power plants. This waste product is a natural pozzolanic material or a reactive aluminosilicate material created from natural processes. The most common production of fly ash is from a dry-bottom boiler that burns pulverized coal. In this process, about 80 percent of all ash leaves the furnace as fly ash and is entrained in the flue gas. The fly ash is then collected in hoppers by means of an electrostatic precipitator as shown in **Figure 2.5** or by a mechanical precipitator. Both collection processes can generate fineness, density, and carbon content variations in the fly ash from hopper to hopper. Although, typical particle size can range from 0.00004 in. (1 μm) to more than 0.008 in. (200 μm) and density of individual particles from less than 62.4 lb/ft^3 (1000

kg/m^3) hollow spheres to more than 187 lb/ft^3 (3000 kg/m^3), coal burned from a uniform source generally produces very consistent fly ash [Huffman, 2003]. A more homogenous material is created when the hoppers are emptied and the fly ash is conveyed to storage.
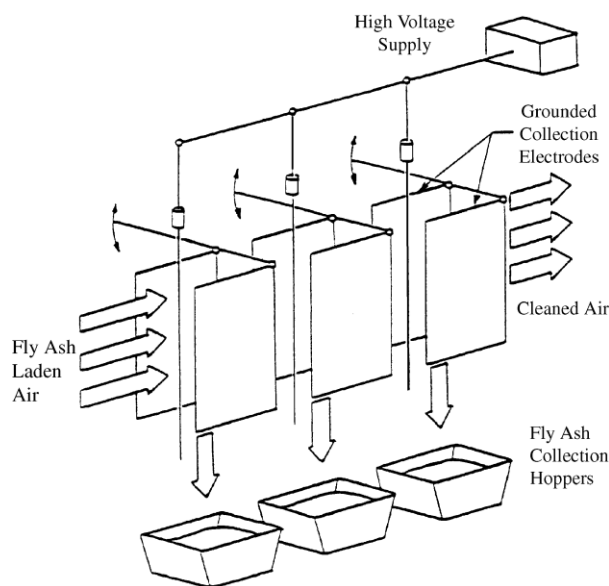
Figure 2.5 - Electrostatic Precipitator Fly Ash Collection Process [Huffman, 2003].

There are two types of fly ash as specified in ASTM C 618-12, "Standard Specification for Coal Fly Ash and Raw of Calcined Natural Pozzolan for Use in Concrete," Class C and Class F. Class C fly ashes are produced from the burning of lignitic coals, while Class F fly ash is the result of the burning of bituminous and sub-bituminous coals. These two types of fly ash are divided into these classes due to their chemical variations. Fly ash is mainly composed of silica (SiO_2), alumina (Al_2O_3), iron (Fe_2O_3), and calcium (CaO). According to ASTM C 618 Class F fly ash contains a minimum of 70% silica, alumina, and iron while Class C must contain a minimum of 50%. A complete table of the chemical composition of the different classes of fly ash can be seen in **Table 2.1**.

Table 2.1 Chemical Composition of Fly Ash as Percent by Weight [Office, 1997]

Component	Class F	Class C
SiO_2	20 – 60	40 – 60
Al_2O_3	5 – 35	20 – 30
Fe_2O_3	10 – 40	4 – 10
CaO	1 – 12	5 – 30
MgO	0 – 5	1 – 6
SO_3	0 – 4	0 – 2
Na_2O	0 – 4	0 – 2
K_2O	0 – 3	0 – 4
LOI	0 – 15	0 – 3

The chemical composition of fly ash has a noticeable impact on the hydration of concrete. Fly ash shows very little reaction when mixed with water and requires what is known as "activators". Alkalis, sulfates, and calcium hydroxide are all used as activators. This leads to a lowered heat of hydration and delayed setting time, which can have a serious impact on finishing and removal of formwork. While the chemical composition of fly ashes may be different, their physical make up is very similar. Both classes of fly ash are very spherical in nature. Under a microscope these particles resemble tiny ball bearings. The spherical nature of these particles results in an increase in the workability of concrete containing fly ash. A microscopic photograph of fly ash can be seen in **Figure 2.6**.
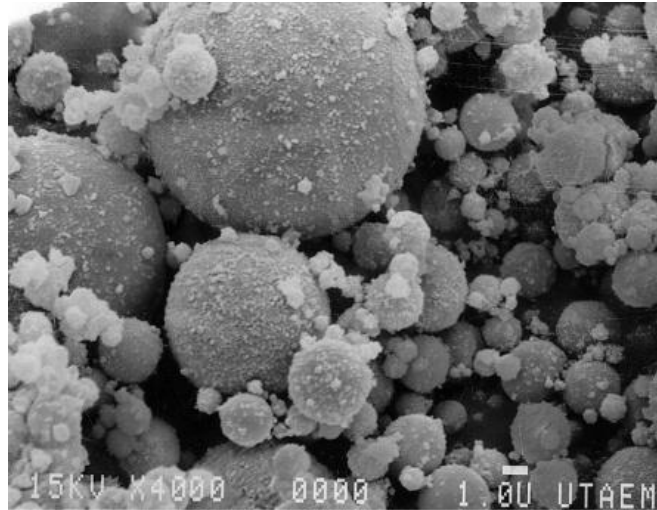
Figure 2.6 - Fly Ash at 4000x Magnification [Huffman, 2003]

The presence of fly ash also has other positive influences on concrete besides workability. Concretes with fly ash show a better plasticity as well as cohesiveness. In addition to the workability increasing, the pumpability of concrete containing fly ash increases as well. The permeability of concrete containing fly ash has been shown to decrease (Myers et al. 1998). . During the hydration process of Portland cement, calcium hydroxide may be leached out of the concrete creating voids which allow water to permeate, which can bring in unwanted and damaging chemicals. The addition of fly ash causes more of that calcium hydroxide to chemically react with water and create C-S-H, thereby preventing the calcium hydroxide from being leached. This creates an overall denser microstructure of the concrete, reducing permeability [Malhorta and Mehta, 2008].

The use of high amounts of fly ash in concrete also has environmental benefits. Currently, a majority of fly ash in the United States is disposed of in landfills. Using higher amounts of fly ash in concrete would considerably reduce the amount of fly ash

that is placed into landfills. Also, the production of Portland cement emits large amounts of carbon dioxide and consume large amount of energy. With fly ash being a by-product that is already produced from creating electricity, using higher amounts could significantly reduce these emissions and reduce energy consumption in the production of Portland cement.

2.2. MECHANICAL PROPERTY TESTING METHODS

2.2.1. Compressive Strength. The compressive strength of concrete is one of the most important of all the mechanical properties. Measuring compressive strength is influenced by many factors including specimen size, curing conditions, load rate, etc. In order to control variations in testing and consequently variations in results, a standard test method was developed by ASTM International. The standard for determining the compressive strength of concrete is outlined in ASTM C 39–11, "Standard Test Method for Compressive Strength of Cylindrical Concrete Specimens." This standard requires cylindrical specimens for testing. The specimens used in laboratory testing measure either 4 in. (102 mm) in diameter x 8 in. (203 mm) in height or 6 in. (152 mm) in diameter x 12 in. (305 mm) in height. The specimens are prepared by filling the molds in equal lifts and rodding each lift a specified number of times. The numbers of lifts and extent of rodding depends on the diameter and cross sectional area, which is specified in ASTM C 192-07 "Standard Practice for Making and Curing Concrete Test Specimens in the Laboratory." After each lift, the mold is also stuck with a mallet to ensure consolidation. After 24 hours in a moist curing chamber, the specimens are de-molded and returned to the moist curing chamber until the proper test date. Common testing dates for measuring a

concrete's strength gain profile are 1, 7, and 28 days after batching. The cylindrical specimens are ground flat or capped before testing. This flat surface reduces localized stress on the specimen. Capping can be done with sulfur capping compound or neoprene pads. Dimensions of the specimens are taken before being loaded at a constant rate until failure. The load recorded at failure is divided by the cross-sectional area to find the compressive strength of the concrete.

2.2.2. Modulus of Elasticity. Due to the nonlinear inelastic behavior of concrete, the modulus of elasticity (MOE) can be different depending on how it is measured. The MOE is the slope of the stress–strain curve between two designated points. An example of the different moduli of elasticity that can be measured can be seen in **Figure 2.7**.
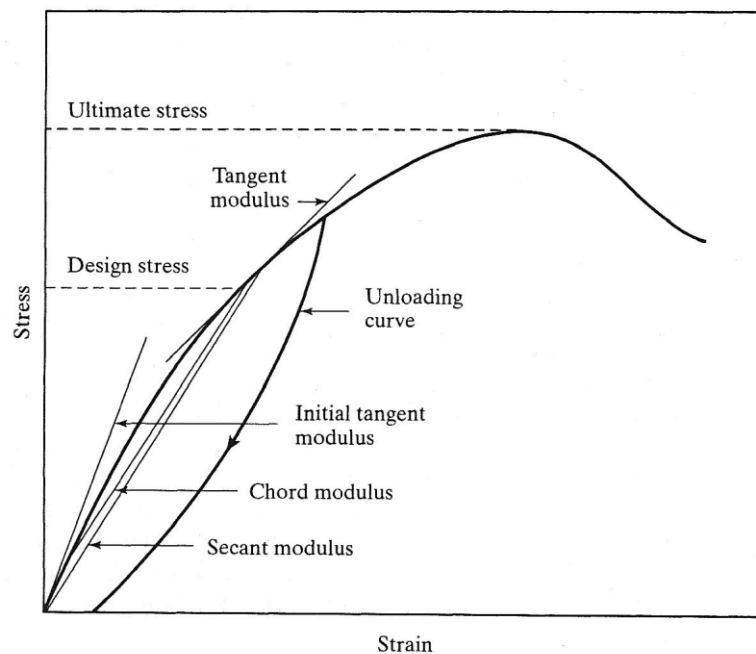
**Figure 2.7 – Typical Stress-Strain Diagram for Concrete,
Showing the Different Elastic Moduli [Mindess et al., 2002]**

In order to standardize the measured modulus of elasticity, ASTM International developed a standard test method ASTM C 469-10, "Standard Test Method for Static Modulus of Elasticity and Poisson's Ratio of Concrete in Compression." This test method measures what is known as the chord modulus of elasticity. The specimens used in this test are the same type used in the compressive strength test. Either the 4 in. (102 mm) or 6 in. (152 mm) diameter cylindrical specimens can be used. Specimens are fabricated and cured in the same manner as the compressive strength specimens. After 28 days of moist curing, specimens are prepared for testing. Using a Compressometer, the strain produced at 40% of the ultimate load is recorded. Also, the stress that produces a measured strain of 0.00005 in./in. is recorded. Using these values, the chord modulus of elasticity can be calculated in accordance with **Eq. 2.2**.

$$E_c = \frac{(S_2 - S_1)}{(\varepsilon_2 - 0.00005)} \tag{2.2}$$

2.2.3. Modulus of Rupture. The modulus of rupture (MOR) is an important property in the calculation of the cracking moment of concrete and thus determining how a concrete member will behave post-cracking. ASTM International has created a standard for testing the modulus of rupture known as ASTM C 78-10, "Standard Test Method for Flexural Strength of Concrete (Using Simple Beam with Third-Point Loading)." This approach is an indirect way to measure the tensile strength of concrete. The specimen has to have an overall depth of a third of the span length. The span length shall be such that it measures three times the distance in between the load points of the testing apparatus.

Also, the specimen shall overhang the supports by at least 1 in. (25 mm). The schematic

diagram in **Figure 2.8** summarizes these requirements.
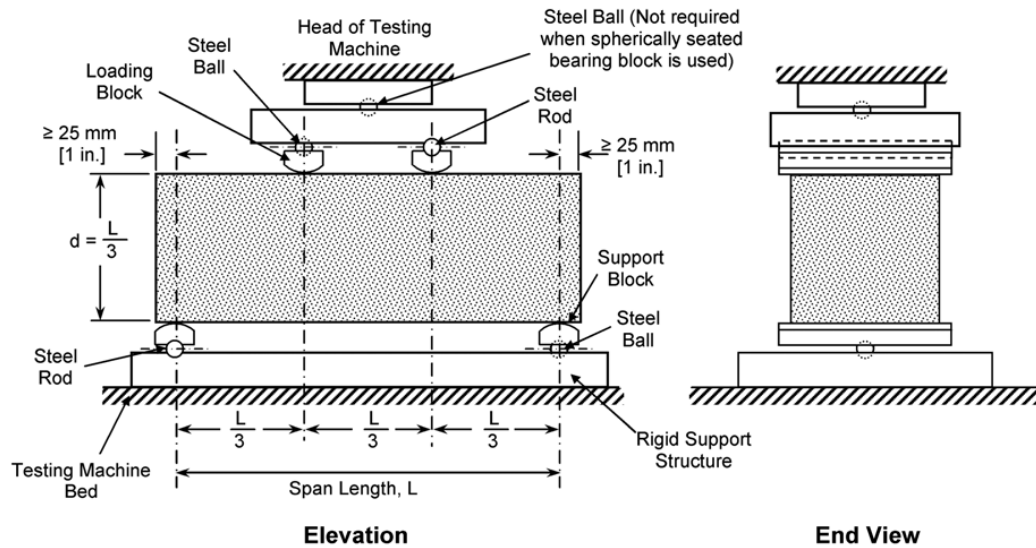
Figure 2.8 - Typical Modulus of Rupture Testing Setup [ASTM C 78–10]

The specimen is then loaded until failure. After testing, the dimensions are

recorded and the modulus of rupture is computed in accordance with **Eq. 2.3**. While this

test method overestimates the "true" tensile strength of concrete, the test does simulate

the most common way concrete is placed into tension, through flexure.

$$R = \frac{PL}{bd^2}$$
(2.3)

2.2.4. Splitting Tensile Strength. While the modulus of rupture test described

in Section 2.3.3 tests for the tensile strength of concrete indirectly, the splitting tensile

test uses a much more direct manner. This test is outlined in ASTM C 496–11, "Splitting

Tensile Strength of Cylindrical Concrete Specimens." The cylindrical specimens measure

either 4 in. (102 mm) in diameter by 8 in. (203 mm) in height or 6 in. (152 mm) in

diameter and 12 in. (305 mm) in height. The method for preparing the specimens used in

the splitting-tensile test is outline in ASTM C 192. Specimens are stored in a moist curing

chamber and tested after 28 days. Diametral lines are drawn on the specimens to ensure

that they are in the same axial plane. The dimensions of the specimens are then taken.

The specimens are then placed on top of a 1 in. (25 mm) wide x 3/8 in. (10 mm) thick

plywood strip within the testing apparatus. A second plywood strip is then placed on top

of the specimen so the two strips align with the diametral lines. This ensures that the load

is distributed in one plane of the specimen. The peak load is recorded and the tensile

strength is then calculated in accordance with **Eq. 2.4**.

$$T = \frac{2P}{\pi LD} \tag{2.4}$$

2.3. DURABILITY OF CONCRETE

2.3.1. Freezing and Thawing. Concrete is a porous material which allows

water to permeate into its microstructure. When concrete containing moisture is subjected

to repeated cycles of freezing and thawing, severe deterioration can occur. Initially

researchers believed that this damage was caused by the expansion of water when it

transitioned into ice. The trapped water would freeze and expand in the capillary pores

and exert hydraulic pressure on the hardened paste. This theory of hydraulic pressure was

proposed by T.C Powers [Mindess et al., 2002]. Later, Powers developed a new theory

based on osmotic pressure [Powers, 1956]. He proposed this theory after observing that

concrete paste, when frozen, shrank first than expanded. He also observed that air entrained cement paste would shrink indefinitely and the same deterioration is observed when liquids that do not expand when frozen were used to saturate the concrete. Investigators developed two possible explanations for these observations. The first is osmotic pressure. As water is drawn to the freezing sites through osmosis, osmotic pressure is built up. This eventually would cause the concrete to crack. Another possible explanation is vapor pressure. The ice that begins to form in the pores has less chemical potential than the supercooled water in the unfrozen pores. This creates a lower vapor pressure. This condition causes the relative humidity at the freezing pores to lower, which draws water towards them to maintain equilibrium. This pressure would also cause the concrete to begin to crack.

The introduction of air entraining admixtures has had a positive effect on the resistance of concrete to freezing and thawing deterioration. The air bubbles in the concrete allow for excess space for the water to move and freeze without damaging the concrete. These bubbles must be spaced at certain intervals to be effective in protecting the concrete. If the bubbles are too far apart, the water cannot move to these "safety valves" and the pressure cannot be relieved. The air-entraining system becomes ineffective in fully saturated concrete due to all the pores and air bubbles containing water. Many other factors influence a concrete's resistance to freezing and thawing attack, the most important of which is the permeability of the concrete. With concretes having a low water/cement ratio and usually a low permeability, freeze/thaw resistance generally increases [Mindess et al., 2002]. This relationship can be seen in **Table 2.2**.

Table 2.2 Effect of w/cm Ratio on the Air Void System in Concrete

w/c ratio	Air content (%)	Spacing factor mm (in.)	Liner expansion per freeze – thaw cycle
0.35	4.8	0.11 (0.0043)	0.00004
0.45	4.7	0.14 (0.0055)	0.00014
0.55	5.2	0.15 (0.0059)	0.00021
0.65	4.9	0.18 (0.0071)	0.00026
0.75	5.3	0.23 (0.0091)	0.00036

1 in. = 2.54 cm.

2.3.2. Chloride Attack. Chloride ions attack the passive layer that forms on reinforcing steel placed within a high pH environment, such as concrete. Chloride ions are most commonly introduced into concrete through deicing salts. These salts can remain on bridge decks for days or even weeks, penetrating into the concrete structure and eventually destroying the passive layer of the reinforcing steel. Corrosion in steel begins with the iron being oxidized at an anode as shown in **Eq. 2.5**.

$$Fe \rightleftarrows 2e^- + Fe^{2+} \tag{2.5}$$

At the cathode, water is reduced into hydroxyl (OH⁻) ions as shown in **Eq. 2.6**.

$$\frac{1}{2}O_2 + H_2O + 2e^- \rightleftarrows 2OH^- \tag{2.6}$$
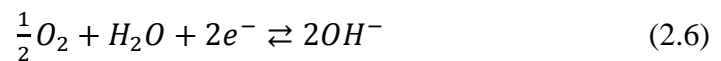
These hydroxyl ions then flow from the cathode to the anode. At the anode, the ferrous ions and the hydroxyl ions react to form ferrous hydroxide as shown in **Eq. 2.7**.

$$Fe^{2+} + 2(OH)^- \rightarrow Fe(OH)_2 \qquad\qquad (2.7)$$

When oxygen and water are introduced the ferrous hydroxide will spontaneously oxidize

into hydrated ferric oxide (rust) as shown in **Eq. 2.8**.

$$2Fe(OH)_2 \rightarrow 2Fe(OH)_3 \rightarrow Fe_2O_3 \cdot nH_2O \qquad\qquad (2.8)$$
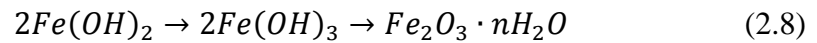
This hydrated ferric oxide, or red rust that is commonly seen, is known to have six times

the volume of the original iron [Broomfield, 2007]. The increased volume induces

expansive stresses in the concrete, eventually leading to cracking and progressive

deterioration. The volume of iron and various forms of oxidized irons can be seen in

Figure 2.9.
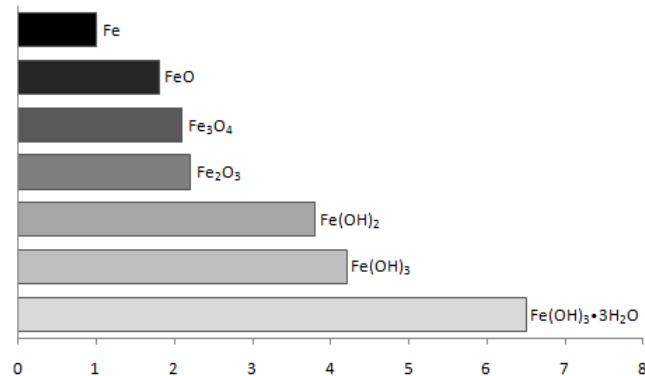
**Figure 2.9 - The Relative Volumes of Various Iron Oxides
from Mansfield [1981], Corrosion 37(5), 301-307.**

This reaction can be largely avoided in concrete structures. Conventional concrete is highly alkaline which allows for the formation of a passive oxide film (FeOOH) on the reinforcement. The $Fe(OH)_2$ is oxidized to create this film as shown in **Eq. 2.9**.

$$2Fe(OH)_2 + \frac{1}{2}O_2 \rightarrow 2\gamma - FeOOH + H_2O \qquad (2.9)$$
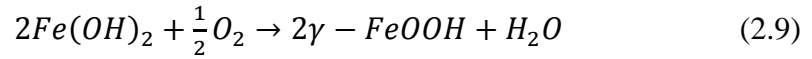
Chlorides effectively destroy this passive layer allowing for the reinforcement to corrode. Chlorides react with ferrous ions to create a soluble iron-chloride complex as shown in **Eq. 2.10**.

$$Fe^{2+} + Cl^- \rightarrow [FeCl\ complex]^+ \qquad (2.10)$$
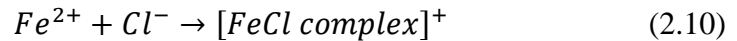
This complex in turn reacts with the hydroxyl to form the ferrous hydroxide which oxidizes into expansive rust as shown in **Eq. 2.11**.

$$[FeCl]^+ + 2OH^- \rightarrow Fe(OH)_2 + Cl^- \qquad (2.11)$$
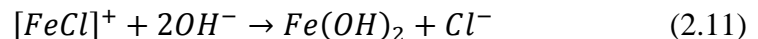
The largest factor influencing the effect of chlorides in concrete is the permeability of the concrete. The permeability relates to the amount and rate of oxygen, moisture, and chloride penetration into the microstructure of the concrete over time. Permeability is most influenced by the water to cementitious material ratio (w/cm). The lower the w/cm ratio of the concrete, the lower the porosity [Powers et al., 1954]. Decreasing the permeability of concrete will improve its durability. Water can carry

harmful chemicals, such as chlorides, into the concrete's pores. The diffusion of chemicals into hardened concrete is described by *Fick's Second Law* as shown in **Eq. 2.12**.

$$\frac{\partial c}{\partial t} = K_d \frac{\partial^2 c}{\partial x^2}$$ (2.12)

Where C is the concentration, t is the time, K_d is the diffusion coefficient, and x is the depth. The solution of this equation is shown in **Eq. 2.13** [Broomfield 2007].

$$\frac{C_{max} - C_d}{C_{max} - C_{min}} = erf\left(\frac{x}{\sqrt{4D_c t}}\right)$$ (2.13)

Where C_d is the chloride concentration at depth (x), x is the specified depth, t is the time, D_c is the diffusion coefficient of concrete, C_{max} is the maximum chloride content of the concrete, C_{min} is the baseline chloride content of the concrete, and erf is the error function. Using this function the chloride penetration over time can be estimated. This equation has proved to estimated chloride contents extremely accurately when compared to field results [Berke and Hicks, 1996]

2.4. DURABILITY TESTING METHODS

2.4.1. Resistance to Freezing and Thawing. In order to evaluate the potentially devastating effects of freezing and thawing cycles, ASTM International developed a standardized test to simulate these conditions in the lab. This test is outlined in ASTM C 666–03 "Standard Test Method for Resistance of Concrete to Rapid Freezing and

Thawing." Specimens used in this test are prisms that are made and cured in accordance

with ASTM C 192. The dimensions requirements of these specimens are specified in

ASTM C 666. The specimens are cured for 14 days before testing unless otherwise

specified. This test subjects the specimens to 300 freezing and thawing cycles. Every 36

cycles, the specimens are removed and properties of the concrete are measured. These

properties include the transverse frequency, total length change, and total weight change.

These specimens can be tested using two different procedures, A or B. Procedure A

specifies that the specimens be surrounded by water during the freezing and thawing

cycles, while Procedure B specifies that the specimens be surrounded by air during

freezing and water during thawing. Between the testing intervals, both the relative

dynamic modulus of elasticity and the durability factor are calculated. Using these values,

the concrete can be evaluated for its durability performance. The test calls for the cycles

to be stopped when the measured durability factor falls below 50. Every Department of

Transportation has its own criteria for acceptable durability factor and sets a minimum

for acceptance. The acceptability criteria for the state of Missouri and for this

investigation will be discussed during evaluation of the different concretes of this study.

      2.4.2. Rapid Chloride Penetration. The diffusion of chlorides can be extremely

damaging, as stated previously. However the process is very slow, and testing the

chloride penetration accurately can take years. In order to test a concrete's ability to resist

chloride penetration, ASTM International developed a testing method that could be

performed much more quickly. This testing method is outline in ASTM C 1202–10,

"Standard Test Method for Electrical Indication of Concrete's Ability to Resist Chloride

Ion Penetration." This test is also known as the Rapid Chloride Test (RCT). The test

specimens consist of concrete disks subjected to a constant voltage to determine their resistance to chloride penetration. The disks are cut from concrete cylinders that are fabricated and cured according to ASTM C 192. The disks, measuring 4 in. (102 mm) in diameter and 2 in. (51 mm) thick, are prepared according to ASTM C 1202 and subjected to 60 V for 6 hours as shown in **Figure 2.10**.

Figure 2.10 - Typical RCT Setup

During the test, the current is recorded every 30 minutes. Using a plot of current versus time, the total charge passed is calculated and used to determine the permeability class of the concrete. There is a correlation between the amount of charge passed and the chloride ion penetrability of concrete. This correlation can be seen in **Table 2.3**.

Table 2.3 Chloride Ion Penetrability Based On Charge Passed [ASTM C1202–10]

Charge Passed (coulombs)	Chloride Ion Penetrability
>4000	High
2000-4000	Moderate
1000-2000	Low
100-1000	Very Low
<100	Negligible

2.4.3. Chloride Content Analysis. While the test outlined in ASTM C 1202 is

an adequate test when the results are required quickly, it does not subject the concrete to

realistic conditions. ASTM C 1202 is only suitable for research and development. Some

studies have indicates that ASTM C 1202 gives false indications for concretes made with

supplementary cementitious materials, such as fly ash, slag, silica fume, and slag [e.g.,

Shi, 2002]. This study showed that cement containing supplementary cementitious

material would yield falsely high results than what was observed in the field. Researchers

found that the change in chemical composition due the addition of supplementary

cementitious material affected the results of the Rapid Chloride Test. In order to properly

evaluate a concrete's ability to resist chloride penetration, it should tested directly using

ASTM C 1543–10, "Standard Test Method for Determining the Penetration of Chloride

Ion into Concrete by Ponding." This test method involves subjecting concrete specimens

to a 5% by weight sodium chloride solution for 120 days. The specimens are then cored

and powder samples are collected to determine the chloride content at multiple levels.

According to Broomfield [2007], it is recommended that a minimum of four data points

be used in developing a chloride profile in order to obtain an accurate representation of

the chloride distribution. A chloride content analysis is then performed on the powder

samples in order to determine the chloride profile of the concrete.

Two types of chloride analyses can be performed on the concrete powder; acid-

soluble and water-soluble. Acid-soluble tests will determine the total chloride content,

including those chlorides trapped in the aggregate and paste (C_3A). Water-soluble tests

will only determine those chlorides free to deteriorate the passive layer of the concrete,

thus promoting corrosion. In some cases, the acid-soluble test will overestimate the

corrosion potential of a concrete and in others provide a reasonable evaluation. ACI has

developed limits on chloride content for new construction for varying applications of

concrete. These limitations can be seen in **Table 2.4**.

Table 2.4 Chloride Limits for New Construction in % Chloride by Mass of Cement [ACI, 2001]

	Test method	
	Acid Soluble	Water Soluble
Concrete Application	ASTM C1152	ASTM C1218
Pre-stressed concrete	0.08	0.06
Reinforced concrete in wet conditions	0.10	0.08
Reinforced concrete in dry conditions	0.20	0.15

For in place structures classifications were developed based on chloride contents

and the corrosion risk. These classifications can be seen in **Table 2.5** [Broomfield, 2007].

**Table 2.5 Correlation Between Percent Water Soluble Chloride
by Mass of Concrete and Corrosion Risk [Broomfield, 2007]**

% Chloride by mass of concrete	Corrosion Risk
<0.03	Negligible
0.03-0.06	Low
0.06-0.14	Moderate
>0.14	High

The chloride profile determined from this test method indicates the concentration of the chloride ions in the concrete as a function of depth from the surface. As stated in Section 2.4.2, chlorides will destroy the passive layer on the reinforcement in the concrete, exposing the steel to elements that will initiate corrosion. The chloride profile determined from this test method will indicate the amount of ions at specified depth to determine a concrete's ability to resist diffusion and therefore chloride ingress. In general, this test is a comparative test and does not necessarily indicate the response of a structure in service.

2.4.4 Concrete Resistivity. Electrical resistance also refers to the ability of concrete to resist corrosion. When hydroxyl ions (OH-) are created at the cathode, they must move to the anode to cause the oxidation process to begin. The slower these ions are transported, the slower the corrosion process. This ionic current is similar to electrical current. Therefore, the rate of corrosion of the reinforcement can be estimated by the electrical resistance of the concrete [Whiting and Nagi, 2003].

Three methods have been developed to analyze the electrical resistance of concrete: single-electrode method, two-probe method, and the four probe method. Of the three methods the two-probe method is the most labor intensive and least accurate

[Broomfield, 2007]. The two-probe method works by measuring the potential between two electrodes by passing an alternating current between them. If aggregates are located near the electrodes this can cause a false reading. Aggregates have a higher resistivity than concrete paste and will therefore cause a reading to be much higher than the actual resistivity. In order to counteract this problem, shallow holes can be drilled to place the electrodes into. However this is what makes the two probe method labor intensive.

The single-electrode method is a more advanced method to determine a concrete's resistivity. This method uses a disk placed on the concrete's surface as an electrode and the embedded steel reinforcement as the second electrode. The resistivity of the concrete is measured using **Eq. 2.14**.

$$Resistivity\ (\Omega cm) = 2RD \qquad\qquad (2.14)$$

Where R is the resistance drop between the embedded reinforcement and the surface electrode, and D is the diameter of the surface electrode.

The third method is the four-probe method developed by Frank Wenner. This method was developed in 1916 and was designed for geophysical studies. This method has become widely accepted by the industry and is known as the Wenner method. The probe used in this method has four equally spaced electrodes on a single rod. The two outer electrodes send an alternating current through the concrete while the middle two electrodes measure the change in potential. The resistivity is then calculated using **Eq. 2.15**.

$$\rho = \frac{2\pi s V}{I} \qquad\qquad (2.15)$$

Where ρ is the resistivity (Ωcm), s is the spacing between the electrodes (cm), V is the voltage (V), and I is the applied current (A). When the current is applied through the concrete it travels in a hemispherical pattern. This can be seen in **Figure 2.11**. This allows for a greater area of concrete to be measured and thus avoids the influence of highly resistive aggregates.
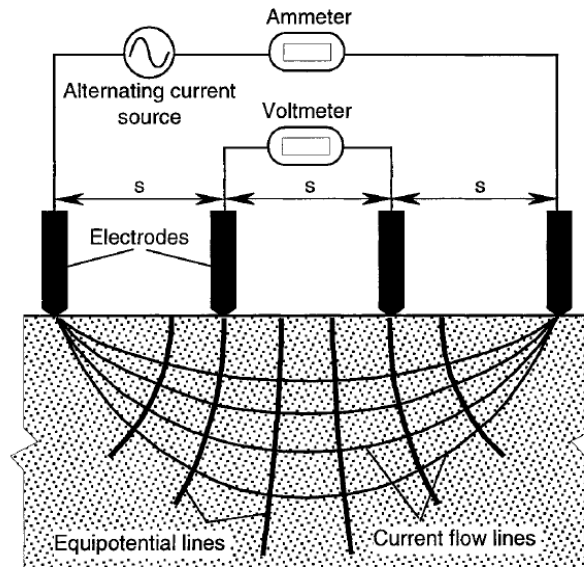
Figure 2.11 - Schematic Representation of the Four-Probe Resistivity Method [Broomfield, 2007]

The four-probe method is based on the theory that the resistivity values measured by the equation above are accurate if the current and potential fields exist in a semi-infinite volume of material [Whiting and Nagi, 2003]. This assumption indicates that larger concrete specimens will yield more accurate results. This condition has been found to be true. Measuring relatively thin concrete members or near edges produces noticeable

errors. It is recommended that the spacing between the electrodes of the probe do not exceed ¼ of the smallest concrete section dimension. Another source of error is the non-homogeneous composition of concrete. While the assumption of the Wenner method is that the material will have a consistent resistivity, this is not the case for concrete. Highly resistive aggregates are surrounded by low-resistivity paste which affects the measurements. According to research, this source of error can be avoided by using a probe where the spacing between electrodes is greater than 1.5 times the aggregate maximum size. This approach will maintain a coefficient of variation less than 5% [Whiting and Nagi, 2003]. A correlation was developed between measured concrete resistivity and the corrosion rate of embedded reinforcement. This classification can be seen in **Table 2.6**. This relationship was developed by Langford and Broomfield in 1987 and is widely used in the field.

Table 2.6 Correlation Between Concrete Resistivity and the Rate of Corrosion for a Depassivated Steel Bar Embedded within the Concrete [Broomfield, 2007]

Concrete Resistivity	Rate of Corrosion
>20 kΩcm	Low
10-20 kΩcm	Low to Moderate
5-10 kΩcm	High
<5 kΩcm	Very High

2.4.5   Scaling Resistance. The presence of salt solutions on concrete can cause additional damage besides corrosion of the reinforcing steel. The surface of the concrete can become pitted and roughened by a mechanism called scaling. In addition to leaving the surface scarred and rough, it can also increase the permeability of the concrete. To

evaluate a concrete's resistance to scaling ASTM has created a test method ASTM C
672–03, "Standard Test Method for Scaling Resistance of Concrete Surfaces Exposed to
Deicing Chemicals." This test method requires specimens to have at least 72 in^2 (46,452
mm^2) of surface area and be at least 3 in. (76 mm) deep. The specimens are broom
finished and a dike is built up around the perimeter of the specimen. This dike must be at
least 0.75 in. (19 mm) tall and approximately 1 in. (25 mm) wide. The specimen is then
moist cured for 14 days and then air cured for 14 days. When the curing duration is over
the surface of the specimen is covered with a solution having a concentration of 5.34 oz
/gal (0.04 g/mL) of anhydrous calcium chloride. The specimen is then subjected to 50
cycles of freezing and thawing. After every 5 cycles, the solution is completely replaced
and the condition of the surface is evaluated. After 50 cycles the surface of the concrete is
evaluated and given a rating based on the scaling resistance. The rating scale can be seen
in **Table 2.7**.

Table 2.7 Rating Scale for Scaling Resistance [MoDOT]

Rating	Condition of Surface
1	No scaling
2	Very slight scaling
3	Slight to moderate scaling
4	Moderate scaling
5	Moderate to severe scaling

2.5. HIGH VOLUME FLY ASH CONCRETE

2.5.1. Mechanical Properties. Through several research investigations, it has

been seen that HVFA concrete performs adequately in the area of mechanical properties.

It has been seen that while conventional concrete reaches relative maximum strength after

28 days, HVFA continues to gain significant strength well after 28 days. This behavior is

due to the increased pozzolanic reaction that occurs with the high amounts of fly ash.

Typical mechanical properties for HVFA concrete using Type I Portland cement are

summarized in **Table 2.8**.

**Table 2.8 Typical Mechanical Properties of HVFA Concrete
Made with ASTM Type I Portland Cement [Malhotra Mehta 2008]**

	Age (days)	Strength (psi)
Compressive Strength	1	1160 ± 290
	7	2900 ± 725
	28	5076 ± 725
Flexural Strength	14	725 ± 72
Splitting-Tensile Strength	28	507 ± 72
Modulus of Elasticity	28	5,076,000 ± 290,000

1 psi = 0.00689 MPa

2.5.2. Durability Performance. It has been found through numerous

investigations that HVFA concrete shows adequate durability performance when

compared to conventional concrete. It should be noted that while HVFA concrete shows

adequate durability performance, the scaling performance has been noted as poor. This

result is due mainly to the tight microstructure and discontinuous pore structure found in

HVFA concrete [Malhotra and Mehta, 2008]. HVFA concrete has performed adequately

in the areas of freeze-thaw resistance and resistance to the penetration of chloride ions.

HVFA concrete has reportedly achieved durability factors as high as 90 when subject to ASTM C 666. A durability factor over 80 is typically considered to be durable concrete. HVFA has also shown a typical charge passing of 1000 coulombs when subjected to the electrical indication of chloride penetration test. Any concrete allowing only 1000 coulombs or less during the ASTM C 1202 test is considered a low permeability concrete and should perform well in the field. According to research done by Marlay [2011], HVFA concrete also showed adequate chloride penetration resistance by ponding as well as a relatively high electrical resistivity when measured using a Wenner probe.

The one area of durability that HVFA concrete may have potential problems is in the area of scaling resistance. Conflicting results have been found in the area of scaling resistance [Malhorta and Mehta, 2008]. Some research has shown that HVFA concrete shows very little scaling resistance when compared to conventional concrete while other research has indicated good scaling resistance [Malhorta and Mehta, 2008]. However field observations have indicated that HVFA concrete shows adequate scaling resistance and laboratory tests are not indicative of the actual response in service [Malhorta and Mehta, 2008].

3. MECHANICAL PROPERTY TESTS

3.1. INTRODUCTION

This section discusses the mechanical property tests used to evaluate the performance of high-volume fly ash (HVFA) concrete. The mechanical property comparison was important because these properties are essential to estimating the behavior of concrete in the field. These also serve as a good indicator of the quality of the concrete. The following mechanical property tests were included in the scope of work of this investigation:

- Compressive Strength of Cylindrical Concrete Specimens (ASTM C 39-11a)

- Static Modulus of Elasticity and Poisson's Ratio of Concrete in Compression (ASTM C 469-10)

- Flexural Strength of Concrete (Using Simple Beam with Third-Point Loading) (ASTM C 78-10)

- Splitting Tensile Strength of Cylindrical Concrete Specimens (ASTM C 496-11)

These are standard tests that are used to investigate the most commonly used mechanical properties of concrete. Running these tests on both the conventional concrete and the specialized concretes will not only assure the quality of the conventional concrete but also will serve as a baseline of comparison for the specialized concretes. These mechanical properties are used in many aspects of design, and the results of these tests will allow investigators to determine how applicable existing formulas are in estimating these properties.

An outline for all the mechanical tests performed on all experimental mixes is shown in **Table 3.1**. The outline identifies the number of test specimens fabricated for

each test for each concrete mix. All of the concrete specimens were moist cured until the designated testing date. The date tested is listed as number of days after batching of the concrete.

Table 3.1 Test Matrix for Mechanical Properties

Material Property	Number of Specimens	Moist Curing Duration, days	Testing Date(s), days
Compressive Strength	9, (3/test age)	1,7,28	1,7,28
Modulus of Elasticity	3	28	28
Flexural Strength	3	28	28
Splitting Tensile Strength	3	28	28

3.2. MIX DESIGN

The design of the HVFA concrete mixes was based on input from MoDOT as well as the results of previous research conducted at Missouri S&T. This research varied the percent of fly-ash replacement in concrete from 50% to 75% [Marlay, Wolfe, 2011]. Two HVFA concrete mixes were investigated. Both mixes used 50 and 75% replacement of cement with a Class C fly ash. One mix contained a relatively high total cementitious content (756 pcy), designated HVFA-70H and the other contained a relatively low total cementitious content (564 pcy), designated HVFA-70L. Due to the carbon content of fly ash, air-entraining admixtures do not always react the same way when used in HVFA concrete. Consequently, this present study examined the durability of HVFA concrete both with and without air entrainment. The low cementitious content HVFA concrete mix had a version both with (HVFA-70LA) and without (HVFA-70L) an air entraining admixture. The final mix designs are shown in **Table 3.5**.

Table 3.5 Mix Design per Cubic Yard for High-Volume Fly Ash Investigation

	Mix Design ID			
	Control	HVFA-70H	HVFA-70L	HVFA-70LA
Cement (Type I) (lb)	564	219	155	155
Fly Ash (lb)	0	511	360	360
w/cm	0.40	0.40	0.40	0.40
Coarse Aggregate, SSD (lb)	1860	1754	1860	1860
Fine Aggregate, SSD (lb)	1240	1080	1240	1240
HRWR (fl. oz)	16.9	21.9	15.45	15.45
Air Entrainment (fl. oz)	3.5	0	0	3.2
CaOH (lb)	0	51	39	39
Gypsum (lb)	0	21	16	16

1 lb = 0.45 kg

1 fl. oz. = 29.57 mL

The HVFA concrete mixes used a Type I cement to match typical cast-in-place concrete construction. Two types of admixtures were also used in the mix design. HRWR was added to the mix in order to achieve the necessary workability while maintaining the design w/cm. In concrete, the cement particles typical carry either positive or negative charges. The attraction between particles causes them to agglomerate. Water is trapped inside these particles and is not able to add to the workability of the concrete. HRWRs place a like charge on the cement particles causing them to repel each other. This frees the water in the paste to add to the workability of the concrete. This apparent increase in water content allows the workability to increase while maintaining relatively low w/cm. It should be noted that the batch water was adjusted to account for any moisture that was present in the aggregate. The total moisture content was found by taking a representative sample of the aggregate and weighing it. The sample was then placed into an oven and dried overnight. The dried sample was then re-weighed and the difference was taken as the total moisture content.

To provide the necessary durability of the concrete, an air-entraining admixture was also used. Concrete that is exposed to freezing and thawing temperatures is at risk of serious deterioration. One of the most effective ways to protect against that is using an air-entraining admixture. This admixture creates an air void system in the concrete paste that is composed of millions of tiny bubbles. This air void system allows for the pressure that builds up due to the freezing of water to be released into these tiny bubbles. However air entrainment was not used in every mix design. Two of the HVFA concrete mixes did not include any entrained air. This step was done because of carbon content issues when using high amounts of fly ash. With such high carbon content, it is sometimes difficult to reach the desired entrained air content. The air entrainment was purposefully left out to investigate the durability performance of the HVFA with just the entrapped air. The air entrainment was added to a third experimental mix. This was done in order to investigate if reaching the desired air entrainment was possible. The air entrainment was placed into the low cementitious content variation in order to maximize its effect due to the minimal amount of carbon found in that mix. These admixtures were added at trial dosages until the desired behavior and air contents were achieved. The proper dosages were established using 3 ft^3 mixes.

The high volume fly ash mix designs also include two supplementary materials, calcium hydroxide and gypsum. The calcium hydroxide was added to the mix in order to offset the retardation of setting time that occurs in concrete containing HVFA. This natural occurrence results in a delayed finishing time and very low early strengths. The addition of calcium hydroxide helps to maintain the hydration at a faster rate. The gypsum was added to the mix to balance out the lack of sulfates present in a high volume

fly ash mix. Typical fly ash contains a very low amount of sulfates. This leads to a delay in the hydration process as well as a decrease in the overall magnitude of the hydration peak. This leads to a decrease in early strength. With the addition of gypsum the sulfate imbalance is corrected leading to a more desirable hydration curve when compared to conventional concrete. The amount of calcium hydroxide and gypsum was determined by previous research done at Missouri S&T, [Ortega, 2012].

Fresh concrete properties were measured during each batching operation, either within the Materials Lab for mixes prepared on site or within the Structural Engineering High-Bay Research Laboratory (SERL) for mixes delivered by a local ready-mix supplier. The location of each mix is stated in **Table 3.6**. These tests were performed to ensure that certain properties were achieved such as workability and air content. The following fresh property tests were performed on all the mixes:

- Slump of Hydraulic-Cement Concrete (ASTM C 143)

- Unit of Weight of Concrete (ASTM C 138)

- Air Content of Freshly Mixed Concrete by the Pressure Method (ASTM C 173)

Typical fresh properties of the HVFA concrete mixes and locations of the pours are shown in **Table 3.6**.

Table 3.6 Location of Pours and Typical Fresh Concrete Properties for

High-Volume Fly Ash Concrete

	Mix Design ID			
	Control	HVFA-70H	HVFA-70L	HVFA-70LA
Slump (in)	5	4.5	4	4.5
Air Content (%)	6.5	NA	NA	5
Unit Weight (lb/ft^3)	143.6	147.5	149.6	144.8
Pour Location	SERL	SERL	SERL	Materials Lab

1 in. = 2.54 cm.

1 lb/ft^3 = 16.02 kg/m^3

3.3. COMPRESSIVE STRENGTH TEST

3.3.1. Introduction. The compressive strength test was used in several different aspects of the research project. It was used as a quality control and quality assurance, (QC/QA) tool. The compressive strength results from the experimental mixes were compared to target values to assure the strengths were within the desired limits. These values can also be compared to other strengths of similar mixes to evaluate behavior. The compressive strength was also used to assure the quality of the concrete by observing any drastic differences between the target and actual strengths. The compressive strength of concrete is also an important factor in many tests that were used in this investigation, such as shear, bond, and creep.

3.3.2. Fabrication. A minimum of 9 compressive strength cylinders were cast for each mix design. All specimens were prepared in accordance with ASTM C 192-07, "Standard Practice for Making and Curing Concrete Test Specimens in the Laboratory" using 4 in. (102 mm) diameter by 8 in. (203 mm) long plastic cylinder molds. The molds were lubricated using form release oil prior to the placement of concrete. The concrete was rodded in order to reduce air voids and to assure the concrete would be sufficiently consolidated. The sides of the mold were also struck smartly for each lift with a rubber

mallet in order to consolidate the concrete. It should be noted that the compressive

strength specimens made with the self-consolidating mixes were not rodded or struck due

to the plastic highly flowable behavior of the concrete. Instead, these mixes were placed

in one continuous lift. Immediately after casting, plastic lids were placed over the molds

and the specimens were covered with plastic. After allowing for 16 to 24 hours of setting

time, the concrete specimens were removed from the molds using compressed air and

placed inside a temperature-controlled moist curing room until the designated testing

date.

    3.3.3. Testing & Procedure. The testing of the compressive strength of the

experimental mixes was performed in accordance with ASTM C 39-11, "Standard Test

Method for Compressive Strength of Cylindrical Concrete Specimens." A minimum of 3

compressive strength cylinders were used at each test age. Testing occurred at 1, 7, and

28 days after batching. These are typical testing dates for compressive strength tests.

Prior to testing, the specimens had to be capped in order to provide a flat surface for

testing. The two methods used to cap specimens in this project were sulfur capping and

neoprene pad capping.

    Neoprene pads were used to cap any specimens constructed with a high strength

concrete mix. Any specimens that were constructed with normal strength concrete were

sulfur capped. Prior to using the neoprene pads, the concrete specimens were ground

smooth using a concrete grinding machine. Once the ends were removed off all rough

spots, the cylinders were placed into steel retaining rings with a neoprene pad between

the specimen and the steel. With the steel retaining rings and neoprene pads on both the

top and bottom of the concrete specimen, it was loaded into the compressive strength

testing machine. Specimens that were sulfur capped were placed into liquid sulfur capping compound to create a smooth liquid cap that hardened within seconds and could be tested in a few hours. At least two hours before the compressive strength test was to occur, the concrete specimens were removed from the moist curing chamber and the moisture was removed from the ends. When the specimens were ready to be capped, an ample amount of sulfur capping compounded was poured into the capping mold. The specimen was quickly held against the mold to ensure it was level and it was gently but quickly lowered in the capping compound. The capping compound hardened very quickly, so capping the cylinders needed to be done in a swift manner. Once the capping compound hardened around the concrete specimen, it was removed and the process was repeated on the other end. Once the specimen was capped on both ends, it was returned to the moist curing chamber. In order for the capping compound to reach its maximum strength, the capped specimens had to sit in the moist curing chamber for a minimum of two hours. After this time, the concrete specimens could be tested for compressive strength.

Before the compressive strength tests were run, the dimensions of the specimens were measured. The diameter was measured three times and the average was used to compute the compressive strength. From the measured diameter, the cross sectional area was calculated. The height was also measured. The specimens were then loosely wrapped in a canvas wrap and placed in the testing apparatus, as shown in **Figure 3.1**. A Forney 600 kip (2670 kN) compression testing machine was used. Steel plates were placed on the load deck in order to minimize the distance traveled. The specimen was then placed in the apparatus, centered, and brought to just below the upper plate.

Figure 3.1 - Compressive Strength Testing Setup

When the setup was complete, the specimen was loaded at a load rate specified for 4 in. (102 mm) diameter specimens. The target load rate was 525 lb/sec. (238 kg/sec.). The specimen was loaded at the specified rate until it could no longer sustain a load and the load rate dropped to a negative value. The machine was turned off and the peak load was recorded. Completed test specimens are show in **Figure 3.2**.

Figure 3.2 - High Strength Compressive Strength Specimens Post-Test

The load was then divided by the cross sectional area to get the measured compressive strength in pounds per square inch. A minimum of three specimens were tested at a given test age and the results were averaged to get the final measured compressive strength.

3.4. MODULUS OF ELASTICITY TEST

3.4.1. Introduction. The modulus of elasticity is an important property to investigate as it is used to determine the anticipated amount of deflection in design. This is important in designing for serviceability of a structure. The modulus of elasticity of concrete is determined by testing specimens in the liner elastic range. Specimens are loaded to a specified stress while the strain is measured. The slope of the stress–strain curve is taken as the modulus of elasticity.

3.4.2. Fabrication. Specimens used to measure the modulus of elasticity were fabricated according to ASTM C 192–07.These are the same type of specimens that were used for compressive strength testing. A minimum of three specimens were created for

each mix design. For the modulus of elasticity test, the specimens could be fabricated

either using 4 in. (102 mm) diameter by 8 in. (203 mm) long cylinders or 6 in.(152 mm)

diameter by 12 in.(305 mm) long cylinders. The two types of cylinder molds can be seen

in **Figure 3.3**. It should be noted that for the SCC mixes, 4 in. (102 mm) x 8 in. (203 mm)

specimens were used, while for the HVFA concrete mixes, 6 in. (152 mm) x 12 in. (305

mm) specimens were used.
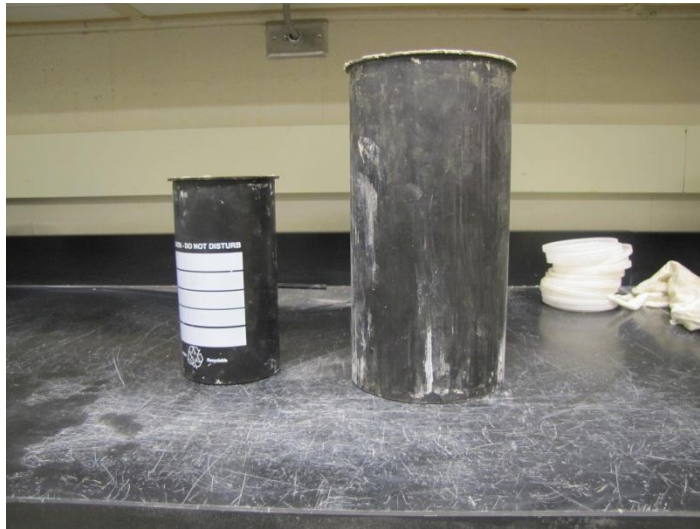
Figure 3.3 – 4 in. (102 mm) x 8 in. (203 mm) Cylinder Mold
Compared to 6 in. (152 mm) x 12 in. (305 mm) Cylinder Mold

Specimens were de-molded after 24 hours and placed in the moist curing chamber

for 28 days before testing. Before the test was conducted, all test specimens were sulfur

capped in the same manner as the compressive strength cylinders.

3.4.3. Testing & Procedure. After the specimens were allowed to cure for 28

days, the specimens were tested in accordance with ASTM C 469–10, "Standard Test

Method for Static Modulus of Elasticity and Poisson's Ratio of Concrete in

Compression." The dimensions of the specimens were measured, and before loading, the

specimen was fitted with a compressometer in order to measure the deflection of the cylinder during loading. A typical compressometer can be seen in **Figure 3.4**.

Figure 3.4 - Typical Compressometer

The specimen was then placed into a compression loading apparatus and loaded at a constant rate. The load was recorded when the deflection of the specimen reached 0.0004 in. (0.01 mm). The specimen was continually loaded until the load reached 40% of the ultimate strength of the concrete. The value of the ultimate strength was determined from compressive strength tests of companion specimens. When the load on the specimen reached 40% of the measured ultimate load, the deflection was recorded. This test was then performed three additional times on the same specimen. The data recorded during the first test run on each specimen was disregarded and only the following three tests were used for averaging. Using these deflections, the strains were calculated and the corresponding stresses were used to calculate the modulus of elasticity using Eq. 3.1.

$$E_c = \frac{(S_2 - S_1)}{(\varepsilon_2 - 0.00005)} \tag{3.1}$$

Where S_2 is the stress measured at 40% of the ultimate load and S_1 is the stress measured when the deflection of the specimen reached 0.0004 in. (0.01 mm) and ε_2 is the strain produced by S_2. The results from the individual tests were then averaged and the averages from the three tests were then averaged to obtain the measured modulus of elasticity.

3.5. MODULUS OF RUPTURE TEST

3.5.1. Introduction. The modulus of rupture test is used to determine the flexural strength or tensile strength of the concrete. This is an important mechanical property to investigate. The modulus of rupture is important in design for estimating the cracking moment of the concrete when subjected to flexure.

3.5.2. Fabrication. The specimens used for the modulus of rupture test were fabricated in accordance with ASTM C 78–10, "Standard Test Method for Flexural Strength of Concrete (Using Simple Beam with Third-Point Loading)." Three specimens were fabricated for every concrete mix. The specimens measured 6 in. (152 mm) x 6 in. (152 mm) in cross section with a length of 24 in. (610 mm). The specimens were filled with two lifts, each lift being rodded 72 times. It should be noted that the SCC was not rodded when specimens were cast. The specimens were cast in one single lift. The specimens were de-molded after 24 hours and stored in a moist curing chamber for 28 days. After 28 days they were prepared for testing.

3.5.3. Testing & Procedure. After 28 days, the specimens were removed from the moist curing chamber. The supports on the testing apparatus were 18 in. (457 mm) apart. In order to align the specimen on the supports, it had to be divided into thirds. The first 3 in. (76 mm) of either end of the specimen were not included in the measuring. This caused the 18 in. (457 mm) span to be divided into 3, 6 in. spans. The load points would be placed on the 6 in. mark and the 12 in. mark, creating the third-point loading. The prepared specimen can be seen in **Figure 3.5**.
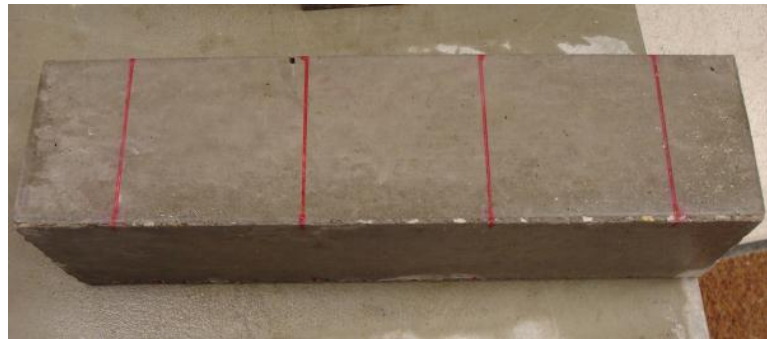
Figure 3.5 - Prepared Modulus of Rupture Specimen

The specimen was rotated and loaded into the testing machine on a formed side to provide the smoothest surface and thus prevent localized forces on the beam. The load was applied at the aforementioned points. A leather pad was placed in between the concrete specimen and the load points in order to help distribute the load. The test setup can be seen in **Figure 3.6**. It is important to note that during the set-up, the specimen was kept moist in order to prevent any internal stresses from developing.

Figure 3.6 - Modulus of Rupture Testing Setup

The load head was then lowered until it made contact with the leather pads. The beam was then loaded at a constant rate until failure. If the beam failed within the middle third, the test was accepted. It should be noted that all beams tested in this investigation failed in the middle third of the beam. A post failure specimen can be seen in **Figure 3.7**. The failure load was recorded and subsequently used to calculate the modulus of rupture using **Eq. 2**.

Figure 3.7 - Modulus of Rupture Specimen Post-Test

The beam was removed from the testing apparatus and its dimensions were measured. The width and depth of the beam were measured three times and averaged. The modulus of rupture was then calculated using **Eq. 3.2**.

$$R = \frac{PL}{bd^2} \tag{3.2}$$

Where P is the peak load, L is the distance between supports, b is the average width of the beam after testing, and d is the average depth of the beam after testing.

3.6. SPLITTING TENSILE TEST

3.6.1. Introduction. ASTM has not yet specified a standardized test to find the direct tensile strength of concrete. There is a standardized test for an indirect tension test known as the splitting tensile test. This test involves loading a cylindrical specimen along its longitudinal axis until failure. This test is thought to measure a greater tensile strength than a direct tensile strength. However it is usually lower than a measured strength from a modulus of rupture test. The splitting tensile test is a good indication of a concrete's tensile strength but should be performed alongside other tests such as the modulus of rupture test.

3.6.2. Fabrication. The specimens used for the splitting tensile test were fabricated in accordance with ASTM C 496–11, "Standard Test Method for Splitting Tensile Strength of Cylindrical Concrete Specimens." A minimum of three specimens were made for each concrete mix. The specimens were made using a 4 in. (102 mm) diameter by 8 in. (203 mm) long cylindrical molds. The specimens used for the splitting

tensile test were the same types of specimens used for the compressive strength test. The

specimens were fabricated according to ASTM C 192. After 24 hours, the specimens

were de-molded and placed in a moist curing chamber for 28 days, at which time they

were then tested.

3.6.3. Testing & Procedure. After the specimens were allowed to cure for 28

days, the specimens were removed from the curing chamber for testing. The diameter and

height of the specimens were recorded. The diameter of the specimen was marked the top

of the specimen. Two lines were then drawn down the long side of the specimen from the

previously drawn line. This was done to assist in lining up the specimen in the testing

apparatus. The specimen was then loaded into the testing apparatus on the line drawn

down its vertical axis. The specimen was placed on a piece of plywood. Another plywood

strip was placed on the top of the specimen between it and the load platen. These strips

were used so the load would be distributed along the axis of the specimen. The test setup

can be seen in **Figure 3.9**.

Figure 3.9 - Typical Splitting Tensile Test Setup

4. DURABILITY TESTS

4.1. INTRODUCTION

This section discusses the durability tests used to evaluate the performance high-volume fly ash (HVFA) concrete. The durability performance of these specialized concretes is a crucial aspect in investigating the possibility of implementing these new materials into transportation-related infrastructure, such as bridges, roadways, culverts, and retaining walls. The following durability tests were included in the scope of work for this investigation:

- Resistance of Concrete to Rapid Freezing and Thawing (ASTM C 666-08)

- Electrical Indication of Concrete's Ability to Resist Chloride Ion Penetration (ASTM C 1202-10)

- Determining the Penetration of Chloride Ion into Concrete by Ponding (ASTM C 1543-10)

- Concrete Resistivity (Non-ASTM)

- Scaling Resistance of Concrete Surfaces Exposed to Deicing Chemicals (ASTM C 672-03)

The outline for the durability tests is shown in **Table 4.1**. The outline identifies the number of test specimens fabricated for each test for each concrete mix. The table also includes the required curing conditions and durations, as well as the specimen age at the start of testing and the duration of the test, if applicable.

Table 4.1 Test Matrix for Durability Performance

Durability Property	Number of Specimens	Moist Curing Duration, days	Dry Curing Duration, days	Testing Date, days	Testing Duration, days
Freezing and Thawing	3	35	0	35	N/A[1]
Electrical Chloride Penetration	2 (4) disk	28	0	28	N/A[2]
Ponding	3	14	14	28	120
Concrete Resistivity	3	14	21	35	168
Scaling	3	14	14	28	50

Notes: 1. Test duration based on cycles
2. Duration of test is 6 hours

4.2. RAPID FREEZING & THAWING TEST

4.2.1. Introduction. The rapid freeze-thaw test was one of the most critical durability tests performed in this investigation. The climate in Missouri is susceptible to multiple freeze-thaw cycles, which is a more severe environment for concrete durability than continuous freezing. The test involves subjecting specimens to multiple freeze-thaw cycles in order to measure the resistance of the material to deterioration caused by the expansion of the free water freezing inside the specimens. This resistance was measured using three parameters: the length change of the specimens, change in the fundamental transverse frequency of the specimens, and mass change of the specimens. A decrease in the values for these parameters indicates freeze-thaw deterioration.

4.2.2. Fabrication. The specimens for the rapid freeze-thaw test were fabricated according to ASTM C 666–03, "Standard Test Method for Resistance of Concrete to Rapid Freezing and Thawing." The molds used in the fabrication of these

specimens were loaned to the project by the Construction Materials Department of the Missouri Department of Transportation (MoDOT) and can be seen in **Figure 4.1**. These stainless steel molds measured 3.5 in. (8.9 cm) in width, 4.5 in. (11.43 cm) in height, and 16 in. (40.64 cm) in length and conformed to ASTM C 666 requirements for specimen dimensions.

Figure 4.1 - Freezing and Thawing Specimen Molds

The ends of each mold contained a threaded hole to install a specialized bolt. This bolt contained a rounded end, and when the concrete specimens were de-molded, the end of this bolt protruded from both either end of the prism as shown in **Figure 4.2**. The embedded bolt provides a mechanism to measure the length change of the concrete prism as it was subjected to freezing and thawing cycles.
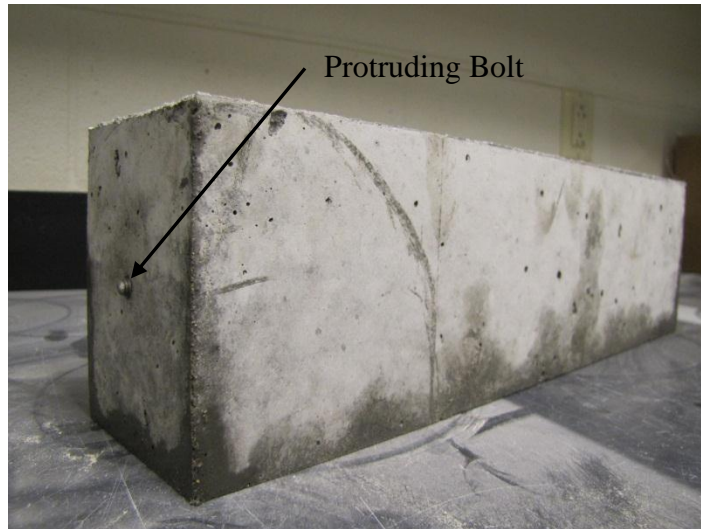
Figure 4.2 - Freezing and Thawing Specimen with Protruding Bolt

Once the specimens were formed and de-molded, they were placed in a

temperature controlled moist curing room for 35 days prior to testing. It should be noted

that this moist curing duration is a standard for MoDOT and a modification from ASTM

C 666. The ASTM specifies that the prisms should be moist cured for 14 days unless

otherwise specified. It should also be noted that the typical MoDOT procedure requires

that specimens that will be subjected to the rapid freeze-thaw test be submersed in a lime

water solution while they cure for the 35 days. However, due to space restraints in the

University laboratory, the specimens were only moist cured. This change was deemed

acceptable provided all specimens received the same treatment. Between 14 and 21 days,

the prisms were transported from the University's moist curing chamber to the

Construction Materials testing lab of MoDOT in Jefferson City, Missouri. To be

transported, the specimens were wrapped in burlap that was saturated in a 5% by weight

lime water solution. The specimens were then placed into a cooler and immediately

driven to the MoDOT lab and placed into the moist curing chamber to complete the 35-

day moist curing regime. All rapid freezing and thawing test were performed by MoDOT employees of the Construction Materials Department.

4.2.3. Testing & Procedure. All specimens were tested in accordance with ASTM C 666, Procedure A. When the specimens reached the appropriate age, they were brought to the target thaw temperature. The fundamental transverse frequency, mass, length, and cross section of the specimen was measured. The freeze-thaw specimens were then subjected to the appropriate freezing and thawing cycles. Each specimen was subject to 300 cycles of freezing and thawing while submerged in water. Every 36 cycles the specimens would be removed at the thawed state and properties of the specimen would be measured. The properties measured were fundamental transverse frequency, length change, and mass change. The specimens were then placed back into the testing apparatus and the cycles continued. The test could be ceased if the specimen deteriorated so extensively that the test could not continue. The relative dynamic modulus of elasticity was then calculated using **Eq. 4.1**.

$$P_c = \frac{n_1^2}{n^2} x 100 \qquad\qquad (4.1)$$

Where P_c is the relative dynamic modulus of elasticity at, c, cycles of freezing and thawing. N_1 is the fundamental transverse frequency after, c, cycles of freezing and thawing and n is the fundamental transverse frequency after 0 cycles of freezing and thawing. Using the relative dynamic modulus of elasticity, the durability factor of the freezing and thawing specimen was also calculated using **Eq. 4.2**.

$$DF = \frac{PN}{M} \tag{4.2}$$

Where DF is the durability factor, P is the relative dynamic modulus of elasticity at N cycles, N is the number of cycles at which the specified value of P is reached or the specified number of cycles is reached, whichever is less, and M is the number of cycles which the test is to be terminated. The higher the measured durability factor, the greater resistance the concrete will have to freezing and thawing attack.

4.3. ELECTRICAL INDICATION TO RESIST CHLORIDE ION PENETRATION TEST

4.3.1. Introduction. Chloride penetration of concrete is one of the leading durability issues facing many concrete specimens. Concrete members that are exposed to chlorides such as concrete piers in the ocean or concrete bridge decks exposed to de-icing salts all face chloride penetration. If sufficient chloride is allowed to penetrate into a concrete member, it can cause the embedded steel reinforcement to corrode and the expanding corrosion product will results in internal stresses, which in turn will cause cracking of the concrete. Over time this will cause concrete spalling and eventual failure. The electrical indication of concrete's ability to resist chloride penetration is a rapid method to determine the permeability of the concrete and its ability to withstand chloride penetration. This test is often used in correlation with the ponding test as it was in this investigation. Due to the ponding test's longer duration, this electrical test is a rapid method to estimate the durability of concrete. This test is also known as the Rapid Chloride Test (RCT).

4.3.2. Fabrication. The test specimens consisted of cylinders fabricated and prepared according to ASTM C 192–07, "Standard Practice for Making and Curing Concrete Test Specimens in the Laboratory." Two 4 in. (10.16 cm) diameter x 8in. (20.32 cm) long cylinders were used for this test for every concrete mix. These cylinders were prepared alongside the compressive strength specimens. These specimens were de-molded after 24 hours and placed in the moist curing chamber for 28 days. In between 14 and 21 days after batching, these cylinders were transported to the Construction Materials testing lab in Jefferson City to finish the curing cycle and begin testing. These specimens were wrapped in burlap that was saturated in a 5% by weight lime water solution. The specimens were then placed into a cooler and immediately driven to the MoDOT lab and placed into the moist curing chamber to complete the 28-day moist curing regime. All electrical chloride tests were performed by MoDOT employees of the Construction Materials Department.

4.3.3. Testing & Procedure. The testing of specimens for the electrical indication of a concrete's ability to resist chloride ion penetration is outlined in ASTM C 1202-10, "Standard Test Method for Electrical Indication of Concrete's Ability to Resist Chloride Ion Penetration." The test specimens consist of 4 in. (102 mm) diameter by 2 in. (51 mm) thick concrete disks. These disks were cut from specimens cast according to ASTM C 192. Two disks were cut from each concrete cylinder, with two concrete cylinders cast from each mix, which resulted in a total of 4 concrete disks for each concrete mix. One disk was cut from the top of the cylinder and the other from the middle. These disks were labeled with the mix design name and noted as either middle or

top. The specimens were allowed to surface dry for at least 1 hour before the sides of the

disks were coated with a setting coating as seen in **Figure 4.3**.

Figure 4.3 - Setting Coating Being Applied to Concrete Specimens

After the coating dried, the specimens were placed into a vacuum desiccator and

vacuumed for 3 hours. The pressure of the vacuum was at least 0.96 psi (6650 Pa). At the

end of the 3 hour desiccation period, de-aerated water was poured into the water stockpot

of the vacuum until the specimen was covered. The stockpot was closed and the vacuum

was maintained for another hour. The vacuum was then turned off and air was allowed to

enter the desiccator. The specimen was then allowed to soak in the de-aerated water for

18 ± 2 hours. The specimen is then blotted dry and placed into the voltage cell. A sealant

is then applied to the specimen-cell boundary. The exposed face of the specimen is then

covered while the sealant is allowed to dry. Once the sealant is dry, the process is

repeated to the other face of the specimen. The final specimen can be seen in **Figure 4.4**.
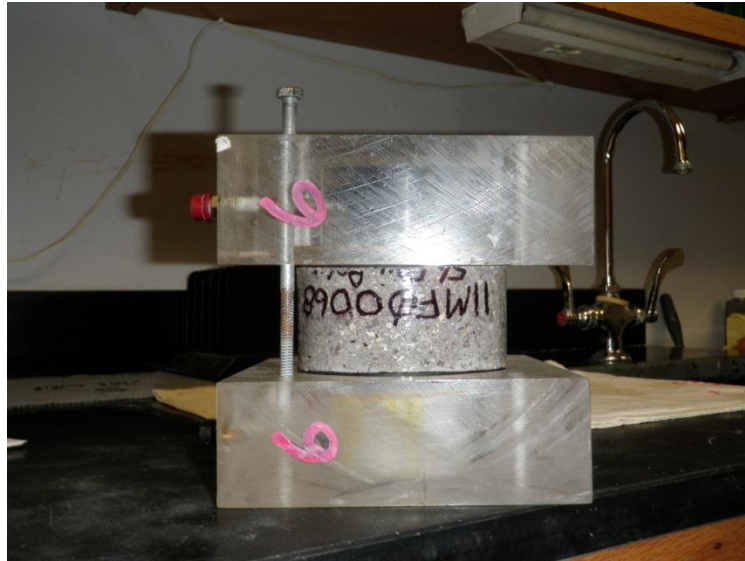
Figure 4.4 - Typical Completed Specimen

The side of the cell that is connected to the negative terminal is then filled with 3.0% NaCI solution while the side connected to the positive terminal is filled with 0.3 N NaOH solution. The test setup can be seen in **Figure 4.5**. The power is then turned on and the voltage is set to 60 V. The initial current is recorded and then recorded at 30 minute intervals.

The test is conducted for 6 hours unless the temperature in the solution exceeds 190°F. This temperature is only exceeded when the concrete is extremely permeable. The data that is recorded is then used to calculate the total charge passed through the specimen in coulombs. This is discussed further during evaluation of the different concretes.

Figure 4.5 – Typical RCT Setup

4.4. PONDING TEST

    4.4.1. Introduction. A serious problem facing Missouri concrete bridge decks is spalling and deterioration caused by chloride penetration and subsequent corrosion of the underlying steel. During winter months, de-icing salts are used to remove snow and ice from bridge and roadway surfaces. The chlorides contained in these de-icing salts diffuse into the concrete, eventually breaking down the passive layer of the reinforcing steel and causing corrosion. The corrosion product expands to approximately six times the original volume, resulting in internal stresses and eventually cracking. Over time, this process will lead to spalling and deterioration of the concrete. The ponding test subjects concrete specimens to a similar environment to investigate the ability of the concrete to resist chloride penetration. This test is a valuable indicator of the resistance of the concrete to chloride ingress and thus the durability of the material. Although this test

requires a longer period of time compared to other methods to predict the resistance of concrete to chloride penetration, it is the most realistic test method.

4.4.2. Fabrication. The concrete specimens for the ponding test were fabricated according to ASTM C 1543-10, "Standard Test Method for Determining the Penetration of Chloride Ion into Concrete by Ponding." Three specimens were made for each concrete mix. The test requires that the specimens have a surface area of at least 45.6 in^2 (30,000 mm^2). The specimens must also be at least 3.54 ± 0.6 in. (90 ± 15 mm). tall. The specimens created for the ponding test in this investigation measured 18 in. (457 mm) wide x 18 in. (457 mm) long x 4 in. (102 mm) tall. Also, the test procedure required a dike along the top of the specimen with a height of at least 0.79 in. (20 mm) high. To accomplish this, a 0.75 in.-thick (19 mm) foam panel measuring 16 in. (406 mm) x 16 in. (406 mm) in plan was placed on a sheet of plywood that would serve as the base of the mold. Walls constructed from 2 in. (51 mm) x 4 in. (102 mm) pieces of wood were then connected to the panel to arrive at the overall dimension of 18 in. (457 mm) x 18 in. (457 mm) in plan. When the concrete was placed in the mold, the foam created a void in what would become the top of the specimen. The foam formed the reservoir for the chloride solution. The concrete was placed into the formwork and consolidated as necessary. After 24 hours, the concrete specimens were de-molded and placed in a moist curing chamber. After 14 days of moist curing, the specimens were transported to a temperature and humidity controlled environment where they would dry cure for another 14 days. After 28 days of curing, the specimens would then begin the ponding test.

4.4.3. Testing & Procedure. The test procedure involved placing a 5% by weight chloride solution into the ponding specimen reservoir. The solution had to be at a depth of 0.6 ± 0.2 in. (15 ± 5 mm). A typical ponded specimen can be seen in **Figure 4.6**. When the required amount of solution was poured into the reservoir, the concrete specimens were covered with plastic sheeting and the sheets were secured with elastic bands to prevent evaporation of the solution.

Figure 4.6 - Typical Ponding Specimen

Every two weeks the specimens were checked to ensure that the proper depth of the solution was maintained. If the reservoir was low, additional solution was added. After 60 days of ponding, the reservoir was vacuumed dry and fresh solution was added. The sheeting was replaced and the specimens were monitored every two weeks. After another 60 days, the chloride solution was vacuumed off and the specimen allowed to air dry. A few days later, a core was taken from the center of the specimen. A typical core and core location can be seen in **Figure 4.7**.

Figure 4.7 - Concrete Core and Resulting Void in the Concrete Specimen

The core was removed using an industry standard core driller with a medium flow of water to ensure proper blade lubrication as well as creating the proper slurry. Powder samples were then taken from the cores at specified depth intervals. The intervals were 0.25 in. (6 mm), 0.75 in. (19 mm), 1.5 in. (38 mm), and 2 in. (51 mm) from the surface of the core. A sample was also taken from the surface of the core. These depths are shown in **Figure 4.8**.
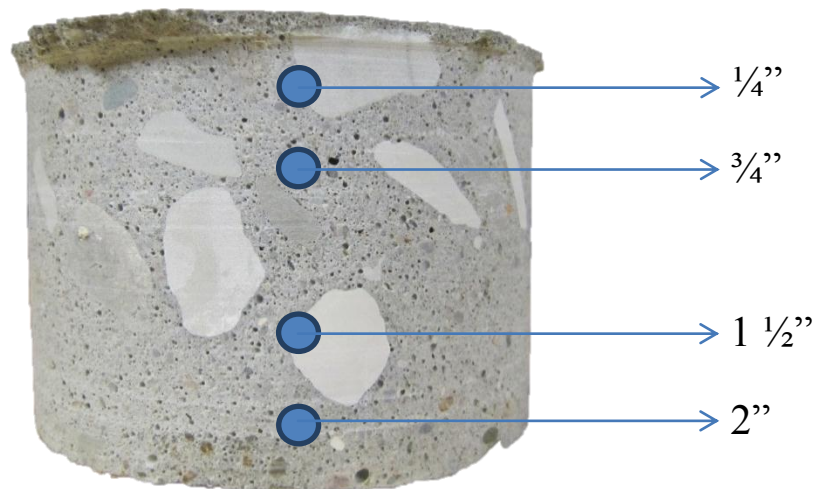
Figure 4.8 - Depths at which Powder Samples Were Collected
1 in. = 2.54 cm.

The samples had to measure at least 0.053 oz. (1.5 g) to be considered sufficient. Samples were collected using a 3/8 in. (9.5 mm) drilled bit at all locations except at the 0.25 in. (6 mm) location. At this location a 3/16 in. (5 mm) drill bit was used. A paper plate was used to collect the dust and a steel plate was placed in between the core and the vice to confine the concrete and prevent spalling. After each hole was drilled, it was sealed using masking tape to prevent cross contamination with the other samples. Samples were also taken from the surface of the core. This was done by drilling the surface of the core to a depth of no deeper than 0.125 in. (3 mm). Samples were collected from several locations on the surface of the core to obtain the necessary sample size. A chloride analysis was then performed on the powder samples to obtain the chloride content in the concrete at the respective sample depths.

The chloride analysis of water soluble chlorides was performed using the Rapid Chloride Testing (RCT) equipment made by Germann Instruments, Inc. The 0.053 oz. (1.5 g) sample was poured into a vial containing 0.304 fl-oz. (9 mL) of the extraction liquid. The vial was shaken vigorously for 5 minutes. The extraction liquid and powder slurry were then filtered into a buffer solution. While the slurry was filtering the electrode was prepared and calibrated. The preparing of the electrode began with filling it with a wetting agent. After any air bubbles were removed the wetting agent was allowed to be released in order to fully wet the circumference of the electrode tip. After the electrode had been refilled with the wetting agent, it had been prepared. In order to calibrate the electrode and build a scale to determine the chloride content of the specimens, the electrode was inserted into four calibration solutions of known chloride content. The four calibration liquids contained 0.005%, 0.02%, 0.05%, and 0.5% chloride content. The

electrode was inserted into each solution and the voltage was read. The four calibration liquids produced a voltage of approximately 100 mV, 72 mV, 49 mV, and -5 mV respectively. This data was used then plotted on a log chart in order to build a scale for the rest of the testing. An example of this log chart can be seen in Appendix B. After the preparing and the calibrating the electrode was ready to use. When the filtering process was complete the electrode was inserted into the vial and was held steady until the voltage reading stabilized. Using the recorded voltage and the scale determine by the log, the chloride content was determined. After every use the electrode was sprayed with distilled water, blotted dry and stored in an empty vial. This data collected from each depth was used to develop a chloride profile and determine chloride penetration into the concrete.

4.5. CONCRETE RESISTIVITY TEST

4.5.1. Introduction. A concrete's electrical resistance may be measured in an attempt to quantify the rate at which a bare, depassivated steel bar, embedded within the concrete, corrodes. The corrosion process is dependent upon the ability of charged ions, such as hydroxyl ions (OH^-), to flow from the cathode to the anode. The faster the ions can flow from the cathode to the anode, the faster the corrosion process may proceed, provided the cathode is supplied with a sufficient amount of oxygen and water. The transport of electricity through concrete closely resembles that of ionic current; therefore, it is possible to classify the rate of corrosion of a bar embedded within concrete by quantifying the electrical resistance of the surrounding concrete.

The four probe resistivity meter, also known as the Wenner probe and shown in **Figure 4.9**, is generally regarded as the most accurate method of measuring concrete resistivity. The probe contains four equally spaced electrodes that are positioned along a straight line. The two outer electrodes send an alternating current through the concrete while the inner electrodes measure the drop in potential. The resistivity is then calculated using **Eq. 3.3**.

$$\rho \;=\; \frac{2\pi s V}{I} \tag{3.3}$$

Where ρ is the resistivity (Ωcm) of the concrete, s is the spacing of the electrodes (cm), V is the recorded voltage (V), and I is the applied current (A).

Figure 4.9 - Canin$^+$ Wenner Probe

4.5.2. Fabrication. The concrete specimens for the resistivity test were fabricated according to ASTM C 1543–10 "Standard Test Method for Determining the Penetration of Chloride Ion into Concrete by Ponding". The molds used to create these specimens were the same molds to create the specimens for the ponding test. The specimens were prepared the same way, using the same procedure. They were cured in the moist curing chamber for 14 days then transported to a humidity and temperature controlled environment to dry cure for an additional 21 days before testing. Testing began when the specimens reached an age of 35 days.

4.5.3. Testing & Procedure. One day prior to the beginning of the test, the specimens were ponded with just enough distilled water to coat the bottom of the reservoir. The specimens sat with water in them for 24 hours. The following day the water was vacuumed off using a shop vacuum cleaner. The Wernner probe was then used to take the initial resistivity measurements. The measurements were taken in a systematic manner, from left to right, then top to bottom, using the Plexiglas template shown in **Figure 4.10**. Three measurements were taken from left to right, once on the far left, once in the middle and once on the far right. Three measurements were then taken from top to bottom, once on the top, once in the middle, and once on the bottom.

These measurements were taken in the same order, once every week. The measurements were taken weekly until the resistivity measurements became constant. However, due to time constraints, the duration of the test was limited to 24 weeks.

Figure 4.10 - Wenner Probe Grid

4.6. SCALING TEST

4.6.1. Introduction. When concrete is exposed to freezing and thawing temperatures and is subjected to de-icing salts, it can deteriorate in the form of scaling. Scaling is defined as a general loss of surface mortar or mortar surrounding the coarse aggregate particles on a concrete surface. This occurs most often on bridge decks and roadways in cold climates. Scaling deterioration reduces the appearance, smoothness, and, most importantly, resistance of the concrete to further degradation.

4.6.2. Fabrication. The specimens used for the scaling test were fabricated as specified by ASTM C 672–03, "Standard Test Method for Scaling Resistance of Concrete Surfaces Exposed to Deicing Chemicals." These specimens are required to be at least 75 in^2 (483.9 cm^2) in plan and at least 3 in. (76 mm.) in depth. The specimen form is shown in **Figure 4.11**. Three specimens were constructed for each concrete mix. It should be noted that scaling specimens were only fabricated for the HVFA concrete investigation. The molds used to fabricate these specimens were provided by the MoDOT

Construction Materials testing laboratory. The molds were formed from two steel

channels connected by a steel pin. A plate was placed at the bottom of the channels.

Figure 4.11 - Scaling Specimen Form

The concrete was placed in the form in one lift and rodded 72 times. The concrete

was placed with approximately one inch of the form remaining exposed. Once the

concrete was placed into the mold and allowed to reach a firm state, the specimens were

broom finished with a medium broom. Then, using the exposed 1 in. (25 mm) of form, a

dike was constructed along the edges of the specimen. The dike was constructed using a

mortar mix consisting of 3 parts fine aggregate, 2 parts Portland cement, and 1 part water.

The dike was constructed by hand using putty knifes for forming. A 1 in. (25 mm.) guide

line was pressed into the edge of the fresh concrete to indicate the boundary of the dike.

Keyways were then placed into the concrete where the dike would be constructed. The

mortar was then placed onto the specimen and the dike was formed. This process can be

seen in **Figure 4.12**.

Figure 4.12 - Scaling Specimen Dike Keyway and Dike Construction

The dike and the specimen were allowed to cure for 24 hours before being removed from the forms. After form removal, specimens were moist cured for 14 days and then air cured for 14 days. A specimen ready for testing is shown in **Figure 4.13**.

Figure 4.13 - Completed Scaling Specimen and Dike

4.6.3. Testing & Procedure. The testing procedure consisted of subjecting the specimen to freezing and thawing cycles in the presence of a saltwater solution within the reservoir formed by the dikes. A chloride solution measuring approximately 0.25 in. (6

mm) deep was placed into the reservoir of the specimen. The specimen was then placed

into a walk-in freezer where it remained for 16 to 18 hours at a temperature of 32°F

(0°C). After that period of time, the specimen was removed from the freezer and placed

in a temperature and humidity-controlled environment of 73.5± 3.5°F (23.05± 2°C) and

45 to 55% R.H. for a period of 6 to 8 hours. This sequence counted as one cycle. Chloride

solution was periodically added as necessary to maintain the proper depth, and the

solution was completely replaced every 5 cycles. After 50 cycles the surface of the

specimens was inspected and the degree of scaling was reported based on the ASTM

standard.

5. HARDENED PROPERTY AND DURABILITY RESULTS

5.1. COMPRESSIVE STRENGTH

The compressive strength was determined in accordance with ASTM C 39-11. A minimum of three replicate specimens were tested for each testing date for each experimental mix. The compressive strength was tested at 1 day, 7 days, and 28 days. The tests were averaged and reported as the compressive strength of the experimental mix. All the mixes were graphed on the same plot for comparison purposes. A strength profile was developed in order to analyze and compare the strength gain of each mix. The individual specimen results of the high volume fly ash mixes can be seen in **Table 5.1**.

Table 5.1 Individual Compressive Strength Results for HVFA Mixes

Batch ID	1 Day Compressive Strength (psi)			7 Day Compressive Strength (psi)			28 Day Compressive Strength (psi)		
Control	1,960	2,130	1,900	4,540	4,840	4,540	5,440	5,360	5,280
HVFA-70H	712	694	742	2,320	2,490	2,390	3,150	3,090	2,890
HVFA-70L	812	845	827	2,710	2,750	2,790	3,480	3,610	3,350
HVFA-70LA	578	702	621	1,730	1,680	1,610	2,330	2,260	2,590

1 psi = 6.89 kPa

The individual results were then averaged and reported as the compressive strength of the experimental mix. The averaged values can be seen in **Table 5.2**.

Table 5.2 Averaged Compressive Strength Results of HVFA Mixes

Batch ID	1 Day Strength (psi)	7 Day Strength (psi)	28 Day Strength (psi)
Control	2,000	4,640	5,360
HVFA-70H	716	2,400	3,100
HVFA-70L	828	2,750	3,480
HVFA-70LA	633	1,670	2,390

1 psi = 6.89 kPa

These values were then plotted in order to develop a strength gain profile for the HVFA mixes. The strength profiles for the HVFA mixes are shown in **Figure 5.1**.
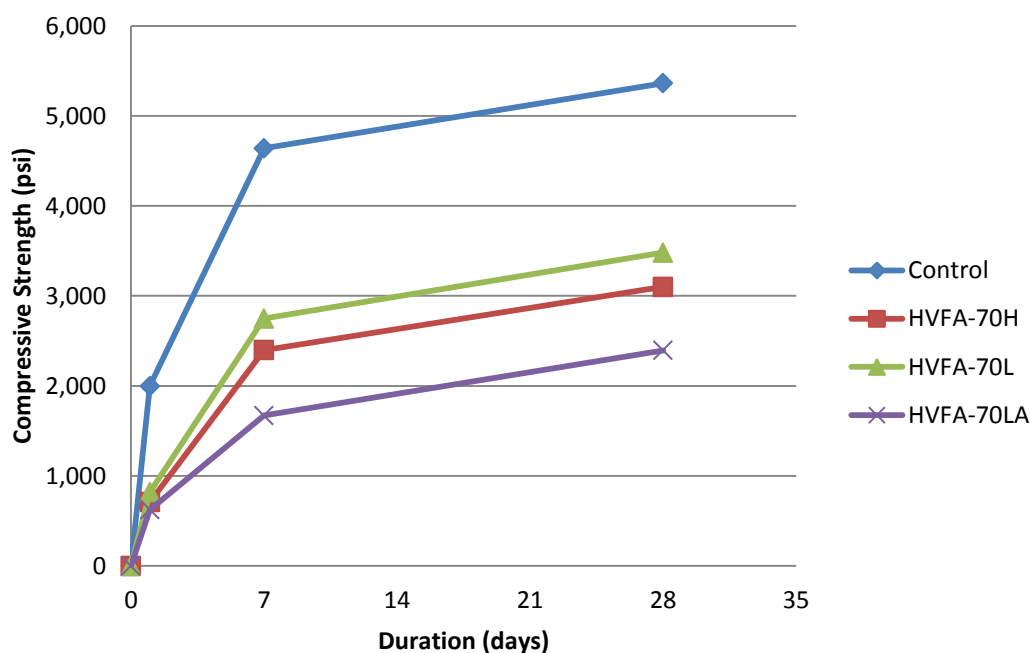
Figure 5.1 - Strength Profile of HVFA Mixes

The strength gain profile shows a large gap between the control mixes and the high-volume fly-ash mixes. The control mix also gained early strength at a much faster rate than any of the variation mixes. Both the HVFA mixes without air entrainment

performed very similar with the mix containing a low cement content doing slightly

better. It should be noted that HVFA-70LA did poorly compared to the other mixes and

did not even reach 3,000 psi (20.7 MPa).

5.2. MODULUS OF ELASTICITY

The modulus of elasticity was tested and calculated in accordance with ASTM C

469-10. Test specimens consisted of both 4 in. diameter x 8 in. long cylinder and 6 in.

(152 mm) diameter x 12 in. (305 mm) long cylinders. The specimens were tested after 28

days. During testing both the load at 50×10^{-6} strain and the length change at 40% of the

ultimate strength were measured. Using these values the modulus of elasticity was

calculated using **Eq. 5.1**.

$$E = \frac{(S_2 - S_1)}{(\varepsilon_2 - 0.000050)} \qquad \textbf{(5.1)}$$

Where S_2 is the stress at 40% of the ultimate load, S_1 is the stress measured at 50×10^{-6}

strain, and $\boldsymbol{\varepsilon_2}$ is the strain at S_2. The results for the control and HVFA-70L experimental

mixes can be seen in **Table 5.3**.

The values for S_2 were based on results of the companion compressive strength

tests. The modulus of elasticity test and compressive strength tests were performed back

to back, so the values for S_2 vary slightly from test to test. Using this data and **Eq. 6.1**,

the modulus of elasticity was calculated and averaged from the two tests. The modulus of

elasticity for the HVFA-70H and HVFA-70LA mixes was calculated using a different

apparatus. The apparatus was calibrated to calculate the modulus and report it on a

printout. For this apparatus to be used, 6 in. (152 mm) diameter x 12 in. (305) long

cylindrical specimens were fitted with a special compressometer. This compressometer

was also fitted with a LVDT to measure the length change of the specimen. Three

replicate specimens were used for this mix. The individual results of the modulus of

elasticity test can be seen in **Table 5.4**. These results were then averaged and can be seen

in **Table 5.5**.

Table 5.3 Individual Modulus of Elasticity Results for Control and HVFA-70L Mixes

Mix Design ID	Specimen ID	Test 1			Test 2		
		S_2 (psi)	S_1 (psi)	ε_2 (x10^{-4})	S_2 (psi)	S_1 (psi)	ε_2 (x10^{-4})
Control	MOE-1	2181	154	6.6	2181	132	6.9
	MOE-2	2163	205	6.1	2163	214	6
HVFA-70L	MOE-1	1395	186	4.1	1395	187	4.1
	MOE-2	1420	152	4.6	1420	147	4.9

1 psi = 6.89 kPa

Table 5.4 Individual Modulus of Elasticity Results for HVFA-70H and HVFA-70LA Mixes

Mix Design ID	Specimen ID	Modulus of Elasticity (psi)
HVFA-70H	MOE-1	3,450,000
	MOE-2	3,500,000
HVFA-70LA	MOE-1	3,450,000
	MOE-2	3,400,000
	MOE-3	3,500,000

1 psi = 6.89 kPa

Table 5.5 Average Modulus of Elasticity for HVFA Mixes

Mix Design ID	Modulus of Elasticity (psi)
Control	3,390,000
HVFA-70H	3,475,000
HVFA-70L	3,163,000
HVFA-70LA	3,450,000

1 psi = 6.89 kPa

The results were also normalized using the respective measured compressive strengths. This step was performed in order to compare the coefficients with the ACI 318-08 recommended value of 57,000, as shown in **Eq. 5.2**.

$$E_c = 57,000\sqrt{f'c} \qquad (5.2)$$

Where E_c is the modulus of elasticity and f'_c is the compressive strength of concrete. The measured modulus of elasticity was divided by the strength of the respective mix and the results can be seen in **Table 5.6**.

Table 5.6 Normalized Modulus of Elasticity for HVFA Mixes

Mix Design ID	Control	HVFA-70H	HVFA-70L	HVFA-70LA	ACI Coefficient
Normalized Results	46,250	62,420	53,610	70,410	57,000

The results of the modulus of elasticity were also compared to the AASHTO
LRFD Bridge Design Specifications. The equation used for AASHTO to estimate the
modulus of elasticity is shown in **Eq. 5.3.**

$$E_c = 33,000 w_c^{1.5} \sqrt{f_c'}$$ (**5.3**)

For normal weight concrete w_c can be assumed as 0.145 kcf. The measured modulus of
elasticity was divided by the strength of the respective mix and the results can be seen in
Table 6.7.

Table 5.7 Normalized AASHTO Modulus of Elasticity for HVFA Mixes

Mix Design ID	Control	HVFA-70H	HVFA-70L	HVFA-70LA	AASHTO Coefficient
Normalized Results	1,463	1,974	1,694	2,232	1,820

5.3. MODULUS OF RUPTURE

The modulus of rupture test was performed in accordance with ASTM C 78-10.
The modulus of rupture was calculated using the formula stated in section 3.5.3. The
values used in the equation measured for each individual test can be seen in **Table 5.7**.

The modulus of rupture was calculated using the values in **Table 5.7** and then
averaged for each concrete type. The average modulus of rupture for the high-volume fly
ash mixes can be seen in **Table 5.8**.

Table 5.7 Individual Modulus of Rupture Results for HVFA Mixes

Batch ID	Specimen ID	L (in.)	Peak Load (lb.)	b_1 (in.)	b_2 (in.)	b_3 (in.)	d_1 (in.)	d_2 (in.)	d_3 (in.)
Control	MOR-1	18	4,561	6.15	6.18	6.15	5.91	5.99	5.93
	MOR-2	18	4,721	6.12	6.12	6.18	5.98	5.98	5.95
	MOR-3	18	5,494	6.19	6.23	6.34	5.90	5.87	5.83
HVFA-70H	MOR-1	18	4,314	6.21	6.26	6.25	5.93	5.96	5.99
	MOR-2	18	4,120	6.11	6.11	6.14	5.95	5.94	5.92
	MOR-3	18	4,085	6.18	6.18	6.17	5.97	5.96	5.94
HVFA-70L	MOR-1	18	5,292	6.22	6.24	6.23	6.09	6.07	5.97
	MOR-2	18	5,571	6.16	6.18	6.20	5.97	5.96	5.95
	MOR-3	18	5,137	6.22	6.18	6.16	6.00	5.95	5.91
HVFA-70LA	MOR-1	18	4,543	6.13	6.12	6.13	5.97	5.97	5.97
	MOR-2	18	5,009	6.19	6.19	6.19	5.95	5.94	5.94
	MOR-3	18	4,791	6.19	6.18	6.19	5.92	5.91	5.92

1 psi = 6.89 kPa
1 in. = 2.54 cm.

Table 5.8 Average Modulus of Rupture Results for HVFA Mixes

Batch ID	Modulus of Rupture (psi)
Control	405
HVFA-70H	343
HVFA-70L	433
HVFA-70LA	395

1 psi = 6.89 kPa

The results were also normalized using the respective measured compressive strengths. This step was done in order to compare the coefficients with the ACI 318-08 recommended coefficient of 7.5, which appears in the equation to estimate the modulus of rupture, as seen in **Eq. 5.4**.

$$f_r = 7.5\sqrt{f'c} \tag{5.4}$$

Where f_r is the modulus of rupture and f'_c is the compressive strength of concrete. While

the coefficient of 7.5 is the most commonly used coefficient, ACI states that any values

between 6 and 12 are acceptable. After the modulus was measured, the values were

divided by the average measured strength of the respected mix. This normalized the

results, and these results were compared to the ACI coefficient of 7.5. The results of the

HVFA mixes can be seen in **Table 5.9**.

Table 5.9 Normalized Modulus of Rupture for HVFA Mixes

Mix Design ID	Control	HVFA-70H	HVFA-70L	HVFA-70LA	ACI Coefficient
Normalized Results	5.5	6.2	7.3	8.1	7.5

The results of the modulus of elasticity were also compared to the AASHTO

LRFD Bridge Design Specifications. The equation used for AASHTO to estimate the

modulus of rupture is shown in **Eq. 5.5.**

$$f_r = 0.24\sqrt{f'_c} \tag{5.5}$$

The normalized results of the HVFA mixes compared to the AASHTO coefficient can be

seen in **Table 5.10**.

Table 5.10 Normalized AASHTO Modulus of Rupture for HVFA Mixes

Mix Design ID	Control	HVFA-70H	HVFA-70L	HVFA-70LA	AASHTO Coefficient
Normalized Results	0.17	0.19	0.23	0.40	0.24

5.4. SPLITTING TENSILE

The splitting-tensile strength of the concrete mixes was tested and calculated in accordance with ASTM C 496-11. This test was performed using 6 in. (152 mm) diameter by 12 in. (305 mm) long cylindrical specimens. These specimens were loaded into the testing apparatus a loaded until failure. The splitting tensile strength was then calculated using **Eq. 5.6**.

$$T = \frac{2P}{\pi l d} \tag{5.6}$$

Where P is the maximum load applied, l is the length of the specimen, and d is the diameter. A minimum of 3 specimens were tested for each mix. The individual test results for the normal strength mixes are shown in **Table 5.11**.

Table 5.11 Individual Splitting-Tensile Test Results for HVFA Concrete Mixes

Mix Design ID	Specimen Number	Length (in.)	Diameter (in.)	Load (lb.)	Splitting Tensile Strength (psi)
Control	1	12.0	6.05	45,560	400
	2	12.0	6.05	39,975	351
	3	12.0	6.07	38,760	339
HVFA-70H	1	12.0	6.03	31,635	279
	2	12.0	6.04	26,550	233
	3	12.0	6.03	32,865	289
	4	12.0	6.04	31,155	273
	5	12.0	6.01	27,165	240
HVFA-70L	1	12.0	6.0	34,530	305
	2	12.0	6.0	35,235	312
	3	12.0	6.0	33,075	292
HVFA-70LA	1	8.0	4.0	7,410	147
	2	8.0	4.0	12,435	248
	3	8.0	4.0	13,980	278

1 in. = 2.54 cm.
1 lb = 0.45 kg
1 psi = 6.89 kPa

The individual splitting-tensile data was then averaged for each mix. The averaged splitting-tensile strength can be seen in **Table 5.12**.

Table 5.12 Averaged Splitting-Tensile Strength for HVFA Mixes

Mix Design ID	Splitting-Tensile Strength (psi)
Control	363
HVFA-70H	263
HVFA-70L	303
HVFA-70LA	224

1 psi = 6.89 kPa

The results were also normalized using the respective measured compressive strengths. This step was done in order to compare the coefficients with the ACI coefficient of 6.7, which comes from the equation to estimate the splitting-tensile strength as seen in **Eq. 5.7**.

$$f_t = 6.7\sqrt{f'c} \qquad\qquad (5.7)$$

Where f_t is the splitting-tensile strength and f'_c is the compressive strength of concrete. The measured modulus of elasticity was divided by the strength of the respected mix and the results can be seen in **Table 5.13**.

Table 5.13 Normalized Splitting-Tensile Strength for HVFA Mixes

Mix Design ID	Control	HVFA-70H	HVFA-70L	HVFA-70LA	ACI Coefficient
Normalized Results	8.6	4.7	5.1	4.6	6.7

5.5. RAPID FREEZING & THAWING

The concrete's resistance to freezing and thawing was tested and calculated in accordance to ASTM C 666-08. During the freezing and thawing cycles, the relative dynamic modulus of elasticity was measured for each of the specimens using the equation stated in Section 4.2.3. Using this data, the durability factor of the specimen could be calculated using the equation stated in Section 4.2.3. The relative dynamic modulus of elasticity and durability factor of each specimen was calculated every 36

cycles. The complete data for all test specimens can be found in Appendix B. The

minimum calculated durability factor was reported as the durability factor for that

specimen, and the values for the individual specimens of HVFA mixes can be seen in

Table 5.14.

Table 5.14 Individual Results of Freezing and Thawing Test for HVFA Mixes

Batch ID	Specimen ID	Initial Frequency	Terminal Frequency	Durability Factor	% Weight Change	Notes
Control	FT-1	1800	1080	20.3	0.02	-
	FT-2	1893	1136	23.5	0.02	-
	FT-3	1942	1165	20.9	0.02	-
HVFA-70H	FT-1	1782	1069	1.83	0.27	corner fell off
	FT-2	1787	1072	2.22	0.27	corner fell off
	FT-3	1739	1043	2.39	0.31	corner fell off
HVFA-70L	FT-1	1881	1129	85.7	-0.004	-
	FT-2	1882	1129	77.8	0.007	-
	FT-3	1886	1132	82.1	0.005	-
HVFA-70LA	FT-1	1761	1057	81.52	-0.683	-
	FT-2	1763	1058	79.61	-0.371	-
	FT-3	1739	1043	44.4	0.18	-

It should be noted that corner of all the freeze-thaw specimens for the HVFA-70H

experimental mix fell off during the testing procedure. This shows the extremely poor

durability performance of this particular mix. The average durability factor was reported

using the three replicate specimens for each experimental mix. The higher the measured

durability factor of the specimen, the better the mix will perform when exposed to cyclic

freezing and thawing. The calculated durability factors for the conventional mixes can be

seen in **Table 5.15**.

Table 5.15 Average Durability Factors for HVFA Mixes

Batch ID	Durability Factor
Control	21.6
HVFA-70H	2.1
HVFA-70L	81.8
HVFA-70LA	68.5

5.6. ELECTRICAL INDICATION TO RESIST CHLORIDE PENETRATION

The testing and calculations for this test were performed in accordance with

ASTM C 1202-10. After the testing was complete, the measured current vs. time was

plotted. A trend line was drawn through the graph and was integrated to calculate the area

under the curve. The graphs plotted for each specimen can be found in Appendix B. An

example of this graph can be seen in **Figure 5.2**.

This area gives the total charge in coulombs to pass through the specimen during

the 6 hour test. Since the diameter of the specimens used did not measure 3.75 in. (95

mm) the charge had to be adjusted using **Eq. 6.8**.

$$Q_s = Q_x \times \left(\frac{3.75}{x}\right)^2 \tag{6.8}$$

Where Q_S is the total charge through a 3.75 in. (95 mm) specimen, Q_X is the total charge

passed through a specimen measuring x inches in diameter, and x is the diameter of the

specimen that is tested. The total charge was then compared to Table 4.1 in ASTM C 1202 to assign a permeability rating, with a range from negligible (indicating the highest resistance to chloride penetration) to high (indicating the lowest resistance to chloride penetration). The corrected results of the individual specimens for the HVFA mixes are shown in **Table 5.16**.

The equation on the graph reads $y = -0.0126x^2 + 1.4316x + 125.19$
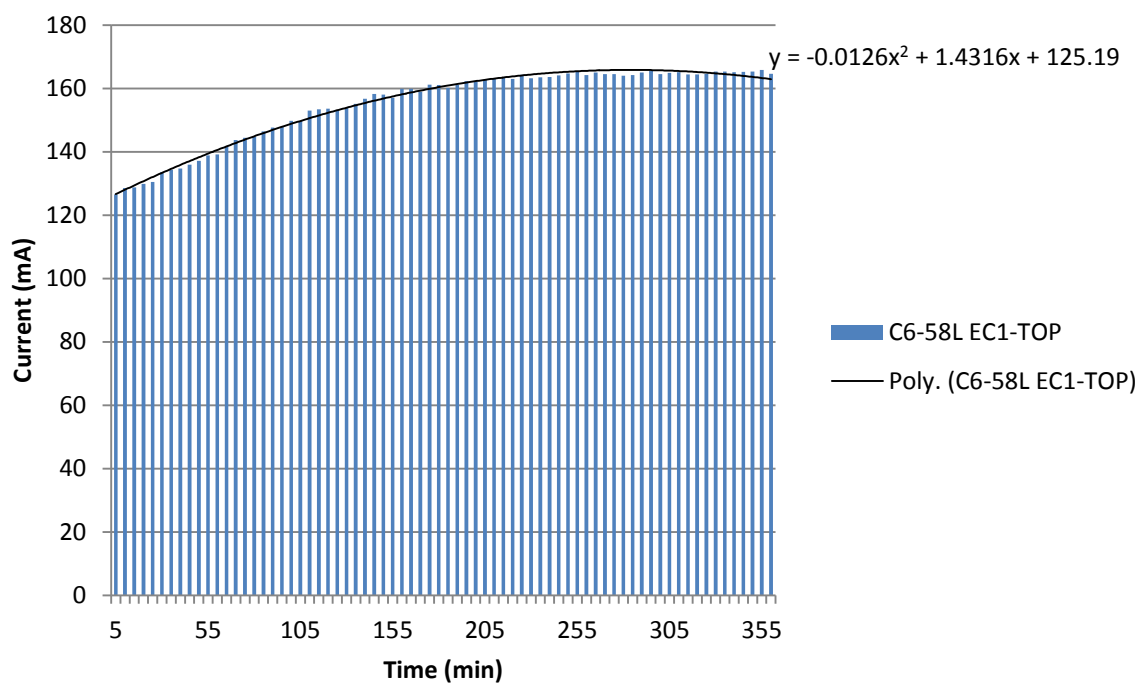
Figure 5.2 - Example of RCT Results

Table 5.16 Individual Results of RCT for HVFA Mixes

	Corrected Charge Passed (Coulombs)				
Batch ID	EC1-TOP	EC1-MID	EC2-TOP	EC2-MID	Notes
Control	4939	4660	4163	4877	-
HVFA-70H	778	583	1445	690	test stopped
HVFA-70L	1067	652	7576	999	test stopped
HVFA-70LA	967	791	1067	652	test stopped

It should be noted that the tests for all specimens for the high-volume fly ash mixes except the control were halted due to excessive voltage or excessive mA. This occurs when the concrete is excessively permeable. While the total charge may appear to be a good indication of permeability, the excessive voltage or mA indicates a high permeability class. The results were then averaged and used to assign a permeability class. The results are shown in **Table 5.17**.

Table 5.17 Averaged Results of RCT and Permeability Class of HVFA Mixes

Batch ID	Charge Passed (Coulombs)	Permeability Class	Notes
Control	4660	High	-
HVFA-70H	874	Very Low	test stopped
HVFA-70L	2573	Moderate	test stopped
HVFA-70LA	869	Very Low	test stopped

The ranges for the classes are as follows; 0-100 for negligible, 100-1000 for very low, 1000-2000 for low, 2000-4000 for moderate, >4000 for high. All three of the high volume fly ash experimental mixes, while showing low permeability class, are actually extremely permeable due to the excessive voltage or mA.

5.7. PONDING TEST

The ponding test was performed in accordance with ASTM C 1543-10. After the ponding duration was complete, cores were taken from the specimens and powder samples collected at specified depths. A chloride analysis was performed on each powder sample to determine the chloride concentration. For each experimental mix, a total of 3

cores were taken from the three individual test specimens, with 5 powder samples taken

from each core. This approach would determine an average chloride profile for each

experimental mix. Using a scale set forth by Broomfield in 2007, the risk of corrosion in

concrete can be determined by the amount of chloride present in concrete. The scale can

be seen in **Table 5.18**.

Table 5.18 Correlation Between Percent Chloride by

Mass of Concrete and Corrosion Risk [Broomfield, 2007]

% Chloride by mass of concrete	Corrosion Risk
<0.03	Negligible
0.03-0.06	Low
0.06-0.14	Moderate
>0.14	High

Using this scale, the concrete mixes were assigned corrosion risk based on the

data collected in the chloride analysis. The averaged data for the HVFA mixes can be

seen in Table **5.19**. The complete table of data can be found in the appendix. This data

was also plotted in **Figure 6.3** with a line indicating negligible corrosion risk.

Table 5.19 Average Chloride Content at Specified Depths of HVFA Mixes

Mix Design ID	Depth (in.)	Chloride Content (%)	Corrosion Risk
Control	Surface	0.045	Low
	0.25	0.047	Low
	0.75	0.039	Low
	1.5	0.031	Low
	2.0	0.033	Low
HVFA-70H	Surface	0.17	High
	0.25	0.37	High
	0.75	0.093	Moderate
	1.5	0.034	Low
	2.0	0.030	Negligible
HVFA-70L	Surface	0.14	High
	0.25	0.24	High
	0.75	0.059	Low
	1.5	0.022	Negligible
	2.0	0.012	Negligible
HVFA-70LA	Surface	0.28	High
	0.25	0.21	High
	0.75	0.13	Moderate
	1.5	0.024	Negligible
	2.0	0.017	Negligible

1 in. = 2.54 cm
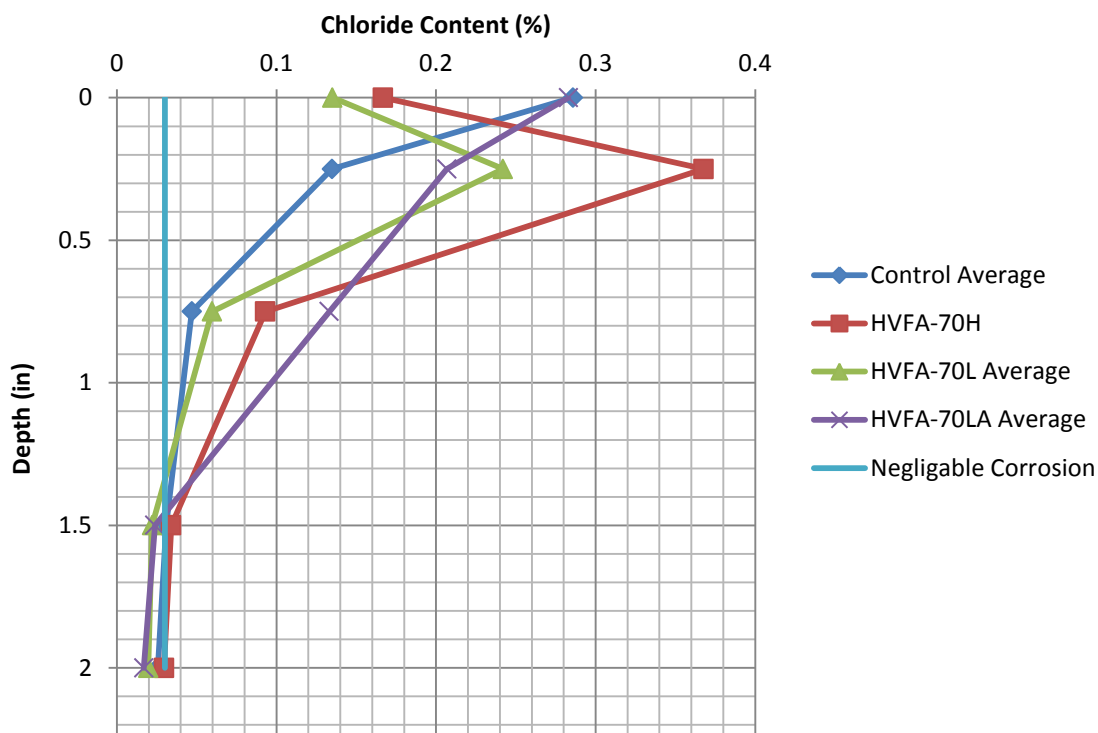
Figure 5.3 – Averaged Chloride Profile for HVFA Mixes

5.8. CONCRETE RESISTIVITY

The concrete resistivity test was a non-ASTM test method. It is, however, an industry standard, and is used quite frequently. The resistivity measurements were measured over a period of 24 weeks. These measurements can be found in Appendix B. The test was performed on three replicate specimens with the results averaged to determine the response of the individual concrete mixes. The averages for each mix were then compared. The individual specimen for the Control, HVFA-70H, HVFA-70L, and HVFA-70LA mixes can be seen in **Figures 5.4**, **5.5**, **5.6**, and **5.7,** respectively.
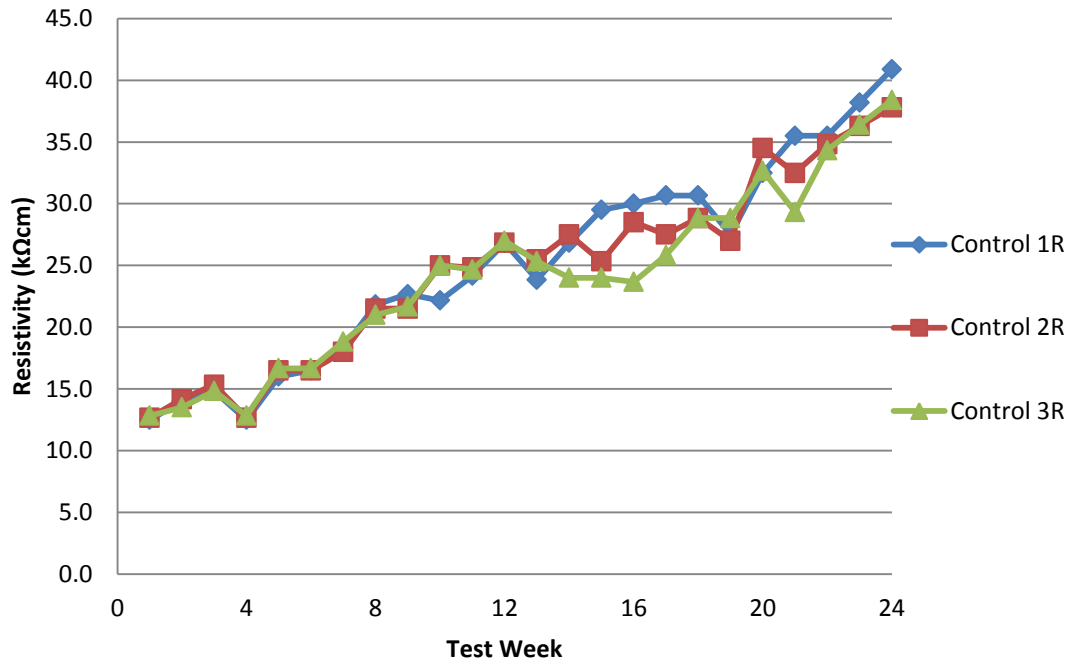
Figure 5.4 – Individual Specimen Results for Concrete Resistivity of Control Mix
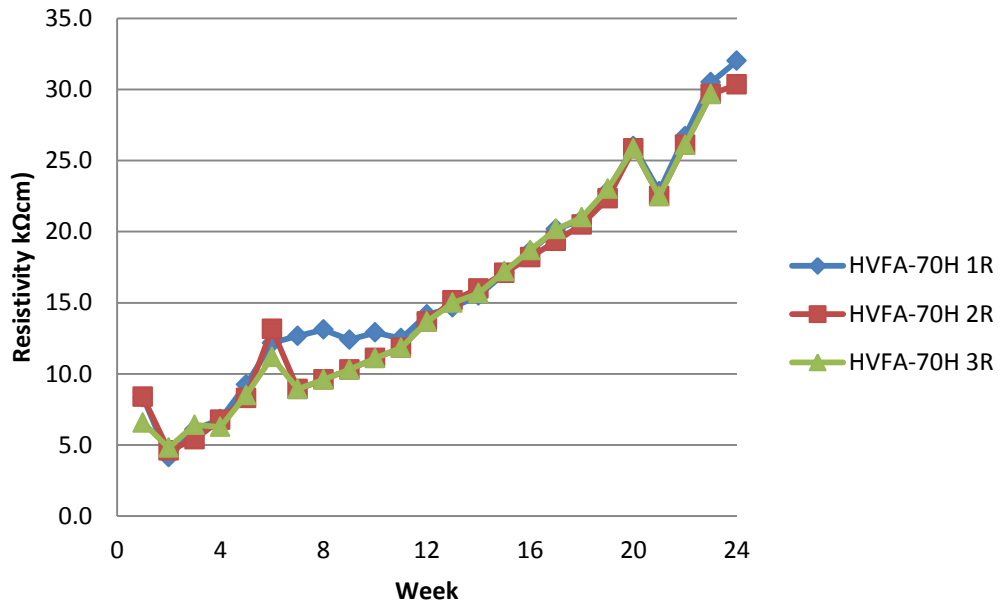
**Figure 5.5 – Individual Specimen Results for Concrete Resistivity of
HVFA-70H Mix**
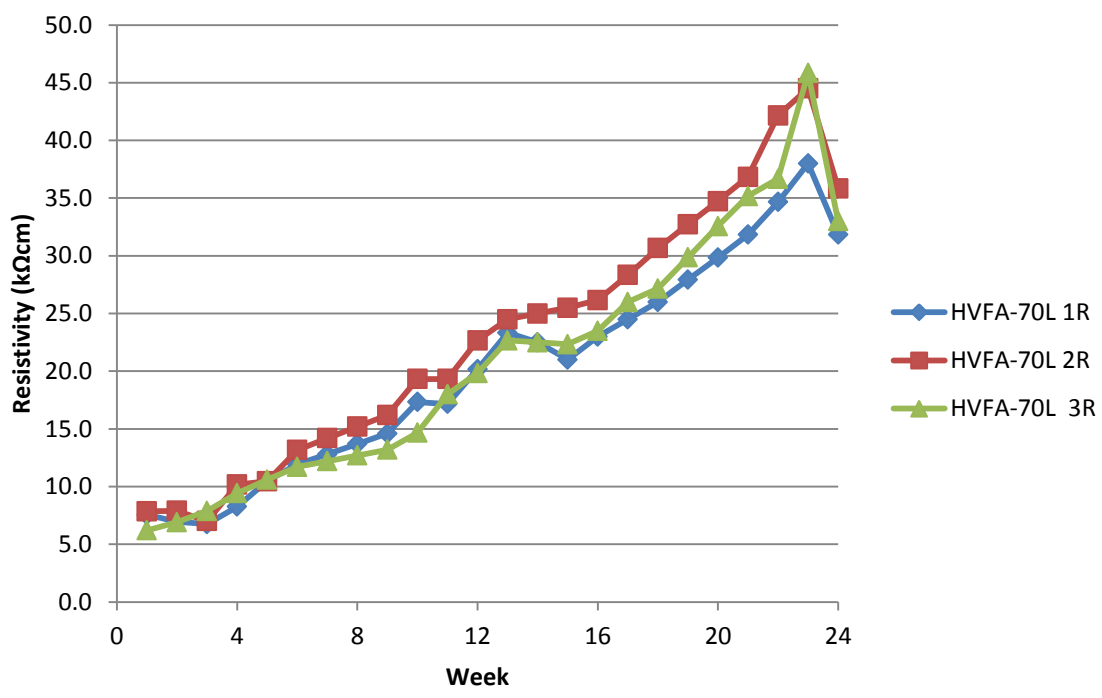
Figure 5.6 – Individual Specimen Results for Concrete Resistivity of HVFA-70H Mix
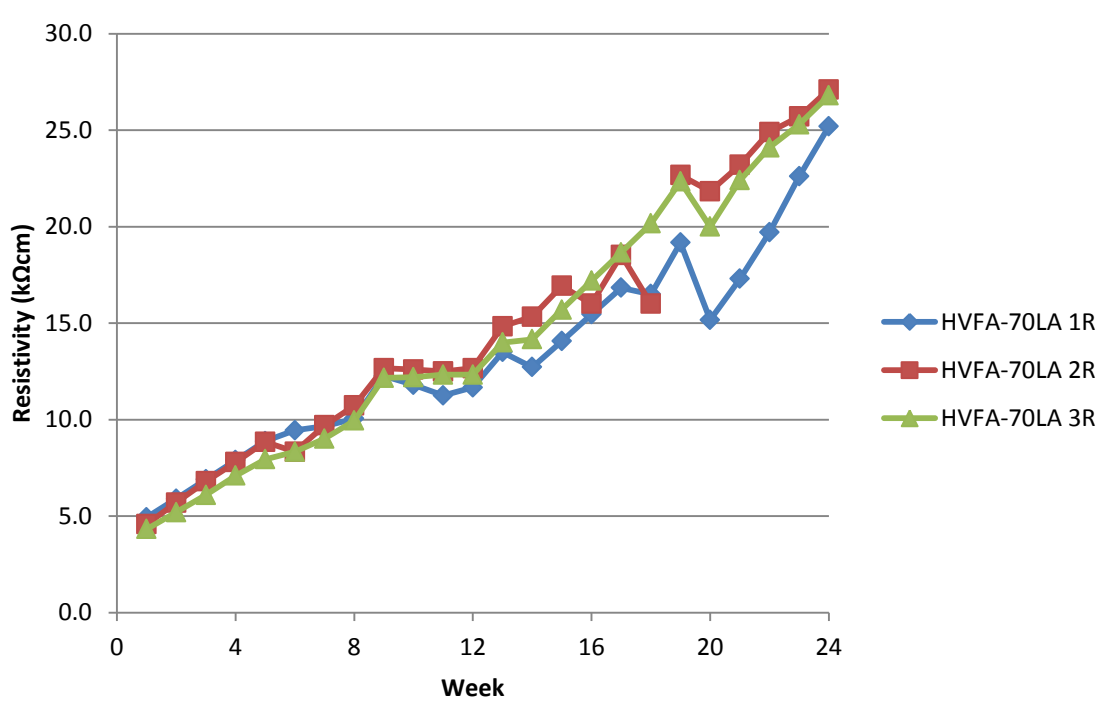
Figure 5.7 – Individual Specimen Results for Concrete Resistivity of HVFA-70LA Mix

The individual results were then averaged and graphed on the same plot for comparison purposes, which are shown in **Figure 5.8**. According to Broomfield, any concrete that has a resistivity greater than 20kΩcm is considered to have low corrosion potential. The final readings were taken at 24 weeks and can be seen in **Table 5.20**.

Table 5.20 Final Resistivity of HVFA Mixes

Mix Design ID	Resistivity (kΩcm)
Control	39.1
HVFA-70H	30.9
HVFA-70L	33.6
HVFA-70LA	26.4
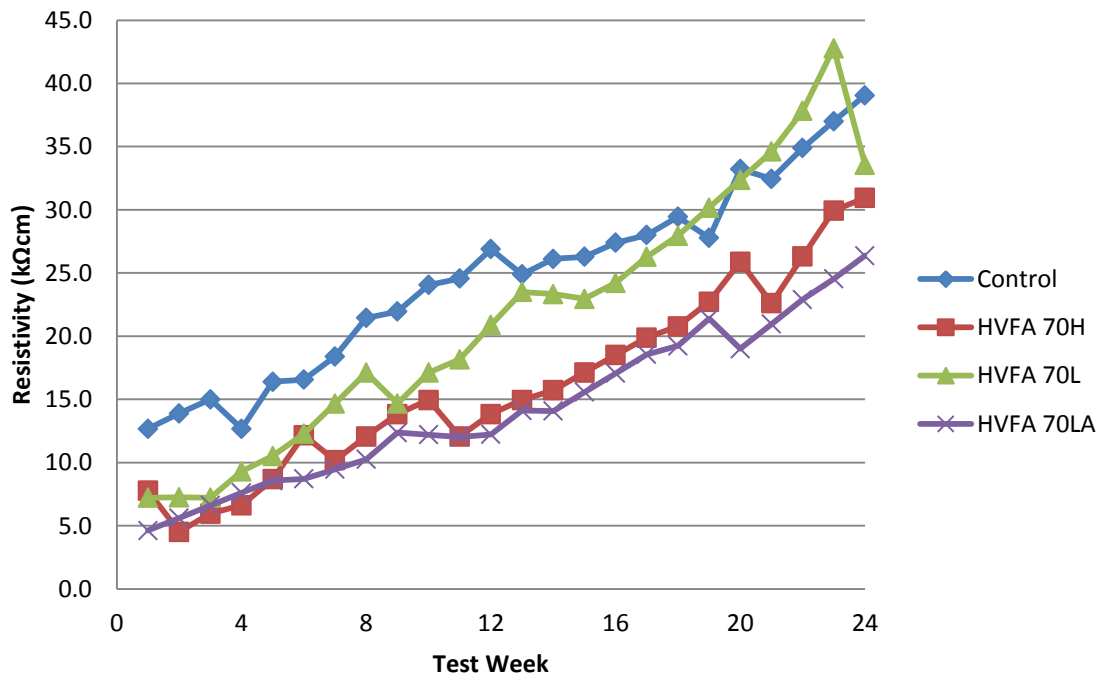
Figure 5.8 – Averaged Resistivity Results for HVFA Mixes

5.9. SCALING

The scaling resistance test was performed in accordance with ASTM C 672-03. After being subjected to 50 freezing and thawing cycles while being ponded with chloride solution, the surface of the specimens were inspected and the appearance assigned a number depending on deterioration. The scale can be seen in **Table 5.21**.

Table 5.21 Scaling Deterioration Classes [MoDOT]

Rating	Condition of Surface
1	No Scaling
2	Very Slight Scaling
3	Slight to Moderate Scaling
4	Moderate Scaling
5	Moderate to Severe Scaling

This scale is determined by ASTM C 672. The deterioration of the surface is evaluated by investigators and is assigned at their discretion. Three specimens were tested for each mix. Each specimen was given a deterioration class and the results of the test were averaged. In the case specimens having different classes, the numbers were averaged and the rounded up to stay conservative. The specimens were subjected to the tests and the results can be seen in **Table 5.22.**

Table 5.22 Averaged Scaling Performance for HVFA Mixes

Batch ID	Condition of Surface
Control	4
HVFA-70H	5
HVFA-70L	5
HVFA-70LA	5

6. EVALUATION OF HIGH-VOLUME FLY ASH CONCRETE

As stated in previous sections, both the Control mix and the HVFA concrete mixes were subjected to the same mechanical property and durability tests. In this way, it was possible to evaluate the performance of the HVFA concrete relative to a benchmark – the conventional mix. If the HVFA concrete mix performed as well or better than the conventional concrete, than it could be reasoned that, due to the positive environmental impact, it would be beneficial to use HVFA concrete in the construction of transportation infrastructure. The results of the mechanical property and durability tests can be found in Chapter 6. An outline of these results can be seen in **Table 6.1**. As stated in previous chapters, the HVFA-70H, HVFA-70L, and HVFA-70LA mix design IDs represent the relatively high total cementitious content HVFA concrete mix, the relatively low total cementitious content HVFA concrete mix, and the relatively low total cementitious content HVFA concrete mix with an air-entraining admixture, respectively. All three HVFA mixes contained a 70 percent replacement of total cementitious material with fly ash.

6.1. MECHANICAL PROPERTIES

For compressive strength, all four mixes were designed to reach 4,000 psi (27.6 MPa) after 28 days. However, only the Control mix reached this goal. All of the mixes containing fly ash showed relatively low early strength gains compared to the Control mix. This behavior is due to the relatively slow pozzolanic reaction typical of fly ash. A statistical t-test was performed on the compressive strength data in order to determine if

there is any statistical difference between the four mixes. The t-test was used to compare

each HVFA concrete mix to the Control mix. The P values between the Control mix and

the HVFA-70H, HVFA-70L, and HVFA-70LA mixes were 0.0002, 0.001, and 0.002,

respectively. Any P value less than 0.05 means the data is statistically different. In other

words, the compressive strength of the Control mix exceeded the compressive strength of

all the HVFA concrete mixes.

Table 6.1 Outline of Results of HVFA Investigation

Test ID	Mix Design ID			
	Control	HVFA-70H	HVFA-70L	HVFA-70LA
28 Day Compressive Strength (psi)	5,363	3,100	3,480	2,394
Modulus of Elasticity (psi)	3,390,000	3,475,000	3,160,000	3,450,000
Modulus of Rupture (psi)	405	343	433	395
Splitting Tensile (psi)	363	263	303	224
Rapid Freezing – Thawing (durability factor)	21.6	2.1	81.8	68.5
RCT (coulombs)	4,660	874	2,573	879
Ponding (Depth at 0.03% Chloride Content, in.)	1.5	2.0	1.3	1.45
Concrete Resistivity (kΩcm)	39.1	30.9	33.6	26.4
Scaling	4	5	5	5

1 psi = 6.89 kPa
1 in. = 2.54 cm

The modulus of rupture, modulus of elasticity, and splitting-tensile strengths are

typically estimated in design using equations based on previous research. These equations

were mentioned in Chapter 6. The results of the modulus of rupture, modulus of

elasticity, and splitting-tensile strengths were subsequently normalized using the

respective compressive strengths of each mix and the resulting coefficients were then

compared to recommended values within ACI standards. A summary of these results can

be seen in **Table 6.2**.

**Table 6.2 Normalized Mechanical Properties Compared to
Respective ACI Coefficients**

	Control	HVFA-70H	HVFA-70L	HVFA-70LA	ACI Coefficient
Modulus of Elasticity	46,250	62,420	53,610	70,410	57,000
Modulus of Rupture	5.5	6.2	7.3	8.1	7.5
Splitting-Tensile Strength	4.9	4.7	5.1	4.6	6.7

The Control mix and the HVFA-70L mix fell considerably short of the empirical

relationship recommended for modulus of elasticity. This result means that in the design

of concrete structures constructed with these concretes, the modulus of elasticity for

either mix would be overestimated. This situation can have negative effects on estimating

deflection and serviceability of concrete in the field. However, both the HVFA-70H and

HVFA-70LA mixes exceeded the empirical relationship. These concrete mixes would

likely perform better in the field than estimated. A statistical t-test was performed on the

modulus of elasticity coefficient data in order to determine if there is a statistical

difference between the four mixes. The t-test was used to compare each HVFA concrete

mix to the control. The P values between the Control mix and the HVFA-70H, HVFA-

70L, HVFA-70LA mixes were 0.045, 0.41, and 0.048, respectively. Any P value less

than 0.05 means the data is statistically different. In other words, the modulus of

elasticity of the Control and all of the HVFA mixes are statistically different. The modulus of elasticity of each specimen was also plotted against compressive strength for comparison with the ACI recommended relationship. Also included in the plot for comparison is data from another HVFA concrete study completed at Missouri S&T. The graph can be seen in **Figure 6.1**.
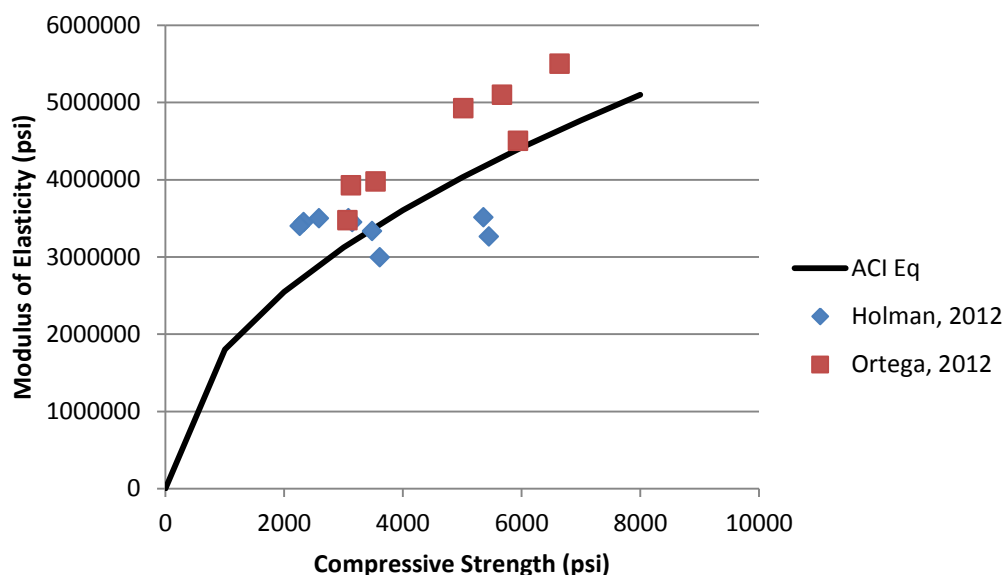
Figure 6.1 - Compressive Strength vs. Modulus of Elasticity

For the modulus of rupture, the Control, HVFA-70H, and HVFA-70L mixes fell below the ACI coefficient of 7.5, although the HVFA-70L was very close (7.3). However, the HVFA-70LA mix exceeded the ACI coefficient of 7.5. It is important to note, however, that the modulus of rupture is highly variable as the coefficient can vary between 6 and 12 [Neville, 1997]. A statistical t-test was performed on the modulus of rupture coefficient data in order to determine if there is a statistical difference between

the four mixes. The t-test was used to compare each HVFA mix to the control. The P

value between the Control and the HVFA-70H, HVFA-70L, and HVFA-70LA mixes

were 0.18, 0.04, and 0.04, respectively. Any P value greater than 0.05 means the data is

statistically equal. In other words, the modulus of rupture of the Control and HVFA-70H

are essentially identical. The P values for the HVFA-70L and HVFA-70LA were less

than 0.05. This means the data is statistically different. The modulus of rupture for each

specimen was plotted against the compressive strength for comparison with the ACI

recommended relationship. Also included in the plot for comparison is data from other

HVFA concrete studies completed at Missouri S&T. The graph can be seen in **Figure**

6.2.
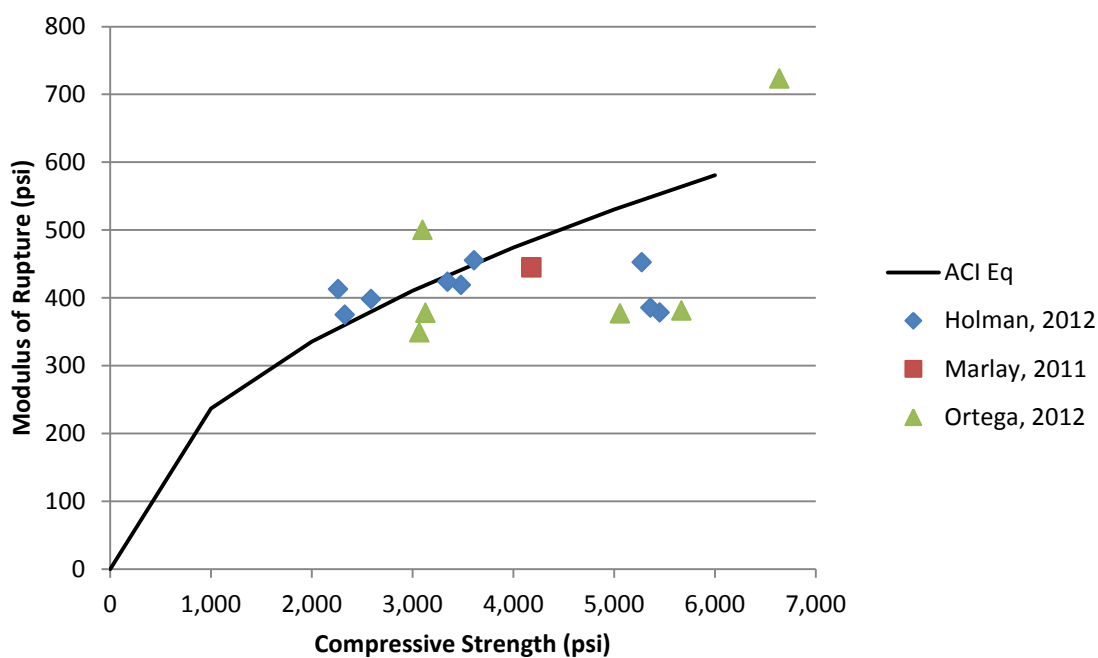
Figure 6.2 – Compressive Strength vs. Modulus of Rupture

For the splitting-tensile strength, all the mixes except for the Control fell below the ACI coefficient used to estimate the splitting-tensile strength. All of the HVFA concrete mixes performed similarly with the calculated coefficients being very close in value. However, splitting-tensile strength is also highly variable with values ranging from 5 to 9.5 [Oluokun, 1991]. A statistical t-test was performed on the splitting-tensile coefficient data in order to determine if there is a statistical difference between the four mixes. The t-test was used to compare each HVFA mix to the control. The P value between the Control and the HVFA-70H, HVFA-70L, and HVFA-70LA mixes were 0.81, 0.48, and 0.74. Any P value greater than 0.05 means the data is statistically equal. In other words, the splitting-tensile strengths of the four mixes are essentially identical. The splitting-tensile strength of the specimens was also plotted against the compressive strength of the concrete. Also included in the plot for comparison is data from other HVFA concrete studies completed at Missouri S&T. The graph can be seen in **Figure 6.3**.

The measured modulus of elasticity and modulus of rupture were also compared to the AASHTO LRFD Design equations used to estimate these mechanical properties. These properties were normalized by dividing the measured values by the respective compressive strength and then compared to the AASHTO equations as mentioned in Chapter 5. A summary of these coefficients can be seen in **Table 6.3**.
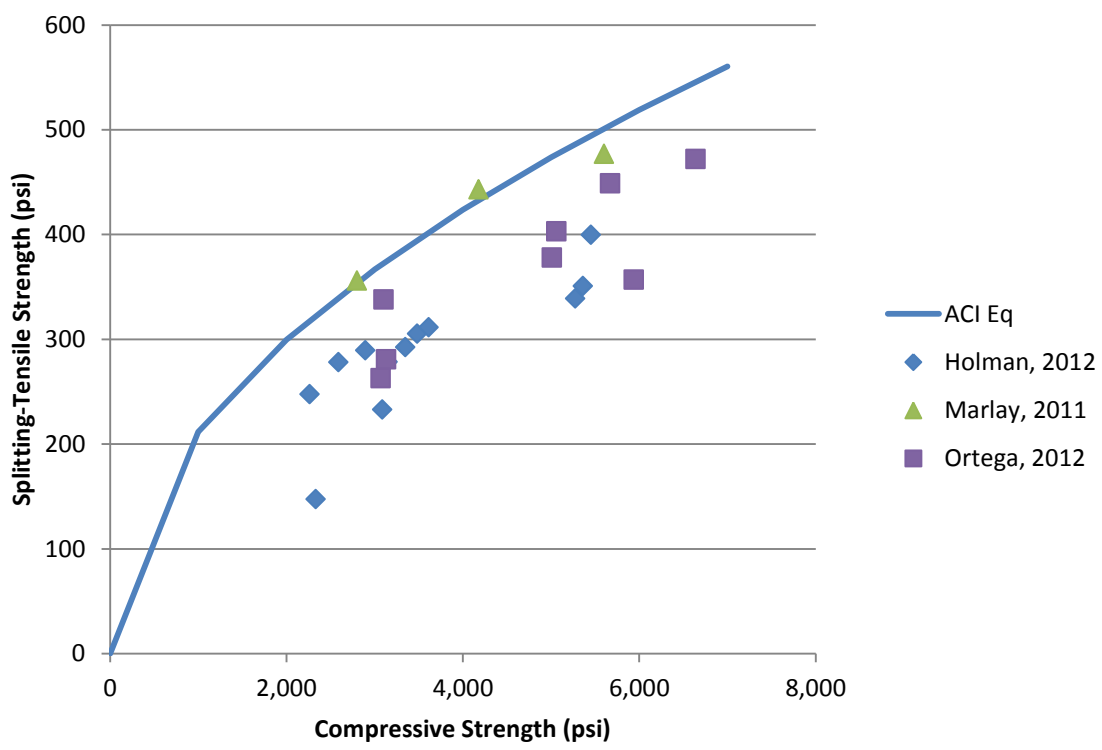
Figure 6.3 – Compressive Strength vs. Splitting-Tensile Strength

Table 6.3 Normalized Mechanical Properties Compared to

Respective AASHTO Coefficients

	Control	HVFA-70H	HVFA-70L	HVFA-70LA	AASHTO Coefficient
Modulus of Elasticity	1,463	1,974	1,694	2,232	1,820
Modulus of Rupture	0.17	0.19	0.23	0.40	0.24

These results also followed a very similar trend as the ACI coefficient comparison. For the modulus of elasticity, both the HVFA-70H and HVFA-70LA showed higher coefficients than the AASHTO recommended coefficient. Only the HVFA-70LA showed a higher coefficient than the AASHTO coefficient.

6.2. DURABILITY PERFORMANCE.

For resistance to freeze-thaw most of the mixes performed very poorly when compared to the minimum set forth by MoDOT, including the Control mix. MoDOT specifies a minimum durability factor of 75, which only the HVFA-70L exceeded. The HVFA-70H mix performed extremely poorly, recording a durability factor of 2.1. Both the HVFA-70L and HVFA-70LA mixes showed much higher performance when compared to the Control mix. Consequently, except for the HVFA-70L mix, the poor freeze-thaw performance was probably more a function of the particular limestone coarse aggregate used in the mixes (Jefferson City dolomite).

With regard to permeability, the mixes showed variable results. The Control mix received a high permeability rating while the HVFA mixes all showed very low permeability. However, all of the tests performed on the mixes containing fly ash were forced to stop due to excessive current or voltage build-up after less than an hour. While the total coulombs passed for these mixes indicate a low permeability, these low numbers are due to early termination of the tests. Two tests performed on specimens containing fly ash did reach the specified test duration of 6 hours and these specimens showed an extremely high total charge passed, indicating high permeability. This result further confirms what other researchers have reported; namely that the RCT indicates false results for concrete mixes contain fly ash [Shi, 2002].

The ponding test also indicated unusual performance of the HVFA concrete mixes. The control mix reached a chloride content of 0.03% at approximately 1.5 in. (38 mm) in depth. This chloride content indicates a negligible corrosion risk. The Control mix also showed a typical chloride profile, with the surface containing the highest

chloride content and decreasing as the depth increases. Both HVFA-70H and HVFA-70L mixes did not show this type of behavior. Both mixes revealed relatively low chloride concentrations at the surface and relatively high chloride concentrations at 0.25 in. (6.4 mm) in depth. These results suggest that mixes containing high amounts of fly ash have higher capillary action than conventional concrete. Also the chloride content decreased significantly after 0.25 in. (6.4 mm) in depth, reaching the 0.03% chloride content goal at approximately 1.5 in. (38 mm). This characteristic would suggest that while HVFA concrete may have high capillary action, these mixes have low diffusion. This was not seen in the HVFA-70LA mix, which showed a relatively typical chloride profile. This mix also reached the 0.03% chloride content goal at approximately 1.5 in. (38 mm). The average chloride profile for all the mixes can be seen in **Figure 6.4**.

With regard to concrete resistivity using the Wenner probe, all of the concrete mixes showed adequate performance. According to Broomfield [2007], any concrete indicating resistivity over 20kΩcm is to be classified as having a low rate of corrosion. All the mixes exceeded this value, with the Control mix having the highest resistivity at 39.1 kΩcm after 24 weeks of testing. HVFA-70L showed the seconded highest resistivity at 33.6 kΩcm, performing slightly higher than HVFA-70H at 30.9 kΩcm, both after 24 weeks of testing. It appears that the addition of an air entraining admixture significantly reduces the resistivity of concrete. The HVFA-70LA mix showed the lowest resistivity at 26.4 kΩcm after 24 weeks of testing, although still above the 20kΩcm standard for a low rate of corrosion. All of the mixes also showed an increase in resistivity over time at approximately the same rate of increase. The average results of this test can be seen in **Figure 6.5**.
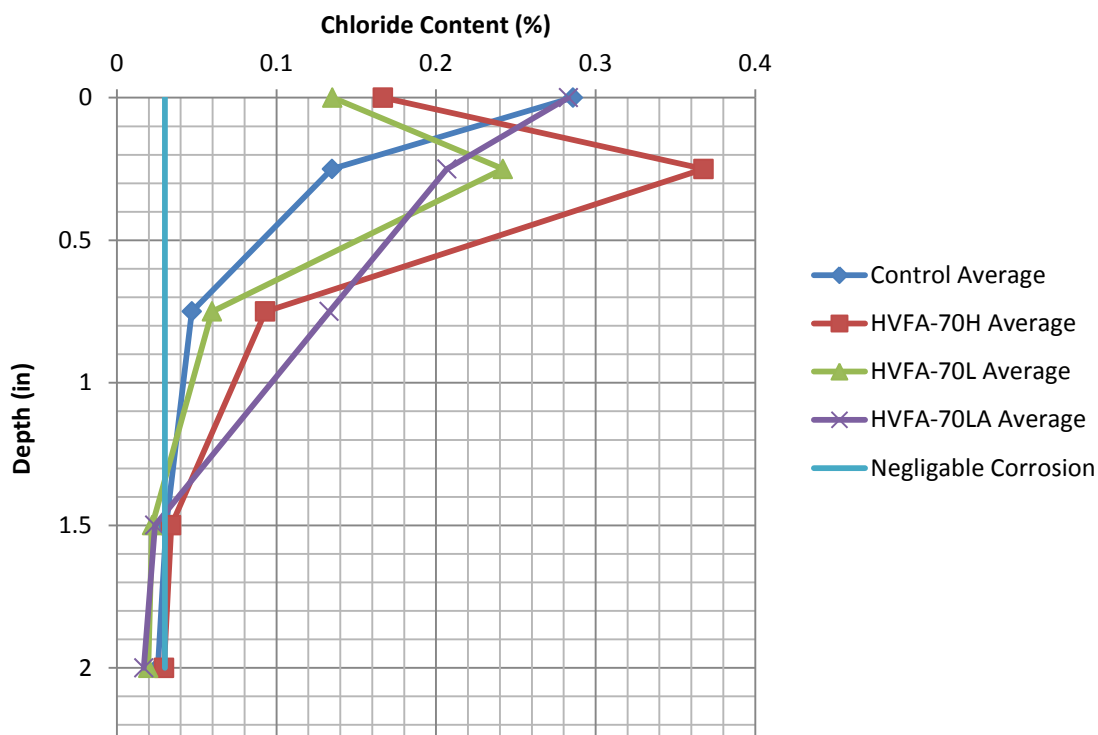
Figure 6.4 – Average Chloride Content vs. Depth of HVFA Mixes
1 in. = 2.54 cm
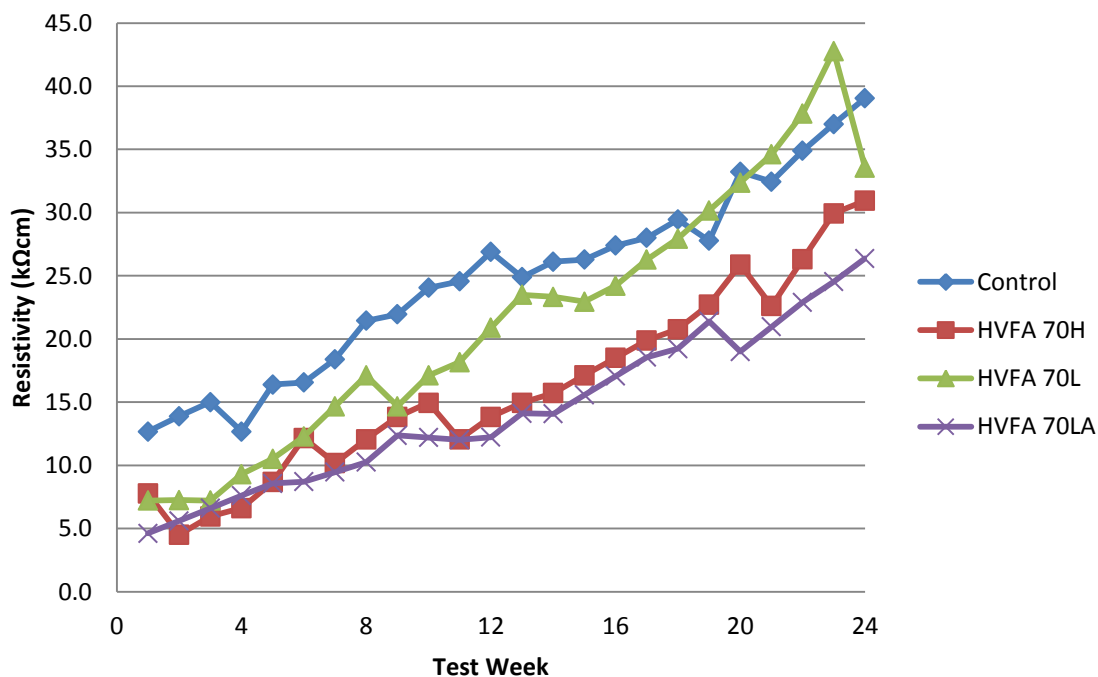
Figure 6.5 – Average Resistivity of HVFA Concrete Mixes

With regard to scaling, all of the HVFA concrete mixes showed very low resistance. All of the mixes containing fly ash reached a rating of 5 within a relatively low number of cycles. This agrees with previous research performed on HVFA concrete, which has consistently shown poor scaling resistance. The Control mix did slightly better, reaching a rating of 4 in deterioration, although the Control completed the 50 cycles of testing while the HVFA concrete mixes did not reach that point in testing due to their rapid rate of deterioration. Many of the scaling panels constructed with HVFA concrete showed deterioration up to 0.25 in. (6.4 mm) in depth. This observation in conjunction with the observations made in the ponding test seems to suggest that HVFA concrete absorbs a high amount of water through capillary action. Two of the three HVFA mixes contained higher chloride concentrations at 0.25 in. (6.4 mm) in depth than at the surface. A highly absorptive concrete would explain both the unusually high chloride concentrations at 0.25 in. (6.4 mm) as well as the severe deterioration of the salt scaling panels.

7. FINDINGS, CONCLUSIONS, AND RECOMMENDATIONS

7.1. FINDINGS AND CONCLUSIONS

The HVFA concretes tested in this investigation showed mixed results relative to the material property and durability testing. All of the concrete mixes containing fly ash showed relatively slow strength gains, including an inability to reach the target strength of 4,000 psi (27.6 MPa) at 28 days. A slow rate of strength gain may be a significant problem in some aspects of construction, although in others, the 28 or 56-day strength is the critical aspect and early age strength is relatively unimportant.

Both the Control and the HVFA-70L mix showed comparable modulus of elasticity. However, both the HVFA-70H and HVFA-70LA showed higher values than the Control mix. When comparing the normalized data, all three HVFA mixes exceeded the Control mix, with only the HVFA-70L mix falling below the recommended ACI coefficient. In regard to the modulus of rupture, only the Control and HVFA-70H mix showed comparable results, with the HVFA-70L and HVFA-70LA mixes performing above the control. In fact, only the HVFA-70L and HVFA-70LA mixes exceeded the recommended ACI coefficient used to estimate the modulus of rupture. In regard to splitting-tensile strength, all three of the HVFA concrete mixes showed comparable results with the Control mix. While all the mixes fell short of the recommended ACI coefficient, all the calculated coefficients for the mixes were comparable; indicating that the HVFA concrete mixes did not suffer any decrease in capacity compared to the conventional concrete.

The mixes containing fly ash all showed variable performance in many of the durability tests. The Control and HVFA-70H showed poor performance for resistance to

freeze-thaw. Both the HVFA-70L and HVFA-70LA significantly exceeded the performance of the Control mix, with the HVFA-70L mix showing slightly better performance than the HVFA-70LA mix. Typically, air entrainment improves a concrete's resistance to freeze-thaw. However, with the higher carbon content of fly ash, the air void system created by air entraining admixtures may be difficult to maintain.

The HVFA concrete mixes all showed poor test results when subjected to the RCT. A majority of the tests performed on the HVFA concrete mixes were terminated before the appropriate time, due to excessive mA or voltage. However, one study has indicated that this test is believed to be invalid for HVFA concrete. The chemical composition of fly ash impacts the test in such a way that excessive mA or voltage can build up during the procedure, forcing the test to be terminated. All of the HVFA mixes showed better performance than the Control mix in the ponding test. All of the concrete mixes containing fly ash reached a chloride content of 0.03% at approximately 1.5 in. (38 mm) in depth, while the Control mix reached a chloride concentration of 0.03% at approximately 2.0 in. (51 mm). However, both the HVFA-70H and HVFA-70L mixes showed very unique chloride content profiles. Both mixes showed lower chloride concentrations at the surface and higher chloride concentrations at 0.25 in. (6 mm) in depth. This observation could indicate that concrete mixes containing high amounts of fly ash have an unusually high amount of capillary action but diffusion characteristics consistent with conventional concrete. HVFA-70LA showed a more typical chloride content profile when compared to the Control mix.

All of the mixes in this investigation showed excellent performance in the aspect of concrete resistivity performance. The Control mix showed the highest resistivity after

24 weeks of testing, measuring 39.1 kΩcm. The HVFA-70H and HVFA-70L mixes both performed similarly, measuring 30.9 kΩcm and 33.6 kΩcm, respectively. The HVFA-70LA performed the lowest, measuring 26.4 kΩcm at 24 weeks, yet still measuring a resistivity higher than that needed to be classified as low rate of corrosion. All of the HVFA concrete mixes showed very poor performance in scaling resistance. All three mixes reached the lowest rating of 5 very early in the testing cycles. This result indicates extremely low durability when exposed to deicing salts in freezing weather.

7.2. RECOMMENDATIONS

After thorough mechanical property and durability testing, it is recommended that HVFA concrete should only be used in applications that are not exposed to salt scaling, such as bridge decks. However, except for the aspect of rate of compressive strength gain, HVFA concrete was comparable in all other aspects of hardened properties tested in this investigation. Unfortunately, HVFA concrete showed very inadequate performance with regard to scaling and inconsistent performance involving chloride penetration. The areas in which HVFA concrete showed adequate durability performance was resistance to freeze-thaw deterioration and concrete resistivity. For freeze-thaw, both the HVFA-70L and HVFA-70LA mixes showed higher performance than the Control mix. The HVFA-70H mix showed extremely low performance, with the specimens falling apart before the end of the test duration. While all of the HVFA mixes measured resistivity lower than the Control mix, all the HVFA mixes performed higher than the level indicating low corrosion risk. While the HVFA mixes showed similar chloride profiles, the observation of higher chloride content at 0.25 in. (6 mm) may suggest that the mechanism of capillary

action and diffusion within HVFA concrete is variable and should be investigated further.

It is recommended that HVFA concrete be used in applications where high early

strengths are not necessary and the concrete elements are not exposed to any

environmental conditions that may cause salt scaling. Alternatively, lower levels of

cement replacement with fly ash – up to 50% – are recommended for the majority of

applications involving transportation-related infrastructure.

APPENDIX

HVFA DURABILITY TEST RESULTS DATA

Table A.1 Control-R1 (Weeks 1-7)

Date	7/19/2011	7/26/2011	8/2/2011	8/9/2011	8/16/2011	8/23/2011	8/30/2011
A1	13	14	16	13	17	17	20
A2	12	13	13	12	15	15	17
A3	14	15	16	14	17	18	20
B1	13	15	15	13	16	17	18
B2	11	13	14	11	15	15	16
B3	12	14	15	12	16	17	19
Average	12.5	14.0	14.8	12.5	16.0	16.5	18.3

Table A.2 Control-R1 (Weeks 8-14)

Date	9/6/2011	9/13/2011	9/20/2011	9/27/2011	10/4/2011	10/11/2011	10/18/2011
A1	23	24	19	25	27	27	27
A2	20	20	20	21	23	21	24
A3	24	25	26	26	30	22	29
B1	24	24	25	25	30	23	28
B2	19	21	19	23	24	23	24
B3	21	22	24	25	27	27	29
Average	21.8	22.7	22.2	24.2	26.8	23.8	26.8

Table A.3 Control-R1 (Weeks 15-21)

Date	10/25/2011	11/1/2011	11/8/2011	11/15/2011	11/22/2011	11/29/2011	12/6/2011
A1	32	32	32	33	32	35	36
A2	26	26	30	29	22	25	31
A3	30	33	34	34	26	38	41
B1	33	32	32	34	33	36	38
B2	26	26	26	27	24	31	30
B3	30	31	30	27	28	30	37
Average	29.5	30.0	30.7	30.7	27.5	32.5	35.5

Table A.4 Control-R1 (Weeks 22-24)

Date	12/16/2011	12/16/2011	12/16/2011
A1	34	36	39
A2	30	33	36
A3	41	44	45
B1	40	42	44
B2	33	36	38
B3	35	38	43
Average	35.5	38.2	40.9

Table A.5 Control-R2 (Weeks 1-7)

Date	7/19/2011	7/26/2011	8/2/2011	8/9/2011	8/16/2011	8/23/2011	8/30/2011
A1	13	14	16	13	17	17	18
A2	11	13	14	11	15	15	17
A3	14	16	17	14	19	18	20
B1	14	16	16	14	17	17	19
B2	11	12	13	11	14	15	16
B3	13	14	16	13	17	17	18
Average	12.7	14.2	15.3	12.7	16.5	16.5	18.0

Table A.6 Control-R2 (Weeks 8-14)

Date	9/6/2011	9/13/2011	9/20/2011	9/27/2011	10/4/2011	10/11/2011	10/18/2011
A1	21	22	25	25	28	26	30
A2	19	19	22	22	23	23	24
A3	24	24	28	26	30	27	30
B1	23	24	26	27	28	28	30
B2	21	19	23	22	28	23	24
B3	21	21	26	27	24	26	27
Average	21.5	21.5	25.0	24.8	26.8	25.5	27.5

Table A.7 Control-R2 (Weeks 15-21)

Date	10/25/2011	11/1/2011	11/8/2011	11/15/2011	11/22/2011	11/29/2011	12/6/2011
A1	27	26	26	28	36	32	35
A2	20	27	25	24	25	27	28
A3	27	35	30	35	28	41	34
B1	31	30	28	34	28	37	36
B2	22	25	24	23	20	28	28
B3	25	28	32	29	25	42	34
Average	25.3	28.5	27.5	28.8	27.0	34.5	32.5

Table A.8 Control-2R (Weeks 22-24)

Date	12/16/2011	12/16/2011	12/16/2011
A1	38	39	41
A2	30	33	34
A3	42	43	44
B1	36	38	39
B2	27	29	31
B3	36	36	38
Average	34.8	36.3	37.8

Table A.9 Control-3R (Weeks 1-7)

Date	7/19/2011	7/26/2011	8/2/2011	8/9/2011	8/16/2011	8/23/2011	8/30/2011
A1	15	15	17	15	17	19	20
A2	12	13	14	12	15	16	18
A3	12	13	15	12	18	17	18
B1	14	14	15	14	18	18	21
B2	11	11	13	11	15	15	18
B3	13	15	15	13	17	15	18
Average	12.8	13.5	14.8	12.8	16.7	16.7	18.8

Table A.10 Control-3R (Weeks 8-14)

Date	9/6/2011	9/13/2011	9/20/2011	9/27/2011	10/4/2011	10/11/2011	10/18/2011
A1	23	24	29	26	28	24	24
A2	21	20	22	23	24	25	19
A3	22	21	25	24	26	22	25
B1	21	25	27	28	30	29	31
B2	20	19	22	23	27	29	24
B3	19	21	25	24	27	23	21
Average	21.0	21.7	25.0	24.7	27.0	25.3	24.0

Table A.11 Control-3R (Weeks 15-21)

Date	10/25/2011	11/1/2011	11/8/2011	11/15/2011	11/22/2011	11/29/2011	12/6/2011
A1	24	25	25	29	35	38	28
A2	20	21	23	23	26	27	21
A3	28	23	34	33	36	37	33
B1	24	27	26	33	30	39	36
B2	20	20	24	31	23	26	28
B3	28	26	23	24	23	29	30
Average	24.0	23.7	25.8	28.8	28.8	32.7	29.3

Table A.12 Control-3R (Weeks 22-24)

Date	12/16/2011	12/16/2011	12/16/2011
A1	36	37	39
A2	26	28	29
A3	35	36	37
B1	46	48	49
B2	32	35	36
B3	31	34	40
Average	34.3	36.4	38.4

Table A.13 HVFA-70H-1R (Weeks 1-7)

Date	10/31/2011	11/7/2011	11/14/2011	11/21/2011	11/28/2011	12/5/2011	12/12/2011
A1	9.4	5.1	7.1	7.1	10	13	14
A2	7.8	3.8	5.4	6.2	9.0	12	12
A3	7.9	4.3	5.0	6.5	8.7	10	11
B1	7.8	3.3	6.6	7.0	11	13	16
B2	7.8	4.3	5.8	7.1	8.0	12	11
B3	9.4	4.0	6.6	7.0	8.7	13	12
Average	8.4	4.1	6.1	6.8	9.2	12.2	12.7

Table A.14 HVFA-70H-1R (Weeks 8-14)

Date	12/19/2011	12/26/2011	1/2/2012	1/9/2012	1/16/2012	1/23/2012	1/30/2012
A1	14	13	13	12	15	16	18
A2	13	12	13	12	13	14	15
A3	12	11	12	12	14	14	14
B1	15	14	13	14	16	15	16
B2	12	10	11	11	12	12	14
B3	13	14	15	14	15	17	16
Average	13.1	12.4	12.9	12.5	14.2	14.7	15.5

Table A.15 HVFA-70H-1R (Weeks 15-21)

Date	2/6/2012	2/13/2012	2/20/2012	2/27/2012	3/5/2012	3/12/2012	3/19/2012
A1	19	21	22	24	24	26	25
A2	16	17	19	21	22	25	21
A3	17	18	19	19	22	27	21
B1	16	19	22	21	23	27	25
B2	15	16	16	17	20	23	19
B3	20	21	23	23	26	28	26
Average	17.1	18.6	20.2	20.8	22.8	26.0	22.8

Table A.16 HVFA-70H-1R (Weeks 22-24)

Date	3/26/2012	4/2/2012	4/9/2012
A1	32	35	33
A2	26	29	31
A3	27	30	30
B1	28	31	33
B2	22	25	28
B3	25	33	37
Average	26.7	30.5	32.0

Table A.17 HVFA-70H-2R (Weeks 1-7)

Date	10/31/2011	11/7/2011	11/14/2011	11/21/2011	11/28/2011	12/5/2011	12/12/2011
A1	7.3	4.7	5.7	7.1	7.9	12	8.1
A2	7.6	4.8	4.8	6	6.2	11	7.4
A3	9.3	4.9	6.1	7.2	9.5	13	9.8
B1	8.5	4.9	6	7	10	14	10
B2	7.6	4.2	4.3	6.4	7.6	13	9
B3	10	4.2	5.4	6.9	8.6	16	9.2
Average	8.4	4.6	5.4	6.8	8.3	13.2	8.9

Table A.18 HVFA-70H-2R (Weeks 8-14)

Date	12/19/2011	12/26/2011	1/2/2012	1/9/2012	1/16/2012	1/23/2012	1/30/2012
A1	9.3	11	12	11	12	15	16
A2	8.1	9.7	10	10	12	13	14
A3	10	12	13	13	14	16	17
B1	11	11	11	12	14	18	19
B2	9.3	10	10	11	13	14	15
B3	9.9	8	11	14	17	15	15
Average	9.6	10.3	11.1	11.8	13.7	15.2	16.0

Table A.19 HVFA-70H-2R (Weeks 15-21)

Date	2/6/2012	2/13/2012	2/20/2012	2/27/2012	3/5/2012	3/12/2012	3/19/2012
A1	17	18	18	20	23	26	23
A2	14	15	17	18	20	20	20
A3	18	19	20	21	21	26	22
B1	21	22	21	23	23	29	24
B2	15	16	19	19	22	25	22
B3	18	19	21	22	25	29	24
Average	17.1	18.2	19.3	20.5	22.3	25.8	22.5

Table A.20 HVFA-70H-2R (Weeks 22-24)

Date	3/26/2012	4/2/2012	4/9/2012
A1	29	31	31
A2	21	23	24
A3	26	30	30
B1	29	31	31
B2	23	26	29
B3	29	37	37
Average	26.1	29.7	30.3

Table A.21 HVFA-70H-3R (Weeks 1-7)

Date	10/31/2011	11/7/2011	11/14/2011	11/21/2011	11/28/2011	12/5/2011	12/12/2011
A1	7.4	4.8	6.4	6.4	8.6	12	9.7
A2	5.7	3.8	6.2	5.2	7.4	10	9.0
A3	6.6	4.2	6	6	9.1	12	7.0
B1	6.6	6.6	6	6.5	8.4	11	9.4
B2	6.5	5	6.2	6.4	8.4	10	8.7
B3	6.6	4.4	7.7	7.1	9.1	12	9.8
Average	6.6	4.8	6.4	6.3	8.5	11.2	8.9

Table A.22 HVFA-70H-3R (Weeks 8-14)

Date	12/19/2011	12/26/2011	1/2/2012	1/9/2012	1/16/2012	1/23/2012	1/30/2012
A1	11	12	12	13	14	15	16
A2	9.6	10	11	11	12	14	15
A3	8.1	9.4	10	11	14	16	16
B1	11	12	12	11	14	15	16
B2	9.5	9.8	10	12	13	14	15
B3	8.4	8.6	12	13	15	16	16
Average	9.6	10.3	11.1	11.8	13.7	15.0	15.7

Table A.23 HVFA-70H-3R (Weeks 15-21)

Date	2/6/2012	2/13/2012	2/20/2012	2/27/2012	3/5/2012	3/12/2012	3/19/2012
A1	18	19	21	21	22	25	23
A2	16	18	18	20	21	24	20
A3	16	17	20	21	24	28	27
B1	17	18	20	21	24	26	22
B2	17	18	19	20	22	24	21
B3	19	22	23	23	25	28	22
Average	17.2	18.7	20.2	21.0	23.0	25.8	22.5

Table A.24 HVFA-70H-3R (Weeks 22-24)

Date	3/26/2012	4/2/2012	4/9/2012
A1	26	29	29
A2	25	28	29
A3	29	32	31
B1	28	29	31
B2	26	27	30
B3	23	33	33
Average	26.1	29.7	30.5

Table A.25 HVFA-70L-1R (Weeks 1-7)

Date	11/11/2011	11/18/2011	11/25/2011	12/2/2011	12/9/2011	12/16/2011	12/23/2011
A1	8.7	6.9	7.5	9.8	11	10	11
A2	7.5	5.7	6.4	6.9	9.7	8.6	9.7
A3	7.6	8.5	6.6	8.4	9.5	12	12
B1	8.4	8.1	5.9	9.6	12	13	13
B2	7	6.7	6.6	5.8	9.8	11	12
B3	6.1	5.8	7.5	9.1	11	17	19
Average	7.6	7.0	6.8	8.3	10.5	11.9	12.8

Table A.26 HVFA-70L-1R (Weeks 8-14)

Date	12/30/2011	1/13/2012	1/20/2012	1/27/2012	2/3/2012	2/10/2012	2/17/2012
A1	12	13	17	18	20	22	21
A2	10	11	14	16	19	19	20
A3	13	14	19	18	22	26	24
B1	14	15	18	19	23	28	27
B2	13	15	13	14	18	21	21
B3	20	20	23	18	19	24	22
Average	13.7	14.6	17.3	17.2	20.2	23.3	22.5

Table A.27 HVFA-70L-1R (Weeks 15-21)

Date	2/24/2012	3/2/2012	3/9/2012	3/16/2012	3/23/2012	3/30/2012	4/6/2012
A1	20	23	26	26	27	29	31
A2	19	19	23	23	25	27	26
A3	22	24	24	25	26	29	33
B1	22	26	26	30	32	32	34
B2	19	21	22	23	25	27	28
B3	24	25	26	29	32	35	39
Average	21.0	23.0	24.5	26.0	27.9	29.8	31.8

Table A.28 HVFA-70L-1R (Weeks 22-24)

Date	4/13/2012	4/20/2012	4/27/2012
A1	34	35	31
A2	32	36	28
A3	35	38	31
B1	36	40	34
B2	30	35	32
B3	41	44	35
Average	34.7	38.0	31.8

Table A.29 HVFA-70L-2R (Weeks 1-7)

Date	11/11/2011	11/18/2011	11/25/2011	12/2/2011	12/9/2011	12/16/2011	12/23/2011
A1	8.1	7.7	7.3	11	11	16	15
A2	7.1	7.2	5.6	9.5	7	12	13
A3	7.9	8.5	9	11	13	12	12
B1	7.1	8.5	6.4	9.6	11	13	14
B2	7	6.2	6	9	8.8	12	13
B3	10	9.3	7.8	11	12	14	18
Average	7.9	7.9	7.0	10.2	10.5	13.2	14.2

Table A.30 HVFA-70L-2R (Weeks 8-14)

Date	12/30/2011	1/13/2012	1/20/2012	1/27/2012	2/3/2012	2/10/2012	2/17/2012
A1	16	17	25	19	22	27	26
A2	13	14	24	17	21	23	24
A3	14	15	26	21	24	26	27
B1	16	17	24	20	23	24	25
B2	15	16	23	19	21	21	22
B3	17	18	23	20	25	26	26
Average	15.2	16.2	24.2	19.3	22.7	24.5	25.0

Table A.31 HVFA-70L-2R (Weeks 15-21)

Date	2/24/2012	3/2/2012	3/9/2012	3/16/2012	3/23/2012	3/30/2012	4/6/2012
A1	27	26	26	31	32	34	39
A2	24	25	25	29	31	32	34
A3	26	27	30	32	33	34	39
B1	25	26	30	30	32	33	37
B2	24	25	26	28	30	32	32
B3	27	28	33	34	37	43	40
Average	25.5	26.2	28.3	30.7	32.7	34.7	36.8

Table A.32 HVFA-70L-2R (Weeks 22-24)

Date	4/13/2012	4/20/2012	4/27/2012
A1	44	46	35
A2	40	38	35
A3	42	47	35
B1	41	43	35
B2	40	41	35
B3	46	52	40
Average	42.2	44.5	35.8

Table A.33 HVFA-70L-3R (Weeks 1-7)

Date	11/11/2011	11/18/2011	11/25/2011	12/2/2011	12/9/2011	12/16/2011	12/23/2011
A1	6.6	7.2	8.7	9.8	11	12	13
A2	5.3	6	6.6	7.2	9.2	10	11
A3	7.1	8.2	7.9	11	11	13	14
B1	5.9	6.1	8.7	8.8	9.7	9.3	10
B2	5.4	5.4	7.2	8.8	8.7	10	11
B3	7	8.6	8.2	11	14	16	14
Average	6.2	6.9	7.9	9.4	10.6	11.7	12.2

Table A.34 HVFA-70L-3R (Weeks 8-14)

Date	12/30/2011	1/13/2012	1/20/2012	1/27/2012	2/3/2012	2/10/2012	2/17/2012
A1	13	14	13	18	20	24	23
A2	12	12	11	14	16	20	20
A3	14	13	13	19	22	23	23
B1	10	14	10	21	20	22	22
B2	12	13	14	16	17	20	19
B3	15	13	27	20	24	27	28
Average	12.7	13.2	14.7	18.0	19.8	22.7	22.5

Table A.35 HVFA-70L-3R (Weeks 15-21)

Date	2/24/2012	3/2/2012	3/9/2012	3/16/2012	3/23/2012	3/30/2012	4/6/2012
A1	20	24	25	28	31	35	34
A2	19	20	24	24	26	31	29
A3	23	24	27	28	30	33	37
B1	22	22	25	26	29	32	32
B2	21	22	23	23	27	31	32
B3	29	29	32	34	36	34	47
Average	22.3	23.5	26.0	27.2	29.9	32.6	35.2

Table A.36 HVFA-70L-3R (Weeks 22-24)

Date	4/13/2012	4/20/2012	4/27/2012
A1	39	45	33
A2	34	39	29
A3	41	50	33
B1	33	40	28
B2	33	41	34
B3	40	60	41
Average	36.7	45.8	33.0

Table A.37 HVFA-70LA-1R (Weeks 1-7)

Date	12/16/2011	12/23/2011	12/30/2011	1/6/2012	1/13/2012	1/20/2012	1/27/2012
A1	5.2	6.2	7.2	8.2	9.2	11	9.4
A2	3.2	4.2	5.2	6.2	8.1	7.1	8.6
A3	5.3	6.3	7.3	8.3	10	9.8	10
B1	5.9	6.9	7.9	8.9	9.2	11	11
B2	4.6	5.6	6.6	7.6	7.6	8.6	9
B3	5.4	6.4	7.4	8.4	9.2	9.2	10
Average	4.9	5.9	6.9	7.9	8.9	9.5	9.7

Table A.38 HVFA-70LA-1R (Weeks 8-14)

Date	2/3/2012	2/10/2012	2/17/2012	2/24/2012	3/2/2012	3/9/2012	3/16/2012
A1	10	12	11	11	13	14	14
A2	7.7	9.6	8.7	8.9	8.6	14	9.3
A3	11	13	12	13	13	14	13
B1	12	14	13	11	14	14	14
B2	8.6	11	11	9.6	9.4	12	11
B3	11	14	15	14	12	13	15
Average	10.1	12.3	11.8	11.3	11.7	13.5	12.7

Table A.39 HVFA-70LA-1R (Weeks 15-21)

Date	3/23/2012	3/30/2012	4/6/2012	4/13/2012	4/20/2012	4/27/2012	5/4/2012
A1	15	18	19	19	22	16	18
A2	13	14	12	13	16	12	14
A3	14	14	17	18	21	16	18
B1	15	16	20	20	22	18	20
B2	13	15	14	13	15	13	15
B3	15	16	19	16	19	16	18
Average	14.1	15.5	16.8	16.5	19.2	15.2	17.3

Table A.40 HVFA-70LA-1R (Weeks 22-24)

Date	5/11/2012	5/18/2012	5/25/2012
A1	20	23	26
A2	16	19	24
A3	21	24	26
B1	22	25	27
B2	17	20	23
B3	22	25	25
Average	19.7	22.6	25.2

Table A.41 HVFA-70LA-2R (Weeks 1-7)

Date	12/16/2011	12/23/2011	12/30/2011	1/6/2012	1/13/2012	1/20/2012	1/27/2012
A1	4.8	5.8	6.8	7.8	8.1	8.2	10
A2	3.7	4.7	5.7	6.7	8.4	7.5	9.3
A3	4.7	5.7	6.7	7.7	9.3	8.2	10
B1	5.3	6.3	7.3	8.3	11	9.2	12
B2	3.6	4.6	5.6	6.6	8.3	7.4	5.9
B3	5.4	6.4	7.4	8.4	8	9.5	11
Average	4.6	5.7	6.8	7.8	8.9	8.3	9.7

Table A.42 HVFA-70LA-2R (Weeks 8-14)

Date	2/3/2012	2/10/2012	2/17/2012	2/24/2012	3/2/2012	3/9/2012	3/16/2012
A1	12	13	13	13	13	19	16
A2	9.2	11	11	11	11	12	13
A3	10	13	13	12	13	15	16
B1	13	14	14	14	14	16	18
B2	9.2	11	11	11	12	12	13
B3	11	14	14	14	13	15	16
Average	10.7	12.7	12.6	12.5	12.7	14.8	15.3

Table A.43 HVFA-70LA-2R (Weeks 15-21)

Date	3/23/2012	3/30/2012	4/6/2012	4/13/2012	4/20/2012	4/27/2012	5/4/2012
A1	18	20	21	21	24	26	28
A2	15	17	17	18	20	19	21
A3	17	19	20	21	22	22	25
B1	19	21	23	24	26	22	24
B2	15	17	18	18	21	19	21
B3	17	17	22	24	23	23	25
Average	16.9	18.5	20.2	21.0	22.7	21.8	23.2

Table A.44 HVFA-70LA-2R (Weeks 22-24)

Date	12/30/2011	1/6/2012	1/13/2012
A1	30	31	33
A2	22	23	25
A3	26	27	29
B1	25	26	28
B2	24	25	27
B3	22	23	20
Average	24.9	25.7	27.1

Table A.45 HVFA-70LA-3R (Weeks 1-7)

Date	12/16/2011	12/23/2011	12/30/2011	1/6/2012	1/13/2012	1/20/2012	1/27/2012
A1	4.4	5.7	6.6	7.6	8.8	8.1	9.3
A2	4	4.4	5.4	6.4	6.8	8.1	7.6
A3	5.2	5.5	6.6	7.5	7.9	10	9.5
B1	4.7	6.3	7.1	8.1	9.2	9.2	11
B2	3.4	4.5	5.5	6.3	6.7	6.4	7.6
B3	4.3	6.1	7.3	8.4	8.3	8.2	9.1
Average	4.3	5.2	6.1	7.1	8.0	8.3	9.0

Table A.46 HVFA-70LA-3R (Weeks 8-14)

Date	2/3/2012	2/10/2012	2/17/2012	2/24/2012	3/2/2012	3/9/2012	3/16/2012
A1	10	13	13	13	12	14	13
A2	9.4	12	12	11	12	13	13
A3	12	12	12	13	13	14	16
B1	11	15	15	14	14	16	17
B2	7.3	10	10	11	11	14	13
B3	10	11	11	12	12	13	13
Average	10.0	12.2	12.2	12.3	12.3	14.0	14.2

Table A.47 HVFA-70LA-3R (Weeks 15-21)

Date	3/23/2012	3/30/2012	4/6/2012	4/13/2012	4/20/2012	4/27/2012	5/4/2012
A1	15	18	17	18	20	19	21
A2	14	16	18	20	21	18	20
A3	18	20	20	22	24	21	23
B1	19	21	22	23	27	24	26
B2	14	15	17	19	22	17	19
B3	14	13	18	19	20	21	23
Average	15.7	17.2	18.7	20.2	22.3	20.0	22.4

Table A.48 HVFA-70LA-3R (Weeks 22-24)

Date	12/30/2011	1/6/2012	1/13/2012
A1	23	24	25
A2	22	23	24
A3	25	26	27
B1	28	29	30
B2	21	22	23
B3	25	26	32
Average	24.1	25.3	26.8
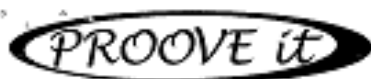
PROOVE it

ASTM C 1202-97

WST CO.

Test-compagny
Testing street 45
CompagnyCity
Some Country

CUMMINS INSTRUMENTS

Test report

Voltage Used:	60
Testing time:	06:00 hour
Charge passed:	5473
Adjusted Charge passed:	4939
Permeability class:	High
Instrument number:	071401
Channel number:	1
Report date:	7/12/2011
Testing by:	TP-SJ
Reference:	B1-EC1 TOP
Sample diameter:	100
Comment:	28 DAY
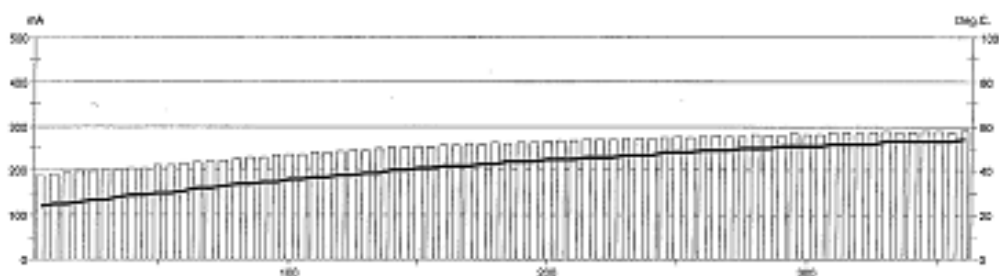
Time	°C	mA	Time	°C	mA	Time	°C	mA	Time	°C	mA
00:05	24	188.8	01:35	35	234.0	03:05	44	261.2	04:35	50	277.7
00:10	25	193.0	01:40	36	236.0	03:10	44	264.3	04:40	50	280.8
00:15	25	194.3	01:45	36	236.8	03:15	44	264.0	04:45	50	279.7
00:20	26	199.0	01:50	37	241.4	03:20	45	264.7	04:50	51	279.0
00:25	27	198.4	01:55	37	240.7	03:25	45	268.1	04:55	51	283.3
00:30	27	201.6	02:00	38	242.2	03:30	45	266.8	05:00	51	282.2
00:35	28	200.5	02:05	38	245.9	03:35	46	269.4	05:05	51	281.1
00:40	29	205.4	02:10	39	245.3	03:40	46	270.3	05:10	52	284.6
00:45	29	205.7	02:15	39	249.0	03:45	46	269.5	05:15	52	284.8
00:50	30	211.1	02:20	40	251.7	03:50	47	272.6	05:20	52	284.0
00:55	30	211.8	02:25	40	252.5	03:55	47	273.0	05:25	52	285.3
01:00	31	217.1	02:30	41	254.4	04:00	47	272.2	05:30	53	287.2
01:05	32	218.1	02:35	41	253.3	04:05	48	275.2	05:35	53	286.4
01:10	32	221.4	02:40	42	257.3	04:10	48	275.7	05:40	53	286.1
01:15	33	224.0	02:45	42	257.4	04:15	48	274.5	05:45	53	288.0
01:20	34	225.2	02:50	42	260.4	04:20	49	276.8	05:50	53	288.9
01:25	34	230.2	02:55	43	258.9	04:25	49	278.3	05:55	53	284.5
01:30	35	230.1	03:00	43	263.1	04:30	49	277.1	06:00	54	289.7

Figure A.1 – Control-EC1TOP RCT Data
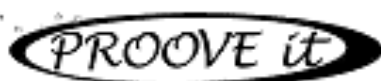
PROOVE it

ASTM C 1202-97

ST CO.

Test-compagny
Testing street 45
CompagnyCity
Some Country

GERMANN INSTRUMENTS

Test report

Voltage Used:	60
Testing time:	06:00 hour
Charge passed:	5163
Adjusted Charge passed:	4650
Permeability class:	High
Instrument number:	071401
Channel number:	2
Report date:	7/12/2011
Testing by:	TP-SJ
Reference:	B1-EC1 MIDDLE
Sample diameter:	100
Comment:	28 DAY
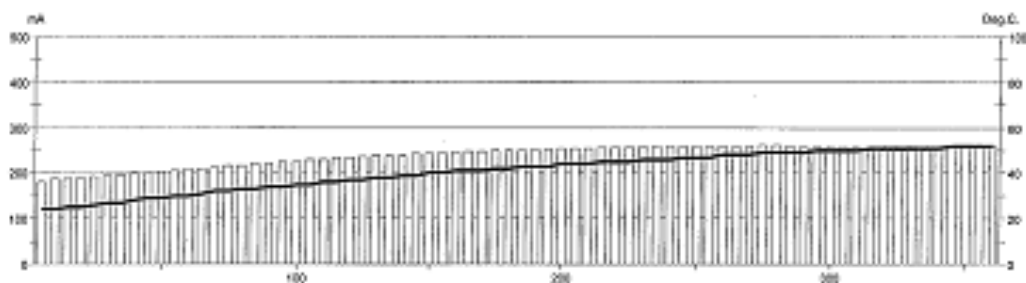
Time	°C	mA	Time	°C	mA	Time	°C	mA	Time	°C	mA
00:05	24	181.4	01:35	34	224.9	03:05	43	251.4	04:35	49	260.4
00:10	24	187.7	01:40	35	225.4	03:10	43	252.2	04:40	49	260.1
00:15	25	189.1	01:45	35	229.2	03:15	43	252.7	04:45	49	259.7
00:20	25	188.8	01:50	36	229.1	03:20	44	254.5	04:50	49	257.5
00:25	26	191.3	01:55	36	233.5	03:25	44	255.1	04:55	50	257.2
00:30	27	193.1	02:00	37	233.7	03:30	44	254.7	05:00	50	257.2
00:35	27	195.5	02:05	37	235.5	03:35	45	257.0	05:05	50	257.5
00:40	28	199.1	02:10	38	238.1	03:40	45	256.6	05:10	50	257.2
00:45	29	199.9	02:15	38	238.6	03:45	45	258.3	05:15	51	256.7
00:50	29	204.2	02:20	39	239.6	03:50	46	257.9	05:20	51	257.3
00:55	30	205.0	02:25	39	242.2	03:55	46	258.0	05:25	51	257.5
01:00	30	208.8	02:30	40	243.2	04:00	46	258.5	05:30	51	257.7
01:05	31	210.9	02:35	40	244.8	04:05	47	258.7	05:35	51	257.5
01:10	32	211.9	02:40	41	245.7	04:10	47	259.7	05:40	51	257.8
01:15	32	216.1	02:45	41	247.1	04:15	47	259.4	05:45	52	257.6
01:20	33	216.0	02:50	41	248.2	04:20	48	260.0	05:50	52	257.9
01:25	33	221.6	02:55	42	249.7	04:25	48	260.0	05:55	52	258.5
01:30	34	221.2	03:00	42	250.6	04:30	48	260.0	06:00	52	259.0

Figure A.2 – Control-EC1MIDDLE RCT Data

PROOVE it

ASTM C 1202-97

ST CO.

Test-compagny
Testing street 45
CompagnyCity
Some Country

Test report

Voltage Used:	60
Testing time:	06:00 hour
Charge passed:	4613
Adjusted Charge passed:	4163
Permeability class:	High
Instrument number:	071401
Channel number:	3
Report date:	7/12/2011
Testing by:	TP-SJ
Reference:	B1-EC2 TOP
Sample diameter:	100
Comment:	28 DAY
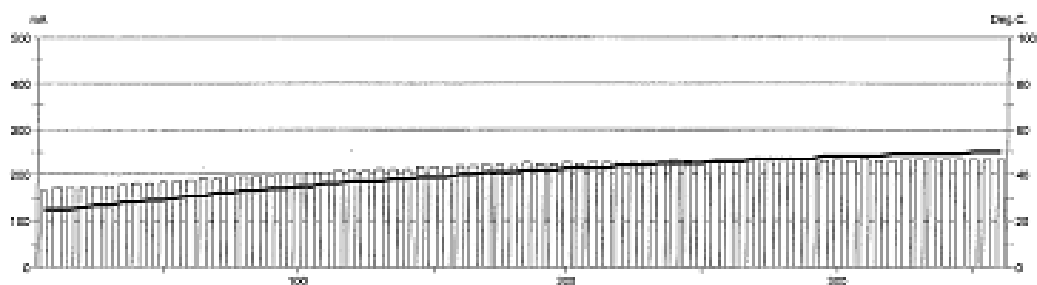
Time	°C	mA	Time	°C	mA	Time	°C	mA	Time	°C	mA
00:05	25	164.3	01:35	34	200.9	03:05	42	224.8	04:35	47	230.1
00:10	25	171.5	01:40	35	201.0	03:10	42	223.0	04:40	47	229.5
00:15	25	170.8	01:45	35	205.4	03:15	42	223.8	04:45	47	234.6
00:20	26	171.8	01:50	36	204.9	03:20	43	236.4	04:50	47	231.6
00:25	27	173.2	01:55	36	206.7	03:25	43	224.0	04:55	48	229.5
00:30	27	174.4	02:00	37	209.5	03:30	43	237.6	05:00	48	234.9
00:35	28	175.6	02:05	37	208.3	03:35	43	226.5	05:05	48	230.9
00:40	28	180.4	02:10	37	212.2	03:40	44	224.8	05:10	48	233.9
00:45	29	180.3	02:15	38	212.0	03:45	44	227.6	05:15	48	230.5
00:50	29	184.0	02:20	38	212.0	03:50	44	229.3	05:20	49	230.2
00:55	30	185.6	02:25	39	216.8	03:55	45	227.0	05:25	49	231.2
01:00	31	187.7	02:30	39	215.8	04:00	45	231.6	05:30	49	233.0
01:05	31	190.9	02:35	39	216.4	04:05	45	228.8	05:35	49	231.2
01:10	32	190.3	02:40	40	219.6	04:10	45	227.5	05:40	49	232.6
01:15	32	195.4	02:45	40	218.0	04:15	46	231.5	05:45	49	231.5
01:20	33	194.6	02:50	41	220.6	04:20	46	231.7	05:50	50	231.6
01:25	33	195.8	02:55	41	221.9	04:25	46	229.9	05:55	50	231.7
01:30	34	199.5	03:00	41	219.7	04:30	47	233.1	06:00	50	232.1

Figure A.3 – Control-EC2TOP RCT Data

PROOVE it

ASTM C 1202-97

ST CO.

Test-compagny
Testing street 45
CompagnyCity
Some Country

Test report

Voltage Used:	60
Testing time:	06:00 hour
Charge passed:	5404
Adjusted Charge passed:	4877
Permeability class:	High
Instrument number:	071401
Channel number:	4
Report date:	7/12/2011
Testing by:	TP SJ
Reference:	B1-EC2 MIDDLE
Sample diameter:	100
Comment:	28 DAY
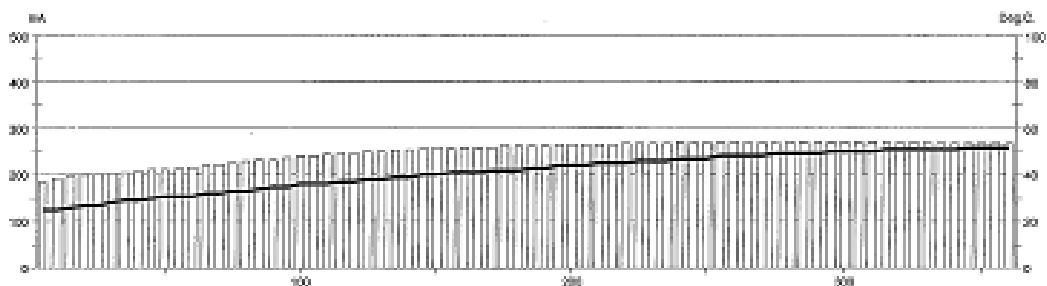
Time	°C	mA	Time	°C	mA	Time	°C	mA	Time	°C	mA
00:05	25	185.3	01:35	35	236.3	03:05	43	263.1	04:35	49	270.1
00:10	25	191.8	01:40	36	239.5	03:10	43	264.1	04:40	49	270.3
00:15	26	195.9	01:45	36	240.0	03:15	44	264.8	04:45	49	270.1
00:20	27	198.5	01:50	36	243.3	03:20	44	265.7	04:50	49	270.4
00:25	27	200.4	01:55	37	245.8	03:25	44	266.0	04:55	50	270.4
00:30	28	203.1	02:00	37	245.7	03:30	45	266.7	05:00	50	270.5
00:35	29	206.2	02:05	38	249.6	03:35	45	266.1	05:05	50	270.4
00:40	29	208.9	02:10	38	250.6	03:40	45	268.4	05:10	50	270.3
00:45	30	211.2	02:15	39	251.6	03:45	46	268.1	05:15	51	270.3
00:50	31	213.1	02:20	39	254.4	03:50	46	268.2	05:20	51	269.9
00:55	31	214.9	02:25	40	256.5	03:55	46	268.9	05:25	51	269.5
01:00	31	216.7	02:30	40	258.9	04:00	47	269.5	05:30	51	269.1
01:05	32	221.9	02:35	41	256.8	04:05	47	269.5	05:35	51	268.3
01:10	32	224.0	02:40	41	259.3	04:10	47	269.5	05:40	51	267.8
01:15	33	225.2	02:45	41	259.5	04:15	48	269.0	05:45	52	266.9
01:20	33	230.0	02:50	42	259.8	04:20	48	269.7	05:50	52	267.1
01:25	34	232.2	02:55	42	262.3	04:25	48	270.4	05:55	52	269.2
01:30	35	233.1	03:00	42	262.9	04:30	48	270.2	06:00	52	268.4

Figure A.4 – Control-EC2MIDDLE RCT Data
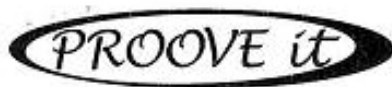
501 Ro114

PROOVE it

ASTM C 1202-97

Test-compagny
Testing street 45
CompagnyCity
Some Country

EST CO.

GIMMANN INSTRUMENTS

DENMARK

USA

Test report

Voltage Used:	60
Testing time:	06:00 hour
Charge passed:	862
Adjusted Charge passed:	778
Permeability class:	Very Low
Instrument number:	071401
Channel number:	3
Report date:	3/28/2012
Testing by:	LG
Reference:	HVFA 1-EC1-TOP
Sample diameter:	100
Comment:	28 DAY
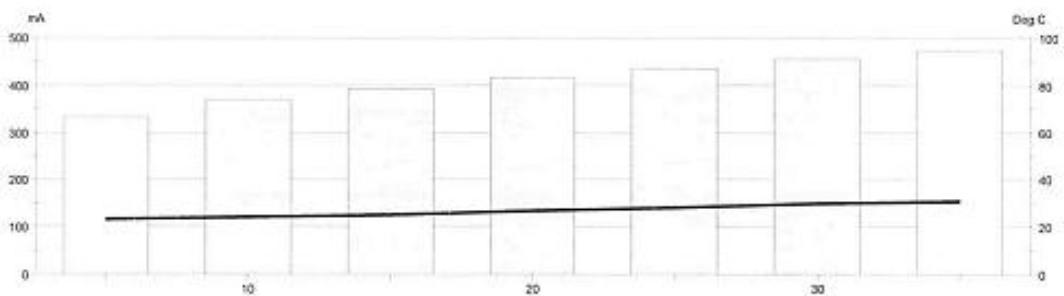
Time	°C	mA	Time	°C	mA	Time	°C	mA	Time	°C	mA
00:05	23	333.6	00:15	25	392.4	00:25	28	435.8	00:35	31	473.5
00:10	24	368.5	00:20	27	414.7	00:30	30	454.6			

Figure A.5 – HVFA-70H-EC1TOP RCT Data
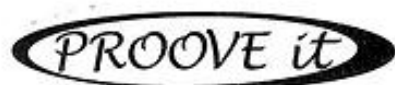
PROOVE it

ASTM C 1202-97

Test-compagny
Testing street 45
CompagnyCity
Some Country

Test report

Voltage Used:	60
Testing time:	06:00 hour
Charge passed:	646
Adjusted Charge passed:	583
Permeability class:	Very Low
Instrument number:	071401
Channel number:	4
Report date:	3/28/2012
Testing by:	LG
Reference:	HVFA 1-EC1-MIDDLE
Sample diameter:	100
Comment:	28 DAY
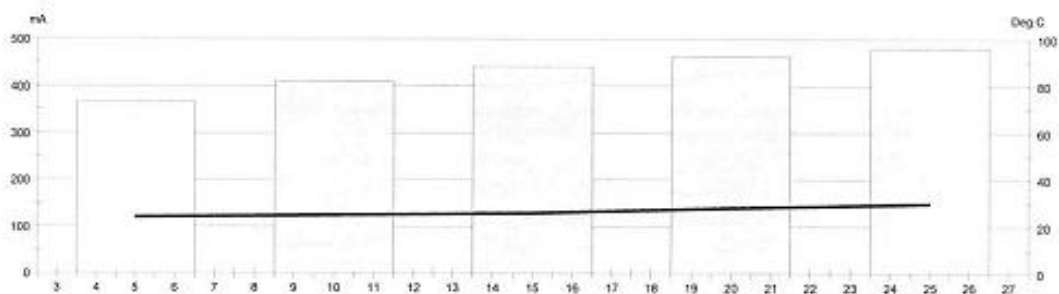
Time	°C	mA	Time	°C	mA	Time	°C	mA	Time	°C	mA
00:05	24	365.4	00:15	26	439.2	00:25	30	479.0			
00:10	25	407.9	00:20	28	462.5						

Figure A.6 – HVFA-70H-EC1MIDDLE RCT Data
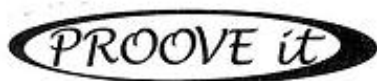
PROOVE it
ASTM C 1202-97

501 Kolla

WEST CO.

Test-compagny
Testing street 45
CompagnyCity
Some Country

GERMAN INSTRUMENTS

Test report

Voltage Used:	60
Testing time:	06:00 hour
Charge passed:	1601
Adjusted Charge passed:	1445
Permeability class:	Low
Instrument number:	071401
Channel number:	1
Report date:	3/28/2012
Testing by:	LG
Reference:	HVFA1-EC2-TOP
Sample diameter:	100
Comment:	28 DAY
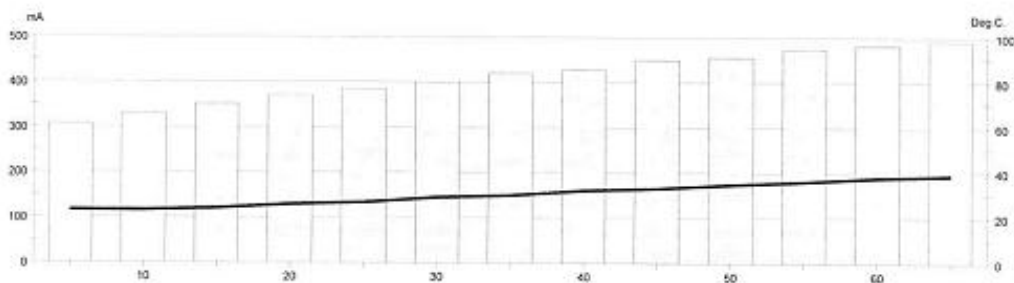
Time	°C	mA	Time	°C	mA	Time	°C	mA	Time	°C	mA
00:05	23	306.9	00:25	27	384.3	00:45	33	448.2	01:05	39	490.7
00:10	23	327.2	00:30	29	399.7	00:50	35	455.0			
00:15	24	350.5	00:35	30	420.1	00:55	36	472.2			
00:20	26	370.6	00:40	32	427.4	01:00	38	482.3			

Figure A.7 – HVFA-70H-EC2TOP RCT Data

PROOVE it

ASTM C 1202-97

Test-compagny
Testing street 45
CompagnyCity
Some Country

Test report

Voltage Used:	60
Testing time:	06:00 hour
Charge passed:	765
Adjusted Charge passed:	690
Permeability class:	Very Low
Instrument number:	071401
Channel number:	2
Report date:	3/28/2012
Testing by:	LG
Reference:	HVFA 1-EC 2-MIDDLE
Sample diameter:	100
Comment:	28 DAY

Time	°C	mA	Time	°C	mA	Time	°C	mA	Time	°C	mA
00:05	23	363.0	00:15	25	417.2	00:25	29	463.4			
00:10	24	386.4	00:20	27	440.6	00:30	31	481.0			
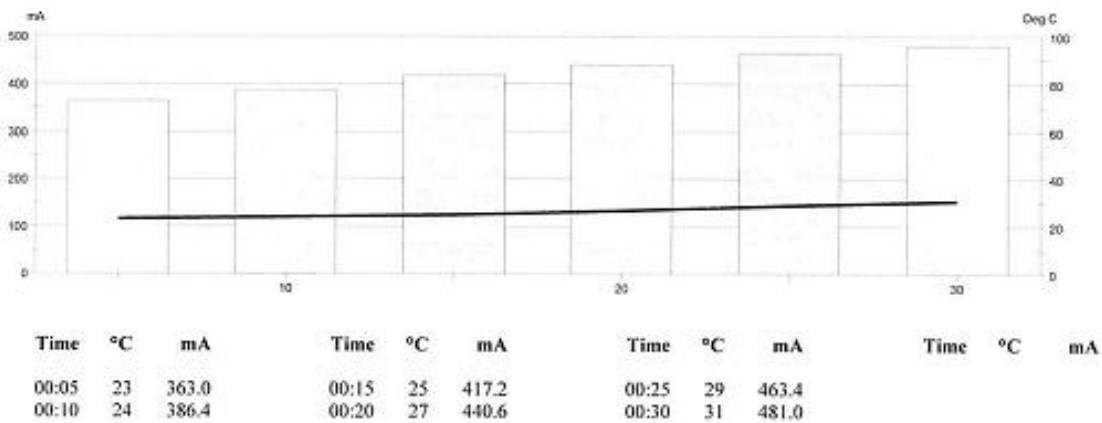
Figure A.8 – HVFA-70H-EC2MIDDLE RCT Data
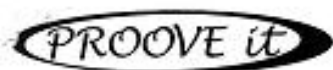
PROOVE it

ASTM C 1202-97

Test-compagny
Testing street 45
Compagny City
Some Country

Test report

Voltage Used:	60
Testing time:	06:00 hour
Charge passed:	7822
Adjusted Charge passed:	7059
Permeability class:	High
Instrument number:	071401
Channel number:	1
Report date:	11/4/2011
Testing by:	LG
Reference:	HVFA-EC1-28 DAY-TOP
Sample diameter:	100
Comment:	---
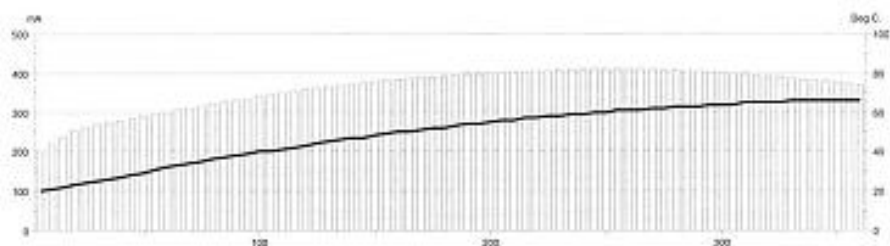
Time	°C	mA	Time	°C	mA	Time	°C	mA	Time	°C	mA
00:05	20	200.3	01:35	39	335.3	03:05	53	394.8	04:35	62	409.3
00:10	21	219.1	01:40	40	340.5	03:10	54	397.0	04:40	63	408.4
00:15	22	237.5	01:45	40	345.5	03:15	54	398.4	04:45	63	407.3
00:20	23	251.6	01:50	41	350.8	03:20	55	400.4	04:50	63	405.9
00:25	24	261.4	01:55	42	354.6	03:25	56	401.1	04:55	64	404.3
00:30	25	268.3	02:00	43	358.0	03:30	56	403.0	05:00	64	402.3
00:35	26	273.0	02:05	44	361.8	03:35	57	404.1	05:05	64	400.0
00:40	27	277.7	02:10	45	366.6	03:40	57	405.6	05:10	65	397.6
00:45	28	283.3	02:15	46	368.9	03:45	58	406.4	05:15	65	395.0
00:50	29	289.7	02:20	47	373.0	03:50	58	407.5	05:20	65	392.5
00:55	31	295.0	02:25	47	375.7	03:55	59	408.9	05:25	65	389.9
01:00	32	300.2	02:30	48	379.5	04:00	59	410.2	05:30	66	387.6
01:05	33	305.6	02:35	49	382.4	04:05	60	410.5	05:35	66	384.8
01:10	34	311.2	02:40	50	384.2	04:10	60	411.1	05:40	66	382.0
01:15	35	315.6	02:45	50	386.7	04:15	61	411.1	05:45	66	379.0
01:20	36	321.1	02:50	51	389.8	04:20	61	410.9	05:50	66	376.3
01:25	37	326.4	02:55	52	391.1	04:25	61	410.5	05:55	66	373.3
01:30	38	330.8	03:00	52	393.6	04:30	62	410.2	06:00	66	370.3

Figure A.9 – HVFA-70L-EC1TOP RCT Data

Figure A.10 – HVFA-70L-EC1MIDDLE RCT Data

PROOVE it

ASTM C 1202-97

ST CO.

Test-compagny
Testing street 45
CompagnyCity
Some Country

GERMAN INSTRUMENTS

Test report

Voltage Used:	60
Testing time:	06:00 hour
Charge passed:	8394
Adjusted Charge passed:	7576
Permeability class:	High
Instrument number:	071401
Channel number:	3
Report date:	11/4/2011
Testing by:	LG
Reference:	HVFA-EC2-TOP-28 DAY
Sample diameter:	100
Comment:	---
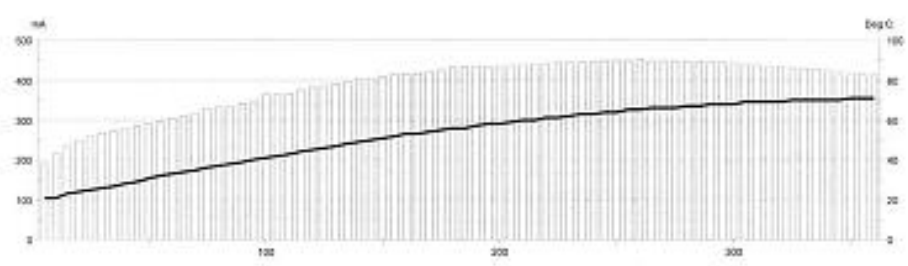
Time	°C	mA	Time	°C	mA	Time	°C	mA	Time	°C	mA
00:05	21	193.5	01:35	40	346.2	03:05	56	432.6	04:35	66	448.6
00:10	21	217.2	01:40	41	363.0	03:10	57	435.1	04:40	67	447.4
00:15	23	235.9	01:45	42	363.1	03:15	58	433.8	04:45	67	446.9
00:20	24	249.8	01:50	43	367.0	03:20	58	435.9	04:50	68	445.0
00:25	25	260.2	01:55	44	373.9	03:25	59	437.4	04:55	68	444.2
00:30	26	267.7	02:00	45	381.1	03:30	60	438.6	05:00	68	441.6
00:35	27	272.5	02:05	46	386.2	03:35	60	440.3	05:05	69	440.1
00:40	28	279.2	02:10	47	390.1	03:40	61	441.8	05:10	69	438.1
00:45	29	285.7	02:15	48	395.4	03:45	61	443.1	05:15	69	435.4
00:50	31	289.9	02:20	49	401.0	03:50	62	444.2	05:20	69	433.6
00:55	32	296.5	02:25	50	404.0	03:55	63	445.3	05:25	70	431.2
01:00	33	302.6	02:30	51	407.8	04:00	63	447.0	05:30	70	428.9
01:05	34	309.9	02:35	52	412.3	04:05	64	448.4	05:35	70	426.5
01:10	35	317.1	02:40	53	414.5	04:10	64	449.4	05:40	70	423.6
01:15	36	327.2	02:45	53	416.7	04:15	65	449.5	05:45	70	420.7
01:20	37	332.0	02:50	54	420.2	04:20	65	450.1	05:50	71	418.0
01:25	38	333.7	02:55	55	423.0	04:25	66	449.6	05:55	71	415.9
01:30	39	340.7	03:00	56	432.5	04:30	66	449.4	06:00	71	413.3

Figure A.11 – HVFA-70L-EC2TOP RCT Data
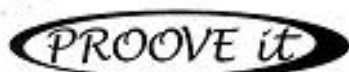
PROOVE it

ASTM C 1202-97

WEST CO.

Test-compagny
Testing street 45
CompagnyCity
Some Country

Test report

Voltage Used:	60
Testing time:	06:00 hour
Charge passed:	1107
Adjusted Charge passed:	999
Permeability class:	Very Low
Instrument number:	071401
Channel number:	4
Report date:	11/4/2011
Testing by:	LG
Reference:	HVFA-EC2-MIDDLE-28 DAY
Sample diameter:	100
Comment:	SHUT OFF 45 MIN DUE TO HIGH mA
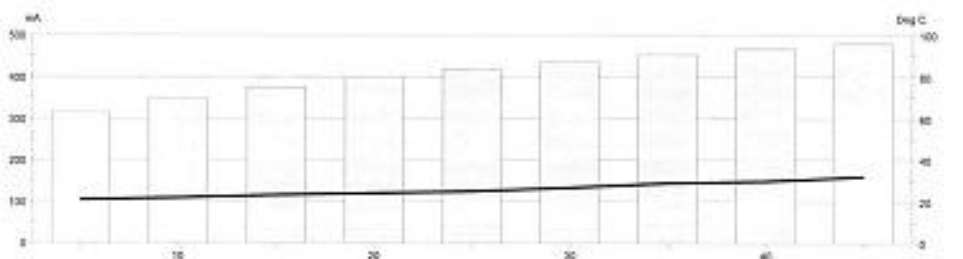
Time	°C	mA	Time	°C	mA	Time	°C	mA	Time	°C	mA
00:05	21	314.0	00:20	24	398.5	00:35	29	452.2			
00:10	22	348.2	00:25	25	418.4	00:40	30	467.2			
00:15	23	374.8	00:30	27	436.2	00:45	32	480.5			

Figure A.12 – HVFA-70L-EC2MIDDLE RCT Data
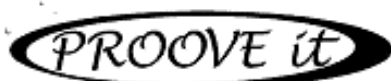
Figure A.13 – HVFA-70LA-EC1TOP RCT Data

PROOVE it

ASTM C 1202-97

Test-compagny
Testing street 45
CompagnyCity
Some Country

GERMANN INSTRUMENTS

Test report

Voltage Used:	60
Testing time:	06:00 hour
Charge passed:	876
Adjusted Charge passed:	791
Permeability class:	Very Low
Instrument number:	071401
Channel number:	4
Report date:	12/13/2011
Testing by:	LG/SB
Reference:	EC1 HVFA3-middle 30day
Sample diameter:	100
Comment:	Turned off due to excessive voltage.

Time	°C	mA	Time	°C	mA	Time	°C	mA	Time	°C	mA
00:05	21	310.0	00:15	22	408.2	00:25	25	455.3	00:35	30	479.5
00:10	21	368.6	00:20	23	436.0	00:30	27	462.3			
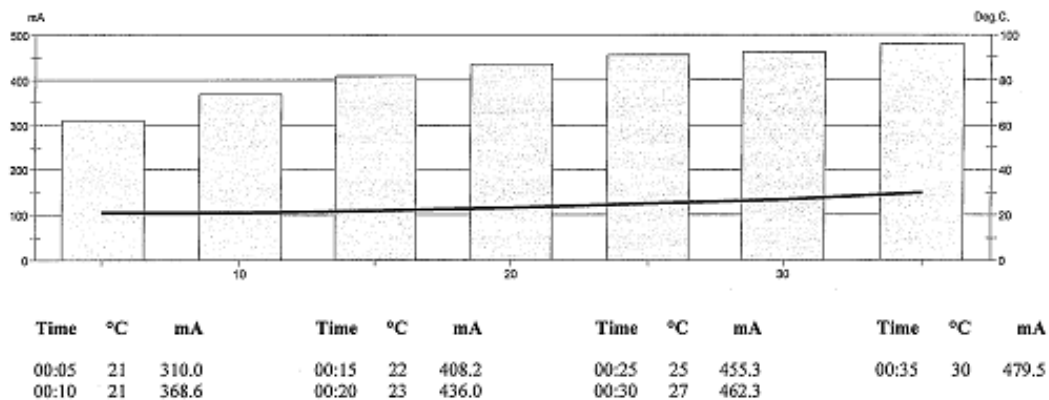
Figure A.14 – HVFA-70LA-EC1MIDDLE RCT Data

Figure A.15 – HVFA-70LA-EC2TOP RCT Data

PROOVE it

ASTM C 1202-97

Test-compagny
Testing street 45
CompagnyCity
Some Country

Test report

Voltage Used:	60
Testing time:	06:00 hour
Charge passed:	722
Adjusted Charge passed:	652
Permeability class:	Very Low
Instrument number:	071401
Channel number:	2
Report date:	12/13/2011
Testing by:	LG/SB
Reference:	EC2 HVFA-middle 30day
Sample diameter:	100
Comment:	Turned off due to excessive voltage.

Time	°C	mA	Time	°C	mA	Time	°C	mA	Time	°C	mA
00:05	21	314.7	00:15	23	392.6	00:25	26	448.2			
00:10	22	358.2	00:20	24	422.1	00:30	28	470.4			
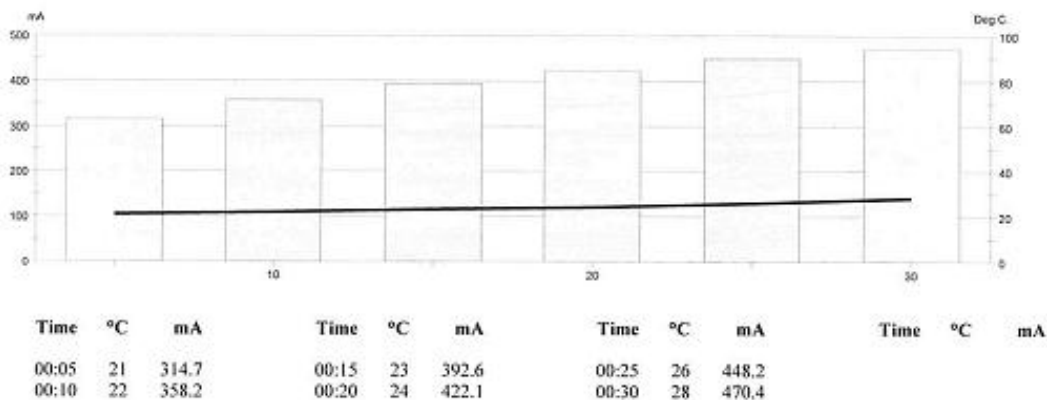
Figure A.16 – HVFA-70LA-EC2MIDDLE RCT Data

Table A.49 Control Chloride Content Data

Depth (in)	Chloride Content (%)		
	Control-1P	Control-2P	Control-3P
0	0.28	0.26	0.31
0.25	0.14	0.15	0.12
0.75	0.06	0.05	0.04
1.5	0.03	0.03	0.03
2.0	0.03	0.03	0.02

Table A.50 HVFA-70H Chloride Content Data

Depth (in)	Chloride Content (%)		
	HVFA-70H-1P	HVFA-70H-2P	HVFA-70H-3P
0	0.16	0.16	0.18
0.25	0.36	0.46	0.31
0.75	0.09	0.07	0.13
1.5	0.05	0.03	0.03
2.0	0.03	0.03	0.03

Table A.51 HVFA-70L Chloride Content Data

Depth (in)	Chloride Content (%)		
	HVFA-70L-1P	HVFA-70L-2P	HVFA-70L-3P
0	0.17	0.14	0.10
0.25	0.22	0.25	0.25
0.75	0.06	0.04	0.08
1.5	0.03	0.02	0.02
2.0	0.02	0.02	0.02

Table A.52 HVFA-70LA Chloride Content Data

Depth (in)	Chloride Content (%)		
	HVFA-70LA-1P	HVFA-70LA-2P	HVFA-70LA-3P
0	0.32	0.30	0.24
0.25	0.18	0.21	0.23
0.75	0.12	0.12	0.17
1.5	0.03	0.03	0.02
2.0	0.02	0.01	0.02

GM23			FREEZE & THAW LEDGER			Preliminary Testing Results @ Zero Cycles						
LAB NO:	UMR-B1		**BEAM ID NO:**		1	**Agg. Description**						
	35 Day Cure											
Initial Weight in Air			9445.5					**Starting Cycle Count**			12710	
						Initial bar reading		0				
Initial Gage Reading								**Date Test Started**		7/19/11		
						Completion Date		8/21/11				
Initial Frequency			1800			**TERMINAL FREQUENCY**			1080			
DATE	**CYCLE #** machine	**Actual cycles**	**Weight**	**Ref. Bar**	**Gage reading**	**Corr. gage reading**	**Frqncy**	**RDM**	**Durab. Factor**	**% Gage Length Change**	**%Wght Change**
7/20/11	12719	9	9447.6				1715	90.78	2.72		0.022
7/21/11	12728	18	9453.8				1676	86.70	5.20		0.088
7/22/11	12736	26	9457.8				1655	84.54	7.33		0.130
7/25/11	12763	53	9477.5				1574	76.47	13.51		0.339
7/27/11	12781	71	9491.2				1497	69.17	16.37		0.484
7/29/11	12799	89	9498.2				1457	65.52	19.44		0.558
8/1/11	12828	118	9505.2				1293	51.60	20.30		0.632
8/3/11	12844	134	9511.2				1104	37.62	16.80		0.696
	Flexural Strength = 356 psi										
	Tangent Modulus = 0.1416 Msi										
	Maximum Strain = 0.0055 in/in										
Totals		134						37.62	20.30	0.00	0.02

Initial Measurements				**Post Break Measurments**					
WIDTH		DEPTH		WIDTH		DEPTH			
				4.567		3.304		21.59	Avg. DF bms 1,2,3
				4.576		3.295		1.71257	Std. dev.
				4.575		3.228			
0.000		0.000		4.573		3.276	Avg.		

Initial Measurements not taken per Steve Jackson

Figure A.17 – Control-FT1 Data

GM23			FREEZE & THAW LEDGER			Preliminary Testing Results @ Zero Cycles					
LAB NO:	UMR-B1		**BEAM ID NO:**	2	**Agg. Description**	0					
	35 Day Cure										
Initial Weight in Air		9974.5				**Starting Cycle Count**			12710		
				Initial bar reading		0					
Initial Gage Reading						**Date Test Started**	7/19/11				
				Completion Date		8/21/11					
Initial Frequency		1893				**TERMINAL FREQUENCY**		1136			
DATE	**CYCLE # machine**	**Actual cycles**	**Weight**	**Ref. Bar**	**Gage reading**	**Corr. gage reading**	**Frqncy**	**RDM**	**Durab. Factor**	**% Gage Length Change**	**%Wght Change**
7/20/11	12719	9	9976.6	0			1787	89.11	2.67		0.021
7/21/11	12728	18	9984.6	0			1771	87.53	5.25		0.101
7/22/11	12736	26	9988.7	0			1759	86.34	7.48		0.142
7/25/11	12763	53	10007.7	0			1703	80.93	14.30		0.333
7/27/11	12781	71	10019.8	0			1644	75.42	17.85		0.454
7/29/11	12799	89	10028.9	0			1577	69.40	20.59		0.545
8/1/11	12828	118	10038.8	0			1423	56.51	22.23		0.645
8/3/11	12844	134	10040.8	0			1374	52.68	23.53		0.665
	Flexural Strength = 248 psi										
	Tangent Modulus = 0.0806 Msi										
	Maximum Strain = 0.0049 in/in										
Totals		134						52.68	23.53	0.00	0.02

Initial Measurements			**Post Break Measurments**		
WIDTH	DEPTH		WIDTH		DEPTH
			4.656		3.373
			4.675		3.413
			4.694		3.478
0.000	0.000		4.675		3.421 Avg.

Initial Measurements not taken per Steve Jackson

Figure B.18 – Control-FT2 Data

GM23			FREEZE & THAW LEDGER				Preliminary Testing Results @ Zero Cycles					

LAB NO:	UMR-B1		BEAM ID NO:		3	Agg. Description		0				
	35 Day Cure											
Initial Weight in Air			9195.0					Starting Cycle Count			12710	
					Initial bar reading			0				
Initial Gage Reading							Date Test Started		7/19/11			
					Completion Date		8/21/11					
Initial Frequency			1942			TERMINAL FREQUENCY			1165			

DATE	CYCLE # machine	Actual cycles	Weight	Ref. Bar	Gage reading	Corr. gage reading	Frqncy	RDM	Durab. Factor	% Gage Length Change	%Wght Change
7/20/11	12719	9	9197.0	0			1835	89.28	2.68		0.022
7/21/11	12728	18	9203.9	0			1813	87.16	5.23		0.097
7/22/11	12736	26	9210.1	0			1787	84.67	7.34		0.164
7/25/11	12763	53	9229.5	0			1696	76.27	13.47		0.375
7/27/11	12781	71	9239.3	0			1617	69.33	16.41		0.482
7/29/11	12799	89	9247.1	0			1540	62.88	18.66		0.567
8/1/11	12828	118	9255.9	0			1417	53.24	20.94		0.662
8/3/11	12844	134	9257.3	0			1263	42.30	18.89		0.678
	Flexural Strength = 350 psi										
	Tangent Modulus = 0.1226 Msi										
	Maximum Strain = 0.0040 in/in										
Totals		134						42.30	20.94	0.00	0.02

Initial Measurements				Post Break Measurments						
WIDTH		DEPTH		WIDTH		DEPTH				
				4.261		3.515				
				4.247		3.514				
				4.221		3.525				
0.000		0.000		4.243		3.518	Avg.			

Initial Measurements not taken per Steve Jackson

Figure A.19 – Control-FT3 Data

GM23			FREEZE & THAW LEDGER				Preliminary Testing Results @ Zero Cycles				
LAB NO:	HV FA1 ROLLA		**BEAM ID NO:**		1		**Agg. Description**				
	35 Day Cure										
Initial Weight in Air			9788.0					**Starting Cycle Count**		13611	
						Initial bar reading		0.2527			
Initial Gage Reading			0.2751					**Date Test Started**	10/31/11		
						Completion Date		12/3/11			
Initial Frequency			1782					**TERMINAL FREQUENCY**		1069	

DATE	CYCLE # machine	Actual cycles	Weight	Ref. Bar	Gage reading	Corr. gage reading	Frqncy	RDM	Durab. Factor	% Gage Length Change	%Wght Change
11/1/11	13620	9	9814.1	0.2534	0.2896	0.2889	1390	60.84	1.83	0.0862	0.267
11/3/11	13638	27	9856.8	0.2530	0.3299	0.3296	758	18.09	1.63	0.3406	0.703
Totals		27									

Initial Measurements				Post Break Measurments					
WIDTH		DEPTH		WIDTH		DEPTH			
4.538		3.518		4.515		3.526		#DIV/0!	Avg. DF bms 1,2,3
4.530		3.521		4.521		3.517		#DIV/0!	Std. dev.
4.543		3.515		4.538		3.553			
4.518		3.511							
4.532		3.516		4.525		3.532	Avg.		

11/3 CORNER FELL OFF

Figure A.20 – HVFA-70H-FT1 Data

GM23			FREEZE & THAW LEDGER			Preliminary Testing Results @ Zero Cycles					

LAB NO: HV FA1 ROLLA **BEAM ID NO:** 2 **Agg. Description** 0

35 Day Cure

Initial Weight in Air 9917.5   **Starting Cycle Count** 13611

Initial bar reading 0.2527

Initial Gage Reading 0.2505   **Date Test Started** 10/31/11

Completion Date 12/3/11

Initial Frequency 1787   **TERMINAL FREQUENCY** 1072

DATE	CYCLE # machine	Actual cycles	Weight	Ref. Bar	Gage reading	Corr. gage reading	Frqncy	RDM	Durab. Factor	% Gage Length Change	%Wght Change
11/1/11	13620	9	9944.7	0.2534	0.2640	0.2633	1304	53.25	1.60	0.0800	0.274
11/3/11	13638	27	9968.6	0.253	0.3018	0.3015	888	24.69	2.22	0.3188	0.515
Totals		27									

Initial Measurements				Post Break Measurments			
WIDTH		DEPTH		WIDTH		DEPTH	
4.555		3.518		4.588		3.523	
4.578		3.511		4.560		3.526	
4.551		3.503		4.574		3.514	
4.558		3.502					
4.561		3.509		4.574		3.521	Avg.

Figure A.21 – HVFA-70H-FT2 Data

GM23			FREEZE & THAW LEDGER			Preliminary Testing Results @ Zero Cycles					
LAB NO:	HV FA1 ROLLA		**BEAM ID NO:**		3	**Agg. Description**		0			
	35 Day Cure										
Initial Weight in Air			9825.6				**Starting Cycle Count**			13611	
						Initial bar reading		0.2527			
Initial Gage Reading			0.1937				**Date Test Started**		10/31/11		
						Completion Date		12/3/11			
Initial Frequency			1739				**TERMINAL FREQUENCY**		1043		

DATE	CYCLE # machine	Actual cycles	Weight	Ref. Bar	Gage reading	Corr. gage reading	Frqncy	RDM	Durab. Factor	% Gage Length Change	%Wght Change
11/1/11	13620	9	9856.3	0.2534	0.2080	0.2073	1229	49.95	1.50	0.0850	0.312
11/3/11	13638	27	9891.9	0.253	0.2459	0.2456	878	25.49	2.29	0.3244	0.675
Totals		27									

Initial Measurements				Post Break Measurments							
WIDTH		DEPTH		WIDTH		DEPTH					
4.548		3.504		4.570		3.504					
4.542		3.492		4.570		3.502					
4.547		3.494		4.569		3.522					
4.569		3.507									
4.552		3.499		4.570		3.509	Avg.				

11/3 corner fell off

Figure A.22 – HVFA-70H-FT3 Data

GM23			FREEZE & THAW LEDGER			Preliminary Testing Results @ Zero Cycles					
LAB NO:	HV FA -2		**BEAM ID NO:**	1	**Agg. Description**	ROLLA					
	35 Day Cure										
Initial Weight in Air		9956.7				**Starting Cycle Count**			13703		
				Initial bar reading	0.2528						
Initial Gage Reading		0.3387				**Date Test Started**	11/10/11				
				Completion Date	12/13/11						
Initial Frequency		1881				**TERMINAL FREQUENCY**	1129				
DATE	**CYCLE # machine**	**Actual cycles**	**Weight**	**Ref. Bar**	**Gage reading**	**Corr. gage reading**	**Frqncy**	**RDM**	**Durab. Factor**	**% Gage Length Change**	**%Wght Change**
11/14/11	13737	34	9952.3	0.2523	0.3350	0.3355	1845	96.21	10.90	-0.0200	-0.044
11/16/11	13756	53	9952.4	0.2531	0.3356	0.3353	1845	96.21	17.00	-0.0212	-0.043
11/18/11	13776	73	9953.8	0.2530	0.3340	0.3338	1849	96.63	23.51	-0.0306	-0.029
11/21/11	13801	98	9955.6	0.2535	0.3370	0.3363	1845	96.21	31.43	-0.0150	-0.011
11/23/11	13819	116	9956.3	0.2533	0.3374	0.3369	1840	95.69	37.00	-0.0112	-0.004
11/25/11	13837	134	9919.0	0.2526	0.3386	0.3388	1842	95.90	42.83	0.0006	-0.379
11/28/11	13864	161	9918.1	0.2530	0.3396	0.3394	1842	95.90	51.46	0.0044	-0.388
11/29/11	13873	170	9918.4	0.2536	0.3406	0.3398	1862	97.99	55.53	0.0069	-0.385
12/2/11	13899	196	9849.6	0.2527	0.3419	0.342	1895	101.49	66.31	0.0206	-1.076
12/5/11	13928	225	9721.7	0.2524	0.3439	0.3443	1910	103.11	77.33	0.0350	-2.360
12/7/11	13944	241	9566.9	0.2521	0.3387	0.3394	1892	101.17	81.28	0.0044	-3.915
12/9/11	13956	253	9556.1	0.2523	0.3478	0.3483	1883	100.21	84.51	0.0600	-4.023
12/12/11	13985	282	9558.8	0.2526	0.3503	0.3505	1757	87.25	82.02	0.0737	-3.996
12/14/11	14003	300	6450.0	0.2533	0.3599	0.3594	1742	85.77	85.77	0.1294	-35.220
Totals		300									

Initial Measurements			Post Break Measurments					
WIDTH	DEPTH		WIDTH		DEPTH			
4.578	3.480		4.591		3.480		#DIV/0!	Avg. DF bms 1,2,3
4.579	3.487		4.616		3.500		#DIV/0!	Std. dev.
4.535	3.486		4.577		3.487			
4.515	3.483							
4.552	3.484		4.595		3.489	Avg.		

Figure A.23 – HVFA-70L-FT1 Data

GM23			FREEZE & THAW LEDGER			Preliminary Testing Results @ Zero Cycles					
LAB NO:	HV FA -2		**BEAM ID NO:**		2	**Agg. Description**		ROLLA			
	35 Day Cure										
Initial Weight in Air			10025.6				**Starting Cycle Count**			13703	
					Initial bar reading		0.2528				
Initial Gage Reading			0.2417				**Date Test Started**		11/10/11		
					Completion Date		12/13/11				
Initial Frequency			1882			**TERMINAL FREQUENCY**			1129		
DATE	**CYCLE #** machine	**Actual cycles**	**Weight**	**Ref. Bar**	**Gage reading**	**Corr. gage reading**	**Frqncy**	**RDM**	**Durab. Factor**	**% Gage Length Change**	**%Wght Change**
11/14/11	13737	34	10022.2	0.2523	0.2446	0.2451	1845	96.11	10.89	0.0213	-0.034
11/16/11	13756	53	10022.1	0.2531	0.2452	0.2449	1841	95.69	16.91	0.0200	-0.035
11/18/11	13776	73	10022.3	0.253	0.2434	0.2432	1851	96.73	23.54	0.0094	-0.033
11/21/11	13801	98	10023.5	0.2535	0.2460	0.2453	1848	96.42	31.50	0.0225	-0.021
11/23/11	13819	116	10023.9	0.2533	0.2461	0.2456	1856	97.26	37.61	0.0244	-0.017
11/25/11	13837	134	10025.8	0.2526	0.2466	0.2468	1855	97.15	43.39	0.0319	0.002
11/28/11	13864	161	10026.3	0.253	0.2482	0.248	1854	97.05	52.08	0.0394	0.007
11/29/11	13873	170	10027.9	0.2536	0.2484	0.2476	1856	97.26	55.11	0.0369	0.023
12/2/11	13899	196	10030.4	0.2527	0.2503	0.2504	1846	96.21	62.86	0.0544	0.048
12/5/11	13928	225	10034.0	0.2524	0.2519	0.2523	1836	95.17	71.38	0.0663	0.084
12/7/11	13944	241	10016.8	0.2521	0.2507	0.2514	1829	94.45	75.87	0.0606	-0.088
12/9/11	13956	253	10018.1	0.2523	0.2530	0.2535	1805	91.98	77.57	0.0738	-0.075
12/12/11	13985	282	10027.0	0.2526	0.2608	0.261	1696	81.21	76.34	0.1206	0.014
12/14/11	14003	300	9962.0	0.2533	0.2645	0.264	1660	77.80	77.80	0.1394	-0.634
1/0/00	0	####		0							
1/0/00	0	####		0							
1/0/00	0	####		0							
1/0/00	0	####		0							
1/0/00	0	####		0							
1/0/00	0	####		0							
1/0/00	0	####		0							
1/0/00	0	####		0							
Totals		300									

Initial Measurements				**Post Break Measurments**					
WIDTH		DEPTH		WIDTH		DEPTH			
4.569		3.480		4.565		3.486			
4.578		3.481		4.563		3.473			
4.549		3.487		4.555		3.472			
4.533		3.474							
	4.557	3.481			4.561		3.477	Avg.	

Figure A.24 – HVFA-70L-FT2 Data

GM23			FREEZE & THAW LEDGER			Preliminary Testing Results @ Zero Cycles					
LAB NO:	HV FA -2		**BEAM ID NO:**		3	**Agg. Description**		ROLLA			
	35 Day Cure										
Initial Weight in Air		10153.3					**Starting Cycle Count**			13703	
					Initial bar reading		0.2528				
Initial Gage Reading		0.2511					**Date Test Started**		11/10/11		
					Completion Date		12/13/11				
Initial Frequency		1886				**TERMINAL FREQUENCY**			1132		
DATE	**CYCLE #** machine	**Actual cycles**	**Weight**	**Ref. Bar**	**Gage reading**	**Corr. gage reading**	**Frqncy**	**RDM**	**Durab. Factor**	**% Gage Length Change**	**%Wght Change**
11/14/11	13737	34	10149.6	0.2523	0.2534	0.2539	1870	98.31	11.14	0.0175	-0.036
11/16/11	13756	53	10149.5	0.2531	0.2521	0.2518	1865	97.79	17.28	0.0044	-0.037
11/18/11	13776	73	10151.2	0.253	0.2503	0.2501	1875	98.84	24.05	-0.0062	-0.021
11/21/11	13801	98	10151.8	0.2535	0.2535	0.2528	1862	97.47	31.84	0.0106	-0.015
11/23/11	13819	116	10152.2	0.2533	0.2536	0.2531	1879	99.26	38.38	0.0125	-0.011
11/25/11	13837	134	10154.4	0.2526	0.2538	0.254	1876	98.94	44.19	0.0181	0.011
11/28/11	13864	161	10153.8	0.253	0.2548	0.2546	1877	99.05	53.16	0.0219	0.005
11/29/11	13873	170	10156.6	0.2536	0.2559	0.2551	1871	98.42	55.77	0.0250	0.033
12/2/11	13899	196	10157.2	0.2527	0.2604	0.2605	1862	97.47	63.68	0.0588	0.038
12/5/11	13928	225	10163.3	0.2524	0.2641	0.2645	1836	94.77	71.08	0.0838	0.098
12/7/11	13944	241	10132.3	0.2521	0.2650	0.2657	1842	95.39	76.63	0.0913	-0.207
12/9/11	13956	253	10059.1	0.2523	0.2654	0.2659	1842	95.39	80.44	0.0925	-0.928
12/12/11	13985	282	10066.2	0.2526	0.2757	0.2759	1715	82.69	77.73	0.1550	-0.858
12/14/11	14003	300	9992.9	0.2533	0.2776	0.2771	1709	82.11	82.11	0.1625	-1.580
1/0/00	0	####		0							
1/0/00	0	####		0							
1/0/00	0	####		0							
1/0/00	0	####		0							
1/0/00	0	####		0							
1/0/00	0	####		0							
1/0/00	0	####		0							
1/0/00	0	####		0							
Totals		300									

Initial Measurements				**Post Break Measurments**			
WIDTH		DEPTH		WIDTH		DEPTH	
4.629		3.494		4.620		3.495	
4.633		3.489		4.598		3.491	
4.620		3.503		4.562		3.495	
4.633		3.501					
4.629		3.497		4.593		3.494	Avg.

Figure A.25 – HVFA-70L-FT3 Data

GM23			FREEZE & THAW LEDGER			Preliminary Testing Results @ Zero Cycles						
LAB NO:	HV FA3		**BEAM ID NO:**		1	**Agg. Description**		ROLLA				
Initial Weight in Air			10102.4					**Starting Cycle Count**			888	
						Initial bar reading		0.2523				
Initial Gage Reading			0.4134					**Date Test Started**		3/5/12		
						Completion Date		4/7/12				
Initial Frequency			1761					**TERMINAL FREQUENCY**		1057		

DATE	CYCLE # machine	Actual cycles	Weight	Ref. Bar	Gage reading	Corr. gage reading	Frqncy	RDM	Durab. Factor	% Gage Length Change	%Wght Change
3/7/12	901	13	10102.6	0.2532	0.4143	0.4134	1676	90.58	3.93	0.0000	0.002
3/9/12	917	29	10092.7	0.2521	0.4132	0.4134	1669	89.82	8.68	0.0000	-0.096
3/13/12	953	65	10093.9	0.2523	0.4149	0.4149	1663	89.18	19.32	0.0094	-0.084
3/16/12	979	91	10094.7	0.2507	0.4141	0.4157	1656	88.43	26.82	0.0144	-0.076
3/26/12	1015	127	10088.6	0.2516	0.4167	0.4174	1648	87.58	37.07	0.0250	-0.137
3/28/12	1033	145	10089.6	0.2519	0.4168	0.4172	1633	85.99	41.56	0.0238	-0.127
3/29/12	1043	155	10090.2	0.2515	0.4172	0.418	1636	86.31	44.59	0.0288	-0.121
4/4/12	1081	193	10092.0	0.2513	0.4172	0.4182	1610	83.59	53.77	0.0300	-0.103
4/6/12	1087	199	10094.0	0.2495	0.4169	0.4197	1609	83.48	55.38	0.0394	-0.083
4/9/12	1113	225	10094.1	0.2518	0.4196	0.4201	1613	83.90	62.92	0.0419	-0.082
4/13/12	1128	240	10065.3	0.2513	0.4183	0.4193	1594	81.93	65.55	0.0369	-0.367
4/16/12	1156	268	10061.2	0.2520	0.4204	0.4207	1598	82.34	73.56	0.0456	-0.408
4/19/12	1179	291	10059.4	0.2524	0.4220	0.4219	1593	81.83	79.38	0.0531	-0.426
4/20/12	1188	300	10033.4	0.2515	0.4208	0.4216	1590	81.52	81.52	0.0513	-0.683
Totals		300						81.52	81.52	0.05	0.00

Initial Measurements			Post Break Measurments					
WIDTH		DEPTH	WIDTH		DEPTH			
4.590		3.512	4.558		3.511		68.52	Avg. DF bms 1,2,3
4.601		3.512	4.578		3.508		20.8907	Std. dev.
4.601		3.512	4.581		3.510			
4.615		3.513						
4.602		3.512	4.572		3.510	Avg.		

3/20/12 Equipment failure the beams had to be put in the walk in freezer for 6 days.

Figure A.26 – HVFA-70LA-FT1 Data

GM23			FREEZE & THAW LEDGER			Preliminary Testing Results @ Zero Cycles						
LAB NO:	HV FA3		**BEAM ID NO:**		2	**Agg. Description**		ROLLA				
Initial Weight in Air			10005.7					**Starting Cycle Count**			888	
					Initial bar reading		0.2523					
Initial Gage Reading			0.2670					**Date Test Started**	3/5/12			
					Completion Date		4/7/12					
Initial Frequency			1763			**TERMINAL FREQUENCY**			1058			

DATE	CYCLE # machine	Actual cycles	Weight	Ref. Bar	Gage reading	Corr. gage reading	Frqncy	RDM	Durab. Factor	% Gage Length Change	%Wght Change
3/7/12	901	13	10003.1	0.2532	0.2679	0.267	1694	92.33	4.00	0.0000	-0.026
3/9/12	917	29	10003.3	0.2521	0.2667	0.2669	1689	91.78	8.87	-0.0006	-0.024
3/13/12	953	65	10003.6	0.2523	0.2690	0.269	1691	92.00	19.93	0.0125	-0.021
3/16/12	979	91	10005.5	0.2507	0.2690	0.2706	1675	90.27	27.38	0.0225	-0.002
3/26/12	1015	127	10000.1	0.2516	0.2711	0.2718	1662	88.87	37.62	0.0300	-0.056
3/28/12	1033	145	9997.2	0.2519	0.2716	0.272	1656	88.23	42.64	0.0313	-0.085
3/29/12	1043	155	9998.0	0.2515	0.2721	0.2729	1643	86.85	44.87	0.0369	-0.077
4/4/12	1081	193	9995.5	0.2513	0.2726	0.2736	1618	84.23	54.19	0.0413	-0.102
4/6/12	1087	199	9991.9	0.2495	0.2723	0.2751	1626	85.06	56.42	0.0506	-0.138
4/9/12	1113	225	9990.1	0.2518	0.2762	0.2767	1613	83.71	62.78	0.0606	-0.156
4/13/12	1128	240	9970.3	0.2513	0.2748	0.2758	1578	80.11	64.09	0.0550	-0.354
4/16/12	1156	268	9971.2	0.252	0.2772	0.2775	1592	81.54	72.84	0.0656	-0.345
4/19/12	1179	291	9969.3	0.2524	0.2780	0.2779	1580	80.32	77.91	0.0681	-0.364
4/20/12	1188	300	9968.6	0.2515	0.2781	0.2789	1573	79.61	79.61	0.0744	-0.371
Totals		300						79.61	79.61	0.07	0.00

Initial Measurements				Post Break Measurments						
WIDTH		DEPTH		WIDTH		DEPTH				
4.569		3.491		4.611		3.477				
4.618		3.501		4.616		3.482				
4.613		3.496		4.610		3.492				
4.601		3.495								
4.600		3.496		4.612		3.484	Avg.			

3/20/12 Equipment failure the beams had to be put in the walk in freezer for 6 days.

Figure A.27 – HVFA-70LA-FT2 Data

GM23			FREEZE & THAW LEDGER			Preliminary Testing Results @ Zero Cycles					
LAB NO:	HV FA3		**BEAM ID NO:**		3	**Agg. Description**		ROLLA			
Initial Weight in Air			9969.8				**Starting Cycle Count**			888	
					Initial bar reading		0.2523				
Initial Gage Reading			0.3015				**Date Test Started**		3/5/12		
					Completion Date		4/7/12				
Initial Frequency			1739				**TERMINAL FREQUENCY**		1043		

DATE	CYCLE # machine	Actual cycles	Weight	Ref. Bar	Gage reading	Corr. gage reading	Frqncy	RDM	Durab. Factor	% Gage Length Change	%Wght Change
3/7/12	901	13	9971.1	0.2532	0.3025	0.3016	1672	92.44	4.01	0.0006	0.013
3/9/12	917	29	9974.1	0.2521	0.3014	0.3016	1659	91.01	8.80	0.0006	0.043
3/13/12	953	65	9977.6	0.2523	0.3044	0.3044	1640	88.94	19.27	0.0181	0.078
3/16/12	979	91	9982.5	0.2507	0.3039	0.3055	1607	85.40	25.90	0.0250	0.127
3/26/12	1015	127	9987.2	0.2516	0.3086	0.3093	1563	80.78	34.20	0.0487	0.175
3/28/12	1033	145	9987.6	0.2519	0.3103	0.3107	1516	76.00	36.73	0.0575	0.179
3/29/12	1043	155	9982.0	0.2515	0.3111	0.3119	1506	75.00	38.75	0.0650	0.122
4/4/12	1081	193	9976.9	0.2513	0.3132	0.3142	1441	68.66	44.17	0.0794	0.071
4/6/12	1087	199	9976.9	0.2495	0.3129	0.3157	1440	68.57	45.48	0.0888	0.071
4/9/12	1113	225	9978.0	0.2518	0.3192	0.3197	1368	61.88	46.41	0.1138	0.082
4/13/12	1128	240	9932.4	0.2513	0.3185	0.3195	1310	56.75	45.40	0.1125	-0.375
4/16/12	1156	268	9933.0	0.252	0.3223	0.3226	1267	53.08	47.42	0.1319	-0.369
4/19/12	1179	291	9901.1	0.2524	0.3236	0.3235	1210	48.41	46.96	0.1375	-0.689
4/20/12	1188	300	9895.9	0.2515	0.3275	0.3283	1159	44.42	44.42	0.1675	-0.741
Totals		300						44.42	44.42	0.17	0.18

Initial Measurements				**Post Break Measurments**						
WIDTH		DEPTH		WIDTH		DEPTH				
4.568		3.538		4.576		3.491				
4.592		3.504		4.566		3.492				
4.581		3.501		4.557		3.502				
4.589		3.515								
4.583		3.515		4.566		3.495	Avg.			

3/20/12 Equipment failure the beams had to be put in the walk in freezer for 6 days.

Figure A.28 – HVFA-70LA-FT3 Data

REFERENCES

ASTM C 39 (2010). Standard Test Method for Compressive Strength of Cylindrical Concrete Specimens. *American Society of Testing and Materials,* West Conshohocken, PA.

ASTM C 78 (2010). Standard Test Method for Flexural Strength of Concrete (Using Simple Beam with Third-Point Loading) *American Society of Testing and Materials,* West Conshohocken, PA.

ASTM C 192 (2007). Standard Test Method for Making and Curing Concrete Test Specimens in the Laboratory. *American Society of Testing and Materials,* West Conshohocken, PA.

ASTM C 469 (2002). Standard Test Method for Static Modulus of Elasticity and Poissons Ratio of Concrete in Compression. *American Society of Testing and Materials,* West Conshohocken, PA.

ASTM C 496 (2004). Standard Test Method for Splitting Tensile Strength of Cylindrical Concrete Specimens. *American Society of Testing and Materials,* West Conshohocken, PA.

ASTM C 618 (2004). Standard Guide for Coal Fly Ash and Raw or Calcined Natural Pozzolan for Use in Concrete. *American Society of Testing and Materials,* West Conshohocken, PA.

ASTM C 666 (2008). Standard Test Method for Resistance of Concrete to Rapid Freezing and Thawing. *American Society of Testing and Materials,* West Conshohocken, PA.

ASTM C 672 (2008). Standard Test Method for Scaling Resistance of Concrete Surfaces Exposed to Deicing Chemicals. *American Society of Testing and Materials,* West Conshohocken, PA.

ASTM C 1202 (2010). Standard Test Method for Electrical Indication of Concrete's Ability to Resist Chloride Ion Penetration. *American Society of Testing and Materials*, West Conshohocken, PA.

ASTM C 1543 (2010). Standard Test Method for Determining the Penetration of Chloride Ion into Concrete by Ponding. *American Society of Testing and Materials,* West Conshohocken, PA.

Office of Research, Development, and Technology, Office of Safety, RDT. (1997). "User Guidelines for Waste and Byproduct Materials in Pavement Construction," *Report No. FHWA-RD-97-148*. Federal Highway Administration, Cortest Columbus Technologies.

V.M. Malhotra and P.K. Mehta (2008). *High-Performance, High-Volume Fly Ash Concrete for Building Sustainable and Durable Structures*. (Third Editon).

Mindess, Sidney, Young, J. Francis, and Darwin, David (2003). *Concrete*. Pearson Education, Inc. (Second Editon)

Powers, T.C., "Freezing Effects in Concrete," in *Durability of Concrete*, SP-47, American Concrete Institute, Detroit, MI, pp. 1-12 (1975)

Shi, Caijun, "Another Look at the Rapid Chloride Permeability Test (ASTM C1202 or AASHTO T277)

Bentz, Dale P. and Ferraris, Chiara F. (2001). Rheology and Setting of High Volume Fly Ash Mixtures. *National Institute of Standards and Technology.* Gaithersburg, MD.

Broomfield, John P. (2007). *Corrosion of Steel in Concrete: Understanding, Investigation and Repair.* Taylor & Francis (Second Edition).

Hopkins, D.S., Thomas, M.D.A., Oates, D.B., Girn, G., Munro, R. (2003). York University uses High-Volume Fly Ash Concrete for Green Building. Department of Civil Engineering, University of Toronto, Canada.

Huffman, Morris and ACI Committee 232. (2003). "Use of Fly Ash in Concrete," *Report No. ACI 232.2R-03.* American Concrete Institute, Farmington Hills, MI.

Sengul, O. and Gjørv, O. (2009). Effect of Embedded Steel on Electrical Resistivity Measurements on Concrete Structures. *ACI Materials Journal, 106(1),* 11-18.

Whiting, D.A. and Nagi, M.A. (2003). *Electrical Resistivity of Concrete - A Literature Review,* R&D Serial No. 2457. Portland Cement Association, Skokie, IL.

Mansfield, F. "Recording and Analysis of AC Impedance Data for *Corrosion* Studies," *Corrosion*, Vol. *37*, No. *5*, *1981*, pp. *301-307*

Berke, N.S. and Hicks, M.C., "Predicting Times to Corrosion from Field and Laboratory Data," Techniques to Assess the Corrosion Activity of Steel Reinforced Concrete Structures, ASTM STP 1276. Neal S. Berke, Edward Escalante, Charles K. Nmai, and David Whiting, Eds., American Society for Testing and Materials, 1996.

Marlay, Kyle M. *Hardened Concrete Properties and Durability Assessment of High Volume Fly   Ash Concrete*. Report. Missouri University of Science and Technology, 2011. Print.

Ortega, Carlos A. *Shear and Fracture Behavior of High-Volume Fly Ash Reinforced Concrete   for Sustainable Construction.* Report. Missouri University of Science and Technology,   2012. Print.

A. M. Neville (1997).   *Properties of Concrete.*   John Wiley and Sons, Inc. (Fourth Edition).

Oluokun, Francis A (1991). "Prediciton of Concrete Tensile Strength from Its Compressive Strength: Evaluation of Existing Relations for Normal Weight Concrete." *ACI Materials Journal*, Vol. 88, No. 3, pp. 302-309.